NASA TECHNICAL TRANSLATION NASA TT F-16,226

PHYSICS OF THE PLANET VENUS

A.D. Kuz'min and M.Ya. Marov

(NASA-TT-F-16226) PHYSICS OF THE PLANET VENUS (Kanner (Leo) Associates) 334 p HC CSCL 03B

N75-26959

Unclas
G3/91 27338

Translation of "Fizika Planety Venera," Moscow, "Nauka" Press, 1974, 408 pages

Reproduced by
NATIONAL TECHNICAL
INFORMATION SERVICE
US Department of Commerce
Springfield, VA. 22151

NATIONAL AERONAUTICS AND SPACE ADMINISTRATION
WASHINGTON, D.C. 20546 JUNE 1975

STANDARD TITLE PAGE

1. Report No. NASA TT F-16,226	2. Government Accession No.	3. Recipient's Catalog No
4. Title and Subtitle PHYSICS OF THE PLANET VENUS		5. Report Date June 1975 6. Performing Organization Code
7. Author(s) A.D. Kuz'min and M.Ya. Marov		8. Performing Organization Report No. 10. Work Unit No. 11. Contract or Grant No. NASw-2481
9. Performing Organization Name and Address Leo Kanner Associates Redwood City, California 94063		13. Type of Report and Period Covered Translation
12. Sponsoring Agency Name and Address National Aeronautics and Space Administration, Washington, D.C. 20546		14. Sponsoring Agency Code

15. Supplementary Notes

Translation of "Fizika Planety Venera," Moscow, "Nauka" Press, 1974, 408 pages

16. Abstract

This monograph summarizes currently-known data on the dimensions, figure, relief, rotation, surface physics, atmosphere, ionosphere and upper atmosphere of Venus. These data have been obtained from measurements made from spacecraft and with the aid of ground-based instruments.

The book contains an analysis of previously-published materials as well as the findings of authors who have made important contributions to the study of Venus.

PRICES SUBJECT TO CHANGE

17. Key Words (Selected by Author(s))	18. Distribution Statement
	Unclassified-Unlimited

19. Security Classif. (of this report)	20. Security Classif. (of this page)
Unclassified	Unclassified

NASA-HQ

Annotation

Fizika planetary Venera, Kuz'man, A.D., M. Ya. Marov, Physics-Mathematics Section, Nauka Press, 408 pages.

This monograph summarizes currently-known data on the dimensions, figure, relief, rotation, surface physics, atmosphere, ionosphere and upper atmosphere of Venus. These data have been obtained from measurements made from spacecraft and with the aid of ground-based instruments.

The book contains an analysis of previously-published materials as well as the findings of authors who have made important contributions to the study of Venus.

The book is for specialists in astronomy and physics, undergraduate and graduate students in these specialties, and specialists in other branches of sciences who are interested in space research.

126 figures, 25 tables and 587 references.

Dedicated to the fond memory of Georgiy Nikolayevich Babakin

Foreword

Questions of the physics of planets have received a significant development in recent years. This has been caused, on one hand, by practical needs connected with the development of space flights and, on the other hand, by the improvement of ground observation techniques and by putting such powerful instruments as unmanned spacecraft into operation. As a result, the study of planets has been enriched with new data, which have a fundamental significance and which have led to substantial progress in our conceptions of the physical characteristics of the planets.

Venus is the planet closest to Earth and is very similar to Earth in mass, size, and the amount of solar energy it absorbs. It has attracted the attention of researchers for many centuries. From 1761, when M.V. Lomonosov discovered an atmosphere on Venus, the results of optical and radio observations have made a great contribution to the study of the physics of this planet; yet it was in the 1950's and 1960's that they developed the most. The work of the Soviet school of astronomers -- radiophysicists and planetologists -- have played a great role in this respect. The results of their work have been set forth in detail in the monographs of V.V. Sharonov, N.P. Barabashov, V.I. Moroz, and A.D. Kuz'min.

Research findings in the last decade have brought forth convincing evidence that Venus is a unique planet, different from other planets in the solar system, primarily in terms of the gaseous atmosphere, heat conditions, and parameters of rotation. Thanks to the launch of spacecraft, great progress has been made in the study of Venus; these spacecraft have allowed atmospheric probes behow the level of the dense clouds that continually wind around the planet. The successes of space-rocket technology have made it possible to set and carry through such experiments.

In recent years, a planned program of Venus research has been carried out in the Soviet Union. Flights began in 1961 with the launch of Venera-1. In 1965, the Venera-2 and Venera-3 stations made flights along flyby and intercept trajectories. In October 1967, while descending by parachute to a level that corresponded to a pressure of about 18 atm, the unmanned Venera-4 station took the first direct measurements of the physical parameters and chemical composition of the atmosphere of Venus. Measurements made by the American spacecraft Mariner-4, which flew by at a distance of about 10,000 km from the center of Venus, probed the atmosphere on the day and night sides of the planet down to the level of critical refraction of radio waves, and thus complemented the Venera measurements. Besides measuring the parameters of the

neutral atmosphere at the altitude of the troposphere and stratosphere, both spacecraft also sent back information about the upper atmosphere and ionosphere of Venus and revealed an interesting feature -- a plasma of solar wind surrounding the planet. The flights of Venera-5 and Venera-6 in May 1969 substantially refined and added to the results of the Venera-4 flight, broadened the area of direct measurements of atmospheric temperature and pressure on the night side, and made it possible to construct a model of the planetary atmosphere with reliable estimates of its surface parameters.

In December 1970, Venera-7 made the first landing on the night side of Venus and transmitted information directly from the planetary surface. In July 1972, Venera-8 landed on the Venusian day side and, while operating on the surface in the extraordinarly difficult conditions of the surrounding medium, took measurements for almost an hour.

The flights of the Venera unmanned stations have elucidated the features of the physical structure of the Venusian atmosphere and have allowed us to make more definite judgments about the mechanisms responsible for the development and maintenance of the planet's peculiar heat conditions.

On April 12, 1973, the President of the USSR Academy of Sciences, Academician M.V. Keldysh, appeared before a solemn convocation devoted to celebrating the Day of Cosmonautics and stated: "A large and important stage in the study of this planet by using unmanned stations has been crowned by the experiments on Venera-8. This stage has reliably established the basic chemical composition and parameters of the Venusian atmosphere down to the surface, we have obtained data about the optical characteristics of the atmosphere, and the first research done directly on the planetary surface has been accomplished."

This fundamentally new information about Venus' physical features, information that has been obtained both by measurements on spacecraft and by optical and radio observations, as well as the possibility of interpreting more reliably the data previously obtained from ground observations, have naturally not been reflected in monographs more than 7 to 10 years old.

This has made it necessary to write this book, which attempts to bring together the latest information about the nature of Venus, information which heretofore has been dispersed in individual articles and reports. The book is based on an analysis of the great amount of material contained in the world literature and on the authors' own findings. It is meant for specialists in planetary astronomy and space physicists, for geophysicists and representatives of related specialties, and it can be of use to engineers and anyone who is interested in space research and the physics of planets.

The authors well know that their work is not an exhaustive account of all the problems that have to do with the physics of the planet Venus. Nor have they set themselves such a task. Rather, their consideration is primarily to give the fullest possible account of research findings up to the beginning of 1973, while at the same time keeping the book at an optimal length. In a whole series of cases, therefore, the reader who wishes to become acquainted in detail with a particular problem is referred to the original work; this is given in the extensive bibliography, which is, however, in no case to be considered a full bibliography. The reader who is prepared, who is well acquainted with the subject, may be dissatisfied because the authors have kept to a descriptive account and thus have not set forth the methodological side of the experiments, as well as the history of the question, in sufficient detail. The justification for this, in our opinion, is that as a rule preference was given to the most recent works, which in many cases contain information on methodology and which generalize the significant results obtained previously.

A.D. Kuz'min has written Chapters I, II, III, and Part 5 of Chapter IV; M.Ya. Marov has written Chapters IV, V, VI and the Appendix.

The authors consider it their obligation to emphasize above all that obtaining fundamental results about the nature of Venus would have been impossible without the immense labors of many research teams, who have enabled unmanned space stations to be built, who have directed their flights, and who have successfully carried out complex experiments in the planetary atmosphere and on its surface. The authors are grateful to Academician A.P. Vinogradov, who initiated this work; to their colleagues in their work, V.S. Avduyevskiy, M.K. Rozhdestvenskiy, V.V. Kerzhanovich, N.F. Borodino, B.Ye. Moshkin, A.P. Ekonomov, N.L. Lukashevich, V.P. Shari, V.I. Polezhayev, Ye.M. Feygel'son, Yu.N. Vetukhnovskaya, O.L. Ryabov and others, with whose cooperation the individual investigations reflected in this book were done; and to their colleagues abroad, who kindly sent in original materials to be included in the book. At various stages in working up and ordering the materials used in the preparation of the monograph, M.A. Butuzova, T.I. Gavrilenko, N.D. Rozman, L.D. Lomakina, and T.I. Popova were of great help; to them the authors express their gratitude.

The authors thank D.Ya. Martynov, V.S. Avduyevskiy, and G.S. Golitsyn, who read the manuscript or individual chapters and who have made number of valuable comments, and V.A. Bronshten, who took on the job of editing the book. All wishes and critical remarks will be accepted with gratitude.

TABLE OF CONTENTS

Foreword ii

Chapter I. Venus as a planet in the Solar System 1

Chapter II. The Rotation and Topography of Venus 6

II.1. Visual Observations 6
II.2. The Fundamentals of Radar Research of Planets 8
II.3 Radar Determination of the Elements of Rotation 19
II.4. The Topography and Relief of the Surface 24

Chapter III. The Physics of the Surface 33

III.1. The Fundamentals of Planetary Radio Astronomy 33
III.2. The Determination of Permittivity, Density and Composition of the Rocks of the Planet's Surface. Surface Microrelief. 39
III.3. Temperature of the Surface 45

Chapter IV. The Structure of the Lower Atmosphere 53

IV.1. The Parameters of the Atmosphere of Venus According to Measurements Made at Long Range 53
IV.2. The Venera Automatic Interplanetary Stations (AIS's) 60
IV.3. The Results of Direct Measurements of Atmospheric Parameters on the Venera Stations and an Analysis of These Results 75
IV.4. The Results of the Mariner-5 Measurements 105
IV.5. Estimates of Water Vapor and Ammonia Content in The Venusian Troposphere From Radio Astronomy Measurements 112
IV.6. The Structure of the Venusian Troposphere and Stratosphere 118
IV.7. On the Nature and Structure of the Clouds 135
IV.8. Several Considerations About the Origin and Evolution of the Atmosphere 149

Chapter V. Optical Properties and Thermal Regime 158

V.1. Conceptions About the Heating Mechanism of Venus 158
V.2. On Energy Balance in the Atmosphere 166
V.3. The Optical Properties of the Venusian Atmosphere 176
V.4. Radiative Heat Exchange in the Atmosphere 204
V.5. Convective Heat Exchange 225

Chapter VI. The Upper Atmosphere 241

VI.1 Fundamental Definitions 241
VI.2. The Neutral Upper Atmosphere and Ionosphere of Venus 244

VI.3. Theoretical Models 255
VI.4. Photochemistry and Dynamics. The Exosphere 264

Appendix. Atmospheric Model of Venus. 274

Bibliography 284

PHYSICS OF THE PLANET VENUS

A.D. Kuz'min and M.Ya. Marov

CHAPTER I. VENUS AS A PLANET IN THE SOLAR SYSTEM /9*

Of the planets in the solar system, Venus is the second closest to the Sun. Its average distance from the Sun is 0.723 astronomical units, i.e., about 1.4 times closer than the Earth. The orbit of Venus is almost circular (eccentricity 0.0068) and is inclined 3°24' in relation to the Earth's orbital plane.

The rotation period of Venus around the Sun (sidereal period) is 224.7 Earth days. The average velocity of the planet's motion in orbit is 35 km/sec.

As it moves in relation to the Sun and Earth, Venus goes through phases (from the standpoint of an observer on Earth) similar to those of the Moon. At inferior conjunction, when Venus is between the Earth and the Sun, the dark side of the planet, unlit by the Sun, is turned toward the Earth. This phase is analogous to the new Moon. At superior conjunction, Venus is almost exactly behind the Sun, and its illuminated side is turned toward the Earth. This phase is analogous to the full Moon. In other positions, Venus passes through all the intervening phases of partial illumination of the disk: these are also analogous to those of the Moon. The maximum angular distance between Venus and the Sun for an observer on Earth (the greatest elongation) is 48°. The time interval between two identical phases, the synodic period, is equal on the average to 584 Earth days or 8/5 of an Earth year. Because of this relation between Venus' synodic period and the Earth year, the conditions for observing the planet repeat themselves every 8 years. A list of Venus conjunctions from 1956 to 2000, which we have borrowed from [120], is given in Table 1.

The visible (from Earth) angular diameter varies within the limits of 63" at inferior conjunction to 10" at superior conjunction. /10

The magnitude of Venus is about 4 and does not depend greatly on the phases of the planet. Even during the day, therefore, the naked eye can see the planet, if its location in the heavens is known.

The reflectivity of the planet depends on wavelength. Fig. 1 illustrates the character of this dependence. Venus is one of the

---

* Numbers in the margin indicate pagination in the foreign text.

terrestrial planets and has about the same dimensions, mass, and average density as Earth. /11

TABLE 1. LIST OF VENUS CONJUNCTIONS, 1956-2000

Inferior conjunction			Superior conjunction		
Year	Date	Visible diameter	Year	Date	Visible diameter
1956	22 June	58"	1957	14 April	10"
1958	28 January	63	1958	11 November	10
1959	1 September	59	1960	22 June	10
1961	11 April	59	1962	27 January	10
1962	12 November	63	1963	30 August	10
1964	19 June	58	1965	12 April	10
1966	26 January	63	1966	9 November	10
1967	29 August	59	1968	20 June	10
1969	8 April	59	1970	24 January	10
1970	10 November	63	1971	27 August	10
1972	17 June	58	1973	9 April	10
1974	23 January	63	1974	6 November	10
1975	27 August	59	1976	18 June	10
1977	6 April	59	1978	22 January	10
1978	7 November	63	1979	25 August	10
1980	15 June	58	1981	7 April	10
1982	21 January	63	1982	4 November	10
1983	25 August	58	1984	15 June	10
1985	3 April	60	1986	19 January	10
1986	5 November	62	1987	23 August	10
1988	13 June	58	1989	5 April	10
1990	19 January	63	1990	1 November	10
1991	22 August	58	1992	13 June	10
1993	1 April	60	1994	17 January	10
1994	2 November	62	1995	10 August	10
1996	10 June	58	1997	2 April	10
1998	16 January	63	1998	30 October	10
1999	20 August	58	2000	11 June	10

ORIGINAL PAGE IS OF POOR QUALITY

The radius of the Venusian cloud layer is 6100 ± 30 km in Martynov's estimate [106] and 6120 ± 7 km in Vaucouleurs' estimate. Dollfus [278, 279], on the basis of an analysis of his own measurements and those of other observers, took note of the dependence of the radius on the phases: as the phase angle decreases, the measured diameter decreases. He explains this dependence as a change in the visible dimensions of the disk because of scattering on particles suspended in the upper atmosphere. The scattering effect is maximum at inferior conjunction, when the Sun in behind the planet, and minimum at superior conjunction. In the first case, therefore, the radius of the cloud layer is measured. Dollfus determined the corresponding angular diameters to be 16.95" ± 0.05" and 16.86" ± 0.05", which corresponds to a radius of 6140 ± 13 km for the scattering layer and a radius of 6115 ± 13 km for the cloud layer.

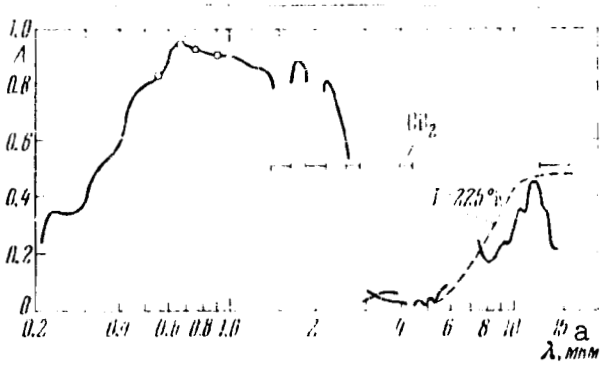

Fig. 1. Reflection and emission characteristics of Venus in the spectral region from 0.2 to 15 μm [338]. Along the ordinate are relative values. The dashed line is equilibrium emission at T = 225°K. The horizontal segments are the location of the strongest CO_2 absorption bands.

Key: a. μm

The measurements by Vaucouleurs and Menzel [532] of the occultation of Regulus gave a radius of 8.506", which corresponds to a linear radius of 6169 km. The error in the determination of this radius is not less than 10 km [107].

The first measurements of the radius of the planetary surface were done by radio astronomy methods and by using a radio interferometer with a high angular resolution; these measurements gave 6057 ± 55 km [83]. Later radar measurements, as well as a combination of radar measurements and Mariner-5 trajectory measurements, allowed us to make this important parameter more accurate and significantly reduced the error in its determination. The results of these measurements, given in Table 2, show good agreement among the data obtained with different methods on various instruments, with an average equatorial radius of 6050 km for the Venusian surface.

/12

TABLE 2. RADIUS OF THE SURFACE OF VENUS

Institution	Date of publication	Radius km	Method of measurement	Literature
California Institute of Technology	1965	6057 ± 55	Radio astronomy	[83]
Lincoln Laboratory	1967	6056 ± 1	Combined processing of all radar measurements 1961-1966	[184]
IRE; USSR Academy of Sciences	1968	6056 ± 15	Radar	[126]
Lincoln Laboratory	1968	6058 ± 1	»	[185]
Arecibo	1968	6052 ± 2	»	[185]
Jet Propulsion Laboratory	1968	6053,7 ± 2,2	»	[128]
Jet Propulsion Laboratory	1968	6052,5 ± 2,5	Trajectory measurements of Mariner-5; radar	[179]

ORIGINAL PAGE IS
OF POOR QUALITY

For calculation of the ephemerides, a radius of 6100 km is accepted; this is 0.956 the radius of Earth.

The planetary figure was measured by radar at a wavelength of 3.8 cm [506]. The resolution of the experiment was 0.5 km in altitude, 1000 km in latitude, and 100 km in longitude. At the equatorial plane, the planetary section approximates an ellipse, and the difference between its semi-major and semi-minor axes is 1.1 ± 0.4 km.[1] The major axis of the ellipse has an angle of 55° (clockwise), with the direction toward the Earth at inferior conjunction. The center of the figure is shifted relative to the mass center by 1.5 ± 0.3 km at a direction away from the Earth at inferior conjunction. The oblateness can be estimated by analyzing the measurement of the Mariner-5 spacecraft's trajectory in the Venusian gravitational field [181], according to which the principal moment is

/13

$$J_2 = \frac{1}{2}[C - (A + B)] = (5 \pm 10) \cdot 10^{-6}.$$

ORIGINAL PAGE IS
OF POOR QUALITY

Here, A, B, and C are the moments of inertia relative to the equatorial and polar axes.

A negative value for J_2 is not likely, since this would be evidence that the planet rotates around its axis with a smaller moment of inertia. It is more probable and within the bounds of error for J_2 to have a positive value. From its value, it is possible to estimate that the difference between the polar radius and the equatorial radius does not exceed several hundred meters. The expected centrifugal hydrostatic polar flattening for Venus is 40 cm.

The most precise determinations of the mass of Venus were made from measurements of the orbits of the Mariner-2 and Mariner-5 spacecraft, which flew by the planet in 1962 and 1967, respectively. According to the Mariner-2 measurements, the relation of the mass of the Sun to the mass of Venus is 408532 ± 37 [178]. According to Mariner-5 measurements, the retrograde mass of Venus is 408522 ± 3 [180].

The weighted mean according to all available measurements using various methods is $M_\odot/M_\varphi$ = 408519 ± 11 [381].

The average density of Venus is 5.27 $g \cdot cm^{-3}$ (for Earth, the corresponding value is 5.52 $g \cdot cm^{-3}$).

The gravitational acceleration on the Venusian surface near the equator is 885 $cm \cdot sec^{-2}$. Escape velocity on the surface is 10.3 km/sec.

---

[1] On Earth, this difference is about 200 m.

No magnetic field has been discovered on Venus: the upper limit on dipole moment is $3 \cdot 10^{-4}$ of the Earth's.

CHAPTER II. THE ROTATION AND TOPOGRAPHY OF VENUS /14

II.1. Visual Observations

The question about the elements of Venusian rotation has been the subject of numerous inquiries: since 1666, i.e., in 300 years, more than 100 articles have been devoted to this subject.

The first determinations of the elements of the planet's rotation were based on attempts to discover constant features on the planetary disk and to follow their apparent motion. After observing the movement of "spots" on the visible disk of Venus, J.D. Cassini concluded in 1666 that its rotation period was 23 hours 21 min. However, subsequent observers of Venus could not discern any surface details on Venus and thus even confirm the presence of "spots."

Sixty years later, F. Bianchini again observed details on the planetary disk and even drew up a map of Venus, which depicted "oceans" and "continents." From the motion of what he thought were constant surface features, he obtained a rotation period of 24 days 8 hours.

For the next 150 years, the majority of observers obtained a value of close to 23 hours for the rotation period of Venus. Schiapirelli obtained a completely different result in 1887. He found that the rotation period was equal to the period of revolution around the Sun (224.7 days) and, consequently, that Venus always had one side turned toward the Sun.

Such a wide discrepancy in determinations of rotation period is caused by the fact that the surface of Venus is covered with a dense cloud layer. The details of the cloud cover itself are so blurred and changeable that it is doubtful whether any such details /15 exist at all.

Observations in the infrared region of the spectrum, which is transparent for several forms of haze and fog, also yielded no results. Nevertheless, photographs taken by Ross in ultraviolet light in 1926 [475] unexpectedly revealed dark bands located almost perpendicular to the terminator. The bands changed position from day to day; this indicated that they were of atmospheric origin. Ross estimated the rotation period at close to 1 month. In 1950-1954, Kuiper [387] confirmed the presence of the bands that Ross had seen. In Kuiper's opinion, the presence of bands indicated a comparatively rapid rotation around its axis. Boyer and Camichel did detailed research on the bands observed in the ultraviolet region of the spectrum.

Boyer [221] took photographs of Venus in 1957, 1959, and 1960 and noted that the details repeated themselves every 4 days. In

order to explain these findings, he advanced the hypothesis that the rotation period of Venus was about 4 days and that the spin axis was approximately perpendicular to the plane of the ecliptic.

Camichel [230] compared his own photographs with those obtained at other observatories and taken at intervals of several hours. In many cases, he discovered a shift in the details, a shift that corresponded to a retrograde rotation.

For a more detailed investigation, Boyer and Camichel [222] put their photographs together and selected the best ones. An analysis of these photographs led them to conclude that there is a continuously existing dark formation in the shape of the letter "Y" laid on its side ⋊ on the visible surface of the planet. The various parts of this formation, which appears on the illuminated part of the disk, created, thanks to rotation, differences in the apparent picture of dark and light zones.

Making use of the observational material gathered at Pic-du-Midi in 1948-1960 and in Brazzaville in 1953-1954, the authors [223] were able to work with data that took in a time period of many years. As a reference point, they selected the point where three bands came together to form the ⋊-shaped feature. Measurements of the shifting of this point on all the collected photographs showed that the feature shifted from photograph to photograph in a retrograde direction with an average velocity of about 100 m/sec. This corresponds to a full revolution around the planet every 4 days. Variations from 3.5 to 4.5 days were noted in this period. /16

B. Smith made similar observations [504, 505] in 1966-1967 at an observatory in New Mexico and verified what the French astronomers had discovered: the rapid movements of formations on the disk of Venus, observed in the ultraviolet spectrum. The average velocity of these formations was 100 m/sec in a retrograde direction. Variations of 10-20% in velocity were observed. No connection between the velocity of movement and the latitude was observed.

In Smith's observations, the clouds did not maintain themselves over several years, as Boyer had reported. According to data from Smith's subsequent observations [505], the lifetime of the ⋊-shaped formation is 10-15 days.

Scott and Reese [489] have recently shown that the ⋊-shaped features are short-lived formations (no longer than 20 days) and are distributed randomly about the surface of the planet. Therefore, what Boyer and Guerin [224] had determined as the rotation period of the cloud cover -- 3.995 days -- is evidently fictitious, caused by the stroboscopic effect of repeated, one-per-day observations made during the short time the planet is visible from a single observatory.

Guinot [330] used a high-resolution interference spectrograph to make independent observations of the velocity with which the cloud formations on Venus move. By measuring the Doppler shift of the lines in the visible region of the planet's spectrum, he determined that the velocity with which the cloud cover moves while making a full revolution around the planet corresponded to 4.1 ± 0.7 days, in a direction opposite to that with which the planet revolves around the Sun.

Other data (e.g., the shift of the line of the terminator caused, according to Goody [313, 325], by strong convective movements) are not numerous and are basically of an indirect character.

Fig. 73 gives exemplary photographs of these ultraviolet details.

Thus, observations in the ultraviolet region of the spectrum /17 have allowed us to estimate the velocity with which cloud formations in the Venusian atmosphere move. But they have given no information about the elements of the rotation of the planet itself. The determination of these parameters has become possible only in the last decade with the aid of planetary radar.

In connection with the fact that the Venusian atmosphere is opaque to visible and infrared radiation and that the possibilities of using descent apparati for research are limited by the complexity of such an experiment, the basic source of information about the surface of Venus is radio astronomy and radar measurement of the planet.

For convenience, basic information about radar astronomy (and in Section III.1, radio astronomy) concerning primarily terminology and the methods of determining basic parameters is given below. Readers familiar with radio astronomy and radar astronomy can skip these sections.

II.2. The Fundamentals of Radar Research of Planets

Radar astronomy arose in the second half of the 1940's from the application of radar methods and techniques to the study of celestial bodies. Its purpose is to study these bodies from the radio signal they reflect; radio transmitting devices used especially for this purpose generate and direct this radio signal.

In its application to planets, an analysis of reflected radio signals makes it possible to determine the permittivity of the material and the character of the surface roughness of the planet, the dimensions of the planet, its figure, its topography, the elements of rotation, the ephemerides, and the orbital parameters.

The determination of the permittivity of the surface material and the character of its roughness is done by measuring the echo intensity and its time-frequency dependence.

For normal incidence, the reflection coefficient R_s of a surface consisting of a dielectric with a complex permittivity $\varepsilon = \varepsilon' + i\varepsilon''$ is determined by the relation /18

$$R_s = \left(\frac{\sqrt{\varepsilon} - 1}{\sqrt{\varepsilon} + 1}\right)\left(\frac{\sqrt{\varepsilon_*} - 1}{\sqrt{\varepsilon_*} + 1}\right). \qquad \text{(II.1)}$$

ORIGINAL PAGE IS
OF POOR QUALITY

Here $\varepsilon_* = \varepsilon' + \varepsilon i''$ is the complex conjugate of permittivity ε.

If $\varepsilon'' < \varepsilon'$ (low electrical conductivity), which occurs for most silicate rocks, (II.1) reduces to the well-known form

$$R_s = \left(\frac{\sqrt{\varepsilon} - 1}{\sqrt{\varepsilon} + 1}\right)^2. \qquad \text{(II.2)}$$

From this, if R_s is known, it is not difficult to calculate

$$\varepsilon = \left(\frac{1 + \sqrt{R_s}}{1 - \sqrt{R_s}}\right)^2. \qquad \text{(II.3)}$$

The value R_s can be determined from measurements of the radar cross section

$$S_r = gR_s\pi R^2, \qquad \text{(II.4)}$$

where πR^2 is the area of the planet's geometric section.

The radar cross section S_r is determined directly from measurement. Transforming the well-known radar equation (cf., for example, [16])

$$P_0 = P_t \frac{GAS_r}{(4\pi r^2)^2}, \qquad \text{(II.5)}$$

where P_t is the power of the transmitter, G is the gain of the transmitting antenna, A is the effective receiving area of the receiving antenna, and r is the distance to the reflecting object, we obtain

$$S_r = \frac{(4\pi r^2)^2}{GA}\frac{P_0}{P_t}. \qquad \text{(II.6)}$$

It is customary to express the results of the measurement of S_r as a fraction of the geometric area of the planet's section

$$\sigma_r = \frac{S_r}{\pi R^2}.$$

ORIGINAL PAGE IS
OF POOR QUALITY

The direction coefficient g characterizes the dependence of the scattered echo on the surface roughness. The value of g is defined by the relation /19

$$g = \frac{4\pi \int_0^{\pi/2} F(\theta) \sin\theta \, d\theta}{\int_0^{\pi/2} \int_0^{\pi/2} \int_0^{2\pi} F(\theta, i, \Phi) \sin\theta \sin i \, d\Phi \, di \, d\theta}. \qquad \text{(II.7)}$$

where $F(\theta,i,\Phi)$ is the scattering function, which shows the dependence of the scattered echo on the angle of incidence θ, the angle of reflection i, and the difference between the azimuths of incident and reflected beams Φ (Fig. 2). Finding this function is possible only theoretically, by examination of the scattering mechanism of a reflecting surface with specific statistically-given roughness, or practically, by suitable experiment.

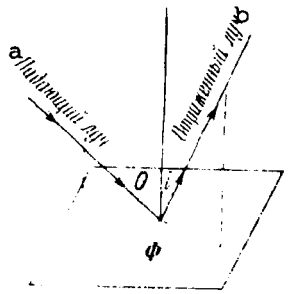

Fig. 2. The geometry of reflected radiation.

Key: a. Incident beam; b. Reflected beam

In radar observations of the planet from the Earth, measurements of $F(\theta,i,\Phi)$ are made only for the partical case of reflection in the direction of the incident beam ($i = \theta$, $\Phi = 0$). The measured value in this is the reflection function $F(\theta)$, which is thus a special case of the scattering function $F(\theta,i,\Phi)$.

The scattering function $F(\theta,i,\Phi)$ cannot be determined by experimentation on Earth. It is therefore necessary to limit oneself to an approximate estimate of the parameter g, an estimate based on the results of the determination of the statistical properties of the reflecting surface from measurement of the reflection function.

For a sphere that is smooth on the scale of a wavelength (a sphere that gives a specular reflection), $g = 1$.

For a surface that consists of many sufficiently large (by comparison to wavelength), randomly inclined, flat, specular- /20

reflecting segments, the reflection is called quasi-specular. The most widely used means of statistically describing such a surface is the following. Let us assume that the true surface differs from the mean surface and that deviations are random, so that deviations from the mean elevation are characterized by a normal distribution with a mean square deviation h_0 or with a mean slope $\bar{\alpha} = h_0/d_0$ of flat, specular-reflecting segments. The horizontal scale of surface roughness is given by the autocorrelated function r(d). Two forms of this function are used: the gaussian

$$r(d) \quad \exp\left| \quad \frac{1}{2}\left(\frac{d}{d_0}\right)^2 \right| . \tag{II.8}$$

ORIGINAL PAGE IS
OF POOR QUALITY

and the exponential

$$r(d) \quad \exp\left| \quad \frac{d}{d'} \right| . \tag{II.9}$$

For a gaussian slope distribution, the direction coefficient of the reflected echo is

$$g \quad 1 \quad \alpha^2 . \tag{II.10}$$

The value $\bar{\alpha}$ is determined on the basis of the reflection function

$$F_g(\theta) \sim \frac{\exp\left| \quad \frac{1}{2}\left(\frac{\theta}{\bar{\alpha}}\right)^2 \right|}{\cos^4\theta} . \tag{II.11}$$

For exponential distribution

$$g \quad 1 \quad \frac{1}{r} . \tag{II.12}$$

The value $C = \frac{d'\lambda}{4\pi h_0}$ is also determined on the basis of the reflection function

$$F_e(\theta) \sim [\cos^4\theta \quad C\sin^2\theta]^{-} . \tag{II.13}$$

The choice between gaussian and exponential slope distribution is made on the basis of a criterion of whether $F_r(\theta)$ or $F_e(\theta)$ corresponds to the experimentally measured reflection function.

For Venus, $\alpha \ll 1$ and $1/C \ll 1$; therefore, it can be assumed /21 with sufficiently good approximation that for quasi-specular reflection, $g \simeq 1$.

For a surface that is rough on the scale of a wavelength and that isotropically scatters the echo as in Lambert's rule

$$F(\theta) = \cos^2\theta, \tag{II.14}$$

the direction coefficient of the reflection is $g = 8/3$.

In treating the results of radar measurements of Venus, it is customary to present the echo as the sum of two components: the quasi-specular, which is caused by specular reflection of flat segments in the region nearest the Earth; and the diffused, which is caused by the isotropic-scattering part of a surface rough on the scale of a wavelength. In such approximation, the total radar cross section σ_r may be represented in the form

$$\sigma_r = g_s R_s (1 - a_d) + g_d R_s a_d \tag{II.15}$$

where a_d is the ratio of the area of those segments of the planet's disk that give a diffused reflection to the cross section area of the planet, g_s and g_d are the direction coefficients of specular and diffused reflections.

By designating b_s and b_d as the ratios of the energy of the specular and diffused components to the total reflected power ($b_s + b_d = 1$) and by assuming, in connection with what was set forth above, that $g_s \simeq 1$ and $g_d = 8/3$, and carrying through simple transformations, we obtain

$$R_s = \left(b_s + \frac{3}{8} b_d\right) \sigma_r \tag{II.16}$$

The values b_s and b_d are determined by experiment.

One may further calculate

$$\left.\begin{aligned} a_s &= \frac{b_s \sigma_r}{R_s}, \\ a_d &= \frac{3}{8} \frac{b_d \sigma_r}{R_s}. \end{aligned}\right| \tag{II.17}$$

ORIGINAL PAGE IS
OF POOR QUALITY

Separation of the quasi-specular and diffused components is done by analyzing the reflection function, which is more conveniently performed on a logarithmic plot: /22

$$\lg F(\theta) \quad f(\lg \cos \theta).$$

It is obvious that with such a construction, the reflection function of the diffused component will have the form of a straight line with an angular slope equal to 2. By extrapolating this straight line, one may obtain the reflection function of the diffused component $F_d(\theta)$ in the whole range of angles θ from 0° to 90°. The value of b_d is determined from the relation

$$b_d = \frac{\int_0^{90} F_d(\theta) \sin\theta \, d\theta}{\int_0^{90} F(\theta) \sin\theta \, d\theta}. \qquad \text{(II.18)}$$

ORIGINAL PAGE IS
OF POOR QUALITY

All the remaining echo is considered quasi-specular and $g \cong g_s = 1$ and $b_s \equiv 1 - b_d$ is assumed for it.

The reflection function may be determined experimentally, on the basis of data from the measurement of range distribution of the echo intensity or by data from measurement of the echo frequency spectrum.

As it is reflected from a spherical planet, the signal becomes longer in time. This is caused by the finiteness of the propagation velocity of electromagnetic waves and by the depth of the reflecting body along the line of sight. It is obvious that the first to be recorded on the receiver will be the echo reflected off that point on the planetary surface closest to the observer on Earth. This point (Fig. 3) is usually called the "subradar point." At time t after the beginning of the pulse of the echo, the energy received will be caused by reflection of those points on the planetary surface that are at a distance ct/2 along the line of sight beyond the subradar point. It is obvious that these points lie on a circumference, the center of which is located on a straight line that passes through the subradar point and the center of the planetary sphere, at a distance of ct/2 from the first. It is not difficult to show that the angle θ under which this circumference is visible from the center of the sphere is related to the echo time delay t by the relation /23

$$t = \frac{2R}{c}(1 - \cos\theta), \qquad \text{(II.19)}$$

where R is the radius of the planet.

ORIGINAL PAGE IS
OF POOR QUALITY

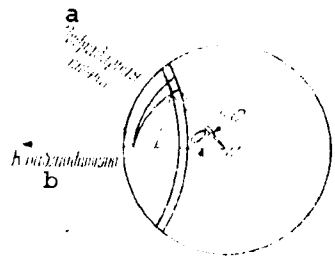

Fig. 3. Geometry of the reflection of a pulse signal from the planet.

Key: a. Subradar point; b. To observer

The greatest delay $t_M = 2R/c$ will occur for an echo from points on the planet's limb ($\theta = 90°$).

By time gating, one can separate out reflection from various regions of the planet and thus study these regions individually. The resolution of such gating is limited by the finiteness of the duration of the impulse τ of the ratio transmitter. It is obvious that the energy of the echo received in the time interval $dt = \tau$ (Fig. 4) corresponds to an echo from a ring (cf. Fig. 3) of angular width $d\theta$, which is determined by the relation

$$dt = \frac{2R}{c} \sin\theta d\theta. \qquad \text{(II.20)}$$

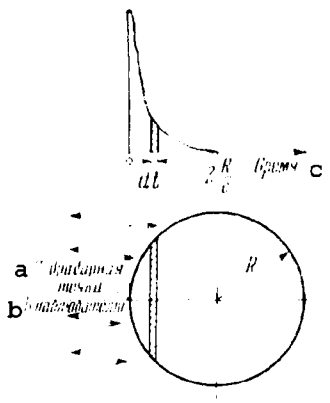

Fig. 4. Schematic representation of the stretching of the echo in time as it reflects from the planet.

Key: a. Subradar point; b. To observer; c. Time

On the basis of this relation one can, by using the measured time spectrum P(t), construct an angular spectrum $P(\theta)$ of the reflection from the rings irradiated by an impulse of duration τ. The area of these rings is /24

$$\Delta S = \pi R c \tau, \qquad \text{(II.21)}$$

i.e., it does not depend on the position of the ring on the sphere. Therefore, the angular spectrum $P(\theta)$ characterizes the reflection not only of rings of identical depth, but also the reflection of a single element of the surface, i.e., it is (after normalization) the sought-for reflection function $F(\theta)$.

In addition to a lengthening in time, the echo differs from the emission also in terms of frequency spectrum. The first difference is caused by a Doppler shift of the mean frequency due to the planet's direct motion with a velocity v relative to an observer and is equal to

$$\Delta\nu = \frac{2v}{c}\nu_0, \qquad \text{(II.22)}$$

ORIGINAL PAGE IS
OF POOR QUALITY

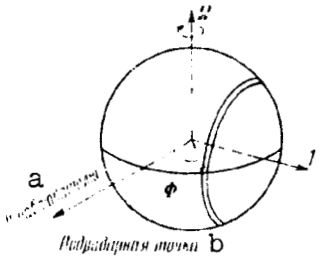

Fig. 5. Geometry of frequency Doppler shift upon reflection from a spinning planet. 1 is the center line of loci of identical Doppler shift.

Key: a. To observer; b. Subradar point

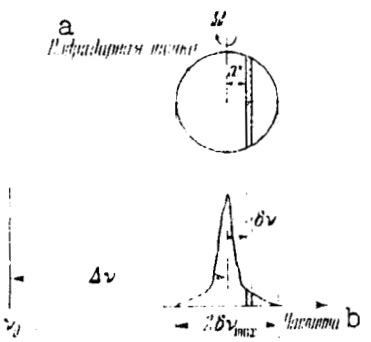

Fig. 6. Schematic representation of the Doppler spread of the spectrum upon reflection from a spinning planet.

Key: a. Subradar point; b. Frequency

where ν_0 is the echo frequency. The second difference is caused by the Doppler spread arising from the planet's rotation.

It is possible to show[1] that on the surface of a sphere the geometric loci of points with an identical linear velocity along the line of sight toward the observer and, consequently, with an identical Doppler shift, are circumferences whose centers are on a straight line that passes through the center of the sphere perpendicular to the plane formed by the direction toward the observer and the planet's rotation axis (Fig. 5). For the observer, these circumferences are segments of straight lines parallel to the projection of the spin axis onto a map surface (Fig. 6).

With the apparent angular velocity of the planet's rotation relative to a projection of the rotation axis onto a map surface Ω, each such segment at a distance x from the projection of the planet's spin axis has an additional linear velocity along the line of sight equal to $2x\Omega$ and an additional Doppler shift in frequency /25

$$\delta\nu \quad \frac{2x\Omega}{c}\nu_0. \qquad \text{(II.23)}$$

The full Doppler spread of the echo spectrum from the entire planet is

$$B \quad \frac{2R\Omega}{c}\nu_0. \qquad \text{(II.24)}$$

where R is the planet's radius.

The connection between the reflection function and the echo frequency spectrum $P(\nu)$ is determined by the relation

[1] Cf., for example, E.R. Mustel', Zvezdnyye atmosfery [Stellar Atmospheres], "Fizmatgiz" Press, 1960, pp. 339-340.

$$P(\nu) \sim \int_0^{\sqrt{\left(\frac{B}{2}\right)^2 - \nu^2}} \frac{P(0)}{\sqrt{\left(\frac{B}{2}\right)^2 - \nu^2 - y^2}} dy. \qquad \text{(II.25)}$$

where

$$0 = \arcsin\left|\frac{2}{B}\sqrt{\nu^2 + y^2}\right|.$$

ORIGINAL PAGE IS
OF POOR QUALITY

The inverse transformation can be done using Abel's integral equation, which gives

$$P(0) \sim \cos\theta \int_{-\frac{B}{2}\sin\theta}^{B/2} \frac{P'(\nu)\,d\nu}{\sqrt{\nu^2 - \left(\frac{B}{2}\sin\theta\right)^2}}. \qquad \text{(II.26)}$$

The full echo power is

/26

$$P_0 = \int_0^{2B/c} P(t)\,dt = \int_{-B/2}^{B/2} P(\nu)\,d\nu. \qquad \text{(II.27)}$$

This entire examination has been done assuming that the planet's atmosphere is transparent and therefore holds only for the radio wave frequency (for Venus $\lambda \gtrsim 20$ cm) for which this assumption occurs. In treating and interpreting measurement results on the shorter waves, it is necessary to take absorption by the atmosphere into account. Absorption decreases the value of the echo $e^{-2\tau}$ times, where $\tau(\lambda,\theta)$ is the optical thickness of the planet's atmosphere at wavelength λ and at a point whose planetocentric angle relative to the subradar point is equal to θ. At $\theta < 85°$, the dependence on θ can be presented in the form

$$\tau(\theta) = \tau(0)\sec\theta.$$

Taking absorption into account, the measured radar cross section is $\sigma_r = \sigma_{r0}e^{-2\tau(\lambda)}$, where σ_{r0} is the radar cross section of a planet with no atmosphere.

The optical thickness is connected with the absorption coefficient by the well-known relation

$$\tau(\lambda, 0) = \int_0^{\infty} \varkappa(\lambda, h)\,dh \qquad \text{(II.28)}$$

In the atmosphere of Venus, the absorption of radio waves is determined primarily by absorption by carbon dioxide and partly by water vapor:

$$\varkappa(\lambda, h) = \varkappa_{CO_2}(\lambda, h) + \varkappa_{H_2O}(\lambda, h). \quad \text{(II.29)}$$

ORIGINAL PAGE IS
OF POOR QUALITY

Absorption by carbon dioxide can be determined from the semi-empirical formula of Ho, Kaufman, and Thaddeus [346]

$$\varkappa_{CO_2}(\lambda, h) = (15.7 f_{CO_2} + 3.9 f_{CO_2} \cdot f_{N_2}) \times \frac{1}{\lambda^2} |p(h)|^2 \left[\frac{273}{T(h)}\right]^5 \cdot 10^{-3} \ (\kappa.м^{-1}), \quad \text{(II.30)}$$

where f_{CO_2} and f_{N_2} are the relative carbon dioxide and nitrogen content in the atmosphere (by volume, pressure or number of molecules), /27 p(h) is full pressure (in $kg \cdot cm^{-2}$) in the atmosphere at altitude h above the surface, and T(h) is the temperature of the atmosphere at altitude h.

Absorption by water vapor can be determined from the quantomechanical formula [25]

$$\varkappa_{H_2O}(\lambda, h) = \left\{2{,}3 \cdot 10^4 \left[e^{-\frac{642{,}219}{T(h)}} - e^{-\frac{643{,}283}{T(h)}}\right] \times \frac{\Delta\nu}{\left(0{,}5176 - \frac{1}{\lambda^2}\right)^2 + 4(\Delta\nu)^2 \cdot \frac{1}{\lambda^2}} + 1{,}577 \cdot 10^3 \frac{p(h)}{T(h)}\right\} \times \frac{p(h)}{\lambda^2 |T(h)|^{1.5}} \ (\kappa.м^{-1}). \quad \text{(II.31)}$$

Here

$$\Delta\nu = 0{,}1693 \rho(h) \left[\frac{T(h)}{300}\right]^{-0.6} \ (см^{-1})$$

is the half-width of the water vapor line $5_{-1} - 6_{-5}$ and ρ is the absolute humidity in g/m^3.

The combination of time gating, which allows us to differentiate an echo from a specific ring on the apparent disk of the planet (cf. Fig. 3), and frequency gating, which allows us to differentiate an echo from a band at a finite distance from the planet's spin axis (cf. Fig. 5), makes it possible to resolve relatively small regions, which correspond to an intersection of these rings and bands, on the planetary disk (Fig. 7). Thus it is possible to study reflectivity distribution on the planetary disk by

ORIGINAL PAGE IS
OF POOR QUALITY

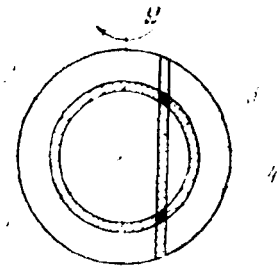

Fig. 7. Schematic representation of the increase in resolution due to time and frequency gating. 1 1 is the subradar point; 2 is the ring resolved by time gating; 3 is the band resolved by frequency gating; 4 are the regions resolved by time and frequency gating.

using ground antennas whose beam width is too large to make such measurements because of angular resolution. The limitation of this method of increasing angular resolution is its ambiguity. The intersection of a ring and a band forms two regions (Fig. 7) which are impossible to separate without additional gating. Such gating can be implemented either by changing the orientation of the regions of ambiguity as the planet rotates, which requires extended measurements, or by using an interferometer system at reception or at transmission.

The angular velocity of the planet's /28
apparent rotation relative to the projection of the spin axis on a map surface Ω can be determined from relation (II.24) by measuring the spectral spreading of echo B.

However, if the reflecting surface is smooth enough (i.e., the parameter of roughness is small at the wavelength at which the study is being done), the main part of the echo reflects from a relatively small (equal to the first Fresnel zone) central part of the planet; reflection off the edges of the disk is quite small. Therefore, measurements of the full width of the echo spectrum require the echo to exceed the noise level significantly; this has still not been achieved in present-day measurements. This difficulty may be overcome by correlating spectral measurements with measurements of echo range distribution. A single measurement, no matter how accurate, allows us to determine only the apparent velocity of the planet's rotation as seen by an observer on Earth, but it does not answer the question about the direction of rotation or the orientation of the spin axis. These parameters can be determined from the way the apparent velocity of the planet's rotation changes over time only from extended radar measurements. The planet's apparent rotation for an observer on Earth results from its true rotation and also the Earth's motion relative to the planet. An analysis of the way the apparent velocity of rotation changes makes it possible also to determine the orientation of the axis and, consequently, the planet's poles of rotation.

If there are regions on the planetary surface that have a reflectivity different from the average, it is possible independently to determine the period, the direction of rotation, and the orientation of the axis -- by measuring the movement of these

regions about the planet's apparent disk. For this, the above-mentioned time and frequency gating is used.

Finally, by measuring the time delay in the arrival of the leading edge of the echo, one can determine the radius of the planet at the subradar point, and through extended observations, the figure and relief of the subradar region of the planet.

II.3. Radar Determination of the Elements of Rotation

The first attempt to observe radio echoes from Venus was made during 2 days in February 1958 by Price et al. [465]. The measurements were made at a wavelength of 68 cm from the 26-m antenna of the Massachusetts Institute of Technology's Lincoln Laboratory (USA). Because of the low signal-to-noise ratio, an echo was discovered only by statistical processing. Of four series of observations subjected to this processing, an echo was evidently revealed in only two. Later measurements made in the same laboratory [448] showed that the astronomical unit had been determined incorrectly. In this connection, Pettengill [449], who was one of the authors of the earlier work [465], suggests that the echo received in 1958 was not from Venus and was caused by some kind of parasitic effect. It is therefore impossible to consider the value of the radar cross section for Venus reliable; this value, according to data from this experiment, was equal to the geometric area of the planet's cross section, i.e., about seven times larger than that obtained in subsequent measurements.

Pettengill and Price's attempt [446] to make radar measurements of Venus near the next inferior conjunction of Venus in 1959 also turned out to be unsuccessful; no echo was discovered.

Evans and Taylor [293] also tried to make radar measurements of Venus in 1959 at Jodrell Bank in England. They reported that they had found an echo that exceeded noise by 2.5 times and that corresponded to a radar cross section of 0.5% and a value for the astronomical unit that agreed with what Price et al. [465] had obtained and that had turned out to be in error. In this connection, it is probable that these measurements were also in error. /30

The first successful radar measurements of Venus were made near inferior conjunction in 1961 by: in the USSR, a team under the direction of Academician V.A. Kotel'nikov [73, 74, 386] at the USSR Academy of Sciences' Institute of Electronics and Radio Engineering; in the USA, by Pettengill et al. [447] at the Massachusetts Institute of Technology's Lincoln Laboratory; at the Jet Propulsion Laboratory of the California Institute of Technology [409, 535, 536]; and in England at the Jodrell Bank Radio Astronomy Observatory [524].

These and subsequent experiments measured the frequency and time spectra of the echoes, the Doppler shift in frequency, echo intensity and depolarization, and echo propagation time.

The elements of the planet's rotation were determined on the basis of measurements (several methods were used) of the angular velocity of its rotation.

The basis of the first method is measurement of the spectral width B of the echo while irradiating the planet with a monochromatic signal of frequency ν_0. The angular velocity Ω is determined from the relation (II.24).

The first measurements of the echo frequency spectrum of Venus were made in 1961 -- in the USSR, in the Institute of Electronics and Radio Engineering of the USSR Academy of Sciences by V.A. Kotel'nikov et al; and in the USA, in the California Institute of Technology's Jet Propulsion Laboratory and in the Massachusetts Institute of Technology's Lincoln Laboratory.

According to measurements made by the IRE [Institute of Electronics and Radio Engineering] of the USSR Academy of Sciences on a frequency of 700 MHz (wavelength 43 cm), the echo spectrum contains two components: narrow-band and wide-band.

The width of the narrow-band component was less than 4 Hz, and its intensity hardly changed throughout the observations. The wide-band component occupied frequency bands up to 400 Hz and changed greatly from day to day. The echo energy of the wide-band component was commensurable with the narrow-band component. /31

By assuming that the narrow-band component was produced by reflection off the surface of Venus and that the size of the reflecting spot was, by analogy with the Moon, equal to 1/10 the visible disk of the planet, the rotation period of Venus was determined to be longer than 100 days.

Measurements of the frequency spectrum in the Jet Propulsion Laboratory and in the Lincoln Laboratory were made with a higher resolution and also showed that the echo spectrum of Venus was quite narrow and corresponded to a rotation period of from 200 to 400 days. The wide-band component of the echo was not discovered in these measurements.

More complete and accurate data were obtained from measurements made near the inferior conjunction of Venus in 1964.

The results of measurements made in the Institute of Electronics and Radio Engineering of the USSR Academy of Sciences [76] correspond to a retrograde rotation of Venus with a period of 230 ± 25 days.

Measurement at Cornell University's Arecibo Ionospheric Observatory put the Venusian rotation period at T = 244.3 ± 2 days, the direction of rotation as retrograde, and the coordinates of the north pole[2] at α = 270.9 ± 1 and δ = 66.4 ± 1 [287].

The second method is based on measuring the velocity with which particular regions of high reflectivity move about the planetary disk.

If there are any formations on the planetary surface whose reflection characteristics in the radio wave range are different from the average, the high resolution attained in radar measurements of Venus by time and frequency gating makes it possible to measure the Venusian rotation by the common geometric method of observing these formations as they move about the visible disk of the planet. The first measurements of this kind were made by Goldstein and Carpenter in 1962 [317].

On the echo spectrum they noted a detail with high reflectivity; moreover, the location of this detail shifted systematically from day to day. Fig. 8 shows the shift of this detail in the spectrum relative to zero frequency, which corresponds to Venus' central meridian. The observation dates are entered on the graph along the ordinal axis. The black rectangles signify good identification of detail; the light rectangles signify doubtful identification. The width of the rectangles characterizes the spectral width of the echo of the detail. /32

The relative constancy of detail is evidence that it is actually caused by some real formation on the surface of Venus and that its motion is the result of the rotation of Venus.

The connection between the apparent angular velocity of the planet's rotation Ω and the shift velocity of details in the frequency spectrum of the echo $\dot{\nu}$ is expressed by the relation

$$\Omega = \frac{\lambda}{2\pi}(\sec\varphi\cdot\sec\psi\dot{\nu}), \qquad \text{(II.32)}$$

ORIGINAL PAGE IS
OF POOR QUALITY

where λ is the wavelength used for the measurement, ϕ and ψ are the planetocentric latitude and longitude of the observed formation.

The longitude of the formation can be estimated by comparing the shift of the detail to the full width of the spectrum. Such an estimate, made from the best spectra near inferior conjunction on the assumption that the maximum width of the spectrum corresponds to reflection from the planetary limb, leads to an apparent

---

[2] According to the recommendation of the International Astronomical Union, the north pole is considered the pole to the north of the ecliptic (more precisely, north of the fixed Laplace plane).

ORIGINAL PAGE IS
OF POOR QUALITY

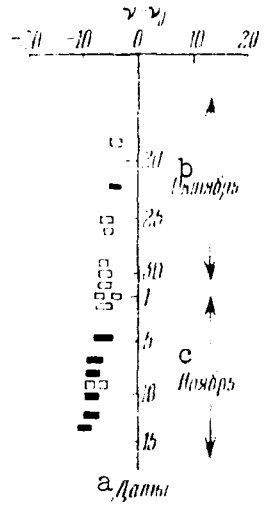

Fig. 8. Frequency displacement of a high-reflectivity detail relative to the central frequency depending on the date.

Key: a. Dates; b. October; c. November

velocity of Venus' rotation $(2.0\ ^{+0.87}_{-0.41})$·radian·$\cdot sec^{-1}$. Assuming that the spin axis is perpendicular to the planet's orbital plane, the data obtained correspond to a direct rotation with a period of 1200 days or a retrograde rotation with a period of $230\ ^{+40}_{-50}$ days. This agrees with the results of spectral spreading measurments. /33

The most accurate data about the elements of Venus' rotation are obtained by determining the time the indicated details of the spectrum appear during several inferior conjunctions. Thus, according to observations of three details of intense reflectivity (made at Arecibo Observatory near the inferior conjunctions of 1964, 1967, and 1969 [369]), the rotation period of the planet is 243 ± 0.1 Earth days, and the coordinates of the pole of the spin axis $\alpha = 272.7 \pm 0.7°$, $\delta = 65.3° \pm 1.0°$.

Carpenter's observations [234] at the Jet Propulsion Laboratory during four inferior conjunctions (1962, 1964, 1966, and 1967) gave a rotation period T = 242.98 ± 0.04 days and coordinates of the north pole $\alpha = 274.1° \pm 3°$, $\delta = 71.4° \pm 1°$ (1950.0).

The next independent estimate of Venus' rotation period was made on the basis of radar measurements of echo fading and amplification at a wavelength of 6 m [380]. According to the characteristic time of these fadings, the rotation period of Venus is estimated to be equal to 180-280 Earth days.

These results show that the rotation period of Venus is equal to or very close to the planet's synchronous rotation relative to Earth (243.16 Earth days). At every inferior and superior conjunction, Venus is always turned with the same side toward Earth.

With retrograde rotation, this corresponds to a solar day duration on Venus of 117 Earth days, i.e., the Venusian year consists approximately of two Venusian solar days.

The synchronous rotation of Venus relative to Earth is apparently caused by the action of the Earth's gravitation on the asymmetrical figure of Venus. For this condition to remain stable, it is necessary that the stabilizing moment of Earth /34

ORIGINAL PAGE IS
OF POOR QUALITY

$$T \quad \frac{\gamma M_{\oplus} M_{\varphi} R^5}{2 a_{AU}^6} k(q) \qquad \text{(II.33)}$$

(γ is the gravitational constant $M_{\oplus}$ and M_{φ} are the masses of Earth and Venus, AU is the astronomical unit, k(q) is the function calculated and tabulated in [316]) be larger than the tidal moment of Venus in the gravitational field of the Sun

$$T \quad \frac{3\gamma M_{\odot}^2 R^5}{a^6} k \qquad \text{(II.34)}$$

(k is the tidal Love numbers determined by the rigidity of the planet, a is the distance from the Sun, whose effect is to brake the rotation of the planet). The asymmetry of the Venusian figure that has been revealed (cf. Chapter 1) is evidently sufficient to assure a difference in the moments of inertia (B - A) relative to the equatorial axes that is necessary to fulfill the condition $T_{\oplus} > T_{\odot}$. Another factor contributing to the synchronization of Venus's rotation to the Earth (Gold and Soter have pointed this out [315] is the diurnal pressure variation in the Venusian atmosphere due to heating by the Sun. The minimum atmospheric pressure and mass occur in the afternoon part of the atmosphere, and the maximum pressure and mass in the morning part of the atmosphere. This distribution of the atmospheric mass creates in the gravitational field the moment $T'_{\odot}$, which is opposite in sign to the moment $T_{\odot}$, i.e., it accelerates the planet's rotation. This decreases the effect of the Sun's tidal moment and makes the synchronization of the Venusian rotation to the Earth easier. Taking the atmospheric moment into account, a condition for the synchronization of Venus' rotation to the Earth is $T_{\oplus} > T_{\odot} - T'_{\odot}$. The moment $T'_{\odot}$, which is created by the planetary atmosphere, is proportional to the rotation period P

$$T'_{\odot} = FP, \qquad \text{(II.35)}$$

where F is a constant for a given planet. In this connection, Gold and Soter think that the evolution of the Venusian rotation period could have occurred as in the following models. As it formed, Venus had a retrograde rotation that was faster than at present. Because of this rapid rotation, the influence of the atmosphere was inconsiderable, the braking moment of the Sun was greater than the synchronizing moment of the Earth /35

$$T_{\odot} - FP > T_{\oplus},$$

and the planet's rotation slowed. The atmospheric moment $T'_{\odot} = FP$ increased, so that at a certain P, which was a multiple of the synodic period, the condition

$$T_{\oplus} > T_{\odot} - FP$$

ORIGINAL PAGE IS
OF POOR QUALITY

obtained, and the rotation of Venus became synchronized to the Earth.

The direction of the Venusian spin axis is close to the pole of its orbit ($\alpha = 276°$, $\delta = 66°$): the deviation of the pole of the planet from the pole of the orbit does not exceed 6°. Therefore, seasonal variations similar to the seasons of the year on Earth should not be strongly marked on Venus.

The International Astronomical Union confirmed in 1970 the recommendation to accept the sidereal period of rotation as equal to 243.0 days and the orientation of the north pole as $\alpha = 273.0°$ and $\delta = +66.0$ (1950.0).

In principle, by analogy with Earth, one can expect changes in the location of the poles over time -- because of precession and nutation. However, the nutation is quite small, and the precession occurs very slowly. Therefore, one can consider the location of the poles as fixed for all practical purposes.

II.4. The Topography and Relief of the Surface

One of the important problems of the physics of Venus is to discover regions on the surface with various physical properties, to determine the location, size, and forms of these regions, and to correlate these data with the other characteristics of the planet.

Because the Venusian atmosphere is opaque for visible and infrared radiation, such information can be obtained either by direct probes using descent apparati or by radio astronomy and radar results.

Descent apparatuses can provide the most complete and accurate information about the properties of the surface in the regions of descent. /36 However, it would hardly be realistic in the foreseeable future to send the hundreds of descent apparatuses needed to resolve this problem.

Radio astronomy measurements made in two polarization planes at several wavelengths could, with sufficiently high resolution, determine the distribution of temperature, permittivity, and elevation above the mean level of the planetary surface. However,

the resolution of the ground radiotelescopes that are available or are being built is not high enough to examine individual regions on Venus.

A very promising means of solving this problem is to increase resolution by installing a radiotelescope on a spacecraft that passes by near the planet or that is inserted into orbit as an artificial satellite. The Soviet AIS [automatic interplanetary station] Mars-3 used this successfully to study Mars [12]; however, it has still not been used to study Venus.[3] Therefore, the only means of examining the details of the Venusian surface is still radar, the high planetary resolution of which is due to frequency and time gating (cf. Section II.2). With this, regions with various reflecting characteristics can be discovered on the planet. The time the front edge of the echo pulse returns can be used also to determine surface elevation at the subradar point; in this way, information about surface relief is obtained.

As mentioned above, in 1962 Goldstein and Carpenter [317] found on the echo spectrum details that correspond to high-reflectivity localities on the planetary surface. In order to determine the location of these localities on the planetary surface, Carpenter used a planetocentric system of coordinates, in which zero was taken to be the meridian that passed through the region of greatest reflectivity, a region Goldstein called the α-region. The direction of the longitude readings was chosen so that the longitude of the central (for an observer on Earth) meridian increased as Venus rotated. In connection with the fact that several observers had used different readings systems and that there was ambiguity in the determination of the Venusian north and south poles, the International Astronomical Union in 1970 accepted the basic postulates of the planetocentric system of coordinates for Venus; accordingly, the north pole of Venus is north of the plane of the ecliptic, and its coordinates are defined as follows: right ascension $\alpha = 273.0°$ and declination $\delta = +66.0°$ (1950.0). Longitudes are considered to increase as time passes for an Earth observer. The zero meridian passes through the α-region and is defined so that the longitude of the central (for an observer on Earth) meridian at 0:00 on June 20, 1964 (Julian day 2,438,566.5) was 320.0°. The planetocentric latitude of the center of the α-region is -30°. A second region of high reflectivity Goldstein named β; it is located near 280° longitude, +20° latitude. /37

In the measurements Carpenter made in the Jet Propulsion Laboratory in 1964 [232], the β-region was resolved into three features

---

[3] The only experiment in installing a radiotelescope on a spacecraft was done by the USA on the Mariner-2, which flew by Venus in 1962. However, the atmosphere of Venus is impenetrable to the wavelengths of 1.35 and 1.9 cm which were used in these measurements. Therefore, the data obtained in this experiment gave no information about the planetary surface.

ORIGINAL PAGE IS
OF POOR QUALITY

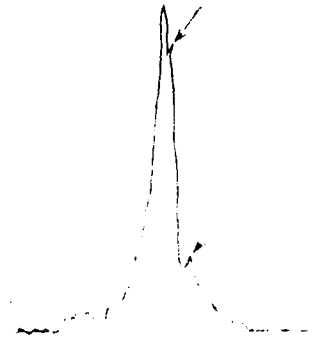

Fig. 9. Frequency spectrum of the reflection from Venus at a wavelength of 12.5 cm. The arrows denote the high-reflectivity areas.

he named B, C, and D. Measurements made near inferior conjunction in 1964 by the USSR Academy of Sciences' Institute of Electronics and Radio Engineering, the Jet Propulsion Laboratory, and the Arecibo Ionospheric Laboratory (USA) confirmed the presence of particular regions of high reflectivity on the planetary surface. An example of a Venusian reflectivity spectrum with these details in given in Fig. 9.

Near three inferior conjunctions of Venus in 1964, 1967, and 1969, measurements were made of three selected details at a wavelength of 70 cm [369]. Two of these details, named Gauss and Hertz, coincide with Carpenter's C1 and D2 details. The third detail, named Maxwell (Venusian latitude 64 ± 2° and longitude 3.5 ± 1°) had not previously been observed. A list of high reflectivity regions and their coordinates are given in Table 3. /38

TABLE 3. DETAILS OF HIGH RADAR REFLECTIVITY ON THE SURFACE OF VENUS

λ = 3.8 cm, Haystack Station, Rogers et al.			λ = 12.5 cm, Jet Propulsion Lab., Goldstein			λ = 12.5 cm, Jet Propulsion Laboratory, Carpenter			λ = 70 cm, Arecibo, Jurgens		
Name of detail	Longitude	Latitude	Name of detail	Longitude	Latitude	Name of detail	Longitude	Latitude	Name of detail	Longitude	Latitude

High reflectivity can be caused by the following features of the study region:

1) differences in surface material and, thus, permittivity;

2) a local elevated area and, thus, less absorption by the atmosphere;

3) a rougher surface texture.

An analysis of the change in the magnitude of high reflectivity at a wavelength of 3.8 cm as the particular region moved along the disk and, consequently, as the angle of reflection changed, showed that the main reason for high reflectivity is surface roughness. However, rough surface features alone cannot explain the quantitatively high reflectivity in the α-region; an increase in permittivity or in elevation is also necessary.

Polarized measurements also show that regions of high reflectivity are rougher (on the scale of the wavelengths of the radar measurements). Anomalously reflecting regions have, in a depolarized echo, a much greater (about ten times) contrast to the surrounding surface than in a polarized echo.

It is difficult at present to give an unambiguous interpretation of these features of the planet. Moreover, available experimental data from radar soundings indicate a considerable roughness on the Venusian surface.

Rogers and Ingalls [473] drew up a detailed map of the Venusian reflecting properties from measurements made at a wavelength of 3.8 cm. So as to avoid any ambiguity between the northern and southern hemispheres (an ambiguity inherent in the time-frequency gating method, cf. Section II.2), the echo was received on two spaced antennas, which operated as a radio interferometer. The /40
width of the interference lobe is equal to 0.1 of the disk of Venus. On the basis of observations made during 5 days in April 1969, a map was drawn up of the reflecting properties of a surface area bounded by longitudes o° and -80° (according to the IAU [International Astronomical Union] system) and latitudes of -50° to +40° (Fig. 10).

Two large circular formations similar to lunar seas were discovered. Their centers are $\lambda = 335°$, $\phi = -28°$ and $\lambda = 312°$, $\phi = -14°$. The first formation was clearly seen on each day of the observations. The second formation was less clear.

In the spring of 1969 and the fall of 1970, Goldstein et al. /41
[320] did independent measurements of reflectivity distribution on the surface of Venus at a wavelength of 12.5 cm. Resolution on the surface of the planet was about 50 km x 50 km; however,

ORIGINAL PAGE IS
OF POOR QUALITY

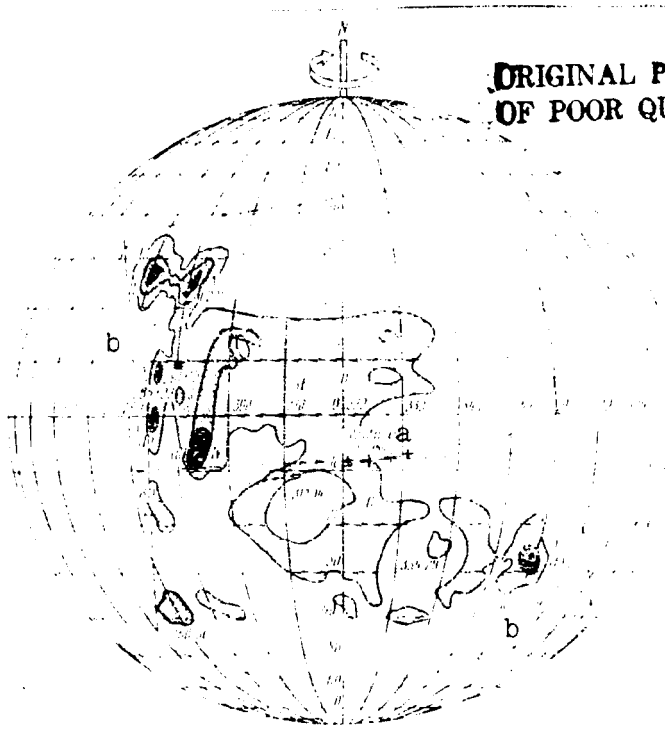

Fig. 10. Reflectivity map of the surface of Venus at a wavelength of 3.8 cm. The dashed line is the edge of the mapped area.

Key: a. Subradar point; b. Region...

ambiguity between northern and southern hemisphere was not entirely ruled out.

The results of the measurements are given in Fig. 11. The ratio of echo intensity in "bright" and "dark" regions is as high as 20:1. Regions of high reflectivity α, β, and δ have a circular shape and a diameter of about 1000 km.

The most detailed measurement of the distribution of reflecting properties and topography of the Venusian surface was made near the inferior conjunction of 1972 [285].

The planetary surface resolution was five times higher than in 1970 -- 10 km. With /42 such resolution, a more detailed examination was made of a region whose diameter was about 1500 km and whose center was at $\lambda = 320°$, $\phi = +2°$. This region is circled in Fig. 11.

The composite radar map in Fig. 12 revealed that in this region there are more than ten ring-shaped craters, with diameters of 35-150 km, and similar in shape to the craters of the Moon. Smaller craters cannot be discovered because of the limitations on resolution.

The first resulting attempt to study the relief of the Venusian surface was undertaken by W. Smith et al. at the Haystack Station [508]. Their radar measurements, made at a wavelength of 3.8 cm and within a limited longitudinal range, revealed the presence of an elevated area about 2 km high and 150 km long on a longitude of about 330°. This elevated area also gives an echo 2.5 times stronger than the surrounding area. At the present time, the Haystack and Arecibo stations are making radar measurements of the topography of the entire equatorial region [231]. The measurements were at wavelengths of 3.8 and 70 cm from August 1967 to

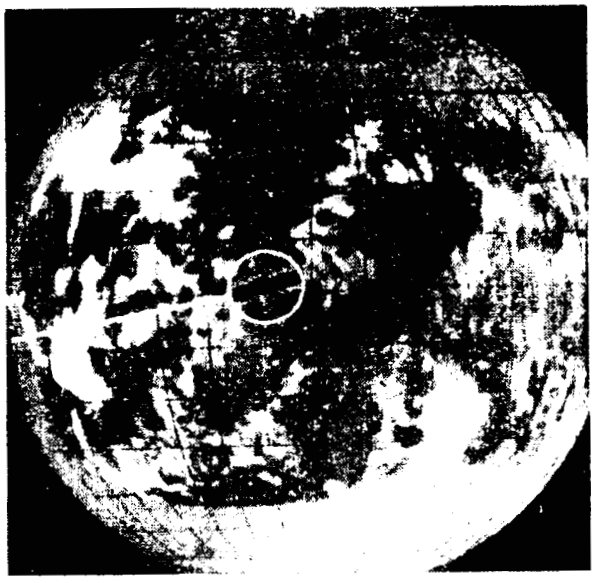

Fig. 11. Reflectivity map of the surface of Venus at a wavelength of 12.5 cm.

November 1970, and they include eight full revolutions of Venus relative to Earth. Changing the latitude of the subradar point during the period made it possible to cover the area of latitudes from -9° to +10°. In the first measurements, the altitude resolution was no worse than 1 km. In the 1970 measurements, the altitude resolution was improved to 150 m. Resolution of the planet's surface was from 200 to 400 km. The results of the measurements are given in Fig. 13.

The most noteworthy finding was an elevated area about 3 km above the mean surface level corresponding to an equatorial radius 6050 ± 0.5 km. The longitude of this region is about 90°. It extends about 6000 km in longitude and at least 500 km in latitude

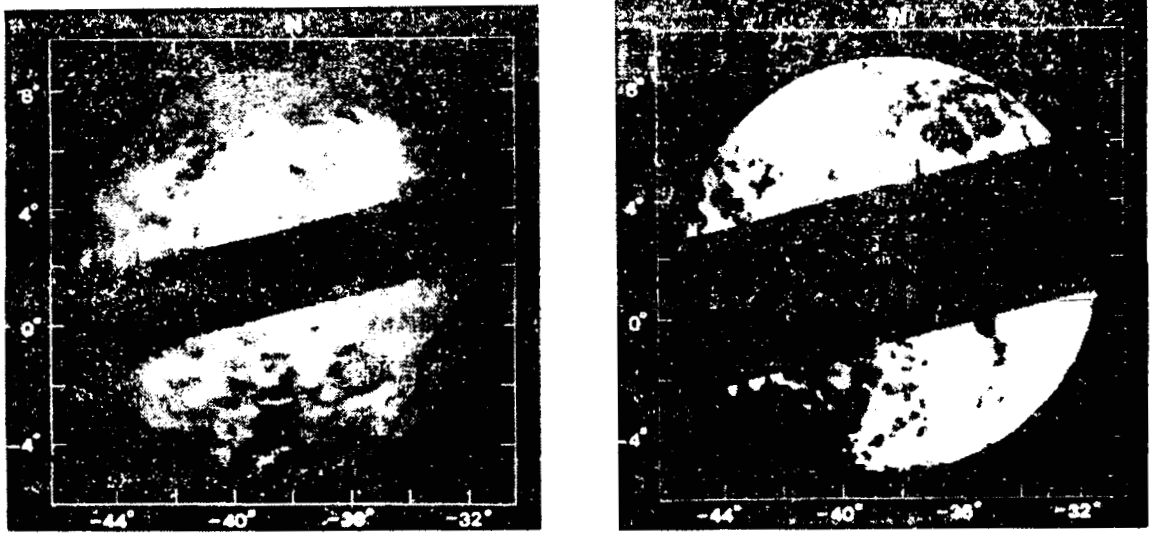

Fig. 12. Large-scale map of the reflection of the area of Venus circled in Fig. 11 (left). An elevation map of the same region (right). Contour interval -- 200 m.

ORIGINAL PAGE IS
OF POOR QUALITY

ORIGINAL PAGE IS
OF POOR QUALITY

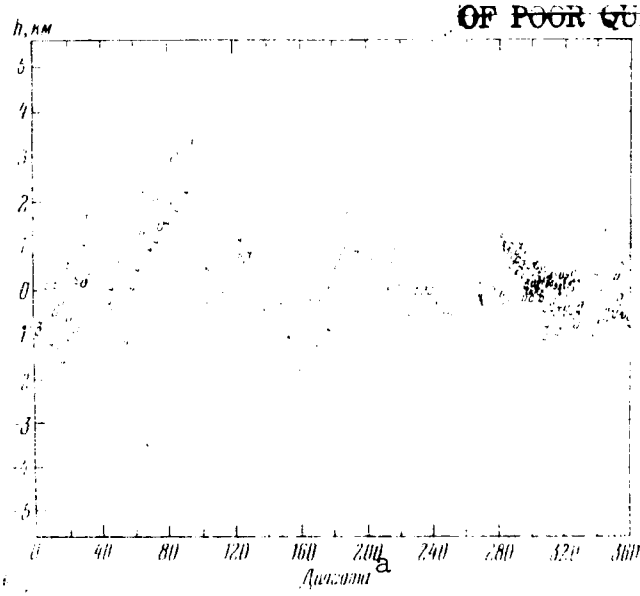

Fig. 13. Elevation profile of the surface of the equatorial region of Venus; according to radar measurements of range. The numerals denote the numbers of revolutions of Venus relative to Earth since August 1967. Zero altitude corresponds to an equatorial radius of Venus of 6050 ± 0.5 km.

Key: a. Longitude

The slopes of this elevated region are uneven. On the side where longitude decreases, the slope is gentle -- a mean angle of about 0.04°. On the side where latitude increases, the slope is much steeper -- a mean angle of about 0.5°.

Measurements of the relief made on various revolutions of Venus agree with each other to within 200-500 m. Rogers et al. [474] made an independent determination of the elevation profile of the Venusian equatorial region from data on the change of radar cross section at a wavelength of 3.8 cm with a planetocentric longitude. Radio waves at this wavelength are strongly absorbed by the Venusian atmosphere. By comparing the radar cross section at this wavelength with that at longer wavelengths, where there is little absorption, it is possible to determine the amount of atmospheric absorption, the thickness of the atmosphere, and, consequently, the elevation of the surface as well. /44

The results of determining an elevation profile in this way (given in Fig. 14) are in qualitatively good agreement with previously cited data on measuring the relief by measuring the radar range (cf. Fig. 13). Longitudinal resolution is 12°. /45

For purposes of calculation, the atmosphere of Venus was taken as adiabatic, $\gamma = c_p/c_v = 12.8$, the temperature gradient $\beta = -8.8$ deg.km^{-1}, the temperature and pressure at mean surface level are 750°K and 90 atm, and the chemical composition is 95% CO_2, 4.6% N_2, and 0.4% H_2O. An increase of 10% in one of the parameters $p(0)$, $T(0)$, β and γ changes the zero level by 3, -8, 1, and 12, respectively. The elevation changes by -3, 18, 7, and 45%, respectively.

ORIGINAL PAGE IS
OF POOR QUALITY

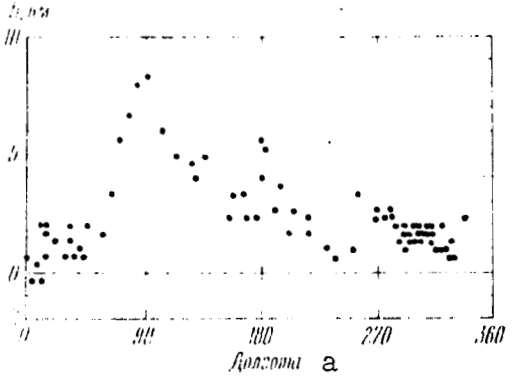

Fig. 14. Elevation profile of the surface of the equatorial region of Venus -- determined from the absorption of radar reflection in the atmosphere.

Key: a. Longitude

It should be noted that the relief determined in this way is averaged over a large area. Therefore, the actual drop in elevation recorded in these measurements can be much greater. In order to evaluate this effect, we did a modeled average for the Caucasus Mountains on Earth; this decreased the actual drop in elevation about twofold. Consequently, if there is a "Caucasus-like" relief on Venus, the elevated areas discovered by radar can correspond to mountains about 6-10 km high. However, because of the high surface temperature, the Venusian crust should be even more active than the Earth's, and, therefore, because of conditions of isostasy, it is not probable that there are such high mountains on Venus.

The next measurements of the Venusian surface relief were made /46 in the above-mentioned radar experiment at the Jet Propulsion Laboratory in 1972 [285]. Echo reception was on two antennas spaced 22 km apart. This made it possible to obtain spectroscopic depiction of the surface with an elevation resolution of 200 m. The processing, done on a computer specially devised for this experiment and with a speed of $5 \cdot 10^7$ operations per second, showed that the craters on Venus were quite shallow. For example, a crater of 150 km diameter has an overall depth of about 0.5 km. The entire study area turned out to be quite flat: the drop in elevation is not in excess of 1 km.

It is important to note that of the three bodies in the solar system -- the Moon, Mars, and Venus -- whose surfaces are strongly cratered, the deepest craters are found on the Moon, which has practically no atmosphere. The craters on Mars, which has a rarefied atmosphere, are smaller. The smallest are on Venus, a planet whose atmosphere is dense. Such a sequence gives reason to suppose that this difference in crater depth on the Moon, Mars, and Venus is caused primarily by the atmosphere. In Goldstein's opinion, the large craters on Venus are of impact origin and were formed when the planet did not have a dense atmosphere. An increase in atmospheric density led to the development of a more intense erosion than on the Moon and Mars, and this made the relief flatter. However, it is impossible to exclude the hypothesis that the craters are volcanically formed.

The Earth does not fit into this sequence. Its atmospheric density is intermediate between that of Mars and Venus, and it has only quite smooth remnants of meteorite craters. A possible reason for this feature can be the predominant role of water erosion, as opposed to wind erosion on Mars and Venus, in the formation of the Earth's relief. The shallowness of Venusian craters can be caused, besides by atmospheric erosion, by volcanic activity filling them with lava.

Radar measurements of relief have dealt only with the equatorial region of the planet. There are no data on the relief of the rest of the surface, which is not covered by these measurements. /47
One can only assume that, because of conditions of isostasy and the density of surface material, it is not very likely that there are mountains on Venus higher than 10 km.

In order to solve this problem experimentally, by methods on Earth, a significant increase in the energy potential of radar devices is necessary. However, the measurements most conducive to results for these investigations will evidently be measurements made by automatic interplanetary spacecraft that are inserted into orbit around Venus.

CHAPTER 3. THE PHYSICS OF THE SURFACE /48

As indicated above, because optical and infrared radiation cannot penetrate the Venusian atmosphere, the study of the surface can be done only by the techniques of radio astronomy and radar and by using descent apparatuses as well. In this regard, Section II.2 briefly sets forth the fundamentals of radar research of planets. Here we set forth the fundamentals of planetary radio astronomy -- as applied to the study of Venus. Readers familiar with radio astronomy can skip this section.

III.1. The Fundamentals of Planetary Radio Astronomy

Any body at a temperature other than 0°K emits electromagnetic waves in a broad spectral range, including radio frequency. This emission arises as the energy of charged particles in random thermal motion changes.

The intensity of radio emission is usually expressed by one of the three following parameters: brightness I, flux density S, and brightness temperature T.

Brightness I characterizes the flux of energy emitted by an element of area of the body under examination (this area subtends a solid angle $d\Omega$ at the observer) per unit frequency band, unit time, and unit area in a direction normal to this area. In a practical system of units, I is expressed as $\omega \cdot m^{-2} \cdot Hz^{-1} \cdot sterad^{-1}$.

For heat emission

ORIGINAL PAGE IS
OF POOR QUALITY

$$I = \varkappa B(T), \qquad \text{(III.1)}$$

where κ and T are the coefficient of absorption and the temperature of the body and B(T) is Planck's emission function. In the general case /49

$$B(T) = \frac{2h\nu^3}{c^2} \frac{1}{\exp\left(\frac{h\nu}{kT}\right) - 1}, \qquad \text{(III.2)}$$

where h is Planck's constant, k is Boltzmann's constant, λ and ν are the wavelength and frequency of the radio emission received.

In the radio frequency range, usually $h\nu << kT$. With this, Eq. (III.2) leads to the simpler form of the Rayleigh-Jeans formula

$$B(T) = \frac{2kT}{\lambda^2}. \qquad \text{(III.3)}$$

whence

ORIGINAL PAGE IS
OF POOR QUALITY

$$I \approx \frac{2kT}{\lambda^2}. \qquad \text{(III.4)}$$

For sources that are small in comparison with the beam width of radio telescopes (which is usually the case for the planets), the measured value is the flux density S, which characterizes the flux of the energy emitted by the entire object under study

$$S = \int_{\Omega_S} I \, d\Omega. \qquad \text{(III.5)}$$

Integration is carried out within the limits of the solid angle of the source Ω_S, since the integral is equal to zero outside these limits. In a practical system of units, S is expressed as $\omega \cdot m^{-2} \cdot Hz^{-1}$.

The determination of brightness or flux density of the radio emission under investigation -- by measuring its power -- requires a knowledge of the transmission bandwidth and the form of the frequency characteristic of the radio receiver. Therefore, the measurement of intensity is done by comparing it to the intensity of absolute blackbody radio emission. The temperature of an absolute blackbody that has the same brightness on a given frequency in a given direction as the source being studied is called the <u>brightness temperature</u> T_B of this source.

For an absolute blackbody, $\kappa = 1$ and the brightness of its emission at a given temperature is maximally /50

$$I = \frac{2kT_B}{\lambda^2}. \qquad \text{(III.6)}$$

By comparing Eqs. (III.4) and (III.6), we obtain the brightness temperature of thermal radio emission

$$T_B = T. \qquad \text{(III.7)}$$

The absorption coefficient $\kappa \leq 1$. Therefore, for thermal emission, always[1]

[1] In the case of nonthermal emission, the brightness temperature is a formal parameter unrelated to the kinetic temperature of the body under investigation. In this case, therefore, it is possible that $T_B > T$. However, there is no pronounced nonthermal radio emission on Venus. We therefore do not examine the mechanics of nonthermal radio emission.

ORIGINAL PAGE IS
OF POOR QUALITY

$$T_B \leq T. \qquad \text{(III.8)}$$

These relations describe the emission of an isothermal body.

Venus has a dense atmosphere that absorbs millimeter and centimeter radio waves, the temperature of which varies with altitude; it is not an isothermal body. In this case, the intensity of emission is defined by the emission transfer equation

$$dI = -\varkappa I\,ds + \varkappa B(T)\,ds$$

or

$$\frac{dI}{d\tau} = -I + B(T), \qquad \text{(III.9)}$$

where

$$d\tau = \varkappa\,ds.$$

The value

$$\tau = \int \varkappa\,ds$$

is called the optical depth of the atmosphere and characterizes the extinction of an electromagnetic wave along the line of sight above a level located at a distance s from the surface of the planet. Inasmuch as for every optical depth τ_s there is a definite value T, /51 one can henceforth write $B(\tau_s)$ instead of B(T). By integrating Eq. (III.9) along the line of sight, we obtain

$$I = \int_0^{\tau} B(\tau)\,e^{-(\tau-\tau)}\,d\tau + I_0 e^{-\tau},$$

or, transferring to brightness temperatures

$$T_B = \int_0^{\tau} T(\tau)\,e^{-(\tau-\tau)}\,d\tau + T_{B0}e^{-\tau}. \qquad \text{(III.10)}$$

Here I_0 and T_{B0} are the brightness and brightness temperature of the surface $\tau = \int_0^{\infty} \varkappa ds$ is the total optical thickness of the atmosphere.

Passing to a more specific distribution of temperature and absorption at altitude h, and considering also the atmospheric

emission reflected off the surface, we obtain the following formula for determining the radio emission of a planet with an atmosphere:

ORIGINAL PAGE IS
OF POOR QUALITY

$$T_B = T_{B\text{surf}} \int_0^\infty T(h)\varkappa(h)e^{-\int_0^h \varkappa(h)\,dh}\,dh + R_S e^{-\int_0^\infty \varkappa(h)\,dh} \int_0^\infty T(h)\varkappa(h)e^{-\int_0^h \varkappa(h)\,dh}\,dh. \qquad \text{(III.11)}$$

Here the first term expresses the emission from the surface, the second the emission from the atmosphere, and the third the atmospheric emission reflected off the surface. R_S is the reflection coefficient of the surface.

The brightness temperature in general, as well as the brightness, depends on the location of the emitting region on the object $T_B = T_B(\phi,\theta)$ and characterizes the distribution of the intensity of radio emission by the source being studied.

The flux density of radio emission is connected with the brightness temperature by the obvious relation

$$S = \frac{2k}{\lambda^2}\int_{\Omega_S} T_B\,d\Omega \qquad \text{(III.12)}$$

For a source with an identical brightness temperature T_B at all points

$$S = \frac{2k}{\lambda^2} T_B \Omega_S \qquad \text{(III.13)}$$

where Ω_S is the solid angle of the radio source.

For sources with dissimilar brightness temperature, the conception of brightness temperature averaged over its solid angle is used:

$$T_B = \frac{1}{\Omega_S}\int_{\Omega_S} T_B(\varphi,\theta)\,d\Omega. \qquad \text{(III.14)}$$

For Venus, one speaks in this case of a brightness temperature averaged over the apparent disk of the planet $T_{B\varphi}$. The brightness

temperature is expressed in degrees Kelvin (absolute scale). The flux density is related to the brightness temperature averaged over the apparent disk by the relation

$$S \approx \frac{2kT_B}{\lambda^2}\Omega_{\varphi} \qquad \text{(III.15)}$$

ORIGINAL PAGE IS
OF POOR QUALITY

where Ω_{φ} is the solid angle of Venus' apparent disk.

The convenience of using the conception of brightness temperature stems from the fact that in the case of thermal emission T_B is related to the kinetic temperature of the source T by a very simple relation; and for a blackbody, it is simply equal to T.

Solving the opposite problem -- that of finding the surface and atmospheric temperatures from the measured brightness temperature of radio emission, which reduces to the solution of the integral equations (III.11) and (III.14) -- is not generally without ambiguity. It is customary, therefore, to set up a model of the atmosphere (for example, a model with an adiabatic distribution of temperature versus height) and vary the parameters of this model (water vapor content, surface temperature, pressure, etc.) so as to obtain the best agreement with the experiment. The number of equations necessary to determine several parameters is obtained from measurements of T_B at various wavelengths, which are selected in such a way that brightness temperature varies with the parameters to be determined. /53

Specifically, on sufficiently long waves (in the decimeter range), as follows from (II.29)-(II.31), the absorption by the atmosphere is small and $\tau \ll 1$. In this case

The brightness temperature of the surface T_{B0} is the angle between the direction toward the observer and the normal to the surface, and R_s is the reflection coefficient.

For a smooth (compared to a wavelength) surface, the reflection coefficients are determined by the Fresnel formulas

$$R_v = \left(\frac{\varepsilon\cos\theta - \sqrt{\varepsilon - \sin^2\theta}}{\varepsilon\cos\theta + \sqrt{\varepsilon - \sin^2\theta}}\right)^2 \qquad \text{(III.17)}$$

for vertical polarization and

$$R_h = \left(\frac{\cos\theta - \sqrt{\varepsilon - \sin^2\theta}}{\cos\theta + \sqrt{\varepsilon - \sin^2\theta}}\right)^2 \qquad \text{(III.17')}$$

for horizontal polarization.

For a spherical planet, the direction of vertical polarization coincides with the radii of the apparent disk. In the general case of random orientation of the polarization of the receiving system

ORIGINAL PAGE IS
OF POOR QUALITY

$$1 - R_s \quad (1 - R_v)\cos^2\gamma + (1 - R_h)\sin^2\gamma. \qquad \text{(III.18)}$$

where γ is the angle between the direction of polarization of the receiving system and the direction from the emitting element to the center of the apparent disk. Considering that the distance of the emitting element to the center of the disk is expressed in a fraction of the radius of the disk, $a = \sin\theta$, and making simple transformations, we obtain /54

$$\begin{aligned} (1 \quad R_v) \quad & \frac{4r\,|\,(1\quad)(\quad)}{(r\,|\,1\quad)^2\,|\,r\quad)^2} \cdot \Big| \\ (1 \quad R_h) \quad & \frac{4\,|\,(1\quad)(\quad)}{(\,|\,1\quad)^2\,|\,r\quad)^2} \Big| \end{aligned} \qquad \text{(III.19)}$$

The solution of the integral equation (III.16) is also ambiguous and requires the setting up of a model of temperature distribution versus depth. However, as a first approximation, one can consider that the principal contribution to the emission is made by layers at a depth corresponding to $\tau = 1$. This depth, called the electromagnetic wave penetration depth, is equal to

$$l_e \quad \frac{\lambda}{2\pi\operatorname{tg}\delta\,|\,\varepsilon}. \qquad \text{(III.20)}$$

where $\operatorname{tg}\delta$ is the tangent of the loss angle and ε is the permittivity of the surface material. In this way, by measuring T_B at several decimeter wavelengths, one can determine the temperature of the Venusian surface layer and how it changes versus depth.

The value of the permittivity needed to interpret the results of measurements can be determined independently -- on the basis of data from radar measurements (cf. Section II.2) and radio astronomy measurements.

The determination of ε by radio astronomy measurements is based on the fact that the Fresnel reflection coefficients depend on ε; consequently, brightness temperature depends on ε as the angle of emission θ changes.

This makes it possible to determine ε by measuring radio brightness distribution on the planetary disk or by measuring the polarization of the radio emission from edges of the planetary

disk. Making such measurements requires a resolution of sufficiently small segments on the planet; this is achieved only by using radio interferometers or by mounting radio telescopes on spacecraft that fly near Venus.

At millimeter and centimeter waves, the optical thickness of /54
the atmosphere is sufficiently large. Therefore, the emission of these ranges originates basically in the atmosphere, and measuring it gives information about atmospheric parameters. In this case, for example, one can set up a model of temperature and pressure distribution of the atmosphere versus altitude (this is obtained from direct measurements by the Venera-4, 5, 6, and 7 AIS's) and then estimate the content of those components of the Venusian atmosphere that have considerable absorption in the radio frequency range (water vapor, water droplets in the cloud layer, ammonia).

On the basis of radio astronomy measurements made at various phase angles of Venus, one can also estimate the diurnal variations in surface and atmospheric temperatures, thereby extrapolating the results of the Venera-4-7 measurements, which were made on the night side of the planet, to the day side. The Venera-8 measurements made on the day side of the planet have confirmed the validity of such extrapolation.

III.2. Determination of Permittivity, Density, and Composition of Rocks of the Planet's Surface. Surface Microrelief

The permittivity ε of the surface material of Venus is determined on the basis of radar and radio astronomy measurements.

The determination of ε from radar data is made by using relation (II.3) according to the reflection coefficient R_s. The value R_s is determined from Eq. (II.4) on the basis of measurement of the radar cross section σ_r, with the contribution of the quasi-specular and diffused components of the echo taken into account.

The results of measurement of the radar cross section are given in Table 4 and are depicted in Fig. 15 in the form of the dependence of σ_r on wavelength λ. A characteristic feature of this dependence is that σ_r is approximately constant in the wavelength range from 7 m to 20 cm and sharply decreases at shorter waves (by about ten times at wavelength 3.8 cm). This decrease is caused by absorption by the Venusian atmosphere. Therefore, the determination of R_s should be made from measurement at wavelength /56
$\lambda \geq 20$ cm, for which absorption by the Venusian atmosphere is sufficiently small. The weighted mean value of the radar cross section in this range is $\sigma_{r0} = 0.15 \pm 0.03$.

Fig. 15 also gives the calculated dependence of σ_r on wavelength λ for a case where the decrease in σ_r is caused by

ORIGINAL PAGE IS
OF POOR QUALITY

TABLE 4. RADAR CROSS SECTION OF VENUS

λ (cm)	Observers	Dates	r
3.6	Karp et al. [372]	VI.1963	0.009±0.003
3.8	Evans et al. [296]	18 I – 27 IV 1966	0.012±0.005
3.8	Evans et al. [297, 298]	1967	0.017±0.010
12.5	Viktor et al. [536]	10 III – 10 V 1961	0.11±0.02
12.6	Goldstein, Carpenter [232, 318]	I V – 17 XII 1962	0.098 $^{0.026}_{0.020}$
12.5	Carpenter [233]	II – VIII 1964	0.115±0.018
23	Evans et al. [294]	21 II – 7 V 1964	0.152±0.09
23	Evans et al. [295]	17 I – 12 II 1966	0.18±0.11
43	Kotel'nikov et al. [74]	18 IV – 26 IV 1961	0.08*
43	Kotel'nikov et al. [75]	20 X – 21 XII 1962	0.157 $^{0.023}_{0.037}$
43	Kotel'nikov et al. [76]	II IV – 30 VI 1964	0.19
68	Pettengill et al. [447]	6 III – 18 VI 1964	0.13±0.05**
70	Dyce [286]	15 II – 3 XI 1964	0.14 $^{0.09}_{0.05}$
600	Klemperer et al. [380]	23 XII – 7 XII 1962	0.2***
784	James and Ingalls [359]	6 XI – 7 XII 1962	0.15±0.07

* Refers only to the narrow-band component of the echo.
** Reworked and refined by Evans et al.
*** Mean values; there are large variations from day to day.

absorption by the atmosphere for the atmospheric model given in Section IV.5. A good agreement between the calculation and the experiment confirms the validity of the original model.

The contribution of quasi-specular and diffused properties can be estimated by analysing the direction properties of the echo. Figs. 16-18 give the results of measuring the properties of echoes from Venus at wavelengths 23 cm [294], 43 cm [76] and 70 cm [286], wavelengths for which there is little absorption by the planetary atmosphere. These measurements generally revealed the presence in reflection functions of a sharp maximum near $\theta = 0°$, which corresponds to a quasi-specular echo; here, the greater part of the echo energy is included in the quasi-specular component. /57

A precise comparative analysis of the reflection functions obtained in various measurements (for example, for the discovery of their dependence on wavelength) is possible only for measurements made with identical resolution. In particular, therefore, the reflection functions of Venus given in Figs. 16-18 cannot be compared directly. However, it is possible to do an analysis of the

ORIGINAL PAGE IS
OF POOR QUALITY

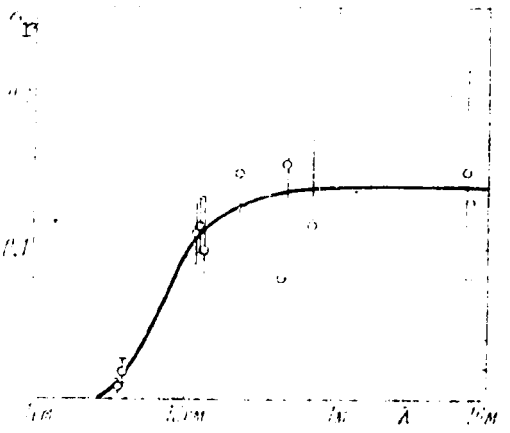

Fig. 15. Measured and calculated dependence of radar cross section of Venus on wavelength.

energy distribution between the quasi-specular b_s and the diffused b_d components of the echo. For convenience in this distribution, as was shown in Section II.2, the reflection functions in Figs. 16-18 are represented in functional form

$$\lg f(\theta) = A + B \lg \cos\theta.$$

An analysis of the results of the measurements shows that at a wavelength of 70 cm, the diffused component is 15% of the full echo energy [286]. At a wavelength of 43 cm, the measured part of the reflection function within the limits $0 < \theta < 50°$ does not contain a component described by the $\cos^2\theta$ rule characteristic of diffused reflection. Assuming that the echo is diffused at $\theta > 50°$, we obtain: the diffused component is 10% of the full echo energy. However, in connection with the lack of measurements in this area, this estimate is approximate. /58

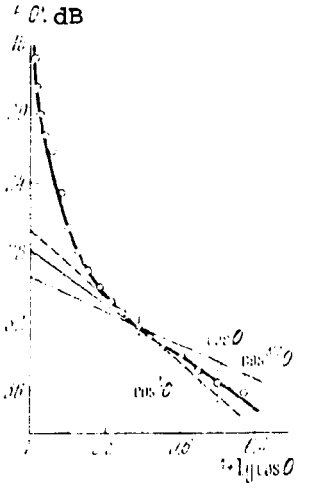

Fig. 16. Reflection function of Venus at a wavelength of 23 cm.

At a wavelength of 23 cm, the diffused component is better approximated by a $\cos^{3/2}\theta$ dependence; however, with an accuracy up to the error of measurement, dependences of the form $\cos^2\theta$ and $\cos\theta$ are also not ruled out. The diffused component, which is determined by integration under the straight line $\lg \cos^{3/2}\theta$, is 11% of the full echo energy.

Thus, at wavelengths $\lambda > 20$ cm, where absorption by the atmosphere of Venus has little influence on the value and character of the echo, $\sigma_{r0} = 0.15 \pm 0.03$, $b_d = 0.1/0.15$ and $b_s = 0.9/0.85$. With this, calculation according to Eq. (II.16) leads to $R_s = 0.14 \pm 0.03$, which corresponds to a permittivity of surface material $\varepsilon = 4.7 \pm 0.8$.

An experiment similar to radar in determining ε from the value of the reflection coefficient for radio waves was carried

ORIGINAL PAGE IS
OF POOR QUALITY

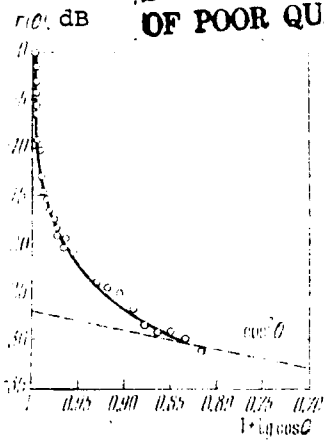

Fig. 17. Reflection function of Venus at a wavelength of 43 cm.

out on the Venera-8 AIS descent apparatus [22] by measuring the echo intensity of a radio altimeter. The value ε obtained is in good agreement with the results of ground radar measurements.

The radio astronomy method of determination of permittivity ε is based on the dependence on ε of the polarization of the radio emission of the surface at the edge of the planet's apparent disk. The high resolution needed for this was attained first through interference measurements of the polarization of Venus' radio emission; Kuz'min and Clark made these measurements in 1964 [83]. However, in interpreting the results obtained, the authors of [83] did not take into account the effect of the atmosphere, which reduced the polarization component of the planetary emission. Therefore ε is underestimated.

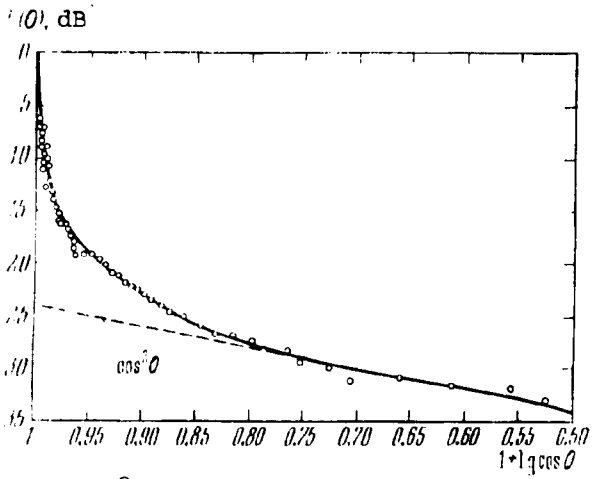

Fig. 18. Reflection function of Venus at a wavelength of 70 cm.

Direct measurements of the Venusian atmospheric parameters, made by Venera 4-8, allow us to determine the absorption by the Venusian atmosphere and to interpret the results of these measurements more correctly [83]. Taking into account absorption by carbon dioxide and water vapor, the relative content of which is $f_{H_2O} = 10^{-3}$, the optical thickness of the planetary atmosphere at a wavelength of 10.6 cm is $\tau_{10.6} = 0.15$. In this, the best agreement between the experimental data [83] and the model calculated for a smooth sphere corresponds to $\varepsilon = 3.0 \pm 0.4$. Calculating the effect of surface roughness gives an additional correction $\Delta\varepsilon = +0.6$. /60

Thus, from the results of polarized radio interferometric measurements [83] and by calculating atmopsheric absorption, the permittivity of the planetary surface is $\varepsilon = 3.6$. By taking a possible indefiniteness in the estimate of water vapor content $\delta f_{H_2O} = \pm 1 \cdot 10^{-3}$, the error in the determination of ε from these measurements is $\delta\varepsilon \cong \pm 1.0$.

Good agreement with radar measurement results rules out the necessity that water vapor be present in the Venusian lower atmosphere and makes it possible, moreover, to estimate an upper bound on water vapor content, as well as on the content of other components that absorb radio waves. Such an estimate will be made further on in Section IV.5.

One could expect that polarized radio astronomy measurements at longer wavelengths, where atmospheric absorption is still smaller, will give more precise data about ε. Preliminary results from recent radio interferometric measurements at a wavelength of 21 cm [217] show that $\varepsilon < 4.5$. However, preliminary processing was done without taking the depolarizing effect of surface roughness into account.

The value $\varepsilon = 4.7 \pm 0.8$ obtained from radar measurements is substantially higher than for the Moon and does not require assumptions about the presence of porous or finely crushed rock, as occurs on the Moon, to explain it. The value $\varepsilon = 4.7$ corresponds to dry silicate rock of the granite or basalt type or to other terrestrial-type dry rock.

Low permittivity decidely rules out Menzel and Whipple's hypothesis that the surface of Venus is a continuous ocean. In addition, water cannot exist as a liquid at the high surface temperature of the planet.

In principle, several oil-type liquids satisfy the value $\varepsilon = 4.7$. However, the hypothesis that the Venusian surface is an ocean of oil is quite artificial. Furthermore, radar measurements have discovered formations on Venus that have high reflectivity persisting over several years, and they indicate that the entire surface of the planet is not liquid. /61

For a solid surface, the results of the determination ε make it possible to estimate the density of surface material of Venus. This assessment is based on the empirical dependence of permittivity ε and density ρ

$$\rho \sim \frac{\sqrt{\varepsilon} - 1}{0.5}, \qquad \text{(III.21)}$$

ORIGINAL PAGE IS
OF POOR QUALITY

obtained by Krotikov [79] for various dry terrestrial rocks. $\rho_{\oplus} = 2.3 \pm 0.4$ g·cm^{-3} corresponds to the value $\varepsilon = 4.7 \pm 0.8$; this is close to the density of terrestrial rocks $\rho_{\oplus} = 2\text{-}3$ g·cm^{-3}. This also gives reason to suppose that the surface material of Venus can be similar to dry terrestrial rock surfaces.

A much lower density for surface rocks than for the mean density of the planet as a whole (5.2 g·cm^{-3}) suggests that Venus,

like the Earth, passed through a stage of differentiation, in the process of which a lighter (compared to deep strata) crust formed.

It is necessary to keep in mind, of course, that the value ε obtained from observations on Earth is averaged over the entire hemisphere of the planet, whose surface can be quite rough. Therefore, this discussion concerns only the mean values of the density of Venusian rock.

A.P. Vinogradov et al. [34] used the AIS Venera-8, whose scientific instrumentation included a gamma-ray spectrograph, to determine the chemical composition of Venusian surface rock. From an analysis of gamma-radiation spectra, the content of natural radioactive elements in Venusian rock is: potassium 4%, uranium $2.2 \cdot 10^{-4}$%, and thorium $6.5 \cdot 10^{-4}$% (percentages by weight). The error in these determinations does not exceed 30%.

Judging from the content of these elements Venusian rock is close to the acidic magma rock of the Earth. The ratio of potassium to uranium content K/U is also quite close to what is characteristic for most magmatic rocks on Earth (on the average, about 10^4). This also indicates a similarity in the processes by which the Earth and Venus formed (the formation of clouds and secondary rocks of non-solar composition). The K/ U ratio for chondrites with primary solar composition is about 10^5, i.e., an order of magnitude higher than for rocks on Earth. /62

An analysis of radar reflection functions makes it possible also to draw several conclusions about the microrelief of the planet's surface. The diffused component of the echo indicates the presence on the planetary surface of regions that are rough for the wavelength at which the measurement is being made, i.e., with anomalies of less than several centimeters in the microrelief. The total area of these sections a_d as determined by the relation (II.17) is about 0.05 of the area of the planetary apparent disk.

The quasi-specular component of the echo indicates that on the surface there are smooth portions, large compared to the wavelength, but inclined relative to the mean surface. The statistical properties of this surface are characterized by the relations (II.8)-(II.13). Fig. 19 gives the distribution curve of the slopes of these flat segments in relation to the mean surface; this curve is obtained from a reflection function of Venus measured at a wavelength of 23 cm [294]. This figure also gives a distribution curve of slopes on the Moon's surface. However, the curve $f(\theta)$ gives the distribution only in one of the vertical sections. The real slope of any facet can be greater; consequently, to determine the mean slope, one should take an average along all vertical sections, i.e., /63

$$\theta = \frac{\int_0^{\pi/2} f(\theta) \cos\theta \sin\theta \, d\theta}{\int_0^{\pi/2} f(\theta) \cos\theta \sin\theta \, d\theta} \qquad \text{(III.22)}$$

ORIGINAL PAGE IS OF POOR QUALITY

ORIGINAL PAGE IS
OF POOR QUALITY

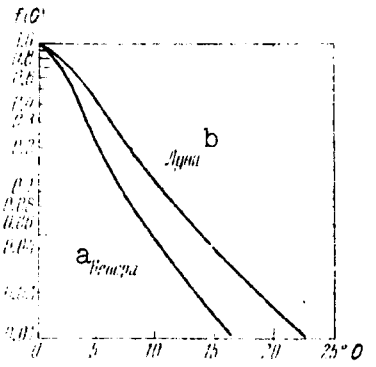

Fig. 19. Probability distribution for slopes of surface $f(\theta)$ of Venus (λ = 23 cm) and the Moon (λ = 68 cm).

Key: a. Venus; b. Moon

Numerical integration of radar measurements results at a wavelength of 23 cm gives $\bar{\theta} = 8.2°$. This value may be slightly underestimated, since in the region $\theta < 2.5°$, the reflection function $F(\theta)$ has not been studied sufficiently.

For the Moon, $\bar{\theta} = 10.2°$ was obtained at this wavelength, i.e., Venusian relief is not as rough as that of the Moon.

An analysis of the data of the Venus measurements at a wavelength of 12.5 cm, done by Carpenter [233] for a gaussian correlation function on the basis of a similar method developed by Daniels [260], leads to a quadratic mean slope of the reflecting surfaces $\bar{\theta} = 6.2°$, which also indicates considerable smoothness on the Venusian surface, as compared to the Moon.

An estimate of the Venusian surface microrelief can be made also by measuring echo depolarization.

As is well-known, for a circularly polarized echo from a smooth sphere, the sense of polarization changes to the reverse. Therefore, if the transmitter emits, for example, a signal with a right circular polarization, the receiving antenna should receive an echo with a left circular polarization. However, a partial depolarization of the signal occurs when it is reflected off a rough surface. This echo component, which is thus characteristic of the roughness of a reflecting surface, can be measured as it returns to an antenna with the same polarization as the transmitting antenna.

The measurements showed that for Venus the relation of nonpolarized to polarized reflection is substantially less than for the Moon (three times less for an angle of incidence of 60°). This indicates that the surface of Venus scatters radio waves considerably less by comparison and that it is smoother on the average than the lunar surface. /64

III.3. Temperature of the Surface

Radio astronomy measurements and the direct measurements made by Venera-7 and Venera-8 have determined the surface temperature of Venus.

Mayer et al. [416] made the first attempt to ascertain the surface temperature of Venus; near the inferior conjunction of 1956, they measured the brightness temperature of Venusian radio emission at a wavelength of 3.15 cm: $\bar{T}_{B\odot} = 560 \pm 73°K$. If the planetary atmosphere is transparent at this wavelength and the radio emission received is the thermal emission from the surface, then the brightness temperature obtained leads to an unexpectedly high surface temperature of about 600°K, more than twice as high as the radiometric temperature of 235°K that was measured previously from infrared emission [450].

The lack of evidence that the Venusian atmosphere is transparent at 3 cm wavelength range[2], the difficulty of explaining such a high surface temperature, and a much lower brightness temperature measured by Kuz'min and Salmonovich [80, 81] and Gibson [310] at a shorter wavelength of 8 mm all provided a basis for a different interpretation of the radio astronomy measurement results offered by Jones [366].

In accordance with this interpretation, it was suggested that the thermal radio emission from the surface of Venus is taken to be in the millimeter range, and Mayer et al. [416] recorded at a wavelength of 3.15 cm an emission of the dense ionosphere of Venus $N_e = 10^9$-10^{10} cm^{-3}, which has a higher kinetic temperature than the surface. In this case, the surface temperature of Venus is about 400°K. In order to resolve this ambiguity, a series of special radio astronomy measurements was made. In 1962, Korol'kev et al. [72], using the large Pulkovskiy radio telescope, and Barath et al., using the radio telescopes mounted on the Mariner-2 spacecraft, measured the radio brightness distribution on the planetary disk and showed that at wavelengths 3 and 1.9 cm Venusian radio emission originates not in the ionosphere but rather in the atmosphere of the planet. Kuz'min and Clark [83], who in 1964 discovered the polarization of Venusian radio emission at a wavelength of 10.6 cm near the edges of the disk, obtained direct evidence of surface radio emission. This made it possible to determine the planet's surface temperature $T_S = 650 \pm 70°K$ [84]. /65

Such a high surface temperature fundamentally changed existing notions about Venus as a twin of Earth, as a planet whose conditions were very similar to those on Earth. Specifically, it is

---

[2] Later radar measurements of Venus and the calculations for an atmospheric model obtained on the basis of the Venera 4-7 AIS measurements showed that at a wavelength of 3 cm, the optical thickness of the planet's atmosphere $\tau \simeq 1.5$ [25], i.e., surface emission is only about 20% of all radio emission received from Venus. Therefore, the brightness temperature measured at this wavelength characterizes the atmospheric temperature rather than the surface temperature.

impossible for proteins to exist at such a high temperature, and this excluded the very tempting possibility of life on Venus, at least, of life on its surface.

The fundamental importance of this finding made it necessary to determine the surface temperature of Venus independently, by a method in which the connection between the measured parameter and the temperature would not depend on an atmospheric model of the planet. The beginning of a program of direct probes of the Venusian atmosphere by the Soviet descent apparati AIS Venera opened up the possibility of making such measurements.

The temperature sensors on these spacecraft made it possible to make measurements with great reliability and high accuracy of the temperature distribution of the Venusian atmosphere by altitude down to the planetary surface.

The AIS descent apparatus Venera-7 made a soft landing on the surface of the planet and thereafter continued to measure the temperature for 23 min [100]. At its landing site, which was located in the equatorial region of the Venusian night side about 1000 km from the morning terminator, the temperature of the near-surface atmosphere was 747 ± 20°K.

With a high gas density and convective heat transfer near the surface, one can assume that there is no marked difference between the surface and atmospheric temperatures. One can, therefore, /66 assume that this measured temperature also holds true for the surface.

Taking errors in measurement and the discreteness of telemetry into account, the surface temperature at this point is T_S = = 740 ± 30°K.

In this way, the notion that the planet Venus has a very hot surface has finally been confirmed, and more accurate data have allowed us to move from qualitative conceptions to the development of quantitative models more suitable to the physical conditions on the planet. In particular, the AIS Venera 4-8 data on the temperature and pressure distribution and the chemical composition of the Venusian atmosphere in local areas of the planet made it possible to interpret more accurately the results of radio astronomy measurements, on the basis of which information obtained about the average temperature of the entire surface of the planet and about the possible diurnal and longitudinal variations in temperature.

The limited nature of the data measured directly at the landing-site region inevitably raises the question of how characteristic these parameters measured in this region are for the planet as a whole.

On Earth, for example, surface temperatures in the Sahara and Antarctic differ by about 130°K, and neither one is characteristic of the Earth as a whole. In principle, then, one may expect similar differences, caused primarily by possible differences in elevation, for Venus also. Radio astronomy measurements made on Earth, measurements in which the measured value is the mean brightness temperature over the planet's apparent disk, make it possible (on the basis of the data the Venera-4-7 obtained from direct local measurements) to determine the surface temperature averaged over the planet's hemisphere that is visible from Earth. Such measurements, if made over an extended period of time and in various light conditions on the planet, can ascertain diurnal temperature variations from day to night.

Table 5 gives the results of measurements of the mean brightness temperature of Venus' dark night side. It includes only measurements[3] in which the antenna was calibrated according to a standard reference or according to reliably measured discrete sources; and the resulting error in measurement does not exceed 15%. An exception is made only for the millimeter range, where, in connection with a smaller relative accuracy of measurements, measurements accurate to 20% are included. /67

Since data about Jupiter's brightness temperature have become more accurate (Jupiter is accepted as a reference source in the millimeter range), and since data about the flux densities of a series of discrete sources [375] used to calibrate measurements in the centimeter range have become more accurate, we have therefore corrected T_B or S to account for that. The corrected values of the brightness temperatures are given in the last column of Table 5.

For the convenience of the reader, the table also gives the original values $\overline{T}_{B\varphi}$ published by the authors (fourth column) and the parameters of the reference sources accepted by the observers (fifth column) and made more accurate in later measurements [375, 548]. For Jupiter, the brightness temperature is in Kelvin degrees; for the discrete sources, the flux density of radio emission is in units 10^{-26} $\omega \cdot m^{-2} \cdot Hz^{-1}$.

A correlation of the results of radio astronomy measurements in the 10 cm wavelength range, in which many quite accurate radio astronomy measurements have been made, and the assumption that Venus' radio emission is basically the emission of its surface, showed that at $\varepsilon = 5$, the mean (over the night side of the planet)

---

[3] One may find summary tables, which include all radio astronomy measurements of the brightness temperature of Venus, in [86] and [540].

ORIGINAL PAGE IS
OF POOR QUALITY

TABLE 5. BRIGHTNESS TEMPERATURE AVERAGED OVER VENUS' APPARENT DISK

Wavelength, cm	Observers	Year	Published $T_{B\Phi}$, °K	T_B or S of supporting source: Accepted by observers	T_B or S of supporting source: Made accurate	Corrected $T_{B\Phi}$, °K
0.225	Yefanov et al. [53, 54]	1967	235±40	Jupiter 120±20		235±40
0.31	Ulich, Cogdell, Davis [527]	1971	386±33	Standard reference		386±33
0.32	Tolbert, Straiton [526]	1963	300 +57 -27	Standard reference		300 +57 -27
0.33	Tolbert, Straiton [526]	1964	320 +56 -36	Standard reference		320 +56 -36
0.8	Kuz'min, Salonomovich [81]	1961	485±65	Jupiter 150	157±8	430±85
0.8	Vetukhnovskaya et al. [23, 24]	1963	511±30	Jupiter 150	157±8	440±35
0.8	Yefanov et al. [53, 54]	1967	375±60	Jupiter 155±23	157±8	410±65
0.82	Vetukhnovskaya, Kuz'min, Losovskiy [26]	1960	428±70	Jupiter 155±23	157±8	465±25
0.835	Thornton, Welch [525]	1962	395±60	Jupiter 155±23	157±8	430±65
0.835	Welch, Thornton [544]	1964	390±45	Jupiter 155±23	157±8	425±50
0.86	Tolbert, Straiton [526]	1963	375±58	Standard reference		375±58
0.97	Griffin, Thornton, Welch [329]	1966	412±55	Standard reference		412±55
1.16	Griffin, Thornton, Welch [329]	1966	395±50	Standard reference		395±50
1.25	Griffin, Thornton, Welch [329]	1966	451±55	Standard reference		451±55
1.31	Vetukhnovskaya et al. [24]	1967	470±40	Jupiter 150	139±6	436±40
1.35	Griffin, Thornton, Welch [329]	1966	530±45	Standard reference		530±45
1.46	Griffin, Thornton, Welch [329]	1966	505±50	Standard reference		505±50
1.6	Vetukhnovskaya et al. [23]	1962	551±60	Taurus 470		551±60
1.65	Griffin, Thornton, Welch [329]	1966	560±51	Standard reference		560±51
1.9	Kellerman, Pauliny-Toth [375]	1966	500±75	Standard source		500±75
1.95	Morrison [433]	1967	595±45	Virgo; 29		595±45
2.07	McCullough, Boland [417]	1963	500±75	Cassiopeia Taurus	--	525±75
2.7	McCullough [418]	1969	612±37	Virgo; 38.4		612±37
3.3	Vetukhnovskaya et al. [23]	1962	575±50	Taurus 560		575±50
3.35	Kuz'min, Dent [85]	1964	650±65	3C 123; 10		
3.52	Dickel [271, 540]	1967	654±36	3C 123; 12.3		689±36
6	Hughes [349]	1966	630±30	Virgo 70 3C 123; 16.9 3C 348; 13	-	630±30
6	Dickel [270, 540]	1966	706±45	3C 218; 13.0		730±46
7.89	Warnock, Dickel [541]	1970	686±38	3C 218; 17.2		686±38

/69

[Table 5 continued on following page]

Wavelength, cm	Observers	Year	Published T_B, °K	T_B or s of supporting source: Accepted by observers	T_B or s of supporting source: Made accurate	Corrected T_B, °K
9.26	Warnock, Dickel [541]	1969	675±38	3C 218; 19.0		675±38
9.6	Kuz'min [82]	1961	660±75	Taurus 760	--	660±75
10.0	Drake [282]	1961	583±50	3C 123; 23.7	3C 123; 25	615±60
10.0	Drake [284]	1962	580±40	3C 123; 23.7	3C 123; 25	610±60
10.3	Vetukhnovskaya [24]	1966	620±30	Taurus 760	--	620±30
10.6	Clark, Spencer [243]	1962	580±60	3C 295; 10.8	3C 295; 11.4	610±60
10.6	Kuz'min, Clark [83]	1964	580±60	3C 48; 7.8	3C 48; 8.6	640±65
11.1	Stankevich [514]	1963	710±35			
11.3	Kellerman [373, 374]	1969	605±30			
12	Warnock, Dickel [541]	1970	701±41	3C 218; 25.2		701±41
13	Boischot, Ginat, Kazes [219]	1962	712±80			
13.3	Warnock, Dickel [541]	1970	670±37	3C 218; 29.5		650±37
21	Boischot, Ginat, Kazes [219]	1962	674±70			
21.3	Kellerman [373, 374]	1969	560±30			560±30
21.4	Drake [284]	1962	542±50	3C 123; 50.1 3C 348; 44.7 3C 353; 50.2	3C 123; 45.9 3C 348; 44.5 3C 353; 51.9	505±50
31.2	Kellerman [373, 374]					
49.7	Muhleman, Berge, Orton [434]	1964	510±50			510±50
70	Gordon, Jauncey, Yerbury [326]	1972	498±33			
		1972	523±28			

TABLE 6. DIFFERENCES IN SURFACE TEMPERATURES OF VENUS' DAY AND NIGHT SIDES

λ, cm	$T_B - T_{B\bullet}$	Observers
11.3	24±50	Kellerman [373, 374]
10.6	−30±30	Kuz'min [82]
10	26±50	Drake et al. [282, 283]
4.52	2±20	Dickel et al. [271]
2.7	0±9	McCullough [418]
1.95	0±25	Morrison [433]
0.86	20±8	Kalaghan et al. [370]
0.82	4±10	Vetukhovskaya et al. [26]
0.35	−22±4	Epstein et al. [290]
0.23	55±60	Yefanov et al. [53, 54]

ORIGINAL PAGE IS
OF POOR QUALITY

ORIGINAL PAGE IS
OF POOR QUALITY

temperature of the surface of Venus is T_S = 720 ± 30°K, i.e., within the accuracy of measurements error, it agrees with the Venera-7 measurements.

Thus, the surface temperature of Venus where Venera-7 landed T_S = 720 ± 30°K can be considered characteristic of the entire dark night side of Venus.

The first information about the surface temperature on the /70
Venusian day side is based on data from radio astronomy measurements of the brightness temperature of Venus near superior conjunction. The results of these measurements are given in Table 6 in the form of the difference between the mean brightness temperatures on the day and night sides of the planet T_{BO} -- $T_{B●}$.

In the 10 cm wavelength range, the radio emission received on Earth originates basically on the surface of Venus. Therefore if the difference T_{BO} - $T_{B●}$ does not exceed the error of measurements at this wavelength, it is evident that the surface and near- /71
surface temperature of the atmosphere of the planet's day side differs little from the temperature of its night side.

This conclusion is confirmed also by the results of recent interferometric radioastronomy measurements of Venus at wavelength 11.1 cm [499]; according to these measurements, the difference between the surface temperatures on the day and night sides of the planet is 18 ± 9°K.

Marov's [97] calculation of the heat regime of the Venusian atmosphere showed that, in connection with the great heat content of Venus's dense atmosphere, the expected temperature change in the near-surface atmosphere from day to night does not exceed 1°K.

With such a massive atmosphere, it is also difficult to expect significant temperature changes by latitude. The radio astronomy measurements that Sinclair et al.[500] made with a resolution of about 1/6 the planet's diameter indicated that the reduction in temperature from the equator to the poles is not more than 12°K.

The first direct measurements of the surface temperature of the Venusian day side (near the morning terminator) were made by the Soviet AIS Venera-8 [103].

At its landing site, the atmospheric temperature was 740 ± 8°K, which agrees (to the error of measurements)with the temperature at the AIS Venera-7 landing site on the planet's night side.

The Soviet automatic interplanetary spacecraft of the Venera series (cf. Chapter 4) have made direct measurements of the chemical composition and the altitude-temperature and -pressure profile, and these measurements have enabled us to interpret the

dependence (obtained in radio astronomy measurements) of the brightness temperature of Venus' radio emission $\bar{T}_{B\varphi}$ at wavelength λ. In the range of wavelengths from 3 mm to 20 cm (given in Table 5), the experimental values $\bar{T}_{B\varphi}$ within the bounds of error agree with what is calculated from formula (III.11) for a model of Venus with a permittivity of the surface $\varepsilon = 4.7$ and with an atmosphere of 97% carbon dioxide and 0.1% water vapor. This obviates the necessity to assume that there are any other components that absorb UHF radiation of this range in the Venusian atmosphere. This question will be examined in detail in Section IV.5. However, at wavelengths longer than 20 cm, the experiment showed a signifi- /72
cant reduction of the measured brightness temperature. This reduction was not predicted theoretically within the framework of the accepted model. The amount of the reduction is about 100°K, i.e., two to three times more than the error of measurements. This discrepancy cannot be explained solely by the dependence of permittivity ε of the surface material on the wavelength, since the value needed for agreement $\varepsilon \approx 13$ is much larger than that measured in the same range by the reflectivity of the planet $\varepsilon \approx 5$. Additional atmospheric absorption of the decimeter radio emission of the planet would reduce the reflection coefficient also; this, too, does not agree with the experiment. In principle, one could obtain agreement between the calculated model and the experiment if one assumes a simultaneous increase in ε and the presence in the atmosphere of an agent that absorbs decimeter radio emission. However, the nature of such an absorber is not clear. Molecular absorption and absorption by a dielectric decrease with wavelength and therefore the presence of such an agent cannot be revealed at shorter wavelengths. Absorption by the ionosphere has the required qualitative dependence; however,the density of the Venusian ionosphere is several orders less than needed for the effect to be noted. Therefore, Muhleman et al [434] and Gordon et al [326] did measurements of the brightness temperature of Venus at wavelengths of 49.4 and 70 cm; the most probable reason for this discrepancy is, in their opinion, underestimated values for the flux densities of the radio emission of the sources on the list of Kellerman et al.[375], sources used as standards in measurements $\bar{T}_{B\varphi}$. This question requires further experimental testing.

ORIGINAL PAGE IS
OF POOR QUALITY

CHAPTER IV. THE STRUCTURE OF THE LOWER ATMOSPHERE

IV.1. The Parameters of the Atmosphere of Venus According to Measurements made at Long Range

Optical and radio measurements are a very effective means of /73 planetary study. The results of optical study of Venus over many years by the classical methods of optical astronomy has produced much valuable information about the physical and chemical properties of the atmosphere, even though they have not provided unambiguous answers to the problem of assigning values to atmosperic parameters in the region below the cloud tops visible from Earth and especially at the planetary surface. This is explained by the fact that the usual difficulties in analyzing long-range measurements, difficulties connected with the solution of the "inverse" problem, are aggravated by the existence of a dense cloud layer. These clouds have a considerable effect on estimates of the effective depth of absorption lines and on the processes of radiative transfer; and the various possible scattering characteristics, the spectrum of particle sizes and the nature of the particles allow a wide variation in the character of reflection from the cloud layer. Moreover, the very boundary of the clouds is not clearly delineated. As a result, atmospheric parameters at the level of the clouds can be calculated with an accuracy up to the idealized models used for the reflection of solar radiation. The development of optical and radio methods on Earth has been aided in recent years by improvements in observation techniques and by the added possibility of more correct interpretation of measurement data from the results of experiments done on spacecraft.

Our purpose here is not to give a systematic survey of the numerous studies that on the eve of space flight contributed to /74 real progress in the study of the Venusian atmosphere; detailed summaries are contained in well-known monographs (e.g.[11, 69, 86, 117, 120, 171, 172]). We will be concerned only briefly with individual works, those that contain estimates of the temperature, pressure, and chemical composition of the atmosphere. Our selection of these works in no way pretends to be comprehensive and in a certain sense reflects the interests of the authors. Other results from ground measurements that are directly related to the problem under discussion and that sometimes determine its status[1] are examined in later sections of this chapter and in the remaining chapters.

Temperature. From a calculation of the thermal balance for the unreflected portion of the Sun's radiant energy and radiation

---

[1] A detailed analysis of data from long-distance measurements can be found in a work by V.I. Moroz [117].

losses, the equilibrium temperature of a rotating planet at the orbit of Venus is

$$T_e = \left[S \frac{(1-A)}{4\sigma a^2} \right]^{1/4} \qquad \text{(IV.1)}$$

ORIGINAL PAGE IS
OF POOR QUALITY

Here $E_S = 1.37 \cdot 10^6$ erg·cm^{-2}·sec^{-1} is the solar constant, A is the integral spherical albedo of Venus, a = 0.723 is the average distance of Venus from the Sun in astronomical units, $\sigma = 5.67 \cdot 10^{-5}$erg·cm^{-1}·deg^{-4} is the Stefan-Boltzmann constant.

From Irvine's [354] photometric measurements, A = 0.77 ± 0.07 and the mean value of T_e = 228°K. The initial results of the temperature measurements in the 8-14 window, made as early as 1924 by Pettit and Nicholson [450], T_B = 240°K, is in good agreement with this estimate. Sinton and Strong essentially confirmed this value, having obtained T_B = 223 ± 10°K in the center of the disk. The measured brightness temperatures correspond to the spectral region of thermal emission and must refer to the level where the emitting layer of the gas becomes optically thick ($\tau \geq 1$). Color temperatures in the 3-14 μm region do not differ practically from the brightness temperature, which indicates a medium containing aerosol. This fact, as well as estimates of the effectiveness of the emission in extremely weak ("hot") CO_2 absorption bands at λ = 9.4 and 10.4 μm give reason to think that the brightness temperature is formed near the level of the clouds. /75

The results of ground-based observations and Mariner-2 data noted a darkening toward the edge of the disk in the infrared region [242, 435, 459, 502]; this can be represented in simple analytic form:

$$I_\lambda(\mu_0) \sim \mu_0^\alpha, \qquad \text{(IV.2)}$$

where $I_\lambda(\mu_0)$ is the spectral intensity in the corresponding region of the spectrum, θ = arccos (μ_0) is the angle between the normal to the surface and the line of sight, and α is essentially a positive number within the limits $0 \leq \alpha \leq 1$. The relation (IV.2) characterizes the usual dependence of the vector of specific intensity of the outgoing radiation on θ and holds true for a wide range of angles at α = 0.50 ± 0.05 [2]. To approximate the

[2] From the results of the recent Mariner 10 radiometric measurements at λ = 45 μm Chase et al [572] found that the darkening toward the edge (within θ < 65°) is well described by the relation (IV.2) at α = 0.16, i.e., $I_{45}(\mu_0) = I_{45}(1.0)\,\mu_0^{0.16}$. The brightness temperature for normal emission ($\mu_0 \approx 1$) is T_B = 255 ± 4°K.

observations, other functions are also assumed; of these, the exponential form gives a good approximation [242].

The infrared brightness temperature of Venus does not reveal any marked dependence on the phases, and the infrared section along the visible equator of the planet consequently should correspond to a true darkening toward the edge. An average over the disk gives $T_B = 220 \pm 10°K$. From the results of measurements in the 8 - 14 μm range, Murray et al [435, 545] came to the conclusion that diurnal temperature variation is practically absent. Fig. 20 shows the isophotes of the planetary disk (with a resolution of about 1/30 of the disk near the subterrestrial point[3]); these were obtained on four successive nights, December 14 - 17, 1962, and then constructed by the authors. These measurements give a two-dimensional picture of Venus's infrared radiation. It is worthwhile to note the general decrease in brightness from center to edge, which corresponds to the approximated form (IV.2) /76 and the symmetry of the contours relative to a diameter lying in Venus's orbital plane. The latter is apparently connected with actual temperature variations on the level of the emitting layer in a latitudinal direction, i.e., with cooling in the direction toward the poles. Actually, for a planet with a slow inherent rotation and a large period of thermal relaxation (cf. Sec. V.2), the /77 latitudinal effect should be considerably less pronounced than the diurnal temperature variations. If the differential accuracy of the determination of the brightness temperature (≈ 1/3°K) is kept in mind, then, on the basis of these measurements, even a small (within 5 - 10°K) excess in the night temperature over the day temperature at the level of the emitting layer near the morning terminator is revealed.

Measurements of the rotational and vibrational temperatures that correspond to the spectral region of the echo have, until very recently, led to values substantially different from the planet's infrared brightness temperature. By analyzing intensity distribution from the energy levels near the rotational-oscillatory CO_2 bands in the region $\lambda = 0.8$ μm, Chamberlain and Kuiper [236] estimated the rotational temperature $T_{ro} = 285 \pm 9°K$. By analyzing these same photographic plates together with Venusian spectra obtained at the Mount Wilson Observatory, Spinrad [509] found, however, that the rotational temperature varies between 250 - 440°K from plate to plate, i.e., from day to day. In the process a correlation was found with pressure (up to P ≈ 6 atm) as determined from the equivalent width of the spectral lines. If the presence of breaks (that lead to a change in the effective depth of band formation) in the clouds is assumed, this variation

[3] This we shall call the point at the center of the planet's visible disk, if the disk is freed of the phase effect. If radar measurements are made on ground antennas, this point coincides with the subradar point discussed in Chapters II - III.

ORIGINAL PAGE IS
OF POOR QUALITY

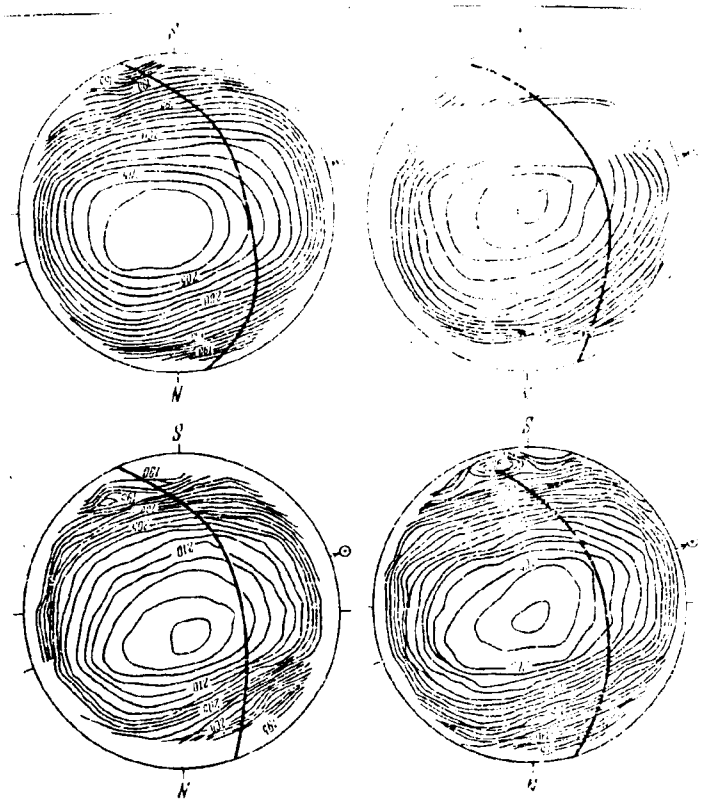

Fig. 20. Isophotes of the disk of Venus according to observations made December 13 - 14, 1962, in the 8 - 14 μm spectral region. The line of the terminator and the direction to the Sun are shown. The values of brightness temperatures are systematically underestimated by 7 - 28°K because of telescope losses.

in recorded temperatures can be explained. In this case, it had to be assumed that the value of the optical path for reflected solar radiation fluctuates more than on a scale height. Chamberlain [238, 240] and Chamberlain and Smith [241] did corresponding theoretical calculations based on computed variations of the equivalent widths of the absorption lines in the bands 8689 A and 1.6 μm. The resulting estimates of rotational temperature essentially depend on the model of reflection used, chiefly on a consideration of the effects of multiple scattering within the clouds. For a simple reflecting model, the value of the temperature determined from the weak band at λ = 8689 Å was T_{ro} = 317 ± 10°K, and with scattering included, T_{ro} = 291 ± 10°K.

Schorn et al. [328, 486, 487] used a quadratic function for the growth curve and the more accurate intensities of the rotational lines measured by Spinrad and found that T_{ro} = 285 ± 46°K. /78
Young and Schorn recently obtained a still lower rotational temperature from an analysis of the weak bands at λλ 7810 and

7884 Å in the Venusian spectrum, bands measured in a wide range of phase angles during 1968 - 1969: $T_{ro} = 244 \pm 3°K$ [551, 552]. Despite the very high accuracy of this estimate, it is also noteworthy that, by contrast to existing notions, the authors did not discover a marked temperature dependence on the phase and time of the observations. This finding is confirmed by measurements in the 8689Å band, which lead to a value $T_{ro} = 238 \pm 1°K$, if the spreading effect of CO_2 lines within the band is not taken into account, and $T_{ro} = 246 \pm 1°K$ if this effect is taken into account. No appreciable temperature variations were discovered for this band also. Thus, although the location of the effective level of line formation in the spectrum of reflected radiation of Venus remains ultimately undetermined, nonetheless, there is serious reason to think that it does not differ strongly (within several kilometers) from the level of the planet's own emission. Apparently, both levels must be located below the cloud boundary visible from Earth.

Pressure. The results of spectroscopic observations and the use of growth curves for saturated and unsaturated lines have yielded an effective value of atmospheric pressure at the cloud level: $P_c \approx 0.1/0.2$ atm [236]. Pressures of several atmospheres have also been reported [509, 511]; for these pressures, as has already been noted, a satisfactory correlation with rotational temperatures has been found.

The other independent source of information about pressure, i.e., a source based on measurements in the visible region of the spectrum, are polarization observations. Dollfus [275] observed a difference in polarization in the red and green regions of the spectrum and interpreted this difference as the result of molecular scattering in the atmosphere at a depth of ≈ 800 m above the cloud tops. The corresponding pressure at the boundary of the cloud layer turned out to be 90 mbar, which is close to spectroscopic estimates. Sagan and Pollack [584] used the results of polarization measurements of Gehrels and Samuelson [309], Coffeen /79 [247], and Coffeen and Gehrels [248] to do a more detailed study of pressure near the observed clouds. At a phase angle of 90° they obtained a value for pressure $P \approx 130$ mbar (for the 0.56 - 0.99 μm region) and $P \approx 35$ mbar (for the 0.36 - 0.99 μm region). These estimates are in satisfactory agreement with each other, if it is kept in mind that they refer to levels where the optical thickness in scattering for CO_2 in corresponding spectral intervals is $\tau \approx 1$.

Before the beginning of space flights, estimates of atmospheric pressure at the surface fluctuated within very wide bounds. The status of the problem is illustrated by Fig. 21, which is borrowed from [268], which itself presents ranges of expected values P_s from estimates by various authors during the period 1960 - 1967. As we see, the minimum value is about 3 atm and the maximum 1000 atm. This uncertainty is connected primarily with the fact that /80

the contents of the gaseous constituents that absorb in the infrared, millimeter and centimeter regions were not known. Specifically, this did not allow us to take advantage of the experimental dependence of the brightness temperature on wavelength. It was evident that only a direct experiment in the planet's atmosphere below the cloud level could yield an unambiguous answer to the question of pressure on the surface of Venus.

ORIGINAL PAGE IS
OF POOR QUALITY

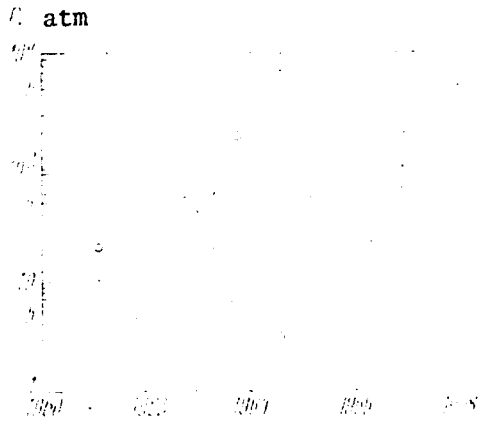

Fig. 21. Values for the atmospheric pressure of Venus at the surface according to various authors, 1960 - 1968 [268]. Authors and dates of estimations of pressure on Venus: January 1961 - Barrett [195]; September 1961 - Öpik [440]; September 1962 - Sagan [478]; March 1963 - Plass and Stull [452]; July 1963 - Ostriker [441]; October 1963 - Cameron [229]; July 1964 - Deirmendjian [266]; July 1964 - Barrett and Staelin [197]; February 1965 - Pollack and Sagan [458]; April 1966 - Staelin and Barrett [513]; November 1966 - Ho, Kaufman, Thaddeus [346].

Chemical composition. By observing absorption bands in the near infrared region of the spectrum, Adams and Dunham [177] in 1932 first discovered the presence of carbon dioxide in the atmosphere of Venus. As is well-known, the intensity of absorption bands indicates the overall gaseous content above the clouds, while the width of individual lines within the band is a measure of the overall pressure at this level. Until recently, relevant analysis led to the conclusion that although the total CO_2 content is about 3000 times greater than in the Earth's atmosphere, it is nonetheless a relatively small component in the Venusian atmosphere [115, 371, 388]. In 1967, however, Belton, Hunten and Goody [215], in interpreting the new, high-quality spectra of Venus they had obtained, took into consideration the effect of multiple scattering of solar radiation by particles within the clouds. It was shown that since this effect substantially changes the width and intensity of CO_2 absorption lines, previous estimates of CO_2 content had been greatly underestimated. Moroz [116] also pointed out the possibility of a high CO_2 content. Connes et al [252, 253] and Gray and Schorn [327, 328] came to a similar conclusion on the basis of high-resolution (up to 10^5 near 1 μm) spectral analyses. Nevertheless,

until Venera-4 made direct measurements, it was assumed that nitrogen, which is widely distributed in the solar system and which is chemically comparatively inert, was the main component of the planetary atmosphere.

ORIGINAL PAGE IS
OF POOR QUALITY

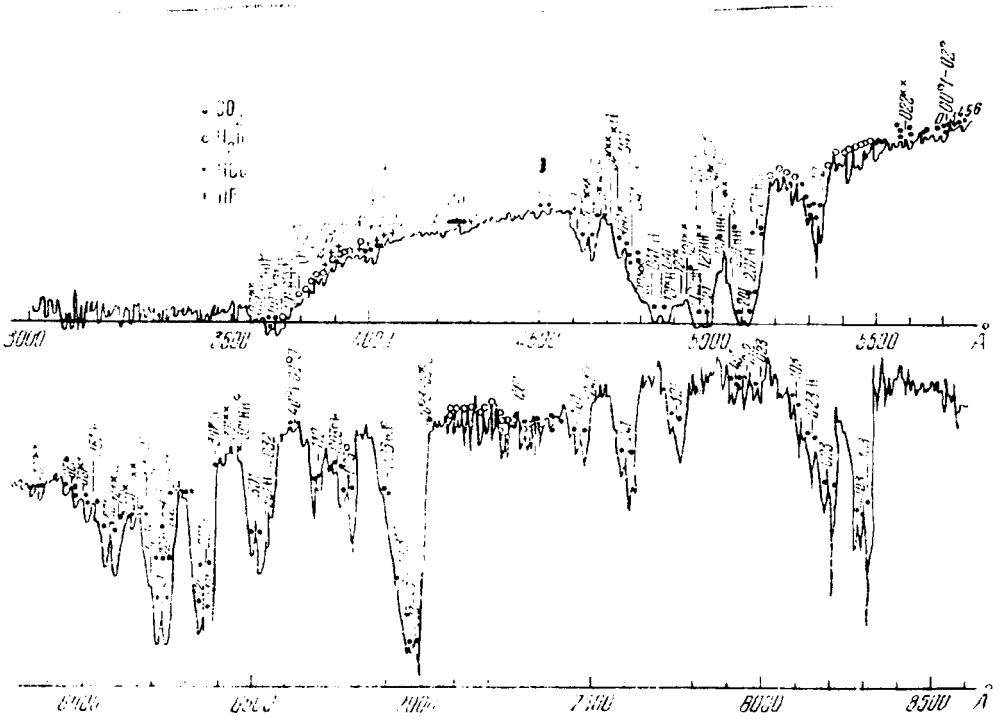

Fig. 22. Venusian spectrum obtained by Kuiper et al from a high-altitude airplane; resolution ≈ 20 cm^{-1}. A spectrum of the Moon's echo is given for comparison, as well as the resulting ratio φ/ζ.

The spectroscopic upper limit for H_2O above the clouds was estimated to have a relative value on the order of 10^{-4}-10^{-5} [211, 391, 510], which is about the same as the water vapor content above the clouds in the Earth's atmosphere. Connes and others' high resolution spectra in the near-infrared region /82 allowed them to confirm what Sinton [502] and Moroz [114] had discovered previously -- the presence of carbon monoxide CO in a relative concentration of ≈ 10^{-3} and to discover hydrogen chloride HCl and hydrogen fluoride HF in relative concentrations of $6 \cdot 10^{-7}$ and $5 \cdot 10^{-8}$ respectively [252, 253]. Fig. 22 gives an example of a spectrum of Venus that Kuiper et al obtained by using the measurements of a Fourier spectrometer from a high-altitude airplane [391-393]. It clearly delineates the

absorption lines that correspond to these characteristic components of the Venusian atmosphere.

IV.2. The Venera Automatic Interplanetary Stations (AIS's)

The conditions for conducting the experiments. Design. The flight trajectories of the Venera-4, Venera-5, Venera-6 and Venera-7 automatic stations were chosen so as to study, at large angles of entry, the planetary atmosphere on the night side near the equatorial plane. Venera-8 was the first to take measurements on the day side of Venus. Table 7 summarizes the basic data about the flights. It also includes data on the Mariner-5 flight. Fig. 23 shows part of the Venusian disk in Mercator projection and marks the areas where the Venera stations descended. The circles indicate the locations of the subterrestrial points, and the stippled lines indicate the locations of the morning terminator at the same times. α and β are the regions of high radar reflectivity; the zero meridian (cf. Chapter II) coincides with the direction toward Earth at inferior conjunction. As is evident from Fig. 23, all the stations descended near the morning terminator. If as time units for Venus we use, by analogy with Earth, the time between two successive solar culminations at a given point as a "Venusian solar day," and the time the Sun moves 15 degrees in longitude as an "hour." When the Veneras-4 to 7 landed near 4:00 or 5:00 in the morning and the Venera-8 about 6-7 in the morning. The region in which the Venera-4 descended was about 1600 km to the north, Venera-7 about 1100 km to the west, and the Venera-5 and Venera-6 near the subterrestrial points. Venera-8 descended about 3800 km southwest of the subterrestrial point.

The design for all the Venera stations was about the same. Fig. 24 shows a general view of one of the Venera stations and designates its basic elements and systems [22]. The upper part of the station (Fig. 24, at left) is an "orbital" module, which delivers the descent apparatus (DA) to the planet. It has a system of correction jets, and on the sides are a highly directive antenna, an astro-orientation sensor with a protective shield and solar battery panels. Also visible are the automatic pneumatic system units with compressed nitrogen bottle, collectors, and control nozzles, a radiator cooler, and a continuous solar orientation sensor. Fig. 25 shows a photograph of one of the Venera stations taken in an assembly shop.

After an analysis of the flight of Venera-4, several changes /85 were made in the design of Venera-5 and Venera-6. The most significant changes were made in the descent apparati of the Venera-7 and Venera-8 stations. By taking into account the results of previous measurements and the limiting estimates of the atmospheric parameters at the surface in accord with a calculated model, the descent apparati were designed in such a way as to

ORIGINAL PAGE IS
OF POOR QUALITY

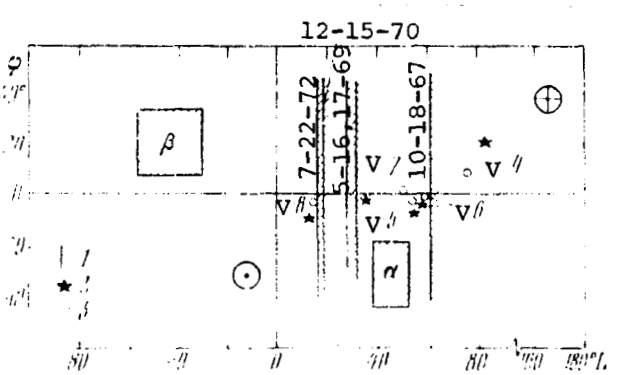

Fig. 23. The near-equatorial part of the Venusian disk in Mercator projection. The position of the zero meridian corresponds with the direction to Earth at inferior conjunction. 1 is the location of the morning terminator on a given date; 2 are the Venera landing sites; 3 is the locations of the sub-terrestrial points; the crossed circle and the dotted circle are the areas where the Mariner 5 spacecraft made atmospheric probes on immersion and emersion.

endure the temperature and pressure of the surrounding medium up to 800°K and 180 atm respectively (for Venera-8 the upper pressure limit was lowered to 120 atm). Because a special heat-resistant cover with the necessary insulating and shock-absorbing properties was strengthened and constructed, the Venera-7 and Venera-8 DA's were about 100 kg heavier, even though the overall weight of the stations was the same as before (about 1180 kg). The design improvements in Venera-8 allowed a significant expansion of the program of scientific measurements made in the atmosphere and on the surface of the planet.

The separation of the descent apparatus from the orbital module was performed about 20,000 to 40,000 km from Venus, and aerodynamic braking in the atmosphere began at a velocity of about 11.2 km/sec^{-1} at angles of about 50-70° to the local horizon. The parachutes opened when the velocity of the apparatus slowed to about 210 m·sec^{-1}, which corresponded to a pressure of about P ≈ 0.6 atm for the surrounding atmosphere. /86

Fig. 26. shows the descent apparatus of the Venera-8 station. It has a slightly oblong shape and contains a sealed, spherical container on the inside; this latter holds the instrumentation, which consists of a radiotelemetry system; instruments for measuring atmospheric and surface parameters; control and heat-regulation units; and power-sources. On the outside the DA is covered with a heat-resistant shield, as well as insulation which protects it from aerodynamic heating upon entry into the atmosphere, during parachute descent, and while on the surface. Heat storage cells are installed on the inner side of the hull. In the upper part of the apparatus, under a release cover is the parachute container. A single-stage parachute system with a release parachute is used. The heat-resistant fabric of the main parachute must withstand temperatures up to 800°K. /87

ORIGINAL PAGE IS
OF POOR QUALITY

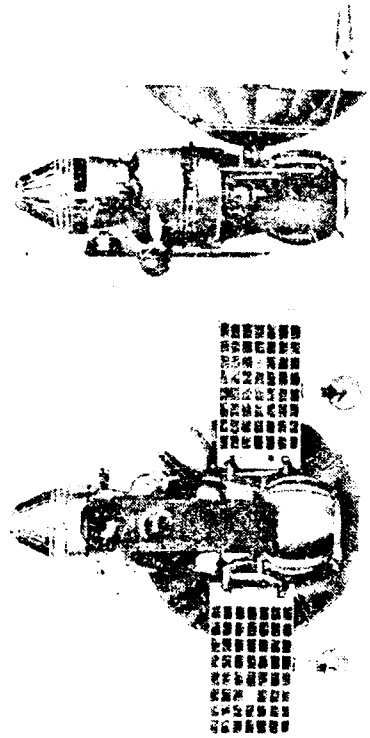

Fig. 24. The automatic interplanetary station Venera-8. 1 -- sensors of the astro-orientation system; 2 -- instrument module; 3 -- correction jet; 4 -- highly directive parabolic antenna; 5 -- poorly-directive antenna; 6 -- descent apparatus; 7 -- solar battery panels.

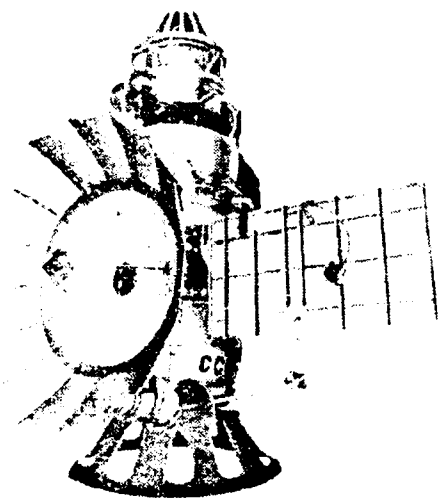

Fig. 25. AIS Venera in an assembly shop.

It had already /88 become evident from the results of the Venera-4 flight that it was advisable to shorten the time of descent in the dense Venusian atmosphere; in order to accomplish this, the canopy area of the parachute was decreased by about an order of magnitude. Of special significance for an apparatus that makes a landing is the time of descent and the problem of maintaining a favorable thermal regime in the instrument container right down to the surface itself. How much heat penetrates inside depends on the time the apparatus is in the atmosphere, inasmuch as heat absorption occurs only due to the inherent heat capacity of the container and the instrumentation inside it. In this regard, (for the Venera-7 and Venera-8 stations), a parachute system with a riffling was chosen so as to pass more quickly through the initial part of the descent in the atmosphere.

The construction of a lander required solutions to a number of complex scientific and technical problems as well as the performance of a great number of theoretical and experimental tests. Above all, this meant the creation of a design able to withstand huge g-forces on entry into the atmosphere, the

TABLE 7. BASIC DATA ON MARINER 5 AND VENERA SERIES

ORIGINAL PAGE IS
OF POOR QUALITY

Spacecraft	Date of experiment	Time (Moscow) of beginning and end of measurements	Region of planet	Remarks
Venera-4	Oct. 18. 1967		Northern hemisphere about 20°N, night side, ≈1500 km from morning terminator	
Mariner-5	Oct.19, 1967		Night side (on immersion), 37°N; θ = 142.3°. Day side (on emersion), 32.4° S; θ = 33.3°	Time indicated in min beginning at closest distance to planet at radio immersion. θ is solar zenith angle.
Venera-5	May 16, 1969		Equatorial region, night side ≈2700 km from morning terminator	Distance between Venera-5 and Venera-6 landing region (≈300 km) figured according to estimates of mathematical expectation of entry points into the atmosphere
Venera-6	May 16, 1969		Equatorial region, night side, ≈2400 km from morning terminator	
Venera-7	Dec. 15, 1970	Landing	Equatorial region, night side, ≈2000 km from morning terminator	
Venera-8	July 22, 1972	Landing	Southern hemisphere (about 10° S) day side ≈600 km from morning terminator	

construction of a strong hull, the calculation and testing of highly efficient heat-resistant and insulating coverings as well as the development of methods and special devices for the ground testing of the DA in conditions that simulate the atmospheric conditions of Venus. The data obtained allowed us to select the optimal parameters of outside heat insulation on various portions of the flight, and to select the proper thickness of the hull and the internal insulation. For the most efficient insulation, porous and honeycomb-shaped materials with the strength needed to withstand high external pressure were used. Avduyevskiy [7] examines questions of heat transfer through porous insulation as applied to the design of descent apparatus.

Another important way to lengthen the life of the apparatus in the hot Venusian atmosphere is to use heat storage cells. The total effective heat capacity inside the apparatus is less than the true heat capacity because of the fact that while it operates, the temperature in all instruments is not equalized. One of the means of heat absorption is the application of evaporator systems. /89 However, conditions on Venus are such that in the range of up to 50°C, the pressure of saturating vapors of possible substances is

ORIGINAL PAGE IS
OF POOR QUALITY

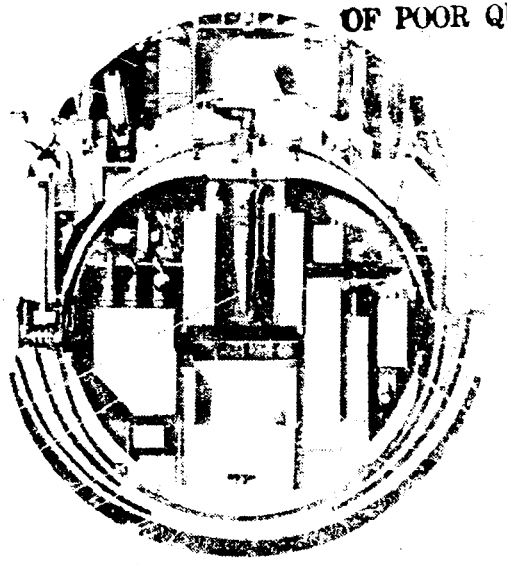

Fig. 26. The descent apparatus of the Venera-8 station. 1. Shock absorber; 2. External heat insulation; 3. Radio transmitter; 4. Hull of the instrument module; 5. Commutator unit; 6. Fan; 7. Duct of the heat regulation system; 8. Distant antenna of the radio transmitter; 9. Parachute container; 10. Main antenna of radio transmitter; 11. Parachute container cover; 12. Release parachute; 13. Main parachute; 14. Radar altimeter antenna; 15. Heat exchanger; 16. Heat storage cells; 17. Internal insulation; 18. Time-program device.

significantly less than the pressure in the surrounding medium, and the removal of vapors under their own pressure is impossible. Therefore, for these heat cells, it was necessary to use a substance whose phase transition occurs at a lower temperature and without a marked change in volume. The crystal hydrate $LiNO_3 \cdot nH_2O$ has such a property -- its phase transition is about 30°C. Upon expansion and heating, this salt absorbs more than 100 kcal/kg, with a change in volume of about 10%. The total heat capacity of this heat storage cell is two times larger than beryllium and six times better than aluminum. Because heat storage cells were installed, the total heat capacity of the DA was successfully increased by 20% [7].

In addition, in order to increase the DA's operating time in the atmosphere and on the surface, special cooling was provided during trajectory so that at the moment of separation from the orbital module, the temperature inside the instrument container was kept within -6/-10°C. A diagram of the AIS Venera heat regulation system is shown in Fig. 27.

Instrumentation. The instruments placed on board the Venera stations, as well as their ranges and errors of measurement, are listed in Table 8. In this chapter we will describe the instrumentation used to measured atmospheric parameters. A description of the photometer is given in Chapter 4, and a description of the gamma-ray spectrometer can be found in [34]. /94

The Venera-4, -5, and -6 stations were equipped with simple gas analyzers of the G-8 and G-10 type to determine the chemical

TABLE 8. INSTRUMENTATION AND MEASURED PARAMETERS OF VENERA SERIES /90

Station	Measured parameter	Instrument	Range of measurement	Error of measurement (mean square error from range of measurements)
Venera-4	Chemical composition of atmosphere	Gas analyzers		
		1. CO_2 (change of heat conductivity of a mixture of atmospher. gases	1%, *)	
		2. CO_2 (KON absorption)	7—100% 2—30%	
		3. N_2 (zirconium absorber)	7—100%	
		4. N_2 (prelim. absorption of CO_2, H_2O at $T \simeq$ $\simeq$ 1000 °C)	2.5—50%	
		5. H_2O (change in elect. conductivity of P_2O_5	>0.1% >0.05%	
		6. H_2O ($CaCl_2$ absorption	>0.7%	
		7. O_2 (burn through of tungsten filament at T ≃ 800°C	>0.4%	
		8. O_2 ($+H_2O$) sublimation of red phosphorus	>1.6%	
	Atmospheric temperature	Resistance thermometers	−60—+60 °C 0—+30 °C	±1.5% ±1.5%
	Pressure	Manometers of the aneroid type	100—5300 mm Hg **) (0.13—7.20 kg·cm^{-2})	±3%

ORIGINAL PAGE IS
OF POOR QUALITY

Venera-4	Atmospheric density	Ionization densimeter	0.5—17 kg·m^{-3} (for CO_2, N_2, O_2 and mixtures	±1.5% (at beginning of range to ±5%) /91
	Altitude above surface	Radar altimeter of decimeter range	~30 km	
	Wind	Onboard radio transmitter (Doppler shift of carrier frequency)	0—∞ m/sec	Not better than ±10 m/sec
Venera-5 Venera-6	Chemical composition of atmosphere	Gas analyzers for CO_2, N_2, H_2O and O_2 content of types 2,4,5,6 and 7 above; with greater accuracy than Venera-4 gas analyzers (+4% for CO_2, +2.5% for N_2; ±0.1% for O_2)		
	Atmospheric temperature	Resistance thermometers	0—+60 °C +150—+370 °C +200—+440 °C	±1.5% ±1.5% ±1.5%
	Atmospheric pressure	Manometers of aneroid type	100—5000 mm Hg (0.13—6.8 kg/cm^2) 500—20000 mm Hg (0.7—27.2 kg·cm^{-2}) 750—30000 mm Hg (1.0—40.7 kg·cm^{-2})	±1.5% ±1.7—2.0% ±1.7—2.0%

* Percentages by volume
** At $g_\oplus$ = 981 cm·sec^{-2}

[TABLE 8. continued on next page]

[TABLE 8. continued]

/92

Station	Measured parameter	Instrument	Range of measurement	Error of measurement (mean square error from range of measurements)
Venera-5	Atmosph.density	Densimeter of tuning fork type	0.5—40 kg·m^{-3}	±3%
Venera-6	Alti ude above surface	Rad altimeter of decimeter range	60 -0km	±5%
	Wind		25 -540 C	±5%
Venera-7	Atmosph.temperat.	Resistance thermometers	0.5 -150 kg·cm^{-2}	±2%
	Atmosph. press.	Manometers of aneroid type	∞ —0 km	±1.5 m/sec (by velocity)
	Altitude above surface	Onboard radio transmitter (Doppler shift of barrier frequency)	0 - ∞	"same"
		"Same"	50—590 C	±1.5%
Venera-8	Atmospher.temp.	Resistance thermometers	200 -435 °C	±1.5%
			395—540 C	±1.5%
			20—605 C	±1.5%
	Atmosph. press.	Manometers of aneroid type	0—59 000 mm Hg (0—80kg/cm^2)	±1—3%
			0—73 000 mm Hg (0—100 kg/cm^2)	±1.5 -2%
			0—110000 mm Hg (0—150kg/cm^2)	±1.5—2%
			0—147000 mm Hg (0—200 kg/cm^2)	±1.5—2%

ORIGINAL PAGE IS
OF POOR QUALITY

/93

Venera-8	Light in atmosphere	Photometer in range 0.4 0.8 microns	10 -10^5 lux	±30%
	Ammonia content in atmosphere	Gas analyzer (color change of tetrabromophenolsulfophthalein on baked silica gel when NH_3 absorption	0.1% at $P<2$ atm	
	Altitude above surface		60—0 km	40.3 -3.4× ×10^{-3} h (m)
	Permittivity of ground ε	"Same"		
	Character of surface rock	160-channel gamma-ray spectrometer (for U, Th, and K content in rock)		
	Wind	Onboard radio transmitter (Doppler frequency shift)	0 - ∞ m/sec	±1 m/sec
	Atmospheric density	Sensor of g-force in relation to time (accelerometer)	~60 -160 km	±20 g

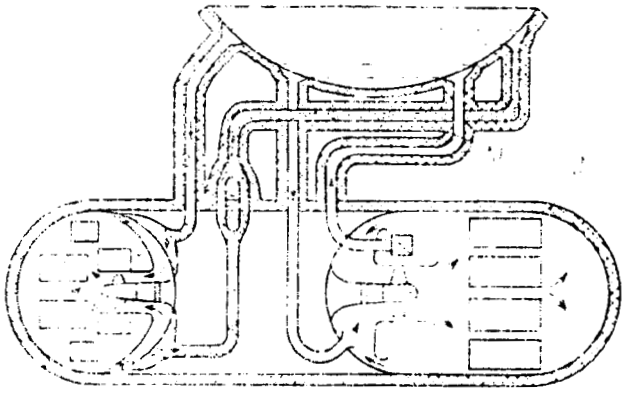

Fig. 27. Diagram of the Venera heat regulation system. 1. Antenna-radiator; 2. Orbital unit; 3. Multi-layered insulation; 4. Cooling circuit; 5. Descent apparatus.

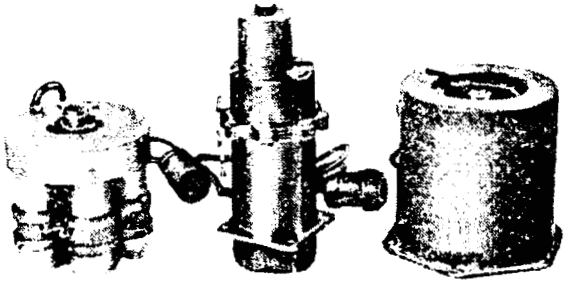

Fig. 28. Composite view of gas analyzers. On the left, the Venera-4 gas analyzer; on the right, the Venera-5 gas analyzer; in the middle, an ammonia gauge.

ORIGINAL PAGE IS
OF POOR QUALITY

composition of the atmosphere. Fig. 28 shows the instruments. Each station had two instruments each in order to make measurements at levels in the atmosphere with various pressures. The following description of this instrumentation and the methods used to measure chemical content is based on the works of Vinogradov, Surkov and their co-workers [29, 31, 32, 153, 154, 537].

In order to determine the content of carbon dioxide, nitrogen (together with the inert gases), oxygen, and water vapor, an amplitude (manometric) method was used. In order to record small (threshold) quantities of H_2O and O_2, the electrolytic and thermochemical methods were used. The reagents were chosen primarily on the following criteria: selectivity for the specified component; a sufficiently high rate of reaction to absorption; /95 stability throughout a comparatively long storage period, in a wide temperature range, and under the impact of considerable g-forces, and the absence of gaseous by-products from the reaction, by-products that would affect the estimate of the content of the defined component.

Good CO_2 absorbers are soda lime, ascarite, potassium hydroxide, sodium hydroxide and calcium hydroxide. all of which possess slightly different absorption characteristics depending on time. Potassium hydroxide (KON) was selected for experiment on the Venera stations as the most acceptable absorber. Its shortcoming is its sensitivity to the presence of moisture. To make absorption speed independent of the degree of drying of

the reagent, a lithium CO_2 absorber (~ 3%) was added to the KON; and to remove any error connected with the absorption of water vapor by the reagent, calcium chloride was put into the other compartment of the cell of the gas analyzer. Within 30 - 50 sec, nearly complete carbon dioxide absorption in the specified volume of the working cell was secured.

Each gas analyzer is a one-time instrument and consists of a set of gas-analyzing cells and an electronics unit. In contrast /96 to G-8 gas analyzers, the number of working cells was increased in the G-10 gas analyzer, and the sensitivity of the manometric sensors was heightened, so as to make measurements when the pressure of the surrounding medium was lower. The operating principle of the gas analyzers is evident from the diagrams in Figs. 29 - 32. These diagrams also show the characteristics of CO_2, O_2 and H_2O absorption by various absorbers as a function of time.

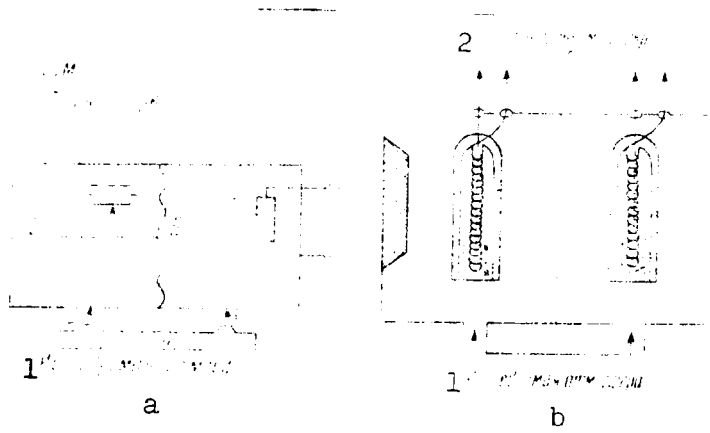

ORIGINAL PAGE IS
OF POOR QUALITY

Fig. 29. The gas-analyzing cells for the determination of CO_2 content in the atmosphere: a) by the manometric method and b) by the heat-conductivity method. 1. The chemical absorber; 2. Manometric device; 3. Potentiometer; 4. Valve[153].

Key: 1. Atmosphere; 2. To electronics unit

The first diagram (Fig. 29a) represents the gas-analyzer cell of a G-8 instrument. On a command from the onboard time-program device, a valve opens, and the atmospheric gas under investigation penetrates into both parts of a cylindrical tube divided by a membrane and evacuated and sealed beforehand. Then the valve /97 closes. In one part there is a chemical absorber of one of several of the atmospheric components; this produces a pressure

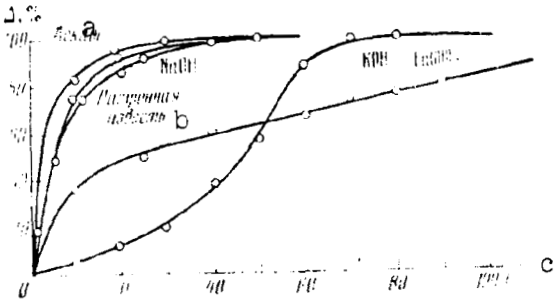

Fig. 30. The CO_2 absorption characteristics of various absorbers vs. time [153]. Key: a. Ascarite; b. Soda lime; c. Sec.

ORIGINAL PAGE IS
OF POOR QUALITY

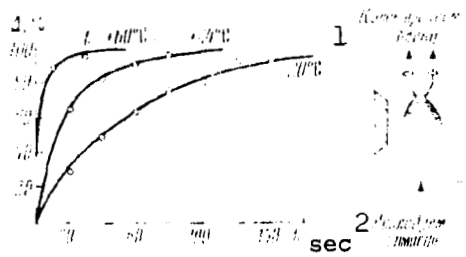

Fig. 31. CO_2 absorption characteristics of white phosphorous vs. time -- at various temperatures (a); and a diagram of the gas-analyzing cell for determination of O_2 content in atmosphere by the thermochemical method (b) [153].

Key: 1. To electronics unit
2. Study atmosphere

differential, and the membrane bulges in one direction or the other; and this is then registered by a potentiometric sensor. To increase reaction speed in several cells an automatic heating of the absorber is provided for after the atmospheric sample is taken and the valve is closed (about 10 sec).

A similar differential (manometric) method is used to determine nitrogen content. In the gas analyzer on board Venera-4, zirconium was used as an absorber. This method is based on the well-known ability of nitrogen to form stable nitrides with metals when heated. The use of this method was to a large extent predetermined by the expectation of a significant nitrogen content in the Venusian atmosphere. A zirconium powder was placed on a crystal capillary and cemented in place by a 20% solution of sodium silicate. In order for the reaction to proceed more intensely (working temperature about 800°C), a zonal mixture was used (aluminum and barium peroxide at a ratio of 2:1). In order to eliminate the influence of CO_2, H_2O, O_2 and Zr absorbents on the readings of the instrument, KON (for CO_2 and H_2O absorption) and phosphorus (for O_2 absorption) were put into the comparison chamber of the gas-analyzer cell. /98

In the gas analyzers of Venera-5 and Venera-6, N_2 was determined by measuring the pressure remaining in the cell after CO_2, O_2 and H_2O absorption. This method is more reliable, since zirconium absorbers are not sufficiently stable in the presence of a large quantity of CO_2. The content of nitrogen and the inert gases (if there are such in the atmosphere) is not sorted out in such a method of analysis.

ORIGINAL PAGE IS
OF POOR QUALITY

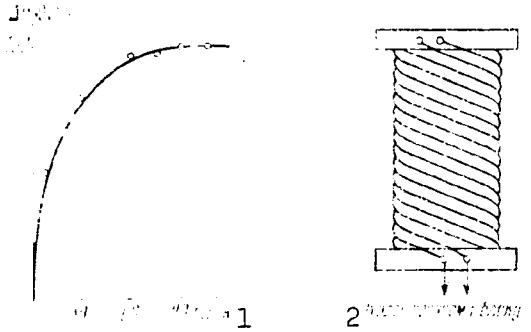

a b

Fig. 32. H_2O absorption characteristics of calcium vs. time (a); and a gas-analyzing cell for determination of H_2O content in the atmosphere by the electrolytic method (b) [153].

Key: 1. t, sec
2. To electronics unit

The second diagram (Fig. 29b) shows the gas-analyzing cell of the G-10 instrument for the determination of small CO_2 content by the heat-conductivity method. This diagram differs from the previous one essentially in that in this case, instead of using a membrane as the sensitive element, platinum filaments were put inside the crystal capillaries and mounted in a balanced bridge circuit. CO_2 absorption in one of the cylinder's compartments led to a change in the heat conductivity from one of the filaments and, consequently, to an imbalance of the bridge, whose magnitude is calibrated in units of CO_2 absorption.

In using the manometric method of determining oxygen and water vapor content, the Venera-4 gas analyzers employed white phosphorus and calcium chloride, respectively, as absorbers. The absorption characteristics of these atmospheric components by these reagents are given in the graphs in Figs. 31 - 32. The white phase of phosphorus was obtained by subliminating the original red phosphorus and was used on the bond (a solution of calcium bichromate and silicate of sodium) with the purpose of securing mechanical strength. Unfortunately, this method does not reveal the presence of an H_2O admixture. The calcium chloride was employed in the form of a screening fraction with a nucleus size of 1 - 3 mm after a preliminary alloying and fragmenting away from moisture.

A more sensitive method for determining oxygen content is the thermochemical method, which was done for all practical purposes on the Venera-4, -5, and -6 AIS's in a variant of the gas-analyzing cell shown in Fig. 31. An electric current, whose size depends on the resistance of the conductor, is passed through a filament of nonmelting metal (tungsten) with a diameter of 12 μm. If there is oxygen within the cell, its reaction with the /99 tungsten either sharply reduces the section of the conductor or burns through it; this enables a threshold determination of O_2 content to be made. This reaction is selective and is not sensitive to CO_2 or N_2.

For a threshold determination of atmospheric humidity, the gas analyzers of Venera-4, -5, and -6 used an electrolytic method. Fig. 32 shows the essential schema of one such gas analyzer cell. This method is based on the change of electrical resistivity in a moisture-absorbing substance; a hydrated phosphoric anhydride was used for this purpose. A 20% aqueous solution of P_2O_5 (metaphosphoric acid) was placed on the outer surface of a glass coil, a dual spiral thread with a pitch of 0.1 mm was cut into the surface; and a platinum filament with a diameter of 0.1 mm was wound onto the glass coil. A voltage feed brings about electrolysis of the metaphosphoric acid, which, as a result of drying, decomposes as in the reaction

$$2HPO_3 + H_2 = \frac{1}{2}O_2 + P_2O_5.$$

ORIGINAL PAGE IS
OF POOR QUALITY

This in turn produces an increased resistance in the absorbing layer. On the other hand, the absorption of moisture brings about a drop in resistance and an increase in the current registered. In order to maintain for an extensive period a low residual moisture over the phosphorus pentoxide after drying, the sensor was located over alkali.

To determine a possible ammonia content in the Venusian atmosphere, Venera-8 carried a gas-analyzer whose operating principle is based on a linear-color method, i.e., on recording the color change of a chemical reagent during a reaction with NH_3. Tetrabromophenolsulfophthalein (a fine-grained yellow powder) on a tempered silica gel was used for this reagent. Under the effect of ammonia, it becomes dark-blue. Any color change /100 was recorded by sulfur cadmium photoresistors. To heighten sensitivity and remove accidental or drift effects, a bridge circuit was built in such a way that the color change of the working reagent was determined in relation to a standard set in a neighboring, sealed compartment of the instrument. Fig. 33 shows a diagram of the gas analyzer.

In order to measure the pressure and temperature of the Venusian atmosphere, the most simple and reliable methods of measuring the thermophysical parameters of a dense gas were used -- with the help of manometers of the membrane (aneroid) type and resistance thermometers [1, 3, 4, 6]. Fig. 34 shows a composite view of instruments of this type. The operating principle of a manometric sensor (Fig. 35a) is based on this property: the elastic deformation of a sensitive element under /102 the effect of external pressure, which is then transformed by a transmitter-multiplier mechanism and a potentiometer into an electric current. Resistance thermometers (Fig. 35b) mounted in balanced bridge circuits served as temperature sensors. Their operating principle is based on the dependence of the ohmic resistance of the sensitive element on temperature change in the medium. A platinum wire was used as the sensitive element of the sensors. The manometers and thermometers were

ORIGINAL PAGE IS
OF POOR QUALITY

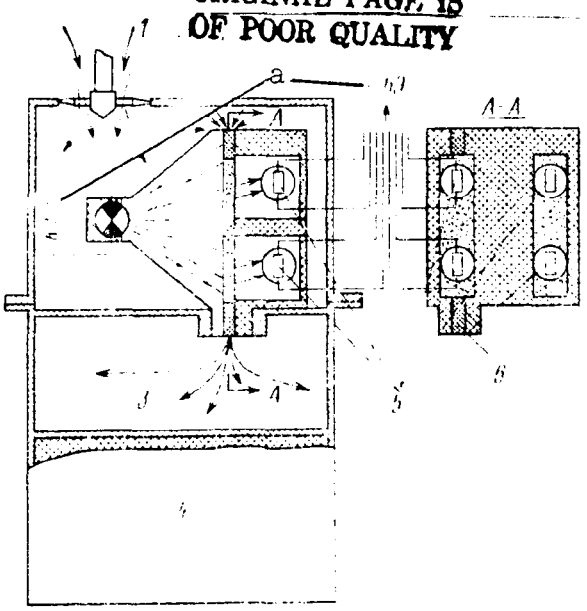

Fig. 33. Diagram of a gas-analyzing cell for determination of NH_3 content in the atmosphere by the colorimetric method. 1. Entry of atmosphere; 2. Measuring chamber; 3. Calibrated capacity; 4. Electronic unit (EU); 5. Photoresistors; 6. Filter [154].
Key: a. To EU.

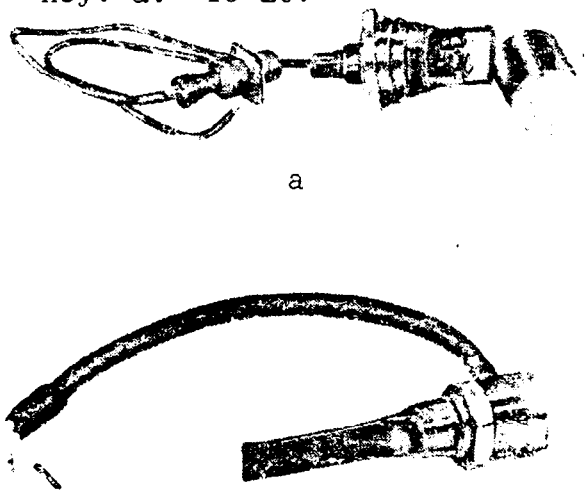

a

b

Fig. 34. Composite view of aneroid manometer (a) and resistance thermometer (b).

tested in a wide range of temperature and pressure variations in the surrounding medium. The error in determining temperature and pressure, estimated as the quadratic mean error of measurements $\sigma_{T(P)}$, was not more than 1.5 - 2.0% of the range of measurement. On individual segments of measurements, it grew because of the discreteness of the interrogation of telemetric commutators.

The Venera-4 - -6 stations also measured the density of the Venusian atmosphere. On Venera-4, Mikhnevich and Sokolov [111] used an ionization densimeter to measure density; and on Venera-5 and Venera-6 [4, 189], Avduyevskiy et al used a densimeter of a tuning-fork type. The ionization densimeter was an ionization chamber of a cylindrical shape; its inner surface was covered with β-active strontium 90. A wire was stretched along the axis of the cylinder. The chamber was completely open to the surrounding space. The operating principle of the densimeter was based on measurement of the size of a current produced by gas ionization inside the cylinder. A constant difference in the potential between the wall of the cylinder and the wire produces a current; the current is proportional to the density of the gas inside the cylinder and, consequently to the density of the gas in the atmosphere. The operating principle of the tuning-fork densimeter is based on variation in the amplitude of the tuning-fork's vibrations with special stimulation as a function of the

density of the medium. The plates of the forks are 0.6 mm thick and 12 mm wide and made of steel. The quality of the tuning fork was ≈ 300. An excitation coil maintains a regime of autovibration at a frequency f = 160 Hz from an oscillator with an electronic feedback; frequency stability is no worse than 1 Hz. A constant energy level on the coil is ensured by an electronic system of amplitude limiters. The amount of variation of the decrement of /103 the fading in the range of measurements was about 30. An electric signal proportional to the amplitude of the oscillation and thus to the density of the medium as well, is taken off the coil, which is secured on one of the plates of the tuning fork.

On the command for the main parachute to open, the radar altimeter with which Venera-4, -5, -6 and -8 were equipped turned on. Measurement of the altitude on the Venera-4, -5, and -6 stations was done according to the principle of frequency modulation. In contrast to the radar altimeter of Venera-4, whose single reading at the moment of parachute deployment was not free of ambiguity, [3, 4] on the Venera-5 and -6 stations, independent frequency filters indicated the moments when the apparatus passed a series of rated altitudes from 50 to 100 km. This method of altitude determination was based on the fact that the difference in frequency between the frequency-modulated echo reflected from the planetary surface and the transmitted frequency-modulated signal was a direct function of altitude. This method made it possible to receive the "envelope" signal in a suitable operating channel of the altimeter; the form of this "envelope" depended on the form of the frequency spectrum of the filter and on the form of the envelope of the spectrum of the pulsed signal. The "envelope" of the signal as it leaves the channel of the receiver reaches a peak when the peak of the frequency spectrum of the filter matches the maximum envelope of the spectrum of the pulsed signal. This characteristic point is determined by the moment when the rated (for a specified channel) altitude above the target surface (at a given reflection coefficient of the surface, which is the result of radar echo data) is reached. In this, the difference between the inherent frequencies of the tuner of the filters of the receiver is within the limits of values that correspond to a difference in altitude of 8 - 10 km.

The radar altimeter on the Venera-8 station operated on the same principle as an instrument of the pulsating type. It was used both to measure altitude above the surface and to estimate from the value of the echo level, the permittivity (density) of the ground.

To determine wind speed in the atmosphere (and on Venera-7 and Venera-8, to define the successive intervals of the parachute /104 descent), data on the Doppler frequency shift of the onboard radio transmitter were used. Kerzhanovich et al [66] have examined methods for analyzing these data. The accuracy (and the possibility) of measuring wind velocity with one-way Doppler information is determined by the frequency stability of onboard oscillators

ORIGINAL PAGE IS
OF POOR QUALITY

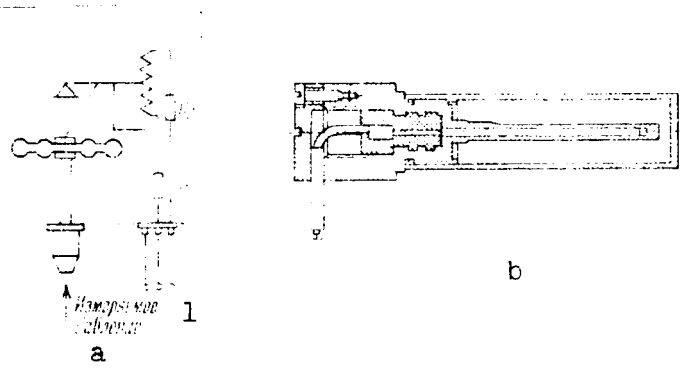

Fig. 35. Diagram of aneroid manometer (a) and design of temperature sensor (b).

Key: 1. Measured pressure

which were used as a standard on the DA. Error is introduced through inaccurate knowledge of the value of the frequency or its unpredictable drift, which can be interpreted as a velocity variation. The main factor influencing the frequency stability of the oscillators is change in the outside temperature. If on the interplanetary segment of the flight the oscillators operate in comparatively favorable conditions, with little temperature fluctuation inside the DA, then during descent when the outside temperature reaches almost 750°K, the temperature inside the DA gradually increases. To decrease temperature-dependent frequency drift, thermostabilized crystal oscillators in Dewar vessels were used in the DA. However, temperature drift in such oscillators during descent can lead to a slowly varying error of measured velocity up to 5 - 7 m/sec. For subsequent correction of the error, a method of calculating temperature-frequency drift was developed that used oscillator characteristics measured on the Earth and telemetry measurements of temperature inside the DA during descent. The remaining error has a smooth, slowly increasing character, and at the end of descent does not exceed 1 - 1.5 m/sec.

Systematic error of velocity measurements is determined by the accuracy with which frequency calibrations during communication periods during interplanetary flight can be used to predict the oscillator frequency at the moment of entry into the Venusian atmosphere. Such a preduction in turn depends on the individual aging of crystal resonators, the number of calibrations made, and the time from the last frequency measurement is made before entry into the atmosphere. The maximum systematic error associated with inaccuracy in extrapolating the frequency of the oscillator to

entry moment is equal to

ORIGINAL PAGE IS
OF POOR QUALITY

/105

$$\begin{vmatrix} -2.8; & 1.-; & 8.5 \\ -2.5; & 10.7; & -1.1 \end{vmatrix} \text{ m/sec}$$

for Venera-4, -5 and -6 respectively.

For Venera-7 and Venera-8, systematic error decreases to $\pm$ 1.5 m/sec when the results of frequency measurements after landing on the planetary surface are used for purposes of calibration. The accuracy of measuring velocity fluctuations is defined by short-time frequency instability and did not exceed 0.3 - 0.5 m/sec for these oscillators. Finally, frequency variation as a result of the refraction of radio waves in the atmosphere introduces a correction of not more than 0.3 m/sec to the velocity on the final stage of descent down to the planetary surface [377].

The instruments placed on the Venera automatic stations have enabled us to make a series of direct measurements in an atmosphere with extremely indefinite values for parameters and with unknown altitude dependence. The complex aims of the first measurements caused them to be rough estimations in some cases. But at the same time the first measurements made it possible to obtain crucial information about the basic physical characteristics of the Venusian atmosphere and to make the transition to a more integrated testing program. In the following sections of this chapter, we will analyze the results of measuring the thermodynamic parameters of the lower atmosphere (troposphere) made on the Venera stations. We will also examine the results of the Mariner-5 measurements, which extended the measured area upwards, into the stratosphere. Our current notions about the planet's atmospheric structure, from the surface to altitudes of about 90 km[1], ultimately rest on these measurements.

IV. Results of Direct Measurements of Atmospheric Parameters on the Venera Stations and an Analysis of These Results /106

Chemical composition. The Venera-4 station made determinations of the gaseous composition at two levels in the atmosphere at $P = 0.6$ kg/cm^2 and $P = 2.0$ kg/cm^2 (2). The gas analyzers of Venera-5 and Venera-6 took samples at levels where $P \approx 0.6$ kg/cm^2; $P \approx 2.0$ kg/cm^2; $P \approx 5.0$ kg/cm^2; and $P \approx 10.0$ kg/cm^2. The Venera-8 station measured ammonia content at atmospheric levels where pressure was $P \approx 2.0$ kg/cm^2 and $P \approx 10.0$ kg/cm^2. The results of

---

[1] Unfortunately, the results of the Mariner 10 flight near Venus on February 5, 1974 were unknown to the authors before they completed work on the manuscript. They were compelled, therefore, to limit themselves to brief mention of the basic results in the appropriate sections of the text or in notes added during proof.

[2] Here and hereafter kg/cm^2 is used; this unit of measurement refers to a technical atmosphere (at.). To transform this into a physical atmosphere (atm), the value in kg/cm^2 should be multiplied by 1.033.

the measurements according to Vinogradov et al [29, 31, 32, 154, 537] are given in Table 9.

From an examination of the data cited in Table 9, one fundamental conclusion ensues: the atmosphere of Venus consists /107 basically of carbon dioxide. Average CO_2 content is 97%. The results of the measurements do not preclude the presence of nitrogen in the atmosphere; the upper limit of nitrogen content (together with a possible admixture of inert gases undifferentiated, as already noted, by the gas analysis method used) is bounded by the threshold value < 3.5% (and probably < 2.0%). As for determination of oxygen content, the most reliable data are those obtained by Venera-5 and Venera-6. They indicate that the oxygen concentration in the Venusian atmosphere is not substantially lower than the threshold value of 0.1%.

The results of measuring the atmospheric humidity of Venus lead to the conclusion that at altitudes of 46 - 54 km, which correspond to a pressure of 0.6 - 2.0 kg/cm^2, the absolute humidity is rather high: ≈ 6/11 mg/ℓ. This corresponds to a relative content for H_2O on the order of 1% by volume; this is close (with an accuracy of up to 2 - 3 times) to the average relative content of water vapor in the Earth's troposphere. As for lower levels in the Venusian atmosphere, the readings of the gas analyzers give only threshold values (more than 0.7 mg/ℓ at 38 km and 30 km), which do not generally contradict the values obtained for humidity. If partial oxygen pressure is put into a barometric formula, relative H_2O content should remain relatively constant. If, though, the basic source of moisture is the clouds, then as gas moves about in the Venusian troposphere (which is consistent, as will be seen later, with the measured temperature profile T(h) with a gradient close to the adiabatic), one can assume a reduction in relative H_2O content by depth. It is more difficult to reconcile a tendency toward reduction in absolute humidity by depth with these notions, if one accepts this threshold estimate as a possible value, to which a mixing ratio $f_{H_2O} \approx 0.007\%$ near 30 km would correspond in this case. The average water vapor content in the entire range of altitudes 30 - 54 km would turn out to be on the order of 0.05% (for details, cf. Section IV.5).

The following value for mean molecular weight corresponds to the content by volume as measured by the Venera stations of the individual atmospheric components

$$\bar{\mu} = 0.97\mu_{CO_2} + 0.02\mu_{N_2} + 0.01\mu_{H_2O}$$

ORIGINAL PAGE IS
OF POOR QUALITY

which is equal in this approximation to $\bar{\mu} \simeq 43.4^{+0.6}_{-0.3}$. The upper and /108 lower limits are possible variants of CO_2 content that are in agreement with measured data. The presence of small admixtures undetermined in gas analysis but identified in spectroscopic data (cf. Table 11 in IV.6 below) does not affect the estimate made for average value $\bar{\mu}$. If the mean content of the basic components remains unchanged, μ can vary appreciably only if inert gases are present.

TABLE 9. RESULTS OF DIRECT DETERMINATION OF GASEOUS COMPOSITION OF THE VENUSIAN ATMOSPHERE (ACCORDING TO [29, 31, 32, 154, 537])

Atmospheric pressure P_2, kg/cm²	Atmospheric temperature T, °C	Altitude above surface (acc. to [102])	Concentration by volume %%				H_2O, mg/ℓ	Spacecraft
			CO_2	N_2	O_2	NH		
								Venera-5
								Venera-
								Venera-
								Venera-
								Venera-
								Venera-5
								Venera-6
								Venera-6
								Venera-8
								Venera-8

ORIGINAL PAGE IS
OF POOR QUALITY

Temperature, pressure and density. Figs. 36 and 37 show the original data from temperature and pressure measurements of the Venusian atmosphere as a function of time on the Venera-4, Venera-5, Venera-6, Venera-7 and Venera-8 stations -- T(h) and P(h) -- these data were obtained by Avduyevskiy et al [1, 3, 4, 6, 186, 187, 189] and by Marov et al [100, 103, 414, 415].

In the first experiment on Venera-4, the temperature was measured at 300 - 535°K and the pressure at 0.6 - 7.2 kg/cm². The dashed line in Fig. 36 shows the extrapolated segment of the measured pressure curve up to the level in the atmosphere where the last temperature measurement was made. The Venera-5 and Venera-6 stations did more comprehensive measurements. There were 50 - 70 measured points P and T made during that stage of the descent of each station where temperature ranged from 300°K to 600°K and pressure from 0.7 kg.cm² to 27 kg/cm². In the process, the measuring ranges of individual instruments overlapped. Since the accuracy of measurements is not identical within the limits of the scale of the instrument and since there is a larger error in sensors /110 with a wide measuring range, these factors are taken into consideration during processing of the data obtained, processing done according to the method of least squares, wherein each individual point is given a corresponding statistical weight. The original points P and T from the measurements of each station were

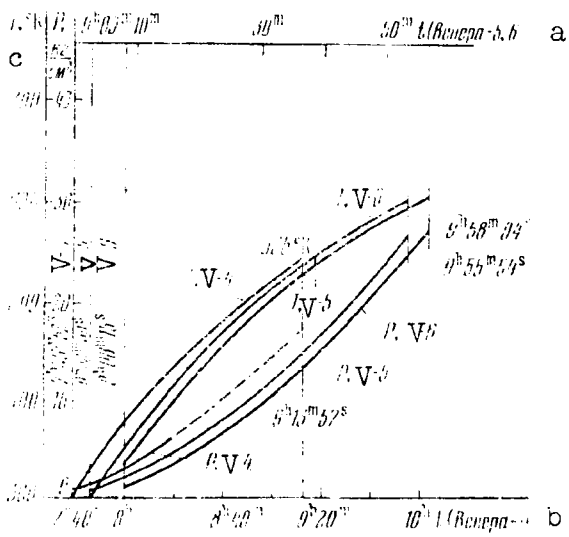

Fig. 36. Atmospheric temperature and pressure vs. time -- according to the measurements of Venera-4, Venera-5, and Venera-6. The solid curves are a polynomial approximation. The elapsed time t for each experiment is Moscow time at reception of signal on Earth. The times of beginning and end of measurements are noted. The dashed line is the portion extrapolated for pressure as measured by Venera-4 until the moment temperature measurements ceased.

Key: a. Venera-5, -6
b. Venera-4,
c. kg/cm^2

ORIGINAL PAGE IS OF POOR QUALITY

approximated by n-degree polynomials. The formal error, which is determined by taking the specified errors of measurement, telemetry discretion, and the processing method into account, does not exceed, for temperature and pressure, σ_{TP} 5 - 10% of the rated values (at n = 2 - 3).

In an experiment on the Venera-7 station (cf. Fig. 37) one instrument measured temperature uninterruptedly from the level T = 333°K down to the planetary surface. But the onboard telemetry commutators did not successively interrogate the various sensors, and unfortunately this did not allow us to make measurements of atmospheric pressure, an altitude profile for which was obtained by calculation. The vertical segments on the curve T(t)(which approximates the experimental data) denote the limiting errors in the measurement of temperature. As is seen from Fig. 37 the temperature increased without interruption and, at the moment of landing on the surface, reached 747°K. Analysis of radio signals by Aleksandrov et al after landing [9] showed that this value remained unchanged for 50 sec; thereupon, a temperature corresponding to the previous telemetry gradient, which was 17°K lower, was recorded. It is possible to explain this change by keeping in mind that the temperature of 747°K was within several degrees of the boundary of transition from one telemetry gradient to another. In this case, even an insignificant change in the conditions of heat transfer between the sensor and the surrounding medium after

landing can bring about a transition to the previous telemetry gradient of T = 730°K. Therefore, a temperature $T_s = 747 \pm 20$°K can be accepted as the most reliable temperature of the Venusian night atmosphere at the surface at the Venera-7 landing site.

This same graph gives the results of temperature and pressure measurements of the Venusian atmosphere on the day side -- as in the data of Venera-8. The designated experimental points correspond to the readings of individual sensors. The solid curves T(t) /111 and P(t) are the results of averaging the experimental points by approximating polynomials. The dashed line designates the principal intervals. The greatest uncertainty occurs at the beginning of measurements of pressure -- because of the significant errors of sensors with large measuring ranges; therefore, in the interval up to $P \lesssim 5$ kg/cm^2, the measurement data were refined by taking into account the additional characteristics of the aerodynamics of parachute descent. The atmospheric temperature and pressure changed smoothly from values of 300°K and 0.7 kg/cm^2 at the beginning of measurements to 743°K and 93 kg/cm^2 at the moment the apparatus landed on the surface; thereafter they remained unchanged. By taking into account possible errors of measurement on the surface at the Venera-8 landing site, we have $T = 743 \pm 8$°K and $P = 93 \pm 1.5$ kg/cm^2.

Fig. 38 shows time vs. the curves of density variation obtained by Venera-4 and Venera-5 [1, 4]. The values for density can be calculated also from the equation of state at a molecular weight μ corresponding to the measured atmospheric composition of Venus. As is evident from Fig. 38, density measurement data do not agree with the results of calculations based on the measured values for pressure and temperature at a constant molecular weight. In the /112 case of Venera-4, an inversion $\rho_{mea}(t)$ occurred in a temperature range of about 380 - 450°, which at a maximum corresponds either to $\mu = 57$ or (assuming a polytropic gas state) to a reading of a conditional polytrope $n = 1.65$ [3]. In the case of Venera-5, the deviation in the profile $\rho(t)$ from what had been calculated was observed from level $T \gtrsim 400$ °C and increased continuously until it reached a maximum value at the end of the descent, at T = 600°K. In the process, the stability condition is not upset; however, using the gas state equation leads, as in the case of Venera-4, to unrealistically high values for μ. The results of repeated laboratory tests did not allow us to reproduce profiles ρ similar to those measured in various CO_2 gaseous mixtures. The phenomena observed while the densimeters were operating cannot be explained unless a hypothesis is introduced about the presence of dust or any liquid or solid admixture in the atmosphere; however, additional substantiation is necessary for this. At the same time, the existence of even relatively small concentrations of such admixtures, which

[3] This last does not agree with notions about the stability of a carbon dioxide atmosphere at these altitudes at corresponding measured values P and T.

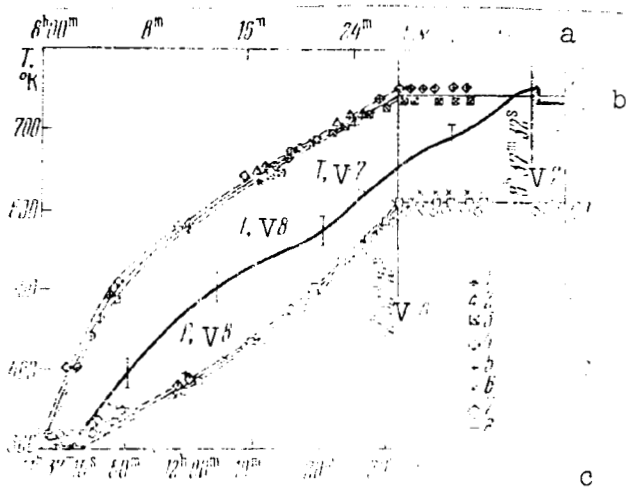

Fig. 37. Atmospheric temperature and pressure vs. time -- according to Venera-7 and Venera-8 measurements. The solid curves are a polynomial approximation, the dashed line is the measuring intervals, the vertical line on curve T, V-7, indicates the maximum possible error of measurements. The designations of the sensors: 1. T1, 50 - 590°C; 2. T2, 200 - 435°C; 3. T3, 395 - 540°C; 4. T4, 20 - 605°C; 5. D1, 0 - 80 kg/cm^2; 6. D2, 0 - 100 kg/cm^2; 7. D3, 0 - 200 kg/cm^2; 8. D4, 0 - 150 kg/cm^2. The vertical lines with the hashing are landing times.

Key: a. Min (Venera-7)
b. kg/cm^2
c. Min (Venera-8)

ORIGINAL PAGE IS
OF POOR QUALITY

have no noticeable effect on the value $\bar{\mu}$ and which therefore do not appear in measurements P in any way, could be determined to have an effect on densimeter readings because of their operating principles.

Determination of descent velocity. Variation with altitude. Data on the descent velocity of the apparatus in the atmosphere and on the distance covered have a direct bearing on analysis of the structure and dynamics of the atmosphere. They enable us to evaluate the character and intensity of atmospheric motion and to obtain altitude profiles of atmospheric parameters when it is impossible to correlate the measured curves T(t) and P(t) at any given moment t to the measured values of altitude above the surface h(t). For these purposes, one may use the results of the measurements of atmospheric parameters as a function of time together with the known relations for atmospheric gas and the aerodynamics of an apparatus descending by parachute [97].

We will assume that /113 the atmosphere of Venus is in conditions of hydrostatic equilibrium and that the aerodynamic drag coefficient of the descent apparatus remains the same during descent. Then, with the known gaseous composition of the atmosphere, the descent velocity and the distance descended during parachute descent as a function of descent time v(t) and z(t) can be calculated accurately from measured P(t)'s and T(t)'s from the hydrostatic and gas state equations and also by using the equation of quasi-uniform parachute descent velocity. The assumption that in a quiet atmosphere, the DA moves with a velocity that is nearly the same as the velocity of quasi-uniform descent,

is completely justified. Nonstationarity can have a small effect only at high velocities of motion, and its effect decreases proportionately to the cube of velocity.

ORIGINAL PAGE IS
OF POOR QUALITY

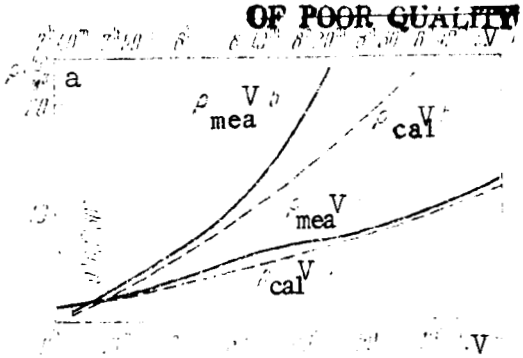

Fig. 38. Atmospheric density vs. time -- according to Venera-4 and Venera-5 measurements (solid curves). The dashed line is calculated according to the hydrostatic equation and measured P and T at $\bar{\mu}$ = 43.4.

Key: a. kg/m^3

The equations have the form

$$dP = -\rho g_{\varphi} dz = \rho g_{\varphi} v dt. \qquad \text{(IV.3)}$$

$$P = \rho \frac{R}{\bar{\mu}} T. \qquad \text{(IV.4)}$$

$$v = V\left(1 - \frac{\rho}{\rho_{DA}}\right) + C_x F \frac{\rho v'^2}{2}. \qquad \text{(IV.5)}$$

where g_{φ} is the gravitational acceleration for Venus (equal to 880 cm/sec^2), M is the mass of the descent apparatus, ρ_{DA} is the mean density of the descent apparatus, $C_x(\alpha)$ is the aerodynamic drag coefficient of a "DA parachute" system at an angle of attack equal to the balance angle α [4], F is the cross section area, v is the descent velocity relative to the surface, v' is the descent velocity relative to the gas, ρ is the atmospheric density, R is the universal gas constant, $\bar{\mu}$ is the mean molecular weight, z is the vertical distance descended, and t is elapsed time.

From (IV.3) we have /114

$$v = \frac{dz}{dt} = \frac{1}{\rho g_{\varphi}} \frac{dP}{dt} = \frac{RT}{\bar{\mu} g_{\varphi}} \frac{d \ln P}{dt}. \qquad \text{(IV.6)}$$

$$z = \frac{1}{g_{\varphi}} \int_{P_1}^{P_2} \frac{dP}{\rho} = \frac{R}{\bar{\mu} g_{\varphi}} \int_{P_1}^{P_2} T \frac{dP}{P}. \qquad \text{(IV.7)}$$

From (IV.5) there follows directly

$$v' = \left[\frac{2 g_{\varphi} M\left(1 - \frac{\rho}{\rho_{DA}}\right)}{\rho C_x F}\right]^{1/2}. \qquad \text{(IV.8)}$$

[4] For the parachutes used on the Venera stations, the value of the angle α was insignificant, i.e., the longitudinal axis of the "DA parachute" system coincided practically with the direction of the oncoming flow.

In this, the vertical and horizontal components of descent velocity are written in the form

$$v'_v = v' \cos \gamma_0; \qquad v'_h = v' \sin \gamma_0, \tag{IV.9}$$

where γ_0 is the planing angle. On parachute descent, one may assume $v'_v = v'$ without much error; i.e. the DA's own motion in the absence of wind is vertical. This does not contradict data from ground tests. Accordingly

$$z = \int_{t_1}^{t_2} v' dt = \frac{2AR}{\pi c_x} \int_{t_1}^{t_2} \left(\frac{T}{p}\right)' dt, \tag{IV.10}$$

where A denotes the aggregate of constants

$$A = \left(\frac{\mu g \pi}{2 c_x R}\right)^{1/2}.$$

ORIGINAL PAGE IS
OF POOR QUALITY

The error of measurement of velocity and distance in these cases is usually a fraction of a meter per second and a fraction of a kilometer respectively.

The time dependences of descent velocity v and distance z for the Veneras-4 - -6, as calculated from (IV.6) and (IV.7) are given in Fig. 39 (the dashed lines are velocity, the solid lines are distance). Calculating v'(t) and z(t) for formulas (IV.8) and (IV.10) gives nearly coincident curves. The atmospheric level where pressure is 0.6 kg/cm^2 is accepted as a basis of integration for distance (up to down). The values for descent /115
velocity are indicated on the same axis. On the right, values for pressure are entered; these correspond to a scale of height z along the ordinal axis in accord with the Venusian atmospheric model given in the Appendix. For convenience in plotting, the time scale on the abscissa is taken to be variable in connection with the substantially different times of the AIS's descent in the atmosphere.

It follows from the calculations that values of velocity on descent into the Venusian atmosphere varied monotonically within the limits 11-3 m/sec for Venera-4, 32-6 m/sec for Venera-5, and 22-6 m/sec for Venera-6. Venera-4 took measurements from the moment the main parachute deployed until radio communications with the station ceased after a descent of 28 km. For Venera-5, this /116
figure is 36.7 km. For Venera-6, this figure is 34.2 km.

The curves z(t) on Fig. 39 accurately correspond to altitudes of those measurements of atmospheric parameters in the interval between the beginning of descent and the termination of radio communications. It is evident that, in order to establish what

levels in the atmosphere the curve z(t) refer to, at least one measurement of the true altitude above the surface during descent or a knowledge of the moment of landing on the surface is needed.

By comparing the Venera-4 measured values T and P with the results of ground radio measurements and Mariner-5 data, it should have been expected that, at the most probable value for the radar radius of Venus, the atmosphere was much deeper than the level at which Venera-4 ceased measurements [3, 87, 95, 291]. The experiments on Venera-5 and Venera-6 make it possible to implement a more reliable correlation to the stages of descent. The arrows on Fig. 39 indicate the distances from each apparatus to the surface; the radar altimeter determined the distances at moments when rated altitude values were passed (h_{15}, h_{25} and h_{35} for Venera-5; h_{16} and h_{26} for Venera-6). These distances allow us to establish a correlation between atmospheric parameters and altitude above the surface. The distances correspond to intervals between the markings on the radar altimeter and can be compared with values for distance calculated from the hydrostatic equation. For easy comparison, the basic data are given in Table 10, where h_{RA} are the altitudes that correspond to the markings on the radar altimeter, Δh_{RA} are the differences in the values for distance, as determined by the markings of the radar altimeter, Δz are segments that correspond to the moments when altitude measurements were made of the distance travelled, as calculated from formula (IV.3).

$$\delta = \Delta h_{RA} - \Delta z,$$

$$\delta\% = \frac{\delta}{\Delta h_{RA}} \cdot 100\%.$$

ORIGINAL PAGE IS
OF POOR QUALITY

As is evident, the segments that each apparatus travelled, which are defined as the difference in altitudes between successive markings on the radar altimeter, are in satisfactory agreement with what is calculated from formula (IV.7). The slight deviations /117
(less than 1.3 km) shown in Fig. 39 and Table 10 are within the bounds of the errors of altitude measurements and can be explained, moreover, by the relief of the locality with a possible sidewise wind drift of the apparati.

Fig. 39 also gives the conditional mean surfaces for each apparatus; these are obtained by an arithmetic averaging of the measured altitudes with weights inversely proportional to the errors of measurements. By making use of the condition that atmospheric pressure is identical on an equipotential level, one can compare the landing-site regions of Venera-5 and Venera-6. As a reference, let us take the equipotential level with pressure /118
$P = 6.6$ kg/cm^2; this was the first reading of the Venera-5 radar altimeter and it was close, at $P = 6.8$ kg/cm^2, to the first reading of the Venera-6 radar altimeter. The location of this level above the conditional mean surface determined from the Venera-5 measurements is $h_{y5} = 40.6$ km; and above the conditional

ORIGINAL PAGE IS
OF POOR QUALITY

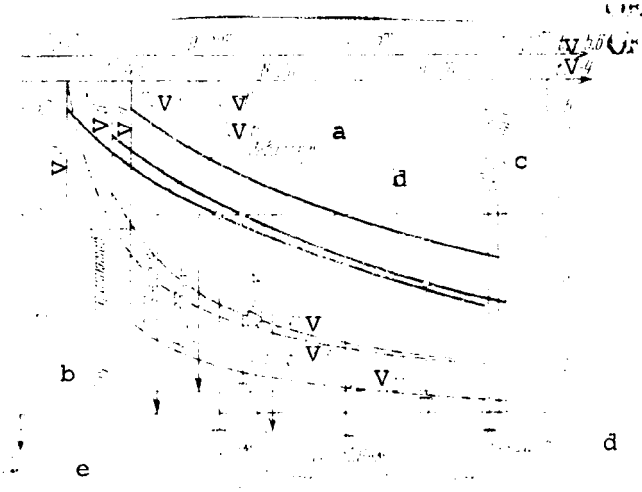

Fig. 39. Descent velocity and distance vs. time for Venera-4, Venera-5 and Venera-6 and relation to altitude above the surface. The solid lines -- the distance z travelled in the atmosphere, the dashed line -- the descent velocity v. The times of parachute riffling and termination of measurements are marked. On the right ordinal axis -- a pressure scale corresponding to the altitude correlation to measured data. The circles on curves z, V-5, and z, V-6, are the moments for which radar altimeters made a determination of altitude above the surface. The vertical line segments correspond to values for altitude. The straight lines with arrows extended below the equipotential level (P = 6.6 kg/cm^2) indicate the local levels and the mean level of the surface according to an aggregate of all altitude measurements.

Key: a. Equipotential level
b. Parachute riffling
c. Termination of measurements
d. kg/cm^2
e. m/sec

mean surface determined by Venera-6 measurements, it is h_{y6} = 33.0 km. When the first readings of the radar altimeters of Venera-5 and Venera-6 are matched in this way, the curves of height vs. time z(t) for both apparati nearly coincide. Taking the following values of measured altitudes into account, the mean (between h_{y5} and h_{y6}) distance from the equipotential level P = 6.6 atm is $\bar{h}$ = 36.8 km. The graph in Fig. 39 illustrates this.

Table 10 gives estimates of how precise the altitude measurements of Venera-5 and Venera-6 were. The quadratic mean error of measurements σ_{RA} is made up of the independent instrument errors σ_i and the methodological errors σ_m. By σ_i is meant the quadratic mean error of the calibration of the radar altimeter, and by σ_m is meant the methodological quadratic mean error of determining altitude from the peak "envelope" while keeping in mind the difference between the law of inverse scattering of radio waves by the planetary surface and specular scattering, as well as the discrete character of the transmissions of "envelopes" in time and amplitude.

The quadratic mean error of the determination of the difference in altitudes h_{15} and h_{16} on the equipotential level is equal to $\sigma_{RA} \approx 1.4$ km, while the quadratic mean error in the determination of distance between the conditional mean surfaces (from Venera-5 and

TABLE 10. RADAR ALTIMETER READINGS AND A COMPARISON BETWEEN THESE READINGS AND THE RESULTS OF CALCULATIONS ACCORDING TO THE HYDROSTATIC EQUILIBRIUM EQUATION

Space-craft	Time	P, kg/cm^2	T, °K	h_{PB}, km	Δ'_{PB}, km	Δz, km
Venera-5	09 22 21 09 37 28 09 55 51*)	6.6 14.8 27.5	450 539 600	30.4 31.9 33.8	3.5 5.1	2.1 3.7
Venera-6	09 25 13 09 38 06	6.8 19.8	461 567	32.1 21.2	10.9	12.2

Space-craft	Δz		T_0		κ		Δh_{PB}	
		$\Delta\kappa$		ΔT_0		$\Delta\kappa$		
Venera-5	7.05 3.5	−0.6 0.3	1.8 1.8 1.8	0.7 0.6 0.3	1.5 1.5 1.5	0.6 0.5 0.2	2.3 2.3 2.1	0.2 0.2 0.5
Venera-6	12.00	−1.3	2.0 2.0	0.6 0.2	2.2 5.0	0.8 1.0	3.0 5.3	1.0 1.1

ORIGINAL PAGE IS OF POOR QUALITY

*Includes extrapolation of the last radar altimeter readings.

Venera-6 data) taking the aggregate of all altitude measurements into account is $\sigma_{RA} \approx 1.0$ km. Errors in estimating h_{y5} and h_{y6}, determined independently for each apparatus, turn out to be variable: for the region of the Venera-5 descent, $\sigma_{RA}^{y5} \approx 1.2$ km, while for the region of the Venera-6 descent $\sigma_{RA}^{y6} \approx 1.4$ km. If the maximum deviations are described by the value 3σ, then we obtain

$$\Delta h_{y5} = \pm 0.6 \pm 2.7 \text{ km}; \quad \Delta h_{y6} = \pm 3.0 \pm 4.2 \text{ km}.$$

The differences δ between Δh_{RA} and Δz, given in Table 10 and viewed as random errors of measurements, stay within the limits $\pm \sigma_{RA}$ from measured altitudes.

The results of this examination provide a reason to begin /119 with a conception of mean surface for that region of the planet which is covered in the measurements of both apparati and which is at the average distance h = 36.8 km from a equipotential level with P = 6.6 atm. According to the measurements of Venera-5 and Venera-6, local surface levels turn out to be situated $\Delta\bar{h}$ = 3.8 km above and below the mean. Taking the previously determined values σ_{RA}^{y5} and σ_{RA}^{y6} into account, it is possible to

designate the values $\zeta = (\Delta\bar{h} \pm 3.4$ km) as the maximum deviations from the position of the mean surface; however, these values are much less probable. It is possible to assume that the difference in the position of local surfaces is connected with the planetary relief in the area of descent. If Venera-5 and Venera-6 set down at a distance $d \approx 300$ km apart from each other (Table 7), a mean slope of the surface $\theta \approx 1.5°$ must correspond to this fall in altitude.

On Venera-7 and Venera-8 the descent velocity of the apparati in the Venusian atmosphere v(t) was determined indirectly: from the frequency deviation of a signal received on Earth from a reference frequency f_o of the onboard oscillator. The curves $v_D(t)$ and z(t), shown in Fig. 40 correspond to the frequency variation recorded. From an examination of the curve $v_D(t)$, it is quite clear how the descent of Venera 7 took place, specifically, the parachute deployed at 8:13:03 and the descent velocity increased at 8:19:08; this is shown in the behavior of the curve T(t) in Fig. 37. Landing occurred at 8:37:32 at a velocity of about 16 m/sec. At this moment, an abrupt change in the frequency of the received signal (a frequency recoil) was recorded; here, the descent velocity relative to the planet of course dropped to zero.

Calculation of the descent velocity was done by various methods using the relations (IV.6) and (IV.8). In addition to the measured temperature $T_{mea}(t)$, a modelled dependence $\rho(h)$, which corresponds to the assumption that the atmosphere in the entire area of descent was adiabatic, was also used. The computed curves are in good agreement with the measured curve v(t) on segments where aerodynamic characteristics differed little from what has been calculated.

The value of distance covered z(t), which was calculated from/120 the measured velocity $v_D(t)$ is shown in Fig. 40 as a solid line. The distance Venera-7 covered from the moment it began measurements until it landed on the surface was $z = 55.1 \pm 3$ km. The indicated deviations are due to the accumulation of errors of measurements v_D (≈ 1.5 m/sec) in the interval of integration. Let us note that, by starting with the assumption that the atmosphere is adiabatic, it is possible to obtain the calculated value z(t) from the measured temperature $T_{mea}(t)$ directly, without resorting to the integration of v(t); this can be done by using the first law of thermodynamics $TdS = di - dp/\rho$, the hydrostatic equation (IV.3) and the isoentropy condition $dS = 0$. Then, in finite increments, we can write

$$\Delta z \approx \frac{\Delta i}{g} \qquad \text{(IV.11)}$$

where i is the gas enthalpy.

ORIGINAL PAGE IS
OF POOR QUALITY

On the whole, the results of calculating with $\bar{\mu} = 43.4$ (the dashed line in Fig. 40) provide evidence that both curves are in satisfactory agreement. At the same time, a slight discrepancy is discovered on the descent between 8:15 and 8:35, while the total distance travelled turns out to be 1.8 km more on the average, $z' = 56.9 \pm 3$ km.

For the Venera-8, descent velocity and the distance travelled are determined by: independent data on the current value of altitude above the surface (according to the measurements of the onboard radar altimeter); measurements of the radial velocity of the apparatus by a one-way Doppler method; and, finally, data on measurements of atmospheric parameters.

The radial component of the descent apparatus's velocity (the total systematic error, the determination of which is within 2 m/sec during the entire descent) varies from 136 m/sec at the beginning to 6.4 m/sec at the termination of descent. The jump in velocity at 11:48:40 is due to the riffling of the parachute, and the jump at 12:32:12 is landing on the Venusian surface. Worthy of note is a pronounced oscillatory movement of the DA after parachute riffling; the oscillations had an amplitude in radial velocity of about 2 m/sec and a period of 1 - 2 sec and died down comparatively slowly (5 - 7 min). Regularly-occurring fluctuations of velocity were subsequently small. Assuming no horizontal drift of the DA prior to landing, the landing velocity of the DA v = 8.35 m/sec corresponds to a radial velocity of 6.4 m/sec at an angle of 37° between the direction to Earth and the local vertical.

Fig. 41 shows the descent velocity v(t) and the altitude above the surface h(t) -- according to the data from radar altimeter measurements and calculated according to equations (IV.6) -- (IV.10). In the last case, the integral of distance travelled is computed from the moment the apparatus landed on the surface. On the portion of descent made with parachute riffled, the descent velocities calculated according to Eqs. (IV.6) and (IV.8) differ by about 20% which is most probably connected with the fact that the constant C_x/M used in the calculations is slightly underestimated. After 11:50:00, the curves v(t) and h(t), which were obtained by various methods, practically coincide. At the same time, a marked difference between the curve n(t) (measured by radar altimeter) and the curve calculated for the descent above 25 - 30 km is noteworthy. If, /122 in the determination of altitude of this portion of the descent, one rules out an error that is substantially larger than the allowable error (cf. Table 8), then one can assume that the planetary region in which Venera-8 began its descent is elevated on the order of 6 km in relation to the region where the apparatus actually landed. The results of radial velocity measurements lead to the conclusion that there was a strong sidewise drift of the apparatus during descent to an altitude of about 15 km. Corresponding estimates of the horizontal component of wind velocity (cf. the

ORIGINAL PAGE IS
OF POOR QUALITY

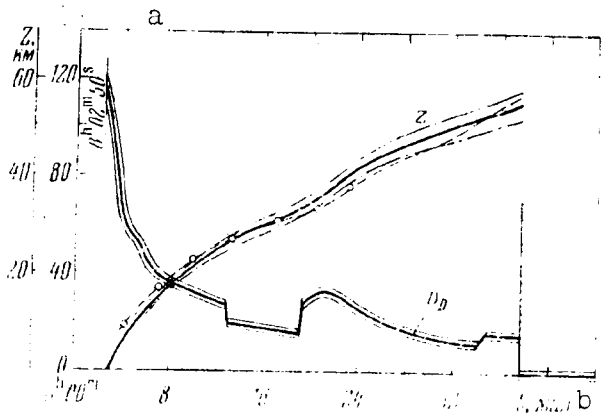

Fig. 40. Descent velocity v_D and distance z vs. time for Venera-7. The narrow lines and the dotted-dashed line are possible errors in the determination of v_D and z. The circles are part of the measurements of the Venera-5 and Venera-6 measurements. The dashed line is z calculated from the measured temperature on Venera-7 assuming an adiabatic model of the atmosphere. The circle with the "horns" is the reference point relative to which the results of measurements of T and P on the Venera AIS are aggregated.

Key: a. m/sec
b. t, min

section on atmospheric dynamics of this chapter) allow us to obtain a value of d ≈ 60 km for horizontal drift of the apparatus during the first 25 minutes of descent. In this case, it is necessary to assume that there is a slope of about 5° between the region where descent began and the landing-site region.

Altitude profiles T, P, and ρ. The results set forth in the previous sections allow us to construct altitude profiles for the temperature, pressure and density of the Venusian atmosphere on the day and night sides in the vicinity of the morning terminator. In so doing, the Venera-7 and Venera-8 measurements make it possible to obtain temperature and pressure distributions as functions of altitude reckoned directly from the surface in the landing site region.

Figs. 42 and 43 show the aggregate curves T(h) and P(h) from the measurements of Veneras-4 - -8. One can /123 make a comparison with the data from Venera-4, -5, and 6 measurements by using a reference point; as such, it is convenient to choose a point where temperature T = 500°K. It is in this region of the atmosphere that most measurements with minimum relative errors have been made. Distributions of T(h) and P(h) from data from Veneras-4 - -6) on both sides of the reference point are determined, as has been seen, by the hydrostatic equation. It is evident that an altitude profile for pressure on the planetary night side for the measured (Venera-7) curve T(h) is determined similarly, provided only one value for pressure at a corresponding temperature is known in the region where Venera-4 - -7 measurements overlap. For the selected reference point, the value P is 10.3 kg/cm^2 according to previous measurements. The profile P(h) from an altitude of 55 km to the surface, a profile calculated by

ORIGINAL PAGE IS
OF POOR QUALITY

taking the real properties of gas at high pressures into consideration, is shown in Fig. 43 by the dashed line. The atmospheric pressure at the surface is P_S = 83.6 kg/cm^2. If Eq. (IV.11) is used for altitude correlation to the curve T(t), the temperature profile below the reference point conforms, as has been seen, to an adiabatic model of the atmosphere, limited by temperature at the surface T_S = 747°K. Temperature distribution vs. altitude corresponds in this model to a value of distance z (z shown in Fig. 40 by the dashed line), which is 1.8 km higher than the value z obtained by integration of v_D during the descent of the apparatus. Let us mention that the difference in altitudes falls within the accumulated error of z during integration as Venera-7 descended from a level where T ≈ 500°K to the planetary surface (cf. Fig. 40). Pressure distributions above and below the reference point essentially coincide in both cases; however, where T(h) = T_{ad}(h) as a result of a large effective depth of the atmosphere, the pressure at the surface (the solid line in Fig. 43) turns out to be P_S = 92.3 ± 15 kg/cm^2.

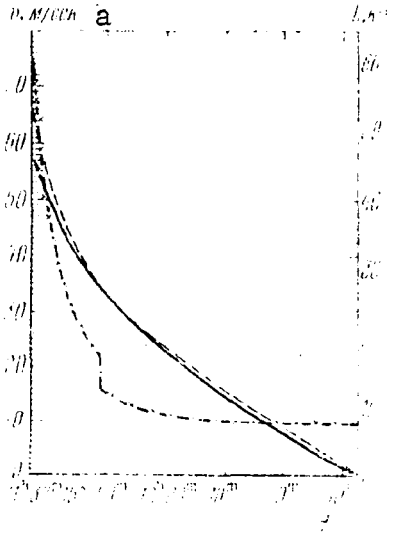

Fig. 41. The variation in descent velocity of Venera-8 v(t) and in altitude above the surface h(t). The solid line is h(t) according to radar altimeter data, the dashed line is h(t) calculated from Eq. (IV.3); the x's are v(t) according to radar altimeter data.

Key: a. m/sec

These deviations take into account any possible limiting errors of measurements. That this value is realistic for the same temperature at the surface is confirmed by more precise data from the Venera-8 measurements. At the landing site of the apparatus, the atmospheric temperature and pressure were T_S = 743 ± 8°K and P_S = 93 ± 1.5 kg/cm^2.

As a whole, the temperature and pressure dependences on altitudes (according to the measurements of all the Venera stations), matched at a reference point where P = 10.3 kg/cm^2, are in good agreement. In examining the results of Venera-8 the following fact is noteworthy: a marked difference between the profiles T(h) and P(h) above 25 km, which were constructed from altitude measurement data made by a /125 radar altimeter, and the profiles that correspond to an altitude correlation in accord with the condition of hydrostatic equilibrium. If the previous assumption that surface relief explains this feature holds true, then the hatched and dashed line in Fig. 43 coincides with

ORIGINAL PAGE IS
OF POOR QUALITY

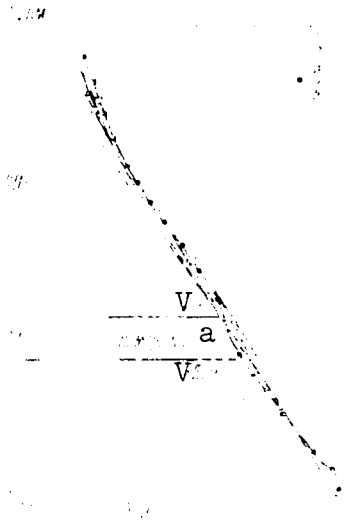

Fig. 42. Curves of atmospheric temperature variation vs. altitude -- according to Venera measurements. 1. Venera-4; 2. Venera-5; 3. Venera-6, 4. Venera-7, 5. Venera-8. The broken line is Venera-8, $T(h_{PB})$.

Key: a. Termination of measurements

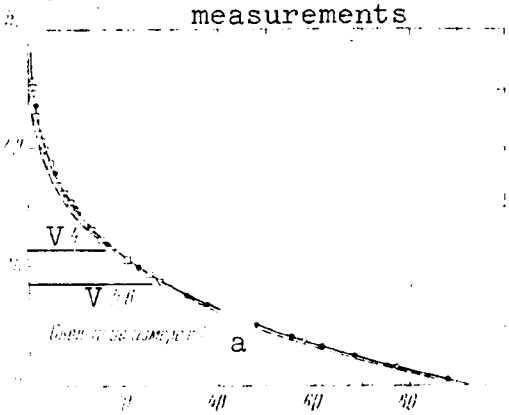

Fig. 43. Curves of atmospheric pressure variation vs. altitude -- as obtained on Venera series. Same designations as in Fig. 42.

Key: a. Termination of measurements
b. kg/cm^2

the solid line. These curves give a physically realistic distribution of atmospheric parameters vs. altitude. The associated altitude profile for atmospheric density $\rho(h)$ and the gradient of density variation vs. altitude $d\rho/dh(h)$, which are calculated from measured T and P at $\bar{\mu} = 43.4$, are shown in Fig. 44. The atmospheric density at the surface of Venus is $P_S = 63.5 \pm 1.5$ kg/m^3.

Gas state in the atmosphere. Graphs of pressure vs. temperature corresponding to data from the Venera apparati, are given in Fig. 45 in logarithmic coordinates. An analysis of these dependences leads to the conclusion that variation of the gas state in the Venusian atmosphere generally /126 corresponds to the polytropic law with an average index of the polytrope $\xi = 1.20/1.25$, which is close to the mean index for the adiabat ($\kappa = 1.23$) at measured parameters of the medium. The calculated (from data of measurements) curve ξ, compared with the variation of the index of the adiabat in the coordinates P -- T, is also shown in Fig. 45.

The adiabatic temperature gradient for a perfect gas is determined from the relation $di/dh = -g$, where $i = i(P, T)$ is the gas enthalpy and is equal to

d (IV.12)

Calculated with a nonperfect gas [36] taken into account, the adiabatic temperature gradient varies in a CO_2

ORIGINAL PAGE IS
OF POOR QUALITY

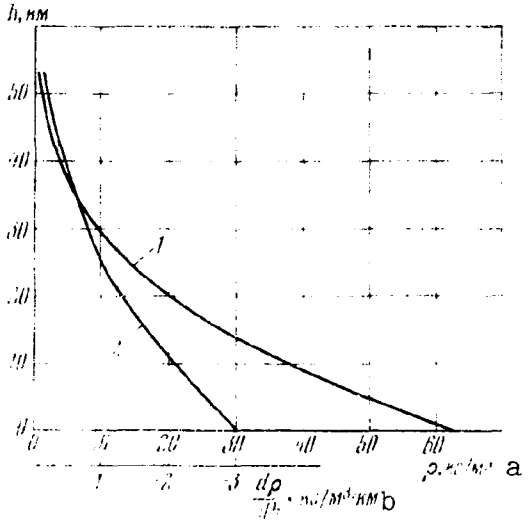

Fig. 44. Atmospheric density vs. altitude ρ(h) (1) and density variation gradient dρ/dh(h) (2) calculated from T(h) and P(h) as measured by Venera-8 (at $\bar{\mu}$ = 43.4).

Key: a. kg/cm^2
b. $kg/m^3 \cdot km$

atmosphere with corresponding P and T from ≈ 10 $deg \cdot km^{-1}$ at the beginning of measurements to ≈ 8 $deg \cdot km^{-1}$ at the surface of Venus: inclusion of possible N_2 content of a few percent does not have an appreciable effect on these values.

The temperature gradient in the Venusian atmosphere $\gamma_i = (dT/dh)_{mea}$ can be determined with rather limited accuracy directly from the measured curve T(h) (Fig. 42); therefore, comparisons of γ_i and γ_a naturally have a qualitative character. Calculations show that the value γ varies from 10.8 $deg \cdot km^{-1}$ at the beginning of measurements, at temperatures T = 300 - 350°K, to 8.6 $deg \cdot km^{-1}$ near levels where the temperature range is 540 - 600°K (where Venera-4 and Venera-5 and -6 respectively terminated measurements, some 20 - 30 km above the surface), and to 8.0 $deg \cdot km^{-1}$ at the surface (Venera-8 data). /127

The results of the Venera-7 and Venera-8 measurements provided convincing evidence that there is no extensive isothermal layer at the surface of the planet -- which had been assumed from an analysis of radio measurements [136]. They allowed us also to rule out assumptions that, because of the increased opacity as a result of the absorption of solar energy by aerosols, the temperature gradient in the real atmosphere can be reduced appreciably as the surface is neared. The obtained dependences (of temperature) on altitude, which are in complete agreement with previous estimates by Avduyevskiy et al [1, 3, 4, 100, 187], allow us to believe that the gas state in the planetary troposphere does not differ practically from the adiabatic -- which directly follows from a comparison of the curves $T_{mea}(h)$ and $T_{ad}(h)$ in Fig. 42. Another, more rigorous confirmation of this conclusion is an analysis of the gas state in entropy diagrams. In essence, such an analysis, made while processing the data of each station's measurements, makes it possible most convincingly to show the correctness of the conclusion that the Venusian lower atmosphere is adiabatic.

ORIGINAL PAGE IS
OF POOR QUALITY

Fig. 45. P vs. T according to Venera measurements. Shown are the corresponding calculated curve of the polytrope index ξ and the theoretical curve of readings of the adiabat κ at the corresponding P and T. Designations same as in Fig. 42.

Key: a. kg/cm^2

On the "entropy-pressure" diagram for 97% CO_2 and 3%N_2 (Fig. 46), the curves of the change of gas state are shown for those portions where Venera-4 - -8 measured P and T. The narrow diagonal lines are isotherms. The thermodynamic parameters of carbon dioxide are here, as previously, taken from [36]. We will note that using the entropy diagram method in an analysis of the thermodynamic state of gas in the Venusian atmosphere from the data of Venera-4 measurements [1, 3, 186] /128 allowed us to estimate a value for pressure at the moment communications with the apparatus ceased -- thus by extrapolation of the curve P(h) to the last measured value of temperature on the assumptions that $(dP/dh)_{P=7.2}$ = const. and that the isoentropies S = const. The value $P = 17.6 \pm 2.8$ kg/cm^2, which was obtained at a level where $T = 535 \pm 17°K$, was confirmed by subsequent measurements.

The change of the parameters of the gas state in the atmosphere should satisfy the stability condition, which can be written in the form

(IV.13)

where S is the entropy of gas. Since for the measured temperature profile the mean value of the temperature gradient $\gamma < 0$, the stability condition assumes the form: $dS/dT \leq 0$. This condition is met, if the curves of the change of state on the entropy diagram have a negative slope or are parallel to the abscissa.

The data from the measurements of the Venera stations do not generally contradict condition (IV.13). Particularly characteristic in this regard is the curve of state constructed from the data /129 from Venera-8 measurements. If the large scale on the entropy

axis is kept in mind, it is possible to maintain that within the measurement error bounds, the gas state in the Venusian troposphere corresponds to isoentropy.

The dynamics of the atmosphere. An analysis of the results of measurements of radial velocity during parachute descent of the apparatus, as well as data from measurements of atmospheric parameters make it possible to obtain an estimate of the horizontal and vertical motions in the Venusian atmosphere.

It is natural to assume that as the apparatus descends in the atmosphere, the radial component of wind velocity enters directly as a factor into the measured (by the Doppler method) radial velocity of the DA; this is as a result of the wind almost completely deflecting the parachute. In order to sort radial velocity out of the measured values of full velocity, it is necessary to subtract all components related to the mutual motion of Venus and the Earth[5] and to their own rotation, as well as to subtract the component of quasi-uniform descent velocity of the apparatus on parachute in a quiet atmosphere. Of course, the inertia of the system and the complex aerodynamic character of descent in a real turbulent atmosphere can lead to a definite difference between the velocity of the parachute and fluctuations in wind velocity. We refer the reader who is interested in this question in detail to the work of Kerzhanovich et al [66] which evaluates the size of this difference on the basis of mathematical modelling of DA motion on parachute in the turbulent Venusian atmosphere.

The geometry of the DA's descent is shown in Fig. 47. Here v is the DA's velocity relative to the surface, u is the wind velocity, v_R and u_R are their radial components, v_V and u_V are their vertical components, and v_h and u_h are their horizontal components. The vertical and horizontal components of the wind velocity -- with coefficients of $\cos\zeta$ and $\sin\zeta$ respectively -- enter simultaneously into the radial velocity; here ζ is the local zenith angle of the Earth in the DA's landing site region:

$$u_R = -u\cos\zeta - u\sin\zeta\cos(\beta_u - \beta_A) \qquad \text{(IV.14)}$$

ORIGINAL PAGE IS
OF POOR QUALITY

A and β_u are the azimuths of the Earth and the wind velocities. The angle ζ is equal to the planetocentric angle between the DA's landing site and the subterrestrial point. Hence, it is clear that the larger the angle ζ, the more the horizontal component contributes and thus the more accurately it is measured. Here the horizontal component is considered to be the horizontal /130

[5] The period of Venus' own rotation is herein assumed to be equal to the synchronic.

ORIGINAL PAGE IS
OF POOR QUALITY

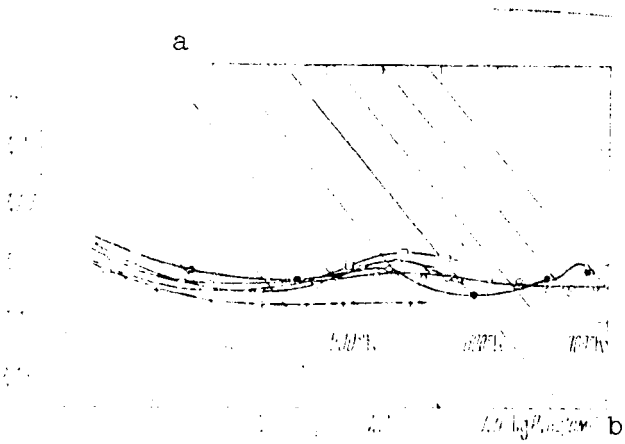

Fig. 46. Curves of change in gas state according to Venera measurements in an entropy diagram for a conditional composition of the atmosphere (97% CO_2; 3% N_2). Designations same as in Fig. 42.

Key: a. kcal/kg·deg
b. kg/cm^2

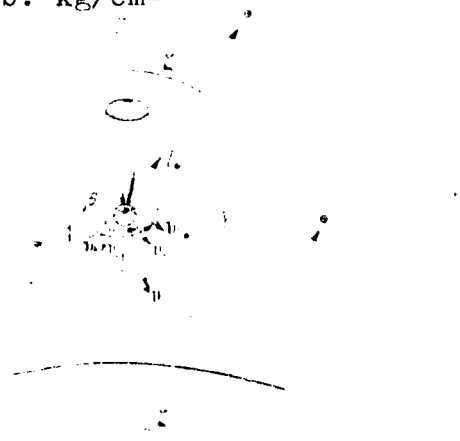

Fig. 47. Geometry of the DA parachute descent into the atmosphere [66]. Text gives explanations of the designations.

velocity component, which lies in a plane containing vectors of the DA's radial velocity and its local vertical. It is evident that the total value for horizontal velocity may be larger due to a component that is orthagonal to the specified plane and therefore does not contribute to v_R. u_h is consequently a lower bound on the horizontal wind velocity in the Venusian atmosphere.

The primary direction of the defined component depends also on the location of the region of descent in relation to the subterrestrial point. It is evident that if the descent takes place near the Venusian equator, then a zonal component of wind velocity is basically determined. If, however, it takes place a substantial distance from the equator, then an appreciable meridianal component may be present. The smaller the angle ζ and and the closer the DA's landing site region to the subterrestrial point (cf. Fig. 23), the more accurate the estimate of vertical velocity. Accordingly, both the vertical and horizontal components of wind velocity can be determined directly from the radial velocity measurements of Venera-4, Venera-7 and Venera-8.

The ambiguity in separating the contributions of the horizontal and vertical components of atmospheric motion can be resolved by several methods[6], all based on /131

[6] It is impossible to perform such a separation for turbulent fluctuations in wind velocity. Here, if needed, hypotheses about the structure of turbulence (for example, of isotropy) can be used.

computing an averaged vertical descent velocity for the DA solely from the measurements of atmospheric temperature and pressure. Basing oneself on these measurements (curves T(t) and P(t)), it is above all possible to estimate the limiting possible intensities of rising or falling flows on descent.

Having used the hydrostatic equation (IV.3), the quasi-uniform descent equation of an apparatus in the atmosphere (IV.5) and the equation of state for a perfect gas (IV.4) (which is accurate to 2 - 3% for CO_2 within the range of measured values for atmospheric temperature and pressure), but disregarding the co-factor $(1 - \rho/\rho_{DA})$ in Eq. (IV.5) as well as taking into account the effect of the expelling force at high densities, we obtain a linear differential equation of the form

$$d(P^{\eta}) = -1\frac{dt}{P^{\eta}} \quad \frac{\eta}{2H}P^{\eta}dt, \qquad \text{(IV.15)}$$

ORIGINAL PAGE IS OF POOR QUALITY

where, as before, $A = \left(\frac{M_{\bar{\mu}}\bar{\mu}}{2C_xFR}\right)^{\eta}$ is a constant determined by the aerodynamic and design parameters of the descent apparatus and is also dependent on $\bar{\mu}$, $H =$ is the scale height $\eta \neq v$ -- v'. It is evident that in the special case of $\eta = 0$, Eq. (IV.15) is reduced to the relation

$$d(P^{\eta}) = -1\frac{dt}{T^{\eta}}, \qquad \text{(IV.16)}$$

or, including (IV.4), to the similar analogous relation

$$dP = B\rho^{\eta}dt, \qquad \text{(IV.17)}$$

where $B = \left(g^{\eta}\frac{2M}{RC_xF}\right)^{\eta}$.

We note that combining Eqs. (IV.3) and (IV.5) provides a convenient method of checking to see whether the measurements of atmospheric parameters from the aerodynamics of parachute descent are internally coherent. This method was used extensively in the processing of the results of the Venera-4 - -6 measurements by Avduyevskiy et al [1, 3, 4, 186, 189]; Obukhov and Golitsyn [124] as well as Golitsyn and Kerzhanovich [46] made an independent examination for several special cases of the generalized Eq. (IV.15). We also note that Eq. (IV.15) and relations (IV.16 and (IV.17) make it possible, in the case of measurements of only one parameter (pressure, temperature, or density), to calculate the values of the other two, provided the design and aerodynamic characteristics of the apparatus and parachute are employed. Specifically, it directly follows from (IV.15) that

$$P = 2A\left(\frac{P}{T}\right)^{\eta} dP. \qquad \text{(IV.18)}$$

/132

where $C = \eta/H$; hence, if for example there are measurements for pressure only and supposing $\eta = 0$, one can determine the temperature[7]

ORIGINAL PAGE IS
OF POOR QUALITY

(IV.18')

In Fig. 48, curves are marked off on the coordinates $P^{1/2}$ and $\sqrt{T}$; these curves correspond to the measured (by Venera-4 - -8) values for pressure and temperature (for Venera-7, temperature and v_D); the solutions to equations (IV.15) with various η may be compared with these values. The conditions $\eta = 0$ and $A = \text{const}$. i.e., a straight line, correspond to the absence of vertical flows in the atmosphere and to a quasi-uniform descent of the apparatus. For Venera-4, these conditions are best met for a group of points lying in the region of pressures (3- 7 kg/cm^2). Taking into account the tolerances in the measurements of P and T, the limiting values $|\eta|$ on this portion are estimated to be not more than 0.2/0.4 m/sec and can grow to 0.5 - 1.0 m/sec at the beginning and end of measurements. The proportionality factor /133 $A \simeq \text{tg}\phi$ in (IV.16) is defined as $C_x/M \simeq A^{-2}$. It is in satisfactory agreement with the computed value of A at $C_x/M = 2.25 \cdot 10^{-3}$ kg^{-1}, which corresponds to the design parameters of the apparatus and the parachute. For Veneras-5 and -6 the experimental points averaged according to all measurements by various instruments still more satisfactorily fall on straight lines. The tangent of the angle of their slope (cf. Fig. 48) is in good agreement with a value A that corresponds to the relation $C_x/M = 1.7 \cdot 10^{-3}$ kg^{-1}. The values η are limited in the basic part of the measuring range by the value $\eta < 0.1/0.2$ m/sec, but at the beginning of descent they turn out to be considerably larger ($\eta \lesssim 1$ m/sec). Here, however, relative errors of measurements (they appear most strongly in derived estimates) can be quite important; therefore, the values obtained for vertical flows should be viewed as upper bounds.

This applies still more to an examination in the same coordinates of the results of Venera-7 measurements. The curve is evidence of a dynamically complex descent, which has several /134 phases; a conspicuous change in coefficient A corresponds to these phases. This change may in principle be attributed to vertical motions and to variations in aerodynamic characteristics. Specifically, variation in aerodynamic characteristics is related to variation in the slopes of the curves in Fig. 48; this variation conforms to the programmed deployment of the parachute on the descent of Venera-7 and Venera-8. In those regions where the values A, obtained from the experimental points, correspond to calculated values ($C_x/M = (1.08/2.23) \cdot 10^{-3}$ kg^{-1} for Venera-7

[7] This estimate makes sense of course only if measurements P(t) are highly accurate.

and $(1.44/2.23)\cdot10^{-3}$ kg^{-1} for Venera-8)[8], the values for vertical flows are estimated from the values $\eta \leq 1.5$ m/sec.

Let us move now to the more comprehensive quantitative estimates of the velocities of atmospheric motions as obtained by Kerzhanovich et al [66, 67, 377, 378].

ORIGINAL PAGE IS
OF POOR QUALITY

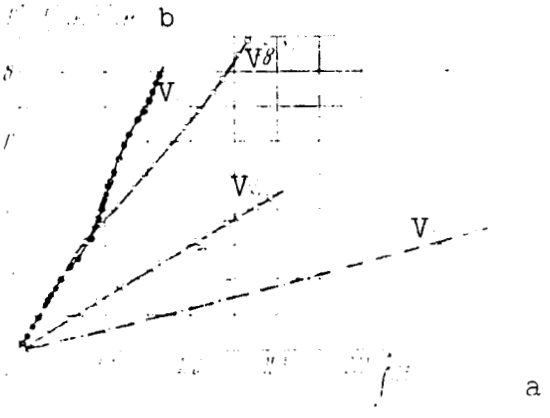

Fig. 48. Results of Venera temperature and pressure measurements in coordinates $P^{1/2}$ and

. Designations as in

Fig. 42. Comparison with calculation according to Eq. (IV.15) for estimation of η.

Key: a. $Sec/deg^{1/2}$
b. $kg^{1/2}/cm$

After subtracting the vertical component of descent velocity, which is calculated according to (IV.6) or (IV.8), the difference between Doppler frequency (radial velocity) and zero can be related only to the effect of wind or the previously specified systematic errors of measurement.

Fig. 49 shows the Doppler differences obtained in experiments on the Veneras-4 - -6 without compensation for temperature drift in the oscillators. Zero wind velocity is zero frequency value. The time of averaging is 6 sec for Venera-4 (Fig.49a) and 10 sec for Venera-5 and Venera-6 (Fig. 49b and 49c).

It is easily seen that /136 frequency variation of the signal received during the first 20 - 23 minutes from Venera-4 had, in contrast to Venera-5, a sharply pronounced non-monotonic character. It is not very probable that this variation was related

[8]Although that portion of the Venera-7's descent near the surface (after 8:34) also has an aerodynamically complex character, it can be used in an analysis of atmospheric dynamics, since the descent velocity for this portion relative to zero at the moment of landing can be calculated with acceptable accuracy. The point is that although the change in the aerodynamic drag coefficient C_x is not known here, it is highly probable that it was insignificant. This is indicated, first of all, by the monotonic change of the average velocity of the DA on this portion, and second, by the small relative increase in the Reynolds' number (less than 15%) when it has a large absolute value ($Re \approx 2.7\cdot10^7$). With such large Reynolds' numbers, motion becomes self-modelling and the value C_x ceases to depend on velocity; this is confirmed by experimental data.

ORIGINAL PAGE IS
OF POOR QUALITY

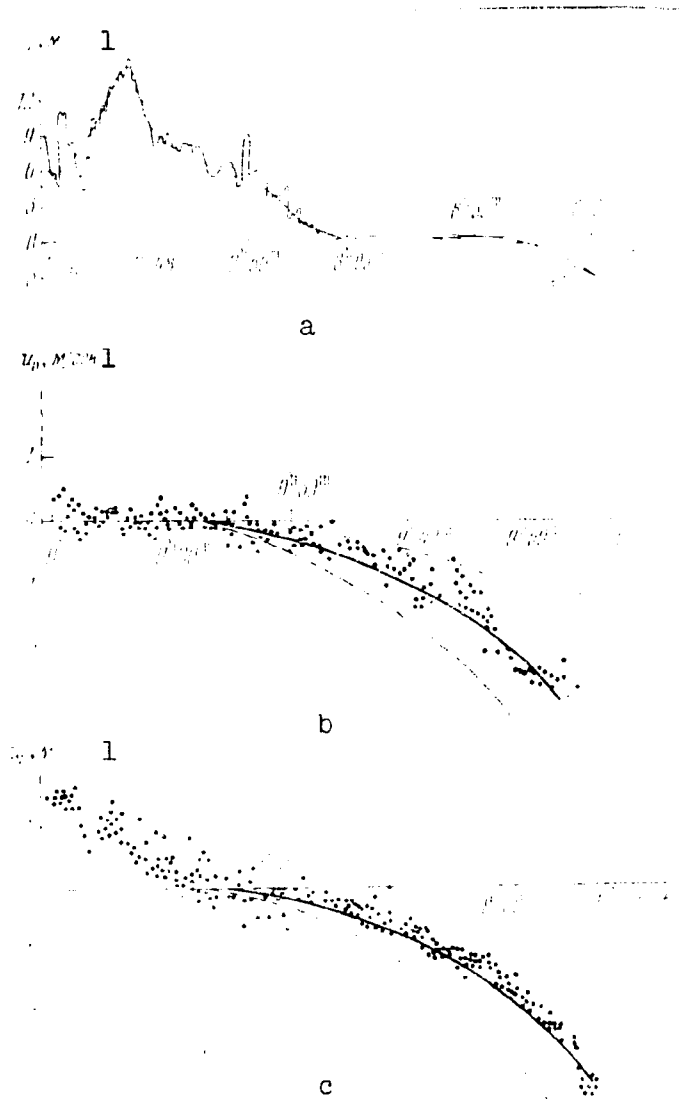

Fig. 49. Variation in radial component of DA velocity u_R vs. time for Venera-4, Venera-5 and Venera-6 (a, b, c). For Venera-5 and Venera-6, the vertical component of velocity u_V is shown, provided $u_R \approx u_V$. The dashed line is the calculated frequency-temperature drift of the oscillator: 1) is the most probable; and 2) and 3) are limiting values [377].

Key: 1. m/sec

to frequency variations in the oscillators themselves or to any other factors that could affect the conditicns of radio wave propagation. One may therefore consider the most likely reason for frequency variations on this portion of the descent was variation in the DA's velocity due to the wind.

ORIGINAL PAGE IS
OF POOR QUALITY

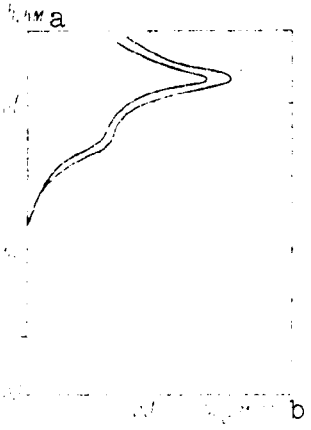

Fig. 50. An altitude profile of horizontal wind velocity u_h. This profile corresponds to the measured radial velocity in Fig. 49a [377]. The horizontal line on the ordinate is the possible systematic error of measurements. Explanation of curves 1 and 2 are given in the text.

Key: a. h, km
b. m/sec

Fig. 50 (curve 1) shows an altitude profile for wind velocity. It was obtained by graphical averaging of the data of the measurements in Fig. 49a -- on the assumptien that all frequency variation is related to the horizontal wind velocity. Curve 2 shows the horizontal wind velocity profile obtained by subtracting the limiting averaged velocity for vertical flow from the radial component of the DA's velocity. As we see, peak wind velocity could have been on the order of 40 - 50 m/sec at an altitude of about 50 km. As altitude decreases, velocity decreases, and below 40 km, it remains approximately constant within the limits of the systematic error shown in Fig. 50.

From the location of the Venera-4 descent region relative to the subterrestrial point (cf. Fig. 23) it follows that the measured velocity has a substantial meridianal component; a wind direction from the pole to the equator corresponds to positive values of this component. If, nonetheless, the latitudinal component is kept in mind and if the measured profile $u_h(h)$ is attributed to a zonal wind, the DA's maximum velocity would have reached no less than 30 m/sec in a direction from the antisolar point to the morning terminator; this coincides with the direction of the planet's own rotation.

Estimates of wind velocity from the data of measurements of radial velocity made in an experiment on Venera-7 are made only for those portions where the DA's descent was close to what was calculated.

Fig. 51 gives a wind velocity profile obtained as the difference between measured values v_R and calculated values v_V for velocity. Below, on the abscissa, is a scale that corresponds to the horizontal component of wind velocity; at the top is the vertical component. A wind from the antisolar point toward the morning terminator or a downward vertical flow correspond to positive values for velocity. The profile is constructed with a spatial averaging of measurements of ≃ 1 km, and the maximum constant systematic error is about 5 m/sec (from u_h).

ORIGINAL PAGE IS
OF POOR QUALITY

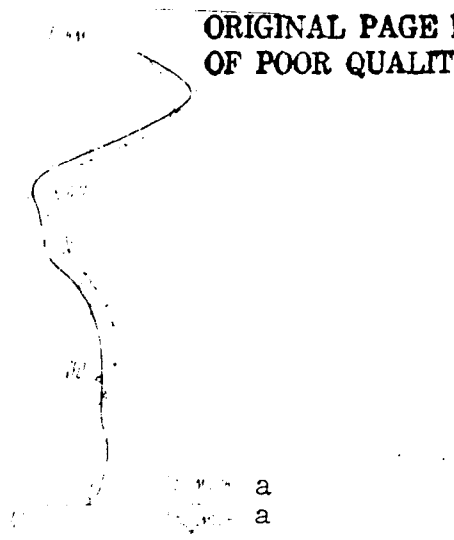

Fig. 51. Altitude profiles for horizontal (u_h) or vertical (u_v) components of wind velocity according to measurements of radial velocity on Venera-7. Curves 1 and 2 are two alternatives of calculating v_V from Eqs. (IV.6) and (IV.8) [377].

Key: a. m/sec

If the entire difference is attributed wholly to the horizontal component of wind velocity u_h, then it follows from an examination of Fig. 51 that the wind velocity reaches 10 - 14 m/sec at an altitude of 45 km and is in the direction of the morning terminator. The further behavior of profile $u_h(h)$ may be interpreted either as an indication that at an altitude of about 42 km the wind velocity changes direction and that at 40 km it is 5 - 7 m/sec or as a reduction in velocity with no change of direction. This is related to the fact that the accompanying systematic error can shift /138 the curves in Fig. 51 as a whole, as article [377] noted. In this case, wind velocity should be higher. Subsequent measurements on Venera-8 make such an assumption more justifiable. They also confirm the possibility of indications that the wind velocity grows to ≃ 100 m/sec at altitudes of 52 - 54 km; these indications were from the measurements of the Venera-7 radial velocity on the initial portion of descent (between 8:02:50 and 8:04:20 Moscow time). If it is presumed that during the

descent only vertical motions occurred, then the corresponding velocities did not exceed 1.2 - 3 m/sec for downward flow and 1 - 1.4 m/sec for upward flow; while below 38 km they remained less than 0.5 - 0.7 m/sec.

Comparison of the measured values v_R and the calculated values v_v for velocity on the final stage of the Venera-7 descent gives rise to the wind velocity profiles at altitudes of 0 - 3.5 km shown in Fig. 52. In order to eliminate the possible influence of short-term fluctuations in velocity, the curves shown are upper bounds obtained from measurements averaged over an interval of 30 sec, i.e., about 500 m, even though wind drag time of the DA on this stage should not exceed 4 - 5 sec. Assuming that $u_h = u_v = 0$ at the surface, it is possible to assume that wind velocity increases smoothly up to 2.5 m/sec (maximum 5 m/sec) at an altitude of 3.4 km. The corresponding possible values for the velocity of upward flow at this altitude would not exceed 0.5 m/sec (maximum 1 m/sec). However, these estimates are in no way appreciably outside the limits of the assumed range of errors of measurements. /139

A Venera-8 experiment made the most complete and accurate measurements of wind velocity. Fig. 53 shows an altitude profile for wind velocity, a profile showing the difference between the measured radial velocity v_R and the calculated vertical descent velocity v_v. The horizontal lines denote the errors of measurements of v_R (the constant systematic error is < 0.2 m/sec, the slowly varying error is from 0 m at the surface to 0.7 m/sec at h ≈ 50 km, and the fluctuation error is < 0.1 m/sec) and the inaccuracy of calculations of v_v according to Eqs. (IV.6) and (IV.8) (from 0.5 m/sec at the surface to 7 - 8 m/sec at h ≈ 50 km). The variation with altitude is analogous to the altitude profiles T(h) and P(h) in Figs. 42 and 43.

Because of the great distance between the landing region and the subterrestrial point, the conditions for determining the horizontal component of wind velocity from Venera-8 data are quite favorable. Since the component of velocity in a direction from the subterrestrial point to the DA (the azimuth of this direction, as reckoned from the direction toward the North pole is $\theta \approx 115°$) was determined from measurements of v_R, then a wind component close to the zonal and directed from the morning terminator toward the day side (i.e., in the direction of the planet's own rotation), as well as a small meridianal component in a direction from the equator toward the South pole[9] should /140

[9] Various values and directions for wind velocity may in principle correspond to the measured component, so that their projection in a "subterrestrial point - DA" direction equals the measured component. Specifically, it is impossible to say anything about a possible orthagonal component. Keeping this in mind, we here speak of the measured component simply as the wind velocity; it is understood in this regard that the wind velocity may in fact be even larger.

ORIGINAL PAGE IS
OF POOR QUALITY

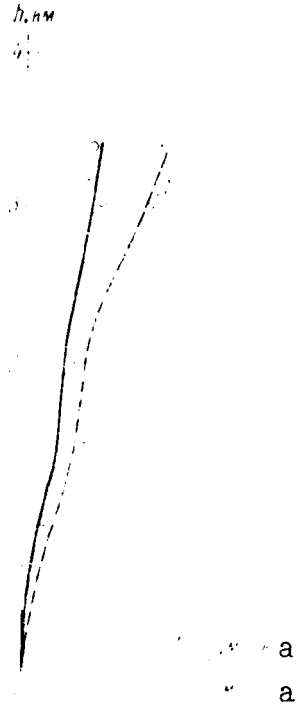

Fig. 52. Wind velocity profile for the near-surface layer of the atmosphere according to Venera-7 data. Curve 1 is the limiting value of the most probable u_h (or u_v) and curve 2 is for the maximum temperature-caused frequency drift of the oscillator.

Key: a. m/sec

correspond to positive values for u_h.

The profile of wind velocity has a series of characteristic features. First, an increase with altitude from $0.5\ ^{+0.25}_{-0.75}$ near the surface to 100 - 140 m/sec at altitudes near 50 km is clearly discerned. Second, there is a region from 18 to 40 km where the wind velocity almost did not change and was 30 - 38 m/sec. We note that such behavior in u_h can be related to the wind turning in a meridianal direction. Third, in the lower troposphere at altitudes of 0 - 10 km, where about half the mass of the atmosphere is concentrated, the wind velocity is less than 3 m/sec (mean velocity $\approx$ 1 m/sec). Altitudes from 11 to 18 km and from 42 to 50 km are regions of abrupt change of wind velocity, with gradients up to 4 - 6 m/sec/km. Here, the lower region (of large gradients of wind velocity) lies essentially lower than the boundary h $\approx$ 32 km; above this, the aerosol component associated with an extensive cloud layer (cf. Section V.4) makes a marked contribution to the attenuation of solar radiation.

Estimates for the near-surface region, as in the case of Venera-7, do not generally go beyond the limits of the possible range of errors, but the range itself is substantially narrowed. Let us remember that the calculated values u_h for Venera-7 were obtained on the assumption that the wind velocity near the surface is zero. If this assumption is not made, then the curves in Fig. 52 show a difference between the wind velocity at a given altitude and the wind velocity in the near-surface region.

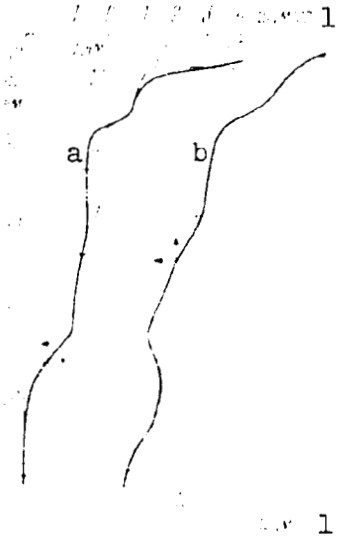

Fig. 53. Altitude profile for horizontal wind velocity according to data from Venera-8 measurements. α is at altitudes 0 - 52 km; δ is for altitudes 0 - 12 km. The horizontal bars are the maximum possible errors of measurement [67].

Key: 1. m/sec

ORIGINAL PAGE IS OF POOR QUALITY

Unfortunately, the upper bound u_h according to Venera-8 data does not also give a value for velocity in the border layer.[10]

We will now turn to /141 the results of an analysis of wind velocity fluctuation [377].

Velocity fluctuations may be obtained by subtracting the averaged values for wind velocity from the wind velocity itself. In so doing, naturally, a definite arbitrariness is assumed; it is connected to the conditionality of dividing the wind velocity into the mean and the fluctuation components and to the inaccuracy of the averaging itself. Therefore, slight corrections that take the DA's inertia into account were introduced into the experimental values for velocity fluctuations [66].

The influence of the system's inertia is important during motion in a less dense medium, i.e., at high altitudes. One of the fundamental parameters that characterize the behavior of a parachute under the impact of turbulence is the drag time of the "parachute - DA" system τ_d. One may define the value τ_d as the time after which a velocity change of the descent apparatus will differ from a change of the wind velocity by not more than 10%. For velocity fluctuations with a characteristic time exceeding the drag time and space scale exceeding the value $l_{min} = \tau_d \cdot v_s$, the DA-parachute system reproduces fluctuations of wind velocity practically without distortion. For small-scale fluctuations of wind velocity, one can make only qualitative estimates of turbulence from the behavior of the DA parachute system. The drag time decreased during descent from 5 to 2 sec for Venera-4, from

[10] It is possible to show that by using the measured wind velocity in the boundary layer, a temperature distribution near the surface can be constructed. However, on this portion of the descent, the difference in velocity for an adiabatic and an isothermal atmosphere does not exceed 0.1 m/sec; consequently, the required accuracy is substantially higher than what has been attained in these measurements.

8 to 4 sec for Venera-5 and Venera-6, from 12 - 15 to 4 - 5 sec for Venera-7 and from 8 to 1 sec for Venera-8. Such differences in values τ_d are connected to a difference in descent velocity: for Venera-4, the difference was about 10 m/sec after parachute deployment, and for Venera-7 it was about 60 m/sec. Correspondingly, the minimum resolved scale of turbulence is: 50 - 10 m for Venera-4, 200 - 10 m for Venera-5 and Venera-6, from 900 - 1000 m to 80 - 100 m for Venera-7, and 500 - 10 m for Venera-8.

The root mean square for wind velocity fluctuations u'_h during descent of Venera-4 up to 8:02 (about 42 km) is 0.75 m/sec /142 (cf. Fig. 49a); at a mean wind velocity of about 20 m/sec for this portion of the descent, this corresponds to a relative intensity of turbulence $\Psi = \sigma u'_h/u_h \approx 0.04$.

Fig. 54 shows the time correlation function of fluctuations of the vertical wind velocity component obtained by 20 min of averaging. The correlation function decreases quickly at $\tau \approx 25$ sec, which corresponds to a scale of turbulence of about 100 - 200 m (if turbulence is considered to be homogeneous) when the mean descent velocity on this portion is ≈ 8 m/sec.

ORIGINAL PAGE IS
OF POOR QUALITY

Fig. 54. Time correlation function of fluctuations in the vertical wind velocity component [377].

Key: a. m^2/sec^2
b. t/sec

As seen from Fig. 49b and Fig. 49c, fluctuations in the vertical component of wind velocity during the descent of Venera-5 and Venera-6 were within the errors bounds of measurements for the whole range of time scales from 2 - 10 sec to 10 - 20 min. The small difference at the beginning of the Venera-6 descent between measured and calculated velocity is probably connected with error in the determination of descent velocity. The root mean square value for fluctuations was practically constant and was equal to 0.28 - 0.32 m/sec for Venera-5 and 0.24 - 0.28 m/sec for Venera-6. The maximum values for fluctuations do not exceed 0.5 m/sec. Assuming isotropic turbulence, the same upper limits are also obtained for fluctuations in horizontal velocity.

If it is assumed that the relative intensity of turbulence $\Psi = \sigma u'_h/u_h$ in the Venusian atmosphere has the same order of magnitude as it has in the Earth atmosphere, it is possible to estimate the value for wind velocity indirectly. According to experimental data [18] the value Ψ depends on wind velocity and altitude; even in the free atmosphere of the Earth it is equal to

0.02 - 0.1 (for Venera-4, $\Psi = 0.04$). Then, at $\sigma u'_h \approx 0.3$ m/sec we obtain a wind velocity of not more than 3 - 15 m/sec throughout the entire descent of Venera-5 and Venera-6; this is of course a rough estimate. It should be noted, moreover, that 0.3 m/sec is the limit of the error of measurements; yet the actual value for fluctuations in velocity was apparently much less. /143

IV.4. The Results of the Mariner-5 Measurements

The American spacecraft Mariner-5 flew past Venus on October 19, 1967 (the day after Venera-4 descended into the atmosphere) at a minimum distance of 4100 km from the planetary surface.[11] Fig. 55 shows a diagram of the Mariner-5 fly-by trajectory in an equatorial projection and Fig. 23 marks the regions where radio probes of the atmosphere on the night and day sides took place. As the spacecraft passed behind the planet, this region was located in the northern hemisphere at latitude 37°N at a solar zenith angle of 142.3°. As it came from behind the planet, this region was located in the southern hemisphere at latitude 32.4°S at a solar zenith angle of 33.3°.

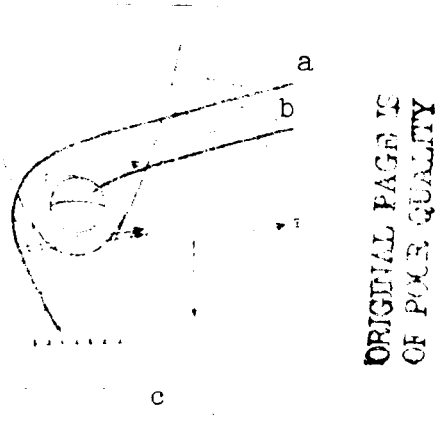

ORIGINAL PAGE IS
OF POOR QUALITY

Fig. 55. Diagram of the fly-by trajectory of the Mariner-5 spacecraft in an equatorial projection. ⊙ and ⊕ designate the directions toward the Sun and the Earth. The dashed line is the conditional boundary of the shock wave. The dotted-dashed line is the ionopause.

Key: a. Mariner-5 b. Venera-4 c. Solar wind

The probing of the atmosphere took place at three ranges of radio waves -- at frequencies f_1 = 49.8 MHz, f_2 = 423.3 MHz, and f_3 = 2297 MHz. Measurements in these frequencies provided information about the parameters of the planet's neutral atmosphere and ionosphere.

The works of Kliore et al and Fjeldbo et al [304, 305, 382, 578] contain a detailed analysis of the method and a description of the characteristics of the radio equipment. We will limit ourselves here to a short account of the fundamental principles directly related to obtaining experimental results.

Fig. 56 shows a diagram that gives some notion about the geometry of radio wave propagation, relation to altitude, and the connection of

[11] See the note on p. 76. The distance between Mariner-10 and the planetary surface at periapsis was 5785 km.

the recorded phase of the received radio signal to the fly-by trajectory of the spacecraft.

ORIGINAL PAGE IS
OF POOR QUALITY

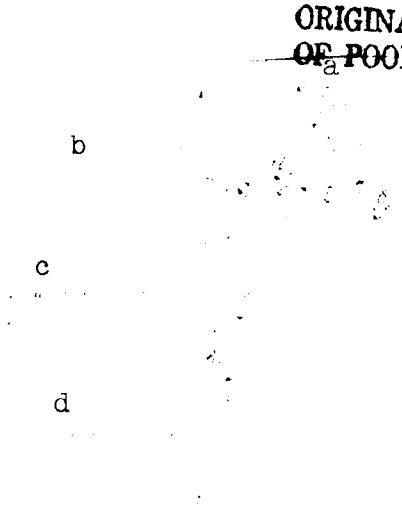

Fig. 56. The geometry of radio-wave propagation and the relation of angles that enable an altitude correlation to be made in a radio refraction experiment [305]. Cf. the text for the explanations of the designations.

Key: a. Spacecraft
b. Planet
c. Ray path asymptotes
d. Ground tracking station

As the Mariner-5 passed behind the planet, the increasing atmospheric density increased the effective path, because of the bending of the radio ray as a result of refraction;[12] defocused the signal as well, because of change in the gradient of the refractive index; and as a result, caused a "blurring" of the radio ray to a large solid angle. The combination of these effects was recorded at ground tracking stations in the form of frequency-phase changes of the radio signal and as a weakening of its power level. The results of these measurements together with data from measurements of trajectory parameters, as well as a prognosis of the spacecraft's motion in the immersion region, provide the necessary starting material for a calculation of atmospheric characteristics.

The limiting altitude /145 resolution achieved in radio occultation experiments is determined by the size of the first Fresnel zone. If there is no atmopsheric refraction, the size of these zones for ranges f_1, f_2, and f_3 were were 14, 5 and 2.4 km respectively. Due to the effects of refraction, the curvature of the wave front increases, and the Fresnel zones instead of becoming circular, become elliptical, wherein the minor axis of the ellipse is oriented in a vertical direction. The altitude resolution is slightly higher in those regions of the neutral atmosphere that cause defocusing; conversely, the

[12] Strictly speaking, not only refraction influences the shift of phase; the difference between radio wave propagation velocity and the speed of light in free space also influences the shift of phase. However, the magnitude of this effect is negligible and it is possible to disregard it.

the resolution is reduced in those portions of the ionosphere that produce focusing.

The detailed structure of the studied region of the atmosphere and its relation to a planetocentric coordinate system depends directly on the accuracy of the trajectory measurements. Although close to Venus the measurements of Mariner-5 location and velocity were made in an incoherent mode (because of the high rate of frequency deviation (up to 50 Hz/sec) and severe defocusing of the signal), predictions of motion upon immersion and emersion were accurate enough to assure a good altitude correlation. Overall frequency variation caused by atmospheric influence only was about 16 kHz.

Frequency change in an electromagnetic wave is related to the velocity of the source by the simple relation

ORIGINAL PAGE IS
OF POOR QUALITY

(IV.19)

where f_s is the transmitted frequency, ϕ is the angle between the velocity vector and the direction to the tracking station, with radio ray bending due to refraction included.

In the actual geometry corresponding to the conditions in which the Mariner-5 experiment was made (cf. Fig. 56), the form of relation (IV.19) becomes more complex when the motion of both the spacecraft and the tracking station are considered -- even though the structure of the relation remains similar. In a cylindrical coordinate system for a dual frequency experiment, it is written in the form [305]

$$\nu_r = \left[f_s \frac{v_{rs}}{c} \cos(\beta_s - \beta_r) - f_s \frac{v_{zs}}{c} \sin(\beta_s - \beta_r) + \right.$$
$$f_s \sin(\delta_s - \delta_r) \frac{v_{rs}}{c} - f_s \frac{v_{zs}}{c} \cos(\delta_s - \delta_r) \Big] -$$
$$- \left[f_s - f_s \frac{v_{rs}}{c} \cos\beta_s - f_s \frac{v_{zs}}{c} \sin\beta_s - f_s \frac{v_{rs}}{c} \sin\delta_s + f_s \frac{v_{zs}}{c} \cos\delta_s \right].$$

(IV.20)

where v_{rs} is the spacecraft velocity in the radial direction, v_{zs} is the spacecraft velocity in the z direction, v_{rt} is the velocity of the tracking station in the radial direction, and v_{zt} is the velocity of the tracking station in the z direction. The angles involved in the above equation are defined in Fig. 56. The angle of refraction α is defined as $\alpha = \delta_r + \beta_r$. The distance from the planet's center of mass to the asymptote in the direction of radio ray propagation, i.e., the shortest distance from the center of

mass to the line of sight a, is expressed in the following form [305]:

/146

$$\cdot \quad (r^2 + a^2)^{1/2} \sin(\beta_e - \beta_r - \gamma).$$

The dependence of frequency variation on the refractive index is expressed by the relation

$$\Delta f_D = \frac{f_0}{c} \frac{d}{dt} \int_{-\infty}^{+\infty} (n - 1)\, dl, \tag{IV.21}$$

where the integration is done along the line of sight l. The measured value Δf_D is in general the sum of two refractive effects -- a positive effect in a neutral atmosphere and a negative effect in an ionized medium. The use of Maxwell equations allows us to obtain an expression for a complex index of refraction whose real part entering into (IV.21) can be presented in the form

$$n = n_n^2 - n_e^2, \tag{IV.22}$$

wherein

ORIGINAL PAGE IS
OF POOR QUALITY

$$n_e^2 = 1 - \frac{e^2 N}{\pi m_e f^2}.$$

Here: n_n and n_e are the coefficients of radio-wave refraction in a neutral and ionized medium; m_e and e are the mass and charge of the electron; and N is the electron concentration along the line /147 of sight. If the spatial coordinates of the transmitter, planet, and receiver are shown, then one may calculate the dependence of the refractive index on the radial distance r, i.e., $n(r) = n_n(r)$, $n_e(r) \approx 0$, from the frequency effects Δf_D which are caused by a neutral gas of variable density. With this aim in mind, one may use the integral equation for optical refraction (a special case of Abel's equation, which connects the values $\alpha(a)$ and $n(r)$), or the slightly simpler "adjustment" method. In the latter case, the atmosphere, presumed to be spherical and symmetrical, is broken into a series of concentric layers; a single point on the experimental curve $\Delta f_D(t)$ corresponds to each one of the layers. For these layers, beginning from the topmost, there are successively computed values n at radial distance r, values that correspond to a bending of the radio ray determined by the angle of refraction α. Since the radio ray passes through all previous layers as it moves to a lower layer, the bending they cause is computed, so that in order to determine the refractive index of this layer, the remaining difference of the corresponding angle of refraction α is used. Repeating this procedure for all layers allows us to obtain the profile n(r).

From the altitude profile of the refractive index (or the refractivity $I(r) = (n - 1) \cdot 10^6$), it is not difficult to calculate

the atmospheric characteristics, if it is kept in mind that the refractive index of atmospheric density is proportional to the condition of hydrostatic equilibrium (IV.3). The density gradients are related to the gradients of the refractive index by

$$\frac{dn}{dr} = c\frac{d\rho}{dr} \qquad \text{(IV.23)}$$

ORIGINAL PAGE IS
OF POOR QUALITY

The coefficient c depends on the chemical composition of the atmosphere. For carbon dioxide c = 0.23 cm^3/g; possible small contributions of N_2 are of little influence. Because the scale height of altitudes vs. density $H_\rho = -\frac{\rho}{d\rho/dr}$, knowing ρ and and $d\rho/dr$ allows one to determine the value H_ρ for all conditional isothermal layers corresponding to the number of division, in whose bounds a constancy of the scale height is assumed. The /148 temperature is easily computed from H_ρ at a specified μ, and the pressure P(h) is determined from the gas-state equation (IV.4). It is evident that the larger the number of layers the curve n(r) is divided into, the more accurately the real temperature and pressure profiles are approximated. The accuracy of the results obtained depends directly also on the errors of the method itself, specifically on the stability of the onboard oscillator. According to [304, 305], the accuracy of measurements is slightly lower at altitudes of more than 70 km, while below this level the error in computed values of T(h) and P(h) is not more than $\pm$ 1%.

Additional information about the atmosphere is given by analysis of measurements of the attenuation of radio signals due to defocusing leading to a decrease in its amplitude. This amount -- the attenuation of the electromagnetic wave -- can be computed from a relation that holds true for an isothermal atmosphere at small bending of the ray:

$$\Gamma(r) \quad \frac{\Phi_0}{\Phi} \quad \frac{L \cdot \ell}{L+\ell} \cdot \frac{(n-1)^2 (2\pi)^3}{\pi^2} \exp\left(-\frac{4}{\pi}\right) \qquad \text{(IV.24)}$$

where Φ_0 is the intensity of the signal in the absence of refraction, Φ is the intensity of the signal with refraction, L is the distance from the observer to the source, and ℓ is the distance from the observer to the planet. The refractive index n refers to the layer from whose base h is reckoned at H = const. By using this method, it is possible in principle to determine altitude profiles for atmospheric temperature and pressure at frequencies f_1 and f_2 independently of radio refraction measurements at frequency f_3. The ground station transmits signals at these frequencies and a transmitter on a spacecraft retransmits this signal; the signal passes therefore twice through the Venusian atmosphere. At frequency f_1, however, the signal was affected quite severely by ionospheric scintillations and multipath propagation and therefore turned out to be ill-suited to the study of the

characteristics of the neutral atmosphere. The data at f_2 may be used for this purpose, if one begins from the assumption that true absorption by the atmosphere is absent and that the radio signal's amplitude varies monotically with decrease in altitude.

The altitude profiles for the atmospheric parameters for the night and day sides -- as obtained from the Mariner-5 radio refractivity measurements -- are shown in Fig. 57 (temperature) /149 and Fig. 58 (pressure) [305]. The results correspond to values of numerical density $n = \rho \bar{\mu}$ assuming 100% CO_2 or 95% CO_2 and 5% N_2; these values are computed from averaged values $\alpha(a) \approx n(r)$ in the limits of layers 0.1 km thick. The curves T(h) and P(h) correspond to the results of measuring the amplitude of the radio signal at frequency f_2 and are generally in good agreement with refractivity data. It should be remembered that error in amplitude measurements grows quickly with decrease in altitude due to the rise in noise level.

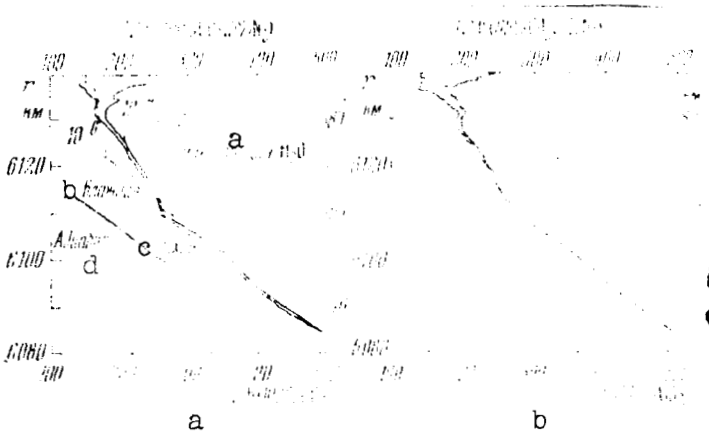

ORIGINAL PAGE IS
OF POOR QUALITY

Fig. 57. Atmospheric temperature vs. planetocentric distance (r) or vs. altitude (h) from the Mariner-5 measurements on the day (a) side and night (b) side of the planet. The results are given in two scales of T and conditionally include a possible difference in atmospheric composition (100% CO_2 and 95% CO_2, 5% N_2). The scale of altitude above the surface is given assuming R_{φ} = 6050 km. The dashed lines are H_2O saturation lines for various mixing ratios f_{H_2O} [305].

Key: a. H_2O concentration
b. Wet
c. Dry
d. Adiabats

The measurements whose results are shown in Figs. 57 and 58 cover a range of altitudes from about 35 to about 90 km. Close to 90 km, there are marked changes in the radio signal due to the influence of the neutral atmosphere. The lower level is the altitude at which super refractive conditions in the atmosphere are reached, i.e., the radius of curvature of a ray is equal to /150 the radius of the planet. Statton [520] examines in detail the peculiarities of optical and radio refraction on Venus.

The Mariner-10 radio refractivity measurements [577] are generally in good agreement with the results shown in Figs. 57 and 58. For this experiment, frequencies of 2295 MHz (similar to f_3 on Mariner-5) and 8415 MHz were used. The noise temperatures of the receivers were 13.4°K and 21.5°K respectively. Immersion occurred on the night side at a point whose coordinates were (in IAU nomenclature) 0.9°N and 69.5°E at a solar zenith distance of the Sun of 117.6°; and emersion occurred on the day side at a point whose coordinates were 56.3°S, 236.4°E at a solar zenith distance of 67.1°. The angle of the maximum ray curvature for the chosen geometry of the fly-by trajectory was 12.6°, which allowed probing at a frequency f_3 to 40 km above the surface (at R_{φ} = 6052 km). At a frequency of 8415 MHz, a rapid fading of the signal was noted at 51 km.

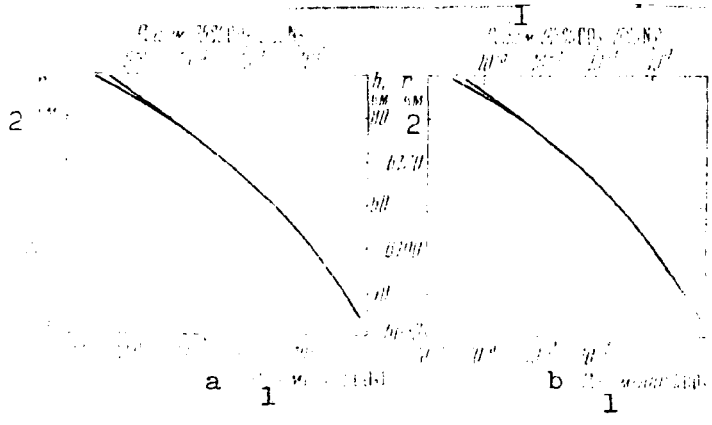

ORIGINAL PAGE IS
OF POOR QUALITY

Fig. 58. Atmospheric pressure vs. planetocentric distance (r) or vs. altitude (h) from the Mariner-5 measurements on the day (a) and night (b) sides of the planet [305]. See explanations for Fig. 57.

Key: 1. atm
2. km

We have not yet dealt with the question of true absorption of radio waves by the Venusian atmosphere. Yet it is possible to obtain specific data about its structure from the character of this absorption.

Loss coefficient profiles at frequency f_3 (in units db/km) /151 as a function of altitude on the planet's day and night sides, profiles obtained by averaging over intervals from 0.5 to 4 km, as shown in Fig. 59 is according to [305]. The loss in radio signal due to defocusing was calculated by using data on measurements of amplitude of the signal at frequency f_2 or by introducing a calculated correction for the magnitude of this effect into the measured values at f_3. In so doing, the remaining fine structure of the profile turns out to be variable; this, generally speaking, does not allow any general conclusions about the relation between individual anomalies and the actual structure of the atmosphere. Nevertheless, it follows from an examination of the curves on Fig. 59 that the losses, which are probably connected with absorption or turbulence, occur below 50 - 54 km; and between 37 and 50 km they are equal on the average to $(4 - 5)\cdot10^{-3}$ db/km. At the same time, two relative maxima, which are localized near 40 and 47 km and which do not appear on the day hemisphere, are noted on the night side. We will devote some attention to the possible causes of this behavior of the radio signal when we discuss the structure of the atmosphere.

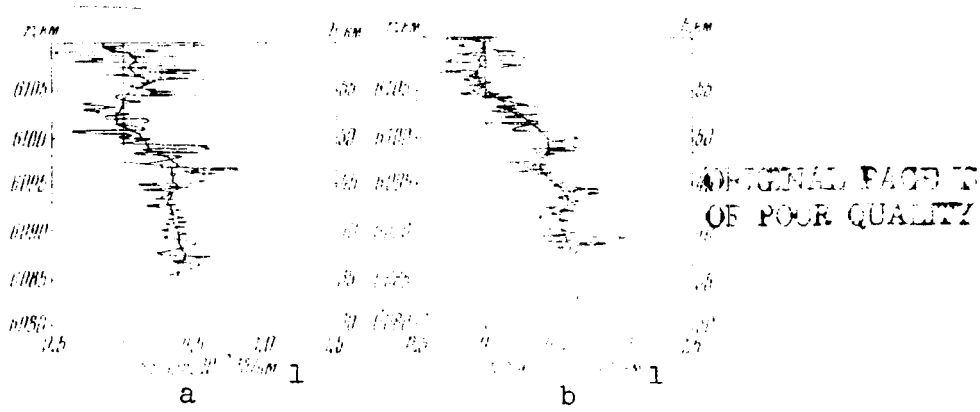

ORIGINAL PAGE IS
OF POOR QUALITY

Fig. 59. Variation in the loss of the radio signal at frequency f_3 (loss coefficient profile) on the day (a) and the night (b) sides of the planet [305]. Cf. explanation in Fig. 57.

Key: 1. Attenuation, 10^{-2} db/km

IV.5. Estimates of Water Vapor and Ammonia Content in the Venusian Troposphere From Radio Astronomy Measurements

Measurements of water vapor content on Venera-4, Venera-5 and Venera-6 refer to the upper regions of the planetary troposphere, where pressures are about 1 atm. It is possible to expect that in connection with phase transitions of water, the altitude distribution of relative water vapor content will not be constant. In the Earth's atmosphere, the relative humidity is highest at the surface

ORIGINAL PAGE IS
OF POOR QUALITY

and diminishes with altitude [166]. This is in connection with the fact that water vapor is formed on the surface of the Earth and then diffuses into the atmosphere. The circulation of water in the Earth's atmosphere is completed by precipitation, such as rain and snow, which transport the water from the clouds to the surface. The circulation of water on Venus is quite different from that on Earth. In the atmosphere of this planet, water cannot exist as a liquid below a level whose temperature and pressure are 430°K and 5.5 atm (cf. Fig. 69). Therefore (if there is no constant source of water formation on the surface due to the process of melting and degassing the substance of the mantle), the formation of water vapor should occur not on the surface, as on Earth, but at a sufficiently high altitude. In this case, water vapor penetrates into the lower troposphere due to diffusion and turbulence, and the relative content of water vapor will decrease as the surface is neared.

The experimental testing of this assumption can be done on the basis of data of radio astronomy and radar astronomy measurements. An analysis of UHF radio emission absorption in the Venusian atmosphere, the amount of which strongly depends on water vapor content, is the basis of such estimation. For a rigorous solution to this problem, it is necessary to know the distribution of water vapor vs. altitude. However, since according to (II.31) absorption by water vapor is proportional to a total pressure P and absolute humidity a, the lower troposphere makes the greatest contribution to this absorption. Therefore, the abundance of water vapor in the lower troposphere determines such absorption.

For a 97% CO_2 atmosphere, whose temperature and pressure are /153 defined by the model given in the Appendix, radar cross section measurements at wavelength 3.8 cm is $\sigma_r = 0.017$, which is in agreement with those determined for longer wavelengths of $\lambda > 20$ cm, that is, $\sigma_{r0} = 0.15$ (the optical thickness of the atmospheere at 3.8 cm wavelength is $\tau_{3.8} = 1.1$). This corresponds to a relative water vapor content in the lower troposphere of $f_{H_2O} = 0.1\%$. In this, the calculated dependence $\sigma_r(\lambda)$ is also in good agreement with the experimental data at the intermediate wavelength $\lambda = 12.5$ cm (cf. Fig. 15). Variations of f_{H_2O} from 0 to 0.2% are possible within the measurement error $\Delta\sigma_r = \pm 0.010$ [144].

In addition, an analysis of the results of measuring the wavelength dependence of the brightness temperature of Venusian radio emission indicates a lower relative water vapor content in comparison to the Venera-4, -5, and -6 measurements, which were made at an altitude of about 50 km.

Fig. 60 (using the data from Table 5) shows the results of /154 measurements $\bar{T}_{B\,♀}(\lambda)$ and a calculation of this dependence for a model for two values of relative water vapor content f_{H_2O} = 0.1% and 0.5%. The experimental data correspond better to the calculation for $f_{H_2O} = 0.1\%$ than for $f_{H_2O} = 0.5\%$.

Janssen et al [360] have made the most recent estimate of water vapor content in the lower atmosphere of Venus. They made special radio astronomy measurements at wavelengths close to the water vapor absorption line. A comparison of the brightness temperature $\bar{T}_{B\varphi}$ that they measured at six wavelengths with the spectrum $T_{B\varphi}(\lambda)$ calculated for $f_{H_2O} = 0$ and 0.5% (Fig. 61) shows that the calculation and the measurements are not in correspondence at $f_{H_2O} = 0.5\%$. (The measured brightness temperature is in agreement with a CO_2 atmosphere with a possible upper limit $f_{H_2O} \leq 0.2\%$). Because there is no gap in the measured spectrum $\bar{T}_{B\varphi}(\lambda)$ at the wavelength of the water vapor absorption line, $f_{H_2O} \leq 0.4\%$. These same authors, using radio interferometry measurements with a base of up to 20,000 wavelengths, made a second, independent estimate of f_{H_2O}. The determination of the limb darkening and the equivalent diameter of the emitting disk at a frequency of 22.1 GHz ($\lambda = 1.35$ cm) and a comparison with the results of measuring the same parameters at a frequency of 25.4 GHz (Fig. 62) likewise do /155 not indicate the presence of water vapor; they are in good agreement only with CO_2 absorption. According to radio interferometry measurements, the upper level of relative water vapor content is $f_{H_2O} \leq 3.5 \cdot 10^{-3}$.

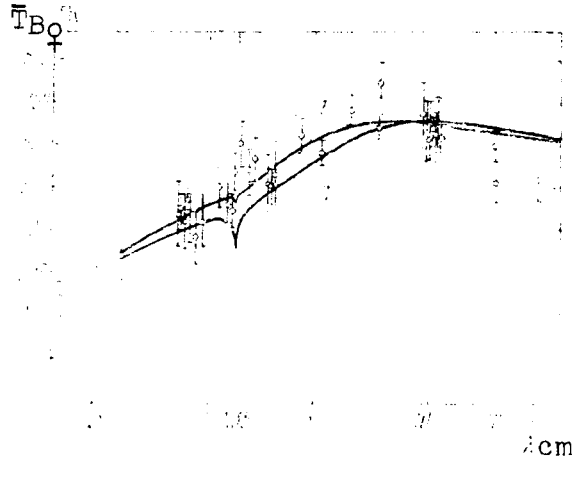

Fig. 60. The measured and calculated dependences of the average (for the apparent disk) brightness temperature of Venus $\bar{T}_{B\varphi}$ at wavelength λ for different water vapor contents: 1) $f_{H_2O} = 0.1\%$; 2) $f_{H_2O} = 0.5\%$.

ORIGINAL PAGE IS OF POOR QUALITY

Thus, according to radio astronomy and radar measurements, the relative water vapor content in the lower atmosphere of Venus is $f_{H_2O} = 0.1 \pm 0.1\%$.

Good agreement between calculated and measured spectra of the radar cross section $\sigma_r(\lambda)$ and the brightness temperature $\bar{T}_{B\varphi}(\lambda)$ for a carbon dioxide atmosphere with an addition of about 0.1% water vapor obviates the need to include any other components that absorb UHF radiation in the composition

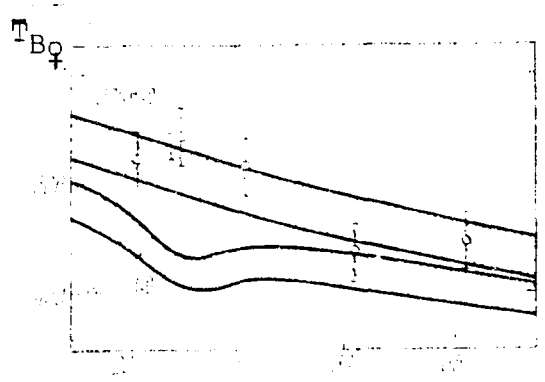

Fig. 61. The measured and calculated dependences of $\bar{T}_{B\varphi}$ on frequency near the resonance line of water vapor absorption for various water vapor contents. The stippled areas are areas of assumed variation in the calculated values of $\bar{T}_{B\varphi}$ within the bounds of errors in determining atmospheric parameters

ORIGINAL PAGE IS
OF POOR QUALITY

of the Venusian atmosphere. Furthermore, it can be said that the content of these components cannot be large, and it is possible to attempt an estimate of the upper limits of their possible content.

One of the components that absorbs UHF radiation can be ammonia; Surkov et al, basing their judgment on data from a Venera-8 experiment, indicate that ammonia is present in the Venusian atmosphere [154].

The character of ammonia absorption depends on pressure. At low pressures, the absorption is of a resonance character and is described by a quantum mechanical formula [88] in which the subscript 1 denotes CO_2 and the subscript 2 denotes NH_3: /156

$$\text{(IV.25)}$$

This formula is obtained by taking into account the shape of the line from the solution of the kinetic equation and making definite assumptions about the character of molecular interaction in binary collisions [55]. Here $I_{JK}(T_c)$ is the intensity of ammonia inversion at temperature T_c (cf. Table 46 in [55]); E_{JK} is the energy of the rotational states of molecules computed from the symmetrical top formula [155]; λ_{JK} are the resonant wavelength of ammonia (cm); J and K are the quantum numbers of symmetrical top; f_2 and f_1 are the relative content by volume of ammonia and carbon dioxide, respectively: the ratio of the cross section of

ORIGINAL PAGE IS
OF POOR QUALITY

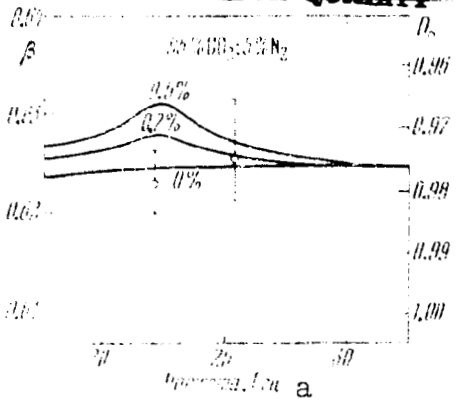

Fig. 62. Measured and calculated positions of the first zero of the interferometric function of the visibility of Venus vs. frequency near the resonance line of water vapor absorption for different relative water vapor contents. For purposes of comparison, this same graph shows the first zero of an uniformly bright disk of the Venusian diameter.

Key: a. Frequency, Hz

CO_2 -- NH_3 molecular collisions to the analogous cross section of NH_3 -- NH_3 collisions is $\sigma_{12}/\sigma_{22} = 0.3$; k is Boltzmann's constant; c is the speed of light.

At pressures greater than 6 - 8 atm, absorption becomes nonresonant and is described by the semiempirical formula of Ben-Reuven [216] as corrected by the results of Morris and Parson's measurements [432].

$$\gamma,\ \mathrm{km}^{-1} = \ldots F(\lambda), \qquad \text{(IV.26)}$$

where

$$F(\lambda) = \ldots$$

/157

$$\ldots$$

$$\frac{1}{\lambda_0} = 0.78\ \mathrm{cm}^{-1}.$$

In order to estimate relative ammonia content f_{NH_3} from radio astronomy and radar data, it is necessary to assume a model for f_{NH_3} distribution vs. altitude.

In the Venusian atmosphere for regions of pressure P = 2 - 10 atm, where Venera-8 did direct measurements of ammonia content, and for the entire atmosphere below that level, total

pressure is less than the pressure of saturated ammonia vapor. Therefore, ammonia can exist in this region only as a gas; consequently, there are no phase transitions. In this case it would be expected that relative ammonia content vs. altitude will be constant.

With the corresponding lower limit of the Venera-8 measurements $f_{NH_3} = 10^{-4}$ and with a constant relative ammonia content vs. altitude, even in the absence of water vapor in the atmosphere, calculation leads to an optical thickness of the Venusian atmosphere at wavelength $\lambda = 3.8$ cm of $\tau = 3.93$. In this case the radar cross section at this wavelength would be

$$\sigma \approx \sigma_0 e^{-2\tau} \approx 6 \cdot 10^{-4},$$

two orders of magnitude less than the measured $\sigma_{3.8} \approx 10^{-2}$ (cf. Table 4). In addition, the brightness temperatures of Venusian radio emission would also turn out to be much lower than what has been measured, while the results of Kuzmin and Clark's polarized radio astronomy measurements [83] could not agree with the calculation no matter what values of surface permittivity are used.

In connection with such disagreement between the results of radar and radio astronomy measurements, [144] solved the inverse problem of determining the upper limit of possible ammonia content in the Venusian atmosphere so as to agree with these results. For a model with a constant relative ammonia content from the surface to a level where P = 2 atm and with no ammonia above this level, the following were obtained: /158

for a dry atmosphere ($f_{H_2O} = 0$) and

$$f_{NH_3} \leq 0.8 \cdot 10^{-5}$$

ORIGINAL PAGE IS
OF POOR QUALITY

for a relative water vapor content $f_{H_2O} = 0.1\%$. With a large water vapor content, the upper limit of f_{NH_3} will be even lower.

In the opinion of Surkov et al [154] the relative ammonia content is at a maximum near the lower boundary of the cloud layer, where Venera-8 made measurements, and decreases as the surface is neared. In this regard, Smirnova [143] examined a model in which $f_{NH_3} = 10^{-4}$ only in the layer where P = 2 - 10 atm and in which it is equal to zero above and below this layer. However, even such a highly artificial model is compatible with the results of radio astronomy measurements -- since the calculated spectrum for this model should have a "gap" near wavelength 1.25 cm up to $T_{B\varphi} = 220°K$, a "gap" which is absent in the measured brightness temperatures of the radio emission of Venus (cf. Table 5).

The upper level of relative ammonia content in the Venusian lower atmosphere, (as obtained from radar and radio astronomy measurements)

$$f_{NH_3} \leq 10^{-7}$$

ORIGINAL PAGE IS
OF POOR QUALITY

agrees with the upper limit of relative content of this molecule in the atmosphere above the clouds, a limit determined from the spectral measurements of Kuiper [69] and Moroz [113].

Because water vapor is present, the Venusian atmosphere, there can be another component that absorbs UHF radiation: water droplets in the cloud layer. A calculation [25, 87] of the effect of absorption by water droplets in the Venusian cloud layer on spectrum $\bar{T}_{B\odot}(\lambda)$ showed that the integral content of water in a liquid phase is:

$$P = \int_{h_1}^{h_2} M_0(h) \exp\left(0{,}04 \int_h^{h_2} \Gamma(h)\,dh\right) dh \approx 0{,}3\ \text{g}\cdot\text{cm}^{-2}$$

This does not contradict the calculation of total water content /159 of the clouds for $f_{H_2O} = 0.5\%$.

With a cloud layer of thickness 7 - 8 km, this total content corresponds to an upper limit of mean water content of the clouds $M_0 \leq 0.4\ \text{g}\cdot\text{m}^{-3}$ (cf. (IV.31)). This estimate, which agrees with the calculated estimate of Obukhov and Golitsyn [123], shows that there are no strong water clouds on Venus and that the cloud layer has no substantial effect on radar and radio astronomy measurements of the planet.

IV.6. The Structure of the Venusian Troposphere and Stratosphere

The data from measurements using spacecraft, complemented by the results of ground-based optical, radio astronomy, and radar measurements, has allowed us to form some definite conceptions about the structure of the Venusian troposphere and stratosphere. Here we will summarize the results of analyzing the experimental data contained in the previous paragraphs of this chapter.

Let us turn first of all to the chemical composition of the atmosphere. Table 11 gives a synopsis of the results of measurements made up to the present. The contents of those components measured by the Venera stations correspond to Table 9. The data from numerous spectroscopic determinations of the content of various components are tabulated; they are based

primarily on measurements in the near-infrared region of the spectrum using simple reflection models[13].

Carbon dioxide is the basic component of the atmosphere. The presence of H_2O, CO, HCl and HF has been identified with certainty, and there are indications that NH_3 is also present. Threshold values are given for other possible components. Among spectroscopic determinations the results of Belton et al [215] come closest to what the Venera-4 measurements enabled us to conclude: that the Venusian atmosphere consists primarily of carbon dioxide. Belton et. al obtained these results by analyzing absorption in the strong lines of the band $\lambda = 1.038$ μm while using a model of spectral line formation that took into account scattering among the clouds. As for nitrogen (and a possible admixture of inert gases), it is possible to say only that nitrogen content does not exceed 2%, which corresponds to a partial pressure of about 2 atm. Even in itself, the fact that nitrogen exists in such quantities in the Venusian atmosphere (almost twice as much as nitrogen content in the Earth's atmosphere) would be of exceptional importance for an understanding of the planet's nature and the conditions in which its atmosphere has formed. /161

Spectroscopy and radio astronomy give water vapor, oxygen, and ammonia contents that are lower than those obtained directly by the Venera spacecraft.

As for water vapor, it is necessary to keep in mind the various levels in the atmosphere to which direct, spectroscopic and radio astronomy determinations refer; this is because of the strong dependence of the H_2O mixing ratio on temperature. Above all, one should take into account the possibility of condensation above the level where gas analyzers measured H_2O content, as well as the possibility of solutions of various compounds forming. This should, accordingly, lead to lower concentrations of water vapor above the saturation level at lower temperatures. The value $7 \cdot 10^{-5}$ (given in Table 11) which corresponds to the spectrogram in Fig. 22, refers to the atmosphere near the visible boundary of the clouds. It should also be noted that the spectroscopic estimates of H_2O content given by various authors differ substantially from each other, depending on what spectral region and what band formation models are used: from less than /162

[13] According to Gray [327], assuming that the Venusian clouds act as a simple reflecting layer can lead to appreciable error in determining the content of atmospheric components; such an assumption underestimates the size of the air mass (up to three times). A detailed analysis of nuerous Venusian spectra has recently been done for various CO_2 bands by L. Young [551]; his analysis indicates that the most acceptable model for Venus is the scattering model proposed by Chamberlain and Kuiper [236] (cf. Section V.3).

2 μm of precipitated water at $\lambda = 1.4$ μm and $\lambda = 2.0$ μm to more than 16 μm in the band $\lambda = 0.82$ μm [442]. These variations (which correspond to relative concentrations from 10^{-6} to 10^{-5} if adjusted to a level with $P \approx 0.2$ atm) are possibly connected, at least partially, to a modification of the growth curve in a scattering atmosphere or with varying opacity in these spectral regions.[14] The results of studying absorption in nearby CO_2 bands ($\lambda = 1.75$ μm; $\lambda = 7820$ and 8689 Å) point toward the second assumption, namely, that opacity in fact depends on wavelength. These variations in H_2O content can also be related to recently discovered [551] substantial variations in the level of CO_2 band formation. In order to interpret more reliably the results of spectroscopic determinations of water vapor content, it is necessary to observe several CO_2 bands of nearly equal intensity in the interval $\lambda = 0.78 - 2.5$ μm while simultaneously measuring absorption in H_2O bands.

/163

An analysis of the results of radio astronomy measurements (cf. Section IV.5) yields an upper limit for H_2O content in the lower atmosphere. It provides evidence that relative H_2O content in the atmosphere below the level where direct measurements were made should be significantly less. Table 11 gives the corresponding estimates.

In connection with his examination of the probable source of N_2 in the atmosphere, Vinogradov indicated that ammonia may be present in the atmosphere and that ammonium salts may be present in the clouds of Venus. If the source of ammonia on Venus is, as on Earth, ammonium chloride of volcanic origin, then it should sublimate at a temperature of about 625°K. The large quantity of carbon dioxide could result in the formation of ammonium carbonate $(NH_4)_2CO_3$, which decomposes at a temperature higher than 330°K and forms ammonia which is slightly oxidized to form N_2 if free oxygen is present in the atmosphere. As temperature decreases below 330°K, the precipitation of ammonium salts can occur. An analysis of the dependence of the change of the equilibrium concentration of saturating NH_3 vapors in the triple diagram $CO_2 - NH_3 - H_2O$ gives rise to notions that the relative content $f_{NH_3} < 3 \cdot 10^{-8}$, which corresponds to the spectroscopic estimate, can in this case be reached at an atmospheric level where temperature is $\leq$ 230°K and pressure $\leq$ 0.1 kg/cm^2 [153a].

Thus by taking phase and chemical transformations into account, it is possible in principle to explain the variation in the results of direct and spectroscopic measurements -- on the

[14] Fink et al recently reanalyzed the results of Fourier spectrometer measurements from a high altitude airplane CV 990 [303]; these results give rise to estimates of relative water vapor content of $0.6 \cdot 10^{-6}$ for a simple reflection model and $1.9 \cdot 10^{-6}$ for a scattering model (cf. Table 11).

TABLE 11. CHEMICAL CONTENT OF THE VENUSIAN ATMOSPHERE

/160

Component	Relative content by volume	Method	Bibliography	Remarks
CO_2	0,97 [illegible]	Venera-4, 5, 6»	[29,31,32]	
N_2 (including inert gases)	$< 2 \cdot 10^{-2}$	Venera-4, 5, 6»	[29,31,32]	
H_2O	$(0.6 \div 4.1) \cdot 10^{-2}$	Venera-4, 5, 6»	[29,31,32]	At $P = 2$ [illegible] $0,6$ kg/cm^2
H_2O	$(1 \div 1) \cdot 10^{-3}$	Radio astronomy	(§ IV, 5)	
H_2O	$\sim 7 \cdot 10^{-3}$	Spectroscopy	[illegible]	
H_2O	$(0.6 \div 2) \cdot 10^{-2}$	Spectroscopy	[illegible]	
O_2	[illegible]	Venera-[illegible]	[31, 32]	
O_2	[illegible]	Spectroscopy	[illegible]	
CO	$(1 \div 3) \cdot 10^{-5}$	Spectroscopy	[illegible]	
HCl	$2 \cdot 10^{-7}$	Spectroscopy	[252]	
HCl	$\sim 10^{-6}$	UAO	[illegible]	At 1 atm-km CO_2
HF	[illegible]	Spectroscopy	[252]	
CH_4	[illegible]	Spectroscopy	[252]	
CH_3Cl	[illegible]	Spectroscopy	[252]	
CH_3F	[illegible]	Spectroscopy	[252]	
C_2H_2	[illegible]	Spectroscopy	[252]	
HCN	[illegible]			
O_3	[illegible]	Spectroscopy	[illegible]	
O_3	[illegible]	UAO	[illegible]	At 1 atm-km CO_2
SO_2	[illegible]	Spectroscopy	[illegible]	
SO_2	[illegible]	UAO	[illegible]	At 1 atm-km CO_2
COS	[illegible]	Spectroscopy	[illegible]	
COS	[illegible]	Spectroscopy	[illegible]	
COS	[illegible]	UAO	[illegible]	At 1 atm-km CO_2
C_3O_2	[illegible]	Spectroscopy	[illegible]	
C_3O_2	[illegible]	UAO	[illegible]	At 1 atm-km CO_2
H_2S	[illegible]	Spectroscopy	[illegible]	
H_2S	[illegible]	UAO	[illegible]	At 1 atm-km CO_2
NH_3	[illegible]	Spectroscopy	[illegible]	
NH_3	[illegible]	Venera-[illegible]	[illegible]	At $P = 2$ [illegible] 10 kg/cm^2
NH_3	[illegible]	UAO	[illegible]	at 1 atm-km CO_2
NH_3	[illegible]	Radio astronomy	(§ IV, 5)	
NO	[illegible]	UAO	[illegible]	1 CO_2
NO_2	[illegible]	Spectroscopy	[illegible]	
NO_2	[illegible]	UAO	[illegible]	At 1 atm-km CO_2
N_2O_4	[illegible]	UAO	[illegible]	
HCHO	[illegible]	UAO	[illegible]	same
CH_3CHO and higher order aldehydes	[illegible]	UAO	[illegible]	same
CH_3COCH_3 and higher order ketones	[illegible]	UAO	[illegible]	same

ORIGINAL PAGE IS
OF POOR QUALITY

condition that the temperature at the level where the corresponding bands form is not greatly different from the phase equilibrium temperature for the given component. However, because of the large difference between the Venera-8 measurements and radar and radio astronomy estimates, the question of ammonia content in the lower atmosphere of Venus requires further research.

The spectroscopic limit of O_2 is in agreement with the threshold estimate made from Venera-6 measurements, which did not reveal the presence of oxygen in relative concentrations larger than or equal to 10^{-3}. It is evident that the spectroscopic limit /164 is more accurate and that the relative O_2 content in the Venusian atmosphere does not exceed $(2-8)\cdot10^{-5}$. The distribution depends on whether absorption occurs in the clouds or above them [213, 214]. Prokof'yev and Petrova [132 - 134] discovered the presence of weak Doppler effects in the wings of the lines of the telluric band of oxygen A (λ 7660Å) and interpreted them as belonging to the spectrum of Venus. Later measurements, however, did not confirm this result.

It is worthy of note that CO and especially HCl and HF, which were discovered by high resolution Fourier spectrometry, are present in the Venusian atmosphere. The relative contents of these components shown in Table 11 include corrections because of the peculiarities of absorption band formation in a heterogeneous cloudy atmosphere as in accord with Belton's [212] theory of growth curves. The measurements refer to the cloud layer (a level with an effective pressure $P_{eff} \approx 35 - 100$ mbar). In this case, therefore, it is natural to ask to what extent these estimates hold true for the atmosphere that lies below, i.e., are these components distributed uniformly vs. altitude?

L. Young [551] has made a careful analysis of the Venusian spectra obtained by Kuiper et al and by others later; his conclusion is that CO is apparently mixed uniformly in the atmosphere at a mixing ratio of $(5.1 \pm 0.1)\cdot10^{-5}$. As for HCl and HF, it is most likely that they are unevenly mixed in the atmosphere, since the effective pressure of formation of the corresponding spectral lines evidently refers to deeper levels in the Venusian atmosphere (slightly deeper for HCl than for HF) than the level of line formation in CO_2 reference bands. The refined estimates of relative HCl and HF content resulting from this analysis are equal to $(4.2 \pm 0.7)\cdot10^{-7}$ and 10^{-8}. As we see, the quantity of CO in the Venusian atmosphere above the clouds (about 13 atm-cm) is about 50 - 100 times higher than mean CO content in the Earth's atmosphere. The quantity of hydrogen chloride and hydrogen fluoride is not large; however, the fact that they exist in such an oxidizing medium as the Venusian atmosphere is of very great interest (on Earth, Cl and F are basically dissolved in the oceans [28, 476]).

Estimates of possible content of carbon suboxide C_3O_2, ozone O_3, hydrocarbons CH_4, C_2H_2, C_2H_4, sulfurous and nitrous compounds SO_2, COS, H_2S, NO, NO_2 and several others are given in Table 11, and they correspond to upper spectroscopic limits of discovery. In addition to data from ground-based spectrometry, it also indicates threshold contents of a series of small admixtures in the atmosphere; these contents were obtained by measurements using a scanning ultraviolet spectrometer mounted in an orbiting astronomical observatory (OAO - A2). Measurements made in the spectral region between 2000 and 3600 Å and with a resolution of about 25 Å yielded estimates of the gaseous components in the Venusian, Martian, Jovian and Saturnian atmosphere, estimates made on the basis of the characteristic absorption lines related to electron transitions in molecules [444]. Because the role of Rayleigh scattering in the ultraviolet region of the spectrum increases, this method allows one to estimate the content of various atmospheric components only in the outer regions of the planetary atmospheres. For Venus, the estimates obtained in this manner refer to a level where the reported thickness of a carbon dioxide atmosphere is about 1 atm-km, i.e., near the visible boundary of the clouds.

By starting with conceptions about the chemical equilibrium between the atmosphere and lithosphere of the planet, and by starting as well with probable equilibrium concentrations among the gases that make up the atmosphere, it is also possible to obtain theoretical estimates of the content of individual atmospheric components. The geochemical upper limits for a model atmosphere with a surface temperature of 748°K and surface CO_2 pressure of 120 atm have been calculated by Lewis [401] for a diverse set of reactions. These limits are given in Table 12 in the form of relative concentrations and are to a significant degree only illustrative, inasmuch as they are based on a series of major assumptions. Thus, by analogy with Earth, a large silicate concentration of the surface rocks of Venus -- in the process of the differentiation and formation of the planetary crust -- is assumed, a concentration that is quite distinct from the relative abundance of the elements throughout the universe. Therefore, quartz plays an important role in the reactions examined. Nevertheless, the data in Table 12 are of definite interest and are noteworthy, for example, because the computed limiting content of /166 such components as CO, H_2O, HCl, and HF is in good agreement with experimental data.

The results of temperature and pressure measurements on Venera-4 - -8 stations are characteristic of the basic features of the structure of the planetary troposphere. An examination of Figs. 42 and 43 shows that the functions T(h) and P(h) on the night and day sides near the morning terminator nearly coincide. Nor, in essence, do the values T_s and P_s obtained at the Venera landing sites differ. Comparative radio astronomy measurements of the brightness temperature of the day and night hemispheres of

TABLE 12. GEOCHEMICAL UPPER LIMITS OF THE RELATIVE CONTENT OF VARIOUS COMPONENTS IN THE VENUSIAN ATMOSPHERE (ACCORDING TO [401]).

Component	Relative content	Component	Relative content	Component	Relative content
CO_2	1	HF	$2 \cdot 10^{-8}$	C_3H_8	$6 \cdot 10^{-21}$
N_2	$5 \cdot 10^{-2}$	CH_4	$7 \cdot 10^{-13}$	SiF_4	10^{-35}
Ar	10^{-1}	NH_3	$8 \cdot 10^{-11}$	Cl_2	$2 \cdot 10^{-21}$
H_2O	$6 \cdot 10^{-4}$	O_2	$8 \cdot 10^{-5}$	SO_2	10^{-16}
CO	$2 \cdot 10^{-3}$	OCS	$8 \cdot 10^{-6}$	NO	10^{-15}
CO_2	$6 \cdot 10^{-4}$	SO_3	$5 \cdot 10^{-7}$	C_4H_8	$8 \cdot 10^{-25}$
H_2	$5 \cdot 10^{-5}$	HCN	$3 \cdot 10^{-11}$	S_2	$8 \cdot 10^{-31}$
H_2S	$8 \cdot 10^{-6}$	$COCl_2$	$8 \cdot 10^{-18}$	F_2	$2 \cdot 10^{-28}$
He	10^{-5}	S_2	$2 \cdot 10^{-8}$		

ORIGINAL PAGE IS OF POOR QUALITY

Venus also point to the absence of diurnal temperature variations in the atmosphere near the planetary surface. Fig. 63. shows the temperature and pressure altitude profiles (constructed from an aggregate of all measurements from the surface to altitudes of 55 km. It also gives Mariner-5 data, data that have been matched to the Venera measurements at a point where pressure $P \approx 4.4$ kg/cm^2.

As we see, the range of altitudes covered by the measurements of spacecraft goes up to about 90 km above the planetary surface. The region in which the Venera and Mariner-5 measurements overlap /167 is about 20 km (290 - 470 °K in temperature and 0.6 - 7 kg/cm^2 in pressure). A comparison of the curves shown in Fig. 57 and 58 indicate that there are also no appreciable differences between the night and day temperature profiles according to Mariner-5. Therefore, the profiles T(h) and P(h) in the troposphere and stratosphere -- shown in Fig. 63 -- correspond to average daily conditions. It is possible to reconcile these profiles with the estimates of stratospheric parameters made from measurements of g-forces before parachute deployment of Venera-8 [566].

Since the Mariner-5 results are not tied directly to altitude /168 above the surface but refer to the distance from the planet's gravitational center, a comparison of Venera and Mariner-5 data in terms of atmospheric parameters (cf. Fig. 63) allows one to obtain a value of planetocentric distance r that corresponds to the level of the surface where the Venera-7 and Venera-8 landed. This value is equal to r = 6051.7 km (for a temperature T_s = 745°K). These values are in good agreement with the results of computing the mean radius of Venus from radar measurements, R_{φ} = 6050 (cf. Section II.4).

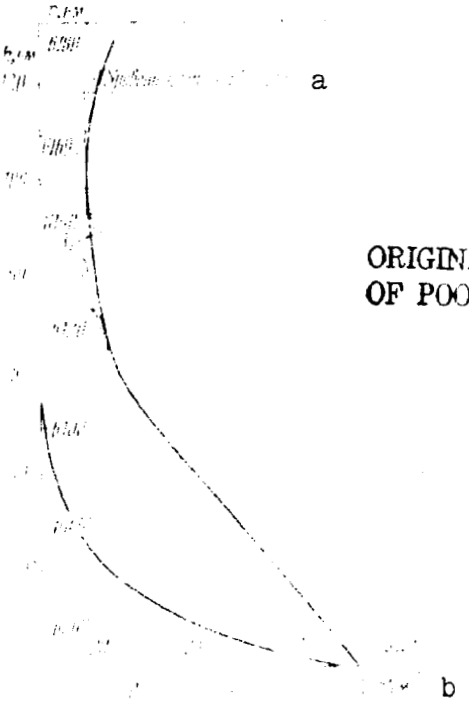

ORIGINAL PAGE IS
OF POOR QUALITY

Fig. 63. Altitude profiles of the atmospheric temperature and pressure of Venus according to all Venera measurements (the thick solid lines) and according to Mariner-5 measurements (dashed line). The dotted-dashed line and the dotted line are the model profiles T(h) as in [99] and [421] respectively.

Key: a. Regulus occultation level
b. kg/cm^2

An examination of the altitude profile T(h) and an analysis of the gas state show that the temperature gradient at altitudes below ≈ 55 km does not differ by and large from a dry adiabatic for the CO_2 atmosphere. A sharp reduction of the temperature fall (up to about 4 deg/km) is observed above 60 km. In addition, small individual fluctuations occur in the 65 - 70 km region. Finally, a rather complex irregular structure with inversion layers occurs between 75 and 90 km. Fjeldbo and Eshleman [305] also note the presence of definite variations in temperature dependence on altitude below 60 km: a certain reduction of dT/dh in the 45 - 50 km region and, on the other hand, a certain tendency toward a super adiabatic close to a level of 35 km. It is difficult to prove or disprove from direct measurement data, whether curve T(h) actually behaves this way, inasmuch as the possible errors of individual measurements are generally commensurable with the value of the assumed feature. The altitude region near 35 km is located near the level of critical refraction, and radio measurements here can be subject to the greatest errors. Variations of T(h) in the 60 - 70 km region can be attributed to the existence of clouds. As for the structural irregularity between 75 and 90 km, it is most probably connected with the choice of boundary conditions in integrating the experimental curve N(h) downwards.

A more detailed profile of atmospheric temperature above 40 km has been obtained from Mariner-10 measurements [577]. A reduction in the temperature gradient above 54 km from $\gamma \approx 9$ deg/km, which /169 corresponds to a dry adiabatic for CO_2 to a value of ~ 3 - 4 deg/km, has been revealed with some certainty, as well as temperature inversions at altitudes 56, 58, 61, and 63 km (with $R_{\varphi} = 6052$ km).

No irregularities were noted above 63 km; this allows the assumption that the regions of the convective-mixing atmosphere extend below this level. Below 55 km, the results of Mariner-10, like those of Mariner-5, are in good agreement with the data from the Venera direct measurements. No appreciable differences in the altitude profiles for temperature and pressure on the day and night side have been noted.

The characteristic variation in dT/dh below 60 km can be explained by beginning with the notion that there are definite admixtures and associated phase transitions (of cloud structure) in the Venusian atmosphere. An analysis of the attenuation of radio emission in the Mariner-5 experiment points to the same possibility (cf. Fig. 59). The magnitude and character of this attenuation are essentially similar on the day and night sides and turn out to be substantially different from what should have been observed in pure CO_2 or in a CO_2 - H_2O mixture at partial pressures corresponding to the results of gas analysis on the Venera stations and to the measured atmospheric temperatures and pressures at these levels. The probable cause for this anomalous absorption is the cloud layer of Venus. It is also possible to assume that additional absorption is related to the presence of localized (at specific levels) admixtures in the Venusian atmosphere.

At a surface temperature of Venus of $T_s \approx 750°K$, various volatile components and compounds could pass into the atmosphere and exist at various levels therein in the form of vapors and condensates. Lewis [400] has discussed in detail the possible equilibrium geochemical reactions for an atmosphere-lithosphere system; and in particular, he has examined the conditions for the formation in the atmosphere of mercury-halogen clouds, which condense at temperatures from 250°K (Hg_2Cl_2) to 450°K (Hg_2I_2). Rasool [467] starting with the proposition that such clouds indeed exist made an effort to find experimental confirmation for this proposition; to do this, he analyzed the altitude dependence of radio wave attenuation measured by Mariner-5. The dots in Fig. 64 show the loss profile as calculated on this assumption. A rather successful correspondence between this interpretation and the features of the measured curve, especially at altitudes 40 - 48 km, should be noted. /170

Golitsyn and Gurvich [575] have examined another probable cause for the scintillations noted in the radio signal, namely the possible presence of turbulent irregularities with a characteristic size of the order of magnitude of $\sqrt{\lambda L_0} \approx 1.25$ km, where L_0 is the distance from the transmitter to the reference point for a given layer in the atmosphere (cf. Fig. 56) and λ is the wavelength. Finally, dust, whose stratification in the Earth's atmosphere is well known, can make a definite contribution to the amount of losses.

It is interesting to note that near 48 - 50 km densimeter measurements have recorded a seeming increase in density. The rather curoius coincidence between this unexplained effect and /171

the increase in radio-wave attenuation is quite possibly not accidental: as has already been noted, the presence of solid or liquid admixtures can influence the readings of densimeters. This is due simply to the principles of their operation.

ORIGINAL PAGE IS
OF POOR QUALITY

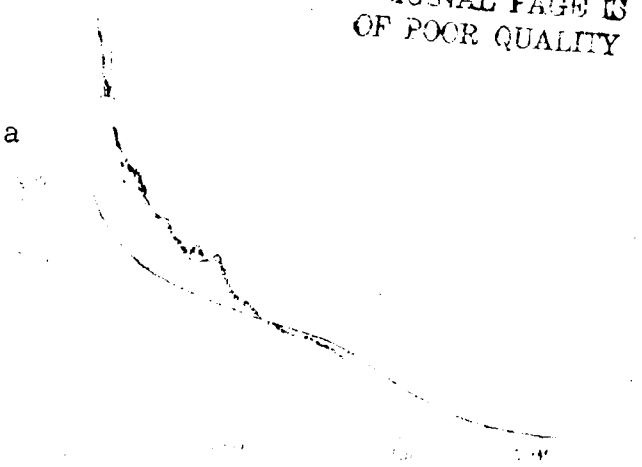

Fig. 64. Centimeter radio-wave attenuation (frequency f_3) in the Mariner-5 experiment. The solid curve is a calculation of the magnitude of the attenuation for pure CO_2. The dashed line is a calculation of attenuation in a CO_2 + 1% H_2O mixture, with induced absorption taken into account and with homogeneous absorbing clouds with absorption coefficients of $1.03 \cdot 10^{-2}$ db/km (from 6098 to 6100.8 km) and $3.29 \cdot 10^{-3}$ db/km (from 6100.6 to 6104.1 km) [382]. The dots are for a calculation assuming the presence of mercury-halogen clouds [467].

Key: a. Attenuation

If it is assumed that there are admixtures in the Venusian atmosphere, admixtures whose distribution vs. altitude is quite probably accompanied by phase transitions, our notions about atmospheric processes in a pure CO_2 medium turn out to be oversimplified; they can be seen, therefore, as a first approximation. The presence of admixtures should be very important for physical structure, thermodynamics, optical characteristics and the thermal regime of the planet's troposphere. The problem of the Venusian clouds, which is surveyed in Section IV.7, is also linked directly to this assumption.

Together with the profiles T(h) and P(h), which have been constructed from the data provided by the measurements on spacecraft, Fig. 63 also shows the extrapolations calculated for temperature at higher altitudes; this has been done in accord with the models suggested by McElroy [421, 422] and Marov [97, 99, 412]. These curves, which have been obtained by using slightly different initial assumptions are alternatives of temperature change in the Venusian stratosphere, i.e., above the tropopause. By tropopause we mean the level near which an abrupt change in the rate of temperature vs. altitude drop occurs, the level where the upper boundary of the clouds is visible from Earth. This region is between 60 - 70 km in altitude. In a certain sense, this level may be viewed as a transition between convective and radiative equilibrium; although it is impossible to rule out here

the presence of limited intensity convective flows due to the mechanism of penetrative conve tion caused by the instability of lower-lying clouds.

By starting with the condition of radiative equilibrium, it is easy to calculate a temperature profile by using the long-wave radiation transfer equation for a gray atmosphere (cf. [50]). Combining this equation with an equation that characterizes the change in optical thickness vs. altitude with the condition of hydrostatic equilibrium taken into account (IV.3) leads to a system of the form /172

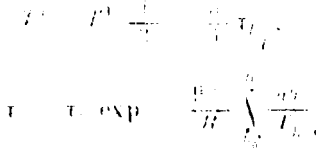

(IV.27)

ORIGINAL PAGE IS
OF POOR QUALITY

(IV.28)

where T_e is the effective temperature of a spinning planet as determined from formula (IV.1); T_h is the atmospheric temperature at level h; τ_h is the optical depth for level h; and τ_{h0} is the optical depth for level h_0.

If $T_h = T_e = 228°K$, we have $\tau_h = 0.7$, i.e., the transmissivity is $p = e^{-0.7} \approx 0.5$. Measurements of the brightness and color temperature in the infrared region of the spectrum refer to this level in the atmosphere; these measurements, as had been noted, lead to values that differ little from T_e; and this in turn indicates a large optical thickness of the emitting layer. The system (IV.27) - (IV.28) makes it possible to calculate temperature distribution above a given level, right up to altitudes where the heat flux is released by the atmosphere without attenuation ($T_h = 0$), and the temperature asymptotically attains the value $T^*_h = T_e/\sqrt[4]{2} \approx 195°K$. For the model in question, this value corresponds to the region of a temperature minimum, which corresponds to the mesopause in the Earth's atmosphere; this region also coincides with the bottom of the thermosphere whichis characterized by a positive temperature gradient due to the direct absorption of solar ultraviolet radiation; direct absorption becomes effective at levels where $\tau_{uv} \lesssim 1$. Since CO_2 absorption begins for all practical purposes in the region that corresponds to a Schuman-Runge continuum, it is not difficult to estimate that at a mean value of the absorption coefficient in the interval $\lambda = 1725$ to 1000 Å, $\bar{S} \approx 10^{-19}$ cm^2 [121], this condition is reached at altitudes where the concentration of particles is $n \lesssim 10^{13}$cm^{-3}, i.e., $h_M \gtrsim$ 105 - 110 km. Thus, the estimates obtained "from the top" and "from the bottom" for the purpose of determining the altitude of the mesopause in the Venusian atmosphere are compatible near the given level. In so doing, the condition corresponding to the position of this transition region from the lower to the upper atmosphere as in the definition given in Section VI.1 is also met rather well.

In essence, a similar result is obtained in a model [421] with a slightly larger temperature gradient in the stratosphere, one which results in $T_M \approx 170°K$. This value is close to the value of the temperature minimum given by the refined data of an analysis of the Mariner-5 measurements [305] ($T_M \approx 150 - 170°K$). It is difficult to estimate the altitude of the mesopause from these data, even though they reveal a definite tendency to locate it lower than the theoretical estimates do (somewhere about 85 - 90 km), i.e., at about the same level as for the Earth). We note that due to the absence of an intervening temperature inversion, as takes place in the Earth's atmosphere as a result of the presence of an ozone layer (ozonosphere), the regions of the stratosphere and mesosphere in the Venusian atmosphere can be considered to coincide, so that the thermosphere begins directly above the stratosphere. Therefore, one can conditionally name this region the stratomesosphere.

The independent estimates of the parameters of the neutral atmosphere, estimates made from data from the photometric observations of the variation of the brightness of Regulus on its occultation by Venus on July 7, 1959, conform to our notions about the rise in temperature above the level h_M. Basically, this method does not differ from the one used to determine atmospheric parameters from the attenuation of the radio signal in the Mariner-5 experiment. For computation of the magnitude of the attenuation of the luminous flux $\Gamma(r)$, therefore, the relation (IV.24) holds true. Vaucouleurs and Menzel [532] determined (at the level of the occultation $r = 6169 \pm 2$ km -- which corresponds to a reduction of e times in the brightness of the star) values for pressure P_R, the scale height H_R and its logarithmic gradient, values that allow one to extend the atmospheric model of Venus from the beginning of the Mariner-5 measurements upwards by about 30 km. These values turn out to be equal to

$P_R \approx (2.6 \pm 0.1) \cdot 10^{-6}$ kg/cm^2

$H_R = 6.8 \pm 0.2$ km; $\frac{d \ln H_R}{dh} = 0.010 \pm 0.002$ km^{-1}.

ORIGINAL PAGE IS OF POOR QUALITY

Martynov and Pospergelis [105] obtained a similar value of the scale height on the level of the occultation ($H_R = 6$ km) by using the same method. However, Martynov considers [106, 107] that it is less reliable to determine altitude from the level of occultation and instead of altitude $h_R = 119 \pm 2$ km (which corresponds to $R_{\varphi} = 6050$ km), he gives a value of $h_R = 116 \pm 10$ km, using an estimate of $R^*_{\varphi} = 6100 \pm 30$ km for the radius of the Venusian cloud layer. At $H_R = 6.8$ km, the temperature and the temperature gradient $dT/dh = T \frac{d \ln H}{dh}$ at the level of the occultation for a

/174

predominantly CO_2 concentration, i.e., assuming that $\bar{\mu} = 43.4$ is maintained at these altitudes, are equal to 300°K and 3 deg/km^{-1}, respectively.

Reconciling all available data for the stratomesosphere and the lower thermosphere (the level to which the occultation of Regulus corresponds) meets with definite difficulties. If T_M = 195°K is assumed, the calculated pressure profile P(h) can be reconciled with the value of P_R; however, appreciable discrepancies are revealed in estimates of T_R and $d\ln H/dh$. The best agreement with the parameters of the stratomesosphere, parameters which are based on previously published Mariner-5 data and on an approximation of radiative equilibrium, is reached at T_R = 220°K and $(dT/dh)_R$ = 2.2 deg/km^{-1} [99, 412]. Hunten and McElroy [350] have suggested that errors in determining H_R and $(d \ln H/dh)_R$ (the errors mentioned by the authors of the photometric measurements) are too optimistic, inasmuch as at the level of the occultation, the concentration of particles is most reliably determined, while derivatives are the least reliably determined. In the McElroy model shown in Fig. 63, therefore, the assumption is that a still larger correction for temperature and the temperature gradient near h_R is possible.

The refined results of Mariner-5 measurements, which result in a much lower temperature of the mesopause, make it difficult to accept the results of Vaucouleurs and Menzel, not only for temperature but also for pressure. In fact, at a lower temperature of the mesostratosphere and thus a smaller H, the fall in pressure with altitude occurs more quickly, (cf. formula (IV.3)); the pressure at the occultation level (according to the model given in the Appendix) therefore is about an order of magnitude smaller than P_R. This result, which does not enable the complete reconciliation of all available experimental data, makes it especially necessary to study the structure of the Venusian atmosphere at altitudes of about 70 - 120 km.

The dynamics of the planetary atmosphere are directly related /175
to the problem of the spatial structure of the atmosphere. The great atmospheric depth, the slow planetary rotation and the small angle of inclination of the equator to the orbit give reason to think that motion and heat exchange in the Venusian atmosphere are not similar to processes in the Earth's atmosphere.

Despite Venus' proximity to Earth, there have been few experimental data about circulation in the Venusian atmosphere up until recently. The most interesting is the well-known, four-day circulation, which was revealed in ultraviolet photographs (cf. Section II.1). Other data (e.g., the shifting of the line of the terminator, caused according to Gierasch and Goody [313], by strong convective movements) are quite few in number and are basically of a peripheral character.

The small number of experiments carried out on the Venera stations, their limited extent in space (500-3000 km) on both sides of the morning terminator) and the relatively brief descent time have not enabled a schema of planetary circulation to be constructed from these data. Because of slow planetary rotation, the great thermal inertia of the atmosphere, and the absence of seasons, circulation on Venus probably has the character of a constant wind system and appears to be much more stable than on the Earth. It is therefore possible to maintain that the results of local experiments can carry over to several of its properties in general, even though purely local conditions can in principle exert a definite influence.

The results of analyzing the experiments carried out on Venera-4, -7, and -8 are summarized in Fig. 65 as in [67]. It is worthy of note that the altitude profiles of horizontal wind are in good agreement with each other. Although, as pointed out in Section IV.3, the wind velocity measured on Venera-8 is higher than those measured on Venera-4 and Venera-7, their profiles have several features in common: an increase in wind velocity with altitude, an almost constant wind velocity at altitudes of 20 - 40 km, the absence of strong winds near the surface. The discrepancies in the data from Venera-4, -7 and -8 can in fact be even smaller, provided the systematic errors of measurements of Venera-4 and Venera-7, as well as the fact that their descents were in different regions, are kept in mind. For Venera-4, it is necessary also to consider that the measured velocity component could have corresponded not only to meridianal movement, as was accepted in the original interpretation, but also to zonal movement in the direction of the retrograde rotation of Venus. These considerations are figured into Fig. 65, in which the Venera-4 (cf. Fig. 50) and Venera-7 (cf. Fig. 51) profiles are shifted as a whole to values that lie within the bounds of systematic error; for Venera-4, the velocity is converted here into a zonal component. The dashed line shows the wind velocity according to the measurements of Venera-7 for that portion of the descent which began directly after the first signal was received from the descent apparatus.

As is seen, the motions are characterized by a gradual rise in horizontal wind velocity from almost zero at the surface to $\approx$ 100 m/sec near 50 km, where the direction of the motion coincides with the planet's own rotation, and where the motion is from the night side to the day side across the morning terminator. The maximum kinetic energy in the lower atmosphere is reached at an altitude of 18 - 20 km. The measured wind velocity at altitudes of 20 - 40 km is equivalent to 90 - 120 m/sec on the Earth's surface; 0.5 m/sec at the surface of Venus corresponds to a wind velocity of 3.5 m/sec at the Earth's surface.[15] It is possible that

---

[15] Equivalence in the sense of velocity pressure $\rho v^2/2$ is meant here, i.e., $v_{\varphi}/v_{\oplus} = (\rho_{\oplus}/\rho_{\varphi})^{1/2}$.

ORIGINAL PAGE IS
OF POOR QUALITY

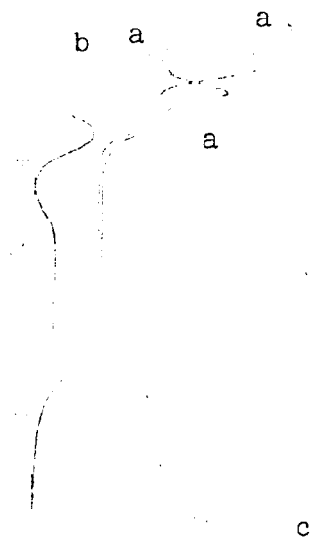

Fig. 65. Horizontal wind profiles as aggregated from the Venera-4, Venera-7 and Venera-8 measurements.

Key: a. Venera
b. km
c. m/sec

horizontal wind velocity on the night side is slightly less than on the day side. The velocities of vertical movements at altitudes up to 50 km in the regions covered by the measurements apparently do not exceed 0.3 - 0.5 m/sec and are probably even less. Judging from the /177 data of Venera-4 and Venera-8 measurements, it impossible to rule out the possibility that there is a meridianal wind from the north pole to the equator and from the equator to the south pole near the morning terminator.

A comparison of the wind velocity profiles obtained and the directions of the measured components leads to the conclusion that motions in the Venusian atmosphere can differ appreciably from schemas of circulation corresponding to various theoretical models (cf. Section V.1 and V.2). It is possible to assume, while making reservations at the same time for the limited experimental data and the possibility of generalizing from local observations, that one of the schemas that satisfy the Venera measurements is the presence in the equatorial zone of the Venusian atmosphere of a circular motion coinciding with the direction of the planet's rotation around its axis.

A similar motion apparently occurs in the atmosphere even at altitudes of about 100 km; it is to these altitudes that UV research on the movement of details on the disk of Venus refer. Wind velocity at these altitudes, as we have seen, corresponds to a mean circulation period of ≈ 4.5 days. About the same period can be typical of motion in the region where the Venera measurements began, while at altitudes of 20 - 40 km, the circulation period can be 12 days and longer. If circulation of this sort actually exists, then the Venera measurements, which refer to various parts /178 of the planet, reflect a latitudinal-temporal motion variability. Measurements of the differential Doppler shift of CO_2 bands in the infrared region [224], measurements that have to do with the visible cloud layer (≈ 60 - 70 km), also indicate the possibility of motions with velocities up to 100 m/sec at these altitudes.

By using the Venera measurements and data from ultraviolet photography and spectroscopic measurements, it is possible to conceive of a "wind model" of the equatorial zone of Venus in the form shown in Fig. 66. The area bounded by the solid lines corresponds to possible variations in wind velocity as determined by various measurements.

ORIGINAL PAGE IS
OF POOR QUALITY

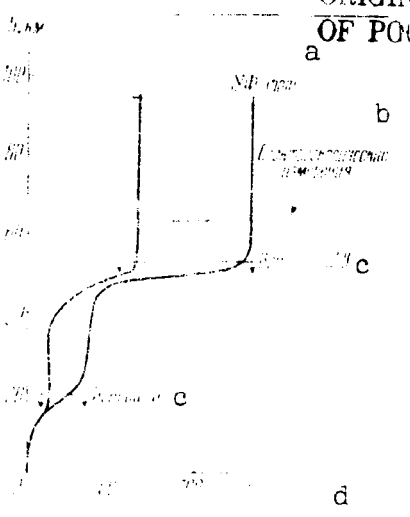

Fig. 66. "Wind model" of the equatorial zone of Venus -- according to aggregate measurements of the Venera series and ground-based observations.

Key: a. UV photography
b. Spectroscopic measurements
c. Venera
d. m/sec

Thus, in the Venusian atmosphere, at least in the layer $\lesssim$ 100 km above the surface, there is apparently a persistent zonal movement of a circulatory type; this motion is characterized by a complex dependence of the increase in the wind velocity gradient on altitude. One may presume that, with the low velocity of the planet's own rotation, horizontal transfer plays a more prominent role in equalizing the irregularly heated areas of the atmosphere (caused by variation in daily insolation) than is the case on Earth, where horizontal velocities are usually less than 0.1 Λ [16] and reaches 1.7 - 1.8 Λ only in the thermosphere, at altitudes of 300 - 350 km [379, 410]. On Venus, this value is reached at 10 km, while it reaches about 50 Λ near 50 km. Furthermore, in contrast to Earth, where seasonal variation brings about a reorganization of stratospheric circulation from the west in winter to the east in summer, on Venus there is evidently a sufficiently persistent flow of gas from the night side to the day side.

These conceptions are confirmed by the results of photographing the planet from onboard the Mariner-10 spacecraft [581]. Successive photographs of Venus with an ultraviolet filter (λ_{max} = 3550 Å) and with a resolution that varied from 130 km to 100 m enabled characteristic features of spatial movements linked directly to the

[16] By Λ is meant the linear velocity of the planet's rotation at the equator.

regions of the upper troposphere and the lower stratosphere to be discovered. /179 Over and above the clearly-traced drifting motions in the equatorial zone, movements which reflect the persisting four-day zonal circulation, (in whose structure are various individual belts up to 100 km wide), an increase in angular velocity with increases in latitude was also discovered, including the formation of clearly distinguishable spiral structures and whirlwinds at the poles (cf. Fig. 73b). At 50° latitude, circulation evidently has a period of about two Earth days and a velocity of ≃ 100 m/sec. At low latitudes, meridianal motion is small, and not localized; large-scale whirlwinds similar to cyclones on Earth have been discoverpd. Within several tens of degrees in latitude and longitude from the subsolar point, there are indications of large-scale cellular convection, which maintain themselves against the general background of persistent zonal motions. The interaction of these two forms of motion can presumably result in the appearance of the disturbances observed in the form of wave movements near the midday meridian.[17]

Unfortunately, very little is now known about the mechanism by which the circular motions are maintained. One can assume that, with a relatively small and variable (by altitude) optical density of the stratomesosphere, the absorption of radiant energy increases with depth and leads to the appearance of intense advection -- due to which an equalization of irregularly heated areas takes place. Gierasch [312] has examined one of the possible mechanisms of this advection. The backward movement of a fluid when it is heated with a slowly rotating heat source (discovered by [586]) can serve as experimental analogy, although the possibility of applying this analogy to the Venusian atmosphere requires additional theoretical and experimental substantiation.

In order to understand dynamic processes in the atmosphere, /180 data on the character and size of the component movements related to turbulent transfer are of great importance. Judging by dynamic conditions and conditions of thermal stratification, one can expect that the inertial range in which turbulence is close to isotropic [112] occupies a larger region of spatial scales in the Venusian atmosphere than in the Earth's atmosphere. In fact, the kinematic viscosity coefficient, whose magnitude determines the microscale of turbulence, is 1.5 - 40 times smaller (as a function of altitude) in the Venusian atmosphere than in the Earth's atmosphere, even near the surface. On the other hand, since the troposphere in the Venusian atmosphere (60 - 70 km) is located 3.5 - 5 times higher

[17] It is impossible to rule out the contention that longitudinal waves are aroused in the stratomesosphere of Venus and that the mixing observed in ultraviolet is partly related to the group velocities of these wave processes. It is known that in Earth conditions such irregular turbulent movements result in group velocities on the order of 10 - 20 m/sec with an amplitude of about 4 km and characteristic wavelengths of up to 50 km (cf. for example [93]).

than in the Earth's atmosphere (11 - 17 km) and since the scale height exceeds that of the Earth, the upper vertical scale of the inertial range in the Venusian atmosphere should not be less than that of the Earth. In addition, the fact that the temperature gradient in the Venusian atmosphere is close to the adiabatic is also conducive to the isotropic character of turbulence [112, 377].

If the turbulence is considered to be isotropic, then the mean square value of the fluctuations of the vertical and horizontal wind components should be nearly identical (more accurately, should differ by $(4/3)^{1/2}$ times). As was noted in Section IV.5, which analyzed the results of the Venera measurements, the characteristic scale of turbulence had a value of 100 - 200 m, which is larger than the value ℓ_{min}; in this case, fluctuations in the horizontal wind component should not for all practical purposes have influenced the vertical velocity of the descent apparatus. Therefore, as a result of the fact that the angle ζ is small (cf. Fig. 47), the observed fluctuations should be related basically to the vertical wind velocity component [66, 377]. The small value of fluctuations below 40 km indicates, first, that convective flows are small, which does not contradict previous estimates of η from temperature and pressure measurements (cf. Fig. 48), and, second, that the gradients of horizontal wind velocity are small (obviously, excluding altitudes from 12 to 18 km, as in accord with Venera-8 data).

The presence of turbulence between 40 and 55 km is in agreement with the large wind velocity gradients observed at these /181 altitudes. If, as a criterion of the development of turbulence, we use a Richardson number

$$Ri = \frac{\beta}{\rho^2 g^2 \left(\frac{1}{\rho}\frac{d\rho}{dh} - \frac{1}{T}\frac{dT}{dh}\right)} \qquad \text{(IV.29)}$$

ORIGINAL PAGE IS OF POOR QUALITY

where $\beta = du_h/dh$ is the wind velocity gradient in a layer with mean temperature $\bar{T}$, then it is highly probable that there is turbulence at altitudes where the condition $Ri < Ri^*$ is met. The critical Richardson number is $Ri^* \simeq 0.5 - 1.0$. Fig. 67 shows Ri numbers calculated from measurements of wind velocity by using previously obtained values of real and adiabatic temperature gradients γ and γ_a according to [377]. As we see, at altitudes of 46 - 53 km, $Ri \lesssim Ri^*$; and below 40 - 45 km $Ri >> Ri^*$ -- which agrees with the observed character of the fluctuations.

IV.7. On the nature and structure of the clouds

The problem of the Venusian clouds continues to be extraordinarily complex and extremely interesting.

The basic source of information about the clouds at present is the optical characteristics of the planet, as observed from

Earth, data on atmospheric structure, and the results of light measurements on Venera-8. Chapter V examines the optical characteristics of Venus on the basis of ground observations and the results of light measurements. It also gives estimates of the expected parameters of the clouds, parameters satisfied by models that interpret the experimental data. Here we will deal with the problem of the clouds primarily from the standpoint of examining /182 the possible components of the Venusian atmosphere.

ORIGINAL PAGE IS OF POOR QUALITY

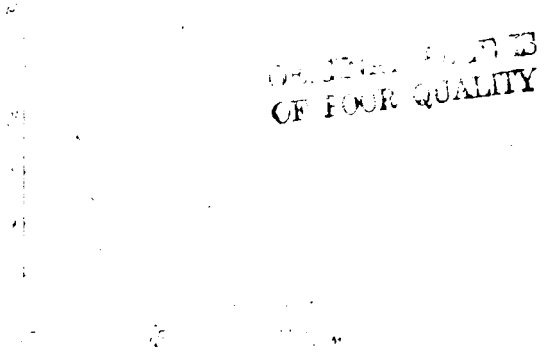

Fig. 67. Richardson number (Ri) vs. altitude -- for measured atmospheric parameters.

Unfortunately, all available data on optical characteristics, chemical composition of the atmosphere, and the altitude profiles T(h) and P(h) do not allow one to come to an unambiguous conclusion about the composition of the Venusian clouds. Until recently, water droplets, ice crystals, and dust have been mentioned as the most probable components. Furthermore, on the basis of comparing laboratory spectra of various substances with Venusian spectra, as well as on the basis of views that have been expressed about the effectiveness of the degassing processes of the hot planetary surface, there have been suggestions that there are more complex condensates in solid and liquid phases in the atmosphere and that the cloud structure is highly stratified.

We note that as a result of the effectiveness of convective and turbulent processes at altitudes where clouds form, the location of their upper boundaries and the mixing ratio of the components that undergo phase transitions cannot remain unchanged -- as Gierasch and Goody have pointed out [313]. This circumstance could make the structure of Venus clouds even more complex.

Of the varous hypothetical aerosols that help make up the Venusian clouds, not all are equally probable. Many are ruled out for one or another reason, resaons founded on experimental data or on comparisons of experimental data with laboratory experiments.

The Venera-8 photometric measurements of the character of the attenuation of solar radiation (cf. Section V.3) and radio astronomy data [464] have definitely repudiated the notion that there is a significant dust content in the atmosphere.

One may rule out dry ice; its condensation temperature is too low to be reached in the Venusian atmosphere. To be sure, if

one begins with the proposition that there is a mesopause with a temperature $T_M \approx 150°K$ as is indicated by an analysis of the Mariner-5 measurements (cf. Fig. 57), then a certain portion of dry ice could be part of the customarily assumed "haze" in the topmost clouds of the Venusian stratomesosphere. /183

The results of comparing observed and laboratory spectral characteristics repudiate any notion of monomeric or partially polymerized C_3O_2; there are no well-manifested narrow minima in the absorption spectrum of solid C_3O_2 at $\lambda = 2.27$ and 2.67 μm, nor is there a broad region of intense absorption between $\lambda = 2.9$ and 3.4 μm [456]. Moreover, the equilibrium vapor pressure above C_3O_2 clouds would significantly exceed the upper spectroscopic limit of gaseous C_3O_2 content (cf. Table 11). For the same reason, and also because of the absence of characteristic indications in the Venusian spectrum (e.g., the absorption region at $\lambda = 2.4$ μm [454]) and the thermodynamic instability in a weakly-oxidizing medium, Lewis [399, 400] rules out hydrocarbons and other organic compounds.

In this regard, Surkov et al [153a] assume that there are hydrated and anhydrous ammonium salts (carbonates and hydrocarbons), which condense at temperatures below 330°K and which are a white substance with a refractive index $m \approx 1.53$, in the clouds. Pure ammonium clouds are impossible, due to the low spectroscopic limit of NH_3 content and their own low refractive index which is incompatible with observations. Starting from the appropriate characteristics of absorption observed in the region λλ 3.0 - 3.3 μm, Kuiper [394] has suggested ammonium chloride NH_4Cl. However, ice crystals are in even better agreement with Venusian spectra in this range; furthermore, the refractive index for NH_4Cl is too high ($m = 1.61$), and this does not agree at all with the estimates that ensue from polarimetric measurements (cf. Section V.3).

Silicates and the products of their reaction with HCl and HF at temperatures $T \lesssim 500°K$, as well as partly hydrated ferrous chloride, have also been mentioned as other possible components of the clouds. It is not likely that they are indeed present, inasmuch as the laboratory characteristics of the reflection of most of these substances is incompatible with the Venusian reflection spectrum.

In addition, if silicate dust were present at the cloud tops, it would be difficult to explain the observed color ("the yellowish tint") of Venus [171, 172]. Accepting the hypothesis that $FeCl_2$ hydrates [394] are present in the clouds would require an H_2O equilibrium mixing ratio approximately one or two orders of magnitude less than the spectroscopic estimate of water vapor content in the Venusian atmosphere. In addition, Cruikshank and Thomson have concluded that identifying the features of the spectrum at about 1 μm, 0.5, and 0.39 μm with the Fe^{2+} electron band is unconvincing [257]. /184

ORIGINAL PAGE IS
OF POOR QUALITY

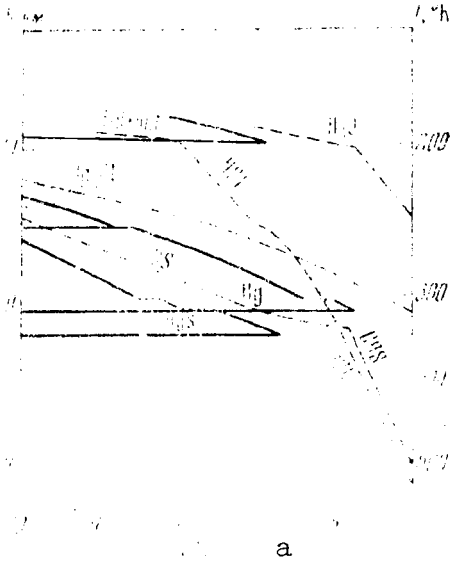

Fig. 68. The structure of the hypothetical clouds in a H, C, N, O, S, Cl, F, Hg system for one of the models at a partial pressure $P_{HG} = 2.10^{-4}$ bar (according to [400]). The solid lines are the clouds; the broken line are gases.

Key: a. kg/cm^2

Finally, let us recall the aforementioned (Section IV.6) hypothesis about the existence of condensates of mercury and mercury-halogen compounds. Fig. 68 shows the location of the corresponding layers in the Venusian atmosphere for one of the models that Lewis has examined [400]. It is interesting to compare this with the curve in Fig. 64, which /185 approximates an altitude profile for radio-wave attenuation in the Mariner-5 experiment. Although this comparison appears to be rather convincing, and while the parameters of the mercury-halogen clouds (particle size $r \approx 20$ μm, density 300 - 400 cm^{-3}) used in the calculations correspond by and large to the characteristics of a dense water cloud on Earth, nevertheless their existence in the Venusian atmosphere is rather problematic.

It would seem natural to examine the most obvious possibility: the formation of water-ice clouds on Venus. A sizeable water vapor content, as determined from the results of gaseous analysis on Veneras-4, -5, and -6 (cf. Table 11) gives reason to assume that H_2O clouds and condensates of a different chemical nature exist on Venus. Fig. 69a shows a phase diagram for H_2O; this allows one to estimate the levels of water vapor condensation and the extent of water-ice clouds for various mixing ratios fH_2O. The dashed curve corresponds in coordinates P-T to pressure and temperature altitude profiles for a model stratomesosphere with $T_M \approx 195°K$. The dotted-dashed line corresponds to the Mariner-5 measurements (cf. Fig. 57). As we see, at a mixing ratio of $f_{H_2O} = 10^{-2}$ for both alternatives of stratomesospheric structure, condensation should begin at temperature $T = 264°K$ and pressure $P = 0.25$ kg/cm^2, i.e., at a level $h \approx 59$ km. As altitude increases and as, accordingly, temperature decreases, vapor-ice phase transitions should predominate over vapor-water phase transitions (if one assumes that no strongly supercooled droplets (theoretically capable of existing in Earth conditions up to a temperature of -40°C) are present [165]).

It follows from Fig. 69a that in the whole stippled region between points 1 and 2 the condition $e = E(T)$ is met, i.e., the

ORIGINAL PAGE IS
OF POOR QUALITY

/186

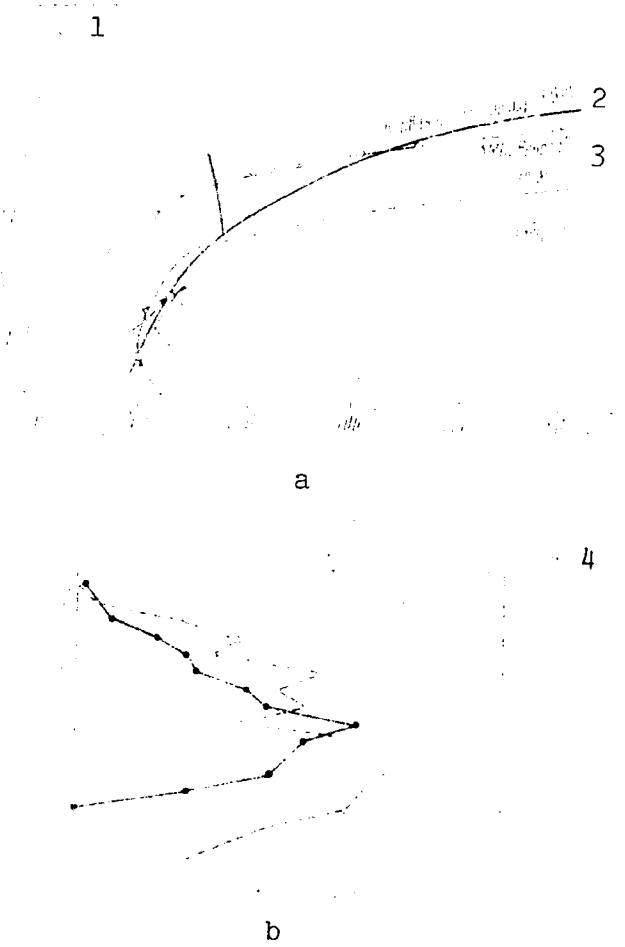

Fig. 69a. Phase diagram of water and the results of temperature and pressure measurements in coordinates P - T (the solid curve with the dots is Venera data; the dashed line is the model stratomesosphere [99]; the dotted-dahsed line is Mariner-5 measurements; the narrow lines are the relative contents of water vapor 1% and 0.1%). The stippled region is the region of H_2O condensation and sublimation. At point 1, T = 264°K, P = 0.25 kg/cm^2, = 59 km. At point 2, T = 198°K, P = $1.40 \cdot 10^{-5}$ kg/cm^2, h = 107 km. At point 3, T = 225°K, P = $2.68 \cdot 10^{-4}$ kg/cm^2, h = 76 km.

Fig. 69b. Distribution of liquid water content (1) and water vapor content (2) vs. altitude in the Venusian atmosphere according to Richter [471].

Key: 1. kg/cm^2
2. H_2O vapor pressure curve
3. Venera AIS
4. g/cm^3

equality of partial water vapor pressure e and the pressure of the saturating vapor E(T) over water or over ice; the thick line 1-2 corresponds to this. Sublimation should thus occur up to a level where temperature T = 198°K and pressure $1.4 \cdot 10^{-5}$ kg/cm^2, i.e., up to an altitude of h ≈ 100 km in a layer more than 40 km thick. It is possible to assume, however, that the effective extent of the clouds is substantially less (≈ 10 km), due to gravitational precipitation of particles in accord with Stoke's law, especially in the upper part of the cloud, where the pressure and ascending flows are small. This agrees with notions about the blurredness of the Venusian cloud tops -- which is well known from ground-based observations [117]. Let us note, too, that the altitude of the cloud tops which corresponds more or less to the level where pressure is about 0.05 atm has been independently confirmed by a series of other arguments; these arguments are related to the interpretation of the reflecting characteristics of Venus and are examined in detail in works [119, 238, 461, 479].

If one begins by assuming that the mixing ratio is $f_{H_2O} \approx 10^{-3}$, then according to the phase diagram in Fig. 69a, in the first case (model distribution), the condition e = E(T) is not met at all, and in the second case (Mariner-5 data), it is met only above that level where temperature and pressure are T ≈ 230°K, P ≈ $6 \cdot 10^{-2}$ gk/cm^2, i.e., beginning from altitude 67 km. From the standpoint of choosing between these possibilities, Fig. 57 is quite characteristic: the dashed line shows the differences in values of γ at the transition from a dry to a wet adiabatic gradient and the absorption lines for various mixing ratios f_{H_2O}. The rather abrupt change in the measured temperature profile at an altitude of about 59 km and its tendency toward a dry adiabat are evidence that condensation and sublimation begin at a mixing ratio ≈ 10^{-2}; this is in agreement with the Veneras-4 - -6 measurements of water vapor content.

The wet adiabatic gradient, with the latent heat of evaporation subtracted, is usually written as (cf. [108]):

ORIGINAL PAGE IS
OF POOR QUALITY

(IV.30)

where γ_a is expressed according to (IV.12) and L = L(T) is the latent heat of phase transition (L ≈ 610 cal/g for vapor-water /188 transition and L ≈ 690 cal/g for vapor-ice transition). In contrast to E(T), L(T) is usually weakly dependent on temperature.

By expressing the derivative dE/dT by the Clausius-Clapeyron equation, and substituting the known numerical values of entry values, Obukhov and Golitsyn [123] have obtained a simplified expression for estimating the role of vapor-water and vapor-ice phase transitions; the purpose here is to determine how the wet adiabatic gradient varies with altitude by extrapolating above the level where the Venera measurements began:

ORIGINAL PAGE IS
OF POOR QUALITY

(IV.30')

(IV.30")

Their computed values E/P for mixing ratios $7 \cdot 10^{-3}$ and 10^{-3} are also in rather good agreement with the experimentally-revealed break in profile T(h) near the condensation level and with its course in the clouds if $f_{H_2O} \approx 7 \cdot 10^{-3}$.

The stippled region between points 1 - 2 in Fig. 69a characterizes the specific moisture content in the liquid and solid phases (water content) of the hypothetical H_2O clouds, as determined from relation

(IV.31)

Substituting the corresponding values gives a mean value of water content of $M_o \approx 0.6$ g/m^3 at $f_{H_2O} \approx 10^{-2}$. It is easier to reconcile the limiting estimate of the total content of liquid water given in IV.5 with the value M_o for $f_{H_2O} \leq 0.5 \cdot 10^{-3}$. As already noted, at a cloud layer thickness of $7 \div 8$ km [123], $M_o \leq 0.4$ g/m^3 corresponds to the value B obtained.

On the basis of an analysis of the absorption of radio emission on the Mariner-5 radio translucence experiment, Richter has obtained interesting results concerning the possible structure /189 of the Venusian cloud layer [471]. Comparing the losses and the refractive coefficient in this experiment with those calculated for a 100% CO_2 atmosphere and assuming that this difference is caused by the presence of water vapor and water droplets, he separated these components and determined altitude profiles of their content (Fig. 69b). The upper limit of the total content of water droplets was

$$B \leq 0.35 \text{ g} \cdot \text{cm}^{-2}$$

which is close to $B \leq 0.3$ g$\cdot$cm^{-3} determined by Kuz'min and Vetukhnovskaya [187].

The hypothesis about H_2O clouds encounters definite difficulties: the results of optical ground-based observations. For this reason, the possibility of water-ice Venusian clouds is subject to serious doubt [119, 183, 336, 469]. We shall review the principal objections to this hypothesis.

In a whole series of works, the possibility of H_2O clouds existing on Venus has been repudiated in connection with the almost complete absence of the depressions in bands λ = 1.5 and 2.0 μm characteristic of ice in the planetary spectrum.

Kuiper [388, 389, 391, 392] has obtained Venusian reflection spectra with a resolution of ≈ 20 cm^{-1} from a high altitude airplane and has cast doubt on the earlier findings of Bottema et al [220], who had found such depressions in spectra with a much lower resolution obtained from a high-altitude balloon. The identification of these spectral characteristics is not an easy task because of the influence of strong carbon dioxide absorbing bands in the same regions, especially near λ = 2.0 μm (the triad of CO_2 bands, cf. Fig. 71a). Sagan and Pollack [461, 479] used the results of solving the equation of radiative transfer using the Schuster-Schwarzschild approximation to do a detailed analysis of the reflection spectrum of a medium in which multiple anisotropic scattering takes place. They concluded that it is possible to attribute the small minima in the spectrum at 1.5 and 2.0 μm to reflection from ice clouds and only partly to absorption in CO_2 bands occurring in the atmosphere above the clouds. They also noted evidence in /190 favor of ice crystals: the very weak reflection throughout the region λλ 3.0 - 3.3 μm. Ice has a fundamental absorption band centered at λ = 3.1 μm.

By studying the laboratory reflection spectra of ice crystals of various size (with varying degrees of dispersion) in the spectral interval 0.9 - 3.4 μm, Plummer [454] has concluded that the depressions at 1.5 and 2.0 μm in the Venusian spectrum can be caused by ice particles with a characteristic size r ≈ 2. This conclusion was made on one rather strong condition, namely, that the optical thickness of the ice cloud is $\tau_c \approx 10$. In interpreting Kuiper's spectrograms, Plummer also assumed [455] that a definite underestimation of the magnitude of the depression was possible -- if as a comparison spectrum the spectrum of the Moon's reflection is used, since the Moon is not a gray reflector. In his estimates, the degree of CO_2 absorption at λ = 1.93 μm and at λ = 2.05 μm differs by 14 and 30%, respectively, from the minimum that Kuiper observed in the Venusian spectrum. This brings the measured character of absorption on Venus closer to ice clouds.

The results of the theoretical analysis done by Hansen and Cheyney [333, 334] using numerical methods can agree with conceptions about the water-ice makeup of the visible clouds only if an approximately 20% depression in the continuum λ = 2.0 μm exists, and only if it is assumed that $\tau_c \approx 10$. At the same time, the results of numerical calculations (using a method of statistical analysis; Krekova et al [560]) of the spectral albedo in the near infrared region (1.4 μm ≤ λ ≤ 3.2 μm) for a cloud layer with $\tau_c \leq 10$ led the authors to the conclusion that in taking account of the combined effect of multiple scattering and absorption due to ice particles and also CO_2 absorption, it is the latter that has

the fundamental influence on the formation of bands λλ 1.5 μm and 2.0 μm; an increase in τ_c has comparatively little effect. Hence, they maintain that the ice particle hypothesis at least does not contradict the measured spectrum of the planet (with averaging at intervals of $\Delta\lambda \approx 0.05$ μm).

The extremely low water vapor content near the cloud tops /191 (the region to which spectroscopic and polarimetric measurements refer) is evidence against the ice-cloud hypothesis.[18] It should be kept in mind, of course, that there is uncertainty in estimating the location of the atmospheric level to which the albedo of Venus belongs in the continuum of the near infrared region of the spectrum, and that there are difficulties in explaining the observed phase dependence of individual absorption lines. It is possible to reconcile a reduction in temperature to 160 - 180°K with a reduction of H_2O mixing ratio down to magnitudes of 10^{-6} - 10^{-7}, which correspond to spectroscopic data, provided that these estimates are for levels with a temperature of about 60°K lower than the customary estimates of the temperature of H_2O absorption line formation. This, however, is hardly likely [119, 551]. The assumption of a homogeneous scattering medium, in particular, scarcely affects the altitude of the level, although it is quite clear from Fig. 57 that there is a rather anomalous atmospheric structure at altitudes of about 60 - 80 km, whereas profiles T(h) are obtained by averagings over spatial dimensions of several hundred kilometers, which is connected to the methodology of measurements [305]. (One of the possible reasons for the behavior of the curve T(h) is that the clouds are not continuous but with significant breaks, i.e., irregular cloud structure within the bounds of a spherical layer of 20 km thickness).

According to polarimetric observations, the refractive index at the cloud tops ($m = 1.44 \pm 0.02$) differs substantially from the refractive index for ice and water droplets ($m = 1.31 - 1.33$). An increase in m may be caused by aqueous solutions of several compounds present in the Venusian atmosphere. Lewis [402] has suggested that the clouds and haze are enriched with an aqueous solution of HCl. As an analysis of corresponding phase diagrams of state shows, spectroscopically determined equilibrium contents /192 of HCl and H_2O in the gaseous phase are met by a 6-molar aqueous HCl solution (25% concentration by weight) at a temperature of about 200°K above the solution. Fig. 70 shows the isopleths of the refractive index of an HCl solution vs. temperature and concentration by weight; these are according to laboratory measurements and the results of calculations according to the Lorentz-Lorenz equation at low temperatures. If there is a 25% HCl solution

---

[18] It is interesting to note that the amount of precipitated water at level $T \approx 250$°K, which corresponds approximately to the H_2O detection level, turns out to be about 40 times smaller than the amount of H_2O recorded in the atmosphere of Mars at a much lower temperature $T \approx 210$°K (cf. [487a]).

and if T ≈ 200°K, the refractive index m ≈ 1.42 is very close to the value obtained for Venus.

ORIGINAL PAGE IS
OF POOR QUALITY

Fig. 70. Isopleths of the refractive index of an aqueous HCl solution vs. temperature and concentration by weight (according to [402]).

Key: a. Ice
b. HCl concentration by weight

The spectral characteristics of an aqueous HCl solution at T = 205°K are in good agreement with the Venus spectrum between 3 and 4.5 μm (cf. Fig. 71) and differ little from the H_2O spectrum. Slight variations in the near ultraviolet region with the addition of HCl could be explained by the presence of hydroxonic acid ions H_3O^+ [338],[19] /193 ions that have a broad absorption band in the region λλ 3 - 5 μm and in a longer wavelength range. The required temperature, however, is much lower than the temperature of spectral line formation T ≈ 250°K, although the presence of H_3O^+ could in principle lead to a change in the intensity of the rotational lines in the CO_2 bands, as well as to a certain difference between measured temperature and temperature on the emission level.

These hypothetical components of the Venusian clouds have all had serious drawbacks; however, this can be overcome within the framework of a hypothesis about a concentrated (≈ 75 - 80%) aqueous solution of sulfuric acid. Both Sill [498] and A. Young

[19] It is appropriate to point out that from the point of view of theory, electrolytic dissociation of acid (HA) is the name for a compound that dissociates in an aqueous solution to form hydrated ions (hydroxonic ions) and an acid residuum: $HA + H_2O \rightleftarrows H_3O + A^-(H_2O)_m$ [227a]. The H_3O^+ ion also has all the general properties of acids. The proton exchange of acid with water consists in the fact that acid can detach H^+ protons, while water combines with them to form an H_3O^+ ion. In aqueous solutions, therefore, there are no free protons, only hydroxonic ions and solvated molecules of water. For example

$$HCl + H_2O \rightleftarrows H_3O^+ + Cl^-,$$
$$HNO_3 + H_2O \rightleftarrows H_3O^+ + NO_3^-,$$
$$H_2O + H_2O \rightleftarrows H_3O^+ + OH^- \text{ (dissociation of water)}$$

[550] have very recently offered this most exotic hypothesis. Polarimetric and spectrometric data are explained by this hypothesis; and it is favored by a number of chemical arguments.

The refractive index of H_2SO_4 clouds (1.442 ± 0.001) corresponds to that determined for Venus. Since the freezing point for sulfuric acid hydrates is about 235 - 250°K, this explains why the cloud particles near the cloud tops retain their liquid-droplet state; this is indicated in polarimetric observations.[20] The remarkable dessicating properties of H_2SO_4 easily explain the reason for the extraordinarily low atmospheric humidity recorded above the cloud layer. Thus, the water vapor pressure over a 75% solution of sulfuric acid is about 1%. From this point of view, nitric and phosphoric acid are far less suitable agents, since they have no chemical affinity with water; furthermore, they have a markedly different refractive index at T ≈ 250°K. /194

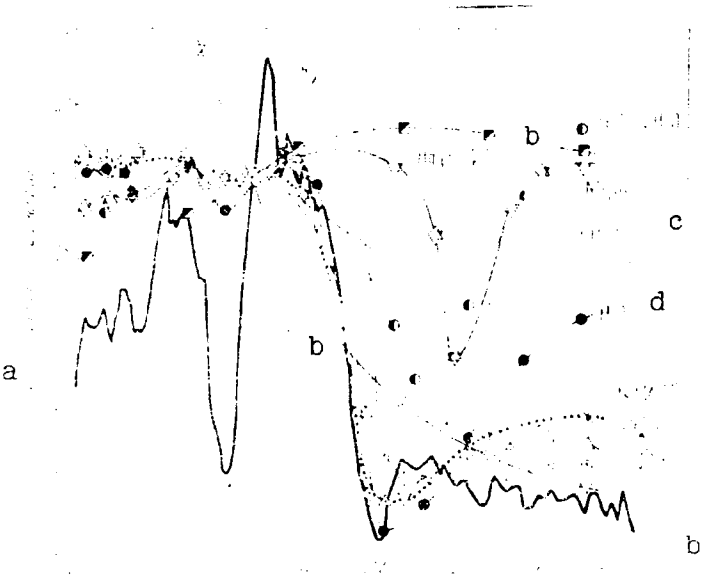

ORIGINAL PAGE IS
OF POOR QUALITY

Fig. 71a. Venusian reflection spectrum (R_λ) in the region 1 - 4 μm in comparison with the spectral characteristics of water, ice, mercury, ferrous chloride, ammonium chloride and aqueous solutions of sulfuric and hydrochloric acid (according to [464a]).

Key: a. Relative reflection
b. μm
c. Liquid
d. Ice

[20] The sphericity and homogeneity of cloud particles results from the fact that the rainbow is clearer with a transition to a shorter wavelength region of the spectrum [337].

A number of spectral characteristics of Venus provide evidence in favor of H_2SO_4 clouds. In particular, the sharp decrease in reflectivity in the spectral region λλ 3.2 = 3.6 μm and the emission spectrum in the region 7 - 14 μm, especially the wide depression at λ = 11.2 μm, are in satisfactory agreement with this proposition. Figs. 71a and 71b reproduce the features /195
of the Venusian spectrum in these areas in comparison to laboratory spectral characteristics of H_2SO_4 hydrates and other compounds. Fig. 71a contains the results of recent measurements of the spectral albedo of Venus in the near infrared region; Pollack et al [464a] made these measurements from a high altitude airplane and using a spectrometer with a circular interference filter and a cooled (to 77°K) PbS detector as a receiver. Analysis of these spectra led the authors to the conclusion that, of all the substances examined, a 75% H_2SO_4 solution is in the best agreement with the reflecting characteristics of Venus in the 3 μm band. The depressions at λλ 1.4, 1.6, 2.0 and 2.8 μm are explained by CO_2 absorption. The measurements show that $R_\lambda = 2.0/R_\lambda = 1.0 \approx 1.6$ is in good agreement with the estimate that Kuiper et al (cf. [555]) obtained previously. Such features do not appear in a laboratory H_2SO_4 spectrum, but Pollack et al [583] note the possibility that there are admixtures dissolved in acid, specifically iron in the form of the trivalent ion Fe^{3+} (present in salt solutions), within the clouds. In order to explain the observed strong reduction of the Venusian spectral albedo in ultraviolet and to explain the yellow tinge of the clouds, Hapke [338] has offered a similar hypothesis with regard to hypothetical clouds enriched with an HCl solution.

The presence of H_2SO_4 is of interest also as a possible /196
explanation for the peculiarities noted in the behavior of measured curves T(h) and ρ(h) and in the character of radio-wave attenuation. Specifically, the discharge of a large quantity of heat during the formation of solutions in the lower-lying atmosphere and at an f_{H_2O} that corresponds to the data of direct measurements should result in a difference between the temperature profile and the adiabatic that is more pronounced than in the case of a wet adiabat. The amount of sulfuric acid needed to form a dense cloud layer is not large; and it is in agreement with the relative abundance of sulfur in the universe as well as with its expected appearance in the atmosphere from the interior through volcanic eruptions. It is difficult otherwise to reconcile the extremely low upper limit of the contents of sulfur compounds with the data in Table 11. At the same time, the breakdown of sulfates at high temperatures in the presence of HCl could prevent them from being used up in the atmosphere as they combine in reactions with surface rocks [550].

At a 76% concentration at a level where P = 50 mbar, $\tau \approx 1$ would assure a uniform layer of droplets 2.2 μm in diameter. In this case the required quantity of H_2SO_4 is, according to Young's estimates, about 0.29 mg/cm^2 or, with respect to CO_2 content,

ORIGINAL PAGE IS
OF POOR QUALITY

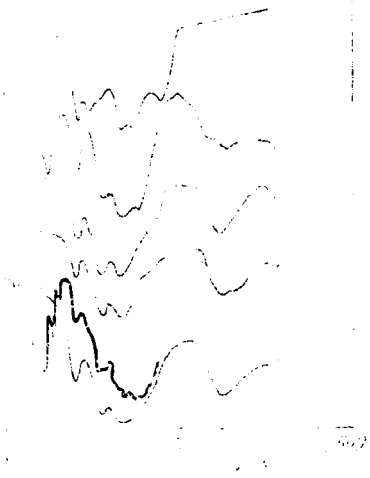

Fig. 71b. Spectrum of Venus' own infrared radiation in the 7 - 14 μm region in comparison with solid and liquid hydrates of H_2SO_4: 1. 100% solid H_2SO_4; 2. 84.5% solid $H_2SO_4 \cdot H_2O$; 3. 73.15% solid $H_2SO_4 \cdot 2H_2O$; 4. 57.7% $H_2SO_4 \cdot 4H_2O$; 5. 10 μm, 78.5% liquid H_2SO_4 [550].

$2.3 \cdot 10^{-6}$. If one assumes constant ratios by weight of H_2O and H_2SO_4 below the level of the visible clouds, and if one assumes that 99% of the water at this level is compounded with sulfuric acid, then at $f_{H_2O} \approx 10^{-3}$ H_2SO_4 content turns out to be about three orders of magnitude larger. The uncertainty in this regard is related to the fact that estimates vary widely about the extent (which depends on the intensity of the mixing process) to which the droplets precipitate.

In a large cloud, the amount of water should increase with depth due to the release of compounded water from the droplets of the solution as temperature increases; this would lead to a change in the concentration of the H_2SO_4 solution. Both the concentration of the solution and the extent of the clouds depend in turn on the total water content in the atmosphere. Estimates of the equilibrium relation between the gas phase and the cloud droplets at various levels in the atmosphere, with constant functions of H_2SO_4 and H_2O by weight at every level, are shown in Fig. 72 according to [550]. If $f_{H_2O} = 10^{-3}$, nearly /197 all the water at $T \approx 273°K$ is still concentrated in droplets, and the 76% H_2SO_4 solution corresponds to the equilibrium vapor pressure. The clouds in this case could extend to the boiling point at T = 533°K and P = 14 atm (h ≈ 26 km); an ~ 98.3% H_2SO_4 solution corresponds to this level. If $f_{H_2O} = 10^{-5}$, then the concentration by weight even at T = 250°K should be no less than 85% (which is less compatible with polarimetry data), while the lower boundary turns out to be at level T = 373°K and P = 2.4 atm (h = 44 km). Finally, with $f_{H_2O} \approx 10^{-4}$, the clouds should end near h ≈ 35 km, where a strong change in the character of attenuation of solar radiant energy vs. depth has been revealed (from Venera-8 data) (cf. Chapter V).

Thus, a series of data provide definite evidence in favor of /198 the notion that the visible clouds could consist of concentrated acid solutions, primarily H_2SO_4. Nevertheless, a more detailed

analysis of this interesting question is necessary, and, of course, direct experimentation as well, before we can draw more definite conclusions about the composition of the Venusian clouds.

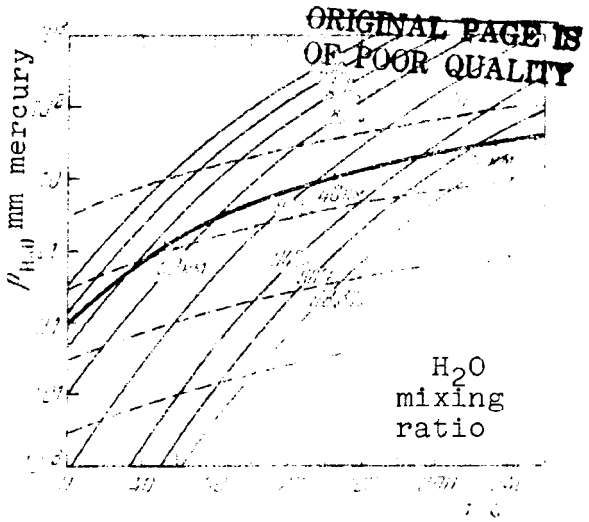

Fig. 72. Diagram of the equilibrium state of H_2SO_4 condensate from the gas phase at various H_2O mixing ratios vs. temperature (according to [550]). The narrow curves -- vapor pressure for various percentage concentrations of aqueous H_2SO_4 solution. The dashed line -- the H_2O mixing ratio for an atmospheric model according to [412]. The dotted-dashed line -- the boiling point. The thick curve -- a model with H_2SO_4 clouds at $f_{H_2O} \approx 10^{-3}$.

The estimated (photographic measurements) altitude of the cloud tops can agree with the value of the "optical radius" of Venus as cited in Chapter 1: $\overset{*}{\varphi} R = 6120 \pm 8$ km [533]. By measuring the equivalent widths of CO_2 bands at $\lambda = 1.6$ μm near the inferior conjunction of Venus, Moroz [119a] has discovered an asymmetry in the position of the band formation level; this can be attributed to the fact that the cloud tops at polar latitudes (the polar tropopause) are 5 - 7 km lower than at equatorial latitudes. /200

As photographic measurements of the crescent of Venus near inferior conjunction have shown [394], the apparent limb of the planet does not coincide with the upper boundary of the comparatively dense layer of haze recorded in the short-wave region of the spectrum. In the red and near-infrared regions, this boundary is $R^{*}_{\varphi}R = 6100$ km, while in ultraviolet region ($\lambda \approx 3600$ Å) $R^{*UV}_{\varphi} = 6145$ km.

The altitude correspondence of "ultraviolet clouds" is directly related to this last estimate. Figs. 73a and 73b show examples of photographs in ultraviolet rays obtained at a New Mexico observatory and during the Mariner-10 flight past Venus. According to Kuiper [394], the strongest contrasts of cloud structures appear in the range 3200 - 4000 Å, with a maximum at $\lambda = 3600$ Å. The atmospheric density at altitudes r = 6120 - 6145 km is sufficient to ensure an appreciable scattering of ultraviolet above the cloud tops. At longer wavelengths ($\lambda > 4000$ Å) scattering predominates, while in the short-wave region, ($\lambda <$ 3200 Å) absorption by atmospheric gases apparently has the most substantial impact. These features are examined more closely in Chapter V.

ORIGINAL PAGE IS
OF POOR QUALITY

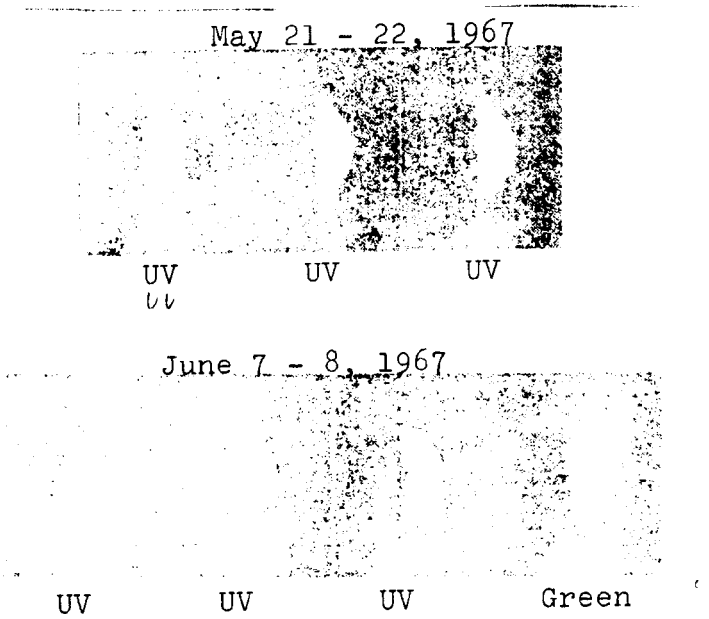

Fig. 73a. Ultraviolet ray photographs of Venus from ground-based observations in New Mexico. For purposes of comparison, the photograph is shown in green light. Below are the times of the observations. B. Smith kindly furnished the photographs.

IV.8. Several Considerations About The Origin And Evolution Of The Atmosphere.

The preceding paragraphs have contained convincing evidence that the Venusian atmosphere is a unique gaseous shell, a shell that is fundamentally different in its most important characteristics from the atmosphere of the Earth. Its basic chemical component is carbon dioxide (in the Earth's atmosphere, relative CO_2 content is 0.03% on the average), the surface temperature is about 500°C and the pressure is almost 100 atm. Naturally, questions have arisen about what led to the development of such unusual conditions, what processes have caused the formation of a massive and hot CO_2 atmosphere and, at the same time, left the planet practically devoid of water. It is important to understand whether the Venusian atmosphere is the necessary product of an earlier stage of evolution or whether existing conditions developed later, as a result of irreversible processes related to the planet's proximity to the Sun.

Based on the hypothesis that the planets of the Solar System formed simultaneously from the agglomeration of the cold material

ORIGINAL PAGE IS
OF POOR QUALITY

of a protoplanetary nebula of gas and dust [21], it is possible to conjecture that the original composition of the planetary atmospheres was about the same as the relative abundance of the chemical elements in the Sun (cf., for example, [528, 529, 571]). Subsequently, however, the most abundant elements, hydrogen and helium, were retained only by the cold giant planets, which formed on the periphery of the Solar System primarily from these gases. Heavier and less widespread elements -- the metals, together with their oxides and sulfides -- entered into the composition of the solid, iron-silicate phase of the terrestrial planets, which were closer to the Sun. Since the Earth, Venus, Mars and Mercury all had relatively small masses, the lightest elements, hydrogen and helium, disappeared into space.

Starting with current conceptions [30, 480], it is possible to maintain that the atmospheric composition of the terrestrial planets was determined primarily by the escape of volcanic gases that accompanied the differentiation of the planet's substance into layers, a process which occurred under the impact of the gravitational potential energy of accretion, density convection in the mantle, and thermal energy of radioactive decay.[22] In the process, easily-melted basalt material was /202 extruded from the mantle in accord with the mechanism of zonal melting; degassing accompanied this extrusion.

Water vapor and carbon dioxide are the basic parts of the volcanic gases formed by chemical reactions at the high temperatures and pressures in the interior of the planet. These gases, the composition of which depends on the conditions in which the reaction takes place (especially the temperature) and on the mass of the relevant substance in the mantle, are dissolved in water in varying degrees and together with the water, are expelled during volcanic eruptions. At the highest temperatures HCl, HF, H_2S, and SO_2 are among the gases expelled; at relatively low temperatures, NH_4CL, $B(OH)_3$, and others are present.

---

[21] In essence, the Kant-Laplace nebular hypothesis, which O. Yu. Shmidt [567] has later surveyed in a slightly different variant, lies at the basis of this conception. A detailed account of the various hypotheses concerning the origins of the planets of the Solar System can be found, for example, in Levin's work [561]. Here we will only remark that, as has been determined experimentally, the relative abundance of the isotopes of various elements is quite similar for the Sun, the Earth and the meteorites, and that this, as well as other cosmogenic and radiogenic data, serves to confirm the hypothesis of a single protoplanetary nebula with a comparatively homogeneous composition. (cf. [65]).

[22] The current hypothesis (for Earth) concerning the tectonics of moving lithospheric plates is now being connected with density convection in the mantle caused by chemical-gravitational differentiation at the surface where the mantle and core of the planet meet (cf. [564, 565]). This is thus an attempt to explain how the Earth's geological development conforms to certain natural laws.

ORIGINAL PAGE IS
OF POOR QUALITY

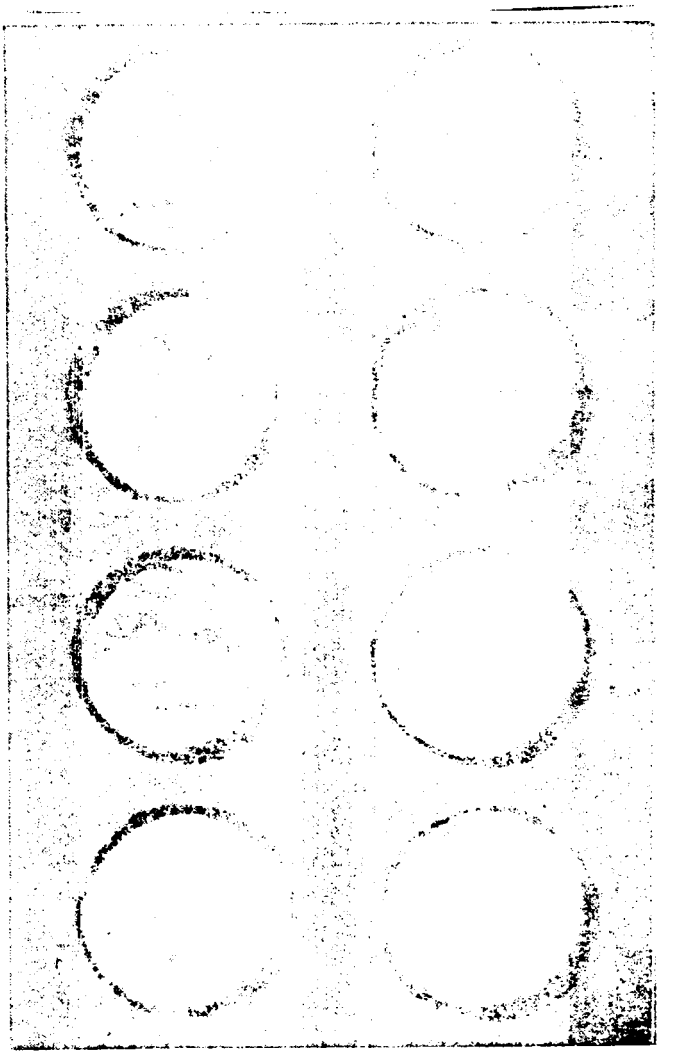

Fig. 73b. Photographs of Venus obtained by Mariner-10 as it flew by the planet; taken at intervals of one day, beginning with t_p + 1 day, where t_p is the time the periapsis was passed. B. Murray furnished the photographs.

The composition of volcanic gases (according to [30]) is cited in Table 13 in order of abundance. Table 13 also indicates the relative content of the basic gases by percentages.

Table 13 shows the predominant role of water, which makes up about 20% by volume of the extrusive basalts. The ratio of relative CO_2 and H_2O content is approximately 5:1. Free /203 nitrogen, oxygen and hydrogen are essentially the secondary products of the reactions.

TABLE 13. COMPOSITION OF VOLCANIC GASES

Group	Gases	Relative content (%)
I	[illegible]	[illegible]
II	[illegible]	
III	[illegible]	
IV	[illegible] and others	

ORIGINAL PAGE IS
OF POOR QUALITY

As is seen, it would seem easier to understand the composition of the Venusian atmsophere, with its overwhelming CO_2 content, in terms of degassing; this is of course less true for the composition of the Earth's atmosphere, in which N_2 and O_2 predominate. It is also possible to understand that the dry Venusian atmosphere contains components such as HCl and HF, which, in conditions on Earth, the rains wash out of the atmosphere and which are dissolved in the oceans or combined in reactions with the solid substance of the Earth's crust; and that it contains sulfur (in confirmation of the H_2SO_4 cloud hypothesis). It is much more difficult to explain the minute quantity of water on Venus, a quantity thousands of times smaller than on Earth.

One clue to why the planets took varying evolutionary paths, traces of which are manifest in the shell of gas that has formed around them, is obviously the position of a given planet in the Solar System and, consequently, its heat balance. In particular, this fact, together with the pressure of solar radiation, has apparently influenced the thermal fractation of the substance in the protoplanetary nebula; this has resulted in a situation where the easily volatile components were depleted in the regions closest to the Sun [561]. It is possible to argue that several billion years ago the composition of the Earth's atmosphere was closer to that of the present Venusian atmosphere than it is to the present Earth's atmosphere, but that it was substantially less dense. According to the most widely accepted hypothesis [30], of decisive importance for the Earth's evolution was photosynthesis, which appeared in the Proterozoic, and which, under the impact of solar short-wave radiation, supplanted abiogenic organic synthesis; this resulted in the appearance of a biosphere and of free oxygen in the atmosphere. According th another conception [565], a more powerful mechanism for carrying oxygen into the atmosphere may be connected with the reorganization of the stoichiometry of ferrous oxides at high pressures and may be caused by the process of density differentiation

ORIGINAL PAGE IS
OF POOR QUALITY

of substances of the mantle at the edge of the Earth's core. This mechanism begins to be effective only after the free iron in the mantle has been completely oxidized; according to calculations for the lherzolitic model of the Earth's mantle, this occurred at the end of the Proterozoic.

The appearance of free oxygen in the Earth's atmosphere must have caused the oxidation of the ammonia contained in the ammonium /204 compounds of volcanic gases as well as the release of free nitrogen into the atmosphere. Since nitrogen is a neutral gas, which does not enter into reactions with surface rocks and which, moreover, has a high threshold of dissociation (which is essential in an atmosphere of small optical thickness), it gradually accumulates in the atmosphere. At temperatures T_e = 275°K, assuming that its original albedo was determined entirely by the surface and corresponded to that of the Moon, i.e., A ≈ 0.07, the Earth retained its water, the basic part of which was concentrated in the oceans. As for the carbon dioxide gas released by degassing from the mantle, since liquid water and a relatively low temperature were present, it accumulated chiefly in the Earth's hydrosphere and the carbonates of sedimentary rocks due to reaction with the metal oxides freed during serpentinization and kaolinization.

The atmosphere of Venus must have gone through a different process of evolution. Evidently, the deciding factor in this regard was Venus' proximity to the Sun. This idea is discussed in detail in the works of Vinogradov [30], Rasool and De Bergh [468] and Pollack [457].

The development of present conditions on Venus probably began when the Sun made the transition to the main sequence when, as is usually suggested, the intensity of its radiation increased by about 30%. Using these notions as a starting point, it would hardly have been possible for climatic conditions favorable to life to appear on Earth had the radius of its orbit been about 10,000,000 km smaller. This is illustrated by a diagram (Fig. 74) taken from [468]; this latter shows how temperature grows from the original temperature T_e in the original planetary atmosphere, which consisted of CO_2 and H_2O in a ratio close to that of the volcanic gases. Although the calculations, which were done according to the radiative transfer equation using the Eddington approximation are only rough estimates, they do allow one to form definite notions about the possible evolution of the Venusian atmosphere. If one begins with the same value A ≈ 0.07, then the equilibrium temperature for Venus according to (IV.1) will be T_e ≈ 325°K; at comparatively /205 low pressures (up to P ≈ 0.2 atm), which evidently correspond to the original planetary atmosphere, this temperature turns out to be higher than the boiling point of water. It is possible that this is one of the basic "boundary" factors that led in the final account to the development of present-day conditions, in which the total water content on Venus is ≈ 10^{-3} of the mass of the Earth's hydrosphere (which is about $2 \cdot 10^{24}$ g [28]). The loss of water by the planet depends on the effectiveness of the dissociation processes at altitudes where the optical thickness in the continuum $\lambda < 2400$ Å (H_2O dissociation is $\tau < 1$. This condition is in turn directly related to the effectiveness

of molecular diffusion, which determines the speed with which water vapor molecules can be delivered to altitudes where dissociation can occur. In conditions on Earth, solar quanta with an energy greater than 5.08 eV, which corresponds to the dissociation threshold of molecular oxygen ($\lambda \geq 2424$ Å), are absorbed at altitudes $h > 100 - 150$ km (although they are present at even higher altitudes, since dissociation time is much longer than diffusion time [438]). CO_2 absorption begins for all practical purposes in the Schuman-Runge continuum (dissociation threshold $\lambda = 1670$ Å) and occurs at a slower rate than for O_2. In an atmosphere with an overwhelming CO_2 content and with practically no O_2, therefore, short-wave solar radiation, which effectively dissociates water vapor, can obviously penetrate deeper, to a level where the absolute content of H_2O molecules is higher. It is possible that a similar situation existed some 1 - 1.5 billion years ago on the Earth, before free oxygen appeared in the atmosphere. At the same time, the fact that the rate of photolysis in Venusian conditions is about 3 - 4 orders of magnitude faster than in present-day conditions on Earth had an undoubted effect on the disappearance of H_2O on Venus [281]. Moreover, it is impossible to rule out the possibility that the temperature of the Venusian stratomesosphere is slightly higher than in the Earth's mesosphere. These factors must have resulted in a more energetic molecular diffusion from below and in an effective dissociation, wherein light hydrogen disappeared from the atmosphere. But oxygen, which diffusion and convection can carry to the lower-lying atmosphere, will combine with the solid substance of the surface rocks. [23] An indirect confirmation that /207 such a mechanism may in fact have existed is, on one hand, the prevalence of CO_2 to comparatively high altitudes and, on the other hand, the existence of a hydrogen corona near Venus with a possible deuterium concentration at its base (due to the fact that it dissipates more slowly) (cf. Chapter VI).

The gradual accumulation of CO_2 and H_2O in the atmosphere and an increase in its density should lead to an increase in temperature

---

[23] Sorokhtin [565] examines the reaction of the thermal dissociation of water vapor over free iron in a regolith-like layer ($3Fe + 4H_2O \rightarrow Fe_3O_4 + 4H_2$); this reaction proceeds at high temperatures simultaneously with the serpentinization reaction and the reaction combining degassed CO_2 and H_2O; this reaction he sees as an additional effective mechanism of water loss, a mechanism active at a comparatively early stage in the evolution of the planet. In order to explain the low oxygen content in the Venusian atmosphere, he suggests that the Fe/FeO ratio in the material of Venus would, if the large degree of thermal fractionation of the protoplanetary nebula is figured in, turn out to be higher than in the material of Earth and that free iron could remain in the mantle of Venus and continue to combine actively with the oxygen discharged as the Venus core grows.

ORIGINAL PAGE IS
OF POOR QUALITY

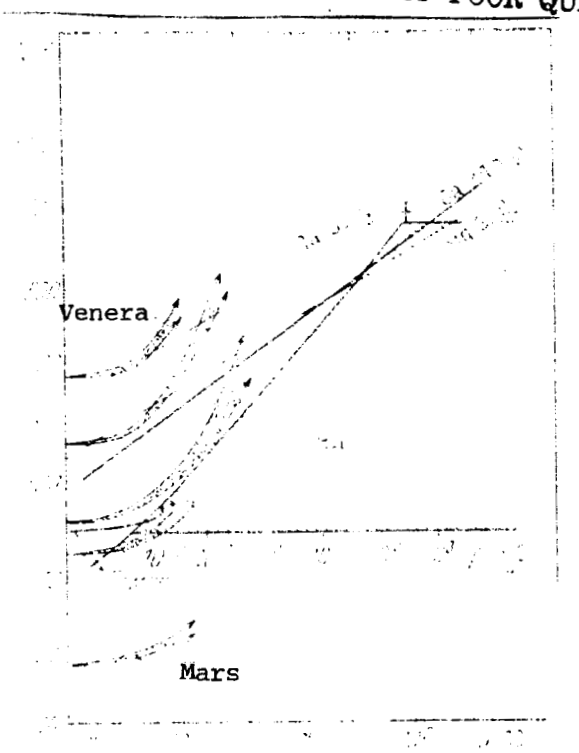

Fig. 74. A diagram showing the change in surface temperature from the original temperature of equilibrium T_e for three planets, a change due to the "greenhouse effect" in a CO_2 and H_2O atmosphere [468]. The curved lines with arrows show the character of the evolution; the narrow curved lines, which correspond to the phase transitions of H_2O, bound a stippled region, inside which water can exist as a liquid. The topmost diagonal lines are the conditions of Wollaston equilibrium. The different evolutionary paths correspond to the various original values of albedo (7 and 20%) for the Earth and, for Venus, to the alternatives of rapid or slow rotation.

due to the development of the "greenhouse effect."

Heating processes, which we will deal with more closely in Chapter V, are intimately linked to the transfer of large quantities of CO_2 and H_2O into the atmosphere. The equilibrium state is determined by carbonate-silicate interaction in the surface layer of the planet -- as in the reactions of Wollaston equilibrium:

$$Ca(Mg)SiO_3 + CO_2 \rightleftarrows Ca(Mg)CO_3 + SiO_2$$

It can be shown that CO_2 content in the Venusian atmosphere is comparable to the total quantity of carbon dioxide tied up in the sedimentary rocks of the Earth's crust, a quantity which, in the estimates of Ronov and Yaroshevskiy [563], is equal to $0.37 \cdot 10^{24}$ g (cf. also [33, 176, 529]).

In fact, as is evident from Fig. 75, the amount of carbon dioxide that passes into the atmosphere corresponds to its equilibrium content according to the diagram of Wollaston equilibrium at a planetary surface temperature of about 750°K. The diagram in Fig. 74 also demonstrates the relationship of the parameters at which the conditions of thermal equilibrium (including H_2O phase transitions) and geochemical (Wollaston) equilibrium can be realized. /208

It is of interest to note that if the temperature on the Earth had increased as high as the Venusian temperature, the pressure of the Earth's atmosphere would have substantially exceeded that at the surface of Venus. This is related to the fact that about 300 atm, the result of evaporation from the oceans (mean depth of the Pacific Ocean is about 3 km), would have been added to a pressure of about 50 atm CO_2, the result of freeing carbon dioxide from the carbonates of the Earth's sedimentary shell [33]. A comparison of the basic volatile components on the Earth and on Venus is given in Table 14. For Earth, both atmospheric content and the content of volatile components combined in sedimentary rocks are shown [351].

TABLE 14. CONTENT OF VOLATILE COMPONENTS (kg/cm^2)

Component	Earth's atmosphere	Total on Earth	Venusian atmosphere
CO_2	$3 \cdot 10^{-4}$	70 ÷ 80	90 ± 15
H_2O	$10^{-3} \div 10^{-2}$	65 ÷ 75	$10^{-2} \div 10^{-1}$
O_2	0,23	~0,23	$< 10^{-4}$
N_2	0,75	~0,75	2
Ar	$1,3 \cdot 10^{-2}$	$\sim 1,3 \cdot 10^{-2}$	
CO	$10^{-6} \div 10^{-7}$	~30	$< 10^{-3}$
H_2		5,7	$< 10^{-3}$
H		$< 10^{-3}$	10^{-7}

ORIGINAL PAGE IS
OF POOR QUALITY

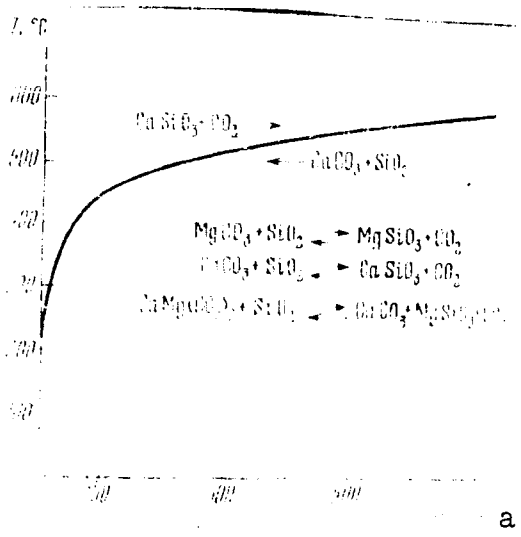

Fig. 75. Calculated CO_2 equilibrium partial pressure vs. surface temperature at Wollaston equilibrium between carbonates and silicates [30].

Key: a. atm

In the light of current conceptions about Venus, it is natural to ask whether the planet is of exobiological interest. This question has been discussed in a number of /206 works (e.g., [483, 580, 583, 585]), whose authors have dealt with the possibility that biologically active forms exist either on the surface or in the clouds. With regard to the surface, one may affirm that most organic molecules that enter into the make-up of biological structures evaporate at temperatures much less than 500°C, that peptides are unstable, and that proteins change their natural properties. Furthermore, there is

no liquid water on the surface. It is possible to rule out, therefore, forms of life similar to those on Earth. It seems rather forced to conceive of "biological refrigerators" or biological structures based on silicon-organic compounds.

Conditions in the clouds are much more favorable. These conditions correspond to a level of about 50 - 55 km on the Earth, excluding of course the prevalent CO_2 content and the almost complete absence of O_2 and N_2. Nevertheless, there are conditions in the clouds for the formation of photoautotrophs. However, since the atmosphere is continuously in motion, there would be some difficulty in maintaining such organisms near a level where conditions are favorable, in keeping them from being carried to the hot atmosphere at lower levels. In order to circumvent this difficulty, Morowitz and Sagan [580] have suggested that there are Venusian organisms in the form of isopycnic balloons filled with photosynthetic hydrogen. In their estimates the diameter of such balloons (which defines their size) would be several centimeters (with a covering about as thick as the membranes in organisms on Earth). /210

Despite their seeming attractiveness, such speculations are in our opinion quite contrived. It is hardly possible to speak seriously about the origin of life in the clouds or about the "remains" of biological forms that once lived on the planet and that have been preserved in the clouds. This of course does not rule out the possibility that at a specific period in its history Venus could have had more favorable conditions, conditions more suited to the existence of life.

V.I. Conceptions About the Heating Mechanism of Venus.

The problem of the optical and thermal regime is one of the most complex problems in the physics of Venus. A successful resolution of this problem will determine not only our understanding of the evolution of Venus and its atmosphere, but also whether we will discover the conditions in which a similar physical mechanism could occur on another planet in the solar system.

Before the beginning of space flight, the great uncertainty with regard to the physical parameters of the planet and the lack of data on the transfer of solar radiant energy in the Venusian atmosphere made it difficult to explain its thermal regime. The discovery of intense microwave emission has given rise to several theoretical models that attempt to explain the physical mechanism responsible for the observed mechanism of radio brightness temperatures. One may tentatively divide these models into those with a hot surface, whose emission in the millimeter range is absorbed by a relatively cooler atmosphere, and those whose radio emission is generated by the atmosphere and whose surface temperature is only a bit higher than that of the Earth. For several years, there has been debate over the acceptability of the physical mechanism upon which this or that particular model has been constructed (cf. Chapter III).

Since it has been difficult to find a convincing explanation for a surface temperature of more than 600°K on a planet that is quite similar to Earth, attempts have been made, beginning with a "hot" atmospheric model, to link observed microwave emission to a /212
hypothetical superdense ionosphere or to gaseous discharges in the atmosphere. Walker and Sagan [538] have subjected these various mechanisms to a persuasive critique, and, in particular, they have shown that it is impossible to explain the observed spectral dependence of radio brightness temperatures in terms of synchotronic or cyclotronic radiation. It is difficult to reconcile the hypothesis of gaseous discharges in the troposphere with the regularity of the emission; furthermore, because of the release of heat during electrical discharges of the required power, the atmosphere would have to be heated to a temperature that exceeds the temperature of the emitting layer [460].

A model with a hot surface has been better substantiated and is supported by the results of optical observations as well. In order to explain the heating of the surface, greenhouse, aeolospheric (friction) and circulation models have been suggested.

In the "greenhouse" model, it is suggested that a definite part of the unreflected solar radiation in the visible region penetrates

to the surface and is then absorbed by the surface[1], while the emission of the surface in the infrared region is captured in the atmosphere by triatomic molecules such as CO_2 and H_2O, which have strong absorption bands in this region of the spectrum. As a result, the surface and the atmosphere are heated to a temperature T_s, which is about the same as the radio brightness temperature of the planet.

Historically, the first such model was that of Wildt (1940), /213 who studied heat transfer in pure carbon dioxide atmosphere of Venus and with a comparatively small optical thickness; he concluded that heating due to the greenhouse effect would not in this case exceed about 50°K [545a].

Sagan's [477, 478] greenhouse model, proposed in 1960, was calculated with integral absorption functions that were contained in the technical literature on boilers and ovens, and it included an attempt to make an approximate calculation of the overlapping of bands within the infrared region he was examining. In a "gray" atmosphere approximation, he obtained estimates of the opacity required to reduce the outgoing heat flux at Ts ≈ 600°K to a value equal to the flux of the absorbed solar radiation, and he showed that the necessary degree of heating is reached in an atmosphere with a high CO_2 content and with 1-10g·cm^{-2} of water vapor present. The atmosphere's opacity to infrared radiation should here be about 99%. If the Milne-Eddington approximation for radiative equilibrium in a "gray" atmosphere (formula (IV.27)) is used, then the required value of optical thickness τ to assure a temperature $T_s \approx 750$°K at $q = E_c(1 - A) \approx 3 \cdot 10^5$ erg·cm^{-2}·sec^{-1} (cf. (IV.1)) turns out to be equal to $\tau \approx 150$; this, generally speaking, is not realistic. However, in the work of Sagan and in the later work of Jastrow and Rasool [361], who did more detailed calculations of radiative transfer in a "gray" approximation, there was no attempt to identify the required opacity with the physical properties of the real atmosphere.

The suggestion that pressure in the tens of atmospheres exists on Venus compelled a more careful estimate of the possible change in

---

[1]The term "greenhouse model" is generally applied to the atmosphere in a figurative sense, and one should guard against the rather widespread error of understanding the term literally, i.e., of making an analogy with greenhouses. In greenhouses, the basic effect is not that the glass prevents the shortwave radiation from escaping, but that there is no convective and circulatory heat exchange. In a free atmosphere, most of the heat is moved about in this way. R. Wood pointed this fact out and confirmed it with his well-known experiment with black cardboard boxes. One was covered by a glass plate, the other by a plate of rock salt (transparent in the long wavelength region). Both boxes were placed in the sunlight, and the resulting temperatures turned out to be virtually identical -- about 55°C (cf. V. Sibruk, Robert Wood, Gostekhizdat, 1946, pp. 130-131).

the characteristics of absorption bands in such conditions. Plass and Wyatt [451] have demonstrated that at high pressures, CO_2 opacity in individual regions of the infrared spectrum increases substantially. Nevertheless, the authors's estimates of radiative transfer were made on the same simple assumptions as Sagan had made in his works. Moreover, the failure to take account of cooling at $\lambda > 20$ μm in the pure CO_2 atmosphere under discussion is too great an oversimplification of the real character of radiative transfer in a CO_2 /214 medium.

The clouds obviously should play an important role in the question of heat exchange on Venus. The first attempt to take their effect on the distribution of radiative fluxes into consideration was undertaken in 1964 by Ohring and Mariano [439], who concluded that if condensed clouds were present, a much lower opacity of the subcloud atmosphere is required. However, in so concluding, they assumed at the same time that there is an adiabatic temperature gradient throughout the atmosphere; and it is hardly possible to reconcile the existence of such a gradient with notions about the moderate opacity of gas for heat radiation with a simultaneous high temperature gradient.

The most rigorous examination of the greenhouse effect in a "gray" planetary atmosphere has been done by Wildt [546], who for the planetary source function $B(\tau,\mu)$, the function that determines the local energy balance at strict radiative equilibrium, obtained an overall solution in the form of the sums of the solution of the homogeneous Milne equation and the Neuman solution with the exponential term:

ORIGINAL PAGE IS
OF POOR QUALITY

(V.1)

where $n = \kappa_\odot/\kappa_c$ is the ratio of the gray absorption coefficients for solar and heat radiation that forms an angle $\theta = \arccos \mu$ with the normal to the surface of an infinitely thick flatly-stratified atmosphere; $\tau = \int \kappa dl$ -- is the optical thickness reckoned from the upper boundary of the atmosphere; πS and πF are the solar and internal heat fluxes respectively of the planet; $f(\tau) = \tau + u(\tau)$ is the normalized solution of the homogeneous Milne equation; and $g(\tau, n/\mu)$ is the normalized Neumann solution of the non-homogeneous Hopfe equation:

(V.2)

Wildt obtained the temperature dependence of the atmosphere as functions of a) the degree of intensity of the greenhouse effect as defined by parameter n and b) the character of the angular distribution of the radiation field as defined by the value μ. According

to these calculations, an example of which is shown in Fig. 76, for $\mu = 0.50$ the surface temperature that corresponds approximately to the radio brightness temperature of Venus is reached in the range log n from 2.5 to 3.0 at values of τ between 100 and 500.

The possibility of attaining such substantial opacity for heat radiation in the Venusian atmosphere, together with the necessary transparency in the visible region of the spectrum, has been subjected to doubt more than once. The strongest argument against the greenhouse model is the possible presence of aerosols -- if there is a large aerosol content in the atmosphere, solar radiation will not reach the surface of the planet. This argument has given rise to the aeolospheric model, which Öpik proposed in 1961 [440]. According to this model, solar energy is absorbed in the upper regions of an atmosphere in convective equilibrium and is transmitted to the planetary surface by the friction between it and dust particles during wind movements. Convection assures that the required number of dust particles (calcium and magnesium carbonates) is maintained in a nitrogen-carbon dioxide atmosphere. In the process, the radio brightness temperature, if it relates to the surface, should not reveal a dependence on phase.

ORIGINAL PAGE IS OF POOR QUALITY

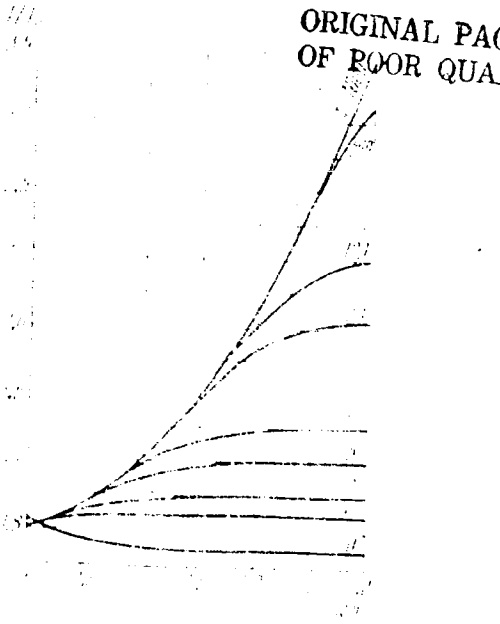

Fig. 76. Surface atmospheric temperature normalized to the effective temperature of the planet vs. log n at $\mu = 0.50$ for values of optical thickness τ according to [546].

The obvious difficulty with the /216 aeolospheric model was that in the regional theory the absorption of solar radiation at the upper boundary of the atmosphere presumes (isothermal equilibrium in the atmosphere) and the absence of radiative heat flux at lower altitudes. The requirement of convective equilibrium should result in the transfer of absorbed energy to lower-lying layers due to convective heat exchange; it should also result in the establishment of a temperature profile close to the adiabatic down to the surface. From this standpoint, the addition of another source of heat release due to friction can turn out to be insignificant.

The regional theory examines the exchange of energy in a limited volume (for example, within a column of gas of unit cross section), and in so doing, disregards the effects of global circulation. Such an approach was fruitful for the Earth's atmosphere, where global circulation influences mainly temperature in the area near

the surface (on the order of 50 m thick, where, according to [50], the greatest daily temperature variations take place). However, it can play a very important role throughout the entire depth of the atmospheric gas, provided that, because of opacity for shortwave radiation, solar radiation is absorbed in a comparatively narrow layer of the atmosphere near the subsolar point.

Goody and Robinson [321] have taken these considerations into account and have attempted to get around the difficulties associated with the aeolospheric model; they have offered their own model of deep circulation in the Venus atmosphere, herein using the analogy with the circulation of the Earth's oceans. In this model, the solar energy absorbed "at the top" of a sunlit atmosphere is transferred to the night side by large scale movements. The flow of gas into the region of the antisolar point and its flow away from the subsolar point cause, accordingly, adiabatic heating and cooling of the gas and, consequently, the establishment of an adiabatic temperature gradient in the atmosphere, the depth of which is determined by the surface temperature. That such a model is possible was confirmed by rather persuasive calculations based on an examination of a system of two-dimensional hydrodynamic equations for uncompressible viscous gas in the Boussinesq approximation. Later, /217
Goody and Robinson used the same formulation to examine the problem of circulation in a meridianal direction, because of which the temperatures of the equatorial and polar regions are equalized [324].

The Goody-Robinson and Öpik models begin with the rather gross assumption that solar radiation is absorbed in a narrow layer in the atmosphere at great altitudes (at the level of the clouds). But the calculations of Samuelson [484, 485] and Pollack [463] have contradicted this assumption. Samuelson studied the radiative transfer in an atmosphere that was in radiative equilibrium and "gray" in two spectral regions of visible and thermal radiation. The values of the single scattering albedo, which were based on data from optical ground-based observations of Venus, were taken to be equal to $\omega_0^V = 0.989$ (weak absorption in the visual region, according to the estimates of Sobolev [145, 147, 148]) and $\omega_0^{IR} = 0.2$ (strong absorption in the infrared region). In such a model, solar radiation penetrates deep into the atmosphere, the existence of a cloud layer notwithstanding. To be sure, the limiting surface temperature, which is reached due to the "greenhouse" effect, in this case turned out to be no higher than 550°K. The reason for the discrepancy between this and the higher values of radio brightness temperatures can be related both to the fact that the effective value of ω_0^V is very close to 1 for the entire thickness of the atmosphere and to the large elongation of the phase function into the forward hemisphere when dust particles are present.

Pollack [462] carried out the opposite task of the theory of transfer in order to determine CO_2, H_2O and N_2 quantities needed to heat Venus to a temperature on the order of 700°K. By so doing,

he determined the temperature gradient in the atmosphere from the surface to the bottom of the clouds. As for the flux of the solar radiant energy incident on the top of a flatly-stratified atmosphere, the value of this flux was corrected for that portion of the radiation that passed through the clouds and the lower-lying molecular sublayer. These corrections took account of scattering and absorption by cloud particles, which were assumed to be ice spheres with $\bar{r}$ = 7.5 μm; the corresponding absorption coefficients were computed by Irvine and Pollack by using the Mie theory [356]. In order to determine the amount of gaseous absorption in the visible region from the upper boundary of the atmosphere to the intervening layer h_n = h/n (at n = 13) characterized by the optical mass of gas along the line of sight $W[h_n(\ell)]$, computations were made of the equivalent width of the absorbing band or several neighboring bands in a range of wave numbers Δv. To account for possible overlapping, a quadratic distribution of absorption by wave number was assumed. /218

TABLE 15. SOURCES OF SOLAR RADIATION ATTENUATION IN THE VENUSIAN ATMOSPHERE (ACCORDING TO [463])

P_s atm								
15	18	0,3250	0,0700	0,1500	0,1571	0,1250	0,0862	0,0538
	43	0,3000	0,0537	0,1200	0,1200	0,2719	0,1172	0,1268
75	18	0,1850	0,0120	0,2000	0,1800	0,1538	0,1020	0,1550
	43	0,2220	0,0210	0,1515	0,2250	0,2410	0,1254	0,1625
300	18	0,0610	0,1360	0,0950	0,2000	0,1715	0,1112	0,2250
	43	0,3000	0,0560	0,0850	0,2500	0,2000	0,1311	0,2780

ORIGINAL PAGE IS OF POOR QUALITY

Although calculations of the profiles of attenuated solar radiation and spectral transparency in the visible and near infrared regions were made with regard to an expected nitrogen atmosphere of Venus (at f_{CO_2} = 0.1 - 10% and f_{H_2O} = 0.01 - 0.1%) for surface pressures P_s = 15, 75 and 300 atm, the results (according to [462]) hold true for a CO_2 atmosphere, provided that accepted values P_s are reduced by about 1.5 times.

These results are partly reproduced in Table 15 for two values of the optical thickness of the clouds, τ_c = 18 and τ_c = 43, which correspond to the estimates of Sagan and Pollack [479]. The values ψ(a), ψ(c), ψ(g) and ψ(x) designate the fractions of solar radiation absorbed, respectively, by the atmosphere; by the aerosols of the clouds; by the surface; and by an unidentified absorber above the visible clouds, an absorber that is effective mainly in the ultraviolet region of the spectrum. ψ'(c) is total absorption in the /219

clouds (by aerosols and gases); and $\psi'(a)$ and $\psi''(a)$ characterize absorption in the atmosphere above and below the clouds, respectively. Obviously, the total absorption is made up of $\psi'(a)$, $\psi''(a)$, $\psi(c)$, $\psi(x)$ and $\psi(g)$.

TABLE 16. REGIONS OF SPECTRAL TRANSPARENCY IN THE VENUSIAN ATMOSPHERE (ACCORDING TO [463]).

$\Delta\lambda$, μm	
P_s = 10 atm	P_s = 200 atm
[illegible]	[illegible]

ORIGINAL PAGE IS OF POOR QUALITY

Data on spectral transparency (Table 16) allow the assumption that although a large region in the range of $\lambda\lambda$ = 0.7 to 1 μm is overlapped by the atmosphere and the clouds, nonetheless, an appreciable portion of solar energy near the maximum of the Planck intensity curve $I(\lambda)$ (at $T \approx 6000°K$) should reach the planetary surface. Calculations also showed that in order to assure the opacity required to obtain high values of T_s and P_s due to the "greenhouse" effect, the atmospheric parameters at the level of the clouds should have a substantial impact. Fig. 77 shows the relation between surface pressure and pressure at the cloud tops P_{uc} vs f_{H_2O} for 97% and 75% CO_2. The solid lines assume a dry adiabatic gradient in the clouds, the dashed line is a wet adiabat. At the most probable values f_{CO_2} = 0.97, $P_s \approx 100$ atm, and with a wet adiabatic gradient, $P_{uc} \approx 0.2 \div 0.3$ atm. Here f_{H_2O} is within the limits 0.005-0.01, which is compatible with the data from the Venera measurements and with the estimates of parameters at the level of H_2O clouds given in Section IV.7. /220

Pollack's calculations are undoubtedly interesting, even though they are based on a number of assumptions, primarily those related to the structure of the atmosphere and to the radiative transfer coefficients (transmission functions) of the medium. Therefore, this attractive conception that the conditions of the "greenhouse" model may indeed occur has remained hypothetical, as has its opposite, on which the Goody-Robinson model is based.

The doubts about whether it is possible to reach the necessary atmospheric transparency in the visible region have led to the idea that surface heating is due to radioactive decay in the interior of the planet. Kuz'min has advanced a similar hypothesis [84],

and Hansen and Matsushima [332] have examined it in more detail. If one begins by solving the heat conductivity equation in soil with parameters that correspond to those on Earth, then, in order to reach a high surface temperature, an unrealistically high temperature gradient in the near-surface layer has to be assumed. In the various estimates of the heat flux from the interior (several orders of magnitude less than solar flux, but noticeably more than for the Earth, where the mean value is ~ 50 erg·cm^{-2}·sec^{-1} [28]), the required heating of the surface can be reached from the condition of heat balance with the atmosphere only if the atmosphere is highly transparent, which in turn is attained only if there is a significant concentration of aerosols. However, this requirement is difficult to reconcile with the observed spectrum of radio brightness temperatures and with radar cross sections [464]. The results of theoretical calculations have also contradicted notions about uniform dust distribution in the troposphere and the localization of aerosols near the surface. Moreover, maintaining the necessary amount of dust requires mixing, which in a state of equilibrium cannot be realized within the framework of such a model. Therefore, the model of radioactive heating was itself rather contrived and has essentially given way, from the point of view of physical validity, to "greenhouse" or circulation models.

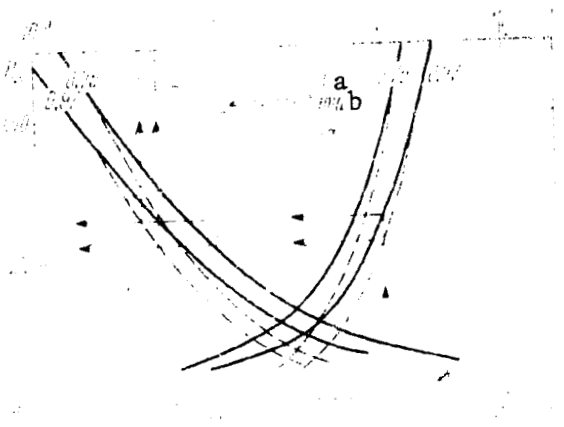

Fig. 77. Pressure at the Venusian cloud tops vs surface pressure P_s and mixing ratio f_{H_2O} [463].

Key: a. dry adiabat
b. wet adiabat

ORIGINAL PAGE IS OF POOR QUALITY

/221

The direct measurements of the Venera spacecraft have opened up the possibility of modelling heat exchange in the Venusian atmosphere, a procedure which can now begin with factual values of gaseous parameters and measured temperature and pressure profiles and need not resort to hypothetical models of atmospheric structure. This has enabled a much better understanding of the characteristic features of the planet's thermal regime, and it has allowed us to obtain a number of important quantitative estimates. The recent works of Avduyevskiy et al. [2, 5, 188], Strelkov [151], Strelkov and Kukharskaya [152], Sagan [482], and Ginzburg and Feygel'son [41] have made a detailed examination of the "greenhouse" mechanism and have attempted to calculate radiative heat transfer in "non-gray" and "window-gray" approximations (i.e., with a choice of individual spectral intervals for a CO_2-H_2O mixture that presumably possesses the least opacity for heat radiation).

Unfortunately, there are few data on CO_2 and H_2O absorption characteristics at high pressures and high temperatures, and this has reduced the reliability of the quantitative estimates obtained. This is particularly true of carbon dioxide.

All these calculations have used the wide-band CO_2 transmission function computed theoretically by Plass et al. [451, 453] and Stull et al. [522] for spectral intervals 50-100 cm^{-1} wide in the region of wave numbers from 1000 to 5000 cm^{-1} in a wide range of gas densities along the optical path, but at P = 1 atm and T = 300°K. A number of works have also used data on CO_2 absorption coefficients in individual bands ($\lambda\lambda$ = 15, 4.3, 2.7, 2.04 μm) in a broader range of temperatures as according to [10, 227, 300, 407]. The matter is slightly simpler with regard to water vapor, for which there are data on absorption coefficients at high temperatures (calculated by Ferriso et al. [301, 302], in addition to the known characteristics of opacity in the long wave region at T = 300°K [262, 445, 515, 549]. As for calculating the dependences of CO_2 and H_2O absorption coefficients on pressure by introducing the factor $(P/P_0)^\nu$ (assuming ν = 1 throughout the range of pressure change $P \gtrless P_0$ = 1 atm), then such an assumption is evidently justified only for large masses of gas. Generally speaking, there is no unanimity among authors about the choice of ν, since it is known that the mean (by mass) size of the absorption coefficient serves as a rough measure of the real absorption capacity of a layer with $P \neq$ const. Specifically, there are indications [348, 462, 482] that H_2O opacity varies nearly proportionally to the first degree of pressure; however, it shows a strong non-linear dependence on the quantity of gas along the line of sight. /222

There has recently been definite progress in refining the characteristics of the transfer of long wave radiation; this is of prime importance for the problem of the Venusian thermal regime. Together with this, the results of the Venera-8 measurements of illumination have made it possible to substantiate assumptions about the extent of the planetary atmosphere's opacity in the visible region, and they have led to specific conclusions with regard to the possibility of attaining energy balance within the framework of heat exchange models.

We will examine these questions in later sections of this chapter.

V.2. On Energy Balance in the Atmosphere

ORIGINAL PAGE IS OF POOR QUALITY

/223

Models of thermal equilibrium. The thermodynamics of a planetary atmosphere are determined by the amount of solar energy at its upper boundary, for which the level P = 0 (which assumes a free surface) is usually used. In the case of Venus, it is convenient to take as the upper boundary of the atmosphere the cloud tops (at

P ≈ 0.1 atm)(and the molecular sublayer), at which the significant portion of the solar radiation that reaches the planet's orbit is reflected.

The thermal energy emitted at temperatures from ~ 800°K to 200°K is concentrated in the spectral region from approximately 2 to 80 μm. It is possible to argue that in this region, especially near temperatures of 200-300°K, the clouds (of whatever condensate that can be expected on Venus) are extremely opaque. Therefore, as noted in Section IV.1, the effective temperature of the planet's emission into space is close to the effective temperature of the emission of clouds (or slightly lower, because of weak opacity in the infrared spectrum of gases above the clouds) and satisfies the condition of radiative balance of the atmosphere at this level. These considerations are supported by the results of radiometric measurements and also by the absence on the planetary disk of individual hot spots, which could be attributed to the emission of lower-lying regions of the Venusian subcloud atmosphere [331, 435, 501, 502]. Above the clouds, the transparency of the Venusian atmosphere increases, evidently because of the settling of condensate and the temperature sensitivity of "hot" CO_2 bands at λ = 9.4 μm and λ = 10.4 μm.

It is necessary to include in the thermal balance both the portion of the solar radiation that passes through the atmosphere and the reemission of solar and thermal radiation due to reflection by the clouds and the atmosphere. Because radiation penetrates through the clouds, the radiative flux of heat into the atmosphere, an influx that is a constantly active non-adiabatic factor, is secured. If there is a regime of radiative equilibrium in the atmosphere, the energy of the shortwave solar radiation should be matched at each level by a flux of outgoing radiation; in conditions of convective /224 equilibrium, the influx of solar energy is matched at every level in the atmosphere by the total heat flux due to outgoing radiation and convective transfer.

The absorption of solar energy as it penetrates into the atmosphere should lead to a heat flux that varies with altitude (in contrast to what happens in stellar atmospheres, cf. [50, 146, 462]). According to the law of conservation of energy, the integrated (over the spectrum) radiative flux at a certain level h in the atmosphere, q(h), is directly related to the amount of solar energy absorbed below this level. In stationary conditions dq/dh = 0, due to the constancy of the total flux vs depth. The spectral regions in which the basic portions of solar shortwave and heat radiation are transferred overlap slightly and

$$q(h) = q_{\odot}(h) + q_{t}(h). \qquad \text{(V.3)}$$

ORIGINAL PAGE IS OF POOR QUALITY

where $q_{\odot}$ (h) is the solar energy flux below level h averaged over a Venusian day, q_t(h) is the heat flux at this level. In turn, $q_{\odot}$ (h) may be presented as

(V.4)

i.e., the solar energy absorbed by the atmosphere and by the surface below level h is made up of the flux of solar radiation reflected from the layers below level h and the radiation that reaches this level $q_{\odot}^{+}(h)$, as well as the downward luminous flux $q_{\odot}^{-}(h)$. An analogous relation is written for the heat flux $q_t(h)$. Since

(V.5)

and the condition of energy balance at the upper boundary of the atmosphere h_∞:

(V.6)

where $q_t^0 \equiv q_t(h_\infty)$ and $q_\odot^0 \equiv q_\odot(h_\infty)$. According to (V.6), the absorbed solar energy and the energy emitted by the planet into space should be equal: /225

(V.7)

ORIGINAL PAGE IS
OF POOR QUALITY

which, after integrating with respect to the entire surface $Q = 4\pi R^2$, gives formula (IV.1), which determines the effective temperature T_e. It is an average value in relation to the spectral brightness temperatures. For Venus, T_e corresponds to the maximum in the Planck curve at $\lambda = 12.7$ μm (at $A = 0.77$ [354]). /226

If one disregards a possible contribution by internal heat sources, the type of heat exchange in the troposphere depends on what portion of the solar energy is absorbed by the atmosphere and the surface. The diagrams in Fig. 78 show this graphically. For each of these diagrams, it is assumed that there are no energy losses of the lower atmosphere to radiation (at the upper boundary $\operatorname{div} q(h_\infty) = 0$).

Diagrams a and b are cases in which the solar radiation $q_\odot^0$ that is not reflected off the upper boundary of the atmosphere h_∞ reaches the surface, i.e., $q_s = q^0 = q_\varphi (1 - A)/4$, where $q_\varphi = E_0/a^2$. Diagram a (radiative equilibrium) ♀ corresponds to ♀ the condition $\partial q/\partial h = 0$, if $(\partial T/\partial h) = (\partial T/\partial h)_{rad}$. In this case the entire area below level h_∞ is filled with equilibrium radiation. The field of equilibrium radiation is isotropic at any point of the body, and the flux of radiation [57]

ORIGINAL PAGE IS
OF POOR QUALITY

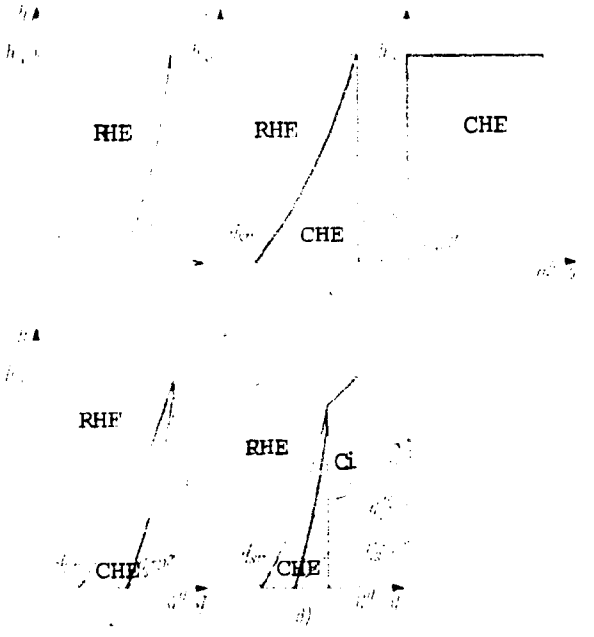

Fig. 78. Diagrams illustrating the possibility of models of heat equilibrium in the Venusian troposphere: a -- radiative equilibrium in an atmosphere transparent in the visible region; b -- convective equilibrium in an atmosphere transparent in the visible region; c -- deep circulation model; d -- radiative-convective heat exchange if uniform absorption of solar radiation by the atmosphere and clouds; e -- radiative-convective heat exchange if non-uniform absorption of solar radiation by the atmosphere and clouds; RHE is radiative heat exchange; CHE is convective heat exchange; CCHE is convective-circulatory heat exchange; and Ci is circulation.

Diagram b (convective equilibrium) corresponds to the condition $\partial q/\partial h \neq 0$, when $\partial t/\partial h = (\partial T/\partial h_{ad}$ and $q(h) < q^0$. We note that, with convection, the quantity of solar energy absorbed by the surface should be larger than in conditions of radiative equilibrium at the same T_s, i.e., $q_s^b > q_s^a$ if $T_s^a = T_s^b$.

Diagram c corresponds to the limiting case, when solar radiation in the visible region does not reach the surface and is entirely absorbed near the upper boundary of the atmosphere ($q_s = 0$); given this, the deep circulation model of Goody and Robinson is possible (cf. p. 161). Diagram d corresponds to an intermediate case, when solar radiation is attenuated more or less uniformly throughout the entire thickness of the atmosphere and when $q_s < q^0$. Diagram e also corresponds to an intermediate case, when absorption takes place only in the cloud layer Δh_c, so that $q_s' < q^0$ or when, after the main absorption has taken place in the clouds, a certain additional attenuation in the atmosphere takes place ($q_s'' < q_s' < q^0$).

In all these intermediate /227
cases for corresponding regions, the field of radiation is also isotropic. The difference with variant (a) is that when solar radiation does not reach the surface at all, heat equilibrium in the atmosphere should come about according to the actual profile of the attenuated radiation $q_{sr} < q^0$. Specifically, the curve $q_s = q_{sr} < q^0$, which is shown tentatively by the dashed line in diagram a, will correspond to a regime of radiative equilibrium. With partial absorption of solar energy in the atmosphere (diagrams c and d), an additional equalization of values of heat flux near h_∞ and the surface temperature can

occur due to advective transfer with large-scale circulation -- to which diagram c corresponds in the limit. It is natural that other cases can in principle be realized, for example an average between a and c or between c and d.

Taking the various contributions of individual members into account (and equating them to zero in limiting cases), each diagram in Fig. 78 will correspond to the local energy balance equation at the surface of the planet, the equation which follows from (V.3) in the form:

(V.8)

ORIGINAL PAGE IS
OF POOR QUALITY

where q_{gv} and q_{gt} are the radiative heat fluxes from gas in the visible and infrared regions, respectively; ε_s^v and ε_s^t are the emission coefficients of the surface in the same regions; T_s is the surface temperature; and q_c and q_{ci} are the effective heat fluxes due to free convection and to forced convection connected with circulation.

Several characteristics of heat exchange. The thermal properties of the atmosphere are to a large degree determined by motions of various dimensions. In global heat exchange, the circulation that arises as a result of instability in the radiative equilibrium state of a motionless atmosphere and as a result of latitudinal and logitudinal variations in the amount of insolation play the main role. A regime of polar-symmetrical circulation, known as a Hadley regime, even at very small velocities of atmospheric motions from the heat source to heat sink, should bring about a resolution of the meridianal temperature gradient and an equalization of the temperature field. Zonal currents can /228 play a definite role in heat exchange between the day and night hemispheres. Circulative transfer is accompanied by radiative-convective heat exchange. Unfortunately, the study of the complex, non-linear structure of equations that describe the processes of large-scale circulation, especially those that calculate the instability of currents that appear and the essential time dependence of turbulent fluxes, is extremely difficult. For a slowly rotating planet such as Venus, Coriolis forces should exert but a weak influence on circulation. Estimates according to the value of the Rossby number Ro [illegible] show that for fluxes on a planetary scale ($L \sim R_\varphi$) in middle latitudes, $Ro_\varphi \simeq 5 - 10$, and the condition of geostrophicity $Ro \ll 1$ is not met.[2] Therefore, the main contribution to heat transfer due to circulation on Venus should come from non-linear advective terms. (cf. [325]).

[2] For Earth, $Ro_\oplus \simeq 0.1$.

Several works have been devoted to a theoretical examination of circulation in the Venus atmosphere; these works describe the structure of meteorological fields either on the basis of the quasi-static approximation of equations of motion (here the atmosphere's own thermal instability is filtered) or by using dimensionless numbers, which were originally developed to describe the regularity of motion in the Earth's atmosphere.

Golitsyn [43,44, 574], using the methods of similarity theory and dimensionality and assigning global parameters such as albedo, solar constant, atmospheric mass etc., estimated the characteristic velocity of motion in the Venusian troposphere as $v \sim 1$ m/sec. This estimate, which is not related to the assumptions that unavoidably accompany theoretical models of circulation, is rather realistic. As we have seen (cf. Section IV.6), it is in good agreement with the measured velocities of horizontal motion in the lower troposphere of Venus.

It is difficult at present to give preference to any one theoretical model developed with regard to the features of global circulation on Venus. It is evident, however, that the mechanism of circulation is not axisymmetric. /229

In the aforementioned Goody-Robinson "deep" circulation model [321, 324], it is shown that motion in the upper troposphere should be from the subsolar point to the antisolar point or from the equator to the pole at a characteristic velocity of $v \approx 30$ m/sec. In Stone's estimate [519] for a similar schema of circulation, $v \approx 5$ m/sec. In the lower atmosphere, motion occurs with a much lower velocity from the antisolar point to the subsolar point or from the pole to the equator.[3] A dimensionless analysis based on all thermal and dynamic values led to the conclusion that the internal vertical flux is adiabatic down to the surface due to turbulent mixing caused by the circulation of the deep layers. However, Hess [345] has cast doubt on the existence of such turbulence in the lower layer of the atmosphere.

Zilitinkevich et al.'s numerical experiments in modelling circulation in a two-level model of the Venusian atmosphere [58, 158] result in a relatively simple two-celled schema, wherein the low-pressure center is on the day side and shifted toward the evening terminator; the high-pressure center is on the night side near the morning terminator. The characteristic wind velocity for the entire atmosphere is about 5 m/sec in this schema, which is in good agreement with Stone's estimate.

---

[3] It is here assumed that opacity in the narrow atmospheric layer where the absorption of solar energy takes place is so high that radiative and turbulent transfers can be "parameterized" as the process of diffusion.

ORIGINAL PAGE IS
OF POOR QUALITY

The concept of a zonal flow that appears as a result of the asymmetrical convective motions resulting from periodic insolation at the upper boundary of the atmosphere has been adopted in the two-dimensional models of Schubert and Young [488] and Gierasch [312]. These models have included the aforementioned (Section IV.6) results of circulation modelling in fluid-filled cylinders where periodic insolation is simulated by a rotating flame [586]; it was here discovered that zonal currents arose and moved in a direction opposite to that of the flame.

Malkus [579] has examined a three-dimensional model and has concluded that it is possible for weak, Hadley-type cells to arise near the top of the troposphere and, because of temperature contrasts between the equator and the poles, for energy and angular momentum to be transferred to high latitudes. The experimental Mariner-10 data on spatial motions can in principle be compatible with this model, provided that substantial influence of a high-pressure subsolar region on the structure of circulation is also assumed. The meridianal pressure gradients that arise in this case should result in the acceleration (with increase in latitude) of flows orthogonal to isobaric surfaces -- with the formation of spiral movements and jet streams. Energy discharge will occur in polar whirlwinds as a result of the convergence of velocity vectors near the poles at low pressures [581].

Thus, there are conceptions that angular momentum transfer in a meridianal direction should play an important role in the dynamics of the Venusian atmosphere. Obviously, the structure of the atmosphere in the equatorial and polar regions will be appreciably different, particularly in terms of temperature profiles, vertical and horizontal velocities, and directions of motion. Further study of these features will help our understanding of the regularity with which present-day climatic conditions on the planet are formed[4].

Vertical heat and mass exchange on a rotating planet are described by the non-stationary heat balance equation, which establishes a relation between the change in heat content per unit volume of gas and the vertical energy fluxes resulting from solar and heat radiation: /231

$$\rho c_p \frac{\partial T}{\partial t} = \nabla \operatorname{grad} T + \dots \qquad \text{(V.9)}$$

[4] The works of Mintz [110, 429] and the monograph of Golitsyn [46] closely examine the status of the problem of general circulation in planetary atmospheres. With respect to Venus, the circulation regime is surveyed in the monograph of Burangulov, Zilitinkevich et al. [554]. In this regard, we devote our attention to problems of convective heat transfer within the framework of cellular and penetrative convection models (cf. Section V.5). In so doing, these models should be seen as mechanisms that can take place on Venus, not as representations of the actual situation in the Venusian atmosphere.

In so doing, the equalization of the temperature field in a horizontal direction is not figured in (in (V.8) $q_{ci} = 0$). The heat flux q = div (λ grad T) can be determined by solving the radiative transfer equation. Into (V.4) may be placed:

$$q_r^{\downarrow}(h < h_0) = 0 \quad \text{and} \quad q_r^{\downarrow} = f(h) \int_0^{\infty} I_\nu^{\downarrow} d\omega d\nu_{h_0}$$

ORIGINAL PAGE IS OF POOR QUALITY

where f(h) is the portion of the solar energy absorbed below level h [462].

The convective term in the left-hand side of (V.9) is formally represented by the expression for free convection:

$$q_c = \rho c_p V \Delta \bar{T} \quad \rho c_p k_H \frac{\partial T}{\partial h} = \gamma_a \qquad \text{(V.10)}$$

where $\Delta\bar{T}$ is the difference between the temperature established in a convective atmosphere at velocity V and the temperature with a gradient equal to the dry adiabatic. γ_a is determined from formula (IV.12), and the coefficient of turbulent diffusion [313].

$$k_H = \nu L^2 \left(\frac{\frac{\partial T}{\partial h} - \gamma_a}{T} \right) \quad \text{at} \quad \frac{\partial T}{\partial h} + \gamma_a < 0.$$

Here L is the scale of the motion, ν is a numerical constant ($\nu \approx 1.4$). It is clear that $k_H = 0$ when the following stability criterion is met[5].

$$\frac{\partial T}{\partial h} \geq \gamma_a \qquad \text{(V.11)}$$

These relations express the condition of heat transfer due to upward free convection in the atmosphere. L ~ H is customarily accepted as a characteristic scale for a deep atmosphere. We note that relation (V.10) corresponds to a Fickian diffusion equation and describes heat transfer by vortexes whose dimensions are small in comparison to L. /232

[5]The Priestley stability criterion $\frac{\partial T}{\partial h} \geq \frac{1}{c_1} \frac{\nu c_2 a^2 \nu}{\ell_0^4}$ is more general; this criterion expresses the fact that in addition to the relation between γ_a and $\partial T/\partial h$, stability depends on the characteristic size of the elementary convective volume ℓ_0 and the intensity of turbulent heat exchange with the surrounding atmosphere (a and ν are the coefficients of temperature conductivity and viscosity, c_1 and c_2 are constants that depend on the shape of the particles). Hence it follows that as ℓ_0 decreases, the vertical temperature gradients needed for convection increase -- because of the rapid dissipation of the energy of floating motion of small volumes in the processes of turbulent mixing. Priestley's theory is applicable outside the boundary layer (cf. [174, 263, 466] for more detail).

If, instead of T, the potential temperature $\theta = T(P_0/P)^{R/\mu C_p}$ is introduced, then (V.10) is rewritten in the form

$$\gamma_a = \gamma_G \frac{\partial \theta}{\partial h} = \gamma_a \qquad \text{(V.10')}$$

ORIGINAL PAGE IS
OF POOR QUALITY

where, due to the empirical constant γ_G Deardorff calls the "countergradient" [264], equalization of the potential temperature is achieved at unchanged entropy. As deviations from hydrostatic equilibrium appear, this constant essentially expresses the fact that $\partial T/\partial h$ differs little from γ_a (a small ΔT) in an unstable convective region where, according to Gierasch and Goody [313], the condition $\frac{\partial T}{\partial h} \gtrsim \gamma_a$ is met. Unfortunately, a similar formalism cannot be applied to horizontal heat and mass exchange and to angular momentum transfer. This can be seen from an examination of meteorological processes in the Earth's atmosphere, where turbulent transfer is linked to large-scale disturbances such as cyclones and anticyclones and where satisfactory parameters for the dynamic structure of horizontal fields are not found [325].

In modelling heat exchange, it is useful to make several preliminary estimates that characterize the thermal inertia of the atmosphere and the depth of diurnal temperature variations. It is easy to show that, at values of measured parameters of the Venusian atmosphere, the difference between temperatures on the day and night sides should be extremely small, which has been noted in [117]. In fact, the supply of heat in column of gas of unit cross section

/233

$$\int_0^{T_0} C_p(T)\,dT = \frac{5}{2} R \int_0^{h} T(h)\,n(h)\,dh$$

is $i_{\varphi}^{\Sigma} \approx 4.2 \cdot 10^{14}$ erg·cm^{-2} $\approx 10^4$ kcal·cm^2. At the same time, the heat loss during the Venusian night (t_N = 58.4 Earth days) is: $\sigma T_{\varphi}^4 t_N \approx 10^{12}$ erg·cm^{-2} $\approx$ 24 kcal·cm^{-2}, i.e., it does not exceed 0.25% of the energy contained in the atmosphere and cannot be very pronounced in any way in the heat balance of the planet. The maximum diurnal temperature variation in the Venusian lower atmosphere at $q_{\odot}^0 = q_{\varphi}(1 - A)/4$ should not exceed $\frac{\Delta T}{T} \sim 1\%$ [6].

Two parameters used to characterize the thermal regime of a planetary atmosphere are directly related to these values: the time of heat relaxation

$$\tau = \frac{mc_p T}{\sigma T^4} \qquad \text{(V.12)}$$

---

[6] It is evident that a similar estimate of the mean diurnal temperature variation in the atmosphere is given by the formula $\Delta T = \frac{gP_s t}{Pc_p}$, where P_s is surface pressure and t is time in days.

which characterizes the time scale of the equalization of temperature anomalies in relation to disturbances from emission [573, 574]; and the time of radiative heat exchange

$$\tau_{T,p} \sim \frac{c_p T}{q(H)} \qquad \text{(V.13)}$$

ORIGINAL PAGE IS
OF POOR QUALITY

which is the characteristic time scale for the upward transfer of energy that compensates for radiative losses at the upper boundary of the atmosphere [398]. Here m is the mass per unit column of atmosphere, q(h) is the rate of cooling per unit of mass from a level on the order of H, i.e., corresponding to ~ 1/3 m. If, for a carbon dioxide atmosphere, $\varepsilon \approx 0.15$ is taken as the efficiency of radiation, then /234

$$\tau_{p,T} \sim \frac{c_p p}{0.3\varepsilon g} \sim 2\tau_{T,p} \qquad \text{(V.13')}$$

The values $\tau_{p,T}$ and $\tau_{T,p}$ for Venus are given in Table 17. For purposes of comparison, the corresponding estimates for the Earth and Mars (according to Leovy and Pollack [398]) are also given.

TABLE 17. CHARACTERISTIC TEMPERATURES AND TIMES OF THERMAL RELAXATION

Planet	m^2, $\frac{J}{m^2\text{-deg}}$	T_s, K	T_c, K	$\tau_{p,T}$, sec	$\tau_{T,p}$, sec
Venus	10^5	230	~500	10^{10}	$2\cdot10^{10}$
Earth	10^5	250	~ 7	10^7	$2\cdot10^7$
Mars	$1.3\cdot10^5$	200	~ 7	$3\cdot10^6$	$6\cdot10^6$

It is interesting that if Venus ceased to receive solar energy, it would take about 65 Earth years to cool, due to heat loss by emission, to a heat content of the Earth's atmosphere ($i_{\oplus}^{\Sigma} \approx 24.5$ kcal·cm^{-2}) that corresponds to the night heat loss on Venus, (provided all remaining parameters stay unchanged). But this estimate is quite rough, because it does not take into account the variation in atmospheric opacity during cooling, the regime of planetary circulation, and violation of the equilibrium conditions of the formation of the gaseous shell of Venus, mainly the equilibrium between carbonates and silicates (cf. Section IV.8)

In one-dimensional formulation of the non-stationary problem (equation (V.9)), it is convenient to take the time coordinate proportional to the angle of the planet's rotation (latitude) and to solve the problem for several values of latitude ϕ, which allows the calculation both of the diurnal change and the latitudinal dependence in the thermal regime of the planet. However, since the time in which Venus makes one revolution around its axis is

small in comparison to the de-excitation of its stored energy, it /235
is possible to construct a calculated schema by starting with the fact that the solar energy incident on the day side at latitude ϕ is absorbed in the midsection of a truncated cone of height $\Delta\phi$ and is averaged over its entire lateral surface at this latitude (which holds true for a rotating planet). The integration over Q of the left-hand part of relation (V.7) in such a calculated schema gives the following law of uniform distribution of solar energy over the surface of a planet at level h (cf. [5]):

ORIGINAL PAGE IS
OF POOR QUALITY

(V.14)

which leads to a T_e^* different from (IV.1). This is formally related to the neglect of contribution q_{ci} to the energy balance in a local region of space. It should be pointed out that, although an analysis of the thermal regime within the framework of a radiative-convective model oversimplifies the actual situation in the atmosphere, it does allow a most complete study of the "inner" dynamic structure of heat exchange.

V.3. The Optical Properties of the Venusian Atmosphere

On the transfer of radiation in the Venusian atmosphere. In order to determine theoretically an altitude distribution of radiant energy in a planetary atmosphere, it is generally necessary to compute the fraction of monochromatic solar radiation absorbed at various levels by atmospheric gases, the surface and the clouds, as well as the fraction reflected into space from the atmosphere, the surface, and the clouds. However, there is very little information about the opacity of gases in the ranges of visible light, since, in order to determine opacity at relatively low absorption coefficients, the sizes of the optical paths required are still practically unattainable in laboratory conditions. Another limitation is the need to do research at a variable density along the optical path, and in the case of Venus, at high gaseous temperatures and pressures as well. Theoretical estimates of solar radiation attentuation by the atmosphere in the visual and near-infrared regions of the spectrum, estimates similar to those given in Table 15, are only approximations.

From the point of view of radiation transfer, it is possible to view the atmosphere as consisting of two phases -- the gaseous and the aerosol. Total radiation attentuation consists of molecular scattering σ_λ^g, selective absorption by individual gaseous components κ_λ, absorption α_λ and scattering σ_λ^a on aerosol. Accordingly

(V.15)

The extinction coefficient and the items that go into it determine the optical thickness:

$$\tau(z) = \int_z^{\infty} \varkappa(z)\,dz \qquad (V.16)$$

ORIGINAL PAGE IS
OF POOR QUALITY

and the single scattering albedo which characterizes the absorption properties of the scattering medium:

$$\omega_0 = \frac{\sigma}{\varkappa}, \qquad (V.17)$$

which, together with the scattering indicatrix $x(\phi)$, make up the fundamental optical characteristics of the atmosphere.

Scattering on gaseous components is most significant in the shortwave region of the spectrum outside the absorption bands, while aerosol scattering predominates in the longwave region. The reader can find a detailed account of the theory of light scattering on small particles in the monographs of Van de Hulst [21], Sobolev [146, 149], Shifrin [173], Rozenberg [138] (cf. also [109, 137, 531]), and the theory of light scattering on large particles in the works of Irvine [353, 357]. Theory shows that because of the incoherence of gaseous and aerosol-particle scattering one may assume the additivity of corresponding components of the matrix of atmospheric scattering $B(\mu, \mu_0)$ for incident and scattered (at angles $\arccos \mu_0$ and $\arccos \mu$) fluxes of radiant energy. Integration (with respect to the angles) of the relation

$$B(\mu, \mu_0) = B_1(\mu, \mu_0) + B_2(\mu, \mu_0) \qquad (V.18)$$

with $B_1(\mu, \mu_0)$ included allows the expression of an effective normalized scattering matrix for a hazy medium in the form (cf., for example, [21, 138]) /237

$$f(\mu, \mu_0) = \frac{\omega_0 \varkappa_1 B_1(\mu, \mu_0) + \omega_0 \varkappa_2 B_2(\mu, \mu_0)}{\varkappa_1 + \varkappa_2} \qquad (V.19)$$

The concrete form of the scattering matrix (the number of independent and non-zero components) is determined by the properties of the scattering medium (particle composition, size, and shape) and depends on wavelength.

Rayleigh scattering is described by the scattering coefficient σ^g and the scattering indicatrix $x(\phi)$, which are expressed by the well-known formulas:

$$\sigma^g = \frac{8\pi^3 (n^2 - 1)^2}{3\lambda^4 N}, \qquad (V.20)$$

ORIGINAL PAGE IS
OF POOR QUALITY

(V.21)

where m is the mean refractive index of the medium, N is the number of scattering molecules per unit volume, ϕ = arccos μ is the angle of scattering. It is clear from formula (V.20) that the role of molecular scattering is especially large in the transfer of visible solar radiation. Figs. 79 and 80 show calculations of τ_p in the interval λ = 0.2 to 1.2 μm for the Venusian atmosphere (according to the basic model given in the Appendix). Fig. 79 shows the dependence of τ_p (rated per unit of pressure) on λ, while Fig. 80 gives the family of curves $\tau_p(\lambda)$ vs altitude. Since Rayleigh scattering is directly proportional to the mass of the scattering gas, on Venus it turns out to be about two orders of magnitude more intense than on the Earth. Near the maximum of the visibility curve ($\lambda_0 \sim 0.5$μm), $\tau_p \approx 30$, which corresponds approximately to the optical thickness of the Earth's clouds. We note that the spectral dependence of σ^g is expressed by the convenient relation evident from (V.20): /238

(V.20')

The calculated values of the scattering coefficient $\sigma^g_{\lambda_0}(h)$ and the optical thickness $\tau_{p\lambda_0}$ as a function of altitude in the Venusian atmosphere are given in Table 18.

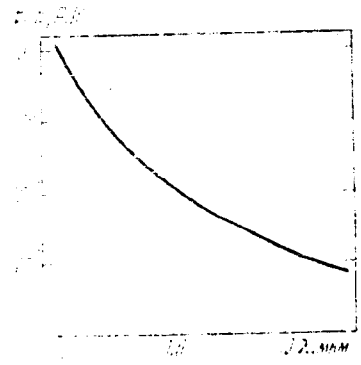

Fig. 79. Variation in optical thickness τ_p vs λ for Rayleigh scattering in the Venusian atmosphere.

Key: a. μm

With the presence of an aerosol component suspended in gas, the optical properties of an atmosphere also depend on the concentration, altitude distribution, size distribution, the nature and the microstructure of the particles. In this case, all 16 components of the scattering matrix can in principle be different. At characteristic particle size $\bar{r} \sim \lambda$, a convenient approximation is given by the Mie theory, which enables a calculation of σ^a as a function of the refractive index m and the parameter $p = 2\pi r/\lambda$. As the aerosol content increases and as this parameter increases, the asymmetry of the phase function grows (the elongation of the scattering indicatrix into the forward hemisphere) due to the deciding influence of the aerosol scattering matrix ; at the same time σ^a and $\alpha\lambda$ increase in comparison to σ^g_λ and κ_λ. /239

Including the polydispersity and the irregularity of the composition of aerosol, the second item in (V.18) can be represented

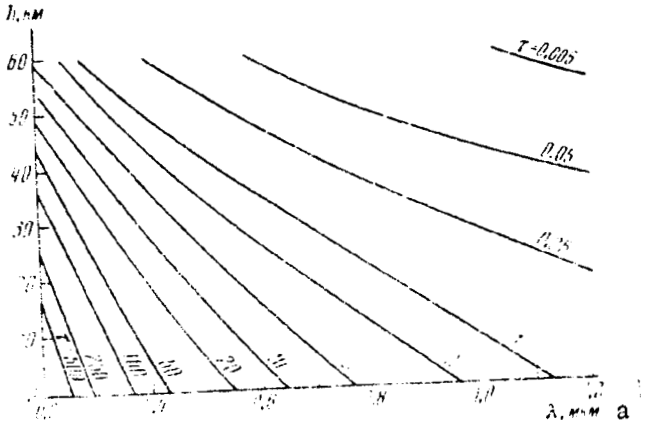

Fig. 80. The family of curves $\tau_p(\lambda)$ for the Venusian atmosphere vs altitude.

Key: a. μm

in the form [138]:

$$P(\gamma, \gamma_0) = \sum_i \int n_i(r) P_i(\gamma, \gamma_0, r) dr \quad (V.22)$$

and by assuming that the orientation of individual particles after integrating over all angles is isoptropic, it is possible to obtain an expression for the scattering cross section:

$$\sigma = \sum_i \int n_i(r) \sigma_i(r) dr \quad (V.23)$$

The density of the size distribution of particles of type y, $n_y(r) = dN_y(r)/dr$ is given by the so-called V-distribution $n(r) = n_0 e^{-tr} r^{\nu}$ or by a Junge

TABLE 18. RAYLEIGH SCATTERING COEFFICIENT $\sigma^g_{\lambda_0}(h)$ (λ_0 = 0.5 μm) AND CORRESPONDING OPTICAL THICKNESS $\tau_p^{\lambda 0}$ VS ALTITUDE (ACCORDING TO [37])

0	165	28,4	24	44	5,0	28	0,2
3	144	23,8	27	37	4,3	31	0,1
6	125	19,7	30	29	3,3	33	0,2
9	108	16,3	33	24	2,6	37	0,1
12	90	13,4	36	19	1,9	40	0,1
15	76	10,9	39	16	1,4	43	0,1
18	64	8,8	42	11	1,1	50	0,1
21	53	7,0	45	8,7	0,7		

ORIGINAL PAGE IS OF POOR QUALITY

function [368, 568] for various values of the parameter of exponential scattering $n(r) = cr^{-(\alpha + 1)}$, where α, t, and ν are constants expressed in terms of the mean and modal radii of the particles. /240

V-distribution is usually realized in Earth clouds, for which (according to [161, 164]), two cases are typical: $r_{mod} \approx 4$ μm; $t \approx 1.5$ μm; $\nu \approx 6$ in the case of Sc, Cu, and Ac clouds and $r_{mod} \approx 7$ μm^{-1}; $t \approx 0.4$ μm^{-1}; $\nu \approx 2$ in the case of St, Ns, and As clouds.

ORIGINAL PAGE IS
OF POOR QUALITY

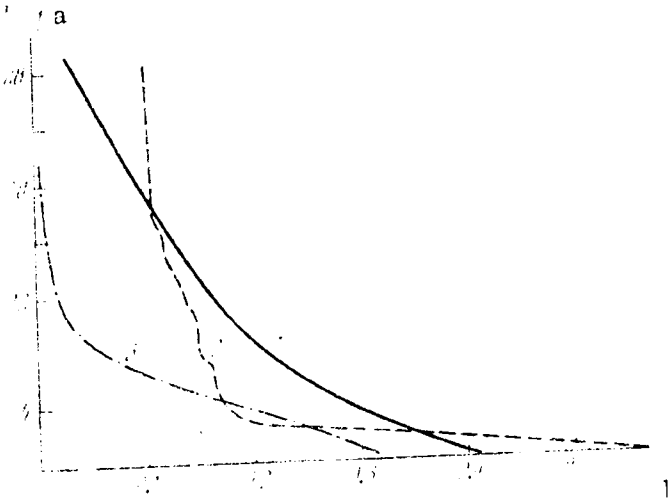

Fig. 81. An example of attentuation of solar radiation in the Earth's atmosphere vs altitude (July 11, 1964, sec θ = 2.85÷1.70). 1 is Rayleigh scattering; 2 is aerosol scattering; 3 is absorption by polyatomic molecules (according to [385]).

Key: a. μm
b. cal/cm^2·min

Observations of the Earth's atmosphere reveal that the dependence of σ^a on λ is satisfactorily approximated by an exponential function of the form:

$$\sigma^a \sim \lambda^{-\psi} \qquad (V.24)$$

in which the exponent ψ varies within rather wide limits as a function of particle size. The Rayleigh law ($\psi = 4$) is met up to $r \lesssim 0.15$ μm, while the value of ψ rapidly decreases and passes through zero as particle size increases, so that scattering in the red region turns out to be more effective than in violet. At $r \gtrsim 1$ μm, the scattering becomes nonselective [171, 175]. /241

For a near-surface layer of the Earth's atmosphere in a weakly hazy medium, $\sigma^a \simeq \lambda^{-1}$ [138]. The attenuation of light in the visible region due to aerosol scattering can exceed attenuation due to molecular scattering by several times (cf. for example [71, 71a, 385]).[7] Fig. 81 shows, as an example, the variation of attenuated radiation with altitude; this dependence corresponds to measurements in the midlatitudes of the USSR in the summer of 1964. As we see, the total attentuation at the Earth's surface exceeds 1.2 cal/cm^2·min; of this, about half is aerosol scattering. As for the true absorption of light by the Earth's aerosols, estimates [62, 64, 142] show it to be comparatively small.

[7] Heightened aerosol content is noted not only at the Earth's surface in the troposphere, but also in the stratosphere and mesosphere (at 10-15 km, about 25 and 80 km) where cirrus, nacreous, and silvery clouds are observed respectively. Hypothetical notions that the source of aerosol on Venus may be volcanic eruptions are developed in [261].

The real and imaginary parts of the combined refractive index, both of which depend on the chemical nature of aerosol, together with the modal radii of the particles, determine the angular dependences of the scattering matrix, specifically, the shape of the scattering indicatrix. An approximation of Rayleigh or isotropic scattering is unsuitable if aerosols are present. The scattering indicatrix are usually expanded in terms of Legendre's polynomials; the longer its elongation, the more terms are to be considered:

$$\sum_{i} x_i P_i(\cos\gamma) \qquad \text{(V.25)}$$

The specific case (V.25) at i = 3, when $x_1 = 0$ and $x_2 = 1/2$, is a Rayleigh indicatrix (V.21). Various other conceptions, which allow the best approximation of greatly elongated indicatrixes frequently encountered in practice, are also used (cf. [149]). A scattering indicatrix that is determined from the Mie formula and averaged over particle sizes given by distribution n(r) is usually called polydispersed. Tables of polydispersed indicatrixes can be found in [51, 267].

In examination of the equation of the transfer of monochromatic radiation non-conservatively scattered by an optically dense dispersive medium, asymptotic methods (cf. [40, 139, 149]) and the Schuster-Schwarzschild approximation, or the so-called two-flux approximation, which leads to two first-order, linear differential equations with constant coefficients, have been widely applied. In these cases, the mean specific intensities in the hemispheres are determined by using the conveniently-tabulated parameters of the scattering indicatrix ℓ or Γ, which characterize its elongation. The parameter ℓ is a function of the mean cosine of the scattering angle x_1: /242

ORIGINAL PAGE IS
OF POOR QUALITY

$$\ell = \frac{1}{x_1} : x_1 = \frac{1}{2}\int_0^{\pi} x(\eta)\cos\eta\, d\eta. \qquad \text{(V.26)}$$

The parameter Γ is the difference between the portions of light scattered into the forward and back hemispheres

$$\Gamma = \frac{1}{2}\int_0^{\pi}\int_0^{\pi} x(\eta,\mu_0)\,d\eta \int_0^{\pi} x(\eta,\mu_0)\,d\eta\, d\mu_0. \qquad \text{(V.27)}$$

It is evident that, with isotropic scattering, $\Gamma = 0$ (analogously x_1).

The item κ_λ, which exerts a strong influence on radiation transfer in absorption bands, is present in expression (V.15). Under normal conditions, there are no such bands in the visible region of a carbon dioxide atmosphere, while in the near-infrared region, there are several weak absorption bands with centers at $\lambda\lambda$ = 0.83, 0.86. 0.92 and 0.96 μm. Water vapor can influence $\lambda > 0.7$ μm even more appreciably; at the same time, estimates of optical thickness in absorption by using values σ_{H_2O} (according,

e.g., to [108]) show that under normal conditions the opacity of water vapor is small for the main part of the solar spectrum. These estimates can vary in the deep layers of the Venusian atmosphere at large P, primarily due to absorption on complexes of CO_2 and H_2O molecules. However, particularly significant is true absorption in the longer wavelength region, which is responsible /243 for the transfer of heat radiation and where the term κ_λ begins to play a definite role. At high pressures and temperatures, a significant contribution is made here, in particular, by continuous absorption at the wings of remote lines and by induced absorption. Section V.4 examines these features.

The characteristics of reflected radiation. Analysis of reflected radiation yields important information about the optical properties of the planetary atmosphere and, in particular, about the relationship among the individual terms of (V.15) in the visible region of the spectrum.

Until recently, the ground-based observations that determined the overall optical properties of the planet (spectral, photometric and polarization characteristics, the distribution of brightness across the disk, change in the visual phase curve) were the only sources of information about solar light transfer on Venus. Unfortunately, these results give no single or simple answer to questions about the relative role of scattering and absorption of radiation in the atmosphere and in the clouds, the structure of the clouds, or the content and nature of the aerosols. It is still more difficult to obtain estimates of the optical regime in the deep layers and, in particular, illumination at the planetary surface -- since the basic part of the photons responsible for the reflecting characteristic of Venus hardly penetrate more than several hundred meters into the clouds [117, 164].

The brilliance of Venus near inferior conjunction means that its scattering indicatrix is strongly elongated into the forward hemisphere. This finding is not unexpected -- in view of the dense cloud layer observed on Venus. As already noted, the presence of a large quantity of aerosols or cloud droplets (or a mixture of the two) with dimensions comparable to or larger than wavelength should result in a marked asymmetry of the phase function for scattering in a hazy medium. This makes it a much more complicated task to obtain, from a solution of the equation of transfer, the characteristics of diffused (depends on the angle) transmission and reflection in such an atmosphere, especially when absorption is taken into account. Romanova [140, 141] and Irvine [358] have examined similar problems. The obstacle to a reliable interpretation of ground-based measurements is above all the absence of data that determine /244 the properties of the elementary scattering matrix of the type (V.19) (the shape, size and concentration of particles, the combined refractive index, the dependence of the degree of polarization on the scattering conditions, the shape of the indicatrix). On the

other hand, in order to obtain estimates of these parameters, it is necessary to use all available observational data.

From an analysis of the polarimetric measurements of Gehrels and Samuelson [309], measurements that show the dependence of polarization p on the phase angle α, Sobolev [147, 148] obtained a value of $x_1 = 2.1$. This corresponds to a mean particle radius $\bar{r} = 1.2$ μm and a refractive index of m = 1.5 (the dependence on m is not strong).

The most complete information about m and $\bar{r}$ has been obtained by Hansen [337], Hansen and Arking [336], and Hansen and Hovenier [576] from a comparison of the polarimetric measurements of Coffeen and Gehrels [248] and Lyot [406] with a calculated model of a cloudy atmosphere, the degree of polarization in which is determined by taking multiple scattering in a Rayleigh medium with spherical particles into account. The values obtained that best satisfy measurement data are shown in Figs. 82a and 82b. These calculations lead to an estimate of the real part of the combined refractive index at the cloud tops (in the range $\lambda_0 = 0.55$ μm) of m = 1.44 ± 0.015. In so doing, they reveal a clear tendency toward a weak decrease in m between the ultraviolet and infrared regions of the spectrum (from m = 1.46 ± 0.015 at $\lambda = 0.365$ μm to m = 1.43 ± 0.015 at $\lambda = 0.99$ μm). The imaginary part, which is determined from the phase matrix for single scattering at $\omega_0 \approx 1$ and $\bar{r} \approx 1$, is negligible. The estimate obtained for mean effective radius of the cloud particles (r = 1.05 ± 0.10 μm for a narrow size distribution)is in good agreement with the Coffeen's calculations using the Mie theory: $\bar{r} = 1.25 \pm 0.25$ μm [247, 249]. Similar values are obtained in [14].

The values of m and $\bar{r}$ and the dependence $m(\lambda)$ satisfy an idealized atmospheric model with homogeneous optical properties in a certain range of altitudes -- which obviously oversimplifies the real situation. Nevertheless, these results significantly narrow /246 the range of parameters on which the optical properties of the clouds depend and at the same time limit the number of possible components and their phase state at the level of reflection. (cf. Section IV.7).

The visual phase curves of Venus obtained by Irvine [354], and Knuckles et al. [383] point to a significant concentration of aerosols in the atmosphere. This concentration, possibly, may not remain constant, if the differences in the phase curves based on 1956 and 1963-1965 measurements are attributed to the optical thickness of the effective scattering layer of a cloudy atmosphere. However, this difference is more probably related to methodological and instrument errors, primarily to averaging over the angles of incident and reflected radiation at large and small phase angles. Fig. 83 shows experimental data and the calculations of Arking and Potter [183] and Galin et al. [37]. Arking and Potter's curves are

ORIGINAL PAGE IS
OF POOR QUALITY

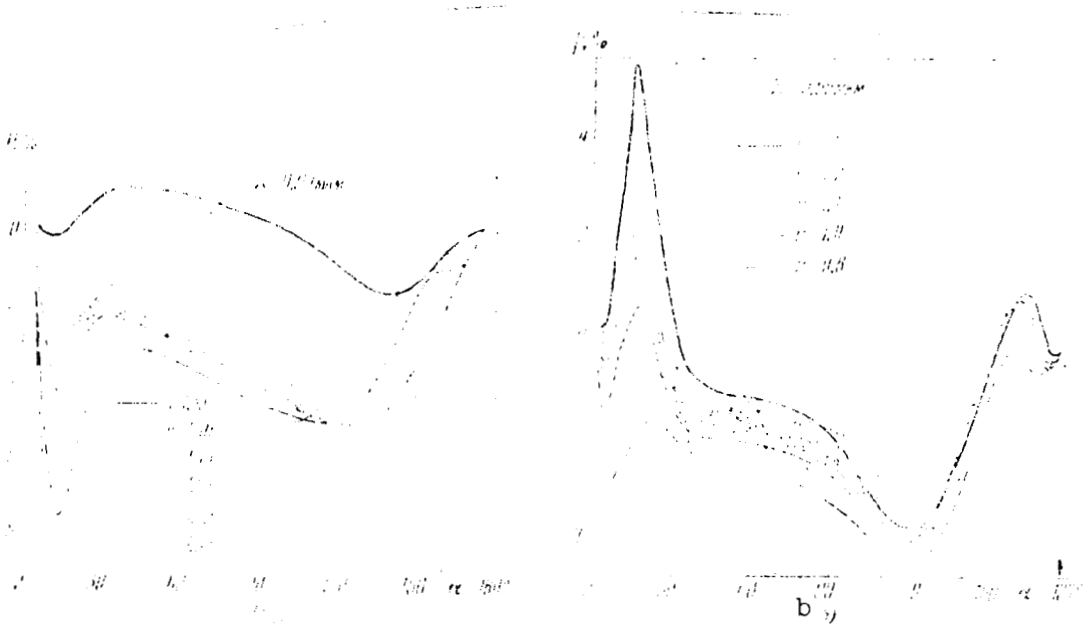

Fig. 82. Polarization vs phase angle: a-Hansen's theoretical curves, which approximate the results of observations by Coffeen and Gehrels at λ = 0.99 μm (the "x's"), at various values of refractive index m. The calculations use particle sizes $\bar{r}$ that give the best agreement with what has been measured at all wavelengths: $\bar{r}$ = 0.7, 0.8, 1.1, 1.2 and 1.2 μm respectively, beginning with m = 1.33. The albedo is taken to be A = 0.90 at λ = 0.99 μm. b is a theoretical approximation of Lyot's observations (the plus signs) and the observations of Coffeen and Gehrels ("x's") at λ = 0.55 μm. Hansen's calculated curves correspond to m = 1.45 at several values of the mean radius of the scattering particles $\bar{r}$ μm [337].

for two limiting cases of conservative scattering in a single-layer atmosphere, in which an infinitely large optical thickness is assured due to purely molecular scattering ($\tau_p = \infty$; $\tau_c = 0$) or to the clouds ($\tau_p = 0$; $\tau_c = \infty$). Galin et al. obtained a segment of a curve using an approximation of a two-layered model with $\tau_c \approx \tau_p = 20$ at a scattering indicatrix of a monodisperse cloud ($\rho = 2\pi r/\lambda = 30$), and it is closer to the experimental data in the range of phase angles $60 \leq \alpha \leq 140°$. However, this does not mean that this ideal model alone satisfies the experiment: for example, in the presence of an /247
aerosol component in a molecular sublayer, the combined effect of two layers can be closer to a model of a homogeneous atmosphere with a polydisperse indicatrix [164].

Fig. 1 shows the basic reflection and emission characteristics of Venus as summarized by Hapke [338]. The curve, which corresponds to a monochromatic spherical albedo $A\lambda$ in the range from 0.2 to 4 μm, is constructed from ground-based spectrometry data and includes corrections for absorption in CO_2 bands. The values of albedo for the region 0.31-1.06 μm are those obtained by Irvine [354, 355]; the values $A\lambda$ (given in Fig. 1) in the near ultraviolet $\lambda \leq 0.3$ μm (according to [182]) and in the near infrared regions of the spectrum (between 0.8 and 1.2 μm[338]) and from 1.2 to 3.5 μm[220, 393]) are normalized to Irvine's values. The data for the infrared region (λ = 3 - 14 μm) are taken in accord with [314, 501] and are listed to the corresponding value of A at λ = 3.2 μm.

The experimental data indicate that true absorption is prevalect in the regions $\lambda > 2.4$ μm and $\lambda < 0.45$ μm, while they are nearly absent in the visible and near infrared spectrum. $A\lambda$ reaches its greatest value in the yellow and red regions of the spectrum, which is probably caused by intense scattering by cloud particles with an albedo per unit of scattering ω_0 that is close to unity. This follows directly from calculations in a homogeneous semi-infinite atmosphere model, provided that Sobolev's asymptotic formula is used [149, 150]; this formula establishes a link between the observed albedo A and the optical parameters of the medium. In the specific case of a semi-infinite scattering atmosphere at $k\tau >> 1$ and $0 < (1 - \omega_0) << 1$

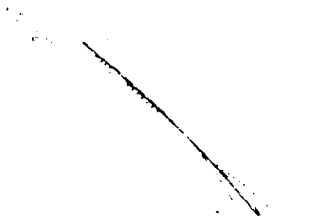

Fig. 83. Visual phase curves of the reflection of Venus: 1-according to observations in 1963-1965 [354]; 2 and 3 calculations for a one-layer atmosphere (2 is $\tau_c = 0$, $\tau_p = \infty$; 3 is $\tau_c = \infty$, $\tau_p = 0$) 4-for a two-layer atmosphere ($\tau_c = 20$, $\tau_p = 20$) [37].

ORIGINAL PAGE IS
OF POOR QUALITY

$$\text{[illegible]} \qquad \text{(V.28)}$$

$$\text{[illegible]} \qquad \text{(V.28')}$$

is a constant determined from the solvable condition of the radiative transfer equation, which describes the light regime in deep layers.[8]

Table 19 gives the values of ω_0 /248 calculated using the monochromatic phase curves of Venus obtained by Irvine et al. [354, 355]. The data in Table 19 are in good agreement with the independent estimates of Sobolev, which give $\omega_0 = 0.989$ in the range of visible light [147, 148]. We note that,

[8] This expression is obtained by expanding the precise formula for k in powers of $\sqrt{1 - \omega_0}$ and keeping terms of the order $\sqrt{1 - \omega_0}$ (cf. [149]).

according to Chamberlain [240], variation in the intensity of the strong band $\lambda = 1.6$ μm as a function of phase also requires that the value of ω_0 in the continuum is close to unity.

TABLE 19. OPTICAL CHARACTERISTICS OF THE VENUS ATMOSPHERE CORRESPONDING TO THE MEASURED ALBEDO A_λ FOR TWO MODELS.

			κ, cm^{-1}	
3417	0,45	0,9815	66	3,4
3580	0,52	0,9871	52	4,5
3626	0,56	0,9891	42	5,4
4155	0,66	0,9937	25	8,4
4573	0,77	0,9970	12	11,7
5012	0,79	0,9975	10	16,6
6263	0,84	0,9988	0,8	60,3
7247	0,93	0,9997	1,2	58,6
8625	0,84	0,9981	2,8	35,8
10350	0,84	0,9981	2,8	35,8
[illegible]	[illegible]	[illegible]	2,8	[illegible]
[illegible]	0,71	[illegible]	[illegible]	[illegible]

ORIGINAL PAGE IS
OF POOR QUALITY

Since $\omega_0 = \sigma/\sigma + \kappa$, or (at $\kappa << \sigma$) $1 - \omega_0 \approx \kappa/\sigma$, where σ and κ are the volume scattering and absorbtion coefficients, the difference between ω_0 and unity should be attributed to true absorption in a semi-infinite scattering medium. Moroz [119] has computed values of the absorption coefficient by volume of the material that makes up the particle, κ^*, from the relation κ^* [illegible]; Table 19 also gives values of κ^*. As is seen, most absorption occurs in the interval 0.3 - 014 μm, while the least occurs at about 0.6 μm; nevertheless, the minimal value of $1 - \omega_0$ (which means κ/σ) is about three orders of magnitude larger than the corresponding value for clouds on Earth in the visible and near infrared regions of the spectrum [163, 335]. If it is assumed that all the radiation not reflected off the planet into space reaches the surface, then the transparency of the Venusian atmosphere should in this case be high -- $R = 1 - \omega_0/\omega_0 = \kappa/\sigma = 10^{-3} - 10^{-2}$ (for clouds on the Earth $R \sim 10^{-7}$). /249

The observed optical characteristics of the Venusian atmosphere can also be explained by beginning with the notion of a conservative atmosphere of finite optical thickness. In this specific case ($k\tau << 1$, $\omega_0 \approx 1$), the Sobolev formula is written as

[illegible] (V.29)

where a is the albedo of the planetary surface. The extreme right-hand column of Table 19 gives estimates of τ that correspond to this model, assuming $x_1 = 2.1$ and $a = 0$. Calculating $a \neq 0$ slightly decreases τ. The more rigorous calculations of Romanova [140] for models of optically thick layers with a strongly-elongated scattering indicatrix lead to a value of the optical thickness of a medium with parameters corresponding to the Venusian atmosphere, $\tau = 65^{+50}_{-20}$. Pollack's calculations of a model of conservative scattering by the Venusian clouds and by a CO_2 and H_2O atmosphere, at $\bar{r} = 7.5$ μm and for two values of the cloud optical thickness in the visual region of the spectrum ($\tau_c = 18$ and 43) show that the optical thickness of the scattering layer and the surface pressure essentially have no influence on the value of A_λ at $\lambda > 1$ μm, i.e., in this region, the clouds completely determine the reflection.

Galin et al. [37] have made interesting calculations of the dependence of the albedo D_λ ($A_\lambda = 2\int D_\lambda(\mu_0)\mu_0 d\mu_0$, where arccos μ_0 is the angle of incidence of solar rays) of a scattering, semi-infinite atmosphere on the optical thickness of the clouds in a two-layered model approximation. It was assumed that the cloud particle size is similar to that on Earth, i.e., rather large ($\bar{r} \sim 5$ μm). /250 Fig. 84 shows that at $\tau_c \leq \tau_p$, the albedo at first decreases (due obviously to the elongation of the indicatrix) and then, at $\tau_c > \tau_p$, as the total optical density of the atmosphere grows $\tau = \tau_c + \tau_p$, it increases. These dependences enable the decrease in A_λ in the region $0.62 \leq \lambda \leq 1$ μm to be explained (because τ_p diminishes with wavelength from 12 to 2 μm) and results in a value of $\tau_c \geq 60$ at $\lambda = 0.626$ μm, where $A_\lambda = A_{\lambda max}$ (cf. Fig. 1). Similar estimates for the shortwave region confirm the fact that true absorption is insignificant as A_λ decreases to $\lambda \approx 0.5$ μm and indicate at the same time that absorption should occur in the clouds and not in the subcloud atmosphere. The computed value $\omega_0 = 0.9987$ at $\lambda = 0.52$ μm, is here close to the value that is given in Table 19. The dots in Fig. 1 show the calculated estimates of A_λ in these conditions according to [37].

The change in A_λ between 0.6 and 0.5 μm can be explained by a one-layer cloudy atmospheric model with a Rayleigh indicatrix and cloud particle size of $\bar{r} \sim 1$ μm (which, as we have seen, is more compatible with polarimetric data; cf. Fig. 82b). It is necessary to assume in this case that true absorption occurs, on the other hand, not in the clouds ($\omega_0^c = 1$), but in the lower-lying molecular atmosphere: the absorption herein should be significant ($\omega_0^p \approx 0.95$). /251 This decrease in the albedo can be attributed to the spectral dependence of the scattering coefficient when particles are small [164]. Fig. 85 shows the calculations[9] for variants of one-layer and two-layer models, when cloud particle size is within $\bar{r} = 0.5 - 1.5$ μm, in comparison with the experimental curve A_λ.

[9] N. L. Lukashevich made these calculations.

ORIGINAL PAGE IS
OF POOR QUALITY

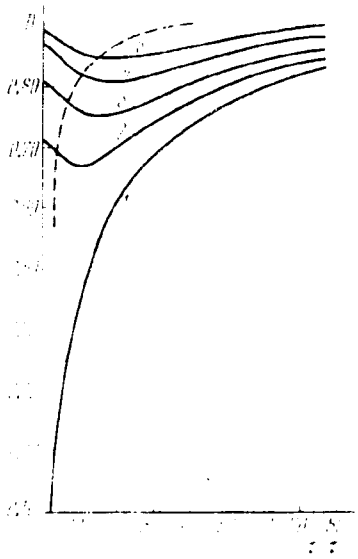

Fig. 84. Flat albedo of a two-layer atmosphere vs τ_c at $\mu_0 = \cos\theta = 1$. The solid curves 1, 2, 3, 4 and 5 are values of τ_p = 0, 5, 10, 20 and 30. The dashed line is a pure Rayleigh atmosphere [37].

As for the sharp decrease in A_λ in the region $\lambda < 0.4$ μm, which was first recorded by Sinton [502] and Evans et al. [502], it is hardly possible to attribute it to absorption in the clouds (since their absorption coefficient in the ultraviolet is very small) and least of all to the subcloud atmosphere. The absorber is probably concentrated in the haze which extends above the boundary of the visible cloud layer and which blurs this boundary. One may identify it with the fraction $\psi(x)$ in Table 15.

Multiple scattering by haze or cloud particles evidently plays an important role in absorption band formation in the observed spectra of Venus, especially in CO_2 band formation. The relative intensity of various absorbers and the variation of absorption bands as a function of the phase of Venus are not in agreement with conceptions of a simple reflecting surface below the gaseous layer of the atmosphere or a homogeneous cloud surface. Since the relative role of scattering and absorbing components is unknown, a good approximation of absorption spectra in the visible and near infrared regions is given by the semi-infinite model of conservative isotropic scattering of Chamberlain and Smith [240, 241], and by Belton's conception [212] of the specific content of the scattering phase. The optical properties of this model correspond to the observed character of the planet's visual albedo at $\tau \geq 20$; as we have seen, this can agree with the values given previously. /252

Let us recall that estimates of the upper and lower boundaries of the Venusian clouds (cf. Section IV.7) give a geometric thickness $\Delta h_c \approx 10 - 20$ km. If it is kept in mind that estimates of τ_c lie mainly within 10-60, then it turns out that the value is $\tau_c/\Delta h_c \approx 1 - 6$ km^{-1}, i.e., the clouds are not overly turbid. The mean value of the volume scattering coefficient is $\bar{\sigma} \approx (2\text{-}5)\cdot 10^{-5}$ cm^{-1}; correspondingly, this is a mean concentration $N \approx \bar{\sigma}/2\pi\bar{r}^2 \approx 600$ cm^{-3} for micron-sized particles. For purposes of comparison, we note that in the Earth's clouds $\sigma \approx 10^{-4}$ cm^{-1}, while the mean concentration of ice crystals with $\bar{r} \approx 20$ μm is of the same order, about 400 cm^{-3} [163, 164].

Measurement of illumination in the atmosphere and at the surface. For the specific conditions of Venus, direct measurements of the Sun's light flux is the only way to make a reliable determination of the altitude dependence of the attenuation of this flux. As we have seen, this is of fundamental importance; it

ORIGINAL PAGE IS
OF POOR QUALITY

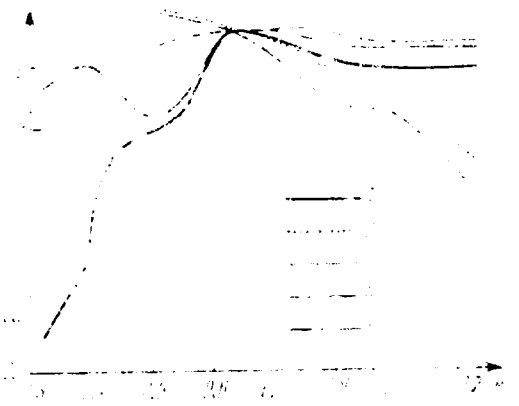

Fig. 85. Monochromatic spherical albedo of Venus. Curve 1-the measurements; curves 2-4-calculations for a two-layer atmosphere at $\bar{r}$ = 0.5, 1, 1.5 μm; curve 5-calculation for a one-layer model at τ_p = 0, $\bar{r}$ = 1 μm.

Key: a. μm

enables us to establish an energy balance of the atmosphere and the reasons for its heating, to explain the structure of the clouds and the optical properties of the atmosphere at various levels, and to determine the degree of illumination at the surface. However, it is very difficult to make optical measurements in the hot, dense Venusian atmosphere. The first such experiment was carried out on July 22, 1972, on Venera-8. Avduyevskiy et al. [8, 190] and Marov et al. [415] /253 have published the basic results of the experiment, and our account here will follow their articles.

The photometers on the Venera-8 were designed to measure light fluxes at sustained high temperatures up to 500°C, at pressures up to 100 atm, and under the impact of the high g-forces that arose when the descent apparatus entered the planetary atmosphere. Since the conditions of light absorption in the atmosphere were not known in advance, the instruments had to be sensitive over a wide range. Two identical instruments, each with its own sensor and electronics unit, were installed in the descent apparatus to ensure that the experiment was reliable.

Fig. 86 shows a picture of the sensor, and Fig. 87 shows its schematic. The light flux from the upper hemisphere entered through a vertically-placed glass light guide 1, which was enclosed in a layer of heat insulation 2, and came to the sensitive element 3, /254 for which a SF2-2 cadmium sulfide photoresistor was used. The radiation receptor which determines the spectral characteristics of the instrument, is on a special mounting 4; this mounting is placed inside the sealed and insulated casing 5, shown in Fig. 86. The temperature of the light sensor 3 was measured using a thermistor. A miniature standard lamp was installed at the side of the upper part of the light guide in order to check the working of the instrument.

The sensors were set vertically in the parachute section of the descent apparatus. Since the open parachute blocked a solid angle of about 0.05 steradian, i.e., about 1% of the field of view of the instruments, its influence on the results of the measurements was negligible. The electronics unit, which was inside the descent apparatus, transmitted signals proportional to the logarithm of the measured illumination in two channels: through the first channel

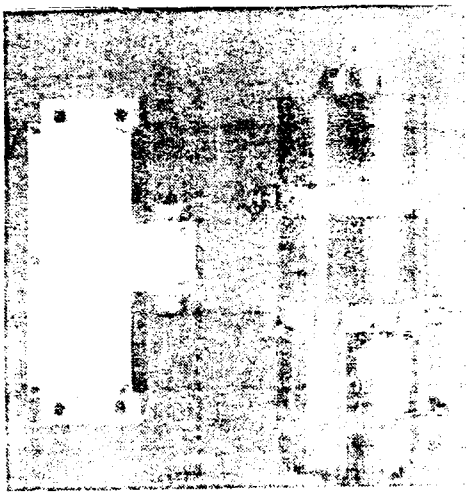

Fig. 86.The Venera-8 photometer.

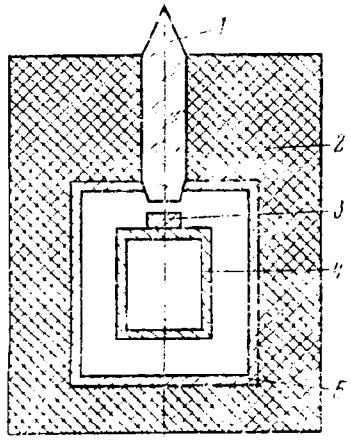

Fig. 87. Schematic of the sensor of the Venera-8 illumination measure. 1 is the light guide; 2 is the heat insulation; 3 is the sensitive element; 4 is the heat-regulation mounting; and 5 is the insulated casing.

as the illumination varied from 1 to 10^3 lux and through the second channel as the illumination varied from 10^2 to 10^5 lux.[10]

The altitude-dependent flux of radiant energy from the upper hemisphere in the spectral interval $\lambda_1 - \lambda_2$ is defined by the expression

$$F(h) = \int_{\lambda_1}^{\lambda_2} \int_0^{2\pi} \int_0^1 I_\lambda(h, \mu_0, \psi)\, \mu_0\, d\mu_0\, d\psi\, d\lambda. \quad \text{(V.30)}$$

where $I_\lambda(h, \mu_0, \psi)$ is the spectral density of the solar radiation at wavelength λ at altitude h above the planetary surface in a unit solid angle in direction l, characterized by an angle with external vertical $\theta = \arccos \mu_0$ and the azimuthal angle ψ reckoned from the solar vertical. /255

Any photometer with an axisymmetrical radiation pattern (indicatrix) $\Xi(\theta)$, a photometer such as that employed on Venera-8, records only a certain fraction W of the radiative flux density incident at the receiving area of the device. This portion W unambiguously determines the output signal of the device. If, in addition to $\Xi(\theta)$, the relative spectral sensitivity of the instrument $S(\lambda)$ is kept in mind, expression (V.30) is conveniently written as

$$W(h) = 2\pi \int_{\lambda_1}^{\lambda_2} \int_0^{\pi} I_\lambda(h, \theta) S(\lambda) \Xi(\theta) \sin\theta \cos\theta\, d\theta\, d\lambda. \quad \text{(V.31)}$$

For the Venus-8 photometer, the function $\Xi(\theta)$ satisfies the normalization condition

$$\int_0^{\pi} \Xi(\theta) \sin\theta\, d\theta = \frac{1}{2}. \quad \text{(V.32)}$$

ORIGINAL PAGE IS
OF POOR QUALITY

[10] These limits correspond to white light.

The form of the sensor's indicatrix $\Xi(\theta)$, which is shown in Fig. 88, is determined by the shape of the top end of the light guide. In order to expand the field of view to 2π steradians, its upper part was made in the shape of a cone with an angle of 60°. The obtained direction pattern provides sufficiently high accuracy if isotropic radiation is replaced by any possible angular distribution of radiation in the Venusian atmosphere at the altitudes of the Venera-8's descent.

The spectral characteristics of the photometer $S(\lambda)$ (Fig. 89) are within the limits $\lambda \approx 0.4$ μm to $\lambda \approx 0.8$ μm, and the effective wavelength is $\lambda_{eff} \approx 0.63$ μm. The spectral characteristics were determined at various temperatures of the photoresistor and at various levels of illumination. The narrow lines in Fig. 89 denote /256 the area corresponding to the error in the determination of the function $S(\lambda)$ and to its variation as the photoresistor was heated during descent to the Venusian surface.

In order to establish the relationship between the readings of the instrument, the degree of illumination, and the temperature of the photoresistors, the instruments were calibrated in a photometric sphere, in which isotropic radiation was produced by a high-pressure 1 kw xenon lamp. The illumination within the photometric sphere was measured by a luxmeter with a selenium photosensor. During calibration, the output signal of the electronics unit was measured at 20-30 points with variations in illumination from 10^5 to 1 lux. These calibration cycles were performed at various temperatures of the sensitive elements, from -10°C to +85°C; this range corresponded to the expected temperature range during descent for the instrument's design. Furthermore, control models of the instruments were heated to 150°C, and the results of their calibration were used to extrapolate the calibration characteristics of the flight models at higher temperatures. /257

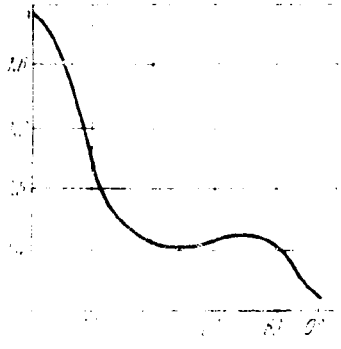

Fig. 88. The indicatrix of the Venera-8 photometer

In order to interpret the results of these measurements, it is necessary to know the proportionality factor between the illumination E in the photometric sphere as measured by the luxmeter and the value of W recorded by the calibrated device. Analysis of the calibration conditions shows that the proportionality factor χ between E and W is determined from the relation

$$\frac{\chi}{\Pi} \quad \frac{K \; \; \;

ORIGINAL PAGE IS
OF POOR QUALITY

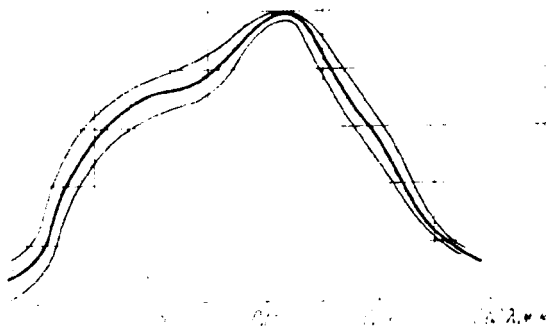

Fig. 89. Spectral characteristics of the Venera-8 photometer.

where K is the sunlight output at Venus and equal to 99 lux/w·m^{-2}; S_{ps} is the spectral sensitivity of the photosensor of the luxmeter; $S(\lambda)$ is the spectral sensitivity of the instrument; B_λ is the energy distribution in the Sun's spectrum ($S(\lambda) \equiv 1$); and $I_\lambda^{x\ell}$ is the energy distribution in the spectrum of the xenon lamp. The value of χ can be found experimentally, by comparing the readings of the instrument, calibrated using a luxmeter and illuminated by the light of a standard lamp ribbon, with the value of W calculated according to (V.31) and calculated to include the geometric factor of the source;

$$W = \frac{G\varepsilon c_1}{\pi R^2} \int_0^\infty \lambda^{-5} \exp\left(-\frac{c_2}{\lambda T_1}\right) S\, d\lambda \qquad (V.34)$$

where G is the area of the lamp ribbon, ε is the coefficient of emissivity, R is the distance from the lamp to the light guide, c_1 and c_2 are radiation constants ($c_1 = 3.74 \cdot 10^{-16}$ w·m^{-2}, $c_2 = 1.438 \cdot 10^{-2}$ m·deg); and T_1 is the temperature of the lamp ribbon.

Both methods result in a value of the proportionality factor of $\chi = 400 \pm 50$ lux/w·m^{-2}, a value that may be used to estimate the illumination created by solar diffused radiation. It is not difficult to see that the full energy of the light flux is $W_\Sigma \approx 4W$. The error of calibration is $\pm 20\%$[11] and remains almost constant throughout the variation of W during descent into the Venusian atmosphere. /258

Table 20 gives the initial results of measuring W vs time. During the descent, there were twenty-seven measurements of illumination and nine measurements of the sensor temperature. The latter made it possible to make the necessary corrections in the determination of W. Also taken into account was an increase of 12% in the sensitivity of the instrument; this increase occurred during the time between calibration and the approach to Venus, and it was discovered two weeks before landing with the help of the standard lamp during communication with the station. Table 20 gives estimates of

[11] This includes luxmeter error (~10%), uncertainty in the value of the factor χ (~15%), the error in the measurements of the sensitive element, and the random distribution of calibrated points.

ORIGINAL PAGE IS
OF POOR QUALITY

the error of measurement δW; these estimates include calibration error and the assumed error in the transmission of telemetry information. The last column in Table 20 gives values of illumination corresponding to the measured values of W in a case where the spectral composition of recorded light flux corresponds to the solar light flux.

Fig. 90 shows W (and the corresponding illumination E, as assumed above) vs altitude above the surface at the landing site at a solar zenith angle of $\theta = 84.5 \pm 2.5°$. The altitude dependence is calculated using the hydrostatic equilibrium equation and measured T and P during the Venera-8 descent. The narrow lines enclose the area of possible deviations of the experimental curves as a result of instrument errors. Random error, determined by the distribution of experimental points around a mean curve, does not exceed 10%.

The graph clearly shows two regions which differ principally in the nature of changes in W(h). At altitudes 0-(32 ± 3)km, the mean value of the derivative dW/dh is six times less than at altitudes above 32 km. If we rule out the influence of density by replacing the true altitude with the corresponding scale height $H = \int_0^h \frac{\rho}{\rho_0} dh$, where ρ and ρ_0 are the density of the gas at altitude h and at the surface, the change in the curve at h = 32 km shows up even more clearly (this is seen in Fig. 91). /259

Even a cursory glance at the altitude dependence of illumination measurements reveals a number of significant regularities. The attenuation of the light flux at altitues 0-32 km and the near-linear character of the curve W(H) gives reason to assume that the reduction of light flux in this region is basically caused by Rayleigh scattering in carbon dioxide. At altitudes above 32 km, the attenuation of light can be explained by assuming a pronounced contribution by aerosols, which are most probably related to the presence of clouds here. As we have seen (cf. Section IV.7), current estimates locate the cloud tops at level $P \approx 0.05$ atm, or at $h \approx 65$-70 km, which is much higher than the altitude at which the descent apparatus began its illumination measurements ($h \approx 50$ km). The Sun was 5.5 ± 2.5° above the horizon, the flux of light energy at the cloud tops was $F^-(h_\infty) = 260 \pm 140$ w/m^2, which is equivalent to readings on the instrument of $W = 65 \pm 35$ w/m^2. Hence it follows that above 50 km the attentuation of light is by about a factor of 7; and between 50 and 32 km by about a factor of three. In the region 32-0 km, light is attentuated by a factor of $\sim$4. /260

Thus, the atmosphere above 50 km is comparable, in terms of optical density, to the lower-lying atmosphere from the surface to 32 km altitude. The optical density of the atmosphere decreases as molecular density increases. The total attenuation of light reaches almost two orders of magnitude and, at the surface, reaches about 1% of the Sun's radiant flux incident at Venus. Since the /261

TABLE 20. LIGHT MEASUREMENTS ON VENERA-8

No. of the measurement	time (Moscow) hour	min.	sec.	W, w/m^2	$\delta W_{,2}$ w/m^2	E, lux
1	11	38	25	10.3		120
2	11	30	31			
3	11	41				
4	11					
5	11	46				
6	11	48				
7	11	50				
8	11	58				
9	11	59				
10	12	00				
11	12	01				
12	12	03				
13	12	10				
14	12	11				
15	12	11				
16	12	12				
17	12	13				
18	12	15				
19	12	15				
20	12	17				
21	12	21				
22	12					
23	12					
24	12					
25	12					
26	12	31				
27	12	32	12			

ORIGINAL PAGE IS
OF POOR QUALITY

albedo of Venus in the visible region is about 80% (cf. Fig. 1), about 20% of the solar energy is absorbed by the atmosphere and the clouds. The diagrams in Fig. 92 illustrate this. Fig. 92 also plots, in relative units, the profiles of total attenuation of solar radiation according to the calculated data in Table 15 for two variants of P_s and τ_c; here $\psi(c) - \psi(x)$ refers to the region above the condensation level for hypothetical H_2O clouds up to the conditional upper boundary at h ≈ 70 km. As we see, the measured profile W(h) differs substantially from the calculated profile; at the same time, the total attenuation of solar light at the surface of Venus -- according to Pollack's [463] estimates for an atmospheric and cloud model -- is only several times higher than the experimental value of W_Σ.

Optical models of the lower atmosphere. The results of measuring the amount and character of attenuation of the flux of solar radiant energy opens up possibilities of obtaining specific information about the optical properties of the atmosphere below the visible boundary of the clouds. Problems of this sort, which are usually called "inverse" problems, belong to the class of ill-posed problems for which significant progress of the theory has recently been made. Most "inverse" problems culminate in the necessity to solve a Fredholm integral equation of the first-kind. Tiknonov's regularization method [156, 157] is widely used as an inversion / 263

ORIGINAL PAGE IS
OF POOR QUALITY

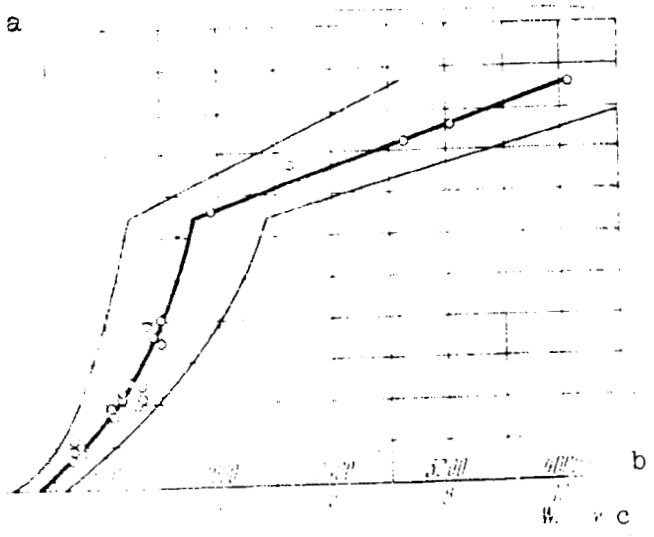

Fig. 90. The measured dependence of W on altitude above the Venusian surface at $\theta = 84.5 \pm 2.5°$. The thick solid curve approximates the experimental points, and the narrow lines bound the area of possible errors of measurement.

Key: a. μm
b. lux
c. w/m^2

algorithm; methods of mathematical statistics are also used [159].

Unfortunately, even in an analysis of reflected radiation, the lack of information about the optical properties of the medium stand in the way of an unambiguous interpretation of the curve W(h), because of the large number of parameters on which the measured profile depends. In these conditions, it is less time-consuming to calculate radiative transfer models by assigning a number of specific parameters of the medium and then to vary the parameters and try to select a profile $\bar{F}(h)$ that is close to the measured profile.

The calculations of Avduyevskiy et al. [8, 190] have confirmed the assumption that the attenuation of light in the atmosphere below $h \approx 32$ km (from ~ 3.5 w/cm^2 to ~ 1 w/m^2) are basically caused by Rayleigh scattering. The functions W (H) are used to estimate the ranges of values that do not contradict the experimental data: the volume scattering coefficient of the medium σ, the single scattering albedo ω_0, the surface albedo a, and the spectral composition of light near level $h \approx 32$ km. It turned out that regardless of the surface albedo (in the interval $a = 0-0.6$) and the spectral composition of the clouds, the scattering coefficient of the atmosphere at altitudes 0-32 km is not more than 30% greater than Rayleigh scattering in CO_2, while $\omega_0 \geq 0.995$.

Lukashevich et al. [92] have done more comprehensive calculations, including an analysis of the optical characteristics of the atmosphere above 32 km, and their findings have helped us to understand what atmospheric model best satisfies the measurement data W (h).

We shall use their work to examine the atmospheric region from /264 the surface to 50 km, viewing it as a two-component medium consisting

ORIGINAL PAGE IS
OF POOR QUALITY

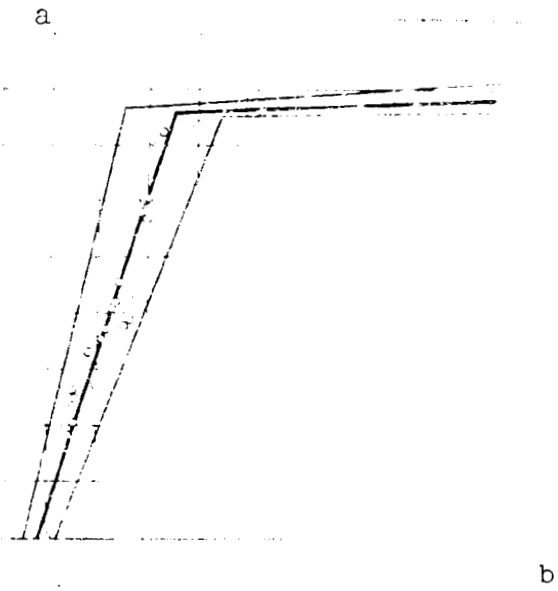

Fig. 91. W vs scale height.

Key: a. km
b. w/m^2

of CO_2 molecules and aerosols of an undetermined nature. The molecular component is known rather well, and the most"workable" (i.e., in agreement with experimental data) optical characteristics of the medium (volume scattering coefficient, single scattering albedo, optical thickness, the parameter of the scattering indicatrix) can give definite information about aerosols.

We shall use the Schwarzschild approximation generalized for non-isotropic scattering. The original relations

$$\int_{\Omega} I(q)\,d\omega = 2F^{+} \int_{\Omega} I(q)\,d\omega = 2F^{-}$$

lead to equations

$$\frac{1}{3}\,\frac{dF^{+}}{dx} = (1-\omega_0)(F^{+} - F^{-}), \qquad (V.35)$$

$$-\frac{1}{3}\,\frac{dF^{-}}{dx} = (F^{+} - F^{-}). \qquad (V.36)$$

where F^{+} and F^{-} are fluxes of ascending and descending radiation, $j = 1 - \omega_0\Gamma$, and Γ is determined from (V.27). Equations (V.35) and (V.36) are obtained on the assumption that the distribution of scattering and absorbing components in the study area of the atmosphere and the scattering law do not vary with altitude, i.e., $\omega_0(h) = \text{const}$; $x(h, \phi) = s(\phi)$. The solution of the system has the form:

$$F^{+} = \left(\frac{1+\sqrt{j}}{1-\omega_0}\right) + \left(\frac{1-\sqrt{j}}{1-\omega_0}\right) + \qquad (V.37)$$

$$F^{-} = \left(\frac{1+\sqrt{j}}{1-\omega_0}\right) - \left(\frac{1-\sqrt{j}}{1-\omega_0}\right) + \qquad (V.38)$$

where c_1 and c_2 are constants of integration.

ORIGINAL PAGE IS
OF POOR QUALITY

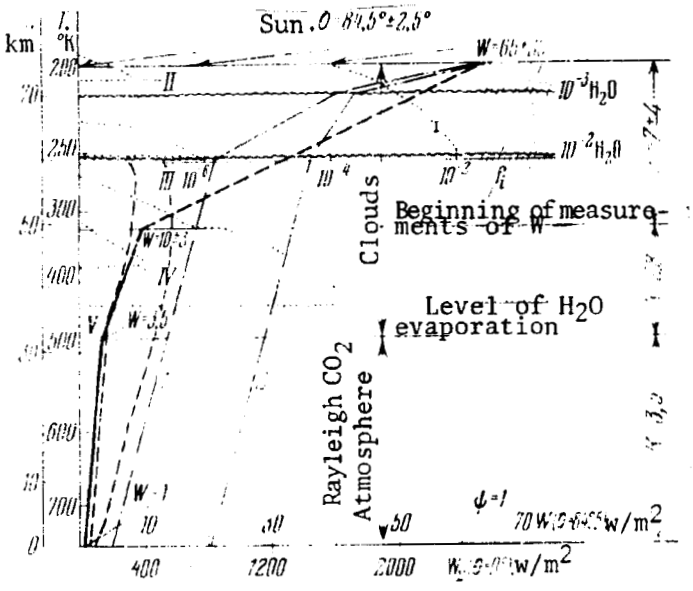

Fig. 92. Attenuation of incident solar energy in the Venusian atmosphere. The thick solid line is the measurements; the thick broken line is an extrapolation to the conditional upper boundary of the atmosphere, at which $W = q_{\varphi}$, $K = W_n/W_{n+1}$ is the attenuation index in the layer $h_{n+1} - h_n$. The wavy lines are the conditional condensation levels corresponding to a content of $f_{H_2O} = 10^{-2}$ and 10^{-3}. The dotted lines are hypothetical clouds: I - H_2O; II - H_2O + HCl; III - $Hg_2Cl_2 \cdot 10^3$; IV - HgS; V - Hg at corresponding values of relative partial pressure of the indicated components f_i (according to Lewis [400]). The stippled area is the area of possible H_2O "precipitation". The dotted-dashed line is the calculated profile of attenuation of solar radiation according to Table 15 at P_s = 200 atm, τ_c = 43 (1) and P_s = 50 atm, τ_c = 18 (2) in relative values (ψ = 1 at the upper boundary). The broken curves are the calculated profiles of total heat radiation at $f_{H_2O}=10^3$ and 10^{-4}(cf. S. V.4). Values of $W(\theta=84.5°)$ and $W_\Sigma(\theta\approx0°)$ are shown on the abscissa.

For purposes of comparison, one may also use the asymptotic method, for example, the Rozenberg formula [139], for descending light flux inside a thick layer: /265

$$[illegible] \qquad (V.39)$$

where u and z are parameters determined in the process of the calculation, wherein

$$[illegible]$$

The parameter $\ell = 4b$, which corresponds to (V.26), must be assigned. The product $\mu_0 g(\mu_0) I_0(\mu) d\omega_0$ is considered a certain constant for a given μ_0.

The boundary conditions at the upper and lower boundaries of the study area are determined, respectively, by the measured value of descending flux and the value of the flux reflected from the underlying surface:

$$[illegible] \qquad (V.40)$$

Here, τ_Σ (h) is the total optical thickness of the layer, whose dependence on altitude is assumed to be in the form τ_Σ (h) $\sim$ P (h).

Fig. 93 shows examples of calculations of the flux of descending solar radiation using the Schwarzschild method (V.37) - (V.38) and by using the asymptotic formula (V.39) for a one-layer homogeneous atmospheric model at

[illegible] eff

τ_Σ τ_Σ eff [illegible]

In order to estimate the accuracy of these approximate solutions, the results of very accurate numerical solutions produced on a Series-4 computer are also given. The calculations lead to several important conclusions about the regularity with which $F^-(h)$ varies as ω_0 decreases, ℓ increases, and as the degree of reflection from the underlying surface changes; they also allow one to estimate the error and convergence of various approximations. It is clear above all that the assumed one-layer model is incompatible with /266 measured data at any ω_0 and $x(\phi)$. Nor is this surprising, since, as we have seen, the experimental profile W(h) leads to conceptions that there are two layers with different attenuation indexes K in the region of measurements. Calculations with various values of a do not reveal any appreciable difference, which confirms the previous conclusion that the surface albedo only weakly influences the structure of the flux. Henceforth, therefore, one may assume $a \approx 0$, i.e., $F^+(\tau = \tau_\Sigma) = 0$, without significant error. In the case of Rayleigh scattering, finally, calculations using formulas (V.37) - (V.38) and (V.39) and calculations using numerical methods yield essentially the same results. Certain differences appear with greatly elongated indicatrixes; according to (56), the error of the two-layer approximation method is 9-12% in reflection and 12-16% in transmission.

ORIGINAL PAGE IS
OF POOR QUALITY

Fig. 93. Variation of illumination with altitude for a one-layer model. The thick solid curve is the measurements, the broken lines are the errors of measurement. The "x's" denote a numerical solution of the transfer equation at $\omega_0 = 1$, $a = 0$ and a Rayleigh indicatrix: 1a-calculations using asymptotic formulas [139] at $\omega_0 = 1$, $a = 0$, $\ell = 4/3$; 1b-calculations using asymptotic formulas [139] at $\omega_0 = 1$, $a = 0$, $\ell = 4$; 2a-calculations using the Schwarzschild method at $\omega_0 = 1$, $a = 0$; 2b-calculations using the Schwarzschild method at $\omega_0 = 1$, $a = 0.85$. Curves 3, 4, 5 and 6 are calculations using the Schwarzschild method at $\Gamma = 0 (j = 1)$, $a = 0$ and $\omega_0 = 0.90$, 0.95, 0.975 and 0.99, respectively. In Figs. 93-95, $F\downarrow \equiv$ [illegible].

Figs. 94 and 95 show calculations for two variants of two- / 267 layer models. They were obtained by solving equations (V.37) - (V.38) at each i-th layer at tabulation over the parameters

$\tau^{(i)}$, $\omega_0^{(i)}$, $j^{(i)}$, where i = 1, 2, wherein 0 - $h_{i=1}$ - 32 km; 32 km $\leq \Delta h_{i=2} \leq$ 50 km. The conditions at the boundary between layers at h = 32 km, in addition to the boundary conditions (V.40), are assigned in this case -- by starting with considerations about the continuity of one-way fluxes:

ORIGINAL PAGE IS
OF POOR QUALITY

(V.41)

In both variants, the lower layer is considered a pure Rayleigh non-absorbing layer with $\tau^{(1)} = \tau_p$, $\lambda_{eff} = 9$, while for the upper layer, the two limiting cases of large and small optical thickness are realized as a function of the predominant role of scattering or true absorption.

As we see, both limiting cases in the choice of specific parameters of the upper layer are in much better agreement with the measured profile W(h). Regardless of these parameters, the results of analyzing the experimental data [8] about the satisfactory approximation of the lower layer of the Rayleigh scattering model, i.e., about its low dust content, are confirmed. A possible deformation of the spectral composition of the flux of radiation at $\lambda'_{eff} > \lambda_{eff}$, as is shown in the calculations, does not change this conclusion. It is noteworthy that these conceptions agree with data on the low wind velocity in the near-surface region of the Venus atmosphere, data obtained from measuring radial velocity during the landing of descent apparati (cf. Section IV.6).

An aggregate of the calculated curves for the upper layer (i = 2) allows one to pick out the parameters that give results closest to actual attenuation of the light flux. An optically thin absorbing atmosphere ($\tau^{(2)} \simeq 3$; $\omega_0^{(2)} < 1$; $\Gamma^{(2)} \geq 0$) corresponds to the first of two alternative models (cf. Fig. 94). It is clear that when $\tau^{(2)} \simeq 3\tau_p^{(2)}$, $\Gamma > 0$ is more likely. A satisfactory agreement with the experimental profile is assured within the range of optical parameters $0.85 \leq \omega_0^{(2)} \leq 0.95$; $0 \leq \Gamma^{(2)} \leq 0.73$. Curves 1b and 2b in Fig. 94 are closest to W(h) at $\omega_0^{(2)} = 0.95$ and $\Gamma^{(2)} = 0$; and at $\omega_0^{(2)} = 0.90$ and $\Gamma^{(2)} = 0.73$, i.e., an increase in the elongation of the scattering indicatrix should lead to an increase in absorption. /269

The second model is associated with a non-absorbing, but strongly scattering upper layer, i.e., a layer with a powerful aerosol component and a greatly elongated indicatrix, so that $\tau^{(2)} >> 1$; $\omega_0^{(2)} \simeq 1$, $\Gamma^{(2)} > 0$. The calculated curves in Fig. 95 vary as a function of $\Gamma^{(2)}$ (curves 1 - 2) and $\tau^{(2)}$ (curves 2-5). A fully acceptable agreement with the experimental profile W(h) is assured at $\tau^{(2)} \simeq 50$; $\Gamma^{(2)} = 0.73$.

It was demonstrated in Section IV.7 that in a hypothetical water-and-ice cloud model, the condensation level as a function of water vapor content in the atmosphere extends above 59 km.

ORIGINAL PAGE IS
OF POOR QUALITY

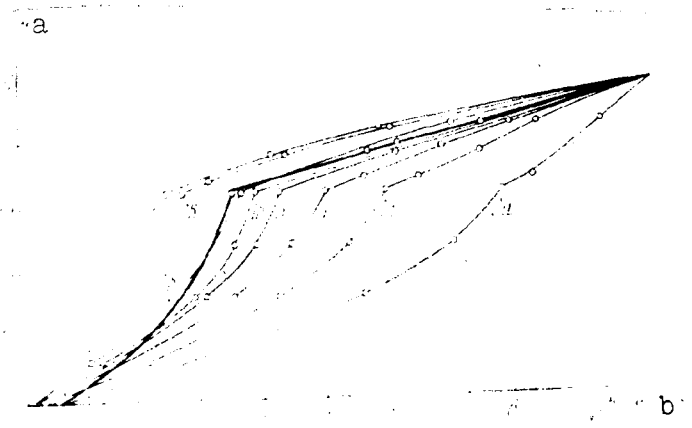

Fig. 94. Illumination vs altitude for a two-layer model. The thick solid curve is the measurements, the remaining lines are calculations. In the lower layer, $\omega_0^{(1)} = 1$, $\Gamma^{(1)} = 0$, $\tau^{(1)} = 9$ in all cases; in the upper layer, the parameters $\tau^{(2)}$, $\omega_0^{(2)}$, and $\Gamma^{(2)}$ assume the following values: $\tau^{(2)} = 3$ (except model 3, where $\tau^{(2)} = 5$); $\omega_0^{(2)} = 0.80$ (model 1b); 0.90 (1b, 2c); 0.95 (1a, 2b, 3, 4); 1.0 (2a); $\Gamma^{(2)} = 0$ (models 2a, 2b, 2c); 0.53 (4); 0.73 (1a, 1b, 1c, 3).

Key: a. km
b. w/m^2

Both models of the 32-50 km layer should in this case be viewed either as the result of penetration of cloud particles into the lower-lying atmosphere or as the result of the presence at these altitudes of clouds consisting of condensates of another chemical nature -- as was discussed in Section IV.7. With an analysis of the characteristics of reflected radiation taken into account, the model of an optically dense upper layer with little true absorption is more realistic; although it is of course impossible to reject an optically thin model, since in the region above 50 km, $\sigma_{clo} >> \sigma^{(2)}$ and $\omega_0^{(2)} < \omega_0^{clo}$ are quite possible. It is interesting to look at a curious phenomenon: water can exist as a liquid at corresponding P and T almost down to the level where a "break" in the curve W(h) is observed. Does this not mean that the measured character of attenuation of light flux is related to the falling of "rain" drops down to the boiling level? Fig. 92 tentatively shows the boundaries of the hypothetical clouds in the Venusian atmosphere and a region of possible H_2O "precipitation."

Assuming that below 50 km there is an optically deep regime, it is possible to obtain an independent estimate of absorption in the layer i = 2. As is known (cf. [139, 149], in this case

ORIGINAL PAGE IS
OF POOR QUALITY

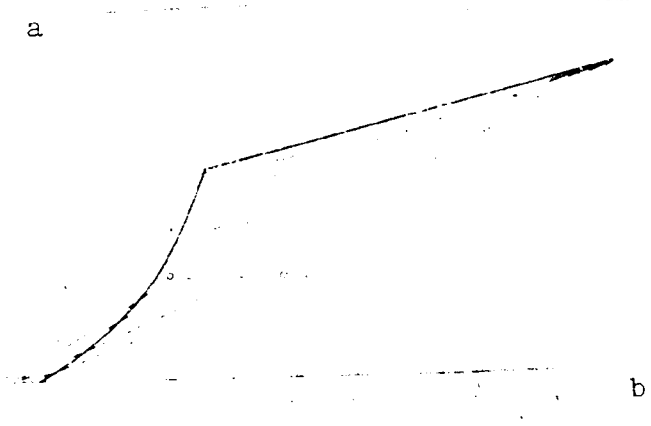

Fig. 95. Illumination vs altitude for a two-layer model. The thick solid curve is the measurements, the rest are the calculations. In the lower layer, $\omega_0^{(1)} = 1$; $\Gamma^{(1)} = 0$; $\tau^{(1)} = 9$ in all cases. In the upper layer: $\tau^{(2)} = 20$ (models 1, 2); 25 (3); 40 (4), 50 (5); $\omega_0^{(2)} = 1$; $\Gamma^{(2)} = 0$ (1); 0.73 (2 - 5).

$$E(h) \sim e^{-kh}, \qquad \text{(V.42)}$$

and if the role of true absorption is small, the parameter k can be determined by using the asymptotic formula (V.28'). It is clear from (V.42) that /270

$$k \sim \frac{1}{\tau} \ln \frac{E(50)}{E(52)},$$

and, at values of optical density corresponding to the two variants of the models examined, we have

$$\tau = 3; \quad \omega_0^{(2)} \leqslant 0.96,$$
$$\tau = 50; \quad \omega_0^{(2)} \geqslant 0.999,$$

which is in good agreement with the estimates of these values cited above.

Our previous judgments (which were based on an analysis of reflected radiation) about the optical properties of the clouds and the subcloud atmosphere do not contradict these optical models. Unfortunately, it is impossible to establish a direct link, since in the presence of dense clouds the lower-lying regions weakly influence the spectrum of reflection. However, it is possible to maintain that the conception of a cloud layer at the reflection level with an optical thickness on the order of several tens and at $0.99 < \omega_0 < 1$ is compatible with measured values of W(h) at h = 49 km.

Article [92] estimates the coefficients of scattering, absorption, and concentration of cloud particles in the layer $\Delta h^{(2)}$ = 32 - 50 km. Since

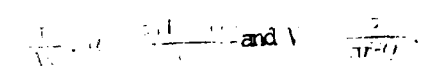

ORIGINAL PAGE IS
OF POOR QUALITY

where Q ≈ 2 is the scattering cross section of the particles, which are assumed to be rather large in the region of the "precipitation," r ≈ 10 μm, we have at $\tau = 3$ ($w_0 = 0.95$):

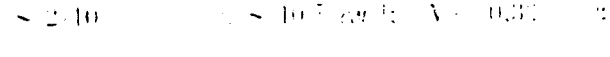

and, at $\tau = 50$ ($w_0 = 0.999$):

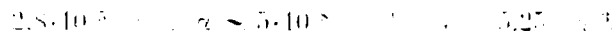

If it is further assumed that r ≈ 1 μm, then we accordingly have N ≈ 30-500 cm^{-3}. Recalling that absorption is equal to /271
$e^{a\bar{l}}$ and that according to [77a] $\bar{l} = n\Delta h$, wherein $1 \leq n \leq 2$ at $\tau \leq 5$ and $3 \leq n \leq 6$ at $10 \leq \tau \leq 100$, it is easy to ascertain to what kind of absorption the obtained values α correspond. For both models, it turns out to be on the order of 50%, i.e., it satisfies measurement data within an order of magnitude (actual absorption is, as we have seen, about 20%).

The conclusion concerning atmospheric transparency, a conclusion made from Venera-8 results, is of fundamental significance. It means that, despite the seeming insignificant value of transmission (~1%), at the surface of the planet one may expect an appreciable (in Earth terms) illumination. In fact, if the illumination of the Venusian surface $E_{\varphi} \approx 400$ lux is compared with the Earth's illumination at the same low position of the Sun, $E_{\oplus} \approx 3000$ lux [171], it turns out that the former is less than the latter only by about an order of magnitude. This comparison is of course very approximate, since it assumes that the spectral composition of the light flux is, for all practical purposes, the same as the Sun's.

Because there are no data on the variation of diurnal illumination on the Venusian surface with the Sun's elevation, we will estimate the illumination on the planet at $\theta \approx 0°$ by analogy with calculations for the Earth's atmosphere in more or less comparable conditions, even though the peculiarities of the light regime in deep layers can introduce specific corrections (cf. [149]). The most probable model of the Venusian atmosphere, a model with a dense cloud layer extending to h ≈ 32 km and with a lower-lying Rayleigh layer, can be viewed as a first approximation of a similar model of an Earth atmosphere with clouds. In addition, estimates of the Venusian surface albedo show that it is not large (probably within a ≈ 0 - 0.6), which allows one to compare the Venusian surface with the Earth's surface with no snow cover.

Fig. 96 shows the family of curves that indicate how the illumination of the Earth's surface without a snow cover varies every day as a function of the zenith angle θ (according to [170]). The dashed line is the cosinusoidal dependence. Values of the Earth's illumination (on scale $E_\oplus$ at left) are given for zenith angles from /272
85° to 35°, since it is usually thought that if the Sun is in a higher position, the illumination for diffused radiation changes only insignificantly. The strong cloud cover on Venus can attenuate solar light more strongly than cumulus clouds on Earth. It is reasonable to assume that there is continuous shade on the Venusian surface, inasmuch as breaks in the optically thick Venusian clouds, breaks through which the Sun might be seen, are not very likely. Apparently, curves 4-9, which do not differ much from a cosine curve, are closest to the conditions that interest us. The extrapolation of curves 4 and 9 (the dotted-dashed lines) give the extreme values of illumination on the Venusian surface, provided they are normalized to the measured value $E = \chi W$ at the landing site at $\theta \approx 85°$. Fig. 96 gives values of W and $E_\oplus$ at other zenith angles on the corresponding ordinal axes.

The approximate character of these estimates of $E_\oplus(\theta)$ is caused by not fully adequate conditions in the Venusian and Earth's atmospheres and by the assumption of identical spectral composition of the light flux that for practical purposes corresponds to the Sun's. In fact, as light passes through a Rayleigh layer of significant /273
optical thickness, a redistribution of energy in the solar spectrum takes place. Less significant are the clouds, in which scattering is predominantly non-selective (cf. p.(179). Fig. 97 shows the deformation of the spectral composition of the light flux as compared to the original distribution of a Rayleigh atmospheric layer with parameters corresponding to the Venusian atmosphere. As we see, the maximum radiation is shifted into the longwave region. However, these estimates are realistic only if τ_λ are not too large even along the line of the beam. In a more realistic Venusian atmosphere, conditions are closer to the light regime in a semi-infinite medium where multiple scattering occurs. If $\omega_0 = 1$, then, as is well-known (cf. [171]), a shift of the spectral composition of the solar radiation into the dark-blue region is possible at the surface -- because of illumination by an atmosphere in which dark-blue quanta predominate. At the same time, since $\omega_0 < 1$ in the dense, multiple-scattering atmosphere of Venus, it is most likely that the shortwave region of the spectrum will experience stronger absorption. This should result in a noticeable change in the color index (a shift into the red region). Biryukov et al. [15] have more closely examined the problem of the spectral composition of the radiation and have estimated the amount of contrast at the Venusian surface.

Estimates of the full flux of solar energy W_Σ that reaches the surface can vary as a function of the deformation of the spectral composition in the Venusian atmosphere, since the starting points of these estimates are the results of measurements in a specific region of the spectrum. A calculation of these features gives

ORIGINAL PAGE IS
OF POOR QUALITY

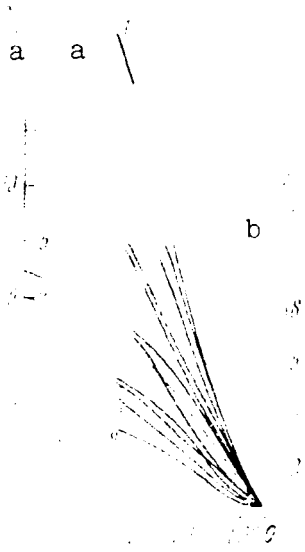

Fig. 96. Variation of illumination on the Earth's surface without snow cover $E_{\oplus}$ with the elevation of the Sun -- for various types of clouds: 1-no clouds; 2a-cirrus clouds Ci, Cs, the Sun in the clouds, ∿1/4 of the sky covered; 2b-same, ∿1/2 covered; 2c-same, entire sky covered; 3-cumulocirrus clouds Cc; 4-altocumulus clouds Ac, entire sky covered; 7-cumulonimbus clouds Cb, entire sky covered; 8-stratus clouds St, solid cloudiness; 9-nimbus coulds Ns, solid cloudiness. The curves are tied to scales of W_{φ}, and $E_{\varphi} = W_{\varphi}$ for $\theta = 84.5°$, the cross is $W/W_{mea} = 1$. The dashed line is a cosine curve. The dashed-dotted line is an extrapolation of curves 4 and 8, which presumably bound the probable conditions of illumination on Venus, at $\theta \approx 0°$.

Key: a. lux
b. w/m^2

$W_{\Sigma} = 2 - 4$ w/m^2 at the landing site on the surface. Fig. 96 shows that at $\theta \approx 0°$, $W^{\varphi}_{\Sigma} = 3.8 - 9.6$ w/cm^2 (in readings of the Venera-8 photometer), or $W^{\circ}_{\Sigma\varphi} = 15.2 - 38.4$ w/cm^2. We find from this that the mean value of the flux of solar energy incident at the Venusian day side is $\overline{W}_{\Sigma\varphi} \approx 10 - 2$ w/m^2. By taking the proportionality factor χ into account as in (V.33), we have E_{φ} ($\theta = 0$) ≈ 1500 - 4000 lux. / 274

V.4. Radiative Heat Exchange in the Atmosphere.

Longwave radiation transfer.

The size and character of radiative heat fluxes in the atmosphere is determined by their physical structure, and, if the chemical composition is known, they can be calculated from actual temperature and pressure values. A knowledge of the functions T(h) and P(h) allows one to make the appropriate calculations for the lower atmosphere of Venus.

Radiative transfer in the spectral region of the planet's own heat emission shows a number of distinctive characteristics. The predominant role is played by gaseous absorption by multiatomic molecules, especially at large optical masses of gas, because (in the Venusian atmosphere) absorption is strongly dependent on the thermophysical parameters of the medium. In expression (V.15) one may then assign

$\sigma^{g} \to 0$ and

Consequently, the problem of determining the attenuation of longwave radiation is reduced primarily to finding the monochromatic opacities of the mixtures of gases found in the Venusian atmosphere --

ORIGINAL PAGE IS
OF POOR QUALITY

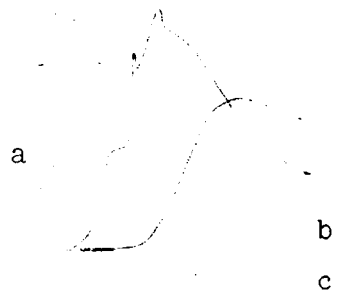

Fig. 97. The spectral distribution of energy in solar light at the boundary of the atmosphere $I_{0\lambda}(1)$ and after passing through a Rayleigh non-absorbing layer (direct beams). $I_\lambda = I_{C\lambda}\, c^{-\tau\lambda}$ at $\tau_\lambda = \tau \overset{\varphi}{p}$ (2).

Key: a. Cal/cm^2-min-μm
b. Cal/cm^2-min-μm
c. μm

CO_2 and H_2O (and also small components, whose influence can be appreciable).

The gaseous absorption of radiation is determined by a number of independent parameters, including the monochromatic absorption coefficient, temperature, total pressure of the medium, partial pressure of the gas, the dependence of spectral line width on admixtures of other gases, the optical path, and the distribution of mass along the optical path. Most of the atmospheric opacity is created by the numerous oscillatory-rotational bands, for which the absorption coefficient varies rapidly as the wave number ν changes. It is necessary in this regard to bring a large number of points into our examination, in order to calculate the total energy flux. Thus, at $P \approx 1$ atm, the half-width of rotational lines is usually less than $10^{-1}cm^{-1}$. This means that maintaining a constant absorption coefficient within the division interval would require an examination of intervals on the order of $10^{-2}cm^{-1}$ wide. In computing total fluxes for the spectral region corresponding to the equilibrium emission at the surface temperature of Venus and to a range of wave numbers from about 10^3 to $10^4 cm^{-1}$, it would be necessary to make a summation over 10^{-5} - 10^{-6} individual points [462]. In a theoretical examination of radiative heat transfer, therefore, there is some question about acceptable methods of averaging monochromatic opacities, methods which would allow a substantial reduction in the number of divisions in this or that wave interval without appreciably reducing the accuracy (especially near the maximum of the Planck curve, where the intensity of emission slowly varies with frequency). /275

For the complex structure of oscillatory-rotational bands, it is customary to assign models of spectral line distribution inside the band. A good approximation to experimental results is given by models of bands in which the intensity and positions of individual lines are statistically distributed. One may find a detailed discussion of this approach in the well-known monograph of Goody [50]. For optically thick gaseous layers, it is also necessary to know the functional dependence of effective band width on optical thickness (growth curve), wherein the fine rotational structure of the bands, which depend in turn on temperature and pressure, are included. At high temperatures and pressures, there are many new features in the spectra of multiatomic molecules, features caused by pressure-induced

ORIGINAL PAGE IS
OF POOR QUALITY

transitions and by states of thermal excitation. One can maintain that in conditions corresponding to the measured parameters of gas in the Venusian atmosphere and with large dimensions of the absorbing layer, absorption even in the wings of the bands is important for the transmission of the subcloud atmosphere.

Experiments with CO_2 and H_2O indicate that for a transmission function of these gases $\Omega_i = \exp\{-\tau_i[\zeta(\ell)]\}$ in the spectral interval $\Delta\nu_i$ if constant pressure P is maintained along the optical path $\zeta(\ell)$, the absorption is well approximated by a power function of the form $\tau_i = c_i u^{r_i} P^{s_i}$ or by its slightly more general modification (including the dependence of opacity on changes in T and P): $\tau_i = c_i \left| \int G_i(T) P^{s_i} \frac{du}{T} \right|^{r_i}$ [204,462, 482]. The function $G_i(T)$, the coefficient c_i and the exponents r_i and s_i are determined from the results of integrating for various temperatures, pressures and optical masses of gas on the line of sight in direction ℓ, and by comparison with experimental data $u(\zeta(\ell)) = \int_0^{\zeta(\ell)} \rho(\zeta)\, d\zeta$. /276

Thus, variation in τ_i as a function of the optical mass of the gas is, in contrast to monochromatic radiation, non-linear. Furthermore, in the general case of a model of mean band opacity in a gaseous mixture, $\bar{\tau}$ is not subject to the superposition rule for monochromatic opacities of an i-th gas $\tau_{\nu i}$. If it is assumed that in each band a specific source of opacity predominates (for example, that caused by water vapor), however, the value of τ_i can be seen as the sum of individual sources of opacity, provided there is no correlation between the positions of individual rotational lines in the bands and that there is no large scale correlation either [50, 462].

Thanks to the works of Gal'tsev, Osipov, and Odishariya [38, 39, 125], there has recently been a great deal of progress in the study of carbon dioxide gas opacity for heat radiation at high temperatures and pressures. For the most part, these are the results of theoretical calculation based on research of the fine structure of CO_2 absorption bands in the infrared region of the sprectrum. They include work on the Fermi resonance of spectroscopic constants for 900 oscillatory states of $C^{12}O_2^{16}$, which are required in order to find line positions and intensities at high temperatures; they include calculations of line position and intensity of 400 oscillatory transitions that lie in the region from 1 to 20 μm and that form bands: 1.2, 1.4, 1.6, 2.0, 2.7, 4.3, 4.8-5.2, 9.4-10.4, and 15 μm; and they include a choice of methodology and a calculation of the parameters needed to determine CO_2 transmission functions at $P \geq 2 - 5$ atm and $295° \leq T \leq 800°K$. /277

It has been shown that in these conditions a computation of the transmission function in the weak line approximation yields sufficiently good agreement with experimental data:

$$\Omega_i = \exp\left(-\frac{\bar{\gamma}}{\bar{d}} u\right). \qquad \text{(V.43)}$$

where S is the mean line intensity in the interval $\Delta\nu_i$, d is the mean distance between lines, u is the content of the absorbing substance under normal conditions (STP)[12], and u is $273/T\ P\ell(\text{atm}\cdot\text{cm})_{STP}$. In this approximation, the values $S/d\ (\text{atm}^{-1}\cdot\text{cm}^{-1})_{STP}$ can be seen as the mean absorption coefficients κ in the interval $\Delta\nu$. For any part of the atmosphere with parameters T_j and P_j, we have

$$\kappa(T; P) \quad \kappa(T)\frac{273}{T}P \tag{V.44}$$

The spectral regions beyond the edges of bands 2.7 and 4.3 μm play an important role in the transfer of its own radiation in the physical conditions of the Venusian subcloud atmosphere. This absorption is determined by the impact of the wings of strong lines in the center of the band (absorption coefficient $\tilde{\kappa}$) and by the weak lines of "hot" transitions. The absorption coefficients beyond the edges of the 4.3 μm band were obtained by direct calculation using a Benedict contour. For the 2.7 μm band, the data obtained experimentally by Berge et al. (cf. [39]) on transmission beyond the edge of the band were used. Beyond the edges of the bands, the transmission function in the following form gives acceptable results

$$\Omega \quad \exp\left\{-\frac{S}{d}u \quad \tilde{\kappa}Pu\right\}. \tag{V.45}$$

wherein the temperature dependence of the absorption coefficient $\tilde{\kappa}$ /278 is expressed by the relation

$$\frac{\tilde{\kappa}(T)}{\tilde{\kappa}(295)} \quad \frac{295}{T}\,\frac{\left(\frac{S}{d}\right)_{\max}(T)}{\left(\frac{S}{d}\right)_{\max}(295)}, \tag{V.46}$$

ORIGINAL PAGE IS
OF POOR QUALITY

where the subscript "max" indicates the value at the edge.

These calculations also included experimental data on induced CO_2 absorption in bands 7.2 and 7.8 μm, which were joined in band 7.5 μm. In thus taking account of induced absorption, one may calculate the transmission for individual spectral intervals $\Delta\nu_i$ from the formula

$$\Omega \quad \exp\left\{\left[\frac{S}{d}u \quad \kappa_{\Delta\nu}(295)\left(\frac{295}{T}\right)^{3}Pu\right]\right\}. \tag{V.47}$$

where $\kappa_{\Delta\nu}$ [295] is the induced-absorption coefficient at $T = 295^{\circ}K$.

---

[12] Under normal conditions, (Standard Temperature Pressure) usually means $T = 273^{\circ}K$ and $P = 1$ atm.

ORIGINAL PAGE IS
OF POOR QUALITY

Fig. 98 shows the distribution of the absorption coefficient κ_{CO_2} vs wave numbers at intervals of $\Delta\nu = 10\ cm^{-1}$ for Venusian atmospheric conditions at the surface (1) at an altitude of 20 km (2), at 40 km (3), and at the cloud level (4), which is conditionally associated with an altitude of $h_0 \approx 60$ km.

The most complete and accessible data on the coefficients of water vapor absorption in the infrared region for optically thick layers in a wide range of temperatures (300-3000°K) are found in the works of Ferriso, Ludwig et al. [302, 404, 405]. [302] tabulates values of κ, calculated by using laboratory emission and absorbtion spectra of H_2O in the interval of wave numbers from 50 to 11,000 cm^{-1}, at every 25 cm^{-1}. The method was as follows: each oscillatory-rotational band for which absorption coefficients were determined was presented as a mean half-width of a spectral line and its broadening in such a way that the total value of the absorption coefficients was equal to the total absorption intensity of the individual band at a given, experimentally-determined temperature. It was assumed that for an optically thick layer of gas, the growth /279 curve can be represented by a statistical model. Calculation of the fine structure of the band was done using the assumption that the corresponding terms were independent of frequency. The various terms to describe fine structure (the terms were obtained from an analysis of optically thick layers) allowed them to compute the broadening of the average (individual bands) lines as a function of temperature. Broadening due to admixtures of other gases was also taken into account, as was non-resonant absorption by H_2O molecules. In the authors' estimates [302], in slowly varying regions of the spectrum the error in computing the absorption coefficients is ±20% and can be slightly larger in regions of more abrupt changes and in the sections between individual oscillatory-rotational bands. Fig. 99 gives an example of the agreement between the measured curves and the experimental results in a fundamental H_2O band at $\lambda = 6.3$ μm at T = 600°K.

By including data on monochromatic absorption coefficients, it /280 is possible to calculate water vapor transmission functions in the intervals $\Delta\nu = 25\ cm^{-1}$ by using, as in the case of CO_2, the weak line approximation. Fig. 100 compares the H_2O absorption coefficients and CO_2 absorption coefficients averaged at intervals of 25 cm^{-1} (according to data for 10 cm^{-1}) for conditions at the planetary surface and for three values of relative H_2O content: 1%, 0.1%, and 0.001% ($f_{CO_2} \approx 100\%$).

Gaseous analysis yields (cf. Table 11) a threshold estimate of less than 2% nitrogen content by volume in the Venusian atmosphere. If nitrogen is present, then with the large total mass of atmospheric gas, a content on the order of a percent will be substantial in absolute units. It should therefore be estimated how essential its influence on the transfer of infrared radiation can then be. Since N_2 molecules are homonuclear, infrared transitions

ORIGINAL PAGE IS
OF POOR QUALITY

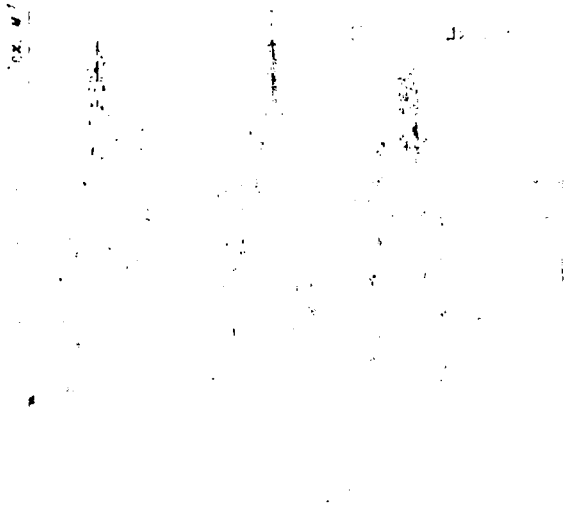

Fig. 98. Distribution of κ_{CO_2} vs wave number for the intervals $\Delta\nu = 10\ cm^{-1}$ up to $\nu = 4200\ cm^{-1}$ and $\Delta\nu = 50\ cm^{-1}$ up to $6000\ cm^{-1}$ in the Venusian atmosphere at the surface (1) and at altitudes of 20 km (2), 40 km (3), and 60 km (4).

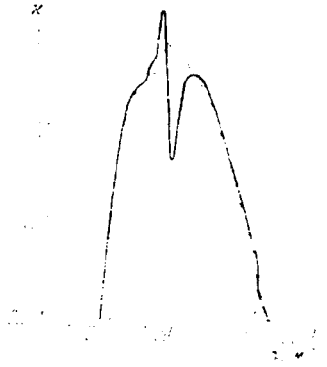

Fig. 99. An example of the agreement between the theoretical profile κ_{H_2O} in the band $\lambda = 6.3$ μm and experimental data. The curve is the calculation, and the circles are the experiment [302].

for them are forbidden. However, at sufficiently high pressures, an induced dipole moment can arise, and hence the induced transitions will have no fine structure. Monochromatic opacity of pressure-induced transitions varies smoothly with wavelength and is proportional to the square of pressure [463]. At pressures corresponding to values at the Venusian surface, the greatest N_2 opacity will be near the CO_2 band at $\lambda = 4.3$ μm and within the rotational H_2O band (17-100 μm). Nevertheless, it will be much lower in comparison to existing CO_2 and H_2O opacities, and it will therefore not exert any appreciable influence on the results of calculations in a carbon dioxide and water vapor model. /281

Available data on opacity characteristics allow calculations of diffused radiative heat fluxes in the subcloud atmosphere of Venus. Marov and Shari [104] and, more recently, Shari [169, 566a] have made such calculations using the aforementioned transmission function of a CO_2 and H_2O mixture. These calculations have enabled previous results to be further refined [2, 5, 97, 188].

The transfer of radiation in the spectral region from 1.2 to 77 μm ($\Delta\nu = 8310 - 130\ cm^{-1}$) has been examined. There are calculations of CO_2 transmission functions for this region, and it is in this region that practically all the intensity of Venus' own surface and atmospheric radiation is concentrated. Here, too, are the most important oscillatory-rotational bands of carbon dioxide and water vapor. In order to take better account of the influence of the latter, the spectral region was broadened to $50\ cm^{-1}$.

ORIGINAL PAGE IS
OF POOR QUALITY

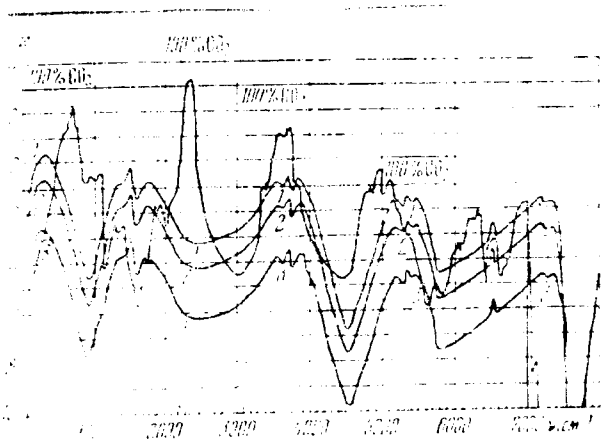

Fig. 100. Distribution of κ_{CO_2} ($\Delta\nu$ = 10 cm^{-1} and 50 cm^{-1}) and κh_2O ($\Delta\nu$ = 25 cm^{-1}) vs wave number for conditions at the Venusian surface at f_{H_2O} = 1% (1), 0.1% (2), and 0.001% (3).

It has been demonstrated /282 in Section V.2 that by taking account of heat content in the Venusian atmosphere, its characteristic time constant (cf. Table 17), and circulatory heat exchange, it may rightly be assumed that temperature distribution does not depend on time of day and that it remains practically the same at different latitudes. Since the radius of Venus is much larger than the examined thickness of layer Z, $R_\varphi >> Z$, in which $Z >> \ell_\nu = \pm 1/\kappa_\nu$, it is possible to disregard the curvature of the atmosphere and to reduce the problem of finding radiative fluxes in the planetary atmosphere to the determination of the transfer of radiant energy within a flat layer of gas. It is also possible to disregard the bending of beams due to refraction, since even with the gaseous parameters at the Venusian surface, the difference between the refractive index m and unity is not large, which Table 21 clearly shows. For zenith angles $\theta \leq \pi/6$, the refraction angles are within $\omega = \Delta m \, tg\theta \leq 30'$. Clearly, refraction greatly influences only beams at small angles to the surface, beams that make no appreciable contribution to the heat flux.

TABLE 21. REFRACTIVE INDEX IN THE VENUSIAN ATMOSPHERE
($m = 1 + \beta(P/T)$; β = 0.13 deg/atm [160])

h, km	m	h, km	m
	1.0172	32	1.0023
	1.0140	36	1.0018
	1.0113	40	1.0013
	1.0090	44	1.0009
16	1.0072	48	1.0005
	1.0056	52	1.0004
	1.0043	56	1.0003
	1.0032	60	1.0001

Thus in this formulation of the problem, the lower atmosphere of Venus is viewed as a flat layer h > 0, which is filled with a substance whose refractive index is m ≈ 1 and whose temperature T(h) varies throughout the thickness of the layer. This layer

is bounded by the surface $h = h_0^-$, from which a flux is emitted; this flux is defined by the integral with respect to the sources (V.7) as the emission of an absolute blackbody at effective temperature T_e[13].

Under these conditions, the equations for spectral intensity of /283 the radiation I_ν^+ into the upper hemisphere (zenith angles $0 \leq \theta \leq \pi/2$) and for the intensity I_ν^- into the lower hemisphere ($\pi/2 \leq \theta \leq \pi$) may be presented in a form similar in terms of assigning boundary conditions [57, 167].

$$\xi \frac{dI_\nu^\pm(h, \xi)}{dh} \quad \varkappa_\nu [I_{p\nu}(h) - I_\nu^\pm(h, \xi)] \qquad \text{(V.48)}$$

where $\xi = \cos\theta (0 \leq \theta \leq \pi/2)$, and $I_{p\nu}$ is the spectral intensity of equilibrium radiation.

A sufficiently general (for these equations) form of the boundary conditions, which model real conditions on the planetary surface h_0^+ and at the lower level of the clouds h_0^-, will be the presence of a single diffused-reflecting surface at $h = h_0^-$ with blackness $\varepsilon^\pm$, which will hereinafter be assumed to be independent of frequency[14]:

$$I_\nu^\pm(h_0^\pm, \xi) \quad \varepsilon^\pm I_{p\nu}(h_0^\pm) \qquad \text{(V.49)}$$

$$\cdot (1 - \varepsilon^\pm) \cdot \frac{\int_0^{2\pi} \int_0^1 I_\nu^\mp(h_0^\mp, \xi) \cos\theta \, d\xi \, d\varphi}{\int_0^{2\pi} \int_0^1 \cos\theta \, d\xi \, d\varphi}$$

ORIGINAL PAGE IS OF POOR QUALITY

If the value $\varepsilon = 1$ is assigned to one surface of the flat layer and the arbitary value $\varepsilon < 1$ is assigned to the other, the system of equations (V.48) with the boundary conditions (V.49) becomes closed.

The solution of this system is expressed in quadratures as /284 follows:

$$I_\nu^\pm(h, \xi) \quad I_\nu^\pm(h_0^\pm, \xi) e^{\int_{h_0^\pm}^{h} \left| \pm \frac{\varkappa_\nu}{\xi}(h') \right| dh'} \qquad \text{(V.50)}$$

$$\int_{h_0^\pm}^{h} \left| \frac{\varkappa_\nu(h')}{\xi} \right| I_{p\nu} \, e^{\int_{h'}^{h} \left| \pm \frac{\varkappa_\nu}{\xi}(h'') \right| dh''} dh'.$$

---

[13] In general case, the level $h_0^- \simeq h_\infty$ lies below the visible boundary of the clouds h_c, and the temperature of radiation at this level is $T_e - T_{h_c}$ even for an optically thick medium such as the lower atmosphere of Venus.

[14] The surface temperature may clearly be taken to be equal to the temperature of the gas at the surface, since at the surface there should be a convective heat transmission that equalizes the temperatures.

ORIGINAL PAGE IS
OF POOR QUALITY

After transformation, we will have

$$\left| \int_{h}^{h_0} \frac{\kappa_\nu dh'}{\xi} \right| \qquad \text{(V.51)}$$

$$I_\nu^{\pm}(h, \xi) = I_\nu^{\pm}(h_0^{\pm}, \xi) \; I_{p\nu}(h_0^{\pm}) e^{-\left| \int_{h}^{h_0} \frac{\kappa_\nu dh'}{\xi} \right|} + \int_{h}^{h_0} e^{-\left| \int_{h}^{h'} \frac{\kappa_\nu dh''}{\xi} \right|} dI_{p\nu}(h') = I_{p\nu}(h_0)$$

By integrating expressions for spectral intensities with respect to frequency intervals $\delta\nu_i$ sufficiently small so as to be able to disregard variation in $I_\nu^{\pm}$ and $I_{p\nu}$ within their limits, we obtain:

$$I_i^{\pm}(h, \xi) = I_i^{\pm}(h_0^{\pm}, \xi) \; I_{pi}(h_0^{\pm}) \Omega_i(h_0^{\pm}, h, \xi) + \int_{h}^{h_0} \Omega_i(h', h, \xi) dI_{pi}(h') \qquad \text{(V.52)}$$

Transmission functions averaged over the frequency intervals $\sigma\nu_i$ enter into the latter expression:

$$\Omega_i(h_1, h_2, \xi) = \frac{\int_{\Delta\nu_i} e^{-\left| \int_{h_1}^{h_2} \frac{\kappa_\nu dh}{\xi} \right|} d\nu}{\int_{\Delta\nu_i} d\nu} \qquad \text{(V.53)}$$

There are serious difficulties involved in obtaining $I_\nu^{\pm}(h, \xi)$ from a formal solution of the equation of transfer (V.51). In the general case κ_ν varies complexly as h varies as a function of temperature, pressure, mass distribution of gas along the beam (cf., for example, [57]). Numerical methods provide much greater opportunities to study the transfer of selective radiation in a medium with variable properties. These methods enable a more efficient calculation of the angular distribution of the field of radiation than is true for cases of diffused or two-flux approximations used in modelling the light regime (V.3). /285

The projection of the vector of monochromatic flux of diffused radiant energy on an altitudinal direction h for a flatly-stratified atmosphere is given by the expression

$$S_\nu(h) = 2\pi \int_0^{\pi} I_\nu(h, \theta) \cos\theta \sin\theta d\theta = 2\pi \int_{-1}^{1} I_\nu(h, \xi) \xi d\xi \qquad \text{(V.54)}$$

For numerical integration (V.54), a Gauss formula is used. This expresses the value of the integral approximately in the form

$$\int_{-1}^{1} g(\xi) d\xi \approx \sum_{i=1}^{n} a_i g(\xi_i).$$

where the angles z_r and the corresponding weight coefficients ω_r do not depend on the choice of an integrand. Here the weights ω_r are determined by the formula

ORIGINAL PAGE IS
OF POOR QUALITY

$$\omega_r = \frac{\Pi_n(z_r)}{\Pi_n'(z_r)}$$

where $\Pi_n(z) = (z - z_1)(z - z_2)\ldots(z - z_n)$, while $\Pi_n'(z)$ designates

$$\Pi_n'(z) = \sum_{r=1}^{n} \omega_r z^{n-1}$$

If the roots of the equation $P_n(z) = 0$ (where $P_n(z)$ are Legendre's polynomials) are taken as z_r, then the corresponding Gauss quadrature formula, which uses n points, will be accurate for all polynomials whose order of magnitude is less than 2n. /286

Table 22 gives the values of the angles z_r and the corresponding weights ω_r for the Gauss formula. The table shows that for even values, $n = 2k$ there are k pairs of roots z_r equal in magnitude and opposite in sign; while, for every pair, there are corresponding weights ω_r that are equal among themselves.

In this case, for a monochromatic diffused flux S_{ν_h} and for an even $n = 2k$, we will have the following instead of (V.54)

$$S_{\nu_h}(h) = 2\pi \int_0^1 I_\nu(h, \xi)\xi\, d\xi \sim 2\pi \sum_{r=1}^{n} \omega_r I_\nu(h, \xi_r)\xi_r \qquad (V.55)$$

$$2\pi \sum_{r=1}^{k} \omega_r I_\nu(h, \xi_r)\xi_r + \sum_{r=k+1}^{n} \omega_r I_\nu(h, -\xi_r)(-\xi_r)$$

$$2\pi \sum_{r=1}^{k} \omega_r \xi_r I_\nu(h, \xi_r) - \sum_{r=1}^{k} \omega_r \xi_r I_\nu(h, -\xi_r)$$

Here, ξ_r are understood to be positive roots. Since negative values of $\cos\theta = \xi$ correspond to a distribution of radiant energy into the lower hemisphere ($I = I^-$), whereas positive values correspond to a distribution of radiant energy into the upper hemisphere ($I = I^+$), it is possible to rewrite (V.55) as

$$S_{\nu_h} \sim 2\pi \sum_{r=1}^{k} \omega_r \xi_r I^+(h, \xi_r) - \sum_{r=1}^{k} \omega_r \xi_r I^-(h, \xi_r) \qquad (V.56)$$

The full flux of radiation in the infrared region of the spectrum is obtained by summation of (V.56) over all frequency intervals $\Delta\nu_i$:

$$S(h) \sim \sum 2\pi \sum \omega_r I^+(h, \xi_r)\Delta\nu_i - \sum \omega_r \xi_r I^-(h, \xi_r)\Delta\nu_i \qquad (V.57)$$

The mean (in the i-th frequency interval) intensities of emission that enter into this expression $I_i(h, \xi_r)$ are determined from the system of equations (V.52) and the boundary conditions (V.49) for k values from Table 22.

TABLE 22. VALUES OF ANGLES z_r AND WEIGHTS ω_r FOR THE GAUSS QUADRATURE FORMULA

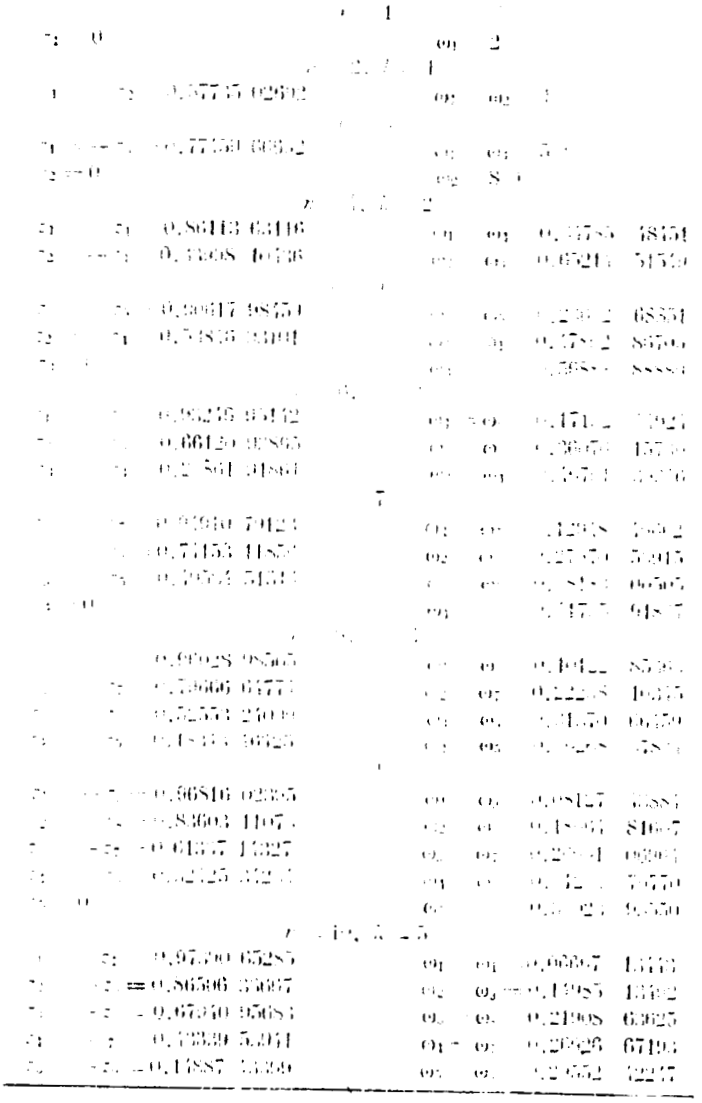

ORIGINAL PAGE IS OF POOR QUALITY

Using the value k = 3 - 4 is fully satisfactory from the point of view of accuracy. An increase in k from 3 to 4 changes the total fluxes at all levels and for all atmospheric compositions by less than 0.5%. Let us introduce the following designations: /288

ORIGINAL PAGE IS
OF POOR QUALITY

$$\tilde{\omega}_i = 2\omega_i \left(\sum_{k=1}^{n} \tilde{\omega}_k + 2 \right),$$

$$\pi I^{\pm}(h, \xi_i) \Delta\nu_i = F_i^{\pm}(h, \xi_i),$$

$$\pi I_p(h) \Delta\nu_i = B_i(h).$$

B_i is the one-way equilibrium radiative flux in the interval $\Delta_{\nu i}$. Using these designations, (V.57) is written as follows:

$$S(h) = \sum_{i} \sum_{k} (\tilde{\omega}_k \xi_k F_i^{+}(h, \xi_k) - \tilde{\omega}_k \xi_k F_i^{-}(h, \xi_k)). \tag{V.58}$$

where, by taking (V.52) and (V.49) into account,

$$F_i^{+}(h, \xi_i) = B_i(h) - [F_i^{+}(h_0^{+}, \xi_i) - B_i(h_0^{+})] \Omega_i(h_0^{+}, h, \xi_i) - \int_{h_0^{+}}^{h} \Omega_i(h', h, \xi_i) dB_i(h'); \tag{V.59}$$

$$F_i^{-}(h, \xi_i) = B_i(h) - [F_i^{-}(h_0^{-}, \xi_i) - B_i(h_0^{-})] \Omega_i(h_0^{-}, h, \xi_i) - \frac{\sum_{k} \tilde{\omega}_k \xi_k F_i^{+}(h_0^{+}, \xi_k)}{\sum_{k} \tilde{\omega}_k \xi_k}. \tag{V.60}$$

As the calculations show (Fig. 101), the integral (with respect to the infrared spectrum) one-way fluxes for the optically dense Venusian atmosphere do not depend substantially on atmospheric composition, especially in models with water vapor included, and they are close to the one-way flux of equilibrium radiation, reflecting the temperature profile in the atmosphere. In order to avoid computing the outgoing flux as the difference between two nearly-equal and large one-way fluxes, let us introduce the values /289

Then, from (V.58), we obtain

$$S(h) = \sum_{i} \left\{ \sum_{k=1}^{n} \tilde{\omega}_k \xi_k F_i^{+}(h, \xi_k) - \sum_{k=n+1}^{2n} \tilde{\omega}_k \xi_k F_i^{-}(h, \xi_k) \right\}. \tag{V.61}$$

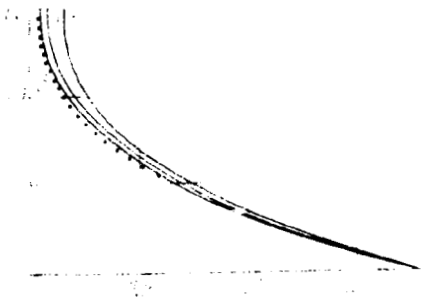

Fig. 101. Intensity variation in the integral (with respect to the spectrum) one-way fluxes $q \equiv S$ vs altitude for various H_2O contents (f_{CO_2} = 100%: f_{H_2O} = 0 (1); 0.001% (2); 0.1% (3). The dots are $S(h) = \sigma T^4(h)$.

Key: a. km.
b. w/cm^2

The differences ΔF_i^+ and ΔF_i^- are determined by system

$$\Delta F_i^+(h, \xi_r) = \Delta F_i^+(h_0^+, \xi_r) + \Omega_i(h_0^+, h, \xi_r) \varepsilon_{i,r} + \int_{h_0^+}^{h} \Omega_i(h', h, \xi_r) dB_i(h'), \quad \text{(V.62)}$$

$$\Delta F_i^-(h, \xi_r) = \Delta F_i^-(h_0^-, \xi_r) + \Omega_i(h_0^-, h, \xi_r) \varepsilon_{i,r} + \int_{h_0^-}^{h} \Omega_i(h', h, \xi_r) dB_i(h').$$

with the boundary conditions:

$$\Delta F_i^+(h_0, \xi_r) = (1 - \varepsilon^{\pm}) \frac{\sum_i \omega_i \Delta F_i^-}{\sum_i \omega_i \xi_r}, \quad \text{(V.63)}$$

If the blackness of the lower boundary of the cloud layer is $\varepsilon_c = \varepsilon^- = 1$ (at $h_0^- = Z$) or if the blackness of the planetary surface is $\varepsilon_s = \varepsilon^+ = 1$ (at $h_0^+ = 0$), the system (V.62)-(V.63) is solvable. If $\varepsilon^- = \varepsilon^+ = 1$, then (V.63) reduces to zero, and (V.62) is reduced to the expression:

/290

$$\left.\begin{aligned} \Delta F_i^+(h, \xi_r) &= \int_0^h \Omega_i(h', h, \xi_r) dB_i(h'), \\ \Delta F_i^-(h, \xi_r) &= \int_Z^h \Omega_i(h', h, \xi_r) dB_i(h'). \end{aligned}\right\} \quad \text{(V.64)}$$

In this case, the total flux of heat radiation is determined from (V.61) in the form:

$$S(h) = \sum_{i=1}^{n} \sum_{r=1}^{k} \omega_i \xi_r \int_0^h \Omega_i(h', h, \xi_r) dB_i(h'). \quad \text{(V.65)}$$

In order to calculate the altitude distribution of the radiative heat fluxes, let us divide the study area of the atmosphere Z into layers ΔH thick with the altitudinal coordinates h_j (j = 0, 1, 2, ...N).

Let us also keep in mind that since the transmission functions in the i-th frequency interval are computed in the weak line approximation, which gives the exponential function

$$\Omega_i(h, h', \xi_r) = \exp\left\{ -\left| \int_{h'}^{h} \frac{k_i(h'')}{\mu} dh'' \right| \right\}.$$

ORIGINAL PAGE IS
OF POOR QUALITY

then for any $h_{j-1} < h_j < h_{j+1}$, the following relation is met:

$$\Omega_i(h_{j-1}, h_{j+1}) = \Omega_i(h_{j-1}, h_j)\,\Omega_i(h_j, h_{j+1}). \tag{V.66}$$

Then, for every j-th level, it is possible to omit equations of the (V.62) type and perform the integration with the boundary conditions (V.63) successively from level to level, using the value $\Delta F^{\pm}$ found at the previous level.

For example, let us demonstrate this for ΔF^{+}: /291

$$\begin{aligned}
\Delta F_i^{+}(h_j) &= \Delta F_i^{+}(h_0)\,\Omega_i(h_0, h_j) - \int_{h_0}^{h_j} \Omega_i(h', h_j)\,dB_i(h') \\
&= \Delta F_i^{+}(h_0)\,\Omega_i(h_0, h_{j-1})\,\Omega_i(h_{j-1}, h_j) \\
&\quad - \int_{h_0}^{h_{j-1}} \Omega_i(h', h_{j-1})\,\Omega_i(h_{j-1}, h_j)\,dB_i(h') - \int_{h_{j-1}}^{h_j} \Omega_i(h', h_j)\,dB_i(h') = \\
&= \left\{\Delta F_i^{+}(h_0)\,\Omega_i(h_0, h_{j-1}) - \right. \\
&\quad \left. - \int_{h_0}^{h_{j-1}} \Omega_i(h', h_{j-1})\,dB_i(h')\right\}\Omega_i(h_{j-1}, h_j) - \int_{h_{j-1}}^{h_j} \Omega_i(h', h_j)\,dB_i(h').
\end{aligned}$$

But the expression in the brackets is $\Delta F^{+}(h_{j-1})$. Therefore, we finally have the following system:

$$\left.\begin{aligned}
&\Delta F_i^{+}(h_0, \xi_r) = (1 - \varepsilon_i)\frac{\sum_{r=1}^{N} \tilde{\omega}_r \xi_r \Delta F_i^{+}(h_0, \xi_r)}{\sum_{r=1}^{N} \tilde{\omega}_r \xi_r}, \\
&\Delta F_i^{+}(h_j, \xi_r) = \Delta F_i^{+}(h_{j-1}, \xi_r)\,\Omega_i(h_{j-1}, h_j, \xi_r) - \\
&\quad - \int_{h_{j-1}}^{h_j} \Omega_i(h', h_j, \xi_r)\,dB_i(h') \quad (j = 1, 2, \ldots, N).
\end{aligned}\right\} \tag{V.67}$$

ORIGINAL PAGE IS
OF POOR QUALITY

$$\left.\begin{aligned}
&\Delta F_i^{-}(h_N, \xi_r) = (1 - \varepsilon_i)\frac{\sum_{r=1}^{N} \tilde{\omega}_r \xi_r \Delta F_i^{-}(h_N, \xi_r)}{\sum_{r=1}^{N} \tilde{\omega}_r \xi_r}, \\
&\Delta F_i^{-}(h_j, \xi_r) = \Delta F_i^{-}(h_{j+1}, \xi_r)\,\Omega_i(h_{j-1}, h_j, \xi_r) - \\
&\quad - \int_{h_{j-1}}^{h_j} \Omega_i(h', h_j, \xi_r)\,dB_i(h') \quad (j = N-1, N-2, \ldots, 0).
\end{aligned}\right\} \tag{V.68}$$

In computing transmission functions for every j-th level h_j of the atmosphere within the altitude region being studied $h_0^- - h_0^+ = Z$, it is necessary to calculate the temperature-pressure dependence of the absorption coefficients: /292

$$\varkappa_j = \varkappa[P(h_j);\ T(h_j)] = \varkappa_{CO_2}(P_j;\ T_j)\frac{P_{CO_2}}{P} + \varkappa_{H_2O}(P_j;\ T_j)\frac{P_{H_2O}}{P}.$$

Here expression (V.44) determines the coefficient κ_{H_2O}; while for the coefficient κ_{CO_2}, relations (V.45)-(V.47), which calculate induced absorption at $\lambda \approx 7.5$ μm and the absorption beyond the edges of bands 4.3 and 2.7 μm should also be taken into consideration, so that

$$\varkappa_{CO_2}(P_j;\ T_j) = \frac{273}{T_j}P\left[\varkappa_{7.5}(295)\frac{295}{T_j}P + \frac{295}{273}\varkappa(295)\frac{\varkappa_{max}(P_j;\ T_j)}{\varkappa_{max}(1;\ 295)}\frac{273}{T_j}P\right] \qquad (V.69)$$

ORIGINAL PAGE IS
OF POOR QUALITY

If it is assumed that inside each cloud layer the temperature and the natural logarithm of the absorption coefficient of the atmospheric gas vary linearly with altitude, then the transmission functions that enter into (V.67) and (V.68) will be expressed in the final form:

$$\Omega(h', h_{j-1}, \xi_r) = \exp\left\{-\left|\int_{h'}^{h_{j-1}} \frac{\varkappa(h'')}{\xi_r}dh''\right|\right\} \cdot \exp\left\{-\left|\frac{\varkappa_{j-1} - \varkappa}{\ln\frac{\varkappa}{\varkappa_{j-1}}}\frac{h_{j-1} - h'}{\xi_r}\right|\right\} \cdot \exp(-\tau),$$

where τ is the optical thickness of layer $\zeta(\ell)$ between levels h_{j-1} and h_j in direction ℓ, the cosine of whose zenith angle is equal to ξ_r^j. Then, for h' that vary within [illegible] we will have

$$\Omega(h', h_{j-1}, \xi_r) = \exp\left\{-\left|\int_{h'}^{h_{j-1}} \frac{\varkappa(h'')}{\xi_r}dh''\right|\right\} = \exp(-\tau\alpha). \qquad (V.70)$$

where /293

$$a = a(T') \qquad \frac{1 - \left(\frac{\nu_{j-1}}{\nu}\right)^{\cdot}}{1 - \left(\frac{\nu_{j-1}}{\nu_j}\right)^{\cdot}}$$

$$T' = T(h'); \quad 0 < a < 1, \quad b = \frac{T - T}{}$$

ORIGINAL PAGE IS
OF POOR QUALITY

If conditions within the layer are homogeneous and thus $\kappa_{j-1} = \kappa_j = \kappa$, the expressions for τ and α will pass to the limit:

$$\tau = \nu \left(\frac{h_{j-1} - h'}{} \right) \qquad (V.71)$$

$$a = \frac{T - T'}{T - T_{j-1}} \qquad \frac{}{}$$

The integrals that enter into (V.67) and (V.68) will then assume the form:

$$\int_{h_{j-1}}^{h_j} \Omega(h', h_j, \xi) \, dB = \int_{}^{} \exp\left[- \tau \, \frac{}{} \right] (T - T'). \qquad (V.72)$$

Calculated profiles of heat fluxes. In order to obtain radiative flux profiles as a function of altitude as according to (V.61), it is necessary to integrate the systems of equations (V.67)-(V.68) with (V.69)-(V.72) taken into account. The results given in [104, 169, 566a] were obtained by integrating with the Simpson method with an automatic choice of step according to a specified relative accuracy (1%) on a Series-6 computer. It was shown that greater accuracy does not make the distribution of total fluxes substantially more precise.

As was expected, the basic part of radiative heat transfer is concentrated in the wave number interval from 100 to 8300 cm^{-1}. The one-way energy flux of the emission of an absolutely black surface at temperature $T_s = 750°K$ has a value of about $1 \cdot 8 \cdot 10^4$ w/m^2 (about the same as the energy flux of the substance $U = 5/2(nkT \cdot \bar{v})$ at $\bar{v} \approx 10$ cm/sec); more than 99.9% of the total flux belongs to this /294 spectral region. In the region 100-6000 cm^{-1}, 99.6% of the energy is emitted by the surface. Therefore, the calculations of the fluxes of heat radiation are carried out with a step of 25 cm^{-1} for the spectral region up to 6000 cm^{-1} (the original CO_2 absorption coefficients calculated for intervals of 10 cm^{-1} were averaged). In the region 6000-8300 cm^{-1} the radiative fluxes for various atmospheric compositions were no more than 2% of that in the region up to 6000 cm^{-1}. Because there were no data on absorption coefficients beyond

ORIGINAL PAGE IS
OF POOR QUALITY

the edges of the 1.4 μm and 1.2 μm bands, it may be assumed that the fraction of heat radiation carried over into the shortwave region 6000-8300 cm^{-1} will still be smaller.

The altitude distribution of the integral (with respect to the spectrum) one-way fluxes for various atmospheric compositions is shown in Fig. 101. As we see, these functions are close to the distribution of a one-way flux of equilibrium radiation reflecting the temperature profile in the atmosphere, and they differ little for various values of humidity. This points to a high optical density of the atmosphere. The total flux of radiation, which is the difference between large-size one-way fluxes, is relatively isotropic and is made up of the fluxes carried over in individual "windows" of transparency. The absorption in these windows is determined by the function $\kappa_{CO_2}(\nu)$ shown in Fig. 98, and it depends as well on H_2O vapor content.

For a pure carbon dioxide atmosphere, the transfer of radiation in the wave number ranges 550-800 cm^{-1}, 1900-2400 cm^{-1}, 3500-4000 cm^{-1} and 4700-5500 cm^{-1} throughout the altitude region under study is negligible. Fig. 102 shows calculations of the altitude distribution of radiative heat fluxes in the remaining intervals of $\Delta\nu$, where the atmosphere is quite transparent. As we see, the contribution of these "windows" is quite variable and depends on altitude. Because of the very large optical density of the atmosphere, radiant energy from the surface and the lower-lying layers contributes little to the flux of heat radiation. The reduction in the screening capacity of the atmosphere, which results in an increase in heat fluxes with altitude and a large anisotropy of the field of radiation, is explained by a reduction in the mass of the absorbing gas and by the dependence of κ_{CO_2} on temperature and pressure. /295

The total flux at the planetary surface S_s is less than 40 w/m^2, and the intervals 100-550 and 800-1400 cm^{-1} make practically no contribution to this value. The remaining intervals contribute no more than 10-15 w/m^2 each. Above 30-40 km the total flux reaches about 700 w/m^2. The "windows" at 1400-1900 cm^{-1}, 2400-3500 cm^{-1}, 100-550 cm^{-1} and 1100-1400 cm^{-1} (listed by the size of contribution) play a definite role here. The first "window", where the maximum of the Planck curve falls (1470 cm^{-1} at T = 750°K), contributes more than 300 w/m^2 and the rest about 200, 120, and 75 w/m^2. /296

The presence of even a relatively small quantity of water vapor in the atmosphere substantially changes the CO_2 absorption spectrum, primarily in the most important "windows" at 1400-1900, 2400-3500, and 100-550 cm^{-1}. Fig. 103 gives an altitude distribution of fluxes of heat radiation in the same spectral intervals as in Fig. 102; this is for a CO_2 atmosphere at a content of $f_{H_2O} = 0.001\%$. Fig. 104 shows the results of similar calculations at $f_{H_2O} = 0.01\%$ (a) and $f_{H_2O} = 0.1\%$ (b). As we see, even at a water vapor content of 0.0001% by volume, the maximum radiative flux in the interval 1400-1900 cm^{-1}

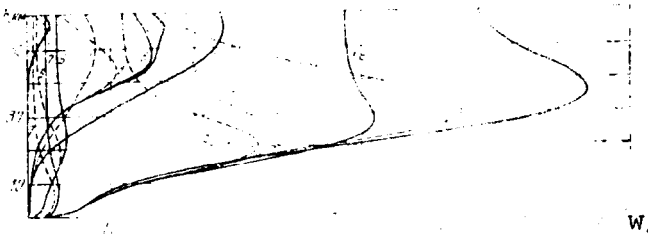

w/m2

ORIGINAL PAGE IS
OF POOR QUALITY

Fig. 102. The successive contribution of individual parts of the spectrum ($\Delta\nu$) to the total flux of heat radiation vs altitude at 100% CO_2, $\varepsilon_s = 1$. Curves 1-7 correspond to the following intervals (in cm^{-1}): 1-100-550; 2-800-1100; 3-110-1400; 4-1400-1900; 5-2400-3500; 6-4000-4700; 7-5500-6000. The solid curves are at $\varepsilon_c = 1$; the broken curves are at $\varepsilon_c = 0.3$, and the dotted curve is at $\varepsilon_c = 0.5$ [566a].

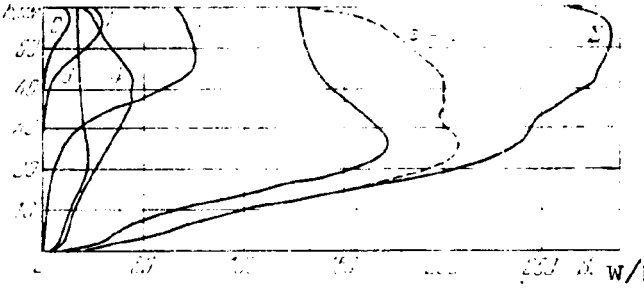

w/m^2

Fig. 103. The successive contribution of individual parts of the spectrum to total flux of heat radiation vs altitude at 97% CO_2 + + 0.001% H_2O. The intervals $\Delta\nu$ 1-6 are designated as in Fig. 102; Σ is the total flux; and the broken curve is total flux at $\varepsilon_c = 0.5$ [556a].

decreases to about 50 w/m^2, while at f_{H_2O} = 0.01% it is less than 5 w/m^2. In the interval 2400-3500 cm^{-1}, this decrease is to 175 w/m^2 (f_{H_2O} = 0.001% and to 70 w/m^2 (f_{H_2O} = 0.01%) respectively. In the longwave portion of the infrared region the H_2O absorption spectrum essentially complements the CO_2 absorption spectrum, and at f_{H_2O} = 0.001% the maximum flux in the interval 100-550 w/m^2 decreases by about four times. In the 800-1100 cm^{-1} interval, water vapor content in the atmosphere up to f_{H_2O} = 0.1% has no appreciable effect on altitude distribution and the size of the heat flux. Transfer in the interval 550-6000 cm^{-1} also changes very little. The total heat flux at the surface is from 20 w/m^2 (at f_{H_2O} = 0.0001%) to 5 w/m^2 (at f_{H_2O} = 0.1%) and is made up of the energy fluxes (in order of size of contribution) within the intervals 2400-3500 cm^{-1}, 4000-4700 cm^{-1}, 5500-6000 cm^{-1}, 1400-1900 cm^{-1}.

It is interesting that in the hot, dense Venusian atmosphere a change of 15-20% in the gas temperature at the surface has comparatively little impact on the value of the radiative heat flux[15].

[15] F. S. Zavelevich has called attehtion to this phenomenon.

ORIGINAL PAGE IS
OF POOR QUALITY

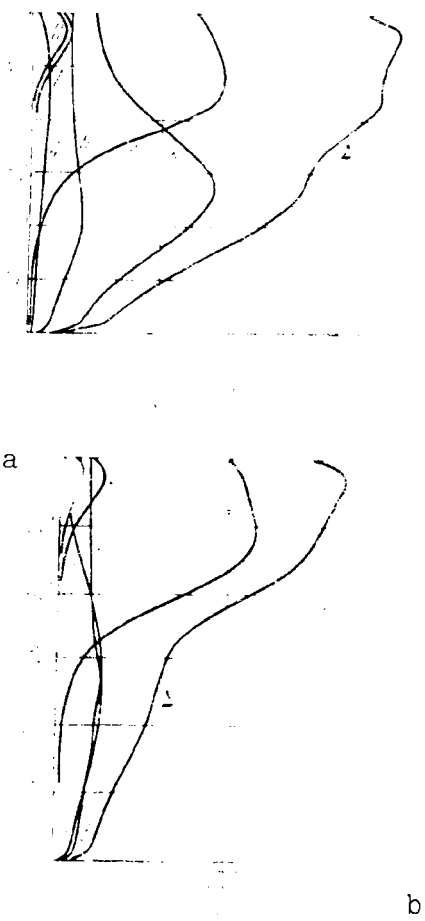

Fig. 104. The successive contribution of individual parts of the spectrum to the total flux of heat radiation vs h at 97% CO_2 + + 0.01% H_2O (a) and at 97% CO_2 + 0.1% H_2O (b) [556a]. Designations the same as in Fig. 103.

Key: a. km
b. w/m^2

At first glance, this seems strange, since the radiative heat conductivity that determines the conditions of transfer is proportional to the cube of the temperature. But in fact, the coefficient of radiative heat conductivity in the lower atmosphere of Venus reaches very high values. With radiative fluxes corresponding to calculations $S = \lambda \partial T/\partial h \approx 200$ w/m^2 and with a characteristic temperature drop from the surface to the boundary of the emitting region $\Delta T \approx 500°K$, the value of /298

$$\lambda_{rad} = \frac{16\sigma T^3}{3}\left(\int_0^\infty \frac{1}{\varkappa_\nu} G'(u)du\right)^{-1}, \text{ where } G'(u)$$

is the Rosseland weight factor and $u = h\nu/kT$) is $\lambda^0_{rad} \approx 5 \cdot 10^3$ cal$\cdot$cm^{-1} sec^{-1}deg^{-1}, which is about 10^8 times larger than the coefficient of molecular heat conductivity in gas under the same conditions. As calculations show (given in Fig. 105), however, it is the temperature gradient, and not the temperature, that basically influences heat flux in the deep Venusian atmosphere. Clearly, the factor G'(u) has the opposite influence on temperature, and, as a result, λ_{rad} does not vary greatly in the specified temperature interval. /299

Let us now compare calculations of total heat fluxes for various models of atmospheric composition with estimates of the effective heat flux reaching the planet from the Sun. Fig. 106 presents corresponding profiles S(h) for a pure carbon dioxide atmosphere and at water vapor contents of 0.001%, 0.005%, 0.01%, and 0.1%. Values of effective temperature calculated from Sections (V.7) or (IV.1) are plotted on the upper horizontal axis. At A = 0.77 ± 0.07, the effective flux of radiation from the Sun is $q^0_\odot = 154 \pm 46$ w/m^2, a value to which $T_e = 228 \pm 17°K$ corresponds.

An examination of the profiles of radiative heat fluxes leads to the conclusion that in a pure carbon dioxide atmosphere, the flux at the cloud tops is more than 3.5 times larger than the limiting value of absorbed solar energy. Beginning with h ≳ 10 km,

ORIGINAL PAGE IS
OF POOR QUALITY

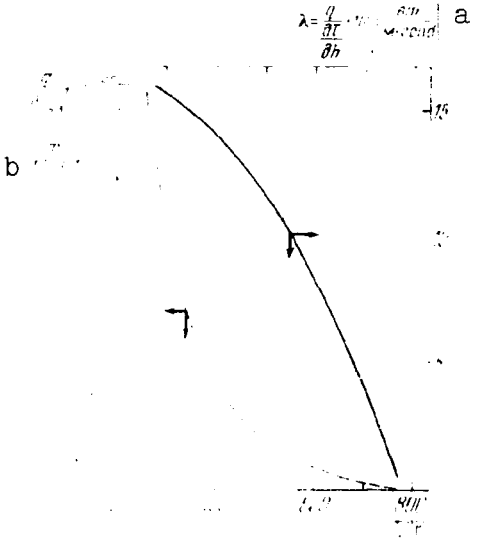

Fig. 105. Variation in the coefficient of heat conductivity in the Venusian atmosphere for the calculated heat flux S(h) (solid curve). The dashed line is the same variation normalized to take account of the temperature dependence $\lambda(T)$ in approximation of radiative heat conductivity. The value of $S_\Sigma(h)$ is given according to Fig. 103.

Key: a. $w/m \cdot deg_4$
b. $w/m \cdot deg^4$

$S(h) > q_e^0$. However, the condition of balance is secured at a content of $f_{H_2O} \approx 0.005\%$, so that the effective heat flux throughout the entire thickness of the study layer does not exceed the Sun's at Venus. /300

Fig. 102 and 103 show the calculations at $\varepsilon_s = \varepsilon_c = 1$, and the dashed lines therein also show calculations of S(h) in individual "windows" for clouds that reflect radiation in the infrared region of the spectrum. Since the emission of a blackbody at the temperature of the clouds is not large, the effective heat flux at the level of the clouds decreases in these cases proportionally to decrease in their blackness ε_c. The internal values of the fluxes are also reduced; however, their maximum values decrease by 15-25% at $\varepsilon_c = 0.5 - 0.3$.

If we make the analogy with the Earth's clouds, then according to Feygel'son [161-163], in an examination of the fluxes of radiation into the hemisphere, the difference between the emission of dense, opaque clouds of water droplets and absolutely black emission in the spectral interval 4-40 μm is not more than 5-10%, with the exception of the window at 8-12 μm, where the difference can reach 15-25%. About a third of solar radiation in the infrared region passes through the Earth's clouds, and if it is considered that, judging by everything, Venus clouds are as dense or slightly denser (cf. Section V.3) than the Earth's clouds, then nearly all the thermal portion of the Sun's spectrum should be contained in the clouds or in the atmosphere directly below the clouds.

Several works have estimated the influence of the altitude of the clouds on radiative fluxes in the Venusian atmosphere. Avduyevskiy et al. [6] have demonstrated that S decreases slightly as h_0 is lowered (and accordingly, as T grows) and that this is especially marked at $\varepsilon_c < 1$. The calculations of Strelkov and Kukharskaya [152], which do not include reflection, also confirm that the clouds contribute little to the distribution of longwave

ORIGINAL PAGE IS
OF POOR QUALITY

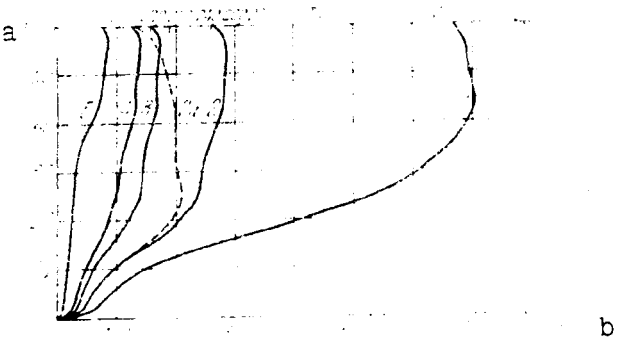

Fig. 106. Total fluxes of heat radiation vs altitude. The solid curves: $\varepsilon_s = \varepsilon_c = 1$; 1-100% CO_2, 2- 97% CO_2 + 0.001% H_2O; 3- 97% CO_2 + 0.005% H_2O; 4- 97% CO_2 + 0.01% H_2O; 5- 97% CO_2 + 0.1% H_2O. The broken line 2a- $\varepsilon_s = 1$, $\varepsilon_c = 0.5$; 97% CO_2 + 0.001% H_2O [566a].

Key: a. km
b. w/m^2

radiation. Pollack [463] has pointed to the increase in the total flux of heat radiation as the temperature and pressure at the level of the clouds decrease. It may be assumed that for low-lying clouds (at $T \gtrsim 300°K$) the downward flux from the clouds exceeds the flux of solar infrared radiation. On the other hand, when the clouds are high, the radiation from the Sun is greater than that of the clouds.

The model under examination /301 has not taken into account the probable lower position of the clouds (a probability, as we have seen, indicated by measurements of illumination). Lowering the level h_0 to an altitude on the order of 30-35 km can have a definite effect on the internal structure of the heat fluxes. At the same time, this will hardly change our basic conclusions, since in the Venusian atmosphere, in contrast to the Earth's atmosphere, it is clearly the opacity of the gaseous medium, not the clouds, that plays the deciding role in the "greenhouse" effect.

An examination of the data given in Fig. 106 shows that in the case of infrared-reflecting clouds, the total heat flux at their level can correspond to the effective flux from the Sun even in a pure CO_2 atmosphere or with an H_2O admixture of 10^{-5}, even though a significant degree of reflection is needed for this. However, the maximum fluxes are reduced only insignificantly in comparison to a model with non-reflecting clouds, and, as the measurements of illumination show, a balance at depth cannot be assured. Assuming that $q_\odot^+ \sim 0$ in (V.4), then in all cases examined an agreement between values of S_s and $\bar{W}_{\Sigma\varphi}$ on the surface is relatively easy to reach; as for the altitude profiles $S(h)$ and $\bar{W}_{\Sigma\varphi}(h)$, the best agreement is reached for a model with $f_{H_2O} = 0.1\%$. With a lower H_2O content, appreciable differences remain (cf. Fig. 92).

These comparisons are conditional, of course, since the Venera-8 experiment measured one-way flux, not the true amount of absorbed solar energy. Opacity needs to be characterized more accurately primarily in those spectral regions where, except for H_2O vapor,

contributions are made by the edges of CO_2 bands, hot transitions of CO_2 bands, and induced absorption in band 7.5 μm. We also need to know that errors result from calculating transmission functions in the weak line approximation through the range of variation in T and P with altitude. Therefore, our conclusions about radiative heat exchange are only as accurate as the transmission functions and heat transfer models used.

V.5. Convective Heat Exchange /302

Basic relations. The previous section demonstrated that radiative heat flux from the surface decreases as altitude decreases, a fact that is related to the attenuation of penetrating solar radiation due to an increasing optical thickness of the atmosphere. Unfortunately, the remaining uncertainty about radiative heat exchange does not allow us at this stage to make a reliable determination of the energy balance in the lower atmosphere and on the surface of Venus. At the same time, since the measured temperature profile is close to the adiabatic, it can be assumed that thermal equilibrium in relation to the profile of penetrating radiation is reached due to additional heat transfer from the lower heated layers of the atmosphere; this compensates for the reduction in radiative heat flux (cf. Fig. 78d, 78e). Free convection can provide such a mechanism. The relation between the flux of attenuated solar radiation at the surface and the total heat flux should in this case be very important for the intensity of convective transfer in the lower atmosphere of Venus.

Another probable cause of added, vertical exchange of energy and equalization of temperature irregularities in the horizontal direction is forced convection, which is related to advective heat transfer in large-scale circulation (cf. equation (V.8)). A certain contribution in this regard can also be made by heat transfer and turbulence-caused motion. On Earth, the average annual heat loss by the surface due to turbulent transfer is about 5%. It is difficult to estimate the effectiveness of turbulent heat exchange between the surface and the atmosphere on Venus, but it should be less than the power of the solar radiation penetrating to the surface.

As already noted (Section V.2), the problem of radiative-convective heat exchange including circulation in the atmosphere, i.e., the interaction between convective elements and motion on a synoptic scale is extremely complex, even for a two-dimensional /303
model; single-precision, numerical computations using available computers are not enough to examine global and local effects. In order to understand the dynamic regime of the Venusian atmosphere, it is of great interest in itself to use the calculations of radiative heat fluxes to examine the mechanism of local heat convection.

The driving force of free convective motions in the gravitational field should be the difference between the temperatures at the boundaries of the studied region of an atmosphere with an unstable stratification. A significant depth of the convective zone and a substantial difference between the temperature profile corresponding to radiative equilibrium and the adiabatic are the basic features of atmospheric convection. In order to calculate these features, it is necessary to examine theoretical models of convective motions in a compressible gas. The works of Polezhayev [127-129] have contributed greatly to the development of such models.

A system of two-dimensional, non-stationary equations (fluid mechanics; the Navier-Stokes equations) that determine motion and heat transfer in a compressible, viscous, heat-conducting, single-component gas in the field of external forces, will have the form (cf. for example, [90]):

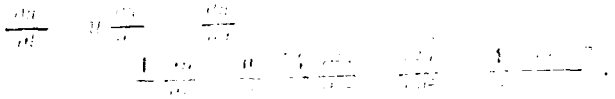

(V.73)

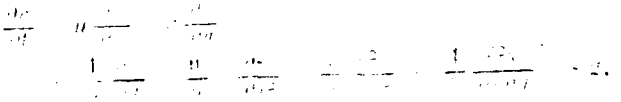

(V.74)

ORIGINAL PAGE IS
OF POOR QUALITY

(V.75)

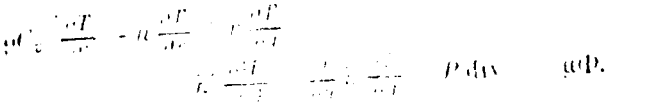

(V.76)

where

/304

is the dissipation function, u and v are the projections of the velocity vector on axes X and Y. In order to close this system, it is necessary to add the equation of state of a perfect gas

$$P = \rho RT \tag{V.77}$$

and the temperature dependences of the coefficients of heat conductivity and viscosity

$$\lambda = \lambda(T); \quad \mu = \mu(T). \tag{V.78}$$

Equations (V.73)-(V.76) are given in dimensionless form as:

(V.79)

ORIGINAL PAGE IS
OF POOR QUALITY

(V.80)

(V.81)

(V.82)

The scalar dimensionless values that enter into the equations are

where a_1 is the speed of sound, which is chosen as a velocity scale /305 (the subscript"1" refers to conditions at the upper boundary). Heat conductivity in a horizontal direction is assumed to be $\lambda' = \text{const}$.

These values and corresponding boundary conditions can yield dimensionless numbers that determine the current and heat transfer convection in a compressible gas:

Ra = GrPr is the Rayleigh number;

Pr = $\mu C_p/\lambda$ is Prandtl's number;

Gr = $C_R C_F \bar{q}_s \frac{\rho L^2}{\lambda^2 T_1}$ is Grashof's number which refers to a supplied heat flux q_s, where $\bar{q}_s = q_s L/\lambda T_1$ is the dimensionless heat flux (Nusselt number), L is the characteristic size of the convective region, and $\nu = \mu\rho^{-1}$ is the coefficient of kinematic viscosity:

K = $g\lambda/C_p q_s$ is the relation of the adiabatic temperature gradient $\gamma_a = -(\partial T/\partial h)_{ad} = g/C_p$ [16] to a given $\gamma = \partial T/\partial h$ or to a radiative $\gamma_{rad} = qs/\lambda$ [17];

---

[16] For the sake of simplicity, here and hereinafter, we will disregard the temperature-pressure dependence of gas enthalpy in the expression for the adiabatic temperature gradient.

[17] In the case where temperature T_2 (i.e., a fixed temperature difference difference T_2-T_1) rather than heat flux q_s is assigned at the lower boundary, Grashof's number and K are determined more conveniently as follows:

or

ORIGINAL PAGE IS
OF POOR QUALITY

The number K is one of the fundamental numbers influencing the /306
intensity of heat convection, which in turn determines the driving force of convective motions in the gravitational field. The numbers κ and Pr define the physical properties of gas. The number C_F is the ratio of free fall velocity from altitude h = L to the speed of sound. It determines the altitude distribution of density and pressure. At the characteristic dimension L ~ H, $C_F \sim 1$. Values of such an order of magnitude can be modelled in numerical calculations. The Rayleigh number Ra is the fundamental dimensionless number, which determines the effect of viscosity during convective motion in the field of external forces. Convective motion in a gas heated from below arises after the mechanical equilibrium determined by the hydrostatic equilibrium equation becomes unstable. In a stratified layer of viscous gas (without taking compressibility into account, $C_F \ll 1$), $Ra < Ra_{cr}$ is the condition of the stability of such equilibrium, where Ra_{cr} is the critical Rayleigh number. In natural convection in a viscous gas heated from below, cellular currents arise in this case at $Ra_{cr} \approx 10^3 - 10^4$. The Jeffreys condition is more general; this condition calculates the value of K and characterizes stability with reference to the number $Ra = \tilde{R}a(1 - K)$.

The system of dimensionless numbers of which C_F is a part is more general than that which follows from Boussinesq equations, which are usually used for convection in a comparatively thin atmospheric layer at the surface. As is well-known, the latter presume that density disturbances do not depend on pressure disturbances and depend linearly on temperature disturbances; changes in density are taken into account only in lifting power. Therefore, calculations of convective transfer in this approximation can be done only when the cell in question (and the fall in ρ) is small. For the conditions with which we are concerned, and with a characteristic cell size on the order of H, the use of Boussinesq equations (C_F not considered) would lead to substantial errors.

In a gas whose density depends on both temperature and pressure, the conditions in which convection arises are more complex. If we consider only the compressibility of the gas, and not its heat conductivity and viscosity, the stability condition is written /307
as in (V.11). As applied to the aforementioned system of dimensionless numbers, this condition can also be presented in the form

$$\eta \cdot (\varkappa - 1) C_p \min K \frac{\varkappa - 1}{\varkappa} \geq 1. \qquad \text{(V.83)}$$

According to Polezhayev's calculations [128], in a compressible, viscous, and heat-conducting gas, the line corresponding to loss of equilibrium and the onset of convection is defined in the plane of the numbers Ra, K or Cr_L, and C_F (at fixed remaining dimensionless numbers). The intensity of convective motions in the atmosphere depend in this case on the distance between a point with coordinates Ra and K, a point that characterizes concrete conditions, and the boundary of stability, which is shown as a curve including the

critical values of Ra^* and K^* ; the intensity is the function

$$\frac{1}{\sqrt{Ra}} f_1(Ra, A, C_R, Pr, z) \qquad (V.84)$$

The intensity of convective motions as obtained in calculations may also be presented in another form, in Re number:

$$f_2(Ra, A, C_R, Pr, z) \qquad (V.85)$$

where $f_2 = f_1 C_R$.

ORIGINAL PAGE IS
OF POOR QUALITY

Since H ≈ 17 km in the lower atmosphere of Venus, the values of Rayleigh number are on the order of $Ra \sim 10^{21} - 10^{22}$. With such large Ra numbers, convective motion is far beyond the threshold of statistical stability and is undoubtedly turbulent. Numerical modelling by Ra number in this range still meets with substantial difficulties. Furthermore, it is impossible to reproduce convective currents at corresponding conditions even in a laboratory experiment[18]. At the same time, however, numerical modelling of the remaining dimensionless numbers with reference to the conditons of the Venusian /308 lower atmosphere and with lower values of Ra number is still possible. In this case, it is possible to obtain several estimates for a model of free convection, assuming that the dependence of dimensionless velocity on the parameters K and C_F remains qualitatively similar.

The most interesting are two limiting cases modelling the development of convective motions in the atmosphere. The first is for relatively weak convective activity in a quiet atmosphere, where the actual temperature gradient is close to the adiabatic. The second case is for maximum intensity of convection arising under the condition that at a certain time in the atmosphere there was an initial temperature profile close to the profile of radiative equilibrium[19]. The convective flux arising in the presence of this profile leads an unstable static atmosphere into a state of convective equilibrium; this equilibrium state corresponds to the first limiting case.

The limiting estimates (obtained in [5, 188]) of such a transition hold true in conditions of high atmospheric transparency for solar radiation, when equality (V.7) or (V.14) is satisfied right down to the surface. This was the purpose of calculating the functions $T_{rad}(h)$ for an atmospheric model with radiative

[18] In order to obatin a large value of C_F, for example, it would be necessary to provide huge values of g freed from various side effects, in particular, from a large Coriolis component while using a centrifuge.

[19] Thus stated, the problem of convective development in an atmosphere originally in a state of hydrostatic and radiative equilibrium was formulated as early as 1913 by Emden (cf. [50]).

equilibrium (Fig. 78a) by integrating the equations of the type (V.58)-(V.60) at $S(h) = q_T^\circ$ (cf. (V.6)), $\varepsilon_s \simeq 1$ and $\varepsilon_c \simeq 0.3 - 0.5$.

The difficulty in solving this problem is that the transfer equation is written for spectral intensity, whereas the condition of radiative equilibrium is integrated with respect to the spectrum. Therefore the function $T_{rad}(h)$ was found by using a method of successive approximations. Because the distribution of gas parameters vary as temperature profiles also vary, the equations of state and hydrostatic equilibrium were also used. In setting the conditions at the upper boundary, a flux of downward radiation F_i^- was calculated, while the values of upward fluxes F_i^+, values necessary to the calculations, at the lower boundary were determined by choosing /309 a surface temperature that satisfied the condition:

ORIGINAL PAGE IS
OF POOR QUALITY

$$\varepsilon \sum B_i(h) \quad (1 \quad \varepsilon) \sum F_i^-(h) \quad q. \qquad \text{(V.86)}$$

Fig. 107. Altitude profiles of atmospheric temperature in conditions of radiative equilibrium:
1-the adiabat;
2-q = 140(ε_c = 0.3); 240 (ε_c = 0.5);
3-q = 125(ε_c = 0.3); 190(ε_c 0.5);
4-q = 105(ε_c = 0.3); 170(ε_c = 0.5) [5].

Fig. 107 shows the temperature distributions obtained for this model at various values of q. As we see, the condition of radiative equilibrium leads to a significant increase in the temperature of the gas near the surface, as well to an increase in temperature gradients with altitude. Particularly large gradients, those that greatly exceed the adiabatic, are reached at the surface. Because convective instability arises in this region, intense convective motions should arise in this region; the smaller K is, the larger these motions are. We will now examine the structure and intensity of currents in models of cellular and penetrating convection.

A model of cellular convection. When the upper boundary of the region under study is restricted, a model of regular (cellular) convection is relatively simple. Avduyevskiy et al. [2, 5, 188] use this approach to model convective activity in the Venusian atmosphere.

Let us assume that convective motion in an infinitely long horizontal layer of gas after loss of mechanical equilibrium is divided into a series of cells, each of whose horizontal dimension

ORIGINAL PAGE IS
OF POOR QUALITY

is close to the depth of the convective zone, i.e., the convection is periodic with a half-period L.[20] Estimates of the intensity of convection can then be reduced to calculations for a single, closed convective cell, whose width is equal to its height H. Depending on the nature of the initial disturbences in the cells, either one-vortex or two-vortex motions can arise. Fig. 108 shows this schematically.

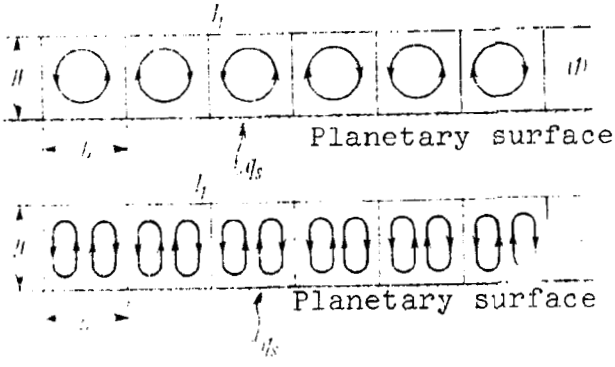

Fig. 108. The structure of the cellular convection in a horizontal layer (L = H):
1-single-vortex cells;
2-double-vortex cells.

Key: a. planetary surface

By taking into account the results of laboratory experiments and numerical experiments, it can be assumed that the lateral surfaces of each individual convective cell (with one or several vortexes) are symmetrical. It is assumed -- by virtue of the conditions of adhesion and non-flow -- that velocities on the upper and lower boundaries of the cell are zero and that the lateral surfaces are insulated from heat.

Thus,

ORIGINAL PAGE IS
OF POOR QUALITY

$$\frac{\partial u}{\partial x} \quad \frac{\partial p}{\partial x} \quad \frac{\partial v}{\partial x} \quad \frac{\partial T}{\partial x} \quad 0. \qquad u = v \quad 0. \qquad \text{(V.87)}$$

/311

It is further held that on the upper surface of the cell the temperature is fixed and equal to T_1 and that on the lower surface of the cell there is a constant heat flux $q_s = \lambda \partial T/\partial y$. The stationary solutions (to be discussed later) of the system (V.77)-(V.82) that correspond to the established character of the thermal regime of the atmosphere are found as a result of establishing the initial disturbances at given original values of velocities u(x, y,0), v(x, y,0) and gas parameters P(x,y,0), T(x,y,0), ρ(x,y,0) related by the equations of state and hydrostatic equilibrium.

---

[20] In a real atmosphere, the size of the cells in cellular convection is influenced by the vertical temperature gradient (especially, the radiative heat inflow and by the anisotropy of turbulent mixing, i.e., the ratio of the vertical and horizontal coefficients of turbulent viscosity. According to estimates made for the Earth's atmosphere, the length of the cells is proportional to $\psi 1/5$, while the time of transition from a laminar regime to a full-fledged convective regime is proportional to $\psi 2/5$, where $\psi = \frac{1}{\theta}\frac{\partial \theta}{\partial y}$ and θ is the potential temperature (cf. [174, 306]).

ORIGINAL PAGE IS
OF POOR QUALITY

There have been calculations of the dependence of the intensity of convection on parameter K for convective motion with one vortex (which is caused by asymmetrical initial disturbances and which has the smallest critical values Gr_L^* , K) and for convective motion with two vortexes (which is caused by symmetrical initial disturbances and which has higher critical values Cr_L^* , K^*) in one and the same region H/L = 1.

The numerical solution of the system of equations (V.77)-(V.82) with these initial and boundary conditions has been carried out by using an unclear difference approach with a spatial approximation of the second order of accuracy; this has been developed by Polezhayev with reference to convective motions of compressible gas at a specified temperature difference across the cell [127, 129][21]. The difference grid h' = 0.05, ℓ' = 0.05 was used (h' and ℓ' are the steps of the grid corresponding to the spatial variables x, y).

Fig. 109 shows the distribution along the horizontal at scale height H/2 of the vertical velocity in the cell for various K for single-vortex convective motion at $Ra = 10^6$.

It is clear from the results that the intensity of convection /312
increases significantly as the ratio of the adiabatic gradient to the given decreases. Fig. 110 shows the maximum amplitude of convective motion as a function of parameter K. The dashed curve 2 shows the corresponding dependence for a two-vortex cell. The maximum amplitude of convective motions in this case turns out to be less than for a single-vortex cell; curve 1 gives an estimate of convective intensity in a viscous gas, an estimate evidently close to the upper limit at specified parameters. For the sake of comparison, curve 3 estimates convective intensity as obtained by using Boussinesq equations without taking viscosity into account (when $Ra = \infty$) for a simplified model of convection [362]. Clearly, at Ra numbers of $10^{21} - 10^{22}$, which correspond to the assumed dimensions of the convective region, the intermediate case between curves 1 and 3 should occur. The required values of Ra can be reached due to corresponding values of viscosity at Re = const (cf. (V.85)).

There are data for the Earth's lower atmospheric layer (about /313
a kilometer) obtained from observations of convective cloudiness from artificial satellites and from high-altitude meteorological towers; these data indicate that cellular structures at $Ra \sim 10^{17} >> Ra_{cr}$ do in fact exist. The works of Ivanov et al. [557-559] explain the appearance of such quasi-cells, whose spatial dimensions are on the order of 1-10 km, by the close relation between large-scale structures and the change in turbulent parameters in a boundary layer with unstable stratification. The existence

---

[21] The general idea of variable directions is at the basis of this approach, which leads to tri-diagonal matrices.

ORIGINAL PAGE IS
OF POOR QUALITY

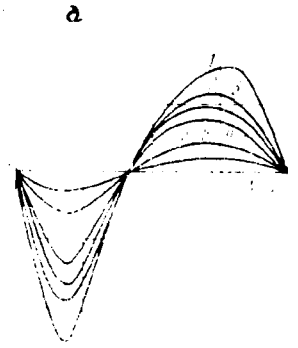

Fig. 109. Profiles of vertical flows vs K:
1-K = 0.0880;
2-K = 0.920;
3-K = 0.945;
4-K = 0.950;
5-K = 0.975;
6-K = 0.990 [188].

Key: a. m/sec

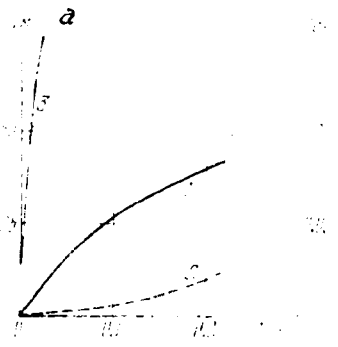

Fig. 110. Maximum velocities of vertical convective motions:
1-single-vortex cell;
2-two-vortex cell;
3-single vortex cell at $\nu = 0$ [188].

Key: a. m/sec

of an ordered structure in the boundary layer of the Earth's atmosphere with a well-developed convection is evidently related also to recorded low-frequency fluctuations of meteorological elements (with time scales on the order of 1000 seconds): these fluctuations contribute noticeably to the dispersion of temperature and the horizonal wind velocity component. This is confirmed by the statistically-based coincidence between the length of the disturbances and the scales of irregularities, which correspond to the spectra of the fluctuations. The replacement of the customary coefficients of viscosity and heat conductivity ν and λ by their turbulent analogues (characteristic of a turbulent medium) will decrease the Rayleigh number by at least 8-9 orders of magnitude. Turbulence thus leads to an increased effectiveness of the processes of exchange and thereby to a reduction in atmospheric stability. These stabilizing factors evidently play an unique feedback role [588, 562].

The results given in Fig. 110 thus allow one to make a qualitative estimate of convective intensity in the lower Venusian atmosphere at Rayleigh numbers close to actual numbers -- provided that convective intensity is fundamentally defined by the value of the parameter K. In the case of viscous gas for the study model at $Ra = 10^6$, large vertical velocities can correspond to comparatively small deviations from static equilibrium (the condition of which is K = 1 in a quiet atmosphere). For example, at K = 0.99 (which at $\gamma_a = 8.5$ deg/km corresponds to a deviation of 0.1 deg/km from the adiabatic gradient), the maximum intensity of convective motions of scale L /314 of the convective cell would reach 1.5 m/sec. If $Ra = \infty$ ($\nu = 0$), a much larger value of vertical velocity, one which corresponds to a value of K = 0.99, is obtained: about 40 m/sec. Since the actual deviations from the adiabatic gradient T in the Venusian atmosphere are apparently much smaller (K is closer to unity), the actual values of the velocity of convective transfer do not reach values within these bounds.

Although the actual range of Ra numbers was not modelled in this calculation, we can try to obtain reasonable qualitative results within the framework of this convective model, if we estimate the value of turbulent viscosity ν_T, passing thereby to the turbulent analogue of the Ra number. For this let us use one of the Richardson-Obukhov empirical relations [122] suggested to describe large-scale turbulent diffusion in the atmosphere:

$$\nu_T(L) \sim \varepsilon^{1/3} L^{4/3}, \tag{V.88}$$

where L is the characteristic size of the atmospheric process, $\varepsilon \approx \alpha q/M$ is the mean specific velocity by which kinetic energy dissipates into heat due to friction. Here $q \sim q_0$ is determined according to (V.7), M is the mass per unit column of atmosphere, and α is a coefficient approximately equal to $\sim 2 \cdot 10^{-2}$ for Earth [46].

If (V.85) is kept in mind, calculations of convective intensity using the system of equations (V.77)-(V.82) can also be represented in dimensionless form [188]

$$\frac{\nu_T L}{\nu}(K) = \frac{\nu_T}{\nu_1}(K) \mathrm{Ra} = 1.41 \cdot 10^3 \frac{\nu_T}{a_1}(K), \tag{V.89}$$

from which we have

$$\frac{\nu_T}{\nu} = \frac{\mathrm{Ra}}{(\nu L)^2} f(K). \tag{V.90}$$

ORIGINAL PAGE IS OF POOR QUALITY

The values of the function $f(K) = 1.41 \cdot 10^3 \nu/a_1(K)$ are determined from calculations using values of molecular viscosity (cf. Fig. 110). According to Brandt's estimates [18], the value of ε for the Earth's troposphere is approximately equal to 5 cm^2/sec^3. This value for this convective layer of Venus (calculating that M is about 10^2 times larger) is accordingly on the order of 1 cm^2/sec^3. Then, at $L \sim 10^4$ m, we obtain /315

$$v \simeq 0.35 f(K)\ m/sec \tag{V.91}$$

Hence, at K = 0.99, we will have v ≈ 1 m/sec.

Let us now estimate the actual value of K and thereby the intensity of convective motions that can actually take place in the lower atmosphere of Venus. Unfortunately, available onboard instruments are unable to measure the extremely small difference between the actual and the adiabatic temperatures $\Delta T = T - T_{ad}$, a difference that determines the value of K. It is possible, however, to obtain an estimate of the order of magnitude of ΔT by beginning with the approximate expression for convective heat flux Δq_c according to (V.10) and by using the calculations of radiative transfer according to the measured temperature profile. As a first approximation,

one can assume that according to order of magnitude, $q_c \sim S \leq 10^2$ w/m^2. Then, by substituting the expression for vertical velocity $v \simeq (2gH\Delta T/T)^{1/2}$ in (V.10), we obtain a formula to determine the mean temperature difference

$$(\Delta T) \simeq \frac{q_c}{\rho C_p \sqrt{2\frac{gH}{T}}}. \qquad \text{(V.92)}$$

ORIGINAL PAGE IS
OF POOR QUALITY

At mean values of atmospheric parameters with altitude of the convective cell ($H \simeq 1.5 \cdot 10^4$ m, $T \simeq 650°K$, $\rho \simeq 45$ kg/m^3, $C_p \simeq 0.24$ kcal/kg·deg), we obtain $\bar{T} \leq 2.5 \cdot 10^{-2}$ deg, whence $1 - K = \Delta T/T \leq 5 \cdot 10^{-5}$. In the range of values $1 - K = 0 - 10^{-2}$ one may approximately represent the function $v/a_1(K)$ (cf. Fig. 110) as the linear function.

$$\frac{v}{a_1}(K) \simeq 0.6(1 - K). \qquad \text{(V.93)}$$

from which: $v \leq 0.01$ m/sec follows. Let us note that the values of v determined according to (V.91) and (V.93) are in good agreement with estimates of the limiting value of vertical motions in the Venusian atmosphere obtained by analyzing the dynamics of the parachute descent of Veneras-4-8 (cf. Section IV.3).

A model of penetrative convection. In the model of cellular convection, the mixing of gas occurs in such a way that a temperature profile with a gradient close to the adiabatic is established in the nucleus of the convective cell. /316

In layers of gas near the lower and upper boundaries, however, the temperature gradient is larger than the adiabatic[22]. The surface temperature T_s is between the temperatures corresponding to the adiabatic and radiative profiles.

The intensity of motions decreases as altitude increases and becomes equal to zero at the upper boundary of the convective cell at height H = 17 km. This result clearly does not reflect the

---

[22] It is known (cf. for example, [50]) that on Earth if the length of the mixing is comparable to the distance from the surface to the bottom of the clouds, there is little effective mixing at the boundaries and that near the boundary of the surface and the clouds a superadiabatic gradient can arise. It should be remembered, however, that in this calculation the obtained character of T(y) is entirely determined by the boundary conditions, not the actual temperature variations with altitude, variations produced by convective instability in the real atmosphere.

actual situation in the Venusian tmosphere and is a consequence of the limitations imposed by the model itself, since it is quite likely that the greatest weakening of convective activity in the Venusian atmospere is marked by the boundary of the clouds. At this level, the condition $\partial q/\partial h \to 0$ is met, which generally agrees with calculations of the altitude distribution of radiative fluxes. One may maintain that heat and mass exchange outside the cell are related to the penetrating character of convective motions. This means that the convective cell's upper boundary, which separates the zones of stable and unstable stratification, is not fixed but shifts upward, up to a certain altitude $h^* > H$, and that, in a stationary regime, the temperature profile in the whole region tends toward the adiabatic[23].

Models of penetrative convection have recently received a great/317 deal of attention [265, 299, 436, 534]. Vlasyuk and Polezhayev have examined one such model with reference to the Venusian atmosphere [35, 130]; and their numerical experiments have produced estimates that develop our conceptions of the mesoprocesses of the atmosphere of this planet.

The difficulties stemming from the great depth of the atmosphere (and, consequently, from the significant variation in density within the studied region) are overcome in part by substituting P, ρ, and T for ln P, ln ρ, and ln T in the original system of equations (V.77)-(V.82). Starting with the conception that motions in a flatly-stratified, uniformly-heated, horizontal layer of gas are periodic, it is assumed that conditions on the lower boundary and lateral surfaces correspond to (V.87), while the upper boundary h^* is determined in this case by the conditions of asymptotic behavior:

ORIGINAL PAGE IS
OF POOR QUALITY

$$T = T_h^{0*}, \quad P = P_h^{0*} \qquad \text{(V.94)}$$

Here T_h^{0*} is the original temperature at level h^*, which depends on the altitude at which convection penetrates into the stable region and which is determined in the course of the calculations. In the system of dimensionless numbers (Gr^{h*}, K(h), C_F^{h*}, L/h, Pr, κ), as before, the parameter $K(h) = \frac{(\kappa - 1) C_F^{h*}}{(dT/dh)^n}$ characterizes stability; clearly, the condition K(h) = 1 corresponds to the boundary between stable (K > 1) and unstable (K < 1) zones.

---

[23] A penetrating convective regime is modelled in laboratory conditions: for example, convection in a layer of water heated from below and kept at zero temperature at the upper boundary. Here, an inversion forms inside the layer at 4°C; this inversion separates the zones of stable and unstable stratification.

Vlasyuk and Polezhayev have examined the structures and intensities of penetrative convection in several models distinguished by: the original depth of the unstable zone for the initial profile of radiative equilibrium, Rayleigh number, the law of variation in viscosity with altitude and vertical stratification of density determined by the parameter of hydrostatic compressibility C_F. Their calculations were done on a Series-6 computer. Of course, as was the case with the model of cellular convection, the results obtained with regard to Venus are rough estimates, since the actual range /318 of numbers Ra, C_F and K(h) is not modelled. At the same time, they revealed a number of interesting features of current and heat exchange in conditions much closer to the actual conditions in the planetary atmosphere.

ORIGINAL PAGE IS
OF POOR QUALITY

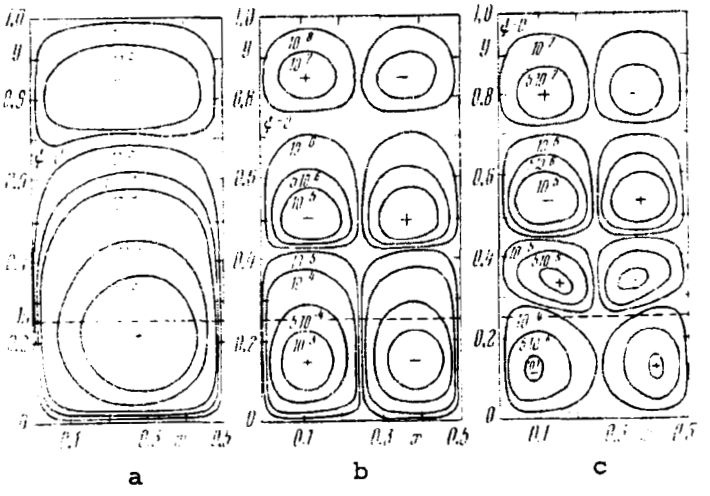

Fig. 111. Flow lines in conditions of penetrative convection for various Ra*: a-Ra* = 10^6; b-Ra* = 10^7; c-Ra* = 10^8; h_1-the boundary between regions of stable and unstable stratification; the pluses and minuses indicate the various directions of motions; velocities are given in units of the speed of sound a_1 [35].

Of these features, one should above all note the possibility that a multi-stage structure of currents can form, so that motions penetrating into the stable zone are blocked by "self-induced" secondary motions in the opposite direction. Fig. 111 shows examples of such structures based on calculating flow lines at Rayleigh numbers from 10^6 to 10^8, C_F = 3 and the original depth of the unstable zone $h_1 = 0.25h^*$. As we see, the weak secondary motions (about three orders of magnitude less than motions in the basic nucleus of the convective cell) are already developed at Ra = 10^6; /319 with further increases in Ra number, horizontal fractionation of the cells and an increase in the number of stages are observed. The horizontal scale of penetrative periodic motions beyond the threshold of stability becomes close to h_1.

ORIGINAL PAGE IS
OF POOR QUALITY

As Ra increases, the difference between the vertical temperature gradient and the adiabatic decreases. Surface cooling due to convective heat transfer increases simultaneously. This is easily seen from the calculations whose results are shown in Fig. 112 relative to the dimensionless temperature $\theta = \frac{T - T_1}{T_2 - T_1}$. The original model in this case differs from the previously-examined large depth of the unstable zone ($h_1 \approx 0.6h^*$), at an initial temperature profile in the lower layer of an atmosphere with a gradient exceeding that of radiative equilibrium. The boundary conditions here come close to the probable lower boundary of the clouds ($h \approx 30$ km), so that convective motions are blocked artificially above and so that the processes in the stable zone are not modelled. The successive change in the altitude profiles of atmospheric temperature (Fig. 112a) and surface temperature (Fig. 112b) corresponds to the establishment of stationary regimes at the indicated Ra values.

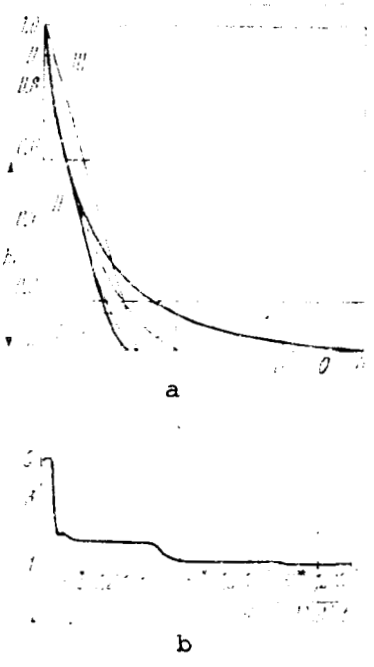

Fig. 112. Temperature change with altitude of the convective region (a) and surface temperature change (heat transfer) as Ra* changes (b): 1-tentative initial profile of radiative equilibrium; 2-adiabat; 3,4, and 5-successive temperature change at transition in Ra* number from 10^5 to 10^7; h_1-region of instability; dotted-dashed line-region with inverse density variation.

The intensity of convective motions in a model of penetrative convection can be approximated by an approximate dependence in a form corresponding to (V.85): /320

$$\frac{\varepsilon h_1}{\nu} = F(\mathrm{Ra}) = b(\mathrm{Ra}^*)^n. \qquad (V.95)$$

Fig. 113 gives this dependence in logarithmic coordinates. The upper and lower straight lines correspond to the previously-described models with $h_1 \approx 0.25h^*$ and $h_1 \approx 0.6h^*$. Correspondingly, in the first case $b = 0.152$ and $n = 0.52$; and in the second case $b = 0.155$ and $n = 0.54$. As was expected, the intensity of convective motions is appreciably higher in the model with the smaller initial values of K(h) in the unstable region of the atmosphere. This is clearly seen in the comparison of the functions (V.95) in Fig. 113.

As with a model of cellular convection of limited depth, in order to estimate the range in which the actual values of ν lie, one may substitute turbulent viscosity for molecular viscosity and assume $\nu_T = \text{const}$. By using equations (V.89) and (V.90) and estimates of

ORIGINAL PAGE IS
OF POOR QUALITY

the actual value of parameter K, it is not difficult to convince oneself that velocities in the nucleus of the convective region in the lower layer of the atmosphere are approximately within the same limits as in a cellular model and that they quickly weaken with altitude. It is also noteworthy that in a model of penetrative convection with ν = constant, there is less asymmetry observed in the rising and falling flows than is the case for a model with $\nu \neq$ const: and that the depth of the adiabatic zone increases at the same Ra (i.e., the ratio h^*/h_1).

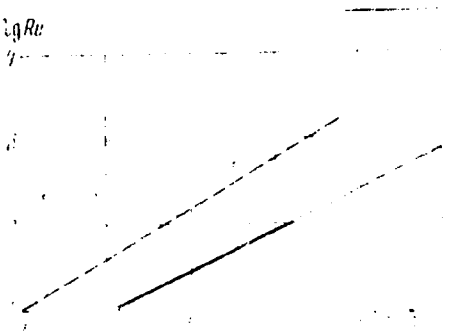

Fig. 113. Change in the maximum intensity of vertical convective motions vs Rayleigh number $Re = f(Ra^*)^n$.
1-a model with motion artificially cut off at h ≈ 30 km;
2-a model with penetrative motions in the entire region at reduced relative depth of the atmosphere h_1/h^* [35].

These features of convection (as accurate as the models used) can have a number of important consequences concerning both the intensity of heat exchange and the structure of the clouds. Well-developed convection in the Earth's atmosphere is accompanied by the formation of dense clouds; it plays an especially important role in the formation of cumulus clouds. Their structure, including the possibility of breaks in the clouds, depends on the relation between the horizontal and vertical heat fluxes, on the presence of a vertical wind shear, on the nature of the underlying surface, and on the flux of the mass in the lower layers and at the condensation level (of cloud streams). On Venus, where the temperature field at the surface and in the /321
lower atmosphere is much more homogeneous, it is not likely that there are such breaks; however, they cannot be ruled out entirely. Since the clouds essentially scatter solar radiation, and since the intensity of atmospheric motions depends directly on the inflow of energy into the atmosphere, the interaction of these processes is of exceptional interest. Let us note that in itself the possibility of breaks in the clouds could have great practical significance from the standpoint of relatively close-range observations of Venus (for example, from the orbit of an artificial satellite).

Further improvement of convective models, especially in models of penetrative convection; the overcoming of computational difficulties related to calculations of deep regions at high values of the compressibility parameter and Ra number; a more precise description

of radiative heat exchange -- all these will allow us to understand better the local structures of meteorological elements, the physical structure and mechanism of cloud formation, and the features of the thermal regime of the Venus atmosphere.

CHAPTER VI. THE UPPER ATMOSPHERE /322

VI.1. Fundamental Definitions

In this chapter we will examine those regions in the Venusian atmosphere above the mesopause: the thermosphere, where the temperature gradient is positive and the mean free path of particles λ is less than the scale height H; and the exosphere, where the temperature remains approximately constant, where $\lambda \geq H$, and where the dispersal of atoms and molecules into outer space may occur. By "the structure of the upper atmosphere," we mean the spatial distribution and temporal variations of its basic macroscopic characteristics -- temperature, pressure, density, and partial concentrations of neutral and ionized components.

It should be noted that the division of the atmosphere into "upper" and "lower" is in a certain sense tentative and that there is no strict terminological definition in this respect. In examining the Earth's atmosphere, we often limit our conception of the lower atmosphere to the region of the troposphere; at the same time, we designate those regions above the troposphere as the upper atmosphere (cf., for example [70]). This no doubt orginates in the notions that dissociation and ionization of atmospheric components play a specific role even in the stratosphere and mesosphere. It is necessary to give a more strict definition of the lower atmosphere: those altitude regions in the planet's gaseous shell in which the condition of local thermodynamic equilibrium (l.t.e.) holds and, consequently, in which the conception of temperature holds true for any finite volume. This means that the populations of rotational and vibrational levels of atmospheric molecules are subject to a Boltz- /323
mann distribution. Deviation from l.t.e. can be important above the level where the probability of spontaneous emission on a single molecule exceeds the rate of collision-caused excitation and is caused basically by the disequilibrium of incident radiation with relation to the kinetic parameters of the atmospheric gas. At these altitudes, the most important photochemical processes are particularly effective, and the "non-insulated" nature of the atmosphere appears in its fullest extent, as an open, rarefied gaseous system subjected to the impact of shortwave solar radiation.

As a starting point, let us estimate the relations of the probability of collisions with nearby molecules (or the time of vibrational relaxation η) and the probability of spontaneous deactivation of the lowest vibrational state of a CO_2 molecule (which corresponds to the fundamental band at $\lambda = 15$ μm with a radiational life-time of the vibrational state $\eta_r \approx 0.4$ sec); a level where the frequency of collisions providing impact deactivation does not exceed 10^5 sec^{-1} corresponds to this transition region. This approximately corresponds to a pressure $P \approx 5 \cdot 10^{-3}$ mbar for the atmospheres of Earth, Venus and Mars [351]. Since the solar energy absorbed above the transition

ORIGINAL PAGE IS
OF POOR QUALITY

level can be removed only by heat conductivity or massive downward transfer, the region of minimum temperature in the atmosphere, a region defined in the case of the Earth as the mesopause, should be located near this level.

It is necessary to keep in mind that attaining the condition $\eta/\eta_r \simeq 1$ does still not mean that deviation from l.t.e. has begun. Corresponding estimates are given in [235]. If ϕ and ϕ^* are the source functions in conditions of l.t.e. and in deviations from it, then the connection between the two is given by the relation

$$\Phi^* = \Phi\left[1 - \frac{\beta}{\gamma}\frac{\eta}{\eta_r}\sqrt{\frac{\gamma}{\beta}}\right]. \qquad \text{(VI.1)}$$

where $\Phi = \frac{B^{(1)}(T)}{B^{(1)}(T_c)} \cdot U^{(1)}$ is the Planck function in the center of the 15-micron band at temperatures of the upper level of the clouds T_c and the atmosphere T; β_0 is the parameter of line structure in the Curtis-Godson approximation

/324

$$\beta_0 = \frac{2\gamma_0 P(0)}{d}\frac{u}{u_0}; \quad u_i = \frac{2S_i}{2\gamma_0 P(0)}\int_0^\infty P\,dh;$$

$$P(h) = P(0)e^{-h/H}; \qquad u_0 = \frac{2S_i H P(0)}{2\gamma_0};$$

A_{0i} is the parameter of band width [289], S_i is the intensity of the i-th band, γ_0 is the mean width of the rotational line per unit pressure, and d is the mean interval between lines.

Estimates show that the value of $\sqrt{\frac{\gamma}{\beta}}$ in (VI.1) is on the order of $0(10^{-4})$ for Venus and Mars; hence, it follows that deviation from l.t.e. is insignificant at altitudes where collision-caused fading predominates over the Doppler spread of the spectral line. Questions of radiative heat exchange in these conditions are examined in detail in [258, 311].

Another important feature that distinguishes the lower atmosphere from the upper atmosphere is that the lower atmosphere is well mixed. This means that the relative concentrations of components not undergoing phase transitions remain the same at all levels, while photodissociation and photoionization can be disregarded -- thanks to the high efficiency of recombination processes. Vertical pressure distribution in this case determines altitude profiles of temperature and concentrations. If diffusion predominates over mixing and violates the constancy of relations among components, then such a possibility is ruled out. For the atmosphere, Dalton's law hold true, as before; however, each component is distributed in the gravitational field with scale height corresponding to its molecular (atomic) weight.

As far as composition is concerned, therefore, it is convenient to divide the planetary atmosphere into two regions: the homosphere and the heterosphere. In the homosphere, the processes of intense turbulent mixing play the deciding role, and the mean molecular weight remains practically constant. In the heterosphere, there is /325 a diffusion-gravitation separation of gases, and the mean molecular weight decreases with altitude. The transition region where complete mixing gives way to diffused separation of gases in the gravity field is located near the base of the thermosphere and is defined as the turbopause.

The estimate of pressure at the level of Venus's occultation of Regulus $P_R = (2.6 + 0.13) \cdot 10^6$ kg/cm^2 (cf. Section IV.6) is an order of magnitude closer to the value of pressure near the turbopause of the Earth's atmosphere. If one starts with the notion that on Venus the turbopause is about on the same level as on the Earth (10-20 km), then the characteristics of the upper atmosphere (to be discussed below) refer to the planet's heterosphere.

The distinguishing features of the upper atmosphere as a gaseous medium at the altitudes of the heterosphere are: its many components and the direct impact of radiation factors with simultaneous chemical transformations of various kinds in conjunction with the processes of heat and mass exchange. Under the impact of intensive solar electromagnetic radiation, the decisive factors in this region are the photochemical processes -- photoionization, photodissociation, the excitation of internal degrees of freedom of atoms and molecules (including electron levels), all accompanied by the reverse reactions of association of atoms into molecules, the recombination of ions, spontaneous emission of photons, and impact deactivization. The properties of gas are formed in the gravitational and magnetic fields: in the process, diffusion and heat transfer (basically, by heat conductivity and to a lesser degree, by emission) play an important role, depending on the effectiveness of transfer coefficients at various levels. The temperature, concentration, and pressure gradients that arise result in the development of macromotions, whose character remains turbulent near the bottom of the thermosphere.

Solar corpuscular radiation, whose importance depends on whether the planet has its own regular magnetic field, can also have a definite impact on the structure and dynamics of the thermosphere. Additional energy sources, such as tidal oscillations and energy dissipation of magnetohydrodynamic and inner gravitational (infrasonic) waves (by analogy with Earth, the fading of these waves occurs in the lower thermosphere) can also play a definite role in the formation of the thermal regime of the upper atmosphere. /326

A theoretical analysis of the structure and dynamics of the upper atmosphere is an extremely complex task. The equations suitable to describe the physical and chemical processes in the

heterosphere should take account of the interrelations and interactions of numerous processes and phenomena. It is reasonable to expect that the most comprehensive and rigorous research can be done within the framework of known methods of the kinetic theory of gases, specifically by starting with a Boltzmann equation whose right-hand side contains integrals of collisions and integrals of reactions [17, 42, 168]. Ivanovskiy et al. have used this approach in their works [59-61], where, in order to solve a system of kinetic equations with a selected and specified complex of reactions, Gred's method of a 13-moment approximation was used [49]. However, the simplifications introduced while resolving specific problems substantially reduce the advantages of these equations. At the same time, as far as macroscopic properties are concerned, the upper atmosphere may be viewed as a continuous medium (at least to altitudes where $\lambda \leq H$), and, in order to describe it properly, one may use generalized equations of multi-component radiative hydrodynamics. The kinetic equation is reduced to these equations if several additional assumptions are made. The generalized hydrodynamic equations for the upper atmosphere can also be formulated "phenomenologically", by using the methods of the thermodynamics of irreversible processes. However, in order to obtain transfer coefficients, this case requires the introduction of the findings of kinetic theory, including the theory of potentials. /327

The works of Marov and Kolesnichenko [96, 98, 101] have analyzed the mathematical structure of equations of multi-component radiative hydrodynamics, transfer coefficients, several assumptions introduced to simplify the original system, and initial and boundary conditions as well. They have developed a generalized method of analysis, which is well suited to describe the structure of the neutral atmosphere and ionosphere of the planet, and which includes recently-developed limited model approaches within the framework of assigning an original distribution of basic components or temperature vs altitude.

One feature of the method, which is illustrated in [97, 411] by examples of the formulation of problems for the thermospheres of Earth and Venus, is the attempt to calculate the heat of reactions for a specific set of photochemical transformations directly within the structure of the energy equation. This method makes possible a better understanding of the physical nature of the planet's thermosphere. Unfortunately, however, it is linked to significant difficulties in computation, which of course limits its practical application.

VI.2. The Neutral Upper Atmosphere and Ionosphere of Venus.

Ground-based observations. Before the beginning of space flight, there was very little information about the upper atmosphere of Venus. Several estimates had been based on the known analogy with the Earth's atmosphere. Calculations of exosperic temperature as a function of CO_2 content (1% or 100%) had led to values of 3000°K to °700K,

respectively [493]. Ground-based observations had enabled the discovery of the luminescence of the night side of Venus, and spectral and photometric measurements had been made in order to explain the reddish-brown "ashen light", which was well-known even from visual observations [120, 172]. It is impossible to rule out the possibility that this luminescence is related to the peculiarities of observations near inferior conjunction, specifically, to the "horn-lengthening" effect [288]. If it is truly connected to the night side of the planet, it may be caused by very weak emissions of the night sky or by stronger emissions excited during aurorae polaris.

It should be emphasized that the identification of individual lines and bands is a very complex problem, even in observations of emissions of the Earth's atmosphere. The progress in this respect /328 during the last 10-15 years has been achieved primarily by substantial progress in technology, in particular, the use of an interferometer to identify emission lines. The problem is simplified when identifying bands, thanks to the possibility of obtaining the relation of intensities and the possibility of sorting out individual lines in a system of bands; even here, however, factors such as atmospheric absorption, the background of the stars, and the zodiacal light with super-imposed Fraunhofer lines influence the reliability of identification [13]. Naturally, these difficulties are magnified in observing the emission spectra of other planets. Yet even these observations are very valuable to an understanding of the physics of the planetary upper atmosphere and the mechanisms of the phenomena occurring therein.

TABLE 23. MEASUREMENTS OF THE INTENSITY OF LUMINESCENCE OF THE VENUSIAN NIGHT SIDE

Filter Characteristics		Intensity of emission of the illuminated side	Noise threshold	Upper level of intensity of luminescence of night side of the zenith
3615	130			
4210	200			
4365	190			
4585	190			
4815	180			
5060	240			
5250				
	150			
5565	170			
6815				
6980	240			
7415	190			
7620	160			
	200			
	250			

ORIGINAL PAGE IS
OF POOR QUALITY

ORIGINAL PAGE IS
OF POOR QUALITY

Kozyrev's spectral observations [68] on the 122-cm telescope at the Crimea astrophysical observatory revealed several emission bands and gave an upper estimate of the luminescence intensity of Venus's night limb in the dark-blue region of the spectrum. As for the intensity of luminescence on the planet's day side, it turned out to be $2 \cdot 10^{-4}$ at a band width up to 12.5 Å. This corresponds to a limiting brightness of about 20 kR; according to Kozyrev's estimates, the intensity of emission bands was about 20% of the Fraunhofer continuum. These threshold values of the nightside brightness are in good agreement with the data of Newkirk [437] and Weinberg and Newkirk [542], who used a coronagraph with a resolution up to 16 Å to make measurements at the high-altitude observatory of the University of Colorado. The first of these measurements revealed what Kozyrev had noted: the emission bands at λ = 4415 Å and 4435 Å and a new band at λ = 4505 Å; however, these were not confirmed by subsequent measurements.

Goody and McCord later used interference filters at the 5-meter telescope at Mount Palomar to make photometric measurements of the night disk of Venus [323]. Table 23 gives their results. The measurements cover the entire visible spectrum from 0.4 μm to 0.8 μm at nearly equal intervals corresponding to the width of the filter $\Delta\lambda$ = 200 Å. The intensity of the luminescence of the day side in the indicated spectral intervals is used as reference points. In the extreme right-hand column are the upper limits of /329
the luminescence of the Venusian night atmosphere at the zenith; these levels correspond to the noise detection threshold (including corrections for the size of the air mass in the center of the aperture m ≈ 3.6). As we see, the upper limits of the intensity of emission lie basically within the range of values from 60 to 200 kR. If the limiting value obtained for the emission is adjusted to the entire continuum 0.4-0.8 μm, the mean value of the brightness is 0.5 kR/Å (more than four orders of magnitude less than the typical brightness of the daytime sky on the Earth: $\sim 10^4$ kR/Å).

These measurements rule out the possibility that there are very bright aurorae polaris (class IV), at least during the period when the observations were made, since the intensity of luminescence in lines O I (5577 Å) and N_2^+ (3914 Å) would in this case be higher than 1000 kR. Unfortunately, the noise threshold is substantially higher than the typical values of characteristic intensities of the luminescence of the night sky on Earth (≈0.2 kR for O I 5577 Å, near 2 kR for red bands of the hydroxyl group and others) and slightly higher than even the brightest lines in the spectrum of daytime luminescence (e.g., O I 6300 Å and Na 5893 Å, which have a maximum brightness of about 50 kR). This prevents us from using these data as a basis for determining the chemistry of the upper atmosphere and the features of the aeronomic processes. /330

ORIGINAL PAGE IS
OF POOR QUALITY

The spectrophotometric rocket measurements of Moos et al. [430] are of importance for the identification of luminescence in the region of the oxygen resonance triplet O I. These authors have discovered a bright emission near 1300 Å (of estimated intensity about 3 kR) in the Venusian spectrum between 1200 and 1800 Å. Subsequent experiments of the same sort by Moos and Rottman [431] have confirmed this result. In the spectrum between 1200-1900 Å, still brighter oxygen emissions over the lighted part of the disk were discovered; these emissions are identifiable with the triplet O I λλ 1302-1304 Å (about 5.7 kR) and the forbidden line of the doublet $^5S - ^3P$ λ 1356 Å (about 3 kR). The intensity of the resonance hydrogen emission in the Lyman -alpha line (L_α) was measured at 24 kR. These findings make it possible to estimate O and H content in the upper atmosphere.

The probable sources of oxygen emissions are resonance scattering of solar photons on O atoms, the impact excitation of O atoms by electrons in the case of λ = 1302-1304 Å, and dissociative excitation of CO_2 together with impact excitation of O by electrons for λ = 1356 Å [521]. Of the other distinctive features of Venus emissions, one of the most interesting is the identification of the weak emission found by Kozyrev with the bands excited during proton bombardment of CO_2 molecules [131].

Until recently, there has been no conclusive evidence about the structure of the Venusian ionosphere. Since Venus is so close to the Sun, the ionosphere was assumed to be much more dense than the Earth's ionosphere, with $N_e \approx 10^7$ cm^{-3}. The discovery of a high /331
radio brightness temperature of Venus inspired a hypothetical ionospheric model [366] with a maximum concentration of electrons up to 10^9 cm^{-3}, i.e., about three orders of magnitude larger than electron density in the F_2 layer of the Earth's ionosphere. To be sure, it was doubtful whether there were such electron concentrations in the Venusian atmosphere, since it would have to be assumed in this case that there is a very powerful source of ionization with a simultaneous small coefficient of recombination. Furthermore, given reasonable assumptions about the vertical structure of the profile N_e, the ionospheric model was not compatible with the results of passage of radar pulses, since it had not been observed that the radar reflection coefficient was dependent on wavelength [538]. Nevertheless, the hypothesis that there is such an ionosphere on Venus has been widely discussed in scientific literature, and, in order to overcome these difficulties, various models, including a "perforated" ionosphere consisting of individual ionized clouds and a "semi-transparent" ionosphere with a variable optical depth for various radio wavelength ranges, have been proposed (cf. [556]). Electron densities in these various ionospheric models have differed from about 10^{10} to 10^7 cm^{-3}.

Measurements from spacecraft. The Venera-4 and Mariner-5 measurements have contributed greatly to available experimental data on the Venusian atmosphere at high altitudes and on its interaction with surrounding space. Their findings were obtained at a time when the level of solar activity, which is characterized by the flux of solar decimetric radio emission, was measured on Earth at $\bar{F}_{10.7} \approx 130 \cdot 10^{-22}$ w·m^{-2} Hz^{-1}, which corresponds approximately to the mean value of this index in the 11-year solar cycle.

Unfortunately, the methods used by Venera-4 and Mariner-5 were unable to determine altitude profiles of the parameters of the neutral atmosphere of Venus above the Regulus occultation level. At the same time, measurements of the ultraviolet luminescence in the atmosphere, luminescence caused by the resonance scattering of solar radiation in spectral intervals including the hydrogen emission line L_α 1216 Å and the oxygen emission triplet O I λ 1302, 1304, and 1305 Å, yielded specific information about the hydrogen and atomic oxygen content in the planet's upper atmosphere. /332

It turned out that the extent of the hydrogen corona in the daytime hemisphere is greater than in the nighttime hemisphere, which could be the result of the lower atmospheric temperature on the night side of Venus. According to the data of Kurt et al. [89, 395] and Barth et al. [198-200], the concentration of atomic hydrogen in the nighttime atmosphere at a distance of about 10,000 km is estimated to be on the order of 50 and 200 cm^{-3}, respectively; this is much lower than H content at the same altitudes in the Earth's atmosphere (10^3-10^4 cm^{-3}, depending on the phase of the solar cycle). It is interesting to note that maintaining such a hydrogen concentration in the Venusian atmosphere could be due to H_2O and HCl dissociation at H_2O and HCl contents (at the level of the visible clouds) corresponding to the results of spectroscopic measurements (cf. Table 11). Fig. 114 shows this change in the content of neutral hydrogen with altitude in the Venusian exosphere on the night side according to [395].

According to Mariner-5 data (Fig. 115), the intensity of luminescence in L_α on the day side grew rapidly as the planet was neared from altitudes 3000 km to 450 km ; this corresponds to a decrease in scale height of about two times. Attempts to explain this fact encounter some difficulties since these attempts require the assumption that the exospheric temperature decreases or that μ increases. The emission mechanism during recombination of hydrogen atoms accompanying the reaction of their photodissociation excitation /333

ORIGINAL PAGE IS
OF POOR QUALITY

$$H_2 + h\nu \rightarrow H(^2S) + H(^2P) \quad (\lambda < 845\ \text{Å}). \qquad \text{(VI.2)}$$

results in an overly high recombination rate or in an unrealistically high concentration of molecular hydrogen in the Venusian exosphere (about 10^{10} cm^{-3} at h ≈ 450 km). Barth [199] has suggested a

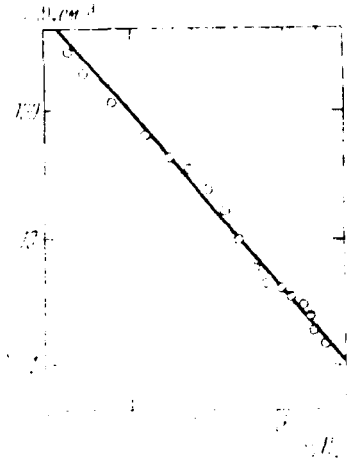

Fig. 114. Concentration of neutral hydrogen vs altitude according to Venera-4 measurements [395].

two-temperature atmospheric model on the day side; however, it is difficult to interpret this model as far as the thermal regime of the exosphere is concerned. Nor is a model of resonance scattering of solar radiation by hydrogen atoms any better in this regard:

$$H(^2S) + h\nu \rightarrow H(^2P) \rightarrow H(^2S) + \lambda 1216\ \text{Å}. \qquad \text{(VI.3)}$$

In this case the rather contrived assumption has been made [201] that one of the atoms produced by dissociation in reaction (VI.2) with excess (epithermal) energy is responsible for the most intense component of the scattered radiation, while the other (heat) is responsible for the less intense component, which reflects the actual value of exospheric temperature. /334

A more original hypothesis explains the observed features of L_α emission as

ORIGINAL PAGE IS
OF POOR QUALITY

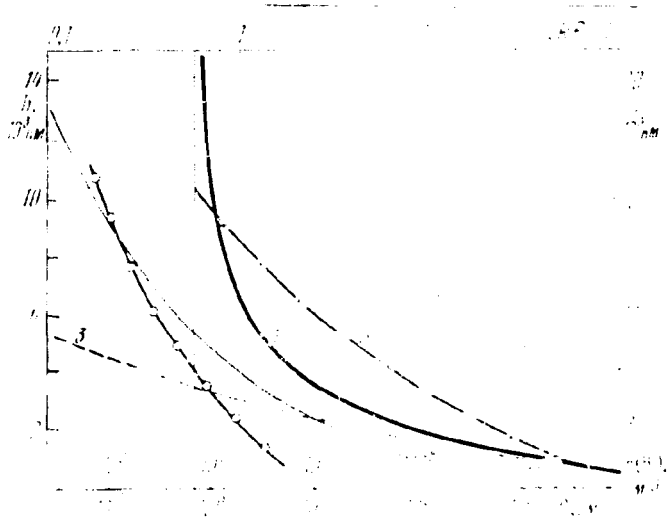

Fig. 115. The intensity of L_α emission vs altitude according to the measurements of Mariner-5 (according to [198]). 1-the total intensity; 2-the calculated profile of emission contributed by atomic hydrogen; 3-the same for molecular hydrogen at T_∞ = 650°K; 4-density H from a calculation of resonance solar L_α radiation; 5-H_2 density from a calculation of the component of emission during H_2 photodissociation. The vertical straight line is the level of the galactic background.

ORIGINAL PAGE IS
OF POOR QUALITY

the result of a predominant deuterium content at the base of the hydrogen corona in accordance with the mechanism of resonance scattering:

$$D(^2S) + h\nu \rightarrow D(^2P) \rightarrow D(^2S) + \lambda 1216\ \text{A}. \qquad \text{(VI.4)}$$

This hypothesis has been discussed in detail by Barth et al. [199, 200], Donahue [280, 281], and McElroy and Hunten [424]. It is necessary in this case to assume that at an altitude of about 500 km the content of deuterium atoms is on the order of $6 \cdot 10^4$ cm^{-3}, while the content of hydrogen atoms at the same time is about $5 \cdot 10^3$ cm^{-3}. At the same time, $n_D/n_H \approx 1$ near 3000 km. What at first glance appears to be an exceptionally high deuterium concentration at $h \approx 500$ km in the Venusian atmosphere ($n_D/n_H \approx 10$) could in principle be explained by fractionation of H and D during thermal dissipation of hydrogen above the turbopause. Clearly, the ratio of fluxes of hydrogen and deuterium dissipation should correspond to the rate at which H and D form due to photolysis. At the base of the Earth's heterosphere, $n_D/n_H \sim 10^{-4}$. In Donahue's estimates [280], it is sufficient to have $n_D/n_H \sim 5 \cdot 10^{-4}$ in the region of mixing in order to obtain a ratio of $n_D/n_H \sim 10$ at the critical level with $T_\infty \approx 700°K$. If diffusion is taken into account at the same time, as was done by McElroy and Hunten [424], it is necessary to increase this estimate by more than three orders of magnitude. This compels the assumption that there is much more deuterium in the lower atmosphere of Venus than there is in the Earth's atmosphere: $n_D/n_H \approx 0.1$.

It is only natural to compare Earth's measurements with the rocket measurements [430, 431]. As it turns out, during the Mariner-5 experiment and later, the intensity of atmospheric luminescence in L_α (according to rocket-based data) remained practically the same, about 24 kR. This value is compatible with the Mariner-5 results only if a hydrogen component alone contributes to the measured luminescence. The deuterium hypothesis if accepted, would increase the intensity of emission by almost four times (to 90 kR, [281]). This would of course make it much less likely that the Venusian atmosphere has a large deuterium concentration, but at the same time it leaves open the question about the causes of the change of signal in L_α, the change which is shown in Fig. 115 and which has given rise to the previously-examined assumptions needed to explain it[1]. /335

By starting with the notion that two predominant components (H or H_2) may cause atmospheric luminescence in L_α, and by using Chamberlain's theory [237] to describe the nature of particle

[1] The measurements of Broadfoot et al. [570] on Mariner-10 did not reveal a similar altitude profile of Lyman-alpha emission. The deuterium hypothesis in accord with mechanism (VI.4) was not thereby confirmed experimentally.

distribution in the planet's exosphere, Barth [199] has obtained estimates of the mean exospheric temperature of Venus $\bar{T}_\infty$. As is seen in Fig. 115, it may be assumed that atomic hydrogen predominates at great distances. In this case the temperature is $T_\infty = 670°K$. Closer to the planet, where the scale height decreases by about two times, nearly the same temperature is obtained $\bar{T}_\infty = 650 \pm 50°K$, assuming that the molecular component is predominant. But temperature estimates for regions closer to the planet encounter the same difficulties, those mentioned previously with regard to the identification of the probable mechanism of emission. A low-temperature model: $\bar{T}_\infty \approx 375°K$ -- itself meets with sizeable difficulties, if it is presumed that atomic hydrogen plays the dominant role (cf. [425, 540]). A temperature of about 650°K is supported by other, independent estimates, in particular, by theoretical calculations of ionospheric models corresponding to measured profiles $N_e(h)$.

According to Kurt et al. [89, 395], the limiting content of atomic hydrogen in the Venusian night atmosphere (adjusted to level $h \approx 300$ km) is $n < 2 \cdot 10^3$ cm^{-3}. Barth et al. [198] have obtained about the same result (with a deviation in estimates of n(O) concentration within an order of magnitude, which does not fundamentally change the following conclusions) for the night and day side of the planet. Compared to O content at the same altitude in the Earth's thermosphere ($n \approx 10^8$ cm^{-3}), these values are 10^5 times smaller on the average, i.e., atomic oxygen should be an extremely small admixture. /336

As we have seen, these findings are not compatible with the rocket-based measurements of Moos et al. [430,431]. The upper limit of n(O) corresponding to the measured intensity of the O I λ 1304 A emission is, according to Stewart [519] (sic) and Thomas [523], close to the content of atomic oxygen in the atmosphere of Mars, i.e., a few percent. Strickland [521] has very recently concluded that the upper limit of the content of O atoms on the line of sight ($\sim 7 \cdot 10^{10}$ cm^{-2}) recorded by Venera-4 gives too low an estimate for the thermosphere of Venus in the region 300-350 km; and he has thereby given substantial support to the findings of Stewart and Thomas. The reason for each underestimation is the failure to calculate intense attenuation of photons at $\lambda = 1304$ Å and at large zenith angles of the Sun θ (on Venera-4 experiment, an angle $\theta \approx 107°$ along the line of sight at an altitude of shade of 300 ± 100 km). According to Strickland's model estimates, nearly total attenuation along the line of sight at $\lambda = 1304$ Å occurs above 500 km, while below 400 km it is entirely due to CO_2 absorption. Therefore, regardless of the distribution of atomic oxygen, the intensity of atmospheric luminescence at $\theta \approx 107°$ will be below the level of detection. Fig. 116 shows the theoretical curves of volume rate of photon generation at $\lambda = 1304$ Å caused by solar radiation at various θ. They give reason to assume that estimates of n(O) in [89, 395] should be increased by factors of three or four, which

would allow them to be reconciled with the data of Moos et al. [430, 431][2].

Nevertheless, in this case, the chemical composition of the Venusian thermosphere is significantly different from the Earth's thermosphere, where atomic oxygen is the basic component near 200-300 km. Thus, complex questions remain, questions related to the need to explain the features of photochemistry on Venus (cf. Section VI.3). /337

The flights of spacecraft have allowed substantial progress to be made in our understanding of the structure of the Venusian ionosphere. Our most comprehensive data are on the altitude distribution and concentration of charged particles on the day and night sides of the planet; these data come from the radio occultation experiments on Mariner-5 [304, 408] and Mariner-10 [577].

The Mariner-5 dual frequency experiment obtained an obvious difference between electron content in the day and night hemispheres (Fig. 117), a fact that indicates that ionization distribution on Venus is not spherically symmetrical [408]. The nighttime ionosphere extrends to altitudes of not less than 3500 km, whereas the daytime ionosphere abruptly terminates near h ~ 500 km The fundamental layers of the Venusian ionosphere are thinner than those of Earth. The maximum electron density on the day side is about two orders of magnitude greater than on the night side. Electron density reaches its maximum on the day side at an altitude of h = 142 km, at $N_{emax} = 5.5 \cdot 10^5$ electron/cm^3. Mariner-10 obtained a similar value: $N_{emax} = 3 \cdot 10^5$ electron/cm^3 at h = 145 km. It obtained at the same time data on the distribution of daytime ionization at altitudes of 200-250 km; the Mariner-5 had been unsuccessful in this.

According to our most up-to-date conceptions, which are based on measurements of the fluctuations of the magnetic field and plasma in circumplanetary space (cf. [52, 226]), the sharp drop (about three orders of magnitude) in concentration from the day side at the level ~500 km[3] results from the interaction between the planet's ionosphere and the solar wind plasma (cf. Section VI.3). The profiles of the nighttime ionosphere can also be explained by the solar plasma surrounding Venus and by the formation of a "plasma tail" on the night side of the planet. A comparison of the measured profile $N_e(h)$ on the night side with the slopes of line segments corresponding

---

[2] The measurements of Broadfoot et al. [570] have shown that emission at λ = 1304 Å is about twice as high as the intensity measured by Moos and Rottman. Also recorded were emissions He λ 584 Å (~600R), to which m(He ~ 10^5 cm^{-3} at h ≃ 200 km) can correspond, as C λ 1657 Å with an intensity of ~10 times greater than that in estimate [427].

[3] According to Mariner-10 measurements, the ionopause extends to an altitude of 530 km [577].

ORIGINAL PAGE IS
OF POOR QUALITY

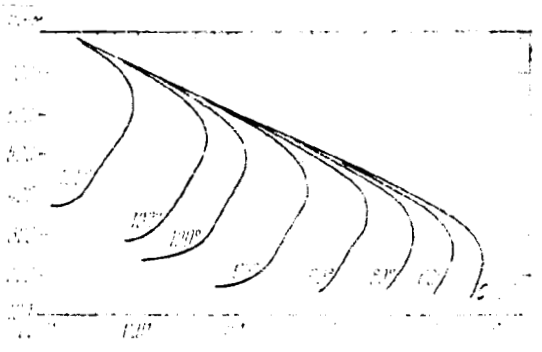

Fig. 116. Theoretical curves of volume rate of photon generation at λ 1304 Å and T = 700°K for various θ, S(h) photon·cm^{-3} sec^{-1} [521].

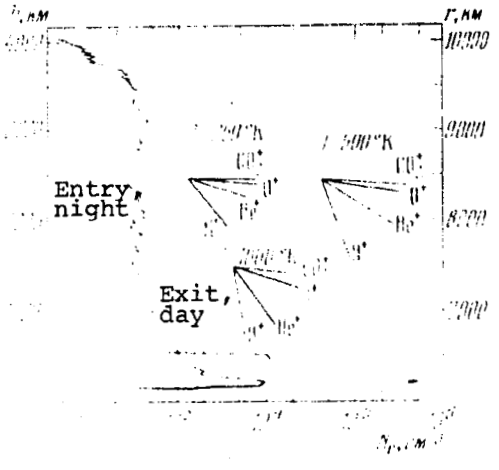

Fig. 117. Profiles of electron concentration on the night and day sides of Venus according to Mariner-5 measurements [408] (frequencies f_2 and f_3). The line segments are scale heights for various ion components and plasma temperature T_p. The dashed line on the daytime profile $N_e(h)$ is the preliminary interpretation of the data. Fig. 118 shows the characteristics of $N_e(h)$ near the maximum in more detail.

to scale heights H_p for various ions at a plasma temperature T_p (Fig. 117) allows us to estimate a probable altitude distribution of ion concentration. /339

The region of the nighttime ionosphere near the ionization maximum was studied by approximating the Mariner-5 attenuation measurements at frequency f_2 (λ = 0.7 μm) with a simple Chapman layer and by varying four free parameters: altitude, maximum electron concentration, and scale heights for ions at the base and top of the layer [304]. Four additional minima observed in the amplitude of the signal were explained by the existence of relatively thin ionization layers with an electron density of $N_e \approx 10^4$ cm^{-3}. These layers should be rather low in the atmosphere: the lowest at pressure P ≈ 1 mbar at h = 88 km (reckoned from R_φ = 6052 km) and the highest near h ≈ 120 km.

The Mariner-10 measurements revealed the existence of two adjoining peaks of electron density in the nighttime ionosphere at altitudes of 120 and 140 km. The value of N_{emax} in the upper peak is about 10^4 electron/cm^3 and slightly less in the lower peak. As for the region between 90 and 120 km, it should be noted that fluctuations in the amplitude of the signal, which had been noted in the Mariner-5 measurements, could have been caused by horizontal irregularities in the Venusian ionosphere, anomalies similar to those which are known to exist in the E layer of the Earth's ionosphere.

Measurements made with the flat and semi-spherical traps on

Venera-4 [47, 48] also yielded estimates of the concentrations of charged particles in the nightside ionosphere. The semi-spherical traps did not record concentrations above a level of detection of $\sim 5 \cdot 10^4$ cm^{-3}; the upper limit of ion density was $\sim 10^3$ cm^{-3} (at h > 300 km) according to data from the flat traps.

Fig. 118 shows altitude profiles of electron concentration in the daytime and nighttime ionosphere according to Mariner-5 data in comparison with the mean profile of N_e in the Earth's ionosphere. As we see, lower values of electron density and a much smaller overall extent of the ionosphere are characteristic for Venus. Another distinguishing feature is the much lower location of ionization /340

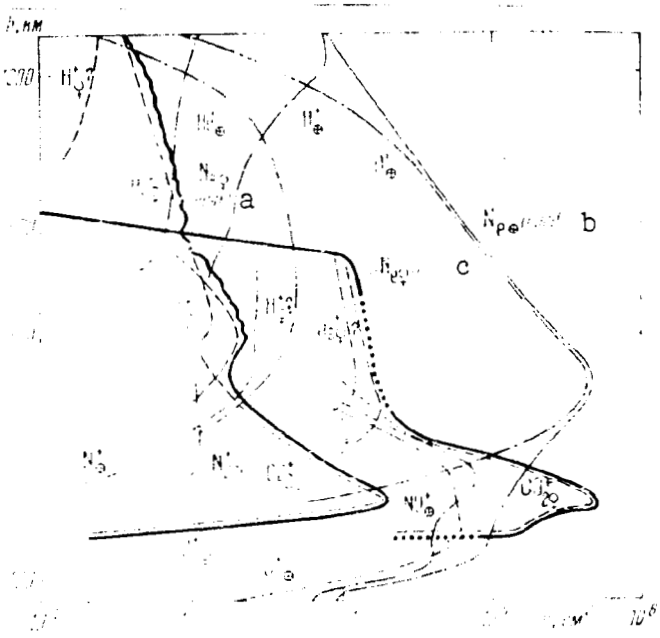

ORIGINAL PAGE IS
OF POOR QUALITY

Fig. 118. Profiles of electron concentration in the atmospheres of Venus and Earth: the thick solid lines are Venus, the Mariner-5 measurements [408]; the thin solid lines are Earth, an ionospheric model for a mean level of solar activity; the dotted-dashed line is ion concentrations for a model of the Earth's atmosphere [62a]; and the dashed line is suggested ion distributions in the Venusian ionosphere.

Key: a. night
b. mean
c. day

maxima (about 100 km lower), which stay at about the same levels on the day and night sides of the planet. Fig. 118 also shows the

altitude distribution of ion components in the Earth's ionosphere according to the model given in the work of Istomin et al. [62a], as well as suggested (quite tentatively) profiles of ion components in the Venusian ionosphere that correspond to the measured profile of $N_e(h)$.

ORIGINAL PAGE IS
OF POOR QUALITY

VI.3. Theoretical Models. /341

Models of temperature and models of compositon. As already pointed out, the study of the physical structure of the upper atmosphere of the planet through the use of full-fledged models generally involves great difficulties. Therefore, simplified approaches have been recently developed. These may tentatively be divided into temperature models and composition models.

The construction of a theoretical temperature profile model requires the establishment of a model of altitude distribution of atmospheric components $n_i(h)$, since the balance of heat energy at various levels in the atmosphere varies as a function of the effectiveness of various aeronomic reactions determined by these distributions. The vertical profile T(h) can be obtained by numerical integration of the stationary energy equation:

$$\frac{d}{dh}\left(\lambda(T)\frac{dT}{dh}\right) = R - A \qquad \text{(VI.5)}$$

with various assumptions concerning the power of heat sources (A) and heat sinks (R). Heating is determined primarily by the absorption of the far ultraviolet solar radiation, and cooling is determined primarily by heat conductivity and reemission in the infrared region of the spectrum.

With a more rigorous formulation of the model problem, the time-dependent energy equation has the form

$$\rho C_p \frac{\partial T}{\partial t} = \frac{\partial}{\partial h}\left(\lambda \frac{\partial T}{\partial h}\right) - \rho C_p \frac{\partial T}{\partial h} - T\sqrt{\frac{1}{T^2}\left(\frac{\partial T}{\partial h}\right)^2 dh} + R - A. \qquad \text{(VI.6)}$$

The second term in the right-hand side of the equation is an approximation of convective heat transfer and the adiabatic effect at vertical motions resulting from thermal expansion and contraction of the thermosphere [96]. The expression for the flow of heat into the thermosphere can be written as follows:

$$A = \sum_{i=1}^{n} n_i \sum \int S_{\nu\infty}\sigma_i(\nu)\varepsilon_i \exp\left(-\sum \int \sigma(\nu)\sec\theta\, dh\right) d\nu, \qquad \text{(VI.7)}$$

where $S_{\nu\infty}$ is the monochromatic flux of radiation at the upper boundary of the atmosphere in the spectral interval from ν to $\nu + d\nu$; /342
$\sigma_i(\nu)$ is the cross-section of photoionization (photodissociation) of the i-th component in the spectral interval form ν to $\nu + d\nu$, θ is the zenith angle of the Sun, and ε_i is the efficiency with which the

ORIGINAL PAGE IS
OF POOR QUALITY

energy of solar radiation absorbed by the i-th component is transformed into heat. The symbol $\sum' \int_{\nu_{rp}}^{\infty}$ designates summation with respect to spectral lines and integration with respect to the continuous spectrum in the ionization (dissociation) continuum $\nu \geq \nu_{rp}$.

The flow of heat into the planetary thermosphere is caused primarily by an excess of energy during the absorption of the shortwave solar radiation that causes the ionization and dissociation of atmospheric components. For reverse recombination processes, reactions of dissociative recombination are very effective as far as the transformation of solar ultraviolet energy into heat is concerned. As analysis of the aeronomic processes in the Earth's thermosphere shows, relatively small components (including intermediate compounds) can make an appreciable energy contribution to the heat balance; however, because there are few data on the composition of the planetary atmosphere at high altitudes, one has to begin by examining only the fundamental and most probable chemical transformations.

The processes of diffusion are usually not examined in temperature models. It is generally assumed that the atmosphere is in gravitational-diffusion equilibrium, and the contents of i-th components (i = 1, ..., j, ..., q) at the turbopause are assigned as boundary conditions. A major shortcoming of this model is that the concentration of $n_i(h)$ remains unchanged as the influx of solar energy varies within rather wide limits. A still more serious shortcoming is that this model does not specify the aeronomic reactions responsible for the heat balance of the thermosphere. This forces us to introduce phenomenological coefficients ε_i into expression (VI.7); estimates of these coefficients involve well-known difficulties and require additional information.

Many attempts have been made to model the Earth's thermosphere /343
by using the approximation described by equations (VI.5)-(VI.7) (cf. [70, 364, 365, 438]). Harris and Priester [339, 340], who began with equation (VI.6), have made substantial progress using this method. The mean value of coefficient ε_i in (VI.7) for an ionization continuum of atomic oxygen as a specific atmospheric component was chosen in such a way that the absolute values and amplitude of diurnal temperature and pressure fluctuations would agree with corresponding values of the parameters determined from the braking of artificial Earth satellites. This value was $\varepsilon_i \approx 0.1$. It was assumed that the outflow of heat is due to what Bates has suggested [207]: a mechanism of infrared emission of atomic oxygen in the magnetic-dipole transitions $O(^3P_1) \rightarrow O(^3P_2) + h\nu(\lambda = 63\ \mu m)$. This mechanism is most effective near 100 km, whence O atoms diffuse from the high altitudes at which the dissociation rate of molecular oxygen is at a maximum and at which collisions are few.

The term R is then expressed as $R = 2\sigma_{12}(T)$.

(VI.8)

where ORIGINAL PAGE IS OF POOR QUALITY $E_{12} = \dfrac{\exp(-E_1/kT)}{\exp(-E_1/kT) + \exp(-E_2/kT)}$.

E_0 and E_1 are the differences of the energy levels of the main (triplet) state of the O atom; w_0, w_1, and w_2 are the statistical weights of the states $^3P_0$, $^3P_1$, and $^3P_2$; σ_{12} is an Einstein coefficient for the transition $^3P_1 - {}^3P_2$; and k is Boltzmann's constant.

The estimates obtained from (VI.8) provide evidence that the intensity of emission is rather high -- about 1 erg·cm^{-2}sec^{-1} -- and it substantially affects the cooling of the lower thermosphere.

It is interesting to note that the shortcomings of a one-dimension formulation of the model problem clearly show up within the framework of this approach. Namely, heat transfer due to advection in the macrocirculatory processes at the altitudes of the thermosphere is not taken into account: the maximum heating of the thermosphere turns out to be localized at 17:00-18:00 local time. This /344 contrasts with experimental data, according to which the phase shift of maximum temperature and pressure values away from the noontime meridian is substantially less. Subsequent alternative calculations of temperature models of the Earth's thermosphere are in better agreement with experimental data when they include atmospheric motions and the more accurate estimates of absorbed shortwave radiation (cf., for example, [218, 307, 341, 342, 556a]. These also take into account the effect of boundary conditions on the time and space characteristics of atmospheric parameters and the structure of the wind field.

Composition models use a slightly different approach. It is known that although the basic composition of atmospheric atoms and molecules is rather limited, the variety of compounds formed as a result of the many photochemical and chemical transformations in the outer regions of the planet's gaseous shell can be quite large. In particular, this is the situation in the Earth's upper atmosphere, whose many reactions have been theoretically studied and confirmed in practice. They are analyzed in detail in works [78,121,206,208,259].

Some of these compounds are stable; others have a limited lifetime. Whether they are present in a specific region of the atmosphere is related to the transformation of absorbed solar energy and to the altitude distribution of atoms and molecules in excited and ionized states, yet their presence depends substantially on mixing, diffusion, and the number of solar quanta of the previously-defined energy threshold ν_{rp} at a given level. It is possible to show, for example, that in the upper regions of the Earth's atmosphere its basic neutral components, oxygen and nitrogen, are not in photochemical equilibrium. In fact, the dissociation time of oxygen at altitudes of 70-100 km, with a dissociation coefficient on the order of 10^{-6} sec^{-1} (which corresponds to a flux of solar radiation at a temperature of T = 4500°K), exceeds $5 \cdot 10^6$sec. For the actual values of the turbulent diffusion coefficient at these altitudes /345 ($K \approx 10^6$ cm^2/sec), diffusion time will be $t_{dif} \approx 10^6$ sec, i.e., less than the time to establish photochemical equilibrium. At great altitudes, molecular diffusion, whose characteristic time rapidly decreases as altitude increases ($t_{dif} \sim nT^{3/2}$), becomes

ORIGINAL PAGE IS
OF POOR QUALITY

quite intense, and deviation from photochemical equilibrium therefore increases even more.

In composition models, it is customary to use an equation of continuity, which takes account of diffusion and chemical reactions, and an equation of diffusion; whereas the profile T(h) is considered given. In a one-dimensional case for a horizontally-stratified atmosphere, the equations have the form [96]:

$$\left(\frac{\partial}{\partial t}\left(\frac{n_i}{n}\right)\right) \quad \left(\frac{\partial}{\partial}\left(\frac{n_i}{n}\right)\right) \quad J \quad \Gamma. \tag{VI.9}$$

$$\frac{\partial}{\partial h} \quad \frac{1}{H} \quad \frac{1}{T}\left(1 \quad \frac{dT}{dh}\right) \quad \sum \tag{VI.10}$$

where

$$\sum n_i m_i$$

$$\sum(\beta_{ij} \quad \alpha_{ij}) W_j$$

$$i = 1, \ldots, N \quad (1)$$

ORIGINAL PAGE IS OF POOR QUALITY

is the generation rate of the i-th component as a result of chemical reactions; n_{ij} and β_{ij} are stoichiometric coefficients; W_j is the resulting rate of the j-th reaction; and J_i is the diffused flux of the i-th component, wherein

$$\sum_{i=1} n_i J_i \quad 0;$$

$H_i = kT/m_i g$ is the scale height of the i-th component; D_{il} is the coefficient of binary diffusion; v is the vertical macroscopic flux rate. Calculating turbulent transfer modifies equation (VI.10), which then assumes the form [96] /346

$$\frac{1}{} \quad \frac{n_i}{D_i + K}\left(\frac{D_i}{H_i} + \frac{K}{H}\right) - \frac{n_i}{T}\left(1 + \frac{D_i}{D_i + K}\alpha_i\right)\frac{\partial T}{\partial h} + \tag{VI.10'}$$

$$+ \frac{D_i}{D_i + K}\sum_{l=1}^{m}\frac{J_l n_i - J_i n_l}{n D_{il}}; \quad D_i = \sum_{l=1}\frac{n_l}{n D_{il}},$$

where K is the coefficient of turbulent diffusion. It was inherently assumed in (VI.10) that fluxes of molecular and turbulent diffusion can be viewed as independent and be added together, i.e. $J_i = J_i^M + \psi_i$, where $\psi_i = -K\left(\frac{\partial n_i}{\partial h} + \frac{n_i}{T}\frac{\partial T}{\partial h} + \frac{n_i}{H_i}\right)$. At v = 0, equation (VI.9) is re-written as:

$$\frac{\partial n_i}{\partial} \quad \frac{\partial}{\partial h} J_i = \sum_{j}^{r}(\alpha_{ij} - \beta_{ij}) W_j \tag{VI.11}$$

If, furthermore, only molecular diffusion is to be studied, then $\psi_i = K = 0$, and the equation of transfer (VI.10') passes to the usual equation of diffusion in the Chapman-Cowling form [168].

The commonly-used method of calculating the structure of the ionosphere is closely related to composition models. In a stationary condition, the equation of continuity (VI.9) relative to the electron concentration N_e is rewritten as:

$$\frac{d}{dz}(N_e v_e) = \Gamma \qquad \text{(VI.12)}$$

ORIGINAL PAGE IS
OF POOR QUALITY

Assuming that in an optically thin atmosphere, the ionization rate is proportional to the density of the corresponding neutral i-th component n_i, and that the recombination rate is proportional to the square of N_e (g and ξ are the proportionality factors), we obtain

$$\frac{d}{dz}(N_e v_e) = g n_i(h) - \xi |N_e(h)|^2. \qquad \text{(VI.13)}$$

The two limiting cases of practical interest are: photochemical equilibrium, which can be obtained at comparatively low altitudes, /347 and dynamic equilibrium, which is reached at greater h. Accordingly, the left-hand side or the second term in the right-hand side of (VI.13) goes to zero, and the altitude-dependent electron concentrations are determined by the formulas [425]

$$N_e(h) = \left|\frac{g n_i(h)}{\xi}\right|^{1/2} \qquad \text{(VI.14)}$$

or

$$N_e(h) = \frac{g n_i(h)}{\xi N_e(h)}. \qquad \text{(VI.14')}$$

Studying the altitude variation of the concentration of neutral components in composition models has turned out to be particularly fruitful for the study of the lower regions of the Earth's thermosphere. Colegrove et al. [250, 251] have numerically integrated the system of equations (VI.10)-(VI.11) with oxygen dissociation and recombination taken into account. In this case, there directly follows from equation (VI.11)

$$\frac{dJ_1}{dh} = 2In_2 - 2\beta_1 n_1^2 n - \beta_2 n_1 n_2 n$$
$$\frac{dJ_2}{dh} = -In_2 + \beta_1 n_1^2 n \qquad \text{(VI.15)}$$

The subscripts 1 and 2 refer to atomic and molecular oxygen, respectively, and n is the total concentration. The diffused fluxes of molecular nitrogen and argon were taken to be equal to zero, $J_3 - J_4 = 0$; and constant values corresponding to $J_5 = 1.7 \cdot 10^6$ cm^{-2} sec^{-1} and $J_6 = 2.5 \cdot 10^7$ $cm^{-2}sec^{-1}$ were assumed for helium and hydrogen fluxes. In system (VI.12)

(VI.12), I designates the coefficient of the oxygen dissociation rate averaged over a day, β_1 is the coefficient of oxygen recombination for the reaction

$$O + O + M \rightarrow O_2 + M.$$

ORIGINAL PAGE IS
OF POOR QUALITY

and β_2 is the coefficient of oxygen recombination for the reaction

$$O + O_2 + M \rightarrow O_3 + M.$$

The coefficient of turbulent diffusion was considered to be independent of altitude and was taken to be $K \approx 5 \cdot 10^6$ cm^2 sec^{-1} by providing the conditions $n(O)/n(O_2) \approx 1$ near $h \approx 120$ km.

The results of modelling for the conditions of diffused equilibrium and disequilibrium indicate that at a given temperature profile, the value of the coefficient of turbulent diffusion in the lower thermosphere plays a most essential role. It is an unique parameter of agreement for the transition region (turbopause), where, by definition, $K = D_{ij}$. The substantial discrepancies in estimates of this coefficient for the Earth's thermosphere depend both on the choice of model and on the validity of the experimental data used for comparison with the results of calculations. In the most recent works of Shimazaki and Kasahara [490] and Shimazaki [491, 492], the results of integrating a non-stationary equation of continuity of the type (VI.9) lead to the conclusion that in order to be compatible with the experimental profiles, it is necessary to assume $k \approx 10^7$ cm^{2}sec^{-1} at altitudes of 140-160 km and $K \approx 5 \cdot 10^6$ cm^{2}sec^{-1} at altitudes of 100-120 km. /348

Modelling the Venusian thermosphere. The task of modelling the Venusian upper atmosphere with so few experimental data is more complicated than the analogous task for Earth, and, furthermore, it requires additional assumptions. On the whole, however, the approach corresponds to approaches to temperature and composition models.

One of the first such attempts was that of Urey [529], who began with the assumption that the atmosphere above the clouds consited for the most part of CO_2 and that the efficiency of dissociation processes had formed an extensive CO and O layer in this region. Kaplan [371], whose estimates led to a mixing ratio of $n(CO_2)/n(N_2) \approx 0.15$, assumed that dissociation had substantially less effect on the establishment of equilibrium concentrations of atmospheric components. The next step was the work of Shimizu [493], in which the altitude profiles $n_i(h)$ were determined from the condition of photochemical equilibrium in an atmosphere consisting of CO_2, O_2, and the products of their dissociation CO and O. Because of the efficiency of oxygen molecule formation during triple collisions, the effect of CO_2 dissociation on the establishment of equilibrium concentrations in the thermosphere was further lessened, and the altitude of the layer where dissociation is greatest was lowered. The reason for this is the screening effect

of O_2 molecules, inasmuch as the absorption coefficient in the Schuman-Runge continuum is larger than in the CO_2 continuum. /349

Shimizu's model, which was closest in type tc composition models, had a serious defect. It did not take account at all of diffusion, which should result in the transfer of CO_2 and O_2 upward and the transfer of CO and O downward and, consequently, to the equalization of "peak" concentrations of individual components, especially O_2. Despite its seeming persuasiveness, the model was unrealistic, since it required a significant content of molecular and atomic oxygen in the Venusian upper atmosphere; as we have seen, this is hardly compatible with current conceptions. Estimates of the altitude profile of the neutral components of the Venusian upper atmosphere made in [118] encounter the same difficulties.

Shimizu overcame these difficulties in a later work [496], which contained not only more accurate estimates of photochemical processes (proceeding from the most probable chemical composition of a thermosphere with prevalent CO_2 content) and molecular diffusion, but also an examination of the processes of turbulent and ambipolar diffusion. His calculations led to the conclusion that since solar radiation in the CO_2 continuum penetrates deeply into the atmosphere, the region near the base of the thermosphere should have a more substantial effect on the altitude distribution of neutral components on Venus than on the Earth. This in turn predetermined the great sensitivity of calculated temperature models to the lower boundary conditions assigned. It is necessary to formulate these conditions below the tropopause, even though it is more convenient to calculate an altitude profile of partial concentrations. The influence of vertical transfer is appreciable at horizontal wind velocities of 10-100 m/sec. The value H^2/K, where H is the scale height, should correspond to the typical time constant of atmospheric circulation R_0/V. At $V \simeq 100$ m/sec, $K \simeq 2 \cdot 10^7$ $cm^2 sec^{-1}$ is obtained. In these conditions, a significant deviation from photochemical equilibrium is observed in the layer where CO_2 dissociation is most efficient (cf. also [494, 495]), and the coefficient K in equation (VI.10) serves as a parameter of agreement for the required concentrations of dissociation products. McElroy [420-422] /350 has calculated a model of the Venusian thermosphere in an approximation corresponding to temperature models. The atmosphere was assumed to consist wholly of carbon dioxide gas. The energy equation in the form (VI.5) was integrated, and in so doing, it was held that the influx of heat (term A) is related primarily to absorption of far ultraviolet radiation in ionization and dissociation CO_2 continuums and that cooling (term R) is related to emission by oscillatory-excited CO_2 molecules.

In addition to heating caused by the absorption of far ultraviolet radiation, infrared radiation absorbed in the 2.0, 2.7, and 4.3 μm bands can also make a definite contribution to the heating

of the Venusian thermosphere. Allowing for the important role played by reemission of absorbed radiation at high altitudes, McElroy estimated the thermal effect of this absorption (the added term A' in (VI.5)) by expressing it in terms of the ratio between the radiation lifetime η_r and the collision lifetime η for corresponding models of bands (cf. VI.1):

$$A' = \gamma(h)\frac{\eta}{\eta_r}. \qquad \text{(VI.16)}$$

ORIGINAL PAGE IS
OF POOR QUALITY

where $\gamma(h)$ is the amount of radiant energy absorbed at altitude h in the corresponding spectral region. Values of η_r for bands 2.0, 2.7, and 4.3 μm are 0.0024, 0.041, and 0.9 sec, respectively. For values of η in the near infrared region of the spectrum it is permissible to use the empirical expression obtained by Chamberlain and McElroy [239] for the 15 μm band but reduced by about two times due to the probable presence of H_2 molecules, which influence the vibrational deactivization of CO_2, in the thermosphere [420]:

$$\eta = \left[3.8\cdot 10^{-3}\exp\left(-\frac{\ldots}{T}\right)n(CO_2)\right]^{-1}. \qquad \text{(VI.16)}$$

As for term R, then as it is found from the equation of transfer in the 15 μm band, it is necessary to keep in mind that in the conditions of the thermosphere the value $1-\frac{\beta_\nu}{\alpha_\nu}$ in (VI.1) becomes significant, i.e., there is substantial deviation from l.t.e. The modelled band structure of Goody and Belton [322] takes this effect into account. McElroy has calculated the value of R as an approximation of the structure by using numerical methods[4]. /351

McElroy's model estimates the mean exospheric temperature at $\bar{T}_\infty \approx 700°K$, which is in good agreement with Barth's findings from measurements of the intensity of atmospheric luminescence in L_α. Hogan and Stewart [347], who also began with an approximation corresponding to temperature models, obtained similar results, with $\bar{T}_\infty = 650 \pm 70°K$. As we see, although the insolation on Venus is twice as high as on the Earth, this additional influx of energy into the upper atmosphere is matched by an even more intense cooling resulting from the high content of CO_2 molecules. The mean exospheric temperature on Venus turns out to be lower than on Earth.

In both models, the level where isothermy begins (the thermopause) is reached near 200 km, and practically coincides with the location of the thermopause in the Earth's atmosphere at the same

---

[4] Dickinson has recently given a detailed analysis of the problem of radiative heat exchange in the infrared region of the spectrum in the Venusian mesosphere [273].

temperature [94, 410, 413]. The concentration of neutral particles $n \approx 10^8$ cm^{-3}, i.e., an altitude of about 250 km, corresponds to the critical level.

Shimizu's results [497] using a non-stationary equation of heat conductivity with a convective term in the form (VI.6) do not differ essentially from these values. In addition to a mean value of $\bar{T}_\infty = 670°K$, he obtained the expected diurnal temperature change and its limiting variations during an 11-year solar cycle while making various assumptions about the efficiency of heat transfer resulting from heat conductivity. Fig. 119 reproduces these results. They indicate that the difference in temperature on the day and night hemispheres can reach almost 400°K and about 600°K depending on the phase of the solar cycle. The latter value is about twice as high as the corresponding estimate in model [422] (Fig. 120). The equalization of temperature irregularities should probably occur due to intense winds with velocities of hundreds of meters per second. As we have seen, the estimates Shimizu made of the probable coefficient of turbulent diffusion $K \sim 10^7$ cm^{2}sec^{-1} (these were obtained for a different model) correspond to these conceptions [496]. /352

It is well known that winds and turbulent transfer have a substantial effect on the space and time characteristics of atmospheric parameters. Wind velocities up to several hundreds of meters per second have been found in the Earth's atmosphere (cf., for example, [209, 379, 403]). In the Venusian thermosphere, such winds are even more probable, if it is kept in mind that because of the planet's slow rotation, the longitudinal temperature gradient should be larger than on Earth. The presence of a horizontal wind should in turn cause intense vertical transfer and have an appreciable effect on the establishment of the thermal regime in both hemispheres. Dickinson [272] has examined a possible schema of circulation in the Venusian upper atmosphere, a schema that leads in particular to a rapid transport of the products of photolysis to the night side. The circulation model of Dickinson and Ridley [274] has further developed these conceptions.

Equalization of temperature and density due to horizontal motions is assumed in the average diurnal model of McElroy [420, 422]. In contrast to this, Hogan and Stewart [347] began with the conception that local radiative equilibrium is established on the night and day sides of the planet for a period of time equal to one Venusian day and that the maintenance of significant gradients of T_∞ and ρ are possible. Therefore, even though they use a generally similar approach to estimation of the sources of the flow of heat energy into the thermosphere, these models use varying values of the coefficient of the efficiency of transformation into heat in expression (VI.7): $\varepsilon \approx 0.60$ in the average diurnal model and $\varepsilon \approx 0.30$ in the local-equilibrium model. In the latter case $\bar{\varepsilon}$ is used as a parameter of agreement in calculating the thermal regime of both hemispheres [425]. The mean exospheric temperature obtained here is about the same, about 700°K. /353

ORIGINAL PAGE IS
OF POOR QUALITY

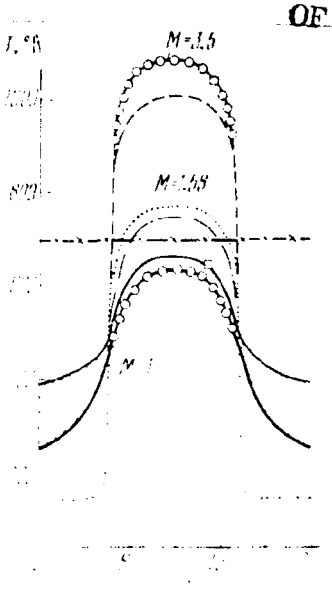

a

Fig. 119. Exospheric temperature of Venus vs time (one day) and level of solar activity according to [497]. The dotted line, the dashed line, and the dotted-dashed line are calculations according to Eq. (VI.5) for values of the coefficient of heat conductivity $\lambda(T) = 0{,}81\ T^{4/3}$; $67\ T^{1/2}$ and $36\ T^{3/4}$ at a solar zenith angle of $\theta \sim 75°$. The solid curve is a calculation according to Eq. (VI.6). The circles are variations during the 11-year solar cycle. M is the parameter of solar activity normalized to a value of $F_{10.7}$ in the minimum of the cycle. The square is Mariner-5 data, to which M=1.58 corresponds. The "x's" are T according to [420].

Key: a. hours

The modelling of the Venusian ionosphere was done in the approximation described by equation (VI.13) and the formulas (VI.14)-(VI.14'). Attempts were made to interpret the daytime profile $N_e(h)$ (as a function of the ionization source) near the principal ionization maximum as one that corresponds to the F_1 or E layer of the Earth's atmosphere. The concentration of neutral particles n in this region was taken to be from 10^{11} to $5 \cdot 10^{12}$ cm^{-3}, with photometric data at the Regulus occultation level taken into account. Article [344] uses a more complex approach to the problem of modelling the daytime ionosphere; it attempts to calculate added heating by solar wind and to estimate the strength of the induced magnetic field in the boundary region. /354

McElroy's calculations [420, 422, 423] provide evidence that favors an F_1-type model, which satisfactorily approximates the measured profile of electron concentrations in the atmosphere below 200 km due to the CO_2^+ ion. The addition of other components (N_2, O_2) results in a marked deviation of the calculated curves from the measured profile $N_e(h)$. The same results give no reason to expect an appreciable concentration of ions of atomic oxygen nor, accordingly, an F_2-type layer, thus agreeing with experimental data about a rapid fall in N_e above the peak of the F_1 layer.

VI.4. Photochemistry and Dynamics. The Exosphere.

The photochemistry of a CO_2 atmosphere. Available experimental data and the results of modelling the thermosphere, as well as theoretical estimates made from the structure of ionization levels compared with measured altitude profiles $N_e(h)$ give reason to assume that a

ORIGINAL PAGE IS
OF POOR QUALITY

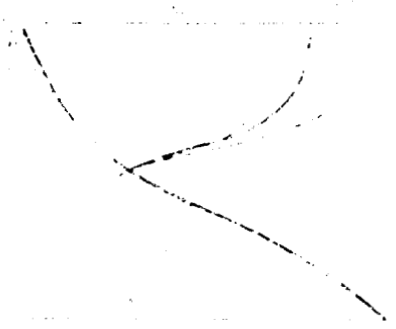

Fig. 120. Temperature T and particle density n vs altitude in the McElroy model [422]. The solid curves correspond the phase of solar cycle activity during the Venera-4 and Mariner-5 flights. The dashed line -- estimates of the limiting cases between the minimum and maximum of the 11-year solar cycle. The square is an estimate of density at the Regulus occultation level.

predominant CO_2 concentration is maintained in the Venusian thermosphere up to ~ 200 km. But an intense dissociation of CO_2 by the solar ultraviolet should occur in a carbon dioxide atmosphere:

(VI.17)

(VI.17')

Reactions of this type at small λ are accompanied by the formation of the products of photodissociation in states of CO_2 excitation $(a^3\Pi)$[5], $CO(A^1\Pi)$, $O(^1S)$ (cf. for example, [245, 397, 416a]) with subsequent spontaneous transitions. At the same time, it is known that the reverse reaction of CO and O recombination as in[6] / 355

(VI.18)

is hardly able to explain the observed stability of CO_2; the coefficient of the rate of this reaction $k_1 < 8 \cdot 10^{-35}$ cm^{6}sec^{-1} at T = 300°K is too small [280]. The association of oxygen atoms occurs about 40 times faster:

(VI.19)

since $k_2 = 3 \cdot 10^{-33}$ cm^{6}sec^{-1} at T = 300°K [470].

The equation of continuity (VI.9) for atomic oxygen in the stationary case and at $J_1 = 0$ is written in a form similar to (VI.12):

(VI.20)

The CO_2 dissociation rate in an optically thin atmosphere is, according to McElroy, $Q(O; CO; h) = 2.2 \cdot 10^{-6} n(CO_2; h)$. The calculation of (VI.18) and (VI.19) gives

---

5 In this case (at λ 1080Å), Cameron bands of CO (a - x) are excited.

6 At the most probable assumption of $M \equiv CO_2$.

By integrating (VI.20), McElroy [421] and Donahue [280] estimated the flux of O atoms at level h_0, where, for the dissociation continuum of CO_2 $\tau \approx 1$, the concentration $n(CO_2) \approx 10^{12}$ cm^{-3}, $Q \approx 2 \cdot 10^{12}$ cm^{-2}sec^{-1}: $|n(0) \cdot v|_{h=h_0} \approx 2 \cdot 10^{11}$ cm^{-2}sec^{-1}. If it is realistic to accept $(v)_{h_0} \leq 10$ cm/sec, the numerical densities of O and CO should then reach $n \geq 2 \cdot 10^{10}$cm^{-3}, which is significantly larger than equilibrium contents n(O), n (CO) and $n(CO_2)$ according to experimental data. The difference between the rates of appearance and disappearance of atomic oxygen at these levels in the thermosphere reaches almost six orders of magnitude [280, 281] and requires either the discovery of a more efficient recombination mechanism or a vertical transfer of O atoms into the atmosphere to a much greater depth. In order to remove this contradiction, McElroy [419, 420] began with the notion of photochemical equilibrium and assumed a recombination mechanism with the formation of an intermediate excited CO_3^* complex accompanying the reaction (VI.17'): /356

(VI.21)

ORIGINAL PAGE IS
OF POOR QUALITY

However, this mechanism, which has been assumed more than once during laboratury study of CO_2 photolysis, has serious shortcomings. It requires that all the oxygen atoms formed in the atmosphere due to dissociation are in an excited state (^{1}D). At the same time, the population of these levels is much lower than the levels in the fundamental state of ^{3}P. Moreover, although the lifetime of the metastable state ^{1}D is long, (96 sec), the process of spontaneous deactivization of O(^{1}D) with the emission of the red doublet can be faster than the recombination process as in (VI.21). Still more efficient is the mechanism of the disappearance of metastable atoms O(^{1}D) in the Venusian thermosphere due to impact deactivation as in :

(VI.22)

Recent results of laboratory experiments by De More [269], Clark and Noxon [244], and Slanger and Black [503] strongly indicate that since CO_2 molecules (at $M \equiv CO_2$ the coefficient of the rate of this reaction is $k_3 \approx 5 \cdot 10^{-11}$ cm^{3}sec^{-1} [553])[7], i.e., the quenching occurs with a rate close to the gas-kinetic rate) can efficiently play the role of the third body in (VI.22), the probability of mechanism (VI.21) is negligible, and the probability of (VI.22) is close to unity. The rather high probability that the excited complex of CO_3^* will decay rapidly should also be kept in mind. McElroy and Hunten [426] have examined the possibility that it is stabilized at the collision-caused emission of a quantum; in this

[7] This reaction at $M \equiv N_2$ is well known for the Earth's thermosphere; it is a type of predissociation reaction.

case, the sequence of reactions (VI.21) is modelled and assumes the /357 form:

$$\left.\begin{array}{l} 2CO_2 + O(^3P) \rightarrow CO_3 + CO_2 \\ CO + CO_3 \rightarrow 2CO_2 \end{array}\right| \qquad \text{(VI.23)}$$

Unfortunately, there are no numerical values of the coefficients characterizing the efficiency of this mechanism. However, it does not seem likely that acceptable values will be obtained, values which in this approach will provide an answer to one of the fundamental problems of the photochemistry of Venus and Mars: how to avoid an accumulation of CO and O_2 in the atmosphere, so as to satisfy the spectroscopic limits of the contents of these components (cf. Table 11).

Donahue [280], and McElroy and Hunten [426] have examined reactions that include intermediate perhydroxyl complexes as alternative recombination processes:

ORIGINAL PAGE IS
OF POOR QUALITY

(VI.24)

However, the coefficient of the rate is $k_4 \approx 10^{-24} - 10^{-23} cm^3 sec^{-1}$, while the formation rate of H atoms, which is determined from the intensity of the emission in L_α ($k_5 \approx 2 \cdot 10^{-3}$ cm sec^{-1}), is several orders of magnitude lower than the value of Q. This makes the sequence of reactions (VI.24) inefficient. The presence of water vapor could significantly speed up the reaction

(VI.25)

in which H_2O is the catalyst. But significant difficulties appear here, too: the relative water vapor content above the clouds according to spectroscopic measurements ($f_{H_2O} \leq 10^{-5}$) is clearly insufficient to secure the required reaction rate of (VI.25). Moreover, according to the estimates of Donahue [280], in order to recombine the products of CO_2 dissociation at a flux of $\sim 2 \cdot 10^{-11}$ cm^{-2} sec^{-1} in the region $n_{CO_2} \geq 10^{18} cm^{-3}$ and at a content of $n_{O_2} \sim 10^{-2} n_{CO_2}$, the required value of k_6 is only $\sim 10^{-43} cm^6 sec^{-1}$.

Coefficients K and ε. The difficulty in finding a mechanism /358 that could rapidly evacuate CO_2 photodissociation products from the dissociation zone by recombining them in the gaseous phase is a definite argument in favor of the assumption that the processes of vertical transfer are quite efficient. The physical nature of

ORIGINAL PAGE IS
OF POOR QUALITY

vertical motions can be related both to the mechanism of global circulation and to the more localized mechanism of penetrative convection, developed and maintained by the instability of lower-lying regions. If there are processes of turbulent diffusion, which hinder diffusion-gravitation separation of gases, then recombination in the presence of a solid phase could play a definite role. Donahue[281] allows for these considerations in his examination of the possibility that the planetary surface has an effect on this process.

The deficit of atomic oxygen in the Venusian thermosphere can be explained if it is assumed that the coefficient of turbulent diffusion is $K \approx 2 \cdot 10^7$ $cm^2 sec^{-1}$, as is shown in the aforementioned calculations of Shimizu. The calculations of McElroy and McConnell [427] for Mars result in a substantially larger value, $K \approx 5 \cdot 10^8 cm^2 sec^{-1}$, assuming that $\frac{n(O)}{n(CO_2)} \sim 10^{-3}$. Assuming transfer down to the surface, velocities of several hundreds of meters per second (!) would correspond to this value. In the case of Venus, however, the dense layer of clouds could serve as this surface; in this regard, $L \sim H$ and the required value of $K \sim 10^7 cm^2 sec^{-1}$. But if the data of Thomas [523] are kept in mind (according to which O content on Mars corresponds to a ratio of $\frac{n(O)}{n(CO_2)} \sim 3 \cdot 10^{-2}$), then for Mars the value of K becomes about an order of magnitude smaller. These estimates are already very close to what is usually accepted for Earth. Nevertheless, it is difficult at present to answer the question of how realistic these values of K are and how they are reached in practice in the atmospheres of Venus and Mars.

The circulation model of Dickinson and Ridley [274] provides additional arguments in favor of the important role played by dynamics in the Venusian thermosphere. Their numerical calculations enable the assumption that both turbulent diffusion and large-scale vertical and horizontal motions (up on the day side and down on the night side) have a significant effect on the establishment /359
of the thermal regime and the equilibrium concentration of components. In this schema, if boundary conditions are assigned at level $P \approx 0.1$ mbar, efficient recombination of CO_2 photodissociation products is assured, so that relative O and CO content near the ionospheric maximum F_1 does not exceed $\sim 2\%$.

It should be noted that if turbulent diffusion and circulation in the Venusian thermosphere indeed play an important role in the Venusian thermosphere, this would be a strong argument against the deuterium hypothesis adduced to explain the dependence (measured by Mariner-5) of the intensity of luminescence in L_α on altitude, since this hypothesis begins by assuming that vertical flows are weak.

The coefficient used in temperature models $\varepsilon \approx 0.60$ is obtained from the calculations of Henry and McElroy [343], who analyzed the

most probable ways solar shortwave radiation is transformed into heat in a CO_2 atmosphere. One can maintain that the basic source of heating of the Venusian thermosphere is "fresh" photoelectrons as they are thermalized and the release of thermal energy during the recombination of CO_2^+ ions. Ionization is caused by photons with energy $E > 13.8$ eV ($\lambda < 902$ Å), which lead to the formation of CO_2^+ in various states of excitation [191]. Ions with energy $E \geq 7$ eV are particularly efficient in the thermal ratio, since in a carbon dioxide atmosphere below this threshold, the most probable is energy loss due to reemission from the vibrational-excitational levels of CO_2 molecules, especially in band $\lambda = 15$ μm. The thermal efficiency of dissociative CO_2^+ recombinations depends to a large extent on the state of excitation of finite products of reaction [425]:

$$CO_2^+ + e \rightarrow \begin{cases} CO(^1\Sigma) + O(^3P) & \text{eV.} \\ CO(^1\Sigma) + O(^1D) & \text{eV.} \\ CO(^1\Sigma) + O(^1S) & \text{eV.} \\ CO(a^3\Pi) + O(^3P) & \text{eV.} \\ CO(^1\Sigma) + O(^3P) & \text{eV.} \end{cases} \qquad \text{(VI.26)}$$

$$CO_2^+ + e \rightarrow \begin{cases} CO(a^3\Pi) + O(^3P) & 0.63 \text{ eV} \\ CO(a^3\Pi) + O(^1D) & 0.35 \text{ eV} \\ CO(^1\Pi) + O(^3P) & 0.28 \text{ eV} \end{cases}$$

ORIGINAL PAGE IS OF POOR QUALITY

Of the ways of transformation given in (VI.26), the most probable/360 is CO formation in the fundamental state ($^1\Sigma$) and O formation in the states (^3P) and (^1D). According to [544], $k_7 = 3.8 \cdot 10^{-7}$ cm^{3}sec^{-1}.

It is assumed that the remaining part of the far ultraviolet radiation is scattered or remitted by the atmosphere, as well as released at lower levels during recombination of photolysis products. Estimates of the energy lost during recombination are rather hypothetical and can significantly change the value of ε. Thus, what Barth et al. [202] discovered on the Mariner-6 and Mariner-7 was completely unexpected and had not been suggested by laboratory experiments: the intense emission of the upper atmosphere of Mars in the Cameron CO bands, together with a pronounced luminescence in CO_2^+ (the doublet CO_2^+ B - X) and $OI^1S - {}^3P$ bands. The calculations of [516, 518] indicated that in this case Mars loses about half the energy of incident far ultraviolet radiation in the form of atmospheric luminescence. This forced a value of $\varepsilon = 0.19/2$ to be used, i.e., $\bar{\varepsilon} \approx 0.1$ in the calculation for both hemispheres, instead of the value McElroy had previously accepted: $\varepsilon = 0.66/2$, i.e., $\bar{\varepsilon} \approx 0.3$.

A similar situation could be expected for Venus also. As in the case of Mars, this leads to a substantial reduction in the exospheric temperature of Venus and to a review of the characteristics of its ionosphere, even though the value $T_\infty \approx 700°K$ and the measured (in 1967) profile $N_e(h)$ are in satisfactory agreement with theoretical calculations at $\varepsilon \approx 0.6$. At the same time, the measurements of atmospheric luminescence in ultraviolet on Mariner-9 in 1971 [203, 517] result in the conclusion that previously-estimated intensities of luminescence in Cameron CO bands were obviously overestimated by about two times (allowing for corrections for instrument calibration and variation in solar activity). Because emission reduced energy losses, the exospheric temperature of Mars should increase from 350° to 420°K, which is less compatible, however, with the model of altitude distribution of oxygen obtained from the /361 same measurements using an ultraviolet spectrometer. This discrepancy can be removed, however, by assuming, for example, that the energy of the excited $O(^1D)$ atom formed during CO_2 photodissociation and CO_2^+ dissociative recombination (reactions (VI.17) and (VI.26)) transforms upon quenching of the excitation not into kinetic energy, but primarily into the energy of CO_2 vibrational excitation, with subsequent emission in the infrared region of the spectrum [517]. The estimate of the value of ε will depend in the final analysis on how correctly these and other possible processes are calculated.

The analogy with Mars is by no means accidental. The features of photochemistry on Mars are apparently quite similar to what occurs on Venus, since the thermospheres of both planets probably consist mainly of CO_2. Therefore, it is customary to examine questions of photochemistry for the Venusian and Mars atmospheres at the same time and to subsume these questions under the general concept of the photochemistry of CO_2 atmospheres. From this point of view, the excellent spectra of Mars in the ultraviolet region ($\lambda\lambda$ = 1100-3400 Å) obtained on Mariner-9 are of great interest; Fig. 121 shows the averaged result of these spectra [203]. The spectrum conveys the basic characteristics of the planet's luminescence, which are extraordinarily important for an understanding of the features of photochemistry in a carbon dioxide atmosphere. A detailed analysis of these features can be found in the original works of Barth and his co-workers [202, 203, 517].

The exosphere and circumplanetary space. In existing estimates, the efficiency of the most probable recombination mechanism of atomic oxygen markedly decreases above about 200-250 km, i.e., near the base of the exosphere. This apparently results in the appearance of a layer of atomic oxygen of relatively small extent (cf. Fig. 117), since near these levels a definite influence should be exerted by helium, assuming, of course, that the crust of the planet is similar to that of Earth and that helium is present in the Venusian atmosphere to about the same extent as in the Earth's

atmosphere ($\sim 2 \cdot 10^6$ atoms $cm^2 sec^{-1}$) [384]. According to [423, 425], the measured profiles of the nighttime Venusian ionosphere above level h ≈ 250 km can be explained by He photoionization on the day side at a rate of $3 \cdot 10^7$ $cm^{-2} sec^{-1}$ and a subsequent horizontal transfer of He^+ ions to the nighttime hemisphere (as in the Dickinson model). In the process, the following sequence of efficient ion-exchange reactions could be assured /362

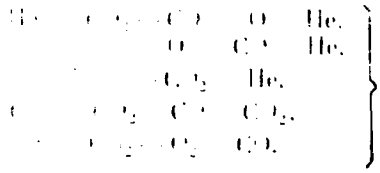

ORIGINAL PAGE IS OF POOR QUALITY

accompanied by the reactions of dissociative recombination (VI.26) and the reaction /363

$$O_2^+ + e \rightarrow O + O$$

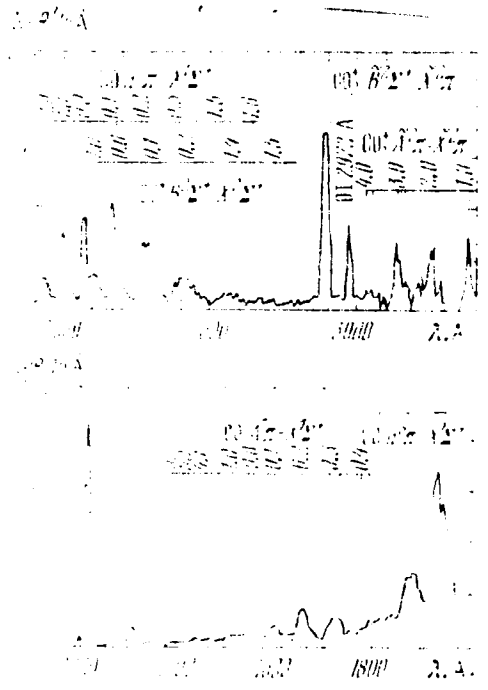

Fig. 121. Spectra of the atmospheric luminescence of Mars in regions 1100-1900 Å and 1900-3400 Å, averaged over 120 measurements at the planetary limb on the Mariner-9. Resolution 15 Å.

The calculations of [246] demonstrate that the transport of about 10% of the helium ions formed on the day side during the planet's interaction with the solar wind secures the necessary balance between helium dissipation and helium appearance resulting from radioactive decay in the interior of the planet. According to Wallace [539], because of the high ionization potential of helium and because of the comparatively low temperature at the critical level, the helium dissipation rate for the Venusian atmosphere is significantly less than that for the Earth's atmosphere. Thanks to this, the ratio of contents $n(He)_♀ / n(He)_⊕ \approx 10^4$. The calculations of [344], which give a value of $\sim 1 (n(He)_♀ \approx 10^8$ $cm^{-3})$ at h ≈ 100 km, are less convincing.

Estimates of the scale height of the nighttime ionosphere (cf. Fig. 117) show that the dominant role of He apparently extends up to 500-700 km, while above this level, the structure of the Venusian atmosphere is determined by the hydrogen content. The altitude distribution of the relative concentrations of components depends on a reliable

interpretation of the mechanism responsible for the measured intensity of the luminescence in the Lyman-alpha line, since this mechanism affects the estimate of exospheric temperature. The plasma temperature T_p is also estimated with this taken into account; this temperature will evidently not differ much from T_∞ on the night side, at least up to h ~ 600-1000 km.

Fig. 122 summarizes existing notions about the structure of the neutral upper atmosphere and ionosphere of Venus up to an altitude of about 1000 km. It shows the profiles n(h) and N_e(h), by starting with the most probable values of scale heights for neutral and ionized components (H_n and H_i). Both experimental data and theoretical estimates were used in estimates of the altitude profile of the neutral atmosphere.

Let us now turn briefly to the problem of Venus's interaction with surrounding space.

According to the measurements of Dolginov et al. on Venera-4, the strength of the planet's own magnetic field is less than 1/3000 of the Earth's [52, 52a]. Venus therefore has no radiation belts /364
(the intensity of the captured radiation is at least 10^6 times less than near the Earth) [530,554a]. By using the measured (by Gringauz et al. [226]) parameters of plasma in the undisturbed solar wind and in disturbed zones near the planet, the formation of a shock wave from the day side and an ionopause are assumed (cf. Fig. 55).

It can be assumed that the energy of the oncoming flux is transformed into magnetic and heat energy in the region inside the shock wave. According to the model of Bauer et al. [192], the strength of the magnetic field increases from about 10 gammas in an undisturbed flux to 40 gammas in the vicinity of the ionopause, whereas the proton temperature increases from $3 \cdot 10^5$ to $4 \cdot 10^6$°K. The ionopause forms in the zone where the solar wind pressure $P_w = nmv^2 = 1.6 \cdot 10^{-8}$ dyne cm^{-2} is counterbalanced by the pressure of ionospheric charged particles and, possibly, by a small pressure from the planet's own magnetic field. In the ideal case of an ionosphere of infinite /365
conductivity, the flows induced by solar wind flux lie on the surface of the ionopause and the region directly adjoining it from the top. Therefore, the resulting induced magnetic field is located outside the ionosphere. A nearly analogous situation apparently holds true even in the more realistic case of an ionosphere of finite conductivity. This is related to the fact that the time of magnetic diffusion t_D is much greater than the time in which the direction of the interplanetary magnetic field changes and is even greater than the length of the Venusian day. As a result, diffusion of the interplanetary magnetic field into the undisturbed ionosphere is negligible. A precise estimate of the extent to which it penetrates requires a combined examination of the effects of change in the direction of the field and the planet's own rotation.

ORIGINAL PAGE IS
OF POOR QUALITY

Fig. 122. The concentration of neutral particles and electrons vs altitude in the Venusian atmosphere. I and II are models of the nighttime ionosphere with various assumptions with regard to the structure of the "plasma tail" [304]. III is a model of the neutral atmosphere. IV is a model of the daytime ionosphere. V is the daytime plasmapause.

If subsequent measurements show that there is an appreciable magnetic field inside the ionosphere, the nature of this field could be various: either related to the existence of a weak magnetic moment of the planet, or to electrical currents arising from large-scale ionospheric irregularities, or, finally, to an increased magnetic diffusion, i.e., a shorter t_D. A situation corresponding to this last case could occur, for example, if the effective distance ℓ_e, at which the magnetic field can be considered homogeneous, turned out to be much less than the value on the order of R_{φ}. Such a possibility can in principle occur if the region studied has a wave structure caused by the turbulent character of the flux at the upper boundary of the ionosphere, with characteristic wavelength $\sim\ell_e \ll R$.

A more detailed examination of the mechanism by which solar plasma surrounds Venus, as well as estimates of the parameters in the boundary region and in the induced "ionopause" (or "magnetopause"), which are themselves of interest, can be found in [47, 192, 246, 512]. The most comprehensive conceptions, which are based on Mariner-5 data, are developed by Ness et al. [582] and by Bridge et al. [569].

There are still many complicated problems in the physics of Venus. Without doubt, spacecraft will play the deciding role in resolving these problems, and it is to be expected that the next few years alone will bring new and significant information. This information, together with further progress in the methods of ground-based measurements and theoretical modelling of the planetary atmosphere, will allow us to expand our conceptions of the structure and physical features of the planet closest to Earth. /366

APPENDIX

/367

Atmospheric Model of Venus

Fundamental Propositions. This model, which has been calculated by Marov and Ryabov [102], establishes numerical values of the basic thermodynamic parameters and other physical characteristics of the Venus atmosphere for the region of altitudes from -6 km to 1000 km.

The chemical compositon of the atmosphere is given in Table 11, according to the direct Venera measurements, the data of ground-based spectroscopy and other estimates. A mean molecular weight $\bar{\mu}$ is assumed for the model by using the following contents by weight of the basic atmospheric components: CO_2 - 97%; N_2 - 2%; H_2O and others - 1%. For this composition, $\bar{\mu} = 43.4$. It is assumed that this value and, thus, the prevalent CO_2 content, remains unchanged up to an altitude of 200 km. Using approximate estimates of atomic oxygen, helium, and hydrogen content in the upper atmosphere (cf. Section VI.2), the profile of change in mean molecular weight shown in Fig. 123 was assumed above this level.

The data from temperature and pressure measurements on the Venera spacecraft, data which cover altitudes from 55 km to the surface, are used as a basis for calculating the parameters of the lower atmosphere. The state of gas remained practically adiabatic throughout the entire region of measurements. Using this, calculations of temperature and pressure in the troposphere correspond to an adiabatic approximation. In the basic calculated model, the value of temperature at the mean surface level is taken to be equal to 750°K. The results of radio measurements are in good agreement with this value. This fact, as well as the absence of pronounced diurnal and latitudinal variations in temperature in the troposphere allow us to apply this model to any point on the surface of the planet. Two additional models -- a maximum and a minimum -- were calculated as limiting cases. They take account of the possible deviations from the mean statistical values of T and P at the level where the results of all Venera measurements are matched (the so-called reference point: cf. Section IV.3).

The altitude profile of temperature and pressure in the Venusian stratosphere up to the region of the temperature minimum (the mesopause) is based on the results of radio refraction measurements of Mariner-5. Accordingly, $T_{mes} \approx 150°K$ has been assumed. In this case, however, disagreement of about an order of magnitude has been discovered in estimates of the value of numerical density at the Regulus occultation level (cf. Section IV.6). This discrepancy is a shortcoming of the model. In constructing the calculated profiles of parameters in the Venusian thermosphere, an estimate of exospheric temperature from the measurements of the resonance mean emission in L_α $T_\infty = 650°K$ has been accepted as a point of departure;

/368

this temperature refers approximately to the mean level of solar activity (the index of decimetric solar radio emission is $F_{10.7} \approx 130 \cdot 10^{-22}$ w·m^2 Hz^{-1}). The profiles T, P, and ρ up to altitudes of 1000 km are calculated from the condition of the constancy of T_∞ in the lower exosphere and the character of the change in $\bar{\mu}(h)$ according to Fig. 123.

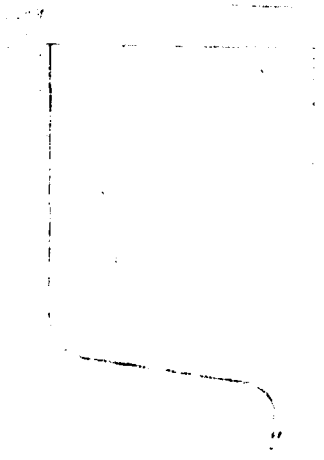

Fig. 123. Model profile of variation of mean molecular weight of the Venusian atmosphere vs altitude.

Because experimental and theoretical data are limited, the altitude profiles of parameters in the stratomesosphere are tentatively taken to be similar to the mean model. Variations of exospheric temperature as a function of variation in solar activity during the 11-year solar cycle (from $F_{10.7} \approx 250$ at a maximum to $F_{10.7} \approx 70$ at a minimum) are, according to current estimates, from 400°K to 900°K (cf. Section IV.4). These values are accepted correspondingly for the minimum and maximum models.

The most valid part of the model is for the region from 0 to 80 km above the surface. It is precisely to this region that the direct measurements of the Venera stations and the Mariner-5 radio probes refer. The model, which is based on available (and rather limited) experimental material, is a preliminary model and will be subject to further refinement as new data are obtained.

Starting parameters. The following values are used in the construction of the model.

Geopotential altitude

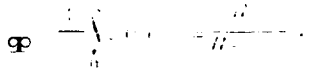

ORIGINAL PAGE IS OF POOR QUALITY

where g(h) and g_0 are the gravitational acceleration on Venus at altitude h and at a mean surface level corresponding to the mean radius of Venus R_φ.

Molecular temperature:

Where T is the kinetic temperature, and M_s and M are the molecular /369 weight of gas at the mean surface level and at altitude h[1].

The molecular temperature gradient at any geopotential altitude:

$$Q = \frac{\Delta T_v}{\Delta h}$$

Values of temperature T and molecular weitht M, which are given in the table as a function of altitude, are taken to be the starting parameters.

Values of physical characteristics of the atmosphere at the surface.

Barometric pressure

Model I (basic model)	$P_s = 9.74 \cdot 10^6$ N/m^2 (99.3 kg/cm^2)
Model II	$P_s = 9.34 \cdot 10^6$ N/m^2 (95.2 kg/cm^2)
Model III	$P_s = 1.02 \cdot 10^7$ N/m2(104.0 kg/cm^2)

Temperature

Model I (basic model)	$T_s = 750°K$
Model II	$T_s = 757°K$
Model III	$T_s = 743°K$
Molecular weight	$M_s = 43.4$

ORIGINAL PAGE IS
OF POOR QUALITY

Physical constants: gas constant
universal R = 8.314 joule/deg.molc

$$\text{specific } R_0 = \frac{R}{M_s} = 191.57 \text{ joule/deg·kg}$$

Coefficient of viscosity for CO_2 at T = 273.16°K in the region of moderate pressures

μ_{T_0} = 0.0146 gm/m·grad

Ratio of heat-capacity at constant pressure and heat-capacity at constant volume in normal conditions

$$\mu_{T_0} = 1365 \cdot 10^{-8} \text{ N·sec/m}^2$$

The functions $C_p(T,P)$, $C_v(T,P)$ are taken according to [36].

---

[1] Here and herinafter M designates the molecular weight, in order to avoid confusion with dynamic viscosity μ.

Acceleration of free fall on the surface

$$g_0 = 8.8 \text{ m/sec}$$

Mean radius of Venus /370

$$R_{\varphi} = 6{,}050{,}000 \text{ m}$$

ORIGINAL PAGE IS
OF POOR QUALITY

Avogadro's number

$$N_A = 6.02470 \cdot 10^{23} \text{ mol}^{-1}$$

Calculated formulas. Values calculated in the tables from the following formulas:

Pressure in an isothermal layer (Q = 0)

$$P = P_* \exp\left[-\frac{g_0 (h_{gp} - h^*_{gp})}{R_0 \cdot T_M n(T, P)}\right],$$

in a layer with a linearly varying temperature (Q = const.)

$$P = P_* \left(\frac{T_M}{T^*_M}\right)^{\frac{g_0}{R_0 n(T, P) Q}},$$

where n(T,P) is the CO_2 compressibility factor [36]. The superscript * shows that the value refers to the lower boundary of the layer under discussion.

Density:

$$\rho = \frac{P}{T_M R_0 n(T, P)}.$$

Acceleration of free fall:

$$g = g_0 \left(\frac{R_{\varphi}}{R_{\varphi} + h}\right)^2.$$

Speed of sound:

$$a = \sqrt{\varkappa R_0 T} = 15{,}52 \cdot \sqrt{T}.$$

Dynamic coefficient of viscosity to altitudes of h ≤ 50 km [36]:

$$\eta = \eta_0 \cdot \frac{T_0 + 198{,}6}{T + 198{,}6} \cdot \left(\frac{T}{T_0}\right)^{1{,}5} = 1{,}2057 \cdot 10^{-5} \cdot \frac{T^{1{,}5}}{T + 198{,}6} \text{ N} \cdot \text{sec/m}^2$$

$$\eta_P = \eta_1 \cdot P^{0{,}5} \cdot \left(\frac{T}{T_1}\right)^{0{,}5} = \frac{T^{0{,}5}}{215{,}16}$$

Dynamic coefficient of viscosity for altitudes of h > 50 km [19]:

$$\mu = \mu_0 \frac{T_0 + 254}{T + 254} \left(\frac{T}{T_0}\right)^{3/2}$$

Kinematic coefficient of viscosity:

$$\nu = \frac{\mu}{\rho}$$

Coefficient of heat conductivity to altitudes of h $\leq$ 50 km [36]:

$$\lambda = \lambda_0 \cdot 10^3 = 0{,}4216 + 1{,}1738 \cdot 10^{-3} T - 1{,}7717 \cdot 10^{-6} T^2 + 1{,}2964 \cdot 10^{-9} T^3 \text{ w/m} \cdot \text{grad}, \quad \lambda_0 = \lambda_{273} \cdot 10^{-3},$$
$$= 1{,}5896 - 0{,}2245\,0 + 0{,}0755 \cdot 10^{-3} \cdot 0^2 - 2{,}5285 \cdot 10^{-6} \cdot 0^3.$$

Coefficient of heat conductivity for altitudes of h > 50 km: /371

$$\lambda = 1{,}51 \cdot 10^{-8} \frac{(1 + 1026 \cdot 10^{-6} \cdot P)\, T^{1/2}}{1 + \frac{254}{T}} \text{ w/m} \cdot \text{deg}$$

Mean free path of molecules:

$$\bar{l} = \frac{\mu}{0{,}499 \bar{W} \rho} = 1{,}255 \nu \sqrt{\frac{\rho}{P}} \text{ (m)},$$

ORIGINAL PAGE IS OF POOR QUALITY

where $\bar{W}$ is the mean arithmetic molecular velocity.

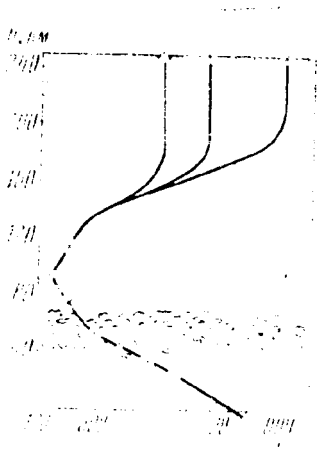

Fig. 124. Temperature profile of the Venusian atmosphere vs altitude for three models.

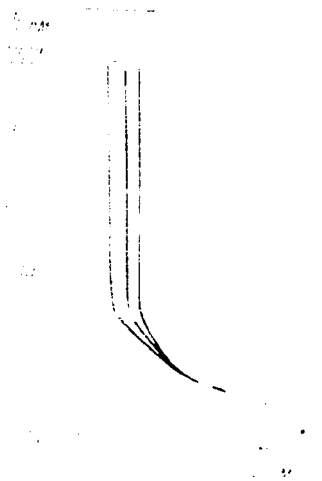

Fig. 125. Pressure profile in the Venusian atmosphere vs altitude for three models.

Scale height:

ORIGINAL PAGE IS
OF POOR QUALITY

Number of particles per unit volume:

Tables. Tables 24-25 give the basic model of the Venusian atmosphere. Altitude profiles of temperature, pressure, and numerical density for the basic, the maximum and the minimum models are shown in Figs. 124-126. On the graphs the basic model I is shown by the "+", model II by the "x", and model III by the diamond. Tables of II and III are given in [102].

For altitudes from -6 to 100 km, values of temperature and molecular weight are given at every two km; for altitudes 100-200 km, every 5 km; for altitudes 200-500 km, every 25 km; and for altitudes 500-1000, every 50 km. In each of these segments of the temperature profile, the gradient of molecular temperature with geopotential altitude is considered constant or equal to zero. The values of pressure P and density ρ are calculated from the equations of hydrostatic equilibrium and gas state, with deviations from ideal gas conditions at high T and P taken into account according to [36].

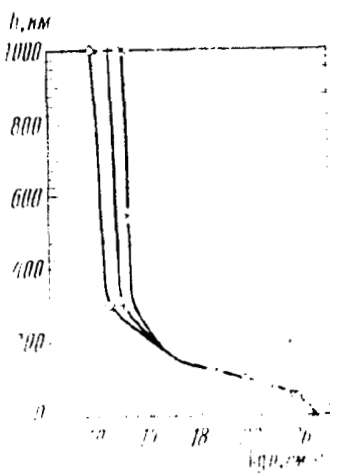

Fig. 126. Density profile of the Venusian atmosphere vs altitude for three models.

The values of the physical parameters of the atmosphere are given in MKS System of Units (and pressure in kg/cm^2 also).

temperature T (deg K)
pressure P (N/m^2)
density ρ (kg/m^3)
speed of sound a (m/sec)
dynamic coefficient of viscosity μ(kg/m·sec)
kinematic coefficient of viscosity ν (m^2/sec)
acceleration of free fall g(m/sec^2)
coefficient of heat conductivity λ (w/m·deg)
number of particles per unit volume n (m^{-3})
mean molecular free path $\bar{\ell}$(m)
scale height H (m)

For the sake of convenience, the relations between units of measurement are given:

pressure 1 N/m^2 = 10:1972·10^{-2} kg/cm^2
density 1 kg/m^3 = 10^{-3} g/cm^3
dynamic coefficient of viscosity: 1 N sec/m^2 = 10 P = 10^3 cP
coefficient of heat conductivity: 1 w/m deg = 2.3866·10^6 kcal/cm sec deg = 0.8598 kcal/m hour deg

TABLE 24. BASIC MODEL OF THE VENUSIAN ATMOSPHERE

h, km	r, km	T °K	P, kg/cm^2	P, N/m^2	ρ, kg/m^3	n, m^{-3}	g, m/sec^2
−6	6044	797	1.4·10^2	1.39·10^7	8.91·10^1	1.2·10^{27}	8.817
−4	6046	781	1.26	1.24	8.13	1.1	8.812
−2	6048	766	1.12	1.10	7.41	1.0	8.806
0	6050	750	9.93·10^1	9.74·10^6	6.73	9.3·10^{26}	8.800
2	6052	734	8.78	8.62	6.09	8.5	8.794
4	6054	718	7.75	7.60	5.51	7.6	8.788
6	6056	702	6.81	6.68	4.96	6.9	8.783
8	6058	686	5.97	5.85	4.46	6.2	8.777
10	6060	670	5.21	5.11	3.99	5.5	8.771
12	6062	654	4.54	4.45	3.57	5.0	8.765
14	6064	637	3.95	3.86	3.18	4.4	8.759
16	6066	621	3.43	3.36	2.82	3.9	8.754
18	6068	604	2.98	2.87	2.50	3.5	8.748
20	6070	587	2.61	2.56	2.20	3.1	8.742
22	6072	570	2.34	2.29	1.97	2.7	8.736
24	6074	553	1.82	1.78	1.69	2.4	8.731
26	6076	536	1.54	1.51	1.48	2.1	8.725
28	6078	519	1.29	1.27	1.28	1.8	8.719
30	6080	502	1.08	1.06	1.11	1.5	8.713
32	6082	484	8.95·10^{-1}	8.78·10^4	9.58·10^0	1.3	8.708
34	6084	466	7.39	7.25	8.18	1.1	8.702
36	6086	448	6.05	5.93	6.96	9.7·10^{25}	8.696
38	6088	430	4.91	4.82	5.89	8.2	8.690
40	6090	412	3.96	3.88	4.95	6.9	8.685
42	6092	394	3.15	3.09	4.13	5.7	8.679
44	6094	376	2.49	2.44	3.42	4.8	8.673
46	6096	358	1.94	1.90	2.81	3.9	8.668
48	6098	340	1.49	1.46	2.28	3.2	8.662
50	6100	317	1.13	1.11	1.81	2.5	8.656
52	6102	300	8.50·10^{-1}	8.24·10^4	1.43	2.0	8.651
54	6104	285	6.47	6.35	1.11	1.5	8.645
56	6106	270	4.86	4.78	8.37·10^{-1}	1.2	8.639
58	6108	263	3.69	3.63	6.21	8.6·10^{24}	8.634
60	6110	254	2.85	2.81	4.53	6.3	8.628
62	6112	246	2.20	2.17	3.26	4.5	8.622
64	6114	239	1.68	1.66	2.32	3.2	8.617
66	6116	232	1.29·10^{-1}	1.25·10^3	1.63	2.3	8.611
68	6118	225	9.99	9.80	1.13	1.6	8.605
70	6120	218	7.73	7.58	7.81·10^{-2}	1.1	8.600
72	6122	211	5.98	5.86	5.31	7.4·10^{23}	8.594
74	6124	204	4.62	4.53	3.57	5.0	8.589
76	6126	197	3.56·10^{-2}	3.49·10^2	2.36	3.3	8.583
78	6128	190	2.72	2.67	1.51	2.1	8.577
80	6130	183	2.07	2.03	9.91·10^{-3}	1.4	8.572
82	6132	176	1.57	1.54	6.56	9.2·10^{22}	8.566

ORIGINAL PAGE IS
OF POOR QUALITY

Table 24 (continued)

km	, km		P, kg/cm^2	P, N/m^2	ρ, kg/m^3	n, m^{-3}	g, m/sec^2
	61	16	1.28	1.25	1.88	5.4	8.561
	61	16					8.555
	61						8.549
	61						8.544
	61						8.538
	61						8.533
	61						8.527
	61						8.522
	61						8.516
	61						8.502
	61						8.489
	61						8.475
	61						8.461
	61						8.447
	61						8.434
	61						8.420
	61						8.406
	61						8.393
	61						8.379
	61						8.366
	61						8.352
	61						8.339
	61						8.326
	61						8.312
	61						8.299
	61						8.286
	61						8.180
	61						7.712
	61						7.687
	61						7.662
	61						7.636
	61						7.508
	61						7.483
	61						7.458
	61						7.433
	61						7.408
	61						6.665
	61						6.481

ORIGINAL PAGE IS
OF POOR QUALITY

TABLE 25. BASIC MODEL OF THE VENUSIAN ATMOSPHERE

h, km	a m/sec	μ N·sec/m²	ν m²/sec	λ w/m·deg	H, m	T, m	M
-6		$3.52 \cdot 10^{-5}$					

Table 25 (continued)

h, km	a m/sec	μ N·sec/m²	ν m²/sec	λ w/m·deg	H, m	$\bar{l}$, m	M
84	200	8.32	2.14	7.85	3775	$1.5 \cdot 10^{-5}$	43.4
86	197	8.01	3.42	7.51	3650	2.4	43.4
88	193	7.68	5.54	7.16	3518	4.0	43.4
90	191	$7.46 \cdot 10^{-6}$	$9.32 \cdot 10^{-3}$	$6.93 \cdot 10^{-3}$	3430	$6.8 \cdot 10^{-5}$	43.4
92	189	7.30	$1.61 \cdot 10^{-2}$	6.76	3365	$1.2 \cdot 10^{-4}$	43.4
94	189	7.30	2.92	6.76	3368	2.2	43.4
96	189	7.35	5.35	6.81	3392	4.0	43.4
98	193	7.68	$1.04 \cdot 10^{-1}$	7.16	3529	7.5	43.4
100	197	8.01	1.96	7.51	3667	$1.4 \cdot 10^{-3}$	43.4
105	206	8.82	8.67	8.40	4011	5.9	43.4
110	214	9.63	$4.39 \cdot 10^{0}$	9.30	4356	$2.2 \cdot 10^{-2}$	43.4
115	222	$1.04 \cdot 10^{-5}$	$1.19 \cdot 10^{1}$	$1.02 \cdot 10^{-2}$	4702	7.5	43.4
120					5049		43.4
125					5433		43.4
130					5941		43.4
135					6631		43.4
140					7503		43.4
145					8533		43.4
150					9667		43.4
155					10838		43.4
160					11968		43.4
165					12984		43.4
170					13822		43.4
180					14825		43.4
190					15053		43.4
200					15101		43.4
225					15222		43.4
250					15855		42.0
275					17210		39.0
300					28188		24.8
325					75761		9.0
350					171803		4.0
375					230863		3.0
400					279196		2.5
425					293088		2.4
450					295356		2.4
475					310573		2.3
500					327182		2.2
525					348015		2.1
550					370974		2.0
575					376573		2.0
600					402331		1.9
650					414341		1.9
700					450222		1.8
750					463272		1.8
800							
900							
1000							

ORIGINAL PAGE IS
OF POOR QUALITY

REFERENCES

1. Avduyevskiy, V.S., N.F. Borodin, V.V. Kuznetsov, A.I. Livshits, M. Ya. Marov, V.V. Mikhnevich, M.K. Rozhdestvenskiy, and V.A. Sokolov, "Temperature, pressure and density of the Venus atmosphere according to the measurements of the Venera-4 automatic interplanetary station," Dokl. AN SSSR 179/2, 310 (1968).

2. Avduyevskiy, V.S., F.S. Zavelevich, M.Ya. Marov, A.I. Noykina, and V.I. Polezhayev, "The thermal regime and convective motions in the lower layers of the Venusian atmosphere," in the coll: Fizika Luny i planet [The physics of the Moon and planets], Nauka, 1972, pp. 383-388.

3. Avduyevskiy, V.S., M.Ya. Marov, and M.K. Rozhdestvenskiy, "The results of measurements of the parameters of the Venusian atmosphere on the Soviet AIS Venera-4," Kosmich. Issled. 7/2, 233-246 (1969).

4. Avduyevskiy, V.S., M. Ya., Marov, and M.K. Rozhdestvenskiy, "The results of measurements on the automatic stations Venera-5 and Venera-6 and a model of the Venusian atmosphere," Kosmich. Issled. 8/6, 871-881 (1970).

5. Avduyevskiy, V.S., F.S. Zavelevich, M.Ya. Marov, A.I. Noykina, and V.I. Polezhayev, "Numerical modelling of radiative convective heat transfer in the Venusian atmosphere," Kosmich. Issled. 9/2, 280-291 (1971).

6. Avduyevskiy, V.S., M. Ya. Marov, and M.K. Rozhdestvenskiy, "Model of the Venusian atmosphere according to the data of direct measurements," in the coll: Fizika Luny i planet [The physics of the Moon and the planets], Nauka, 1972, pp. 254-261.

7. Avduyevskiy, V.S., "Several scientific and technical problems of the creation of the landers of the Venera series," Report at the XXIV Congress of the MAF, Baku, October 8 - 13, 1973.

8. Avduyevskiy, V.S., M. Ya. Marov, B. Ye. Moshkin, and A.P. Ekonomov, "The results of direct measurements of illumination in the atmosphere and on the surface of the planet Venus during the flight of the AIS Venera-8," Dokl. AN SSSR 210/4-6 799-802 (1973).

9. Aleksandrov, Yu. N., O.N. Rzhiga, and A.M. Shakhovskoy, "Studies of the radio signals transmitted by the Soviet interplanetary station Venera-7 during landing on the surface of Venus, with the use of a digital computer," Kosmich. Issled. 9/6, 904-911 (1971).

10. Allen, K.U., Astrofizicheskiye velichiny [Astrophysical values], I.L., 1960.

11. Barabashov, N.P., Issledovaniye fizicheskikh usloviy na Lune i planetakh [Studies of the physical conditions on the Moon and planets], Khar'kov University, Khar'kov, 1952.

12. Basharinov, A.E., Yu. N. Vetukhnovskaya, V.P. Galaktionov, I.B. Drozdovskaya, S.T. Yegorov, M.A. Kolosov, V.D. Krotikov, N.N. Krupenio, A.D. Kuz'min, V.A. Lodygin, L.I. Malafeyev, Ye.I. Omel'chenko, V.S. Troitskiy, N.Ya. Shapirovkaya, A.M. Shutko, and O.B. Shchuko, "The results of observing the radio emission of the planet Mars according to the data of the experiment on the AIS Mars-3," Kosmich. Issled. 11/5, 803-806 (1973).

13. Bates, D.R., "The airglow of the atmosphere," in the coll: Fizika verkhney atmosfery [Physics of the upper atmosphere], Ed. by G.A. Ratcliffe, Fizmatgiz, Moscow, 1963.

14. Buryukov, Yu.L. and L.G. Titarchuk, "On determining the characteristics of scattering particles in the Venusian atmosphere on the basis of photometric measurements," Kosmich. Issled. 10/4, 576-579 (1972).

15. Biryukov, Yu. L., A.S. Panfilov, and L.G. Titarchuk, "Estimates of the optical characteristics of the atmosphere of Venus with reference to the problem of photographing its clouds and surface," in the coll: Kosmicheskaya ikonika [Space iconometry], Nauka, 1973, p. 106.

16. Bogomolov, A.F., Osnovy radiolokatsii [The fundamentals of Radar], Sov. Radio, 1954.

17. Boltzmann, L., Lektsii po teorii gazov [Lectures on the theory of gases], Gostekhizdat, Moscow, 1956.

18. Brent, D., Fizicheskaya i dinamicheskaya meteorologiya [Physical and dynamical meteorology], Gostekhizdat, 1938.

19. Bretshnayder, S.T., Svoystva gazov i zhidkostey [The properties of gases and fluids], Khimiya, 1966.

20. Bronshten, V.A., "The nature of Venus (a survey)," Astr. Vestnik 1/1, 4-27 (1967).

21. Van de Hulst, G., Rasseyaniye sveta malymi chastistami [The scattering of light by small particles], I.L. Moscow, 1961.

22. "Venera-8; the results of its journey into space," Pravda, No. 254, September 10, 1972.

23. Vetukhnovskaya, Yu.N., A.D. Kuz'min, B.G. Kutuza, B. Ya. Losovskiy, and A. Ye. Salomonovich, "Measurements of the spectrum of the radio emission of the night side of Venus in the centimeter range of wavelengths," Izv. vuzov. Radiofizika 6/5, 1054-1056 [1963).

24. Vetukhnovskaya, Yu. N., Radioastronomicheskiye izmereniya Venery i nekotoryye rezul'taty ikh interpretirovaniya na osnove dannykh AIS Venera-4 [Radio astronomy measurements of Venus and several results from an interpretation of these measurements on the basis of AIS Venera-4 data], Dissertation, FIAN, 1969.

25. Vetukhnovskaya, Yu. N., A.D. Kuz'min A.P. Naumov, and T.V. Smirnova, "Determination of the parameters of the Venusian atmosphere at the mean surface level according to radio astronomy and radar measurements," Astron. Zh. 48/1, 146-156 (1971).

26. Vetukhnovskaya, Yu. N., A.D. Kuz'min, and B. Ya. Losovskiy, "Measurements of the phase change of the radio emission of Venus at wavelength 8.2 μm," Astr. Zh. 48/5, 1033-1037 (1971).

27. Vinichenko, N.K., N.Z. Pinus, S.M. Shmeter, and Shur, G.N., Turbulentnost' v svobodnoy atmosfere [Turbulence in a free atmosphere], Gidrometeoizdat, Leningrad, 1968.

28. Vinogradov, A.P., Vvedeniye v geokhimiyu okeana [Introduction to the geochemistry of the oceans), Nauka, Moscow, 1967.

29. Vinogradov, A.P., Yu. A. Surkov, K.P. Florenskiy, and B.M. Andreychikov, "Determination of the chemical composition of the Venusian atmosphere by the Venera-4 interplanetary station," Dokl. AN SSSR 179/1, 37-40, (1968).

30. Vinogradov, A.P., "Atmospheres of the planets of the solar system," Vestnik Moskovskovo universiteta, ser. geologiya, 4, 3-14 (1969).

31. Vinogradov, A.P., Yu. A. Surkov, and B.M. Andreychikov, "Studies of atmospheric composition on the Venera-5 and Venera-6 automatic stations," Dokl. AN SSSR 190/3, 552-554 (1970).

32. Vinogradov, A.P., Yu. A. Surkov, B.M. Andreychikov, O.M. Kalinkina, and I.M. Grechishcheva, "The chemical composition of the Venusian atmosphere," Kosmich. Issled. 8/4, 578-587 (1970).

33. Vinogradov, A.P., and V.P. Volkov, "On Wollaston equilibrium as a mechanism determining the atmospheric content of Venus," Geokhimiya 7, 755 (1971).

34. Vinogradov, A.P., Yu. A. Surkov, F.F. Kirnozov, and V.N. Glazov, "The content of naturally-occurring radioactive elements in Venusian rock according to the data of the Venera-8 automatic station," Geokhimiya, 1, 3 (1973).

35. Vlasyuk, M.P., and V.I. Polezhayev, Issledovaniye statsionarnoy pronikayushchey konvektsii szhimayemogo gaza v atmosfere [Studies of stationary penetrative convection of a compressive gas in the atmosphere], Preprint of IPM, No. 46, 1972.

36. Vukalovich, M.P., and V.V. Altunin, Teplofizicheskiye svoystva dvuokisi ugleroda [Thermophysical properties of carbon dioxide], Atomizdat, 1965.

37. Galin, V. Ya., N.L. Lukashevich, and Ye. M. Feygel'son,"The reflection of solar light from the atmosphere of Venus," Dokl. AN SSSR 197/2, 315-318 (1971).

38. Gal'tsev, A.P. and M.A. Odishariya, "CO_2 absorption bands at 7.2, 7.8, 9.4, 10.4 and 15 μm at increased pressure," Izvestiya AN SSSR, Fizika Atmosfery i Okeana 6/9, 881-888 (1970).

39. Gal'tsev, A.P. and V.M. Osipov, "Calculation of the transmission of infrared CO_2 bands at high temperatures and pressures. The band system 9.4 - 10.4 μm," Izvestiya AN SSSR, Fizika Atmosfery i Okeana 7/8, 857-870 (1971).

40. Germogenova, T.A. and N.V. Konovalov, "Asymptotic characteristics of the solution of the equation of transfer in the problem of an unhomogeneous layer," Zh. Vychisl. Matem. i Matem. Fiziki. 14/4 (1974).

41. Ginzburg, A.S., Ye. M. Feygel'son, "Several optical properties of the Venusian atmosphere and the regime of radiative equilibrium," Kosmich. Issled. 7/2 , 258-265 (1969).

42. Girshfel'der, D., Ch. Kertiss, and R. Berd, Molekulyarnaya teoriya gazov i zhidkostey [Molecular theory of gases and fluids, I.L. 1961.

43. Golitsyn, G.S., "Estimates of several characteristics of general circulation in the atmospheres of the planets of the terrestrial group," Izvestiya AN SSSR, ser. Fizika Atmosfery i Okeana 4/11, 1131-1138 (1968).

44. Golitsyn, G.S., "Dimensionless theory for large-scale motions of planetary atmospheres," Dokl. AN SSSR 190/2, 323-326 (1970).

45. Golitsyn, G.S. and V.V. Kerzhanovich, V.V. "Mutual relationships of atmospheric parameters measured on a spacecraft: the descent velocity of a spacecraft," Kosmich. Issled. 9/6, 896-903 (1971).

46. Golitsyn, G.S., Vvedeniye v dinamiky planetnykh atmosfer [Introduction to the dynamics of planetary atmospheres], Gidrometeoizdat, 1973.

47. Gringauz, K. I., V.V. Bezrykikh, L.S. Musatov, and T.K. Breus, "Plasma measurements made near Venus on the Venera-4 spacecraft," Kosmich. Issled. 6/3, 411-419 (1968).

48. Gringauz, K.I., and T.K. Breus, "Comparative ionospheric characteristics of the planets of the terrestrial group -- Mars, Venus, and the Earth," Kosmich. Issled. 7/6, 871-890 (1969).

49. Gred, G., "On the kinetic theory of rarefied gases," in the coll: Mekhanika [Mechanics], Series 4, No. 71, 61, I.L. 1952.

50. Goody, R., Atmosfernaya radiatsiya [Atmospheric radiation], Mir, Moscow, 1966.

51. Deirmendjian, G., Rasseyaniye elektromagnitogo izlucheniya sfericheskimi polidispersnymi chastitsami [Scattering of electromagnetic radiation by spherical polydisperse particles], Mir, 1971.

52. Dolginov, Sh. Sh., Ye. G. Yeroshenko, and L.N. Zhuzgov, "Studies of the magnetic field from the Venera-4 interplanetary station," Kosmich. Issled. 6/4, 561-575 (1968).

52a. Dolginov, Sh. Sh., Ye. G. Yeroshenko, and L.N. Zhuzgov, "The magnetic field near Venus," in the coll: Fizika Luny i planet [The physics of the Moon and planets], Nauka, 1972, pp. 283-288.

53. Yefanov, V.A., A.G. Kislyakov, I.G. Moiseyev, A.I. Naumov, "The radio emission of Venus at wavelengths 2 μm and 8 μm," in the coll: Fizika Luny i planet [The physics of the Moon and planets], Nauka, 1972, pp. 352-354.

54. Yefanov, V.A., A.G. Kislyakov, I.G. Moiseyev, and A.I. Naumov, "The radio emission of Venus at wavelengths 2.25 and 8 μm," Astr. Zh. 46/1, 147-151 (1969).

55. Zhevakin, S.A., and A.P. Naumov, "On the coefficient of absorption of electromagnetic waves by water vapor in the range 10 - 2 cm," Izv. vuzov, Radiofizika 6, 674-694 (1963).

56. Zege, E.P. O dvukhpotokovom priblizhenii v teorii perenosa izlucheniya [On the two-flux approximation in the theory of transfer of radiation], Minsk, 1971.

57. Zel'dovich, Ya. B., and Yu. P. Rayzer, Fizika udarnykh voln i vysokotemperaturnykh gidrodinamicheskikh yavleniy [The physics of shock waves and high temperature hydrodynamic phenomena], Nauka, Moscow, 1966.

58. Zilitinkevich, S.S., A.S. Monin, V.G. Turikov, and D.V. Chalikov, "Numerical modelling of the circulation of the Venusian atmosphere," Dokl. AN SSSR 197/6, 1291-1294 (1971).

59. Ivanovskiy, A.I., A.I. Repnev, and Ye. G. Shvidkovskiy, Kineticheskaya teoriya verkhney atmosfery [Kinetic theory of the upper atmosphere], Gidrometeoizdat, Leningrad, 1967.

60. Ivanovskiy, A.I., V.A. Marchevskiy, and A.I. Repnev, "A three-component model of a quiescent atmosphere," Trudy TsAO, No. 81, 10-26 (1969).

61. Ivanovskiy, A.I., A.I. Repnev, Ye. G. Shvidlovskiy, "Fluid mechanids equations for a model of a quiescent thermosphere," Trudy TsAO, No. 81, 3 (1969).

62. Ivlev, L.S., N.S. Bursakova, and O.M. Surikov, "Measurements of the distribution of atmospheric aerosols in the near-Earth layer," Problemy Fiziki Atmosfery, 6, 77-86, Leningrad University, Leningrad, 1968.

62a. Istomin, V.G., M Ya. Marov and V.V. Mikhnevich, "Scientific and practical aspects of studies of the structure of and variations in the parameters of the Earth's upper atmosphere," Meteorologiya i Gidrologiya, 6, 3-9 (1969).

63. Kargin, B.A., L.D. Krasnokutskaya and Ye. M Feygel'son, "Reflection and absorption of the Sun's radiant energy by cloud layers," Izv. AN SSSR, ser. Fizika Atmosfery i Okeana, 5, 505-517 (1972).

64. Kastrov, V.G., "Absorption of solar radiation in the lower troposphere," Trudy Tsentr. Aerol. Observ. No. 32, 73 (1959).

65. Kaula, U., Vvedeniye v fiziky planet zemnoy gruppy [Introduction to the physics of the planets of the terrestrial group], Mir, Moscow, 1971.

66. Kerzhanovich, V.V., B.N. Andreyev, and V.M. Gotlib, "Wind velocities and turbulence in the Venusian atmosphere obtained from the measurements of the Doppler velocity of the Venera-4 and Venera-6 automatic interplanetary stations," Kosmich. Issled. 10/2, 261-273 (1971).

67. Kerzhanovich. V.V., and M. Ya. Marov, "Circulation and dust content of the atmosphere of Venus according to the measurements of wind velocity on the AIS Venera-8," Dokl. AN SSSR 215/3 (1973).

68. Kozyrev, N.A., "On the airglow of the Venusian night sky," Izvestiya Krymskoy Astrofiz. Observ. 12, 169-176 (1954); in the collection: Voprosy astrofiziki [Problems of astrophysics], Kiev, 1965, pp. 12-13.

69. Kuiper, G., Atmosfery Zemli i planet [Atmospheres of the Earth and planets], I.L., 1951.

70. Kondrat'yev, K. Ya., and O.P. Filipovich, Teplovoy rezhim verkhnikh sloyev atmosfery [The thermal regime of the upper layers of the atmosphere], Gidrometeoizdat, Leningrad, 1960.

71. Kondrat'yev, K. Ya., Radiatsionnyye kharakteristiki atmosfery i zemnoy poverkhnosti, Gidrometeoizdat, Leningrad, 1969.

71a. Kondrat'yev, K.Ya., I. Ya. Badinov, L.S. Ivlev, and G.A. Nikol'skiy, "The aerosol structure of the troposphere and stratosphere," Izv. AN SSSR, ser. Fizika Atmosfery i Planet 5/5, 480 (1969).

72. Korol'kov, D.V., Yu. N. Pariyskiy, Yu. N. Timofeyeva, and S.E. Khaykin, High-resolution radio astronomy observations of Venus," Dokl. AN SSSR, 149/1 65-67 (1963).

73. Kotel'nikov, V.A., V.M. Dubrovin, M.D. Kislik, Ye. B. Korenberg, V.P. Minashin, V.A. Morozov, N.I. Nikitskiy, G.M. Petrov, O.N. Rzhiga, and A.M. Shakhovskoy, "Radar observations of Venus," Dokl. AN SSSR 145/5, 1035-1038 (1962).

74. Kotel'nikov, V.A., V.M. Dubrovin, V.A. Morozov, G.M. Petrov, O.N. Rzhiga, Z.G. Trunova, and A.M. Shakhovskoy, "Radar observations of Venus in 1961," Radiotekhnika i electronika 7/11, 1860-1872 (1962).

75. Kotel'nikov, V.A., V.M. Dubrovin, B.A. Dubinskiy, M.D. Kislik, B.I. Kuznetsov, I.V. Lishin, V.A. Morozov, G.M. Petrov, O.N. Rzhiga, G.A. Sytsko, and A.M. Shakhovskoy, "Radar observations of Venus in 1962 in the Soviet Union," Dokl. AN SSSR 151/3, 532-535 (1963).

76. Kotel'nikov, V.A., Yu. N. Aleksandrov. L.V. Apraksin, V.M. Dubrovin, M.D. Kislik, B.I. Kuznetsov, G.M. Petrov, O.N. Rzhiga, and A.V. Frantsesson, "Radar observations of Venus in 1964 in the Soviet Union," Dokl. AN SSSR 163/1, 50-53 (1965).

77. Kotel'nikov, V.A., "Radar observation of the planets," Vestnik AN SSSR, 2, 39-43 (1964).

77a. Krasnokutskaya, L.D., and Ye. M Feygel'son, "Calculations of fluxes of solar infrared radiation in a cloudy atmosphere," Izv. AN SSSR, ser. Fizika Atmosfery i Okeana 8/5 (1972).

78. Krasovskiy, V.I., "The chemistry of the upper atmosphere," in the coll: Iskusstvennyye sputniki Zemli [Artificial Earth satellites], AN SSSR, 17, 3-18 (1963).

79. Krotikov, V.D., "Several electrical characteristics of the Earth's rocks and a comparison with the characteristics of the surface layer of the Moon," Izv. Vuzov. Radiofizika 5/6, 1057-1061 (1962).

80. Kuz'min, A.D., and A. Ye. Salomonovich, "The radio emission of Venus in the 8 μm range of wavelengths," Astron. Zh. 37/2 297-300 (1960).

81. Kuz'min, A.D., and A. Ye. Salomonivich, "Observations of the radio emission of Venus and Jupiter at wavelength 8 μm," Astron. Zh. 39/4, 660-668 (1962).

82. Kuz'min, A.D., "Measurements of the brightness temperature of the illuminated side of Venus at wavelength 10.6 cm," Astron. Zh. 42/6, 1281-1286 (1965).

83. Kuz'min, A.D., and B.G. Clark, "The polarization measurement and the distribution of the brightness temperature of Venus at wavelength 10.6 cm," Astron. Zh. 43/3, 595-617 (1965).

84. Kuz'min, A.D., Radioastronomoicheskiye issledovaniya [Radio Astronomy Studies], Dissertation, FIAN, 1965.

85. Kuz'min, A.D., and U. Dent, "Measurement of brightness temperature and the polarization of the radio emission of Venus at wavelength 3.75 cm," Astron. Zh. 43/3, 692-694 (1966).

86. Kuz'min, A.D., Radiofizicheskiye issledovaniya Venery [Radio physical studies of Venus], VINITI, Moscow, 1967.

87. Kuz'min, A.D. and Yu. N. Vetukhnovskaya, "Venera-4 and the interpretation of radio astronomical measurements of Venus," Kosmich. Issled. 6/4, 590-597 (1968).

88. Kuz'min, A.D., A. D. Naumov, and T.V. Smirnova, "Estimate of ammonia content in the subcloud atmosphere of Saturn according to radio astronomy measurements," Astr. Vestnik 6/1 13-18 (1972).

89. Kurt, V.G., Ye. K. Sheffer, and S.B. Dostovalov, "Studies of ultraviolet radiation on the AIS Venera-4," in the coll: Fizika Luny i planet [The physics of the Moon and planets], Nauka, 1972, pp. 275-278.

90. Landau, L.D. and Ye. M. Livshits, Mekhanika sploshnykh sred [The mechanics of continuous mediums], Gostekhizdat, 1953.

91. Lomonosov, M.V., "The appearance of Venus on the Sun, observed in the St. Petersburg Imperial Academy of Sciences, May 26, 1761, St. Petersburg, 1761," Polynoye sobraniye sochineniy [Collected works], Vol. 4, AN SSSR, 1955, pp. 361-376.

92. Lukashevich, N.L., M. Ya. Marov, and Ye. M. Feygel'son, "On the interpretation of illumination measurements in the Venusian atmosphere," Kosmich. Issled. 12/2, 272-278 (1974).

93. MacDonald, G.G.F., "Motions in the upper atmosphere," in the coll: Geofizika (Okolozemnoye kosmicheskoye prostranstvo) [Geophysics; near-Earth space], Ed. by G.S. Golitsyn, Mir, 1964, p. 465.

94. Marov, M. Ya. "On the temperature and density of the thermosphere during the deep minimum period of solar activity," Kosmich. Issled. 6/1, 110-118 (1968).

95. Marov, M. Ya. "The atmosphere of the planet Venus," Vestnik AN SSSR 5, 72-81 (1969).

96. Marov, M. Ya. and A.V. Kolesnichenko, Osnovy matematicheskogo modelirovaniya planetnykh atmosfer. Chast' I, Sistema uravneniy mnogokomponentnoy gidrodinamiki dlya opisaniya neytral'noy verkhney atmosfery planety [The fundamentals of mathematical modelling of planetary atmospheres. Part I, A system of equations of multicomponent fluid dynamics for the description of the neutral upper atmosphere of a planet], IPM preprint, AN SSSR, Moscow, 1969.

97. Marov, M. Ya. Fizicheskaya struktura atmosfery Venery [Physical structure of the Venusian atmosphere], Dissertation, IPM, Moscow, 1970.

98. Marov, M. Ya. and A.V. Kolesnichenko, Osnovy matematicheskogo modelirovaniya planetnykh atmosfer. Chast' II, Sistema uravneniy mnogokomponentnoy plazmoy dlya opisaniya ionosfernykh protsessov [The fundamentals of mathematical modelling of planetary atmospheres. Part II, A system of equations of multicomponent plasma for the description of ionospheric processes], IPM preprint, AN SSSR, No. 19, Moscow, 1970.

99. Marov, M. Ya. "Model of the Venusian atmosphere," Dokl. AN SSSR 196/1, 67-70 (1971).

100. Marov, M. Ya., V.S. Avduyevskiy, M.K. Rozhdestvenskiy, N.F. Borodin, and V.V. Kerzhanovich, "Preliminary results of the study of the Venusian atmosphere by the AIS Venera-7," Kosmich. Issled. 9/4, 570-579 (1971).

101. Marov, M. Ya. and A.V. Kolesnichenko, "On the question of modelling a planetary heterosphere," Geomagnetizm i Aeronomiya 11/1, 40-50 (1971).

102. Marov, M. Ya. and O.L. Ryabov, Model' atmosfery Venery [Model of the Venusian atmosphere], IPM preprint, AN SSSR, No. 39, Moscow, 1972.

103. Marov, M. Ya., V.S. Avduyevskiy, V.V. Kerzhanovich, M.K. Rozhdestvenskiy, N.F. Borodin, and O.L. Ryabov, "Measurements of temperature, pressure, and wind velocity in the Venusian atmosphere on the AIS Venera-8," Dokl. AN SSSR 210/3, 559-562 (1973).

104. Marov, M. Ya., and V.N. Shari, Perenos dlinnovolnogo izlucheniya v nizhney atmosfere Venery [Transfer of long-wave radiation in the lower atmosphere of Venus], IPM preprint, AN SSSR, No. 23, 1973.

105. Martynov, D. Ya. and M.M Pospergelis, "Note on the photometric analysis of the structure of the Venusian atmosphere," Astron. Zh. 38/3, 558-561 (1961).

106. Martynov, D. Ya. "On the radius of Venus," Astron. Zh. 39/4, 653 (1962).

107. Martynov, D. Ya., "Again on the radius of Venus," Astron. Vestnik 3/2, 82-84 (1969).

108. Matveyev, L.T., Osnovy obshchey meteorologii, Fizika atmosfery [Fundamentals of general meteorology, the physics of the atmosphere], Gidrometeoizdat, 1965.

109. Minin, I.N. and V.V Sobolev, "On the theory of light scattering in planetary atmospheres," Astron. Zh. 40/3, 496-503 (1963).

110. Mints, I., "Estimates of general circulation in the atmospheres of the Earth and planets," in the book of Kellogg, W., and C. Sagan, Atmosfery Marsa i Venery [The atmospheres of Mars and Venus], I.L., Moscow, 1962.

111. Mikhnevich, V.V. and V.A. Sokolov, "Model of the Venusian atmosphere according to the results of direct measurements of temperature and density," Kosmich. Issled. 7/2, 220-232 (1969).

112. Monin, A.S. and A.M. Yaglom, Statisticheskaya gidromekhanika [Statistical fluid mechanics], Part 2, Nauka, Moscow, 1967.

113. Moroz, V.I., "The infrared spectrum of Venus (1 - 2.5 μm)," Astron. Zh. 40/1, 144-153 (1963).

114. Moroz, V.I., "New observations of the infrared spectrum of Venus (λ 1.2 - 3.8 μm)," Astron. Zh. 41/4, 711-719 (1964).

115. Moroz, V.I., "The phase effect of the strong CO_2 absorption bands in the Venusian spectrum" Astronomical circular No. 305, October 12, 1964.

116. Moroz, V.I., CO_2 bands and several optical properties of the Venusian atmosphere," Astron. Zh. 44/4, 816-827 (1967).

117. Moroz, V.I., Fizika planet [The physics of planets], Nauka, Moscow, 1967.

118. Moroz, V.I., and V.G. Kurt, "The atmosphere of Venus (a comparison of astronomical observations and direct experimentation)," Kosmich. Issled. 6/4, 576-585 (1968).

119. Moroz, V.I. Atmosfera Venery [The atmosphere of Venus], UFN, 104/2, 255-296 (1971).

119a. Moroz, V.I., "The polar tropopause of Venus," Astron. Zh. 48/3, 570-577 (1971).

120. Mur, P., Planeta Venera [The planet Venus], I.L. Moscow, 1961.

121. Nikole, M., Aeronomiya [Aeronomy], Mir, Moscow, 1964.

122. Obukhov, A.M., "On energy distribution in the spectrum of turbulent flux," Izv. AN SSSR, ser. Geograf. i Geofiz. 5/4-5, 453 (1941).

123. Obukhov, A.M. and G.S. Golitsyn, "An estimate of the lower boundary and thickness of the cloud layer on Venus," Kosmich. Issled. 6/5 759-764 (1968).

124. Obukhov, A.M. and G.S. Golitsyn, "The dynamics of the descent of automatic stations in planetary atmospheres as a means of checking measurement data," Kosmich. Issled. 7/1, 150-155 (1969).

125. Osipov, V.M., Teoreticheskiye issledovaniye IK-spektra CO_2 pri vysokikh temperaturakh i davleniyakh [Theoretical studies of the CO_2 infrared spectrum at high temperatures and pressures], Dissertation, 01.051-Geofizika, Leningrad, 1971.

126. Petrov. G.M., Opredeleniye astronomicheskoy yedinitsy po radiolokatsionnym nablyudeniyam planet, provodivshimsya v Sovetskom Soyuze v 1961, 1962 i 1964 gg [Determination of the astronomical unit from radar observations made in the Soviet Union in 1961, 1962 and 1964), Dissertation, IRE, 1968.

127. Polezhayev, V.I., "Numerical solution of a system of two-dimensional nonstationary Navier-Stokes equations for compressible gas in a closed region," Izv. AN SSSR, Mekhanika Zhidkosti i Gaza, 2, 103-111 (1967).

128. Polezhayev, V.I., "Numerical solution of a system of two-dimensional, nonstationary, Navier-Stokes equations of compressible gas in a closed region," Izv. Sibirskogo Otd. AN SSSR, ser. Tekhnich. Nauk. 3/13 73-80 (1967).

129. Polezhayev, V.I., "Current and heat exchange during natural convection of gas in a closed region after loss of hydrostatic equilibrium" Izv. AN SSSR, Mekhanika Zhidkosti i Gaza, 5, 124-129 (1968).

130. Polezhayev, V.I. and M.P. Vlasyuk, "Model of penetrative convection of a compressible gas in a deep atmosphere," Dokl. AN SSSR 201/3 552-555 (1971).

131. Polyakova, G.N., Ya. M. Fogel', and Tsyu Yu-mey, "Spectra of the luminescence of rarefied molecular gases excited by a mixed beam of protons and hydrogen atoms," Astron. Zh. 40/2, 351-362 (1963).

132. Prokof'yev, V.K., and N.N. Petrova, "The presence of oxygen in the Venusian atmosphere," Izvestiya Krymskoy Astrofiz. Observ. 29, 3-14 (1963).

133. Prokof'yev, V.K., "The presence of oxygen in the Venusian atmosphere," II, Izvestiya Krymskoy Astrofiz. Observ. 31, 276-280 (1964).

134. Prokof'yev, V.K., "The presence of oxygen in the Venusian atmosphere, III, Izvestiya Krymskoy Astrofiz. Observ. 34, 243-251 (1965).

135. Rzhiga, O.N., "The results of radar studies of the planets," Kosmich. Issled. 7/1, 84-91 (1969).

136. Rzhiga, O.N., "Analysis of the brightness temperature spectrum and the structure of the lower atmosphere of Venus," Astron. Zh. 47/3, 566-576 (1970).

137. Rozenberg, G.V. "The light characteristics of the thick layers of a scattering medium with little specific absorption," Dokl AN SSSR 145/4, 775-777 (1962).

138. Rozenberg, G.V., Sumerki [Twilight], Fizmatgiz, 1963.

139. Rozenberg, G.V., "The optical properties of the thick layers of a homogeneous scattering medium," in the coll: Spektroskopiya svetorasseivayushchikh sred [The spectroscopy of light scattering mediums], Minsk, 1963.

140. Romanova, L.M., "The solution of the equation of transfer of radiation with a scattering indicatrix strongly different from the spherical," Optika i Spektroskopiya 13/3, 429; 13/6, 819 (1962).

141. Romanova, L.M. "Photon distribution by paths in the flat layer homogeneous hazy medium," Izv. AN SSSR, ser. Fizika Atmosfery i Okeana 1/10, 1014, 1022-1038 (1965).

142. Selezneva, Ye.S., Atmosfernyye aerozoli [Atmospheric aerosols], Gidrometeoizdat, Leningrad, 1966.

143. Smirnova, T.V., Radioastronomicheskiye issledoyvaniya atmosfer Venery, Yupitera i Saturna [Radio astronomy studies of the atmospheres of Venus, Jupiter and Saturn), Dissertation, MFTI, 1973.

144. Smirnova, T.V., and A.D. Kuzmin, "Estimate of water vapor and ammonia content in the lower atmosphere of Venus according to radar measurements," Astron. Zh. 51/3 (1974).

145. Sobolev, V.V., "On the optical properties of the Venusian atmosphere," Astron. Zh. 21/5, 241-244 (1944).

146. Sobolev, V.V., Perenos luchistoy energii v atmosferakh zvezd i planet [The transfer of radiant energy in the atmospheres of stars and planets], Gostekhizdat, 1956.

147. Sobolev, V.V, "Studies of the Venusian atmosphere," I, Astron. Zh. 41, 97-103 (1964).

148. Sobolev, V.V., "Studies of the Venusian atmosphere," II, Astron. Zh. 45/1, 169-176 (1968).

149. Sobolev, V.V., Rasseyanie sveta v atmosferakh planet [The scattering of light in planetary atmospheres], Nauka, 1972.

150. Sobolev, V.V., "The optical properties of the Venusian atmosphere," in the coll: Fizika Luny i planet [The physics of the Moon and planets], Nauka, 1972, pp. 391-393.

151. Strelkov, G.M., "On the greenhouse effect in the Venusian atmosphere," Kosmich. Issled, 4/4, 581-591 (1966).

152. Strelkov, G.M., and N.F. Kukharskaya, "The greenhouse effect in the Venusian atmosphere," Kosmich. Issled, 7/2, 247-257 (1969).

153. Surkov, Yu. A., B.M. Andreychikov, O.M. Kalinkina, I.M. Grechishcheva, D.M. Sheynin, and A.I. Mochalkin, "The instruments on Venera-4, Venera-5 and Venera-6 for the study of the atmo heric composition of Venus," Kosmich. Issled. 8/5 777-783 (1970).

153a. Surkov, Yu. A., B.M. Andreychikov, O.M. Kalinkina, and I.M. Grechishcheva, "The cloud layer of Venus," in the coll: Ocherki sovremennoy geokhimii i analiticheskoy khimii (k 75-letiyu akad. A.P. Vinogradov) [Essays on Contemporary Geochemistry and Analytic Chemistry (on the 75th birthday of academician A.P. Vinogradov), Nauka, 1970, p. 17.

154. Surkov, Yu. A., B.M. Andreychikov and O.M. Kalinkina, "Ammonia content in the Venusian atmosphere according to the data of the automatic station Venera-8," Dokl. AN SSSR, 213/2, 296-298 (1973).

155. Tauns, Ch., and A. Shavlov, Radiospektroskopiya [Radiospectroscopy], I.L., Moscow, 1959.

156. Tikhonov, A.N., "On the solution of ill-posed questions and the methods of regularization," Dokl. AN SSSR 151/3, 501-504 (1963).

157. Tikhonov, A.P., "On the regularization of ill-posed questions," Dokl. AN SSSR 153/1, 49-52 (1963).

158. Turikov, V.G. and D.V. Chalikov, "A calculation of the general circulation of the atmosphere of the planet Venus," Izv. AN SSSR, Fizika Atmosfery i Okeana 7/7, 705-722 (1971).

159. Turgin, V.F., V.P. Kozlov, and M.S. Malkevich, "Studies on the methods of mathematical statistics for the solution of ill-posed questions," UFH 102/3, 345-386 (1970).

160. Fabelinskiy, I.L., Molekulyarnoye rasseyaniye sveta [The molecular scattering of light], Nauka, Moscow 1965.

161. Feygel'son, Ye. M., Radiatsionnyye protsessy v sloistoobraznykh oblakakh [Radiati processes in strata-like clouds], Nauka, Moscow, 1964.

162. Feygel'son, Ye. M., Spektral'noye otrazheniye radiatsii oblakami [The spectral reflection (by clouds) of radiation], Trudy GGO, No. 166, 1964.

163. Feygel'son, Ye. M., Luchisty teploobmen i oblaka [Radiative heat transfer and the clouds], Gidrometeoizdat, 1970.

164. Feygel'son, Ye. M., "Several optical properties of the Venusian atmosphere and the possibility of interpreting photometric and polarization measurements," Kosmich. Issled. 10/3, 411-422 (1972).

165. Fligl', R. and G. Buzinger, Vvedeniye v fiziky atmosfery [Introduction to atmospheric physics], Mir, Moscow, 1965, p. 134.

166. Khrgian, A. Kh., Fizika atmosfery [Physics of the atmosphere], 2nd edition, Nauka, Moscow, 1972.

167. Chandrasekar, S., Perenos luchistoy energii [The transfer of radiant energy], I.L., Moscow, 1953.

168. Chapman, S., and T. Cowling, Matematicheskaya teoriya neodnorodnykh gazov [The mathematical theory of non-homogeneous gases], I.L., Moscow, 1960.

169. Shari, V.P., Rol' "okon prozrachnosti" v perenose teplovogo izlucheniya i luchistom pritoke tepla v podoblachnoy atmosfere Venery [The role of "transparent windows" in the transfer of thermal radiation and the radiative heat inflow in the subcloud atmosphere of Venus], IPM preprint, AN SSSR, No. 11, 1974.

170. Sharonov, V.V., Tablitsy dlya rascheta prirodnoy osveshchennosti i vidimosti [Calculation tables for natural illumination and visibility], Moscow-Leningrad, 1945.

171. Sharonov, V.V., Priroda planet [The nature of the planets], Fizmatgiz, Moscow, 1958.

172. Sharonov, V.V., Planeta Venera [The planet of Venus], Nauka, 1965.

173. Shifrin, K.S., Rasseyaniye sveta v mutnoy srede [The scattering of light in a hazy medium], Gostekhizdat, 1951.

174. Shmeter, S.M., Fizika konvektivnykh oblakov [The physics of convective clouds], Gidrometeoizdat, Leningrad, 1972.

175. Shuleykin, V.V., "Materials on the optics of a strongly-scattering medium," Zhurnal Geofiziki 3, 145 (1933).

176. Adamčik, J.A., and A. Draper, "The temperature dependence of the Urey equilibrium and the problem of carbon dioxide content in the atmosphere of Venus, Planet. Space Sci. 11/11, 1303 (1963).

177. Adams, W.S., and M. Dunham, "Absorption bands in the infrared spectrum of Venus, Publ. Astron. Soc. Pacific 44, 243, 1932.

178. Anderson, J.D., G.W. Null, and C.T. Thornton, "The evaluation of certain astronomical constants from the radio tracking of Mariner-2," Celestial Mech. and Astrodyn., N.Y., London. Acad. Press, 1964, pp. 131-155.

179. Anderson, J.D., L. Efron, R.M. Goldstein, W.G. Melburne, D.A. O'Handley, G.E. Pease and R.C. Tausworthe, "Radius of Venus as determined by planetary radar and Mariner-5 radio tracking data," Astron. J. 73/10, Part 2, 162, 1968.

180. Anderson, J.D., G.E. Pease, L. Efron, and R.C. Tausworthe, "Determination of the mass of Venus and other astronomical constants from the radio tracking of Mariner-5," Astron. J. 73/2, Part 2, 2, 1968.

181. Anderson, J.D., and L. Efron, "Mass and dynamic oblateness of Venus, Bull. Amer. Astron. Soc. 1, 231-232 (1969).

182. Anderson, R.C., J.G. Pipes, A.L. Broadfoot, and L. Wallace, "Spectra of Venus and Jupiter from 1800 to 3200 Å, J. Atmos. Sci. 26, 874-888 (1969).

183. Arking, A. and J. Potter, "The phase curve of Venus and the nature of its clouds, J. Atmos. Sci. 25/4, 617-628, (1968).

184. Ash, M.E., I.I. Shapiro, and W.B. Smith, "Astronomical constants and planetary ephemerides deduced from radar and optical observations, Astron. J. 72/3, 338 (1967).

185. Ash, M.E., R.P. Ingalls, G.H. Pettengill, I.I. Shapiro, W.B. Smith, M.A. Slade, D.B. Campbell, R.B. Dyce, R. Jurgens, T. W. Thompson, "The case of radar radius of Venus, J. Atmos. Sci. 25/4, 560-563 (1968).

186. Avduyevsky, V.S., M. Ya. Marov, M.K. Rozhdestvensky, "Model of the planet Venus based on results of measurements made by the Soviet automatic interplanetary station Venera-4," J. Atmos. Sci. 25/4, 537-545 (1968).

187. Avduyevsky, V.S., M. Ya. Marov, and M.K. Rozhdestvensky, "The atmosphere of the planet Venus on the results of the measurements made by the Soviet automatic station Venera-4," Space Research IX, North Holland Publ. Co., Amsterdam, 1968.

188. Avduyevsky, V.S., M. Ya. Marov, A.I. Noykina, V.I. Polezhayev, and F.S. Zavelevich, "Heat transfer in the Venusian atmosphere, J. Atmos. Sci. 27/4, 569-579 (1970).

189. Avduyevsky, V.S., M. Ya. Marov, M.K. Rozhdestvensky, "The tentative model of the atmosphere of the planet Venus based on the results of measurement of space probes Venera-5 and Venera-6," J. Atmos. Sci. 27/4, 561-568 (1970).

190. Avduyevsky, V.S., M. Ya. Marov, B.E. Moshkin, A.P. Ekonomov, "Venera-8: Measurements of solar illumination through the atmosphere of Venus, J. Atmos. Sci. 30/6, 1215-1218 (1973).

191. Bahr, J.L., A.J. Blake, J.H. Carver, V. Kumar, "Photoelectron spectra and partial photoionization cross sections for carbon dioxide," J. Quant. Spectr. Rad. Trans., 9, 1359 (1959).

192. Bauer, S.J., R.E.Hartle, J.R. Herman, "Topside wind of Venus and its interaction with the solar wind," Nature 225, 533-534 (1970).

193. Barath, F.T., A.H. Barrett, J. Copeland, D.E. Jones, and A.E. Lilley, "Microwave radiometers," Science 139/3558, 908 (1963).

194. Barath, F.T., A.H. Barrett, J. Copeland, D.E. Jones and A.E. Lilley, "Mariner-2 microwave experiment and results," Astron. J. 69, 49 (1964).

195. Barrett, A.H., "Microwave absorption and emission in the atmosphere of Venus, Astrophys. J. 133, 281 (1961).

196. Barrett, A.H., and A.E. Lilley, "Mariner-2 microwave observations of Venus, Sky and Telescope 25/4, 1-4 (1963).

197. Barrett, A.H., and D.H. Staelin, "Radio observations of Venus and their interpretations, Space Sci. Rev. 3, 109 (1964).

198. Barth, C.A., J.B. Pearce, K.K. Kelly, L. Wallace, W.G. Fastie, "Ultraviolet emissions observed near Venus from Mariner-5," Science 158/3809, 1675 (1967).

199. Barth, C.A., "Interpretation of the Mariner-5 Lyman-alpha measurements, J. Atmos. Sci. 25/4, 564 - 567 (1968).

200. Barth, C.A., L. Wallace, I.B. Pearse, "Mariner-5 measurement of Lyman-alpha radiation on Venus, J. Geophys. Res. 73, 2541 (1968).

201. Barth, C.A., Paper presented at the IAGA Inter-Commission Symposium on aeronomic ionization processes, Madrid, September, 1969.

202. Barth, C.A., C.W. Hord, J.B. Pearce, K.K. Kelly, G.P. Anderson, and A.I. Stewart, "Mariner-6 and -7 ultraviolet spectrometer experiment: upper atmosphere data," J. Geophys. Res. 76, 2213-2227 (1971).

203. Barth, C.A., A.I. Stewart, C.W. Hord, A.L. Lane, Mariner-9 ultraviolet spectrometer experiment: Mars airglow spectroscopy and variations in Lyman-alpha," Icarus 17, 457-468 (1972).

204. Bartko, F., R.A. Hanel, "Nongray equilibrium temperature distributions above the clouds of Venus, Astrophys. J. 151 365-378 (1968).

205. Basharinov, A.E. et al., "Microwave radiometry of Mars from orbiter space probe, Icarus 17/2, 540-542 (1972).

206. Bates, D.T. and M. Nicolet, "The photochemistry of atmospheric water vapor, J. Geophys. Res. 55/3, 301 (1950).

207. Bates, D.R., "The temperature of the upper atmosphere," Proc. Phys. Soc. 64/3818, 805 (1951).

208. Bates, D.R., and M. Nicolet, "Ion-atom interchange," J. Atmos. Terr. Phys. 18/1, 65 (1960).

209. Bedinger, J.F., "Measurements on winds above 200 kilometers," J. Geophys. Res. 75/3, 683 (1970).

210. Beebe, R.F., "Ultraviolet clouds on Venus. Observational bias," Icarus 17/3, 602-607 (1972).

211. Belton, M.J.S., and D.M. Hunten, "Water vapor in the atmosphere of Venus, Astrophys. J. 146, 307-308 (1966).

212. Belton, M.J.S., "Theory of the curve of growth and phase effect in a cloudy atmosphere: applications to Venus," J. Atmos. Sci. 25, 596-609 (1968).

213. Belton, M.J.S., L.A. Broadfoot, and D.M. Hunten, "Upper limit to O_2 on Venus," J. Atmos. Sci. 25/4, 582 (1968).

214. Belton, M.J.S., D.M. Hunten, "A search for O_2 on Mars and Venus: a possible detection of oxygen in the atmosphere of Mars," Astrophys. J. 153, 963-974, (1968).

215. Belton, M.J., D.M. Hunten, and R. Goody, "Quantative spectroscopy of Venus in the region 8000 - 11,000 Å," in: Atmospheres of Venus and Mars, Edited by J.C. Brandt and M.B. McElroy, Gordon and Breach Publishers, New York-London, pp. 9-97.

216. Ben-Reuven, A., "Transition from resonant to nonresonant line shape in microwave absorption, Phys. Rev. Letts. 14/10, 349 (1965).

217. Berge, G.L., D.O. Muhleman, and G.S. Orton, "High resolution interferometric observations of Venus at three radio wavelengths, Icarus, 17/3, 675-681 (1972).

218. Blum, P., I. Harris, and W. Priester, "On the physics of the neutral upper atmosphere," Report prepared for the COSPAR International Reference Atmosphere CIRA 1970, Inst. for Space Studies, Goddard Space Flight Center, NASA, March 16, 1970.

219. Boischot, A., M. Ginat, I. Kazes, "Observations of the radiation of Venus and Jupiter at wavelengths 13 cm and 21 cm," Astrophys. 26/4, 385 (1963).

220. Bottema, M., W. Plummer, J. Strong and R. Zander, "The composition of the Venusian clouds and implications for model atmospheres," J. Geophys. Res. 70, 4401 (1964); Astrophys. J. 140, 1640 (1964).

221. Boyer, Ch., "Observations in Brazzaville," Astronomie 74, 376-378 (1960).

222. Boyer, Ch., and H. Camichel, "Photographic observations of the planet Venus," Ann. Astrophys. 24/6, 531-535 (1961).

223. Boyer,, Ch. and H. Camichel, "Photographic studies of the rotation of Venus C.r.," Acad. Sci. 260/3, 809 (1965).

224. Boyer, Ch., and P. Guérin, "Studies of the 4-day retrograde rotation of the visible cloud layer of Venus," Icarus 11, 338-355 (1969).

225. Boyer, Ch. and P. Guérin,"On the irregularities of the 4-day rotation period of the Y-shaped cloud formations in the upper atmosphere of Venus and their correlation to the slow rotation of the planet, C.r. Acad. Sci. 273/3, B154- B157 (1971).

226. Bridge, H.S., A.J. Lazarus, C.W. Snyder, E.J. Smith, L. Davis, P.J. Coleman, and D.E. Jones, "Mariner-5: Plasma and magnetic fields observed near Venus," Science 158, 1669-1673 (1967).

227. Burch, D.E., D.A. Gryvnak and D. Williams, "Total absorptance of carbon dioxide in the infrared, Appl. Optics 1/6, 759 (1962).

227a. Bronsted, J.N., Chem. Rev. 5, 231 (1928).

228. Caldwell, J., "Retrograde rotation of the upper atmosphere of Venus, Icarus 17, No. 3, 608-616, 1972.

229. Cameron, A.G.W., "The origin of the atmosphere of Venus and the Earth, Icarus 2/3, 249 (1963).

230. Camichel, H., "Observations at Pic-du-Midi," Astronomie 74 378-381 (1960).

231. Campbell, D.B., R.B. Dyce, R.P. Ingalls, G.H. Pettengill, and I.I.Shapiro, "Venus: topography revealed by radar data," Science 175, 514-516 (1972).

232. Carpenter, R.L., "Study of Venus by CW radar," Astron. J. 69/n 1, 2 - 11 (1964).

233. Carpenter, R.L., "Study of Venus by CW radar results of the 1964 conjunction, Astron. J. 70/134 (1965); 71/2, 142-152 (1966).

234. Carpenter, R.L., "A radar determination of the rotation of Venus, Astron. J. 75/1, 61-66 (1970).

235. Cess, R.D. and V. Ramanathan, "Radiative transfer in the atmosphere of Mars and that of Venus above the cloud deck," J. Quant. Spectrosc. Radiat. Transfer 12/5, 933-945 (1972).

236. Chamberlain, J.W. and G.P. Kuiper, "Rotational temperature and phase variation of the carbon dioxide bands of Venus," Astrophys. J. 124, 399 (1956).

237. Chamberlain, J.W., "Planetary coronal and atmospheric evaporation," Planet. Space. Sci. 11, 901 (1963).

238. Chamberlain, J.W., "The atmosphere of Venus near its cloud tops," Astrophys. J. 141, 1184 (1965).

239. Chamberlain, J.W., M.B. McElroy, "Martian atmosphere: an interpretation of the Mariner occultation experiment," Science 152, 3718 (1966).

240. Chamberlain, J.W., "Behavior of absorption lines in a hazy planetary atmosphere," Astrophys. J. 159/1, 137-158 (1970).

241. Chamberlain, J.W. and G.R. Smith, "Interpretation of the Venusian CO_2 absorption, Astrophys. J. 160/2, 755-765 (1970).

242. Chase, S.C., L.D Kaplan, and G. Neugebauer, "The Mariner-2 infrared radiometer experiment," J. Geophys. Res. 68, 6157 (1968).

243. Clark, B.G. and C.L. Spencer, "Some decimeter observations of Venus during the 1962 conjunction," Astron. J. 69/N 1, 59 (1964).

244. Clark, I.D. and J.F. Noxon, "Photodissociation of CO_2 on Mars," J. Geophys. Res. 75, 7307-7310 (1970).

245. Clark, I.D.,"The chemical kinetics of CO_2 atmospheres," J. Atmos. Sci. 28 847-858 (1971).

246. Cloutier, P.A., M.B. McElroy, and F.C. Michel, "Modification of the Martian ionosphere by the solar wind, J. Geophys. Res. 74, 6215-6228 (1969).

247. Coffeen, D.L., "Optical polarization of Venus," J. Atmos. Sci. 25, 643 (1968).

248. Coffeen, D.L., and T. Gehrels, "Wavelength dependence of polarization.XV. Observations of Venus," Astron. J. 74/3, 433-445 (1969).

249. Coffeen, D.L., "Wavelength dependence of polarization. XVI. Atmosphere of Venus," Astron. J. 74/3, 446-460 (1969).

250. Colegrove, F.D., F.S. Johnson, and W.B. Hanson, "Eddy diffusion and oxygen transport in the lower thermosphere," J. Geophys. Res. 70, 4931 (1965).

251. Colegrove, F.D., F.S. Johnson, and W.B. Hanson, "Atmospheric composition in the lower thermosphere," J. Geophys. Res. 71, 2227 (1966).

252. Connes, P., J. Connes, W.S. Benedict, L.D. Kaplan, "Traces of HCl and HF in the atmosphere of Venus," Astrophys. J. 147/3, 1230-1237 (1967).

253. Connes, P., J. Connes, W.S. Benedict, and L.D. Kaplan, "Carbon monoxide in the Venusian atmosphere," Astrophys. J. 152/3, 731-743 (1968).

254. Cruikshank, D.P., "Sulfur compounds in the atmosphere of Venus, II: upper limit for the abundance of COS and H_2S," Ariz. Univ. Commun. Lunar Planet. Lab. 6/3, 199-200 (1967).

255. Cruikshank, D.P. and G.T. Sill, "The infrared spectrum of carbon suboxide. Part II: region 2 - 25 microns," Commun. Lunar Planet. Lab 6/3, 204-205 (1967).

256. Cruikshank, D.P. and G.P. Kuiper, "Sulfur compounds in the atmosphere of Venus: I: an upper limit for the abundance of SO_2," Ariz. Univ. Commun. Lunar Planet. Lab. 6/3, 195-198 (1967).

257. Cruikshank, D.P. and A.B. Thomson, "On the occurrence of ferrous chloride in the clouds of Venus," Icarus 15/3, 497-503 (1971).

258. Curtis, A.R., and R. M. Goody, "Thermal radiation in the upper atmosphere," Proc. Roy. Soc. A. 236, 1205, 193 (1956).

259. Dalgarno A., Charged particles in the upper atmosphere," Ann. Geophys. 17/1, 16 (1961).

260. Daniels, F.B., "Theory of radar reflection from the Moon and planets, J. Geophys. Res. 66/6, 1781 (1961).

261. Davidson, G.T., and A.D. Anderson, "Venus: volcanic eruptions may cause atmospheric obscuration," Science 156/3783, 1729-1730 (1967).

262. Davis, P.A. and W. Vieze, "A model computing infrared transmission through atmospheric water vapor and carbon dioxide," J. Geophys. Res 69, 3785 (1964).

263. Deardorff, J.W. and G.E. Willis, "The free-convection temperature profile," Quart. J. Roy. Met. Soc. 93/396, 166-175 (1967).

264. Deardorff, J., "The counter-gradient heat flux in the lower atmosphere and in the laboratory," J. Atmosph. Sci. 23, 503 (1966).

265. Deardorff, J.W., G.E. Willis, and D.K. Lilly, "Laboratory investigation of nonsteady penetrative convection," J. Fluid Mech. 35, pt. 1 (1969).

266. Deirmendjian, D., "A water cloud interpretation of Venus' microwave continuum, Icarus 3/2, 109-120 (1964).

267. Deirmendjian, D., "Electromagnetic scattering on spherical polydispersions," Appl. Opt. 3/2 (1964).

268. Deirmendjian, D., "Introductory comments on Venus' lower atmosphere," in: The atmospheres of Venus and Mars, Ed. by J.C. Brandt and M.B. McElroy, Gordon and Breach Sci. Publ., 1968, pp. 15-20.

269. De More, W.B., "The efficiency of CO_3 formation in the Martian and Venusian atmosphere," J. Geophys. Res. 75, 4898 (1970).

270. Dickel, J.R. "6 cm observations and the microwave spectrum of Venus," Icarus 6/3, 417-426 (1967).

271. Dickel, J.R., W.W. Warnock, and W.J. Medol, "Lack of phase variation of Venus," Nature 220/5173, 1183 (1968).

272. Dickinson, R.E. "Circulation and thermal structure of the Venusian thermosphere," J. Atmos. Sci. 28, 885-894 (1971).

273. Dickinson, R.E., "Infrared radiative heating and cooling in the Venusian mesosphere. I: Global mean radiative equilibrium," J. Atmos. Sci. 29, 1531 (1972).

274. Dickinson, R.E. and E.C. Ridley, "Numerical solution for the composition of a thermosphere in the presence of a steady subsolar antisolar circulation with application to Venus," J. Atmos. Sci. 29, 1557 (1972).

275. Dollfus, A., "Polarization studies of planets," Suppl. Ann. d'Astrophys. 4, 117 p (1957).

276. Dollfus, A., "Polarization studies of planets. In: Solar System III (Planets and satellites)," Ed. by G.P. Kuiper and B.N. Middlehurst, Univ. of Chicago Press, Chicago, 1961.

277. Dollfus, A., "Synthesis on ultraviolet survey of clouds in Venusian atmospere. In: Atmospheres of Venus and Mars," Ed. by C. Brandt and M.B. McElroy, Ed. Gordon and Breach Publ. House, New York, 1968.

278. Dollfus, A., "Visual determination of the diameter of Venus," C.R. Acad. Sc. Paris 267, Ser. B, 1304 (1968).

279. Dollfus, A., "New optical measurements of planetary diameters. Part II. Planet Venus, Icarus 17/1, 104-115 (1972).

280. Donahue, T.M., "The upper atmosphere of Venus: a review," J. Atmos. Sci. 25/4, 568-573 (1968).

281. Donahue, T.M., "Aeronomy of CO_2 atmospheres: a review," J. Atmos. Sci. 28/6, 895-900 (1971).

282. Drake, F.D., "10-cm observations of Venus near superior conjunction," Publ. NRAO 1/11, 165 (1962).

283. Drake, F.D., 10-cm observations of Venus near superior conjunction," Nature 195/4844, 894 (1962).

284. Drake, F.D., "Microwave observations of Venus in 1962-1963," Astron. J. 69/1, 62 (1964).

285. Driscoll, E., "Our cratered sister planet," Sci. News. 104, 72-73 (1973).

286. Dyce, R.B., "Some radar characteristics of Venus at 430 MHZ," Prog. of Caltech -- JPL Lunar and Planetary Conference, 1965, pp. 172-177.

287. Dyce, R.B., G.H. Pettengill, and I.I. Shapiro, "Radar determination of the rotation of Venus and Mercury," Astron. J. 72/3, 351 (1967).

288. Edson, J.B., "The twilight zone of Venus," Adv. Astr. and Astrophys. 2, 1-42 (1963).

289. Edwards, D.K. and W.A. Menard, "Correlations for absorption by methane and carbon dioxide gases," Appl. Optics 3, 847 (1964).

290. Epstein, E.E., J.P. Oliver, S.L. Soter, R.A. Schorn and W.J. Wilson, "Venus: On the inverse variation with phase in the 3-4 mm emission during 1965 through 1967," Astron. J. 73/4, 271 (1968).

291. Eshleman, V.R., J.D. Anderson, A. Kliore, and R.B. Dyce, "Venus -- lower atmosphere not measured," Science 162, 661 (1968).

292. Evans, D.C., A. Boggess, R. Scolnik, "The reflectivity of Venus and Jupiter in the middle ultraviolet," Astron. J. 70/321 (1965).

293. Evans, J.V., and G.N. Taylor, "The electron content of the ionosphere in winter," Proc. Roy. Soc. 263/1313, 189 (1961).

294. Evans, J.V., R.A. Brockelman, J.C. Menry, G.M. Hude, L.G. Kraft, W.A. Reid, and W.W. Smith, "Radio echo observations of Venus and Mercury at 23 cm wavelength," Astron. J. 70/1, 486-501 (1965).

295. Evans, J.V., R.A. Brockelman, E.N. Dupont, Hanson, L.B., and W.A. Reid, "Radar observations of Venus," Astron. J. 71/9, 897 (1966).

296. Evans, J.V., R.P. Ingalls, L.P. Rainville, and R.R. Silva, "Radar observation of Venus," Astron. J. 71/9, 902 (1966).

297. Evans, J.V., "Variations in the radar cross section of Venus," Astron. J. 73/3, 125-134 (1968).

298. Evans, J.V. and R.P. Ingalls, "Absorption of radar signals by the atmosphere of Venus," J. Atmos. Sci. 25/4, 555-559 (1968).

299. Faller, A.J. and R. Kaylor, "Numerical studies of penetrative convective instabilities," J. Geophys. Res. 75/3 (1970).

300. Ferriso, C.C., "High temperature spectral absorption of the 4.3 micron CO_2 band, " J. Chem. Phys. 37/ N 9, 1955 (1962).

301. Ferriso, C.C., and C.B. Ludwig, "Spectral emissivities and integrated intensities of the 2.7 μ CO_2 band between 1200° and 1800°K," J. Opt. Soc. Amer. 54/5, 657-662 (1964).

302. Ferriso, C.C., C.B. Ludwig, and A.L. Thomson, "Empirically determined infrared absorption coefficients of H_2O from 300 to 3000°K," J. QSRT 6/3, 241 (1966).

303. Fink, V., H.P. Larson, G.P. Kuiper, and R.F. Poppen, "Water vapor in the atmosphere of Venus," Icarus 17, 617-631 (1972).

304. Fjeldbo, G., and V.R. Eshleman, "Atmosphere of Venus as studied with the Mariner-5 dual radio frequency occultation experiment, Radio Science 4/10, 879-897 (1969).

305. Fjeldbo, G., Kliore, A.J., R. Eshleman, "The neutral atmosphere of Venus as studied with the Mariner-5. Radio occultation experiments," Astron. J. 76/2, 123-140 (1971).

306. Foster, T.D., "Onset of manifest convection in a layer of fluid with a time-dependent surface temperature," Phys. Fluids 12/12, pt. 1 (1969).

307. Friedman, M.P., "A three-dimensional model of the upper atmosphere," Smithsonian Astrophys. Obs. Spec. Rep. No. 250, 1967.

308. Gale, W.A., Sinclair, A.C.E. "Polar temperature of Venus," Science 165/3900, 1356-1357 (1969).

309. Gehrels, T., and R.E. Samuelson, "Polarization phase relations for Venus," Astrophys. J. 134/3, 1022, 1024, (1961).

310. Gibson, J.E., "The brightness temperature of Venus at 8.6 mm," Astrophys. J. 137/2, 611-619 (1963).

311. Gierash, P. and R. Goody, "An approximate calculation of radiative heating and radiative equilibrium in the Martian atmosphere," Planet. Space Sci. 15/1465 (1967).

312. Gierasch, P.J., "The four-day rotation in the stratosphere of Venus: a study in radiative driving," Icarus 13/1, 25-33 (1970).

313. Gierasch, P. and R. Goody, "Models of the Venusian clouds," J. Atmos. Sci. 27/2, 224-245 (1970).

314. Gillett, F.C., F.J. Low, and W.A. Stein, "Absolute spectrum of Venus from 2.8 to 14 microns," J. Atmos. Sci. 25/4, 594-595 (1968).

315. Gold, T., and S. Soter, "Atmospheric tides and the resonant rotation of Venus," Icarus 11, 356-366 (1969).

316. Goldreich, P., and S.J. Peal, "Spin orbit coupling in the Solar System," Astron. J. 71, 425-438 (1966).

317. Goldstein, R.M., and R.L. Carpenter, "Rotation of Venus: period estimated from radar measurements," Science 139/3558, [Illegible] (1963).

318. Goldstein, R.M., "Venusian characteristics by Earth-based radar," Astron. J. 69/1, 12 (1964).

319. Goldstein, R., "Preliminary Venus radar results," J. Res. Nat. Bur. Standards 69D, 1623 (1965).

320. Goldstein, R.M., and H.C. Rumsey, "A radar image of Venus," Icarus 17/3, 699-703 (1972).

321. Goody, R.M., and A.R. Robinson, "A discussion of the deep circulation of the atmosphere of Venus," Astrophys. J. 146, 339-355 (1966).

322. Goody, R.M., and M.J.S. Belton, "Radiative relaxation times for Mars, a discussion of Martian atmospheric dynamics," Planet. Space Sci. 15, 247-256 (1967).

323. Goody, R., and T. McCord, "Continued search for the Venusian airglow," Planet. Space Sci. 16, 343-351 (1968).

324. Goody, R., and A. Robinson, "The deep circulation. Report presented at the 4th Arizona Conference on Planetary atmospheres," Tucson, 2-4 March, 1970.

325. Goody, R.M., "Motions of planetary atmospheres," Ann. Rev. Astron. Astrophys. 7, 303-352, 1969. Russian translation in the coll: Issledovaniya atmosfer Marsa i Venery [Studies of the atmospheres of Mars and Venus], Ed. by K. Ya. Kondrat'yev, Gidrometeoizdat, Leningrad, 1970.

326. Gordon, J.J., D.L. Jauncey, and M.J. Yerbury, "The brightness temperature of Venus at 70 centimeters," Astrophys. J. 183/3, 1035-1080 (1973).

327. Gray, L.D., "On the amount of carbon dioxide in the atmosphere of Venus," I. Icarus 8, 518 (1968).

328. Gray, L.D., and R.A. Schorn, "High dispersion spectroscopic observations of Venus. I. The carbon dioxide bands near 1 micron," Icarus 8, 409-422 (1968).

329. Griffin, P.H., D.D. Thornton, and W. J. Welch, "The microwave spectrum of Venus in the frequency range 18-36 Gc/sec," Icarus 6, 175 (1967).

330. Guinot, B., "Measurements of the rotation of Venus," Compt. Rend. 260, 431 (1965).

331. Hanel, R., M. Forman, G. Stambach and T. Meilleur, "Preliminary results of Venusian observations between 8 and 13 microns," J. Atmos. Sci. 25/4 586-593 (1968).

332. Hansen, J.E., and S. Matsushima, "The atmosphere and surface temperature of Venus: a dust insulation model," Astrophys. J. 150, 1139 (1967).

333. Hansen, J.E., and H. Cheyney, "Near-infrared reflectivity of Venus and ice clouds," J. Atmos. Sci. 25/4, 629-633 (1968).

334. Hansen, J.E., and H. Cheyney, "Comments: On the composition of the Venusian clouds," J. Geophys. Res. 73, 6136 (1968).

335. Hansen, J.E., and J. Pollack, "Near-infrared light scattering by terrestrial clouds," J. Atmos. Sci. 27/2, 265-281 (1970).

336. Hansen, J.E., A. Arking, "Clouds of Venus: evidences for their nature," Science 171/3972, 669-672 (1971).

337. Hansen, J.E., "Information contained in the intensity and polarization of scattered sunlight," Inst. for Space Studies Rpt. September, 1972.

338. Hapke, B., "Venusian clouds: a dirty hydrochloric acid model," Science 175, 748 (1972).

339. Harris, I., and W. Priester, "Time dependent structure of the upper atmosphere," J. Atmos. Sci. 19, 286 (1962).

340. Harris, I. and W. Priester, "On the diurnal variation of the upper atmosphere," J. Atmos. Sci. 22, 3 (1965).

341. Harris, I., "Horizontal energy transport in the thermosphere," Transactions AGU 47, 459 (1966).

342. Harris, I. and W. Priester, "The structure of the thermosphere and its variations," Meteorological monographs 9, 72 (1968).

343. Henry, R.J.W., and M.B. McElroy, "Photoelectrons in planetary atmospheres. In: The atmospheres of Mars and Venus, Gordon and Breach, New York, 1968, 251-279.

344. Herman, J.R., R.E. Hartle, and S.J. Bauer, "The dayside ionosphere of Venus," Planet. Space Sci. 19 443-460 (1971).

345. Hess, S.L., "The hydrodynamics of Mars and Venus. In: The atmospheres of Mars and Venus," Ed. by J.C. Brandt and M.B. McElroy, Gordon and Breach, New York, 1968, pp. 109-131.

346. Ho, W., I.A. Kaufman, and P. Thaddeus, "Laboratory measurement of microwave absorption in model of atmosphere of Venus," J. Geophys. Res. 71, 5091 (1968).

347. Hogan, J.S., and R.W. Stewart, "Exospheric temperatures on Mars and Venus," J. Atmos. Sci. 26, 332 (1969).

348. Howard, I.N., D.E. Burch, and D. Williams, "Infrared transmission of synthetic atmospheres, I-IV. J. Opt. Soc. Am. 46, 186-190, 237-245, 334-338, 452-455 (1956).

349. Hughes, M.P., "Planetary observations at a wavelength of 6 cm, Planetary Space Sci. 14/10, 1017 (1965).

350. Hunten, D.M., and M.B. McElroy, "The upper atmosphere of Venus: the Regulus occultation reconsidered," J. Geophys. Res. 73, 4446 (1968)

351. Ingersoll, A.P. and C.B. Leovy, "The atmospheres of Mars and Venus, Annual Review of Astronomy and Astrophysics, (Ed. by Leo Goldberg), 9, 147-182, Palo Alto, Calif. (1971).

352. Ingalls, R.P., and J.V. Evans, "Scattering properties of Venus at 3.8 cm," Astron. J. 74, 258 (1969)

353. Irvine, W.M., "Multiple scattering by large particles," Astrophys. J. 142, 1563 (1965).

354. Irvine, W.M., "Monochromatic phase curves and albedo for Venus," J. Atmos. Sci. 25/4, 610-616 (1968).

355. Irvine, W., T. Simon, D. Menzel, C. Pikoos and A. Young, "Multicolor photoelectric photometry of the brighter planets. III. Observations from Boyden Observatory," Astron. J. 73/9, 807 (1968).

356. Irvine, W.M., J.B. Pollack, "Infrared properties of water and ice spheres," Icarus 8, 324-360 (1968).

357. Irvine, W.M., "Multiple scattering by large particles II. Optically thick layers," Astrophys. J. 152, 823 (1968).

358. Irvine, W.M., "Diffuse reflection and transmission of cloud and dust layers," J. Quant. Spectr. Radiative Transfer 8, 471 (1968).

359. James, J.C., R.P. Ingalls, and L.P. Rainville, "Radar echos from Venus at 38 Mc/sec," Astron. J. 72/8, 1047 (1967).

360. Janssen, M.A., R.E. Hills, D.D. Thornton, and W.J. Welch, "Venus: new microwave measurements show no atmospheric water vapor," Preprint (1973).

361. Jastrow, R., and S.I. Rasool, "Radiative transfer in the atmosphere of Venus and Mars." Space Research 3 (Proceedings of the COSPAR symposium, W. Priester, Ed), North Holland Publ. Co., Amsterdam, 1963, 1036.

362. Jeffreys, H., "The instability of a compressible fluid heated from below," Proc. Cambr. Phil., Soc. 20, 170 (1930).

363. Jenkins, E.B., D.C. Morton, and A.V. Sweigart, "Rocket spectra of Venus and Jupiter from 2000 to 3000 Å," Astrophys. J. 157, 913-924 (1969).

364. Johnson, F.S., "Temperature distribution of the ionosphere under the control of thermal conductivity," J. Geophys. Res. 61, 71 (1956).

365. Johnson, F., "Temperature in the high atmosphere," Ann. Geophys. 14/1 (1958).

366. Jones, D.E., "The microwave temperature of Venus," Planet. Space Sci. 5/2, 166 (1961).

367. Jones, D.E., D.M. Wrathall, and B.L. Meredith, "Spectral observations of Venus in the frequency interval 185.5-24. 0GHz, Publ. Astron. Soc. Pacif. 84/499, 435-442 (1972).

368. Junge, Ch., "The size distribution and aging of natural aerosols as determined from electrical and optical data on the atmosphere," J. Meteorol. 12/1, 13 (1955).

369. Jurgens, R.F., "Some preliminary results of the 70 cm radar studies of Venus," Radio Sci. 5/2, 435-442 (1970).

370. Kalaghan, P.M., K.N. Wulfsberg, L.E. Telford, "Observations of the phase effect of Venus at 8.6 mm wavelength," Astron. J. 73/10, pt. 1 (1969).

371. Kaplan, L.D., "A new interpretation of the structure and CO_2 content of the Venusian atmosphere," Planetary Space Sci. 8/1, 23 (1961).

372. Karp, D., W.E. Morrow, and W.B. Smith, "Radar observations of Venus," Icarus 3/5-6, 473 (1964).

373. Kellerman, K.I., "Radio observations of Mercury, Venus, Mars, Saturn and Uranus," Radio Science 69D, No. 12, 1574 (1965).

374. Kellerman, K.I., "The thermal radio emission from Mercury, Venus, Mars, Saturn and Uranus," Icarus 5, 478 (1966).

375. Kellerman, K.I.,I.I.K. Pauliny-Toth, P.J.S. Williams, "The spectra of radio sources in the revised 3C Catalogue," Astrophys. J. 157/1, Pt. 1, 1-34 (1969).

376. Kellerman, K.I., and I.I.K. Pauliny-Toth, "Observations of the radio emission of Uranus, Neptune, and other planets at 1.9 cm," Astrophys. J. 145/3, 954-957 (1966).

377. Kerzhanovich, V.V., M. Ya. Marov, M.K. Rozhdestvenskiy, "Data on dynamics of the subcloud Venus atmosphere from Venera spaceprobe measurements," Icarus 17, 659 (1972).

378. Kerzhanovich, V.V., M. Ya. Marov, M.K. Rozhdestvensky, and V.P. Lysov, "Dynamics of the Venus atmosphere from Venera-8 spaceprobe measurements," Report presented at XVI-th COSPAR meeting, Konstanz, FRG, May 1973.

379. King-Hele, D.G., D.W. Scott, and D.M.C. Walker, "Upper atmosphere rotational speed and its variation with height," Royal Aircraft Establishment Technical Report 69263, Nov. 1969.

380. Klemperer, W.K., G.R. Ochs, and K.L. Bowles, "Radar echoes from Venus at 50 Mc/sec," Astron. J. 68/1, 22 (1964).

381. Klepczynski, W.J., P.K. Seidelman, and R.L. Dunkombe, "The Masses of the principal planets," Advances in the Astronautical Sci. 29, p.1, 133-170 (1971).

382. Kliore, A., D.L. Cain, G.S. Levy, Fjeldbo, G., and S.I. Rasool, "Structure of the atmosphere of Venus derived from Mariner-5 S-band measurements," Space Research IX, North Holland Publ. Co., Amsterdam 1968.

383. Knuckles, C.F., M.K. Sinton, and W.M. Sinton, "UBV photometry of Venus," Lowell Obs. Bull. 5, 153 (1961).

384. Knudsen, W.C., and A.D. Anderson, " He^4 and Ar^{40} in Cytherean atmosphere," J. Geophys. Res. 74, 24, 5629-5641 (1969).

385. Kondratiev, K. Ya., G.A. Nicolsky, I.K. Badinov, and E.D. Andreyev, "Direct solar radiation up to 30 km and stratification of attenuation components in the stratosphere," Appl. Optics 6/2, 197 (1967).

386. Kotelnikov, V.A., "Radar contact with Venus," J. Brit. I.R.E. 22/4, 293 (1961).

387. Kuiper, G., "Determination of the pole of rotation of Venus," Astrophys. J. 120, 603 (1954).

388. Kuiper, G.P., "Infrared spectra of stars and planets, I: Photometry of the infrared spectrum of Venus, 1-2.5 microns, Comm. Lunar Planet. Lab., 1 (15), 83 (1962).

389. Kuiper, G.P. and F. Forbes, "High altitude spectra from NASA CV 990 Jet. I: Venus, 1-2.5 microns, resolution 20 cm," Commun. Lunar Planet. Lab. 6/99, 201 (1967).

390. Kuiper, G.P., G.T. Sill, and D.P. Cruikshank, "The infrared spectrum of carbon suboxide, Part I: Region 1 - 2.5 microns," Commun. Lunar Planet. Lab. 6/99, 201 (1967).

391. Kuiper, G.P. "Results of recent high altitude flights," Paper presented at the Second Arizona Conference on Planetary Atmospheres, Tucson, 11-13 March, 1968.

392. Kuiper, G.P. "Infrared spectra of Venus from high altitude aircraft," Short communication at the XII meeting of COSPAR, Prague, 1969.

393. Kuiper, G.P., F. Forbes, D. Steinmetz, and R. Mitchell, Commun. Lunar Planet. Lab 6/100, 209 (1968-69).

394. Kuiper, G.P., "On the nature of the Venusian clouds. In Planetary atmospheres, IAU Symposium No. 40 (C. Sagan, T.C. Owen and H.J. Smith, Eds) D. Reidel, Dordrecht, Holland (1969).

395. Kurt, V.G., S.B. Dostovalow, and E.K. Sheffer, "The Venusian far ultraviolet observations with Venera-4," J. Atmos. Sci. 25, 668 (1968).

396. Law, S.E. and D.H. Staelin, "Measurements of Venus and Jupiter near 1 cm wavelength," Astrophys. J. 154/3, pt. 1, 1077 (1968).

397. Lawrence, G.M. "Photodissociation of CO_2 to produce $CO(a^3\Pi)$," J. Chem. Phys. 56, 3435 (1972).

398. Leovy, C.B. and J.B. Pollack, "A first look at atmospheric dynamics and temperature on Titan," Icarus 19/2, 195-201 (1973).

399. Lewis, J.S., "Composition and structure of the clouds of Venus," Astrophys. J. 152, L79-L83 (1968).

400. Lewis, J.S. "Geochemistry of the volatile elements on Venus," Icarus 11, 367 (1969).

401. Lewis, J.S., "Venus: atmospheric and lithospheric composition," Earth Planet. Sci. Lett. 10, 73 (1970).

402. Lewis, J.S., "Refractive index of aqueous HCl solutions and the composition of the Venusian clouds," Nature 230/5292, 295-296 (1971).

403. Lloyd, K.H., C.H. Low, B.J. McA aney, D. Rees, R.G. Roger, "Thermospheric observations combining chemical seeding and ground-based techniques, I. Winds, turbulence and the parameters of the neutral atmosphere," Planet. Space Sci. 20/5, 761 (1972).

404. Ludwig, C.B., C.C. Ferriso, W. Malkums, F.P. Boynton, "High temperature spectra of the pure rotational band of H_2O,"J. QSRT 5, 697 (1965).

405. Ludwig, C.B., C.C. Ferriso, C.N. Abeyta, "Spectral emissivities and integrated intensities of the 6.3 fundamental band of H_2O, J. QSRT 5/2, 281 (1965).

406. Lyot, B., "Polarization studies of the planets and of several substances on Earth," Ann. Obs. Paris (Meudon) 8, 161 (1926).

407. Malkums, W., "Infrared emissivity of carbon dioxide (4.3 μ)," J. Opt. Soc. of America (1963).

408. Mariner Stanford Group."Venus: Ionosphere and atmosphere as measured by dual-frequency radio occultation of Mariner-5," Science 158/3809, 1678 (1967).

409. Maron, I., G. Luchak, and W. Blitzstein, "Radar observation of Venus," Science 134/3488, 1418 (1961).

410. Marov, M. Ya. and A.M. Alferov, "Structure and motion of the thermosphere deduced from satellite drag," Space Res. 12, Academie-Verlag, Berlin, 1972, 823-840.

411. Marov, M. Ya. and A.V. Kolesnichenko, "On the simulation of the heterosphere of the planet. Comparison of the Earth and Venus thermospheres," Report submitted at XII Assembly of International Association of Geomagnetism and Aeronomy, Madrid, Spain, 1969.

412. Marov, M. Ya., "Venus: A perspective of the beginning of planetary exploration," Icarus 16, 415 (1972).

413. Marov, M. Ya., and A. M. Alpherov, "Diurnal variations in the thermosphere," Space Research XII, Academie-Verlag, Berlin, 1972, 337-341.

414. Marov, M. Ya., V.S. Avduyevsky, V.V. Kerzhanovich, M.K. Rozhdestvensky, N.F. Borodin, and I.L. Ryabov, "Venera-8: measurements of temperature, pressure and wind velocity on the illuminated side of Venus," J. Atmos. Sci. 30/6, 1210-1214 (1973).

415. Marov, M. Ya., V.S. Avduyevsky, N.F. Borodin, A.P. Ekonomov, V.V. Kerzhanovich, V.P. Lysov, B.E. Moshkin, M.K. Rozhdestvensky, and O.L. Ryabov, "Preliminary results on the Venusian atmosphere from the Venera-8 descent module," Icarus 20, 407-421 (1973).

416. Mayer, C.H., T.P. McCullough, and R.M. Sloanaker, "Observations of Venus at 3.15 cm wavelength," Astrophys. J. 127/1, 1-10 (1958).

416a. McConnell, J.C., and M.B. McElroy, "Exitation processes for Martian airglow," J. Geophys. Res. 75/34, 7290-7293 (1970).

417. McCullough, T.P., and J.W. Boland, "Observations of Venus at 2.07 cm," Astron. J. 69/1, 68 (1964).

418. McCullough, T.P., "Phase dependence of the 2.7 cm wavelength radiation of Venus," Icarus 16, 310-313 (1972).

419. McElroy, M.B., "The upper atmosphere of Mars," Astrophys. J. 150, 1125 (1967).

420. McElroy, M.B., "The upper atmosphere of Venus," J. Geophys. Res. 73, 1513 (1968).

421. McElroy, M.B.,"The upper atmosphere of Venus in light of the Mariner-5 measurements," J. Atmos. Sci. 25/4, 574 (1968).

422. McElroy, M.B., "Structure of the Venusian and Martian atmosphere," J. Geophys. Res 74/1, 29-41 (1969).

423. McElroy, M.B.,and D.F. Strobel, "Models for the nighttime Venusian ionosphere," J. Geophys. Res. 74, 1118 (1969).

424. McElroy, M.B., and D.M. Hunten, " The ratio deuterium to hydrogen in the Venusian atmosphere," J. Geophys. Res. 74, 1720 (1969).

425. McElroy, M.B., "Ionization processes in the atmospheres of Venus and Mars," Preprint of the Kitt Peak National Observatory, Tucson, Arizona, 1970.

426. McElroy, M.B., and D.M. Hunten, "Photochemistry of CO_2 in the atmosphere of Mars," J. Geophys. Res. 75, 1188-1201 (1970).

427. McElroy, M.B., and J.C. McConnell, "Dissociation of CO_2 in the Martian atmosphere," J. Atmos. Sci. 28, 879-884 (1971).

428. Melbourne, N.C., D.O. Muhleman and D.A. O'Handley, "Radar determination of the radius of Venus," Science 160, 987 (1968).

429. Mintz, Y., "Temperature and circulation of the Venusian atmosphere," Planetary Space Sci. 5, 141 (1961).

430. Moos, H.W., W.G. Fastic, and M. Bottema, "Rocket measurement of ultraviolet spectra of Venus and Jupiter between 1200 and 1800 Å," Astrophys. J. 155, 887-897 (1969).

431. Moos, H.W., and G.I. Rottman, "O I and H I emissions from the upper atmosphere of Venus," Astrophys. J. 169, 6127 (1971).

432. Morris, E.C. and R.W. Parsons, "Microwave absorption by gas mixtures at pressures up to several hundred bars," Austr. J. Phys. 23, 335 (1970).

433. Morrison, D., "Venus: absence of a phase effect at a 2-centimeter wavelength," Science 163/3869, 815 (1969).

434. Muhleman, D.O., G.L. Berge, and G.S. Orton, "The brightness temperature of Venus and the absolute flux-density scale at 608 MHz," Astrophys. J. 183/3, 1081-85 (1973).

435. Murray, B.C., R.L. Wildey, and J.A. Westphal, "Infrared photometric mapping of Venus through the 8-to-14-micron atmospheric window," J. Geophys. Res. 68, 4813 (1963).

436. Musman, S., "Penetrative convection," J. Fluid Mech. 31, pt. 2 (1968).

437. Newkirk, G., "The airglow of Venus," Planet. Space Sci. 1, 32-36 (1959).

438. Nicolet, M., "The thermosphere," Ann. Geophys. 15/ N 1, 1 (1959).

439. Ohring, G., and J. Mariano, "The effect of cloudiness on a greenhouse model of the Venusian atmosphere," J. Geophys. Res. 69, 165 (1964).

440. Öpik, E.J., "The aeolosphere and atmosphere of Venus," J. Geophys. Res. 66, 2807 (1961).

441. Ostriker, J.P., "Radiative transfer in a finite gray atmosphere," Astrophys. J. 138/1, 281 (1963).

442. Owen,, T., "A search for minor constituents in the atmosphere of Venus," J. Atmos. Sci. 25, 583-585 (1968).

443. Owen, T., and H. P. Mason, "Spectroscopic studies of the atmospheres of Mars and Venus." Paper presented at the Symposium on the Physics of the Moon and planets, Kiev, 15-22 October 1968, In the coll: Fizika Luny i planet [Physics of the Moon and planets], Nauka, 1972, pp. 330-334.

444. Owen, T. and C. Sagan, "Minor constituents in planetary atmospheres: ultraviolet spectroscopy from the Orbiting Astronomical Observatory," Icarus 16/3, 557-568 (1972).

445. Palmer, C.H., "Experimental transmission functions for the pure rotation band of water vapor," J. Opt. Soc. Amer. 50, 1232 (1960).

446. Pettengill, G.H., and R. Price, "Radar echoes from Venus and a new determination of the solar parallax," Planet. Space Sci. 5/1, 71 (1961).

447. Pettengill, G.H., H.W. Briscoe, J.V. Evans, E. Gehrels, G.M. Hyde, L.G. Kraft, R. Price, and W.B. Smith, "A radar investigation of Venus," Astron. J. 67/4, 181 (1962).

448. Pettengill, G.H., "Radar observations of Venus," Space Res. III, North Holland Publ. Co., 1963.

449. Pettengill, G.H., R.B. Dyce, and A. Sancher, "Radar measurements on the Arecibo 1000-foot antenna." Report at the 45th Annual Assembly of the American Geoph. Union, Washington, April, 1964.

450. Pettit, E., and S. Nicholson, "Temperatures of the light and dark sides of Venus," Publ. Astron. Soc. Pacif. 67/398, 293 (1955).

451. Plass, G.N. and V.R. Wyatt, "Carbon dioxide absorption for path lengths applicable to the atmosphere of Venus," Aeronutronic Publication No. U 1844, 1962.

452. Plass, G.N., and V.R. Stull, "Carbon dioxide absorption for path lengths applicable to the atmosphere of Venus," J. Geophys. Res. 68/ N 5, 1355-1363 (1963).

453. Plass, G.N. and G.W. Kattawar, "Calculations of reflected and transmitted radiance for Earth's atmosphere," Appl. Opt. 7, 361 (1968).

454. Plummer, W.T., "Infrared reflectivity of frost and the Venusian clouds," J. Geophys. Res. 74, 3331 (1969).

455. Plummer, W.T., "The Venusian spectrum: new evidence for ice," Icarus 12/2, 233-237 (1970).

456. Plummer, W.T., "Venus clouds: infrared reflectivity of several suggested materials," Preprint 1970.

457. Pollack, J.B., "A nongray calculation of the runaway greenhouse: implication for Venus, past and present." Preprint of Space Sci. Division Ames Research Center, NASA, Moffett Field, California 1971.

458. Pollack, J.B. and C. Sagan, "The microwave phase effect of Venus," Icarus 4/1, 62-103 (1965).

459. Pollack, J.B. and C. Sagan, "The infrared limb darkening of Venus," J. Geophys. Res. 70/18, 4403-4426 (1965).

460. Pollack, J.B. and C. Sagan, "A critical test of the electrical discharge model of the Venusian microwave emission," Astrophys. J. 150, 699 (1967).

461. Pollack, J.B. and C. Sagan, "The case for ice clouds on Venus," J. Geophys. Res. 73, 5943-5949 (1968).

462. Pollack, J.B. "Temperature structure of nongray planetary atmospheres," Icarus 10, 301-313 (1969).

463. Pollack, J.B., "A nongray CO_2 - H_2O greenhouse model of Venus," Icarus 10 314 (1969).

464. Pollack, J.B and D. Morrison, "Venus: determination of of atmospheric parameters from the microwave spectrum," Icarus 12/3 376-390 (1970).

464a. Pollack, J.B., E.F. Erickson, F.C. Witteborn, C. Chackerian Jr., A.L. Summers, W. Van Camp, B.J. Baldwin, C.G. Augason, and L.J. Caroff, "Aircraft observations of Venus' near-infrared reflection spectrum: implications for cloud composition." NASA _ Ames Research Center, SSD preprint, 1974.

465. Price, R., P.E. Green, T.J. Goblick, R.H. Kingston, L.G. Kraft, G.H. Pettengill, R. Silver, and W.B. Smith, "Radar echoes from Venus," Science 129/3351, 751-753 (1959).

466. Priestley, C.H.B., "Buoyant motion in a turbulent environment," Austral. J. Phys. 6/3 (1953).

467. Rasool, S.I., "The structure of Venusian clouds -- summary, Radio Sci. 5/ N 2, 367-368 (1970).

468. Rasool, S.I. and C. De Bergh, "The runaway greenhouse and the accumulation of CO_2 in the Venus atmosphere," Nature 226/5250, 1037-1039 (1970).

469. Rea, D.G., and B.T. O'Leary, "On the composition of the Venusian clouds," J. Geophys. Res. 73/2, 665-675 (1968).

470. Reevs, R.R., G. Mannella, and P. Harleck, "Rate of recombination of oxygen atoms," J. Chem. Phys. 32, 632 (1960).

471. Richter, K.R., "Enchanced microwave absorption in the lower atmosphere of Venus," Radio Sci. 7/4, 443-447 (1972).

472. Rogers, A.E.E., T. Hagfors, R.A. Brockelman, R.P. Ingalls, J.I. Levine, G.H. Pettengill, and F.S. Weinstein, "A radar interferometer study of Venus at 3.8 cm," Lincoln Lab. Techn. Report N 444, Mass. Inst. Technol., 1968.

473. Rogers, A.E., and R.P. Ingalls, "Radar mapping of Venus with interferometric resolution of the range-doppler ambiguity," Radio Sci. 5/2, 425-433 (1970).

474. Rogers, A.E.E., R.P. Ingalls, and L.P. Raintree, "The topography of a swath around the equator of the planet Venus from the wavelength dependence of the radar cross section," Astron. J. 77/1, 100-103 (1972).

475. Ross, F.E., "Photographs of Venus," Astrophys. J. 68, 57 (1928).

476. Rubey, W.W., "Geologic history of sea water: an attempt to state the problem," Bull. Geol. Soc. America 62, 1111 (1951).

477. Sagan, C., "The radiation balance on Venus," Calif. Inst. of Tech. Rept. 32-34 (Abstract in: Astron. J. 65/6, 352-353, 1960).

478. Sagan, C., "Structure of the lower atmosphere of Venus," Icarus 1, 151 (1962).

479. Sagan, C., and J.B. Pollack, "Anisotropic nonconservative scattering and the clouds of Venus," J. Geophys. Res. 72/2, 469 (1967).

480. Sagan, C., "Atmospheres, origins of Earth and planets," International Dictionary of Geophysics, Pergamon Press, Oxford, 1967.

481. Sagan, C., "An estimate of the surface temperature of Venus indpendent of passive microwave radiometry," Astrophys. J. 149, 731 (1968). Erratum: Astrophys. J. 152, 1119 (1968).

482. Sagan, C., "Gray and nongray planetary atmospheres: structure, convective instability and greenhouse effect," Icarus 10, 290-300 (1969).

483. Sagan, C., "The trouble with Venus." In: Planetary Atmospheres," IAU Symposium N 40, D. Reidel, Dordrecht, Holland, 1971.

484. Samuelson, R.E., "Greenhouse effect in semi-infinite scattering atmospheres: Application to Venus," Astrophys. J. 147, 782-798 (1967).

485. Samuelson, R.E., "The particulate medium in the atmosphere of Venus," J. Atmos. Sci. 25/4, 634-643 (1968).

486. Schorn, R.A., L.D. Gray, and E.S. Barker, "High dispersion spectroscopic observations of Venus, III. The carbon dioxide band at 7820 Å," Icarus 10, 241-257 (1969).

487. Schorn, R.A., L.D.G. Young, and E.S. Barker, "High-dispersion spectroscopic observations of Venus. The carbon dioxide band at 10362 Å," Icarus 12, 391 (1970).

487a. Schorn, R.A., C.B. Farmer, and S.L. Little, "High-dispersion spectroscopic studies of Mars. III. Preliminary results of 1968-69 water vapor studies," Icarus 11, 283 (1969).

488. Schubert, G., and R.E. Young, "The 4-day Venusian circulation driven by periodic thermal forcing," J. Atmos. Sci. 27, 523-528 (1970).

489. Scott, A.H., and E.J. Reese, "Venus: atmospheric rotation," Icarus 17/3, 589-601 (1972).

490. Shimazaki, T. and A. Kasahara, "Dynamic effects on height in the upper atmosphere," Space Research VII. North Holland Publ. Co. Amsterdam, 1967 p. 1210.

491. Shimazaki, T., "Dynamic effect on atomic and molecular oxygen density distribution in the upper atmosphere: a numerical solution to equations of motion and continuity," J. Atmosph. Terr. Phys. 29, 723-747 (1967).

492. Shimazaki, T., "Dynamic effect on height distribution of neutral constituents in the Earth's upper atmosphere: a calculation of atmospheric model between 70 km and 500 km," J. Atmosph. Terr. Phys. 30, 1279 (1968).

493. Shimizu, M., "Vertical distribution of neutral gases on Venus," Planetary Space Sci. 11, 268-273 (1963).

494. Shimizu, M., "The atomic and molecular processes in the upper atmosphere of planets," Rept. Ionosphere Space Res. Japan 20, 271-288 (1966).

495. Shimizu, M., "The recombination mechanism of O and CO in the upper atmosphere on Venus and Mars," Icarus 9, 593-597 (1968).

496. Shimizu, M., "A model calculation of the Cytherean upper atmosphere," Icarus 10/1, 11-25 (1969).

497. Shimizu, M., "Exospheric temperature of Venus. Institute of Space and Aeronautical Science University of Toyko," Report No. 455, Tokyo, September 1970.

498. Sill, G.T., "Sulfuric acid in the Venusian clouds," Commun. Lunar Planet. Lab. 9/171, 191-198 (1972).

499. Sinclair, A.C.E., J.P. Basart, D. Buhl, W.A. Gale, and M. Liwshitz, "Interferometric determination of the temperature distribution and atmospheric profiles on Venus." Report to the Second Symposium on the Atmospheres and Surface of Planets, Woods Hole, USA, 1968.

500. Sinclair, A.C.E., J.P. Basart, D. Buhl, W.A. Gale, and M. Liwshitz, "Preliminary results of interferometric observations of Venus at 11.1 cm wavelength," Radio. Science 5/2, 347-354 (1970).

501. Sinton, W.M., J. Strong, "Radiometric observations of Venus," Astrophys. J. 131, 470 (1960).

502. Sinton, W.M., "Infrared observations of Venus," Mem. Soc. roy. sci. Liege 7, No. 1, 300-310, Disc. 364-368 (1963).

503. Slanger, T.G., G. Black, "The CO_2 photolysis problem," Trans. Amer. Geophys. Union 51, 786 (1970).

504. Smith, B.A., "Rotation of Venus: continuing contradictions," Science 158/3797, 114-116 (1967).

505. Smith, B.A., "Rapid motions of ultraviolet clouds on Venus," Report at the Symposium on the Physics of the Moon and planets, Kiev, 1969. In the coll: Fizika Luny i planet [The physics of the Moon and planets], Nauka, 1972, pp. 324-325.

506. Smith, B.A., Personal communication, 1973.

507. Smith, W.B., "Radar observations of Venus, 1961 and 1959," Astron. J. 69, 42-48 (1964).

508. Smith, W.B., R.P. Ingalls, I.I. Shapiro, and M.E. Ash, "Surface-height variations on Venus and Mercury, " "Radio Sci. 5/2, 411-423 (1970).

509. Spinrad, H., "Spectroscopic temperature and pressure measurements in the Venusian atmosphere," Publ. Astron. Soc. Pacific 74/418, 187-201 (1962).

510. Spinrad, H., and S.I. Shawl, "Water vapor on Venus -- a confirmation," Astrophys. J. 146 328 (1966).

511. Spinrad, H., "Resolution of a CO_2 "hot band" in the Venusian spectrum," Astrophys. J. 145/3, 943 (1966).

512. Spreiter, J.R., A.L. Summers, and A.W. Rizzi, "Solar wind flow past nonmagnetic planets -- Venus and Mars," Planet. Space Sci. 18/9, 1281-1299 (1970).

513. Staelin, D.H., and A.H. Barrett, "Spectral observations of Venus near 1-centimeter wavelength," Astrophys. J. 144/1, 352 (1966).

514. Stankevich, K.S., "Observation of Mars and Venus at 11.1 cm," Austral. J. Phys. 23/1, 111 (1970).

515. Stauffer, F.R., and T.E. Walsh, "Transmittance of water vapor -- 14 to 20 microns," J. Opt. Soc. Amer. 56, 401 (1966).

516. Stewart, R.W., and J.S. Hogan, "Empirical determination of heating efficiencies in the Martian and Venusian atmospheres," J. Atmos. Sci. 26, 330 (1969).

517. Stewart, A.I., C.A. Barth, C.W. Hord, and A.L. Lane, "Mariner-9 ultraviolet spectrometer experiment: structure of Mars upper atmosphere," Icarus 17, 469-474 (1972).

518. Stewart, A.I., "Mariner-6 and -7 ultraviolet spectrometer experiment: implications of CO_2^+, CO and O airglow," J. Geophys. Res. 77, 54 (1972).

519. Stone, P.H., "Some properties of Hadley regimes on rotating and nonrotating planets," J. Atmos. Sci. 25/4, 644-657 (1968).

520. Stratton, A.J., "Optical and radio refraction on Venus," J. Atmos. Sci. 25/N 4, 666 (1968).

521. Strickland, D.J., "The O I 1304 and 1356 Å emissions from the atmosphere of Venus." Laboratory for Atmosph. and Space Phys., Univ. of Colorado, Rept. 1973.

522. Stull, V.R., P.J. Wyatt, and G.N. Plass, "The infrared transmittance of carbon dioxide," Appl. Optics 3/2, 243 (1964).

523. Thomas, G.E., "Neutral composition of the upper atmosphere of Mars as determined from the Mariner UV spectrometer experiments,"J. Atmos. Sci. 28, 859-868 (1971).

524. Thomson, J.H., J.E.B. Ponsonby, G.N. Taylor, and R.S. Roger, "A new determination of the solar parallax by means of radar echoes from Venus," Nature 190/4775, 519-520 (1961).

525. Thornton, D. D., and W.J. Welch, "Radio emission from Venus at 8.35 mm," Astron. J. 69/1, 71 (1964).

526. Tolbert, C.W., and A.W. Straiton, "35 Gs/c and 94 Gs/c Cytherean radiation," Nature 204/4965, 1242 (1964).

527. Ulich, B.L., J.R. Cogdell, and J.H. Davis, "Planetary observations at millimeter wavelength," NASA Techn. Rept. No. NGL-006-72-1, 31 Jan 1972.

528. Urey, H.C., "The origin and development of the Earth and other terrestrial planets," Geochim. et cosmochim. acta 1/4/516, 209 (1951).

529. Urey, H.C., "The atmospheres of the planets." Handbuch der Physik [Physics Handbook], Springer-Verlag, Berlin, 52, 363, 1959.

530. Van Allen, J.A., S.M. Krimgis, L.A. Frank, and T.P. Armstrong, "Venus: an upper limit on intrinsic magnetic dipole moment based on absence of a radiation belt," Science 158, 1673-1675 (1967).

531. Van de Hulst, H.C., "Scattering in a planetary atmosphere," Astrophys. J. 107, 220 (1948).

532. Vaucouleurs, G. de, and D.H. Menzel, "Results of the occultation of Regulus by Venus," July 7, 1959; Nature 188/4744, 28-33 (1960.

533. Vaucouleurs, G. de, "Geometric and photometric parameters of the terrestrial planets," Icarus 3/3, 187 (1964).

534. Veronis, G., "Penetrative convection," Astrophys. J. 137/N 2 (1963).

535. Victor, W.K., and R. Stevens, "Exploration of Venus by radar," Science 134, 46-48 (1961).

536. Victor, W.K., and R. Stevens, "The 1961 JPL Venus radar experiment," IRE SET-8, No. 2, 84 (1962).

537. Vinogradov, A.P., Yu. A. Surkov, and C.P. Florensky, "The chemical composition of the Venusian atmosphere based on the data of the Interplanetary Station Venera-4," J. Atmos. Sci. 25/4, 535 (1968).

538. Walker, R.G., and C. Sagan, "The ionospheric model of the Venusian microwave emission: an obituary," Icarus 5 105 (1966).

539. Wallace, L., "Analysis of the Lyman-alpha observations of Venus made from Mariner-5," J. Geophys. Res. 74, 115 (1969).

540. Warnock, W.W., and J.R. Dickel, "The revised microwave spectrum of Venus," Preprint. 15 Jan 1969.

541. Warnock, W.W., and J.R. Dickel, "Venus: measurements of brightness temperatures in the 7-15 cm wavelength range and theoretical radio and radar spectra for a two layer subsurface model," Icarus 17/3, 682-691 (1972).

542. Weinberg, J.L., and G. Newkork, "Airglow of Venus: a reexamination," Planet. Space Sci. 5, 163-164 (1961).

543. Welch, W.J. and D.D. Thornton, "Recent planetary observations at wavelengths near 1 cm," Astron. J. 70/2, 149 (1965).

544. Weller, C.S., and M.A. Biondi, "Measurements of dissociative recombination of CO_2^+ ions with electrons," Phys. Rev. Letters 19, 59-61 (1967).

545. Westphal, J.A., R.L. Wildey, and B.C. Murray, "The 8-14-micron appearance of Venus before the 1964 conjunction," Astrophys. J. 142/2, 799 (1965).

545a. Wildt, R., "Note on the surface temperature of Venus," Astrophys. J. 91, 266-268 (1940).

546. Wildt, R., "The greenhouse effect in a gray planetary atmosphere," Icarus 5/24 (1966).

547. Wright, W.H., "Photographs of Venus made by infrared and by violet," Publs. Atron. Soc. Pacif. 39/230, 220-221 (1927).

548. Wrixon, G.T., W.J. Welch, and D.D. Thornton, "The spectrum of Jupiter at millimeter wavelength," Astrophys. J. 169/1, 171-183 (1971).

549. Wyatt, P.J., V.R. Stull, and G.N. Plass, "Infrared absorption of water vapor," Aeronutronic Rept. No. SSD - TDR - 62 - 127, 11 (1962).

550. Young, A.T., "Are the clouds of Venus sulfuric acid?" Icarus 18, 564-582 (1973).

551. Young, L.D.G.,"High resolution spectra of Venus," Icarus 17, 632 (1972).

552. Young, L.D.G. and R.A. Schorn, "High dispersion spectroscopic observations of Venus during 1968 and 1969. I. The carbon dioxide bands at 7810 Å and 7884 Å," Acta Astron. 21/3, 329-363 (1971).

553. Young, R.A., G. Black, and T.G. Slanger, "Reaction and deactivation of O (^{1}D)," J. Chem. Phys. 2/1-3 (1968).

554. Burangulov, N.I., S.S. Zilitinkevich, V.V. Kerzhanovich, S.S.Monin, M.K. Rozhdestvenskiy, A.S. Safray, V.G. Turikov, and D.V. Chalikov, Dinamika atmosfery Venery [The dynamics of the Venusian atmosphere], Leningrad, 1974.

554a. Vernov, S.N., A. Ye. Chudakov, P.V. Valukov, Ye. V. Gorchakov, P.P. Ignat'yev, N.N Kontor, Yu. I. Logachev, G.P. Lyubimov, A.G. Nikolayev, and N.V. Pereslegina, "The measurements of cosmic rays and the search for radiation belts near Venus," in the coll: Fizika Luny i planet [The physics of the Moon and planets], Nauka, 1972, pp. 397-402.

555. Harris, D.L., "Integral photometry and colorimetry of the planets and their satellites," in the coll: Planety i sputniki [Planets and their satellites], Ed. by G. Kuiper and B. Middlehurst, I.L., 1963.

556. Danilov, A.D., "Radio astronomy research and current conceptions about the Venusian atmosphere," Kosmich. Issled. 2/1, 121 (1964).

556a. Izakov, M.N., Doctoral dissertation, IKI AN SSSR, 1973.

557. Ivanov, V.N., A. Ye. Ordanovich, and L.I. Petrova, "Large-scale structure and its interaction with small-scale turbulence in the near-Earth layer," Izv. AN SSSR, Fizika Atmosfery i Okeana 7/3, 261-269 (1971).

558. Ivanov, V.N., and A.Ye. Ordanovich, "Certain feedbacks arising during turbulent cellular convection in the atmosphere," Izv. AN SSSR, Fizika Atmosfery i Okeana 8/11, 1216-1220 (1972).

559. Ivanov, V.N., A. Ye. Ordanovich, and L.I. Petrova, "Several features of the spectra of wind velocity and air temperature in the low-frequency range during convection," Izv. AN SSSR, Fizika Atmosfery i Okeana 9/8, 787-800 (1973).

560. Krekova, M.M., G.M. Krekov, G.A. Titov, and Ye. M. Feygel'son, "The possibility of calculating the spectral albedo of Venus in the near-infrared range," Kosmich. Issled 11/14, 607-611 (1973).

561. Levin, B. Yu., Proiskhozhdeniye Zemli i planet [The origin of the Earth and planets], Nauka, 1970.

562. Monin, A.S., Prognoz pogody kak zadacha fiziki [Weather forecasting as a problem of physics], Nauka, 1970.

563. Ronov, A.B., and A.A. Yaroshevskiy, "The chemical structure of the Earth's crust," Geokhimiya, 11, (1967).

564. Sorokhtin, O.G., Priroda tektonicheskoy aktivnosti Zemli i proiskhozhdeniye okeanov [The nature of the Earth's tectonic activity and the origin of the oceans], Doctoral dissertation, Moscow, 1973.

565. Sorokhtin, O.G., Global'naya evolyutsiya Zemli [The global evolution of the Earth], Nauka, Moscow, 1974.

566. Cheremukhina, Z.P., S.F. Morozov and N.F. Borodin, "Estimate of the temperature of the Venusian stratosphere according to data on the g-forces of the automatic station Venera-8," Kosmich. Issled. 12/2, 264-271 (1974).

566a. Shari, V.P., "Fluxes of heat radiation in the lower atmosphere of Venus," Kosmich. Issled. (1974) (in print).

567. Shmidt, O. Yu. Chetyre lektsii o teorii proiskhozhdeniya Zemli [Four lectures of the theory of the Earth's origin], 3rd Edition, AN SSSR 1952.

568. Yunge, Kh., Khimicheskiy sostav i radioaktivnost' atmosfery [The chemical composition and radioactivity of the atmosphere], Mir, 1965.

569. Bridge, H.S., A.J. Lazarus, J.D. Scudder, K.W. Ogilvie, R.E. Hartle, J.R. Asbridge, S.J. Bame, W.C. Feldman, G.L. Siscoe, "Observations at Venus encounter by the plasma science experiment on Mariner 10," Science 183/4131, 1293-1296 (1974).

570. Broadfoot, A.L., S. Kumar, M.J.S. Belton, and M.B. McElroy, "Ultraviolet observations of Venus from Mariner-10: Preliminary results," Science 183/4131, 1315-1318 (1974).

571. Cameron, A.G.W., "A new table of abundances of the elements in the solar system" In: Origin and distribution of the elements, (Editor L.H. Ahrens), pp. 125-143, Pergamon Press, 1968.

572. Chase, S.C., E.D. Miner, D. Morrison, G. Münch and C. Neugebauer, "Preliminary infrared radiometry of Venus from Mariner-10," Science 183/4131, 1291-1292 (1974).

573. Gierasch, P.J., R. Goody, and P. Stone, "The energy balance of planetary atmospheres," Geophys. Fluid Dynamics 1/1, 1-13 (1970).

574. Golitsyn, G.S., "A similarity approach to the general circulation of planetary atmospheres," Icarus 13, 1 (1970).

575. Golitsyn, G.S., and A.S. Gurvich, "An estimate of refractive index fluctuations in the Venusian atmosphere from Mariner-5 data," J. Atmos. Sci. 28/1, 138-140 (1971).

576. Hansen, J.E., and J.W. Hovenier, "Interpretation of the polarization of Venus," J. Atmos. Sci. 1974 (in print).

577. Howard, H.T., G.L. Tyler, G. Fjeldbo, A.J. Kliore, G.S. Levy, D.L. Brunn, R. Dickinson, R.E. Edelson, E.L. Martin, R.B. Postal, B. Seidel, T.T. Sesplaukis, D.L. Shirley, C.T. Stelzried, D.N. Sweetnam, A.I. Zygielbaum, P.B. Esposito, J.D. Anderson, I.I. Shapiro, and R.D. Reasenberg, "Venus: mass, gravity field, atmosphere and ionosphere as measured by the Mariner-10 dual-frequency radio system," Science 183/4131, 1297-1301 (1974).

578. Kliore, A., G.S. Levy, D.L. Cain, G. Fjeldbo, and S.I. Rasool, "Atmosphere and ionosphere of Venus from the Mariner-5 S-band radio occultation measurement," Science 158, 1683-1688 (1967).

579. Malkus, W.V.R., "Hadley-Halley circulation on Venus," J. Atmos. Sci. 27, 529 (1970).

580. Morowitz, H., and C. Sagan, "Life in the clouds of Venus?", Nature 215, 1259 (1967).

581. Murray, B.C., M.J.S. Belton, G.E. Danielson, M.E. Davies, D. Gault, B. Hapke, B. O'Leary, R.G. Strom, V. Suomi, and N. Trask,"Venus: atmospheric motion and structure from Mariner-10 pictures," Science 183/4131, 1307-1315 (1974).

582. Ness, N.F., K.W. Behannon, R.P. Lepping, Y.C. Whang, and K.H. Schatten, "Magnetic field observations near Venus: preliminary results from Mariner-10," Science 183/4132, 1301-1306 (1974).

583. Sagan, C., "Life on the surface of Venus?", Nature 216/5121, 1198 (1967).

584. Sagan, C. and J. Pollack, "On the structure of the Venusian atmosphere," Icarus 10/2, 274-289 (1969).

585. Sagan, C., "Life," Encyclopedia Britannica, 1970.

586. Schubert, G. and J.A. Whiteheed, "Moving flame experiment with liquid mercury: possible implications for the Venusian atmosphere," Science, 163 71-72, 1969.